171(4), 2017



COMBUSTION ENGINES



AVL X-ion™
Modular data acquisition platform

Adapts. Acquires. Inspires.

AVL X-ion™ is the new high-speed data acquisition platform dedicated to powertrain development.
It is a modular acquisition system that can be easily adapted to different units under test and environments, and that will help manage the growing powertrain complexity.
Powertrain developers can now quickly match acquisition systems to the units under test, thus harmonizing test cells and standardizing test processes.
This new platform combines indicating, optical and e-Power analysis technologies into a single package.

Your added value:

- Increased efficiency based on reduced number of tools in the test facility and in the office
- Enables testbed versatility, reduces changeover and retooling times
- Stress-free transition to electrified powertrains
- Future-proof investment thanks to evolutionary module concept

www.avl.com/x-ion, info@avl.com

PTNSS Supporting Members
Członkowie wspierający PTNSS

BOSMAL Automotive Research and Development Institute Ltd
Instytut Badań i Rozwoju Motoryzacji BOSMAL Sp. z o.o

Motor Transport Institute
Instytut Transportu Samochodowego

The Institute for Sustainable Technologies
Instytut Technologii Eksploatacji

Institute of Aviation
Instytut Lotnictwa

Automotive Industry Institute
Przemysłowy Instytut Motoryzacji

The Rail Vehicles Institute TABOR
Instytut Pojazdów Szynowych TABOR

Institute of Mechanised Construction and Rock Mining
Instytut Mechanizacji Budownictwa i Górnictwa Skalnego

Institute of Logistics and Warehousing
Instytut Logistyki i Magazynowania

Industrial Institute of Agricultural Engineering
Przemysłowy Instytut Maszyn Rolniczych

AVL List GmbH

Solaris Bus & Coach S.A.

Air Force Institute of Technology
Instytut Techniczny Wojsk Lotniczych

COMBUSTION ENGINES

A Scientific Magazine

2017, 171(4)

Year LVI

PL ISSN 2300-9896

Editor:

Polskie Towarzystwo Naukowe Silników Spalinowych
43-300 Bielsko-Biała, Sarni Stok 93 Street, Poland
tel.: +48 33 8130402, fax: +48 33 8125038
E-mail: sekretariat@ptnss.pl
WebSite: http://www.ptnss.pl
Papers available on-line: http://combustion-engines.eu

Scientific Board:

Prof. Krzysztof Wisłocki – Chairman, Poland

Prof. Ewa Bardasz – USA
Prof. Bernard Challen – UK
Prof. Zdzisław Chłopek – Poland
Prof. Giovanni Cipolla – Italy
Prof. Jan Czerwiński – Switzerland
Prof. Vladimir Hlavna – Slovakia
Prof. Kazimierz Lejda – Poland
Prof. Hans Peter Lenz – Austria
Prof. Helmut List – Austria
Prof. Jan Macek – Czech Republic
Prof. Elena R. Magaril – Russia
Prof. Janusz Mysłowski – Poland
Prof. Andrzej Niewczas – Poland
Prof. Marek Orkisz – Poland
Prof. Dieter Peitsch – Germany
Prof. Stefan Pischinger – Germany
Prof. Roger Sierens – Belgium
Prof. Andrzej Sobiesiak – Canada
Prof. Richard Stobart – UK
Prof. Robin Vanhaelst – Germany
Prof. Michael P. Walsh – USA
Prof. Piotr Wolański – Poland
Prof. Mirosław Wyszyński – UK

Editorial:
Institute of Combustion Engines and Transport
Poznan University of Technology
60-965 Poznan, Piotrowo 3 Street
tel.: +48 61 2244505, +48 61 2244502
E-mail: papers@ptnss.pl

Prof. Jerzy Merkisz, DSc., DEng. (Editor-in-chief)
Miłosław Kozak, DSc., DEng. (Editorial Secretary for Science) – papers@ptnss.pl
Ireneusz Pielecha, DSc., DEng. (Technical Editor)
Krystyna Bubacz, MSc. (Proofreading Editor)
Wojciech Serdecki, DSc., DEng. (Statistical Editor)
and Associate Editors

Contents

Aoyagi Y. Improvement of BSFC and effective NO_x and PM reduction by high EGR rates in heavy duty diesel engine (CE-2017-401) 4

Piekarski W., Kuranc A. Exhaust emissions and fuel consumption in a chassis dynamometer load test in the aspect of modification of an engine controlling system (CE-2017-402) 11

Osipowicz T., Lisowski M. The influence of corrosion phenomena on operational parameters of modern fuel injectors CI-engines (CE-2017-403) 17

Merkisz-Guranowska A. Product recycling of automotive parts – trends and issues (CE-2017-404) 24

Grabowski Ł., Wendeker M., Barański G., Duk M. Study of the efficiency of on-board electricity generation in the city bus (CE-2017-405) 29

Wysocki O., Kropiwnicki J., Czyżewicz J. Analysis of the possibility of determining the general characteristics using the operational data of a vehicle engine (CE-2017-406) 33

Rybak A., Hunicz J., Krzaczek P., Golimowski W., Marcinkowski D. Effect of different biofuels on common rail injector flow rate (CE-2017-407) 39

Zadrąg R., Kniaziewicz T. Utilization of the zero unitarization method for the building of a ranking for diagnostic marine engine parameters (CE-2017-408) 44

Worsztynowicz B. Influence of the method of implementing the forced air flow through the cooling system on the temperature of the coolant in heavy-duty engines (CE-2017-409) 51

Korczewski Z., Marszałkowski K., Rudnicki J. The concept of research on ecological, energy and reliability effects of modified marine fuel oils application to supply compression-ignition engines in real conditions (CE-2017-410) 56

Bebkiewicz K., Chłopek Z., Szczepański K., Zimakowska-Laskowska M. Estimating pollutant emission from motor vehicles in the years 2000–2015 (CE-2017-411) 62

Szrama S., Kadziński A. Hazard identification process in the selected analysis domain of the F100 turbofan engines maintenance system (CE-2017-412) 68

Kropiwnicki J., Dominiczak P., Kneba Z., Makowski S., Cieśliński J.T., Ziółkowski M. Analysis of the possibilities of using of DME fuel in motor boat drive systems (CE-2017-413) 74

Doustdar O., Wyszynski M.L., Tsolakis A., Mahmoudi H. Bio-ketones from lignocellulosic biomass: experimental investigation on fuel properties, combustion and emission characteristics of cyclopentanone blends with diesel in compression ignition engine (CE-2017-414) 81

Wirkowski P.J., Kniaziewicz T. Evaluation of marine gas turbine engine parameters in terms of issue of missions of exhaust toxic fumes (CE-2017-415) 87

Bebkiewicz K., Chłopek Z., Szczepański K., Zimakowska-Laskowska M. Evolution of national annual pollutant emission from motor vehicles in Poland (CE-2017-416) 92

Alqahtani A., Wyszynski M., Mazuro P., Xu H. Evaluation of the effect of variable compression ratios performance on opposed piston 2-stroke engine (CE-2017-417) 97

Wróblewski P. The effect of the distribution of variable characteristics determining the asymmetry of the sealing rings sliding surfaces on the values of friction loss coefficients and other selected parameters of oil film (CE-2017-418) 107

Mrozik M., Danilecki K. Environmental assessment of the production process of internal combustion engines (CE-2017-419) 117

Bebkiewicz K., Chłopek Z., Stosio G., Szczepański K., Zimakowska-Laskowska M. Evolution of national annual pollutant emission from motor vehicles in Poland (CE-2017-420) 121

Kałużny J., Merkisz J., Stepanenko A., Wróblewski E., Gapiński B., Piasecki A., Gallas D. Piston assembly in the most powerful 2.0l diesel engine – case study of the current tribological system and innovative concepts for the future (CE-2017-421) 127

Chłopek Z., Samson-Bręk I. Analysis of the ecological effects of biogas use of to supply the internal combustion engine in the electricity generation process – result of LCA analysis (CE-2017-422) 134

Faber J., Brodzik K. Elemental analysis as an important tool for fuels and biofuels quality control (CE-2017-423) 140

Stawecki W., Merkisz J., Bajerlein M., Daszkiewicz P. New technologies of enhanced plastic for use in rail vehicles to reduce noise emissions (CE-2017-424) 145

Flekiewicz M., Kubica G., Marzec P. The possibilities of using DME (BioDME), as an additive to conventional gaseous fuels in SI engine (CE-2017-425) 150

Chłopek Z., Biedrzycki J., Lasocki J., Wójcik P., Samson-Bręk I. Modelling of motor vehicle operation for the evaluation of pollutant emission and fuel consumption (CE-2017-426) 156

Kolodziej C., Wallner T. Combustion characteristics of various fuels during research octane number testing on an instrumented CFR F1/F2 engine (CE-2017-427) 164

Bebkiewicz K., Chłopek Z., Stosio G., Szczepański K., Zimakowska-Laskowska M. Study on sensitivity of national annual pollutant emission from passenger cars to traffic patterns (CE-2017-428) 170

Bera P. Torque characteristic of SI engine in dynamic operating states (CE-2017-429) 175

Gis W., Waśkiewicz J. Development of the international freight transport sector in Poland against the background of the EU market (CE-2017-430) 181

Skowron M., Pielecha I., Wisłocki K. Optical tests as the basis for creating mathematical models to delay opening of CIDI injectors (CE-2017-431) 185
Skarbek-Żabkin A. Effect of the addition of synthetic fuel on the selected physico-chemical properties of the fuel for the diesel engines (CE-2017-432) 193
Fiedkiewicz Ł., Pielecha I., Wisłocki K. Use of the gas ionization signal for combustion process diagnostics in the cylinder of a spark ignition engine (CE-2017-433) 196
Piątkowski P., Lewkowicz R., Ściegienka R., Mysłowski J. The impact of intake channel geometry on in-cylinder swirl (CE-2017-434) 201
Weber M. The influence of high efficiency engines and hybrids on exhaust systems (CE-2017-435) 207
Śmieja M., Wierzbicki S., Mamala J. CAN network in real time on board systems (CE-2017-436) 211
Pojawa B. Energetic state parameters measurements of LM 2500 naval gas turbine for modeling and simulation purposes (CE-2017-437) 215
Ambrozik A., Kurczyński D., Łagowski P., Warianek M. External speed–torque characteristics of Fiat 0.9 TwinAir petrol- and CNG-fuelled engine (CE-2017-438) 222
Bielaczyc P., Szczotka A., Woodburn J. Exhaust emissions of particulate matter from light-duty vehicles – an overview and the current situation (CE-2017-439) 227
Sitnik L.J. Statistic of fuel consumption in test and in natural operation of vehicles (CE-2017-440) 239
Kulczycki A. Theoretical approach to modeling the combustion process in turbine engines fuelled by alternative aviation fuels con-taining various components/biocomponents (CE-2017-441) 245
Stawecki W., Bajerlein M., Daszkiewicz P. Modern high-resistance alloy steel used in railway transport (CE-2017-442) 250
Ambrosewicz-Walacik M., Tańska M., Walacik M., Nitkiewicz S. Production of fuel blends from diesel oil and waste products (CE-2017-443) 255
Borowczyk T., Spadło M. The issues of designing of construction features of the internal combustion cam engine (CE-2017-444) 260
Szczepański T., Skarbek-Żabkin A., Dziedziak P. Impact of the road conditions on the amount of braking energy (CE-2017-445) 265
Cisek J. The influence of non-cooled exhaust gas recirculation on the diesel engine parameters (CE-2017-446) 269
Balawender K., Konieczny D., Kuszewski H., Lejda K., Lew K., Wojewoda P. The effect of physicochemical properties of fuels on ecological param-eters of a diesel engine (CE-2017-447) 274
Szymański G.M., Misztal W. Analysis of measurement points sensitivity of vibration signals on the stand of jet engine (CE-2017-448) 279
Cisek J. The influence of non-cooled exhaust gas recirculation on the indicator diagrams and heat release parameters in diesel engine cylinder (CE-2017-449) 283

Editor
Polish Scientific Society of Combustion Engines
43-300 Bielsko-Biała, Sarni Stok 93 Street, Poland
tel.: +48 33 8130402, fax: +48 33 8125038
E-mail: sekretariat@ptnss.pl
WebSite: http://www.ptnss.pl

The Publisher of this magazine does not endorse the products or services advertised herein. The published materials do not necessarily reflect the views and opinions of the Publisher.

© Copyright by
Polish Scientific Society of Combustion Engines
All rights reserved.
No part of this publication may be reproduced, stored in a retrieval system or transmitted, photocopied or otherwise without prior consent of the copyright holder.

Subscriptions
Send subscription requests to the Publisher's address.
Cost of a single issue PLZ30 + VAT.

Preparation for print
ARS NOVA Publishing House
60-782 Poznań, ul. Grunwaldzka 17/10A

Circulation: 700 copies.

Printing and binding
Zakład Poligraficzny Moś i Łuczak, sp. j., Poznań, ul. Piwna 1

The journal is registered in the Polish technical journals content database – **BAZTECH** www.baztech.icm.edu.pl

The journal is listed in the international database **IC Journal Master List** – **Index Copernicus** www.indexcopernicus.com

Declaration of the original version
The original version of the Combustion Engines journal is the printed version.

Papers published in the ***Combustion Engines*** quarterly receive 13 points as stated by the Notification of the Minister of Science and Higher Education dated 31 December 2015.

Cover
I – Bentley – triple-charged 4.0-litre V8 engine
background – Gigapixel (*fot. www.bentleymedia.com*)
IV – Porsche Panamera Turbo – Direct fuel injection
(*fot. www.caricos.com*)

Article citation info:
AOYAGI, Y. Improvement of BSFC and effective NO_x and PM reduction by high EGR rates in heavy duty diesel engine. *Combustion Engines*. 2017, **171**(4), 4-10. DOI: 10.19206/CE-2017-401

Yuzo AOYAGI

CE-2017-401

Improvement of BSFC and effective NO_x and PM reduction by high EGR rates in heavy duty diesel engine

The test engine was a turbocharged 10.5L engine with an intercooler. A performance target was set at a rated power of 300 kW (BMEP = 1.7 MPa) and peak torque of 1842 Nm (BMEP = 2.2 MPa). Emission targets were set at a level of near future and stringent regulation standards in Japan. The engine was equipped with new technologies such as a high pressure common rail system, FCD piston, a high pressure ratio VGT and an aftertreatment system. The high and low pressure loop EGR system was installed and this system with a VGT had a high performance and could increase an EGR rate in order to reduce $BSNO_x$ while maintaining the satisfied BSFC and PM performance simultaneously not only in the steady state condition but also in the transient condition.

Key words: *diesel engine, exhaust emissions, turbocharger, fuel injection*

1. Introduction

Now diesel engines still have considerable advantages in regard to engine power, fuel economy and durability for commercial vehicles when compared with other types of internal combustion engines. These advantages along with the continuous refinement have led diesel vehicles to the widespread use as prime movers for heavy-duty vehicles. At the present time however, a reduction of exhaust emissions such as NO_x, PM and CO_2 is essential, to meet more stringent emission regulations [1], and several breakthrough technologies will be required.

The author's study has aimed at establishing a new combustion concept for clean diesel engines for the new future emission regulations and both wide range and high EGR rates under the high boost pressure, their effects on the engine performance, $BSNO_x$ and PM are discussed.

New A.C.E. Institute Co., Ltd. (New ACE) was established in 1992 and has researched the improvement of thermal efficiency and exhaust emissions in heavy duty diesel engines (HDDE) by single cylinder engines [2–6]. In 2004 New ACE participated the Japanese national project named Super Clean Diesel (SCD) Engine and has added six cylinder engines in its research. In this paper the author has reviewed the research of these 10 years focusing on the improvement of thermal efficiency and exhaust emissions of a heavy duty six cylinder engine [7–9].

2. Clean technologies for diesel engine

A history of Japanese emission standards for heavy duty diesel vehicles is shown in Fig. 1. Japanese emission standards started as a D6 mode in 1974 and changed to a D13 mode in 1994 year. In 2005, a JE05 started as a first transient test cycle. WHTC started as a new Japanese emission regulation from autumn of 2016. A reduction of exhaust emissions is now going by the adoption of new technologies such as turbocharging, intercooling and the common rail fuel injection system, which allows a high pressure injection [10–13]. Further improvement on these technologies will be carried out going forward [2, 4, 5, 7–9]. Catalysts are indispensable for the reduction of exhaust emissions from diesel engines and it is also necessary to minimize engine-out exhaust emissions [12]. Accordingly, it is very important to combine effects of both combustion improvement and aftertreatment systems efficiently [7, 8, 12]. A history of clean diesel technologies for heavy duty engines is shown in Fig. 2.

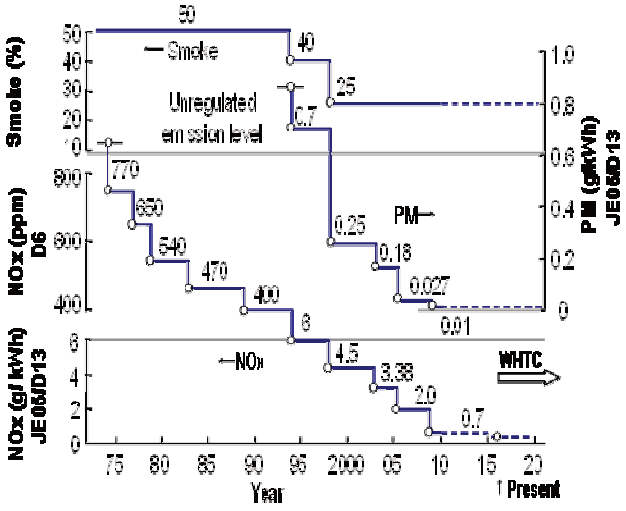


Fig. 1. History of Japanese emission standards for heavy duty diesels

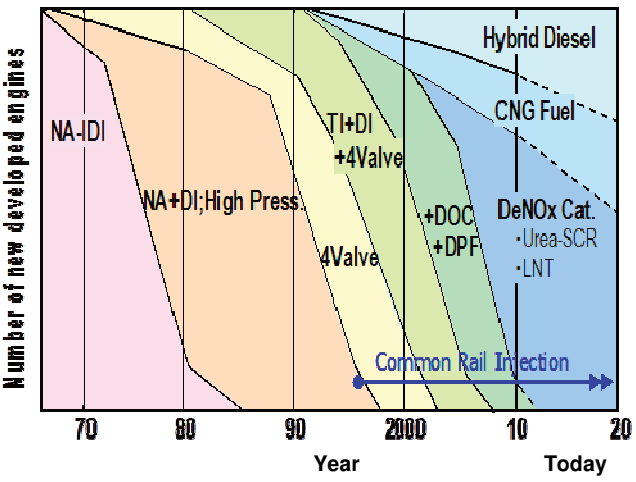


Fig. 2. History of clean emission technologies in heavy duty diesels in Japan

3. Targets of project

The research objectives are low emissions and a high engine performance, and the target emissions are $BSNO_x$ = 0.2 g/kWh and PM = 0.01 g/kWh with aftertreatment systems under the Japanese JE05 transient test cycle. The engine-out emission targets without aftertreatment systems are $BSNO_x$ = 1.0 g/kWh and PM = 0.10 g/kWh under the same test cycle. This target will be achieved by means of combustion improvement and new technologies such as a high pressure common rail system, FCD (Ductile cast iron) piston [10], a high pressure ratio VGT and a combination of high and low pressure loop EGR [7, 8]. After minimizing engine-out exhaust emissions the author will use aftertreatment for the reduction of exhaust emissions from diesel engine [7, 8, 12]. This policy for reduction of exhaust emissions is shown in Fig. 3.

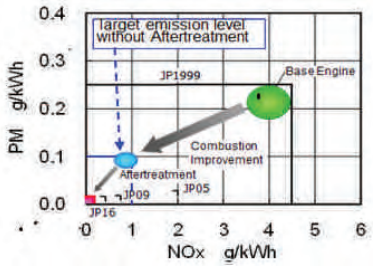


Fig. 3. Strategy of clean emissions

4. Combustion concepts

For the emissions reduction and the high thermal efficiency, many engine components and systems should be improved. Combustion concepts are useful and efficient to develop a brand new engine. The combustion concepts for clean diesel engines have been accomplished and are presented in below. The explanations are as follows;

(1) Lean combustion is necessary for the complete burning, using large quantities of O_2 in a low combustion temperature.

(2) A high boost intake pressure is necessary for combustion in high air density.

(3) A fuel injection in high air density is necessary for reducing exhaust smoke because of a fall of the peak of the fuel/air ratio in a spray.

(4) A high pressure fuel injection is required for a smoke reduction through fine atomization.

(5) A high BMEP engine is needed for a reduction of friction and heat loss.

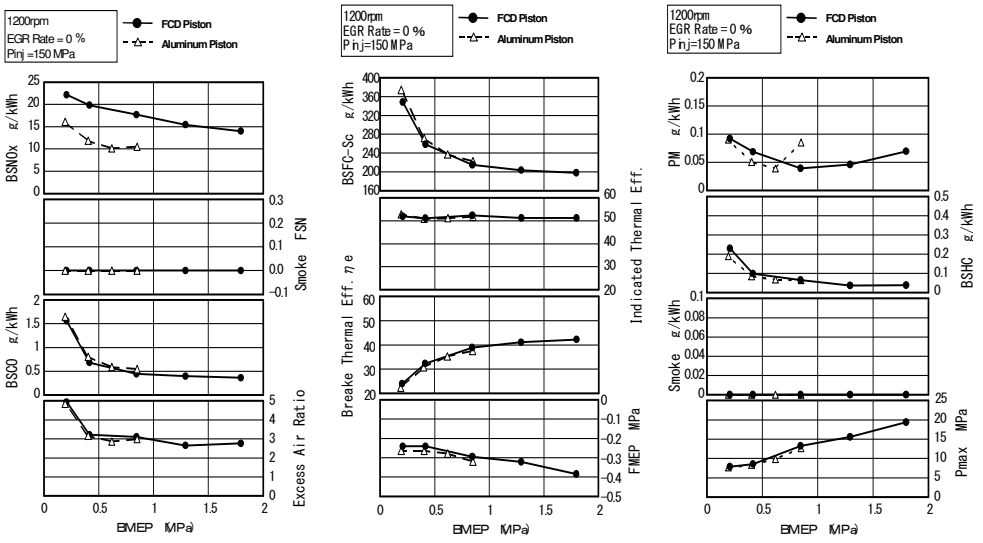
(6) A high EGR rate at a wide speed range and a wide load range is necessary for a drastic $BSNO_x$ reduction.

New technologies are intended for use for the clean diesel engine. Some of these technologies are controlled electronically.

5. New engine and specifications

The author has adopted FCD piston for strength and thermal efficiency instead of aluminum alloy piston and shows the experimental results between FCD piston and aluminum alloy piston by a single cylinder engine before making the six cylinder engine in Fig. 4. Though $BSNO_x$ of FCD is two times of aluminum alloy piston, BSFC of FCD is lower than aluminum alloy because of obtaining high BMEP.

The research engine was modified for high BMEP and a high intake boost pressure from Hino P11C [10]. The engine specifications are presented in Table 1. The newly employed technologies for the engine are shown in Table 2. A schematic of the engine system is illustrated in Fig. 5. A test engine was an in-line six-cylinder turbocharged and intercooled engine with a displacement of 10.5 L, composing of a variable geometry turbocharger (VGT), various cooled EGR systems with a combination of High Pressure Loop EGR (HPL-EGR) and Low Pressure Loop EGR (LPL-EGR), intake-air throttle valves and a back-pressure control valve (BPCV). The VGT is a prototype and had the maximum compressor pressure ratio of 5.0, and this is twice as much as the ordinary turbocharger (approx. 3.0). In Fig. 6 the author shows comparison of compressor map between a current and a high pressure ratio one (SCD).



a. Emissions b. BSFC and FMEP c. PM, BSHC and Smoke

Fig. 4. The comparison of FCD piston and Aluminum alloy piston in combustion characteristics

Table 1. Specifications and targets of clean diesel engine

Engine Type		DI, In-Line 6
Bore × Stroke		Φ 122 mm × 150 mm
Displacement		10,520 cm^3
Compression Ratio		15.3
Swirl Ratio		1.0–9.0
Injection Nozzle		Φ 0.139 mm × 8-155°
Max Output	Engine Speed	2000 rpm
	Output	298{405} kW {PS}
	BMEP	1.7 MPa
Max Torque	Engine Speed	1400 rpm
	Output	1842{188} Nm {kg m}
	BMEP	2.2 MPa

Table 2. Technologies for clean emissions

No.	New technologies
1	High boosting SCD Turbocharger
2	FCD piston & strong structure engine
3	200 MPa common rail injection system
4	High & low combined pressure loop EGR
5	EGR valve and intake air valve
6	High efficiency EGR cooler
7	Variable Valve Actuation
8	Variable Swirl system
9	Efficient SCD after-treatment
10	SCD Electronic control system for JE05

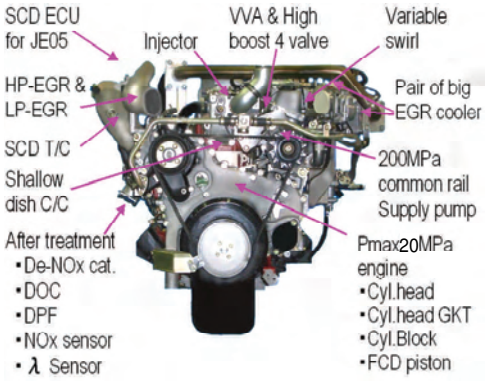


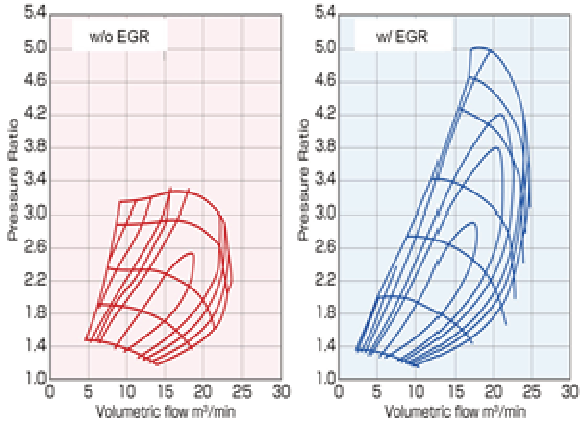
Fig. 5. New engine for clean emissions and its new technologies

As aftertreatment systems, a Lean-NOx Trap (LNT+ DOC) was used for reducing BSNOx and a catalyzed DPF was used for reducing PM from exhaust gases. In Japan low sulfur diesel fuels with the standard sulfur content of less than 10 ppm were used as test fuels, and today they are commercially available. Actual test fuels were the 7 ppm sulfur content. Furthermore, low sulfur engine oil containing 0.26 mass% of sulfur was used as lubricant oil.

6. Experimental measurement for HDDE

An engine performance was measured using a dynamometer system with data acquisition and control systems (FAMS-8000 series; Ono Sokki Co. Ltd.). Exhaust emissions were measured using an emissions analyzer (MEXA-7100DEGR; Horiba Instruments Ltd.).

Smoke was measured using smoke meters (Tsukasa Sokken Co. Ltd. and AVL Co., Ltd.) during the steady state test. An AVL opacimeter was used to measure smoke in the transient test. Particulate matter (PM) was measured using a micro-tunnel (DLT-1303; Horiba Ltd.). An intake air flow rate was measured by a laminar flowmeter (Tsukasa Sokken Co. Ltd.). Cylinder pressure sensing was performed using a pressure transducer (Type 6043A; Kistler Instruments AG). A combustion analysis for the rate of heat release and others was performed using an analyzer (DS-2000 series; Ono Sokki Co. Ltd.).



a. Current Comp. Map b. SCD Comp. Map

Fig. 6. Comp. map comparison of current and new VGT/C

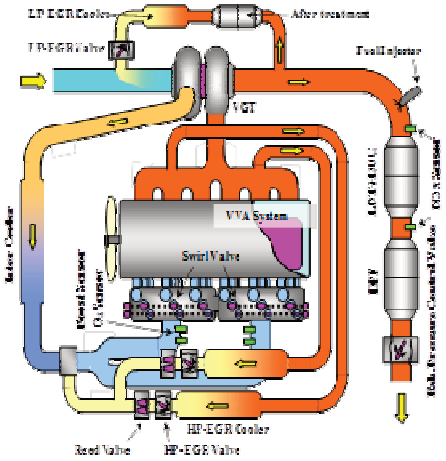


Fig. 7. Layout of new engine for clean emissions

7. Experimental result

7.1. Definition of EGR rate

The EGR rate is defined as shown below:

$$\text{EGR Rate} = \frac{[CO_2]\text{in} - [CO_2]\text{atm}}{[CO_2]\text{exh} - [CO_2]\text{atm}} \times 100\,\%$$

$[CO_2]$ signifies the CO_2 concentration. CO_2 concentrations were measured by an emission analyzer at each point: $[CO_2]$in was measured at the intake manifold inlet; $[CO_2]$exh was measured at the exhaust outlet of a turbocharger; and $[CO_2]$atm was measured in the test room. The $[CO_2]$atm value of 0.04% was used as the atmospheric CO_2 concentration.

7.2. Effects of HPL and LPL-EGR on turbocharging

Fig. 8a shows an intake fresh air flow rate Ga without EGR gas, a boost pressure Pb, a turbocharger (T/C) speed and an exhaust gas flow rate Gt from top in changing total EGR rates. In this case, EGR rates were changed at fixed VGT nozzle closing. Though the EGR rate was the same value, a HPI (High Pressure Index) was varied. A fraction of HPL-EGR in the combination of HPL-EGR and LPL-EGR is designated as a HPL-EGR index and is represented as HPI (%) shown in the definition in the previous section. The EGR rates were compared in four conditions: HPI = 0%, 40%, 60% and 100%, which are marked with ▲,●,◆ and ■ without a back pressure control valve (BPCV) and △,○ and ◇ with a BPCV respectively to increase the EGR rate. HPI = 100% means using HPL-EGR only, whereas HPI = 0% denotes the use of LP-EGR only. This HP-EGR index is defined by the following equation

$$\text{HPI}\ \ \% = \frac{\text{HP-EGR Rate}}{\text{HP-EGR Rate} + \text{LP-EGR Rate}} \times\ 100\ \ \%$$

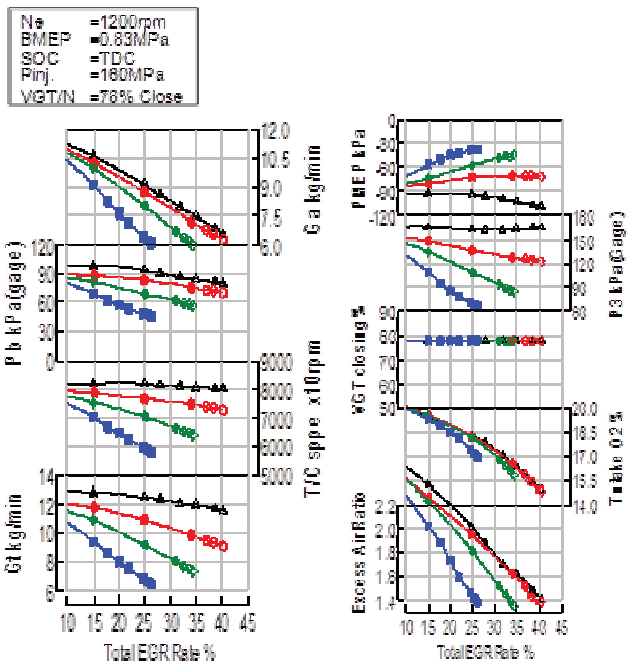
Test conditions were an engine speed at 1,200 rpm, a 40% load (BMEP = 0.83 MPa), a fuel injection pressure at 160 MPa, fuel ignition timing at TDC and VGT nozzle closing fixed at 78%. This is the condition which is frequently used in the JE05 Japanese transient test cycle.

In case of HPI=100% (HPL-EGR only), the EGR rate was limited to 26% and the Gt of HPL-EGR rapidly decreased to EGR rate 26%. On the contrary, in case of the combination of HPL-EGR and LPL-EGR with the BPCV, the EGR rate (HPI = 60, 30, 0%) increased to 40% and the Gt of the combination of HPL-EGR and LPL-EGR gradually decreased to EGR rate 40%. This reason is as follows; In case of LPL-EGR, the Gt to the turbine was the same quantity when the EGR rate increased. On the contrary, in case of HP-EGR, the Gt to the turbine was lower quantity when the EGR rate increased, and the Ga and Pb rapidly went down.

Fig. 8b shows a pumping mean effective pressure (PMEP), a pressure before the turbine operation (P3), VGT nozzle closing, an intake O_2 concentration and an excess air ratio from top. Conditions were the same as Fig. 8a. The values of the P3, intake O_2 and the excess air ratio had the same tendency shown as Fig. 8a when the EGR rate increased. However, the PMEP had a different tendency when the EGR rate increased. When the EGR rate increased, the PMEP of LPL-EGR increased. On the contrary, the PMEP of HPL-EGR decreased when the EGR rate increased. This means that the BSFC in LPL-EGR might be deteriorated.

7.3. Effect on BSFC by EGR

Fig. 9 represents $BSNO_x$, smoke, and brake specific fuel consumption (BSFC) from top at fixed VGT nozzle closing with a various EGR rates. Test conditions were the same as before. These results were compared with the same smoke level of FSN = 0.5. $BSNO_x$ was reduced by approximate 50% ($BSNO_x$ from 2.0 g/kWh to 1.0 g/kWh) compared with the case of HPL-EGR only. The BSFC in LPL-EGR increased when the total EGR rate increased. On the other hands, in case of HPI = 60% (green line) in the combination of HPL-EGR and LPL-EGR, the BSFC was able to be improved in comparison with HPL-EGR only (blue line) without smoke deterioration.



a. Ga: intake air quantity, Pb, T/C speed, Gt: Gas quantity,

b. PMEP, P3, VGT nozzle closing, intake O_2 and excess air ratio

Fig. 8. Experimental results of HPL-EGR and LPL-EGR in changing the total EGR rate

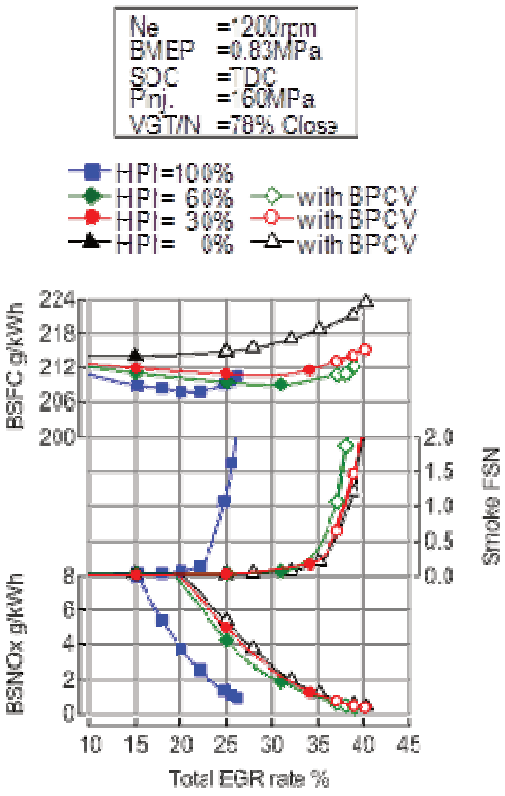


Fig. 9. Experimental results of BSFC, Smoke and $BSNO_x$ in changing the total EGR rate

7.4. Operation lines with EGR

Fig. 10 represents operating lines on the compressor map of the high pressure ratio turbocharger with EGR (red line) and without EGR (black line) when changing the load from 20% to 100% (BMEP 0.44 to 2.2 MPa) at an engine speed 1200 rpm. With the 20% load, the EGR rate was 44%, and this value is relatively high. With the 100% load the EGR rate decreased to 24% when the load ascended to 100%, and the HPL-EGR index was approx. 50% with a combination of HPL-EGR and LPL-EGR. It is noteworthy that the operating line without EGR moved from the center of the map to the surge line side when the EGR rate increased. It must be considered that the operating line of the high EGR rate approach to surge lines as the EGR rate increases, and it is necessary to develop countermeasures of this phenomenon.

Fig. 11 shows the operating lines in the full load condition with EGR at the engine speed from 800rpm to 2,000 rpm. At 800 rpm, the EGR rate was 23% with HPI = 16%, and at 2000 rpm, the EGR rate was 15% with HPI = 43%. At the low engine speed, the EGR rate was high and the value of HPI was 10%, which is relatively low because of small air quantities. As the engine speed increased, the EGR rate became lower such as 15% at 2000 rpm and the value of HPI was 42%, which is relatively high because of large air quantities. It is important to increase the EGR rate at the high engine speed in order to reduce $BSNO_x$ emissions.

7.5. Result of transient test cycle

In Japan, the JE05 transient test cycle has been used for emission standards since 2005 to 2016 autumn. Fig. 12 shows the results under the JE05 transient test cycle. Orange lines represent the results with original engine specifications, which are before the transient cycle tuning test, and black lines represent with improved engine specifications, which are after the transient cycle tuning test. The peaks of opacity and $BSNO_x$ were eliminated by observing the results of transient test cycle. It is improved gradually by HPL-EGR and LPL-EGR incorporated with improvements on the VGT-response, injection-timing, valve-timing and etc.

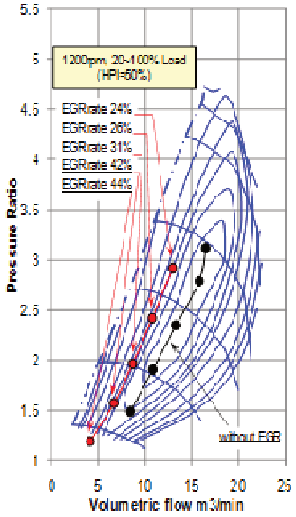


Fig. 10. Operating lines with and without EGR on the compressor map in changing loads at 1200 rpm

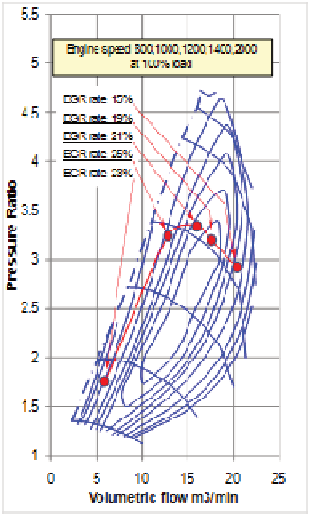


Fig. 11. Operating lines with EGR on the compressor map in changing the engine speed with 100% load

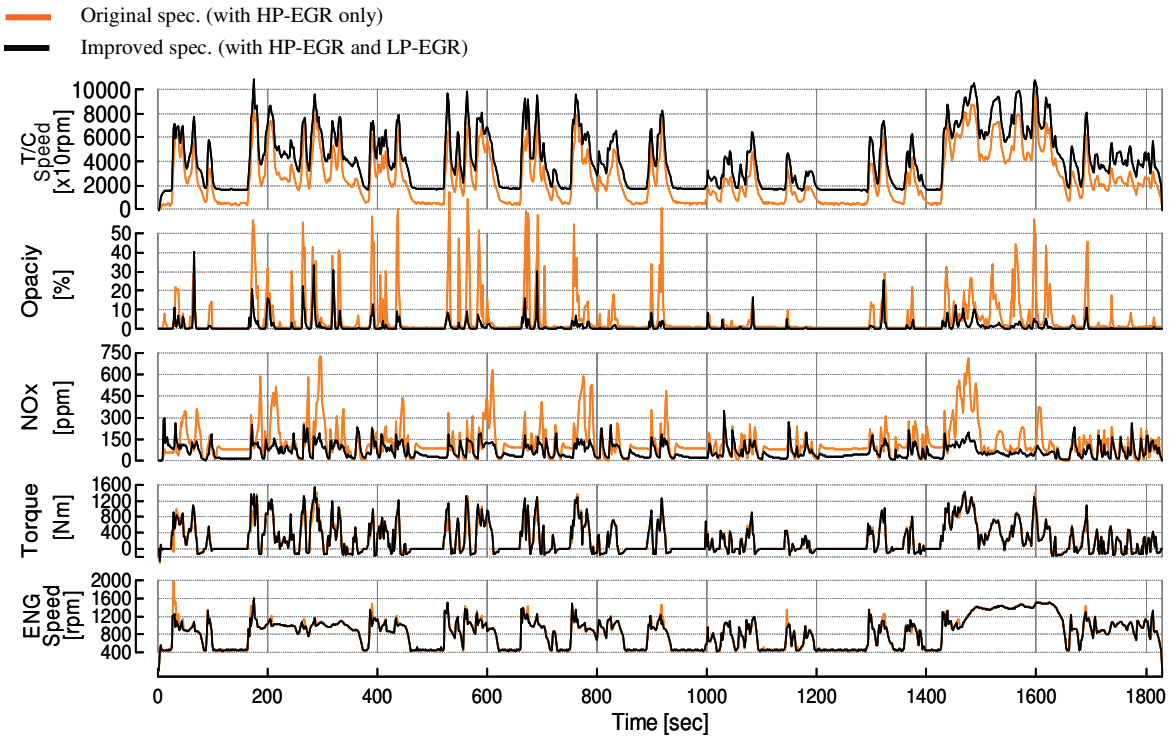


Fig. 12. Experimental results under JE05 transient test cycle in comparison between the original engine specs. and the improved engine specs

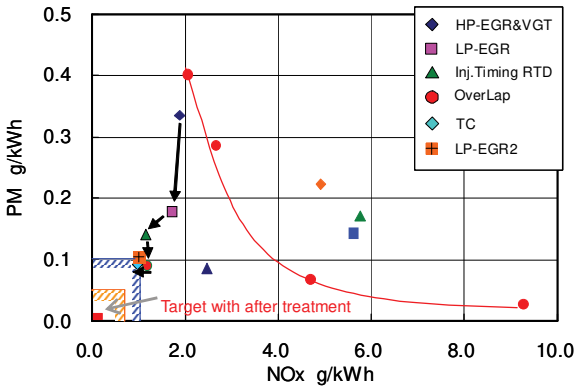


Fig. 13. Final experimental emission results from the original engine by transient test cycle

Fig. 13 represents a summary of the results under the JE05 transient test cycle showing $BSNO_x$ and PM trade-off relations. When boosting with a VGT, HPL-EGR and LPL-EGR and engine-out exhaust emissions were reduced to the effective range of after-treatment systems. The curved red line in Fig. 13 shows a trade-off by changing the HPL-EGR valve positions: 5%, 10%, and 15% before the turning test. After the turning test, approx. 47% of PM, 10% of $BSNO_x$ and 1.4% of BSFC were reduced by the combination of HPL-EGR and LPL-EGR comparing with the HPL-EGR only.

Finally, this engine satisfied the emission targets; $BSNO_x$ = 0.2 g/kWh and PM=0.01 g/kWh with the after-treatment systems, which include a LNT, a DOC and a DPF. Thus, this engine has achieved the emission targets by employing advanced technologies for the reduction of exhaust emissions.

8. Conclusion

The author at New ACE has studied the enhancement of the engine performance and the reduction of exhaust emissions by inducting substantial air into the cylinder with high EGR rates for the high boosted and intercooled diesel engine. As a result of the experiments, the following facts were derived:

- FCD piston combined with high rate EGR gives good exhaust emissions and improved thermal efficiency.
- The high boost pressure VGT (pressure ratio 5) with high EGR rates under the condition of a high injection pressure caused no significant degradation of the performance but yielded a high thermal efficiency.
- By using the high EGR rates, the $BSNO_x$ reached a lower emission level than without EGR and no increase of smoke and PM was observed at this experiment.
- The combined EGR system of HPL-EGR and LPL-EGR used for this study had a high performance, which increases the EGR rate while maintaining BSFC and the boost pressure, and decreased $BSNO_x$ and PM simultaneously not only in the steady state condition but also in the transient condition.

Acknowledgment

This research was done under the auspices of the annual research fund of New A.C.E. Institute Co., Ltd. and the project to promote Research and Development of Next-generation Environmentally Friendly Heavy Duty Vehicles of the Ministry of Land, Infrastructure, Transport and Tourism, to which we are grateful.

Nomenclature

BMEP	brakes mean effective pressure, MPa
BSFC	brake specific fuel consumption, g/kWh
BSNOx	brake specific NOx, g/kWh
FSN	filter smoke number, -
Ga	air flow rate without EGR gas, kg/min
Gt	exhaust gas flow rate, kg/min
Ne	engine speed, rpm
Pb	boost pressure, kPa (gauge)
Pinj	fuel injection pressure, MPa
PM	particulate matter, g/kWh
PMEP	pumping mean effective pressure, MPa
Smoke	smoke, %
T/C speed	turbocharger rotation speed, ×10 rpm
BPCV	back pressure control valve
[CO2]atm	CO2 concentration in atmosphere, %
[CO2]exh	CO2 concentration in exhaust gases, %
[CO2]in	CO2 concentration in intake gases, %
DOC	diesel oxidation catalyst
DPF	diesel particulate filter
LNT	lean NO_x trap
HPL-EGR	high pressure loop EGR
LPL-EGR	low pressure loop EGR
HPI	HPL-EGR rate in total EGR rate
JE05	heavy duty diesel transient test cycle in Japan
VGT	variable geometry turbocharger

Bibliography

[1] MORI, K., NAKAKITA, K., AOYAGI, Y. et al. Diesel engine development (in Japanese with English Summary). *Journal of JSAE*. 2016, **70**(1), 58-67.

[2] AOYAGI, Y., OSADA, H., MISAWA, M. et al. Advanced diesel combustion using of wide range, high boosted and cooled EGR system by single cylinder engine. *SAE Technical Paper*. 2006, 2006-01-0077.

[3] OSADA, H., AOYAGI, Y., YAMAGUCHI, T. et al. Diesel combustion by means of variable valve timing in a single cylinder engine. *Proceedings of the seventh COMODIA*. 2008, 35-42.

[4] OSADA, H., AOYAGI, Y., SHIMADA, K. et al. Reduction of NO_x and PM for a heavy duty diesel using 50% EGR rate in single cylinder engine. *SAE Technical Paper*. 2010, 2010-01-1120.

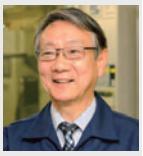
[5] AOYAGI, Y., OSADA, H., SHIMADA, K. et al. Enhancement of thermal efficiency and reduction of exhaust emissions in a heavy duty diesel engine (in Japanese with English Summary). *Journal of JSAE*. 2011, **65**(9), 58-65.

[6] FUJINO, R., AOYAGI, Y., OSADA, H. et al. Direct observation of clean diesel combustion using a bore scope in a single cylinder HDDE. SAE Technical Paper. 2009, 2009-01-0645.

[7] ADACHI, T., AOYAGI, Y., KOBAYASHI, M. et al. Effective NO_x reduction in high boost, wide range and high EGR rate in a heavy duty diesel engine. *SAE Technical Paper*. 2009, 2009-01-1438.
[8] KOBAYASHI, M., AOYAGI, Y., ADACHI, T. et al. Effective BSFC and NO_x reduction on super clean diesel of heavy duty diesel engine by high boosting and high EGR rate. *SAE Technical Paper*. 2011, 2011-01-0369.
[9] AOYAGI, Y., KOBAYASHI, M. Effective NO_x and PM reduction by means of high and low pressure loop EGR in heavy duty diesel engine. *FISITA 2016*, F2016-ESYB-020.
[10] TSUJITA, M., NIINO, S., ISHIZUKA, T. et al. Advanced fuel economy in Hino New P11C turbocharged and charge-cooled heavy duty diesel engine. *SAE Technical Paper*. 1993, 930272.
[11] STOVER, T.R., REICHENBACH, D., LIFFERTH, E. The Cummins signature 600 heavy duty diesel engine. *SAE Technical Paper*. 1998, 981035.
[12] KNECHT, W. European emission legislation of heavy duty diesel engines and strategies for compliance. *Proceedings of the Thermo-and fluid dynamic Processes in Diesel Engines* (THIESEL 2000), 289-302.
[13] KEMNITZ, P., MAIER, O., KLEIN, R. Monotherm, a new forged steel piston design for highly loaded diesel engine. *SAE Technical Paper*. 2000, 2000-01-0924.

Yuzo Aoyagi, DEng. – Counsel, New A.C.E. Institute Co., Ltd. and Temporal Lecturer of Okayama University, Japan.

e-mail: *Aoyagiyz1@jcom.zaq.ne.jp*



Article citation info:
PIEKARSKI, W., KURANC, A. Exhaust emissions and fuel consumption in a chassis dynamometer load test in the aspect of modification of an engine controlling system. Combustion Engines. 2017, **171**(4), 11-16. DOI: 10.19206/CE-2017-402

Wiesław PIEKARSKI
Andrzej KURANC

CE-2017-402

Exhaust emissions and fuel consumption in a chassis dynamometer load test in the aspect of modification of an engine controlling system

The article presents calculations of exhaust emissions and fuel consumption under test conditions on a chassis dynamometer test bench. The study describes the realization of the tests and the methodology of the calculation of the exhaust gas flow and the estimation of the fuel consumption based on exhaust emissions. The presented research results and their analysis describe the emission scale of selected gaseous fumes components during full engine load and the fuel consumption associated with such tests. Similar emissions occur during a rapid acceleration of a vehicle in road conditions.

Key words: *emission tests, CO_2 emissions, fuel consumption, chassis dynamometer, vehicle load tests*

1. Introduction

Considering a very wide spectrum of automotive impact on the environment, many problems still need to be analyzed and resolved. Emissions and road noise issues are still significant, especially at the stage of dynamic development of road infrastructure in Poland. Exhaust gases toxic components emission become a serious nuisance of most Polish cities. Photochemical smog is no longer just a problem of large Silesian agglomerations, but it is also known in Cracow, Poznan, Warsaw or Lublin. The effects of the presence of transport are very burdensome also outside the cities. Between the years 2010 and 2014, the length of national roads and motorways increased twice, reaching 1488 km and 1556 km at the end of 2014 [1]. Roads are built into new areas and introduce hazardous emissions and noise which is particularly important for high speed routes. Acoustic screens are being built to minimize the noise consequences but their aesthetics and landscape composition are not sufficient enough. Acoustic screens, apart from their technical function, should be as natural as possible, which can be achieved using the appropriate plant species [2]. These solutions have a more natural look and can also assimilate gaseous pollutants.

Other serious hazards that have grown up in recent years are problems with the utilization of automotive used fluids. Studies on used engine oils exploited in tractors and agricultural machinery indicate that these oils are only slightly recycled and that a huge part of them goes directly into the environment. The problem is very important because the oils are very harmful due to heavy metals content and other mutagenic impurities [3].

Changes in Poland after accession to the European Union influenced the total number of vehicles has doubled. The expansion and modernization of the machine park has been noted also in agriculture. As for a number of cars (513 units) per 1000 inhabitants we are typical Europeans. It is estimated that the number of passenger cars in Poland is over 20 million [4]. Many of them are in possession of young people who, use the opportunity to work abroad during the holiday season, and then buy cars and bring them to Poland.

As the number of vehicles increases, there is a growing demand for automotive services, not only for vehicle repair but also for their modifications. The modifications that can be seen at a first sight are external, but more often, it is about to improve the dynamic or economics of an engine. In order to properly perform such upgrades, a special equipment is needed to measure the effectiveness of the treatments [5]. Chassis dynamometer is an example of such devices. There were several stands of this type in Poland at the beginning of the century. Nowadays they are becoming increasingly popular for diagnostic reasons as they allow vehicles to be tested under load conditions in a laboratory without the need for road test drives which are less susceptible to perform measurements. The capabilities offered by chassis dynamometers greatly enhance the process of diagnosing the technical condition of an engine and a powertrain system. Moreover a proper regulation of a gas powered engine also requires appropriate testing, not only in aspect of its dynamic performance, but also in terms of emission of harmful exhaust components and fuel consumption.

The results of emission measurements obtained during load tests are very interesting. Examples of such tests can be found in the literature [6]. It should be noticed that such loads can also be present in road conditions, during intense vehicle acceleration. It is very important that the results significantly differ from the emission levels of given components commonly reported in the results of homologation tests or road tests [7–10].

2. The objective and scope of research

The purpose of the study was to determine the mass of exhaust gases emitted to the environment and the fuel consumption during load tests related to the determination of engine performance characteristics with use of a chassis dynamometer test bench.

The paper presents the load tests realization and the results of exhaust emission tests for two twin vehicles, one of which has been modified in the area of the engine controller. Results of exhaust emissions and fuel consumption were obtained by calculations based on the volumetric shares of selected exhaust components, measurement of intake manifold air flow and on the basis of the carbon balance method.

The scope of measurements included registration of several parameters such as:

- power on wheels – N_w, (kW),
- power loss N_l, (kW),
- engine speed – n, (min^{-1}),
- engine oil temperature – T, (°C),
- stream of air mass flowing through the intake manifold – q_{air}, ($g \cdot s^{-1}$),
- volumetric shares of gaseous exhaust components – CO, CO_2, O, (%) and HC, NO_x, (ppm).

3. Methods of research

Two similar vehicles Skoda Octavia 1U were the objects of the study. Each vehicle was fitted with a 1.9 dm^3 direct-injection turbodiesel ASV engine of maximum torque 235 Nm at 1900 min^{-1}) and maximum power output of 81 kW at 4150 min^{-1}. The engines were equipped with exhaust gas recirculation system, variable turbine geometry (VTG) and reactor DOC (Diesel Oxidation Catalysts). Vehicles were of similar age (A – 2002 and B – 2001), while the mileage indicated by the odometer was slightly different (A – 253,000 km, B – 226,000 km). Before the measurements, the vehicles were diagnosed and approved for further testing. It should be noted that in the case of a vehicle B, there has been previously incorporated software modifications into the engine controller to raise the maximum torque and the maximum power output. Each vehicle had been produced to comply with Euro 3 standard but the exploitation process and the modifications could change that.

After the tested vehicle was installed at the test stand, a gas analyzer and a data link cable were connected to the vehicle. Engine oil temperature and cooling air were also monitored. Next, a steady load driving test was carried out to bring up the engine to a stabilized heat state. Prior to the proper measurement unnecessary energy consuming devices has been switched off and then the load test with the data registration begun.

Vehicle tests were carried out using MAHA's MSR 500 chassis dynamometer, dedicated for vehicles with a maximum engine power up to 250 kW. This is a one-drum stand with a drum diameter of 500 mm, which can work in a discrete or load mode. The second mode, due to the way the measurement is carried out, is similar to the inertia method, but in addition to the inertia mass of the accelerated wheels and rollers, an additional brake load is added. This type of dynamometer work was used due to its similarity to an intensive acceleration in road conditions. The device in this mode performs a measurement of the rotational speed of the rollers driven by the vehicle wheels. The same time electronically controlled eddy-current brakes introduce additional load to the rollers an wheels [11, 12].

For the person conducting the test its procedure is reduced to accelerating the vehicle on the test stand with the use of fourth or fifth gear at fully pressed acceleration pedal. Then, after reaching the maximum speed for a given gear, the clutch is disengaged and free-run is being performed to measure the power loss in the powertrain system. So the test method is similar to inertial road tests [5].

Another instrument used in the study was the MAHA MGT5 vehicle exhaust gas analyzer, which allows continuous measurement of the volumetric shares of five exhaust components. It has been classified by OIML (Organization Internationale de Métrologie Légale) as a 0 Class analyzer. The manufacturer of the chassis dynamometer and the analyzer provided the possibility of their cooperation, so the results of the measurement of the exhaust gas composition were recorded using dedicated software.

The procedure utilizes a vehicle diagnostic system and a DLC (Data Link Connector) interface. When the vehicle is connected to the control panel of the dynamometer, the information about the engine operating parameters can be recorded and used for further calculations. In this case the most important were the signals from the engine crankshaft speed sensor and the mass air flow meter. It should be added that thanks to the above mentioned communication with the vehicle controller via the DLC connector it is also possible to register the engine operating parameters in the road traffic conditions. The results of such tests can also be used to evaluate the vehicle dynamic parameters and to determine the external characteristics of an engine - similarly to the chassis dynamometer [5, 13].

4. Methods of calculations

A number of conversions were made to determine the fuel consumption and emissions. Due to the equipment and methods used, the calculations required some assumptions and simplifications.

The exhaust gas analyzer used in the studies performs measurements of the volumetric shares of selected exhaust components. The shares combined with the information about the exhaust gas flow give an opportunity to learn about the amount of given gas emitted. However, the amount of exhaust can be determined by taking into account the air flowing through the engine intake manifold and the fuel dose. The mass of exhaust gases is the sum of the mass of air and the fuel to be burned. Instead of the direct information about the fuel dose, the composition of the exhaust gases can be used to determine the excess air factor λ and then to make the necessary calculations.

By default, the value of λ is determined by assumption that the fuel is petrol, for which the substitution formula can be written as $C_1H_{1.7261}O_{0.0175}$ [14]. Diesel fuel with substitution formula $C_1H_{1.86}O_{0.005}$ [15] has a different composition and therefore the values λ calculated automatically by the analyzer cannot be used. The measured CO, CO_2, HC, O_2 and NO_x volumetric concentrations and the Brettschneider formula should be used to determine the correct value of the excess air ratio [14–16]. The next step is to determine the volumetric shares of N_2, H_2O and Ar to complement the information on the composition of the exhaust gases. The shares of these components can be obtained basing on the combustion reaction for hydrocarbon fuel with air ($\lambda > 1$). The relations between volumetric and mass ratios of the exhaust gaseous components and the mass of exhaust gases were calculated as in the cited literature [16]. Calculations were performed for each set of data recorded during the measurements.

For example, for engine A, when the speed reached 3000 min^{-1} and the torque and engine power were respectively 237.08 Nm and 74.48 kW, the excess air factor λ reached the instantaneous value of 1.555. This value was

determined based on the instantaneous composition of the exhaust gas registered for the mentioned conditions and for the given fuel ($C_1H_{1.86}O_{0.005}$). The reaction of the combustion process took the form (1), where the individual coefficients determine the moles of the component.

$$C_1H_{1.86}O_{0.005} + 2.274 \cdot O_2 + 8.449 \cdot N_2 + 0.108 \cdot Ar \rightarrow \\ \rightarrow 1 \cdot CO_2 + 0.930 \cdot H_2O + 8.449 \cdot N_2 + 0.108 \cdot Ar + 0.812 \cdot O_2 \quad (1)$$

Taking into account individual coefficients for combustion products and treating their sum as 100%, the molar ratios of the given components were determined, respectively: 8.23% – H_2O, 8.85% – CO_2, 74.77% – N_2, 0.96% – Ar and 7.19% – O_2. These are the main components of the exhaust gas of a diesel engine that works with excess of air. These calculations do not take into account information about shares of other exhaust components than mentioned above, which are due to imperfections in the real combustion process. It was, however, simplified and assumed that their shares were small and did not significantly affect the overall exhaust flow. Subsequently, molar masses and determined molar proportions were used to obtain the mass shares of the given components. Summing up results in the time domain, the total masses of the emitted gaseous components (including carbon monoxide and carbon dioxide) were determined.

5. Fuel consumption

Two-way reasoning can be used to determine the fuel consumption. First way (by lambda) sets that we know the stoichiometry of the burning process. Basing on the formula for diesel fuel ($C_1H_{1.86}O_{0.005}$) and the combustion reaction for the stoichiometric mixture ($\lambda = 1$) the air-fuel ratio (AFR) equals 14.46. That means that the mass of exhaust gas is greater than the mass of air by the mass of fuel, which in this case is 1/14.46 of the mass of air. However, the tested diesel engine operates with an excess of air and therefore the actual composition of the air/fuel mixture can become known if the right value of λ, determined by the composition of the fumes, is used.

The other way (by carbon) leads to similar data that can be obtained using the carbon dioxide and carbon monoxide emissions. It can be assumed that the emissions are results of burning fuel of known composition. If, during the test, as a result of burning of the fuel given with formula $C_1H_{1.86}O_{0.005}$, the engine emits mass of carbon dioxide m_{CO2} and mass of carbon monoxide m_{CO}, then basing on the molar masses of the substances, the mass of fuel necessary to achieve the CO and CO_2 emissions can be calculated. The number of moles of carbon introduced with the fuel equals the sum of the moles of carbon dioxide and carbon monoxide produced by the combustion. In turn, the number of moles of fuel is the mass of fuel consumed divided by the molar mass of the fuel. Similarly, the number of moles of carbon dioxide is the mass of carbon dioxide divided by its molar mass. The same is true for carbon monoxide. According to that, the mass of fuel consumed can be expressed by the dependence (2).

$$m_{fuel} = \mu_{fuel} \cdot \left(\frac{m_{CO_2}}{\mu_{CO_2}} + \frac{m_{CO}}{\mu_{CO}} \right) \quad (2)$$

where: m_{fuel} – mass of fuel consumed, (g), m_{CO}, m_{CO2} – mass of emitted carbon monoxide and carbon dioxide, (g), μ_{fuel} – molar mass of the substitution fuel molecule, ($g \cdot mol^{-1}$), μ_{CO}, μ_{CO2} – molar mass of carbon monoxide and carbon dioxide, ($g \cdot mol^{-1}$).

6. Measurement results

As the results of measurements and calculations, the fuel consumption and mass emissions of the selected components of the exhaust gases were determined for two twin diesel engines, one of which was modified by the engine control software (engine B). Calculations and analysis of the results were narrowed to a common rotational speed range of 1450 min^{-1} to 4050 min^{-1}. The power characteristics N and torques M of the tested engines were supplemented by the air mass flow through the intake manifold (Fig. 1) and the volumetric ratios of selected gaseous fumes components (Fig. 2) and presented as functions of rotational speed n.

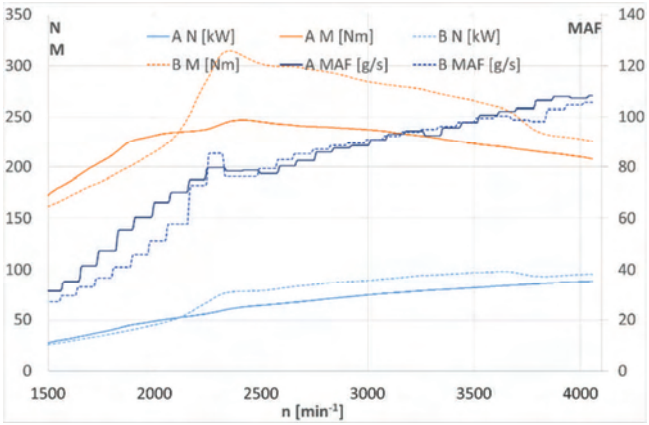


Fig. 1. Power, torque and air flow during the test for engines A and B

Table 1. Results of the tests and calculations

Parameter	Symbol	Unit	Engine A	Engine B
Power max	N_{max}	kW	88.3	97.9
Engine speed of N_{max}	n_N	min^{-1}	4050	3650
Torque max	M_{max}	Nm	246.8	314.7
Engine speed of M_{max}	n_M	min^{-1}	2400	2350
Mass of Fumes	m_{fume}	kg	2.512	2.452
Mass of CO_2	m_{CO2}	kg	0.374	0.433
Mass of O_2	m_{O2}	kg	0.205	0.109
Mass of CO	m_{CO}	g	0.603	5.367
Mass of HC	m_{HC}	g	0.028	0.001
Mass of NO_X	m_{NOx}	g	2.749	3.209
Mass of fuel (by carbon)	$m_{fuel\,C}$	kg	0.119	0.140
Volume of fuel (by carbon)	$V_{fuel\,C}$	dm^3	0.142	0.167
Mass of fuel (by lambda)	$m_{fuel\,\lambda}$	kg	0.110	0.131
Volume of fuel (by lambda)	$V_{fuel\,\lambda}$	dm^3	0.131	0.156

The tests results and further calculations have been gathered in Table 1. The data show that an approximately 90 kW diesel engine during ca. 30 seconds of a full power load test at the chassis dynamometer utilizes about 150 ml of diesel fuel of 0.84 $kg \cdot dm^{-3}$ density. More details can be found by analyzing additional graphs (Figs 1–4).

By the analysis of the data presented in Fig. 1 it can be followed that the engine with modified control software

develops about 27% higher torque and about 11% higher maximal power than the unmodified one. Simultaneously, it can be also seen that the maximum power in case of engine B appears at lower rotational speed (3650 min^{-1}). It is also important that in the speed range of 1500 to 2100 min^{-1}, the modified engine torque is lower than the factory one. In the rest of the observed speed range the modified engine torque is higher. That can be affected by similar changes of the mass air flows for the engines. These are due to differences in the turbochargers operating ways of those engines. In case of engine B the characteristic drop of torque is observed at speed of 3750 min^{-1}. It is implicated by a drop of air mass flow observed simultaneously and influences the drop of power drop. These also affect the final exhaust emissions presented in Table 1.

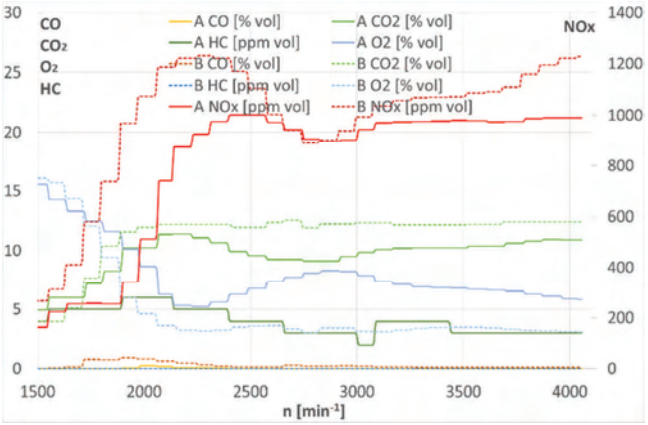


Fig. 2. Volumetric shares of the measured compounds during the test of engines A and B

In Fig. 2, changes in volumetric proportions of selected components of the exhaust gases recorded during the test can be observed. There are differences in emissions of individual components resulting from increased fuel doses for engine B, which are strongly reflected in CO_2 and O_2 emissions. The maximum values for CO_2 are for engines A and B respectively 11.4% and 12.57%. It can be noticed that CO_2 content varies about 2–3% for engine A and for engine B it mainly stays constant (ca. 12.5%). In case of engine A oxygen presence drops to 5% at 2200 min^{-1} and then raises to about 8% at 2900 min^{-1} and then slightly drops to 6%. In case of engine B oxygen content drops to 3.5% at 2100 min^{-1} and stays close to that level till the end of the test. The shares of CO_2 and O_2 for engine B can confirm a tuner's efforts to utilize the oxygen maximally. The changes in combustion conditions (local mixture enrichment, higher pressure, higher temperature) are also seen in emissions of CO (A – max 0.24% and B – max 0.93%) and NO_x (A – max 1001 ppm and B – max 1232 ppm).

Fig. 3 illustrates the changes in the proportions of the main components of the exhaust gases emitted by engine B. Compared to Fig. 2, the illustration (Fig. 3) also includes data on the volumetric shares of N_2, H_2O and Ar. The shares were obtained basing on the substitution fuel formula $C_1H_{1.86}O_{0.005}$, calculated air excess coefficient λ, assumed air composition and the formula of the combustion process reaction. The high level of water vapor content (ca. 11%) and the low content of oxygen (ca. 3%) can suggest that the tuner did his best to uncover the potential power of the engine. It also indicates that the modified engine is very close to the smoke limit.

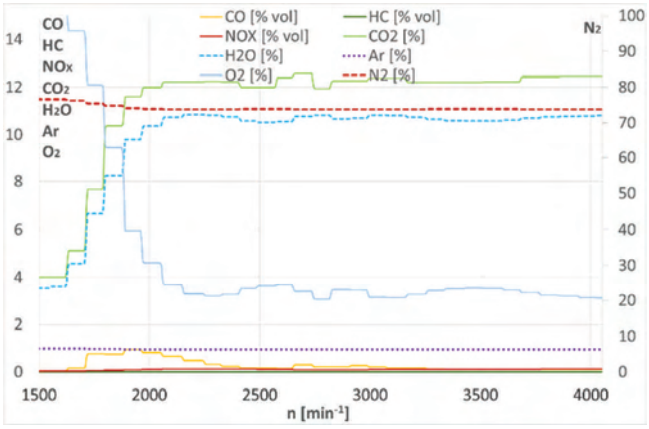


Fig. 3. Calculated volumetric shares of the main fumes compounds for the test of engine B

A summary of the measurements and performed calculations is illustrated in Fig. 4 showing the masses of the selected exhaust gas components emitted during the comparative tests of the engines.

It should be noted that the value of overall exhaust gas emissions should be similar for the compared engines. These engines are loaded at the same time and at the same rotational speed range. The displacement capacity and the boost systems are the same and should result in similar mass of pumped gases.

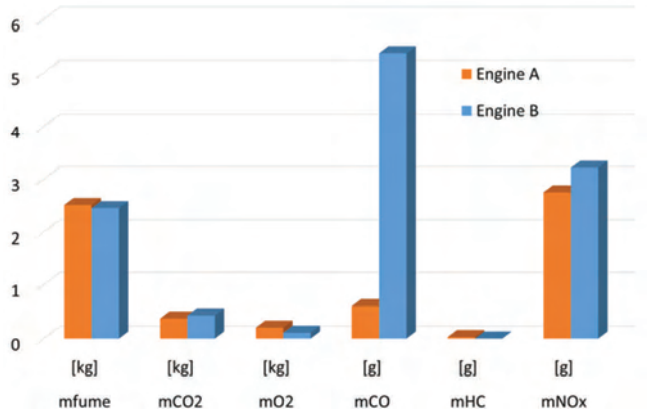


Fig. 4. Mass of the fumes compounds emitted during the test for engines A and B

In this case, however, we have to deal with separate objects of different technical stages, and hence the differences observed in the total mass of the exhaust gases can also be observed. Designated values (2.512 kg and 2.452 kg) indicate that the unmodified engine (A) emits slightly more (about 2.4%) of exhaust gases than the modified engine (B). This is due to the greater amount of air supplying engine A what can be noticed in the initial test phase (Fig. 1).

The next results obtained for the several exhaust components are already in line with the predictions. The CO_2 mass is about 16% higher for the modified engine (B), and

translates into an increase in its power. The increase in CO_2 emissions correlates significantly with the decrease in O_2 emission, too. In the case of the modified engine, the higher CO (about 9 times) and NO_x (about twice) emissions confirm the deterioration of the combustion process conditions.

7. Summary and conclusions

Load tests related to the designation of an engine external (operational) characteristics resemble extreme loads that may occur on the road. However, they differ significantly from the conditions of homologation tests, but one can try to compare them by specifying the emissions in relation to the distance traveled. Regarding the speed at the roller stand, it was found that the vehicles drove about 850 m during the test period.

Comparing the test results to vehicle manufacturer data (CO_2 – 135 g/km) and the limits resulting from the approval standard (Euro3; CO – 0.64 g/km and NO_x – 0.50 g/km [17]) it obviously should be noted that in case of both cars the analyzed load test period results in significantly higher CO_2 emissions due to the maximal load. The real distance traveled during the test is about 850 m, but due to the manufacturer's declared CO_2 emissions it corresponds to driving of about 3.25 km for engine A and about 3.77 km for B. In case of engine A the emission of CO reaches 0.71 g/km, whereas in case of engine B it is ca. nine times higher (6.31 g/km). Emissions of NO_x (A – 3.23 g/km and B – 3.77 g/km) are also high and corresponds to a distance of about 7 km.

It should be emphasized, however, that the comparison to the abovementioned limits (Euro 3) is just indicative and that the standard limits are not foreseen for emission tests during determining engines external characteristics.

Moreover, the following conclusions can be drawn regarding the two engines and the selected parameters of their performances and exhaust emissions:

- engine with modified control software develops about 27% higher torque and about 11% higher power than unmodified one,
- increase in engine power is occupied by increased fuel consumption, which is calculated by carbon balance higher by approx. 18% (according to the lambda coefficient the difference is about 19%),
- considerations for calculating fuel consumption based on CO_2 emissions can be used in reverse, i.e. when estimating CO_2 emissions based on fuel consumption,
- the effect of enrichment of the fuel mixture (fuel dose) in case of engine B is clearly observed in emitted CO and CO_2 – in case of carbon monoxide the emitted mass is nearly nine times greater than in case of engine A,
- the emission of nitrogen oxides is also higher (by 17%), it can be explained by the influence of the air/fuel mixture enrichment, which implicates the increase of maximum temperature and maximum pressure in the combustion chamber – the parameters mostly responsible for nitrogen oxides formation,
- in case of engine B the lower overall mass of the exhaust gases is observed in the test. It is certainly the result of similar difference in the air supplying mass flow. The difference of the flow noticed within the speed range from 1500 to 2100 min^{-1} may be an effect of changed regulation of the turbocharger.

Referring to the research and methods employed, it should be stressed that the mass of the components emitted depends on the method of carrying out the load test. The longer period the engine is being loaded, the greater amount of mass of the exhaust gases is emitted. It is very important in any comparisons of emissions based on tests performed on different dynamometer test stands.

Nomenclature

AFR air/fuel ratio
CO carbon monoxide
CO_2 carbon dioxide
DLC data link connector
HC hydrocarbons
NO_X nitrogen oxides
OIML Organization Internationale de Métrologie Légale
λ excess air coefficient

Bibliography

[1] GUS, Transport/Ogółem/Sieć komunikacyjna, 2014. [Online]. Available: swaid.stat.gov.pl/TransportLacznosc_dashboards/Raporty_predefiniowane/RAP_DBD_TRANS_2.aspx (accessed: 03.01.2017).

[2] SZYSZLAK-BARGŁOWICZ, J., SŁOWIK, T., ZAJĄC, G., PIEKARSKI, W. Inline plantation of virginia mallow (Sida hermaphrodita R.) as biological acoustic screen, *Rocznik Ochrona Srodowiska*. 2013, **15**(1).

[3] ZAJĄC, G., SZYSZLAK-BARGŁOWICZ, J., SŁOWIK, T. et al. Designation of chosen heavy metals in used engine oils using the XRF method. *Polish Journal of Environmental Studies*. 2015, **24**(5).

[4] GUS, Transport/Drogowy/Pojazdy drogowe, 2014. [Online]. Available: swaid.stat.gov.pl/TransportLacznosc_dashboards/Raporty_predefiniowane/RAP_DBD_TRANS_7.aspx (accessed: 03.01.2017).

[5] KURANC, A. Badania mocy silnika pojazdu z wykorzystaniem metod inercyjnych. *Autobusy: technika, eksploatacja, systemy transportowe*. 2012, **13**.

[6] WENDEKER, M., GĘCA, M., BARAŃSKI, G., SOCHACZEWSKI, R. Badania pojazdu EURO 5 przy pełnym obciążeniu silnika. *Autobusy: technika, eksploatacja, systemy transportowe*. 2012, **13**.

[7] COLLINS, J.F., SHEPHERD, P., DURBIN, T.D. et al. Measurements of in-use emissions from modern vehicles using an on-board measurement system. *Environmental Science & Technology*. 2007, **41**(18).

[8] MAZANEK, A. Badania porównawcze emisji toksycznych składników gazów wylotowych z silnika o zapłonie samoczynnym zasilanego ON i B10. *Nafta-Gaz*. 2010, **66**(9).

[9] MERKISZ, J., ANDRZEJEWSKI, M., PIELECHA, J. The effect of applying the eco-driving rules on the exhaust emissions. *Combustion Engines*. 2013, **155**(4).
[10] NITA, J., BORCZUCH, A. Preliminary evaluation of correlation of CVS and modal techniques in homologation tests of vehicle with regard to exhaust-gas toxic components emission. *Journal of KONES Internal Combustion Engines*, 2003, **10**(1-2).
[11] VIERLING, F. Modern performance and emission test procedures – principles, technology, application. Bad Wörishofen. 2010.
[12] MAHA, MSR single roller dynamometer. *Original Operating Instructions*. 2011.
[13] KURANC, A. Chosen examples of investigations upon the combustion engines taken with the modern diagnostic testers, *Eksploatacja silników spalinowych*. 2007.
[14] MAHA, Motor gas tester MGT 5 five-gas tester. *Technical Handbook*. 1999.
[15] Dz. U. UE L42, Tom 55, Regulamin nr 83 Europejskiej Komisji Gospodarczej Organizacji Narodów Zjednoczonych (EKG ONZ) – Jednolite przepisy dotyczące homologacji pojazdów w zakresie emisji zanieczyszczeń w zależności od paliwa zasilającego silnik. 2012.
[16] KURANC, A. Exhaust emission test performance with the use of the signal from air flow meter. *Eksploatacja i Niezawodnosc – Maintenance and Reliability*. 2015, 17(1).
[17] DIESELNET, Emission Standards: Europe: Cars and light trucks, 2017. [Online]. Available: /www.diesel-net.com/standards/eu/ld.php#stds (accessed: 24.03.2017).

Wiesław Piekarski, DSc., DEng. – Faculty of Production Engineering at University of Life Sciences in Lublin.

e-mail: *Wieslaw.Piekarski@up.lublin.pl*



Andrzej Kuranc, DEng. – Faculty of Production Engineering at University of Life Sciences in Lublin.

e-mail: *Andrzej.Kuranc@up.lublin.pl*



Article citation info:
OSIPOWICZ, T., LISOWSKI, M. The influence of corrosion phenomena on operational parameters of modern fuel injectors CI-engines. *Combustion Engines*. 2017, **171**(4), 17-23. DOI: 10.19206/CE-2017-403

Tomasz OSIPOWICZ
Maciej LISOWSKI

CE-2017-403

The influence of corrosion phenomena on operational parameters of modern fuel injectors CI-engines

The article describes the influence of corrosion phenomena on operational parameters of common fuel injectors. Paper has been presented and describes Common Rail fuel injectors, their structure and work principles. Main fuel injectors parameters, like injection dosage, back leakage and injection delay are discussed. It has been presented the elements of injectors which have influence on dosages magnitude and how the corrosion phenomena influences on its. The elements of injectors, which have an influence on dosages magnitudes, are presented and the effect of their corrosion is discussed.

Key words: *corrosion phenomena, fuel dosages, Common Rail system, fuel injector*

1. Introduction

Corrosion phenomena is an undesirable process of destroying materials. This process is driven by a combination of chemical, electrochemical, microbiological and mechanical factors. The results of corrosion phenomena on mechanical objects is increased wear, which has a major impact on working parameters [2] of fuel injectors. Harsh environmental conditions, like extreme pressures, temperatures and fuel moisture that are encountered by fuel injectors accelerate this deteriorating effect [8]. Since all fuel injectors are made from a tool steel (both electromagnetic and piezoelectric injectors share this property) the choice of material or injector type does affect the speed of corrosion, and unfavorable environmental conditions remain a primary driver for corrosion. The corrosion types are mainly: pit, expansion joint corrosion and specific aspect corrosion in moving medium in fuel injectors. Pit corrosion is the form of located medium fit in results appearing local loss material – pits. Damages trigger off pit corrosion on precise elements make the leaks. Intensive local corrosion in covered places or slats (cracks) metal elements expose on acting medium is expansion joint corrosion [4]. The main factor which makes this type of corrosion is unequal access to oxidant. It appears under seals, washers and gaskets in fuel injectors. Pit and expansion joint corrosion are sometimes compared and treated as the same type. The mechanism is similar but the appearing reason of expansion joint corrosion are slats or crack and pit corrosion appears themselves. The corrosion in moving medium depends on the speed of flowing liquid. It is examined for specific conditions: laminar flow, turbulent flow and cavitation corrosion. Liquid flow influences the speed of corrosion. In addition the corrosion is accompanied by metal erosion phenomena. Connecting the effects of mechanic liquid impact on metal called erosion corrosion. Therefore it can be said that the corrosion phenomena is increased by erosion, which in turn depends on the speed of liquid flow and temperature inside the fuel injector [4].

Turbulent fuel flow increases the damaging effect on injector elements. Its parts corrode quickly when faced against an intensive flow, which exceeds a certain speed threshold.

Fast flow through variable cross-section may lead to cavitation, which is the formation of vapor cavities in areas, where local pressure drops. When such cavity experiences a pressure-increase it implodes, generating an intensive shockwave, which damages metallic surfaces. This effect is called a cavitation corrosion, and is frequently encountered in fuel injectors [2, 4].

The last sort of corrosion that occurs in fuel injectors is friction corrosion. It mainly appears in precise elements because of a sliding motion of these elements. Figure 1 presents the sort of corrosion phenomena in fuel injectors.

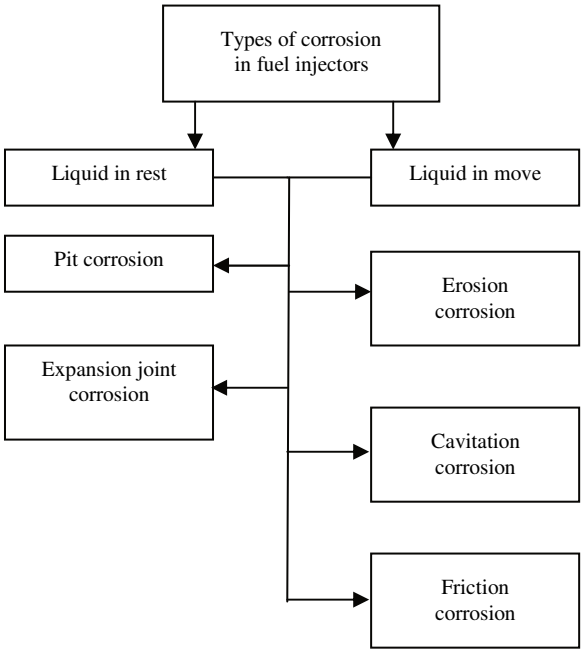


Fig. 1. Types of corrosion in fuel injectors

2. Analysis of fuel injector operational parameters

Fuel injector is a device which deliver fuel to combustion chamber CI-engine. Its main task is to supply an engine's combustion chamber with a specific fuel dosage under given pressure. So injector is responsible for spray and fuel distribution. Modern CI-engines are equipped with Common Rail system. This solution separates the work of pressure pump and fuel injectors through high pressure

accumulator. It allows steering of system pressure, injection time and timing [3, 5].

The fuel injectors parameters could be divide into operational and diagnostic. Operational parameters directly influence CI-engine work. These are injection and return dosages. Diagnostic parameters allow to determine technical condition of fuel injector. Figure 2 presents the research protocol of piezoelectric Continental VDO Siemens fuel injector on Zapp CRU2i test bench.

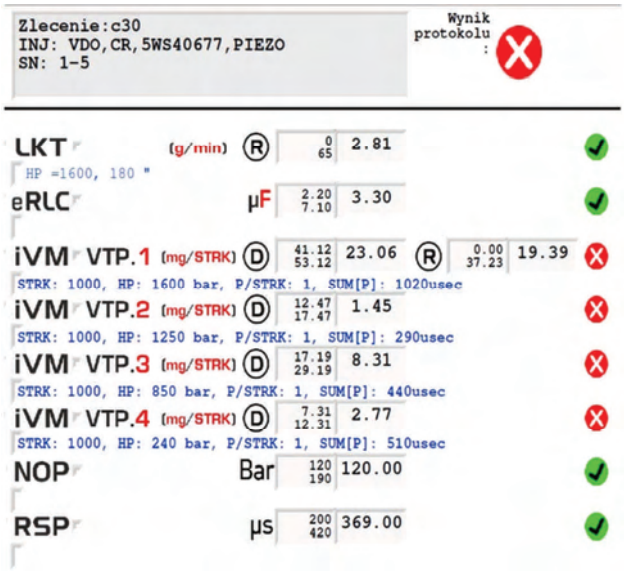


Fig. 2. The protocol of research fuel injector on Zapp CRU 2i test bench

The operational parameters are VTP 1 – 4 injection dosages and return dosage by VTP 1 test. VTP 1 – 4 are the types of dosages. VTP 1 is a full load dosage under 160 MPa system pressure within 1020 µs. This mensuration is at maximum engine load and it also includes return dosage Correct return dosage at maximum load guarantees, that it will stay correct for all other pressure levels, therefore it is not measured in tests VTP.2-4.

The VTP 2 is an initial dosage test. This test is performed under 125 MPa pressure and low injection time of 290 µs. This is very important dosage and regulate is as the first, because depend from range of movement steering valve.

VTP 3 is a middle load dosage under 85 MPa system pressure and 440 µs injection time. The last VTP 4 is idle speed dosage under 24 MPa pressure and 510 µs injection time. It should be noted that the difference between all injectors on engine in this dosage amount 0.5 mg/STRK. If higher differences would be encountered the engine would work unsteadily.

Figure 2 also depicts diagnostic parameters. LKT is an injector leak test in rest. This is very important parameter, since a condition of inner sealing and precision elements can be determine base on its analysis. Only back leakage was measured during this test. Test eRLC is an electrical test. Electrical capacity, insulation resistance between pins by 100 V and ground resistance by 250 V in piezoelectric injectors are measured. NOP is nozzle open pressure test. This parameter measures what level of pressure opens injector nozzle. RSP is delay fuel injection parameter. This is a time between steering electrical element and starting spraying [1, 6, 7]. Figure 3 presents fuel injector diagnostic parameters. Entrances parameters are injection pressure, time and frequency. Output parameters are injection return dosages, injection delay, nozzle open pressure and temperature. Temperature involves injection and return fuel temperature and injector body temperature. This parameter is very important, because it shows the area of injector damage.

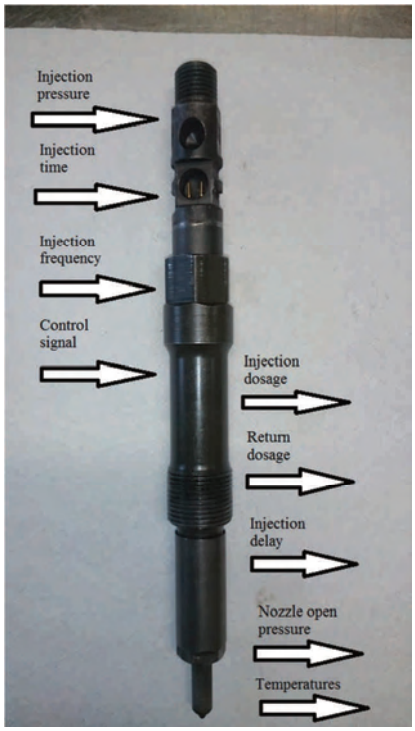


Fig. 3. Fuel injector diagnostic parameters

3. Presentation of test stand

Tests have been performed on tests bench Zapp CRU 2i (Fig. 4), which allowed for measurements of the following parameters:

- fuel injector delay,
- nozzle open pressure,
- injection and return dosages,
- electric parameters.

Research of the effects of corrosion were carried out using the FL150/70 laboratory microscope (Fig. 5).



Fig. 4. Zapp CRU 2i test bench



Fig. 5. Laboratory microscope FL150/70

4. Test results

Corrosion phenomena are examined in two aspects:

- when the fuel injector is out of order and needs to be repaired,
- when the fuel injector works but its operating parameters are not correct.

In the first case there are many signs of corrosion, especially on precision elements. Figures 6–8 present the corroded parts of Bosch fuel injector.

A B

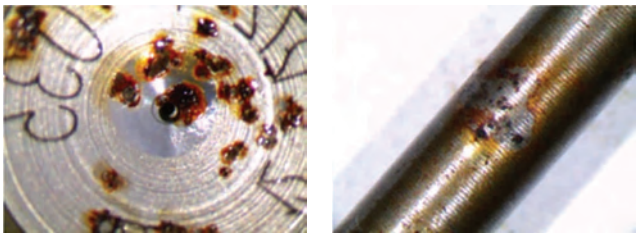


Fig. 6. A –steering valve, B – not working part of the needle

A B

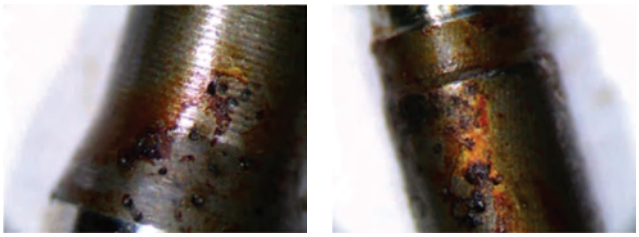


Fig. 7. A – not working part of the injector piston, B – precision element of the injector piston

A B

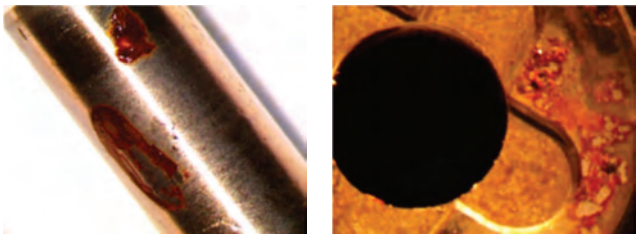


Fig. 8. A – precision element of injector needle, B – sealing surface on injector body between injector nozzle and injector body

Damages due to corrosion, which are presented in Figs 6–8, qualify elements to replacement. Fuel injector valve presented in Fig. 6 is damaged and due to pits it lost tightness. Not working parts of injector's needle and piston are very corroded (Figs 6, 7). Observations point to the conclusion that a quality of the fuel was of poor quality, with large amount of moisture. Precision element of injector needle (Fig. 8) has been effaced and polluted. There are methods depending on shining precision element but not by so huge damages. These defects influence the fuel injectors operational parameters, which became leaky against return dosages, what is easily observed on the test bench Problem begins when engine work but unsteadily in middle load when there is no correction capacity to read. It may be cause because of huge difference between injection dosages.

A B



Fig. 9. A – injector needle spring, B – spring in electromagnetic solenoid

A B

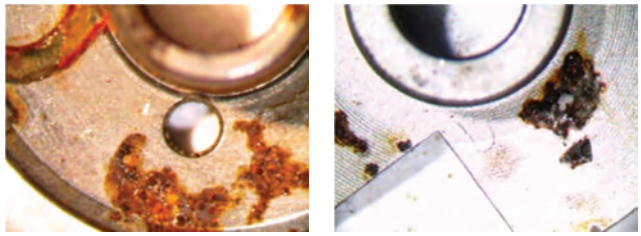


Fig. 10. A – elements of electromagnetic system valve, B – elements of electromagnetic system plate

A B

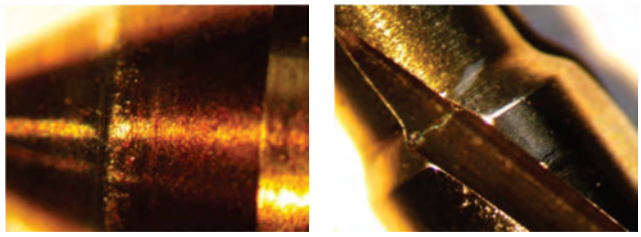


Fig. 11. A – corroded fuel injector needle, B – fuel intake channels damaged by cavitation corrosion in Delphi injectors

Figure 9 A presents injector needle spring with visible corrosion, which affects operational characteristics of the injector and has a direct impact on injection dosages. Nevertheless it is still possible to regulate dosages through washers over injector needle. Spring in the solenoid depends on the return dosage. Results show that decreasing the thickness of the solenoid's washer by 20% doubles the return dosage. Corroded injector valve elements (Fig. 10) could change fuel injector work parameters like injection dosages, delay nozzle open pressure. Figure 11 presents the corroded fuel injector needle and damaged fuel intake channels in Delphi injectors caused by cavitation.

Although the tested injector still works, all presented symptoms lead to deterioration of operational parameters of the injector and have a non-negligible impact on its performance.

Table 1. Test results of good working electromagnetic Bosch fuel injector research

Electromagnetic Bosch fuel injector no. 0445110320				
eRLC	Resistance [0.3–0.7 Ω]		Inductance [115–375 µH]	
	0.4		294	
RSP	Injection delay [200–500 µs]			
	434			
NOP	Nozzle open pressure [14 – 21 MPa]			
	19			
Test	Injection dosage		Return dosage	
Leak test [mm^3/H] 170 MPa, 300 s	0		0–80 [300 s]	9.44
IVM 1 [mm^3/H] 160 MPa, 800 µs	41.16–52.4	44.72	5–82	28,59
IVM 2 [mm^3/H] 60 MPa, 630 µs	8–15.68	11.06		
IVM 3 [mm^3/H] 60 MPa, 640 µs	0.88–6.48	3.60		
IVM 4 [mm^3/H] 60 MPa, 275 µs	0.24–2.96	0.84		

Table 2. Test results of faulty electromagnetic Bosch fuel injector research

Electromagnetic Bosch fuel injector no. 0445110320				
eRLC	Resistance [0.3–0.7 Ω]		Inductance [115–375 µH]	
	0.4		294	
RSP	Injection delay [200–500 µs]			
	674			
NOP	Nozzle open pressure [14–21 MPa]			
	23			
Test	Injection dosage		Return dosage	
Leak test [mm^3/H] 170 MPa, 300 s	0		0–80	48.73
IVM 1 [mm^3/H] 160 MPa, 800 µs	41.16–52.4	42.63	5–82	63,23
IVM 2 [mm^3/H] 60 MPa, 630 µs	8–15.68	8.14		
IVM 3 [mm^3/H] 30 MPa, 640 µs	0.88–6.48	1.05		
IVM 4 [mm^3/H] 60 MPa, 275 µs	0.24–2.96	0.11		

Table 3. Test results of good working piezoelectric Bosch fuel injector research

Piezoelectric Bosch fuel injector no. 0445116024				
eRLC	Resistance [175–200 kΩ]		Capacitance [1.80–5.60 µF]	
	182		2.30	
RSP	Injection delay [100–420 µs]			
	208			
NOP	Nozzle open pressure [12–19 MPa]			
	14			
Test	Injection dosage		Return dosage	
Leak test [mm^3/H] 160 MPa, 85 s	0		0–1	0.33
IVM 1 [mm^3/H] 180 MPa, 800 µs	36.10–44.25	39.17	2–18	9,18
IVM 2 [mm^3/H] 80 MPa, 190 µs	0.24–2.16	1.22		
IVM 3 [mm^3/H] 30 MPa, 535 µs	1.68–5.20	4.27		
IVM 4 [mm^3/H] 80 MPa, 490 µs	12.24–18.00	16.31		

Table 4. Test results of faulty piezoelectric Bosch fuel injector research

Piezoelectric Bosch fuel injector no. 0445116024				
eRLC	Resistance [175–200 kΩ]		Capacitance [1.80–5.60 µF]	
	186		2.98	
RSP	Injection delay [100–420 µs]			
	387			
NOP	Nozzle open pressure [12–19 MPa]			
	23			
Test	Injection dosage		Return dosage	
Leak test [mm^3/H] 160 MPa, 85 s	0		0–1	12.54
IVM 1 [mm^3/H] 180 MPa, 800 µs	36.10–44.25	42.64	2–18	34,75
IVM 2 [mm^3/H] 80 MPa, 190 µs	0.24–2.16	0.34		
IVM 3 [mm^3/H] 30 MPa, 535 µs	1.68–5.20	1.84		
IVM 4 [mm^3/H] 80 MPa, 490 µs	12.24–18.00	9.34		

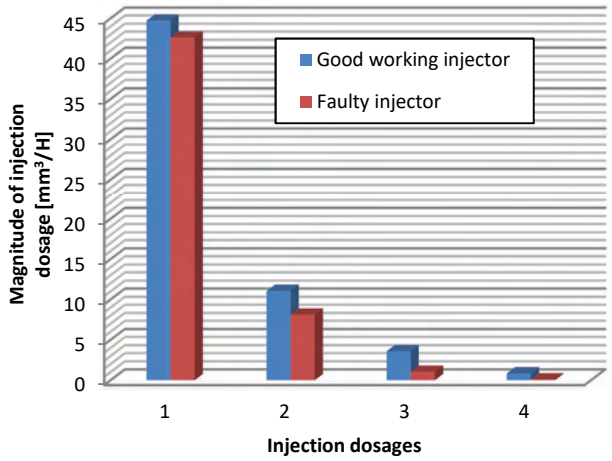


Fig. 12. Injection dosages comparison between faultless and faulty electromagnetic Bosch fuel injector; 1 – full load dosage, 2 – medium load dosage, 3 – idle speed dosage, 4 – initial dosage

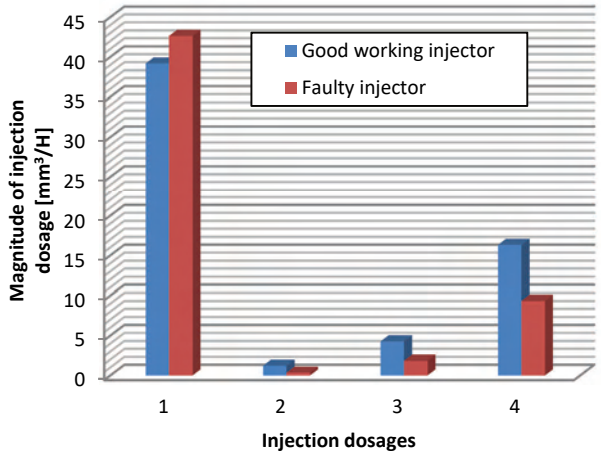


Fig. 13. Injection dosages comparison between faultless and faulty piezoelectric Bosch fuel injector 1 – full load dosage, 2 – initial dosage, 3 – idle speed dosage, 4 – medium load dosage

Table 5. Test results of faultless electromagnetic Denso fuel injector research

Electromagnetic Denso fuel injector no. 095000 – 758				
eRLC	Resistance [0.4–3.8 Ω]		Inductance [300–4000 µH]	
	1.20		570	
RSP	Injection delay [390–680 µs]			
	605			
NOP	Nozzle open pressure [12–28 MPa]			
	21			
Test	Injection dosage		Return dosage	
Leak test [mm^3/H] 170 MPa, 45 s	0		0–60.8	25.48
IVM 1 [mm^3/H] 160 MPa, 1080 µs	36.27–53.33	49.37	0–69	35,18
IVM 2 [mm^3/H] 80 MPa, 760 µs	12–20	16.47		
IVM 3 [mm^3/H] 25 MPa, 820 µs	2.67–6.4	3.48		
IVM 4 [mm^3/H] 80 MPa, 400 µs	0.8–3.47	2.17		

Table 6. Test results of faulty electromagnetic Denso fuel injector research

Electromagnetic Denso fuel injector no. 095000 – 758				
eRLC	Resistance [0.4–3.8 Ω]		Inductance [300–4000 µH]	
	1.39		465	
RSP	Injection delay [390–680 µs]			
	710			
NOP	Nozzle open pressure [12–28 MPa]			
	26			
Test	Injection dosage		Return dosage	
Leak test [mm^3/H] 170 MPa. 45 s	0		0–60.8	48.62
IVM 1 [mm^3/H] 160 MPa, 1080 µs	36.27–53.33	41.97	0–69	75,08
IVM 2 [mm^3/H] 80 MPa, 760 µs	12–20	12.94		
IVM 3 [mm^3/H] 25 MPa, 820 µs	2.67–6.4	2.15		
IVM 4 [mm^3/H] 80 MPa, 400 µs	0.8–3.47	0.38		

Table 7. Test results of faultless electromagnetic Delphi fuel injector research

Electromagnetic Delphi fuel injector no. EJBR – 02301Z				
eRLC	Resistance [0.2–0.6 Ω]		Inductance [60–110 µH]	
	0.40		87	
RSP	Injection delay [300–495 µs]			
	427			
NOP	Nozzle open pressure [13–23 MPa]			
	13			
Test	Injection dosage		Return dosage	
Leak test [mm^3/H] 140 MPa, 120 s	0		0–40	2.02
IVM 1 [mm^3/H] 140 MPa, 700 µs	31.83–46.33	38.75	0–40	18,50
IVM 2[mm^3/H] 80 MPa, 600 µs	14.43–31.35	22.03		
IVM 3[mm^3/H] 23 MPa, 573 µs	0.3–5.55	2.84		
IVM 4[mm^3/H] 40 MPa, 462 µs	1.18–7.91	4.69		

Table 8. Test results of faulty electromagnetic Delphi fuel injector research

Electromagnetic Delphi fuel injector no. EJBR – 02301Z				
eRLC	Resistance [0.2–0.6 Ω]		Inductance [60–110 µH]	
	0.35		74	
RSP	Injection delay [300–495 µs]			
	475			
NOP	Nozzle open pressure [13–23 MPa]			
	17			
Test	Injection dosage		Return dosage	
Leak test [mm^3/H] 140 MPa, 120 s	0		0–40	34.97
IVM 1 [mm^3/H] 140 MPa, 700 µs	31.83–46.33	42.29	0–40	55,18
IVM 2 [mm^3/H] 80 MPa, 600 µs	14.43–31.35	15.86		
IVM 3 [mm^3/H] 23 MPa, 573 µs	0.3–5.55	0.64		
IVM 4 [mm^3/H] 40 MPa, 462 µs	1.18–7.91	2.12		

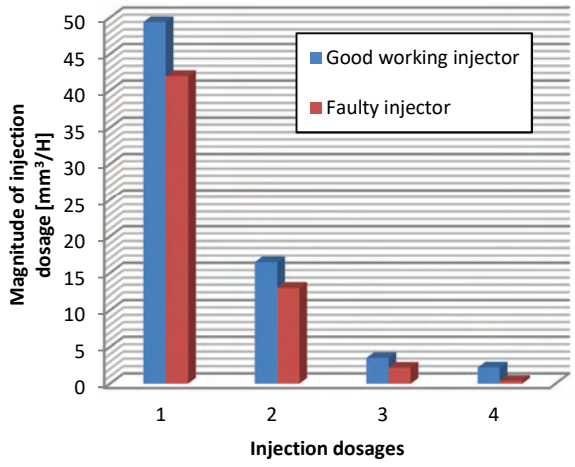


Fig. 14. Injection dosages comparison between faultless and faulty electromagnetic Denso fuel injector 1 – full load dosage, 2 – medium load dosage, 3 – idle speed dosage, 4 – initial dosage

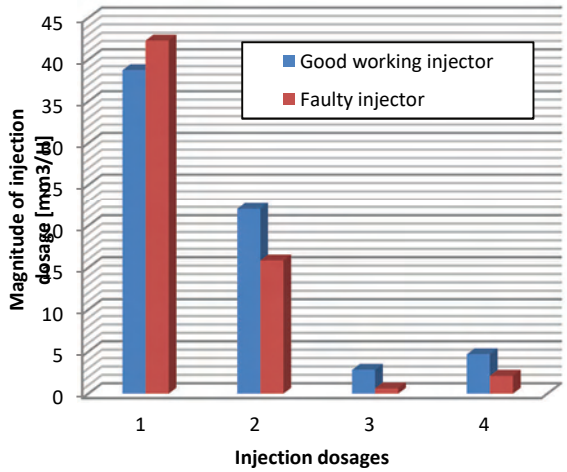


Fig. 15. Injection dosages comparison between faultless and faulty electromagnetic Delphi fuel injector 1 – full load dosage, 2 – medium load dosage, 3 – idle speed dosage, 4 – initial dosage

Table 9. Test results of faultless piezoelectric Continental fuel injector research

Piezoelectric Continental fuel injector no. A2C59511603				
eRLC	Resistance [175–200 kΩ]		Capacitance [2.20–7.10 µF]	
	187		3.35	
RSP	Injection delay [200–420 µs]			
	257			
NOP	Nozzle open pressure [12–19 MPa]			
	15			
Test	Injection dosage		Return dosage	
Leak test [mm^3/H] 160 MPa, 180 s	0		0–65	4.31
IVM 1 [mm^3/H] 160 MPa, 1100 µs	55.45–67.45	61.15	0–40	10,19
IVM 2 [mm^3/H] 70 MPa, 380 µs	10.82–15.82	13.82		
IVM 3 [mm^3/H] 70 MPa, 140 µs	0.5–4.51	2.79		
IVM 4 [mm^3/H] 25 MPa, 520 µs	3.28–8.28	6.17		

Table 10. Test results of faulty piezoelectric Continental fuel injector research

Piezoelectric Continental fuel injector no. A2C59511603				
eRLC	Resistance [175–200 kΩ]		Capacitance [2.20–7.10 µF]	
	178		2.96	
RSP	Injection delay [200–420 µs]			
	643			
NOP	Nozzle open pressure [12–19 MPa]			
	21			
Test	Injection dosage		Return dosage	
Leak test [mm^3/H] 160 MPa, 180 s	0		0–65	18.53
IVM 1 [mm^3/H] 160 MPa, 1100 µs	55.45–67.45	56.31	0–40	27,92
IVM 2[mm^3/H] 70 MPa, 380 µs	10.82–15.82	8.53		
IVM 3[mm^3/H] 70 MPa, 140 µs	0.5–4.51	0.65		
IVM 4[mm^3/H] 25 MPa, 520 µs	3.28–8.28	2.76		

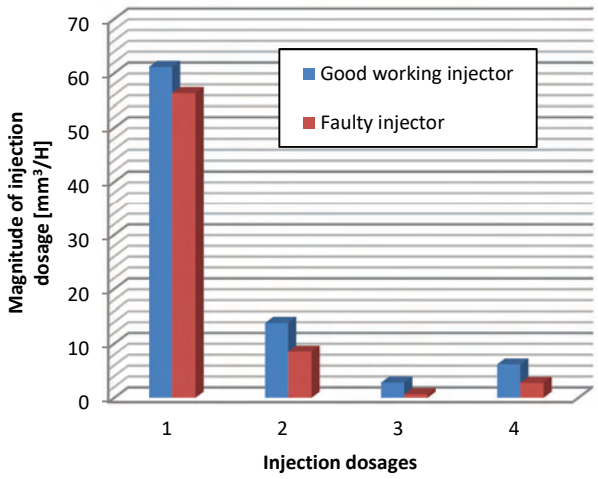


Fig. 16. Injection dosages comparison between faultless and faulty piezoelectric Continental fuel injector 1 – full load dosage, 2 –medium load dosage, 3 – initial dosage, 4 – idle speed dosage

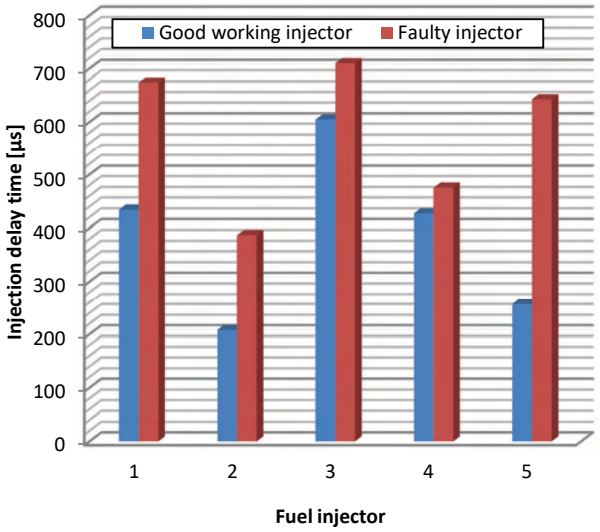


Fig. 17. Comparison of RSP parameter between faultless and faulty fuel injectors 1 – electromagnetic Bosch fuel injector, 2 – piezoelectric Bosch fuel injector, 3 – electromagnetic Denso fuel injector, 4 – electromagnetic Delphi fuel injector, 5 – piezoelectric Continental fuel injector

Tables 1–10 present the results of tests of the number of different fuel injectors. Tests have been made in the fuel injections systems diagnostic and repair laboratory using the test bench Carbon Tech CRU 2i. Main fuel injectors parameters like injection and return dosages, electric values, nozzle open pressure and injection delay (RSP) were measured.

Figures 12–16 present results of fuel injector dosages tests for a set of fuel injectors under different operational conditions, i.e. full load, medium load, idle speed and initial dosages. It is evident that in all the cases corrosion resulted in decreased fuel dosages, what is especially visible for idle-speed tests. Corrosion pollution change work characteristic of injector needle in the nozzle. Figure 17 presents results of RSP parameter measurements. Injection delay is important indicator, which depends on injector construction. The fastest are piezoelectric fuel injectors. Too long injection delays influence on combustion process.

5. Conclusion

Corrosion phenomena is a process which slowly damages metal elements. There are a few types of corrosion processes in fuel injectors. This problem should be examined in two aspects: when liquid is in rest or when it is in move. Fuel injector parts wore out during operation because of erosion, cavitation and friction. The conditions like high pressure, high temperature, poor fuel quality (its pollution and humidity) intensify corrosion. All fuel injectors are made with the same material and magnitude of corrosion depends on medium not on the type of injector. Extensive and deep corrosion pits on precision elements result in loss of fuel tightness. Results of tests of various fuel injectors (Table 1–10) show that corrosion phenomena influences fuel injectors parameters. Corroded precision elements (Figs 6–8) increase leaks what affects return dosage. High inner leaks may lead to unsealing of the whole injection system. Corroded nozzle with idle and steering valve af-

fects injector operational parameters like: injection dosages, nozzle open pressure and injection delay.

Electromagnetic and piezoelectric fuel injectors have been tested and analyzed. Corrosion phenomena has similar effect on both of them. The tests of modern fuel injectors consist of checking injection and return dosages. If precision elements are damaged return dosages increase, what makes injector valve and nozzle very important. Corrosion, cavitation and friction trigger damaging phenomenon which slowly destroys them. The first sign of injector failure is loss of micro dosages when operating in low pressure, short injection time conditions (e.g. 25 MPa and 250 μs).

The results of corrosion phenomena are decrease of initial dosages especial for idle speed and medium engine load.

Idle speed dosage is very important as fuel injector diagnostic parameter. If the differences between idle speed dosages are higher than 0.5 mm^3/H then the fuel injector's elements are already worn and the electronic diagnostics is able to notice this deterioration. The corrosion pollution change range of movement injector idle in the nozzle, what has an impact on injection dosages and nozzle open pressure (NOP). If corrosion pits aren't extensive and deep (Fig. 11) it should be possible to repair injector. The repair involves very accurate cleaning in ultrasonic washers and regulation. When damage is extensive it is necessary to replace elements. Another very important fuel injector operational parameter is injection delay time (RSP). This is the time between electric steering fuel injector and when it starts spraying. Piezoelectric fuel injectors have the shortest delay. Short RSP enables generation of more injections during a single cycle. Too long injection delay compounds combustion process what influences on engine work. Corroded injector components extend injection delay.

Nomenclature

CI compression ignition
CR common rail system

Bibliography

[1] AMBROZIK, A., AMBROZIK, T., ŁAGOWSKI, P. Fuel impact on emissions of harmful components of the exhaust gas from the CI engine during cold start up. *Eksploatacja i Niezawodnosc – Maintenance and Realiability.* 2015, **17**(1), 95-99.

[2] BASZKIEWICZ, J., KAMIŃSKI, M. Korozja materiałów. *Oficyna Wydawnicza Politechniki Warszawskiej*. 2006.

[3] GÜNTHER, H. Common Rail – Systeme in der Werkstattpraxis. Technik, Prüfung, Diagnose. *Bad Wörihofen: Krafthand Verlag Walter Schultz GmbH*. 2012.

[4] HRYNIEWICZ, T., ROKOSZ, K. Podstawy teoretyczne i aspekty praktyczne zjawiska korozji. *Wydawnictwo Uczelniane Politechniki Koszalińskiej*. 2010.

[5] Zasobnikowe układy wtryskowe Common Rail. Informator Techniczny Sterowanie silników ZS. Robert Bosch GMBH. *WKiŁ.* 2005, 2009.

[6] OSIPOWICZ, T., ABRAMEK, K.F., STOECK, T. Testing of modern common rail fuel injectors. *Combustion Engines*. 2015, **162**(3), 688-694.

[7] OSIPOWICZ, T. Diagnosing Common Rail fuel injectors using fuel micro – doses. *Teka. Commission of Motorization and Energetics in Agriculture.* 2015, **15**(1), 61-64.

[8] OSIPOWICZ, T. Diagnosis Diesel Common Rail fuel systems. *Autobusy, Technika, Eksploatacja, Systemy Transportowe.* 2016, **8**, 129-130.

Tomasz Osipowicz, DEng. – Faculty of Mechanical Engineering and Mechatronics at West Pomeranian University of Technology.

e-mail: *Tomasz.Osipowicz@zut.edu.pl*



Maciej Lisowski, DSc., DEng. – Faculty of Mechanical Engineering and Mechatronics at West Pomeranian University of Technology.

e-mail: *MLisowski@zut.edu.pl*

Article citation info:
MERKISZ-GURANOWSKA, A. Product recycling of automotive parts – trends and issues. *Combustion Engines*. 2017, **171**(4), 24-28.
DOI: 10.19206/CE-2017-404

Agnieszka MERKISZ-GURANOWSKA

CE-2017-404

Product recycling of automotive parts – trends and issues

Remanufacturing is a dynamically developing area of the automotive industry. It allows the original equipment manufactures to diversify their activities and sell manufacturer-warrantied subassemblies through a dealership network but at lower prices compared to new products. The paper presents the process of remanufacturing of automotive subassemblies and characterizes the benefits for the industry and vehicle end-users. Examples have been shown of the activities of vehicle manufacturers in the area of product recycling and development of remanufacturing technologies.

Key words: *recycling, remanufacturing, automotive parts*

1. Introduction

The automotive industry is one of the key sectors of economy in developed countries. The worldwide vehicle fleet counts over 1.2 billion vehicles, out of which almost 910 million are passenger vehicles [7]. Each year, nearly 70 million passenger vehicles and another 22 million light-duty trucks and heavy-duty trucks are manufactured. It is estimated that by 2035 the number of vehicles will double.

The production, sales and service maintenance of vehicles are factors of economic growth in the world. The input of the automotive industry in the worldwide economy amounts to almost 2 trillion euros [8], which means that if we compared it to the GDP of a country, the automotive industry would be the seventh economy worldwide. The automotive industry plays and important role in the global use of natural resources, emissions to the atmosphere, water and soil, let alone production of waste. Recycling plays a significant role in the reduction of this environmental impact.

The dependence of the automotive sector on raw materials and some noble metals may in the future become a limitation of its development thus the supply management is a strategic challenge for this sector. The automotive sector is, for example, the largest consumer of lead. Its uses 60% of the world's production of this metal. Aside from the problems related to the possible shortages in the supplies of some metals – whether rare or not – the growth of the global demand for raw materials inevitably leads to increased prices. The implementation of a principle of material reuse, whenever there exists such an opportunity, not only leads to material and energy savings, prevents generating waste but also brings economic benefits. Additionally, such a policy remains in line with the principles of circular economy being introduced in the EU member states.

Circular economy assumes limited generation of waste and environment pollution resulting from the consideration of the relevant needs already on the design stage of the goods. It distinguishes two types of components: biological, to be reentered to the biosphere and technical – designed in such a way as to enable its reuse without entering the biosphere. Such an approach remains in opposition to the traditional concept of economy based on linear model referred to as "take, make, dispose", in which each product has a limited period of operation. Circular economy puts more pressure on reuse, repair, renewal and recycling of materials.

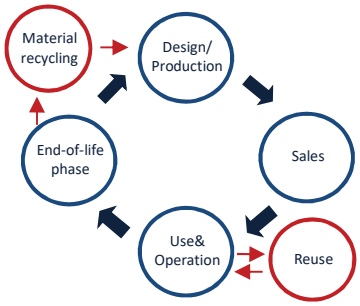


Fig. 1. Diagram of circular economy

Waste recycling may be carried out as product recycling or material recycling. Product recycling consists in restoring the technical parameters of parts or subassemblies so that they could be reused as spare parts in other vehicles in operation. These parts may come from on-going service maintenance or from end-of-life vehicles. Material recycling involves processing of waste to obtain secondary raw materials or other products used in the industry. As for end-of-life vehicles, some disassembled parts (e.g. mirrors, bumpers) may be ready for refitting in other vehicles. Other parts disassembled during service procedures, must undergo remanufacturing. This is particularly the case for engines, engine aggregates, suspension systems, drivetrains. Remanufacturing is most often carried out on such components as fuel systems, hydraulic systems, cylinder heads, crankshafts, starter motors, alternators or transmissions.

The process of remanufacturing consists in restoring the original properties of end-of-life parts that are identical to the properties of a new product by a combination of such processes as disassembly, application of regenerative layers, renewal, repair and refitting. The said procedures result in the extension of the period of operation. Contrary to product recycling, remanufacturing requires direct manpower, development of appropriate technology and use of raw materials.

Remanufacturing is a dynamically developing area within the automotive industry. It allows the original equipment manufacturers to diversify their operations and provides them with a competitive tool in the fight with budget, aftermarket spare part suppliers. The value of the remanufactured automotive part market is to reach 130 billion euros by 2020 [5]. The greatest share in this market

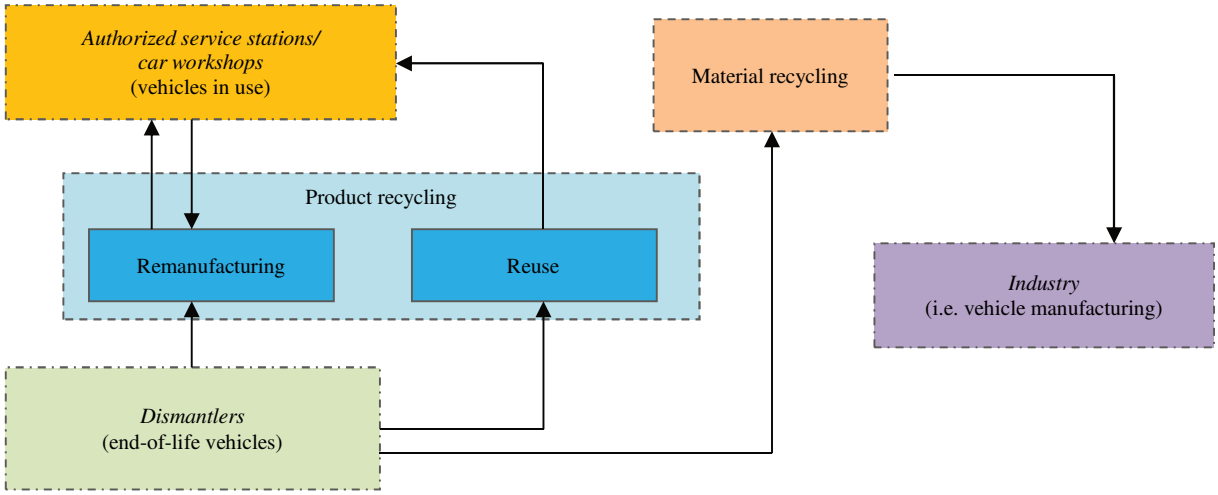


Fig. 2. Recycling flows in vehicle life cycle diagram

has the United States, while the most rapidly advancing market with the annual growth index of 25% is Asia. This sector employs 31 thousand people in the US and approx. 43 thousand people in Europe [6]. According to the estimations of European Association of Automotive Suppliers (CLEPA) and European Remanufacturing Network, the market of remanufactured parts in Europe is worth between 8 and 10 billion euros per annum [2, 4]. The entire European market of remanufacturing of the vehicles, machines and equipment is estimated at approx. 30 billion euros at a total employment level of 190 thousand people [4]. The greatest share have: aerospace (42%), automotive (25%), heavy-duty and off-road (14%) together constituting over 80% of the European remanufacturing market. Unfortunately, the relation between the revenues from remanufacturing to the revenues from the entire sector (sale of remanufactured and new parts) is still rather poor and amounts to 1.9%. For the aerospace, subassembly remanufacturing already constitutes 11.5% of the market value but for the automotive sector this index is a mere 1.1%.

Table 1. Remanufacturing market in Europe by sector [4]

Sectors	Turnover (bn euro)	Firms	Employment	Intensity
Aerospace	12.4	1000	71000	11.5%
Automotive	7.4	2363	43000	1.1%
Heavy duty and off road	4.2	581	31000	2.9%
Electronic & electrical equip.	3.1	2502	28000	1.1%
Furniture	0.3	147	4000	0.4%
Machinery	1.0	513	6000	0.7%
Marine	0.1	1	1000	0.3%
Medical equipment	1.0	7	7000	2.8%
Rail	0.3	3	3000	1.1%
Total	29.8	7204	192000	1.9%

In the European market, the largest stakeholder is Germany with the share in total sales on the level of 2.4 billion euros. France, Spain and Great Britain with Ireland follow immediately with an approx. 10 % share in the market. A slightly smaller share is held by Italy and the countries of Central and Eastern Europe.

2. The advantages of product recycling

Product recycling brings benefits to both the manufacturers and the vehicle end-users. For the manufacturers, the most crucial issue is the savings of the resources, hence the production costs.

In comparison to new parts, the production of regenerated parts saves [3]:

– 80% of energy,
– 88% volume of water,
– 92% mass of chemical products,
– 70% mass of waste.

The durability of the components after remanufacturing should not significantly differ from that of new parts and should at least reach 80% of their durability. However, vehicle manufacturers performing the remanufacturing at their own facilities (factory remanufacturing), subject the remanufactured parts to the same quality tests applied to new parts and guarantee the same durability and functionality. Remanufactured parts are covered with the same manufacturer warranty as the new ones.

The costs of remanufacturing should not exceed those of new parts. Otherwise, the remanufactured parts would not generate demand and the entire process would be economically unjustified. The total costs of remanufacturing should not exceed 60% of the costs of manufacturing of a new part. Most often, the costs fall in the range from 40 to 60% of the costs of a new part [6]. The savings on the cost of production result from the avoidance of production processes such as casting or melting (energy and thus money saving). The energy savings during a remanufacturing may reach up to 85% of the energy necessary to manufacture a new part.

From the point of view of the end-user, the main advantage is the competitive price of the remanufactured items. The price of a remanufactured part is usually50–70% of a new part depending on the required expense.

Remanufacturing requires qualified manpower. Compared to the production of new parts, this type of activity does not involve advanced automation. In combination with the savings on the processing costs, it results that this type of activity is conducted relatively close to the sources of waste, hence is not 'delocalized', thus contributing to creat-

ing new employment opportunities and the development of local economy.

Selling remanufactured parts and subassemblies to customers as an alternative to new products is also a trading argument for workshops and authorized service centres. It allows a repair of older vehicles using spare parts whose durability corresponds to the durability of the repaired vehicle at an acceptable cost that corresponds to the vehicle residual value. This extends the life cycle of vehicles whose further operation would be economically unjustified if repaired with new parts (when the cost of repair exceeds the vehicle residual value). Besides, for parts whose production was seized, remanufacturing is the only way to obtain them.

There are many challenges for business entities dealing with remanufacturing. The most important ones are: the perception of remanufactured parts by the customers as parts of lower quality, irregular supply of used subassemblies, resistance of the manufacturers of the original equipment, no access to product information and possible limitations in the application of remanufactured parts in warranty-covered products. Vehicle manufacturers who conduct remanufacturing by themselves are somewhat privileged, as they can obtain the used parts from their network of authorized service workshops, which ensures more stable sales and facilitates the logistics. They also have full access to information regarding the product and their clients have more trust in them if the parts are covered with a vehicle manufacturer warranty. Even the original equipment manufacturers must allow for irregular supplies of certain subassemblies for remanufacturing and different quality of the product at the beginning of the process.

Table 2. Comparison of remanufacturing and manufacturing of parts

Category	Remanufactured parts	New parts
Production cost	Low	High
Energy consumption	Low	High
Price for user	Low	High
Automation	Low	High
Labour intensity	High	Low
Quality	High	High
Material supplies for production (timing and quantity)	Uncertain	Stable
Perception by the customer	Bad	Good

3. The process of remanufacturing

The regeneration starts with a preliminary assessment if a product is fit for further use. This inspection is decisive of the profitability of the remanufacturing, quality of the remanufactured parts and, simply, whether the process will be performed or not. The subassemblies are disassembled and their individual components are degreased and cleaned. The next step is a detailed evaluation of the technical condition of each of the components. The most important stage is proper remanufacturing of the components that consists in restoring their original properties and applying regenerative layers (chroming, ironing etc.). Some components are renewed and some are repaired. During remanufacturing of engines, only the engine block, the crankshaft and the connecting rods undergo the process, while the cylinder head, the injection pump and the turbocharger are new. The subassembly is then refitted. The last stage is the testing of individual parts and the entire subassembly to make sure it complies with the specifications of the original equipment.

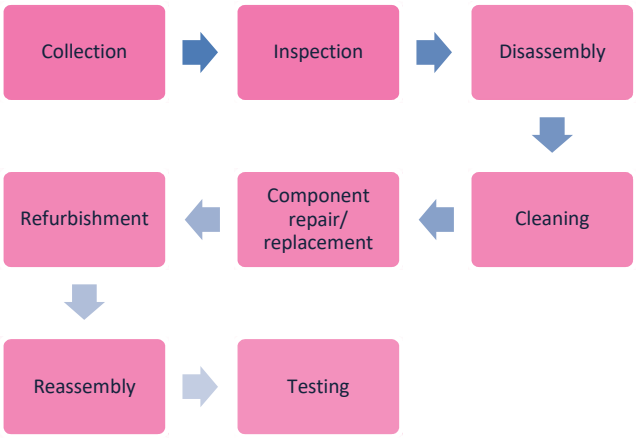


Fig. 3. Remanufacturing process

The disassembly is performed manually due to the versatility of the disassembled components and the necessity of selecting proper tools for the process. The longer the time of disassembly, the higher the cost of labor, which has a negative impact on the economic account. Parts that have been designed to allow for future disassembly (Design for Disassembly) reduce the costs of remanufacturing. In order to determine the optimum methods of disassembly, different solutions are applied such as the petri-net approach or the and/or graph serving the purpose of generating sequences of operations and hierarchical modular modelling.

Another process influencing the course of remanufacturing is cleaning of the parts. Currently commonly used methods are high temperature decomposition, shot blasting and high pressure water cleaning. A new alternative and, at the same time environment-friendly, method is supercritical carbon dioxide (SC–CO_2) cleaning that is very useful in removing oil stains from the engine components and aluminium parts.

The key process during remanufacturing, however, is the restoration of the technical parameters and applying regenerative layers. One of the methods is honing (cross-hatch). This is a technology of bore machining consisting in eliminating material surplus from the inner surface of a bore with abrasive stones. Other methods include surface processing based on laser metal alloy powder hardfacing that allows forming new layers and their quenching, which makes the layers more resistant to stress, ensures greater hardness and operational durability. One of the most recent methods is Plasma Transferred Wire Arc (PTWA) involving application of corrosion resistant material with the method of thermal plasma. The use of PTWA consists in applying a thin layer of material on the worn and porous components of an engine such as the cylinders. The corroded areas with material loss are filled and then polished and restored to the original dimensions.

The logistic chain related to remanufacturing of parts is a typical example of reverse logistics that includes all elements connected to the flow of products whose owner or user no longer wishes to use and forwards them back to the manufacturer distribution network or any other collectors

[9]. Contrary to waste disposal, it focuses on such flows that aim at recovery of the product or waste through its repair or another form of reconditioning.

The logistic chain serving the purpose of collecting parts for remanufacturing and their distribution as spare parts includes selected links of a logistic chain of conventional distribution of new parts and those of the recycling networks of end-of-life vehicles. For parts disassembled in service operations, return shipments are used in modes of transport supplying new parts. Parts disassembled from vehicles for dismantling are forwarded to remanufacturing facilities via dedicated transport.

4. Recycling of vehicle parts on selected examples

A European leader among the automotive car manufacturers is Volkswagen AG. It started remanufacturing parts, including engines in 1947. The first products available after remanufacturing were cylinders, fuel pumps, carburettors, steering boxes and clutch pressure plates.

Ever since, the concern facilities have reconditioned approx. 7.7 million engines, 2.5 million transmissions and 68 million additional components [13]. Upon assessment, the disassembled engines and transmissions are subjected to remanufacturing at the Volkswagen works in Kassel or, if they are not good for product recycling, they are forwarded to material recycling. The basic activity of the Volkswagen works in Kassel is production of new manual and automatic transmissions (the facility supplies 4 million transmissions per annum for the entire VW group), exhaust systems and other subassemblies for the Passat, Polo and Golf models. Kassel also hosts a distribution centre of original parts. The combination of activities of part manufacturing and logistics facilitates a reduction of costs and capital expenditure related to remanufacturing of engines and transmissions.

In 2011 Volkswagen opened the first engine remanufacturing facility outside of Germany. The potential of the facility located in Dailan in East China is 15000 units per annum. 70% of the material mass is reused. Engines subjected to reconditioning are 50% cheaper compared to new engines and are sold under the brand Volkswagen Genuine Exchange Parts operating in the same scheme as Volkswagen Original Parts. The parts are remanufactured with an industrial method and are quality checked locally in the facility in terms of dimensions and operating parameters to ensure safety, technical standards and durability. Therefore, the manufacturer provides warranty identical to that issued for new parts.

The portfolio of parts and components available within the Volkswagen Passenger Cars brand's Genuine Exchange Parts is regularly extended. Currently the portfolio includes approx. 10 thousand items for passenger vehicles and light duty-trucks sold under the brands of Volkswagen and Audi. Thanks to the idea of part remanufacturing, Volkswagen guarantees supplies of spare parts for a minimum of 15 years from the moment of seizing serial production of a given model. The prices of these parts are, on average, lower by 40% compared to new parts. Remanufacturing of engines at the Volkswagen facilities allows saving approx. 7000 tons of steel [12]. The amount of steel contained in the regenerated engine to date would suffice to build 50 Eiffel Towers and 162 Golden Gate bridges[13].

The Renault company is another player having its facility specializing in part remanufacturing. The facility located in Choisy-le-Roi, France began its operations in 1949. It initially reconditioned combustion engines exclusively. In 1989, it extended its operations to injection pumps, then gearboxes (2003), injectors (2010) and turbocompressors (2013). The remanufactured parts are used only for repairs of vehicles already in operation. A customer can purchase a new or a remanufactured part at an authorized service workshop. The regenerated parts cover 70% of reference mechanical parts for 90% of the vehicle models manufactured under the brand of Renault. Collectively, Renault offers 19 product families – mechanical, electronic, parts for the brake systems and air conditioning systems. Remanufactured parts are a proposal mainly targeting owners of vehicles older than 4 years. The prices are 50 to 70% of new parts.

Out of 120 used engines retrieved from end-of-life vehicles or damaged engines obtained from the service networks, on average, 100 remanufactured engines return to the market. The saving on the energy related to the delivery of the remanufactured engines reaches up to 70% compared to the production of new units.

Parts forwarded to the Choisy-le-Roi facility are sorted in the following way[3]:

- 43% of the part mass is reused in reconditioned subassemblies,
- 48% of the part mass is processed in foundries belonging to the group and is used for production of new parts,
- 9% of the remains is subject to other forms of recovery.

The facility does not generate any waste for disposal.

The Choisy-le-Roi facility employing 325 workers remanufactures spare parts of the market value of over100 million euros, which includes [3]:

- 14700 engines,
- 21200 transmissions,
- 32700 injection pumps,
- 151300 injectors,
- 3500 cylinder heads.

Toyota automaker also has a wide portfolio of remanufactured spare parts [10]. They are available at all European Toyota authorized services. The used parts coming from the dealer service networks are forwarded to the European distribution centre and then directly to the entities dealing with the process of remanufacturing .

Part remanufacturing has been performed in Toyota since 2001 when a business entity under the name of Ecoline Corporation was created responsible for the sales of used parts (including the remanufactured ones). In the European market, the reconditioned parts under the brand name of Toyota have been available since 2002 when remanufactured air-conditioning compressors and power assisted steering gears were introduced. A year later, the offer was extended by engines (with and without aggregates) and cylinder heads. Today, the following remanufactured subassemblies (tested and admitted for use by the Toyota standards) are available:

- engines,
- starter motors,
- alternators,
- complete clutch assemblies,

– automatic transmissions,
– air-conditioning compressors,
– steering gears.

Each year Ecoline sells almost 50 used parts [11]. The sales of some remanufactured parts are much higher than the sales of new parts. Each year, service repairs rely on 3780 reconditioned transmissions (the sales of new transmissions are approx. 100 per annum) and the power assisted steering counts 10000 units per annum against 4700 new ones [11].

Ford uses a proprietary patented technology of Plasma Transferred Wire Arc developed at its research and innovation centre in Aachen, Germany. Ford has performed durability tests of the engines remanufactured with this method. The tests have confirmed the engine parameters, the durability and quality of the layer application after a mileage of 400 000 km [1]. The warranty for reconditioned engines is the same as for the new ones. A downside of the PTWA process is the cost that is higher compared to the cost of remanufacturing with conventional methods. An advantage is the savings on the materials used in the reconditioning process and a reduction of the emission of CO_2 by 50% compared to the production of new engines.

The market of subassembly remanufacturing has also been penetrated by Chinese companies. The possibilities of utilizing used parts are limited in China (due to a ban on use of parts retrieved from end-of-life vehicles), yet, the Chinese government has permitted a pilot activity in the area of vehicle part remanufacturing. In 2008 the first 14 companies were authorized and certified by the National Development and Reform Commission and the further 28 in 2013 [14]. These companies mainly deal with the reconditioning of engines, transmissions, alternators, and steering gears. China remanufactures approx. 110 thousand engines, 60 thousand transmissions and a million of starter motors.

5. Conclusions

The supply of recycled materials and investing in recycling technologies have good prospects for the future. Product recycling in the form of part remanufacturing, however, is very often a more profitable solution in terms of reduction of waste negative impact on the environment, savings on energy and raw materials. Despite investments that require developing technologies and performing regenerations of engines and other subassemblies, this activity is also profitable for the vehicle manufacturers. It allows increasing the sales figures related to spare parts that are offered at reduced prices, retaining customers at authorized service networks (owners of older vehicles) and ensuring stability of spare part supplies at acceptable costs for those that are no longer manufactured.

Clients and vehicle users also put increasing pressure on part remanufacturing. In 2015, the US Senate passed a law (Federal Vehicle Repair Cost Savings Act) that imposes on Federal Agencies the necessity to use (if possible) remanufactured parts when maintaining fleets of vehicles. The total vehicle fleet of the Federal Government reaches 580 thousand vehicles and the annual expenses for vehicle maintenance reach 975 million US dollars [4].

Bibliography

[1] BOAGEY, R. Automotive Remanufacturing. *Professional Engineering*. 2017, **02**, 31-32.

[2] CLEPA European Association of Automotive Suppliers, clepa.eu/what-we-do/publications/ (accessed 13.03. 2017).

[3] Ellen Mac Arthur Foundation. De l'économie circulaire appliquée a l'industrie automobile. www.ellenmacarthurfoundation. org/ fr/news/de-leconomie-circulaire-appliquee-a-lindustrie-automobile-le-cas-pratique-de-lusine-de-choisy-le-roi (accessed 15.03.2017).

[4] European Remanufacturing Network, Remanufacturing Market Study, European Commission, Brussels, 2015.

[5] Global Industry Analysis INC., The Global Automotive Parts Remanufacturing Market, www.strategyr.com/ MarketResearch/Automotive_Parts_Remanufacturing_Market_ Trends.asp (accessed 21.03.2017).

[6] LEE, C.-M., WOO, W.-S., YOUNG-HWA, R. Remanufacturing: Trends and Issues. *International Journal of Precision Engineering and Manufacturing-Green Technology*. 2017, **4(1)**, 113-125.

[7] Organisation Internationale des Constructeurs D'automobiles, Vehicles in use report, www.oica.net/category/vehicles-in-use/ (accessed 25.02.2017).

[8] Organisation Internationale des Constructeurs D'automobiles, Economic contributions, www.oica.net/category/economic-contributions/ (accessed 25.02.2017).

[9] STOCK, J.R. Development and implementation of reverse logistics programs. Council of Logistics Management, Oak Brook, USA, 1998.

[10] Toyota Motor Corporation. Recycling of cars, Europe. Toyota Motor Marketing Europe Environmental Affairs Office, Brussels, 2002.

[11] Toyota Motor Corporation. Vehicle recycling. Environmental Affairs Division Toyota Motor Corporation, 2014.

[12] Volkswagen Group. Group Management Report 2014, annualreport2014.volkswagenag.com/group-management-report/sustainable-value-enhancement/environmental-management/recycling.html (accessed 15.03.2017).

[13] Volkswagen Singapore, www.volkswagen.com.sg/en/service/genuine-parts-accessories/genuine-exchange-parts.html (accessed 18.03.2017).

[14] WEI, S., CHENG, D., SUNDIN, E., TANG, O. Motives and Barriers of the Remanufacturing Industry in China. *Journal of Cleaner Production*, 2015, **94**, 340-351.

Prof. Agnieszka Merkisz-Guranowska, DSc. – Faculty of Machines and Transport at Poznan University of Technology.

e-mail: *Agnieszka.Merkisz-Guranowska@put.poznan.pl*



Article citation info:
GRABOWSKI, Ł., WENDEKER, M., BARAŃSKI, G., DUK, M. Study of the efficiency of on-board electricity generation in the city bus. *Combustion Engines*. 2017, **171**(4), 29-32. DOI: 10.19206/CE-2017-405

Łukasz GRABOWSKI
Mirosław WENDEKER
Grzegorz BARAŃSKI
Mariusz DUK

CE-2017-405

Study of the efficiency of on-board electricity generation in the city bus

This paper discusses the methodologies to investigate the efficiency of on-board electricity generation in the city bus. The research object, i.e. the Mercedes Conecto was tested under steady conditions. A chassis dynamometer, i.e. the MAHA LPS 3000 LKW provided the same conditions during the entire research. The paper presents the samples of the measurements performed at a single operating point of a given crankshaft speed and torque. This operating point was specified in line with the guidelines for the WHSC test. In our study, an electrical load was changed with an extra receiver, or a light bulb, at a fixed amount of fuel. The electrical loads were 0.4 kW, 1.6 kW and 2.8 kW. The research results enabled us to specify the amount of fuel to generate 1 kWh of electrical energy.

Key words: *efficiency, engine, city bus, electrical energy*

1. Introduction

The transportation sector is the second largest energy consumer with its consumption of about 30% of total global consumption [1]. The IEA report [10] states that 19% of global energy consumption is for road transportation that, in turn, produces 23% of global CO_2 emissions. Energy consumption by transportation, especially road, has increased much in the past few decades. Crude oil is the primary fuel and hydrocarbons capable of covering the primary energy demand [11].

Vehicles are chiefly driven by compression-ignition internal combustion engines which show high torque over a wide range of speed, which enables efficient daily passenger transportation. The city bus drives about 250 km per day in a medium-sized city in Poland and its typical drive proceeds in the following stages, in order of their frequency: idling, accelerating and braking, and steady-state driving. At the same time, the diesel engine remains a main source of mechanical energy in transportation. Its developed control system and highly efficient working process of more than 40% make it widely used. [16]. The generated energy is chiefly used to drive the vehicle, but also multiple engine-driven receivers such as an air conditioner's compressor, a brake system's compressor or alternators for which there are very often installed two or three receivers of a more than 10 kW total power. These devices should be powered by the adequate on-board generated amount of energy. This means that on-board generated electricity consumed by the city bus is a large share of its total energy consumption. The research results [8] show that the city bus consumes between 15 kWh and 30 kWh of electricity a day. This range of consumption depends on on-board devices, i.e. an air-conditioner, ticket machines, monitors. It should also be remembered that electric power demand in vehicles is constantly increasing [4] for example, due to applying electric power steering [5]. This trend has been clearly visible for the last two decades [17]. Car alternator efficiency reaches 70%, but due to transient operating conditions defined by rotational speed and current load, the average alternator efficiency is much lower than the maximum. It is estimated to range between 50% and 62% [2, 3]. There have been many attempts to improve the efficiency of alternators [7, 12] however, the solution to reduce mechanical losses due to powering 3 alternators is to use only one but large.

Given that the 12-meter bus consumes 35 l of fuel per 100 km and its average mileage is 250 km per day, its chemical energy consumption in fuel is 875 kWh per day. About 5% of that could be spent to generate electric energy. Obviously, this amount also depends on engine load. The drive unit dedicated to buses shows high displacement, which, unfortunately, causes high exhaust gas flow rate and considerable mileage fuel consumption defined in kg/100 km or dm^3/100 km. Continuously changed loads cause, therefore, the larger than in constant-speed driving increase in emissions of toxic substances like PM, NO_x, CO and CO_2. It should also be noted that for every liter of diesel used there is emitted about 2.6 kg of CO_2 [6]. The results [14] show that the passenger transportation sector in the Lower Fraser Valley in British Columbia, Canada consumed 19 050 GWh of energy in just one year. This consumption contributed to 5.47 million tons of CO_2 emissions. A significant share of this emission, especially by city buses, is due to their electricity demand. The amount of fuel used and CO_2 emitted depends, among others, on the total electricity generation efficiency in an electrical way and is the product of the efficiencies of the engine, the transmission belt and the alternator.

Therefore, this research aimed at determining the on-board electricity generation efficiency of a city bus under the defined engine operating conditions and varied alternator electric loads enabled by a chassis dynamometer.

2. The research object and test stand

The research object is a bus owned by Miejskie Przedsiębiorstwo Komunikacyjne Lublin S.A. It is the Mercedes Conecto LF with the OM 926 LA inline 6-cylinder diesel engine of a maximum power of 205 kW (278 hp) and a displacement of 7.23 dm^3, see Figure 1. The engine satisfies Euro IV emission standard with the use of the BlueTec technology based on injecting a special liquid, AdBlue, into the catalytic converter to burn out exhaust gas. Electricity is generated by two alternators of a total maximum current of 200 A (vehicle's electrical installation, punchers, monitor-

ing system and displays) and a 140-watt alternator installed in air-conditioned vehicles.



Fig. 1. Research object at the chassis dynamometer

The chassis dynamometer MAHA LPS 3000 LKW enables repetitive measurement conditions and test bench simulations reproducing road conditions, both steady and transient, to investigate the drive unit. This type of research enables also non-weather dependent measurement conditions, and there is no need to deliver the research vehicle to the research road section. Moreover, test bench research allows us to use measuring instruments more efficiently and research conditions are repetitive, which can be hardly possible in typical road conditions. Accordingly, we have managed to perform steady state measurements, which is a basic assumption behind this research [13].

Figure 1 shows a schematic diagram of the test bench: MAHA LPS3000 LPS chassis dynamometer, SEMTECH exhaust gas analyzer, National Instruments data acquisition system.

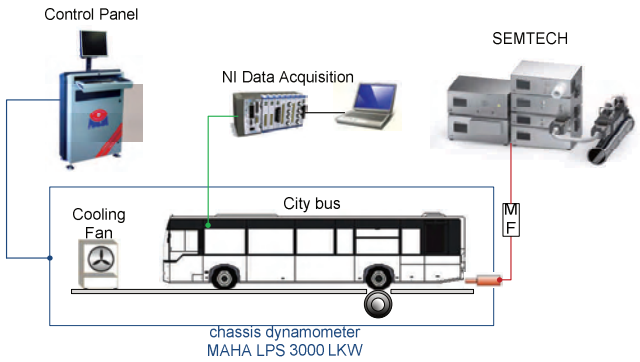


Fig. 2. Test bench

The system for data acquisition, analysis and archiving consisted of:

- real-time controller NI CompactRIO-9024,
- CAN Interface Module NI 9862,
- data acquisition card module NI CompactRIO-9118,
- data acquisition card.

The data from the CAN interface module of the engine control unit were sent in line with the FMS (Fleet Management Systems Interface) standard. Connected to the data acquisition system CompactRIO, the LEM HTR 300-SB current transducer was installed on the cable that connects alternators and a battery.

3. Research scope and aim

The steady-state test cycle was a sequence of measurement points of defined speed and torque at which the engine is investigated in line with the World Harmonized Stationary Cycle (WHSC) [15]. Steady-state research is if vehicle's speed is constant, i.e. crankshaft speed is constant, and an accelerator pedal is in a constant position, which corresponds a fixed dose of fuel. A linear WHSC cycle consists of several standard phases of crankshaft speed and load that are calculated into reference values for a specific engine in line with a calibration curve of operating parameters. The engine needs to operate for a defined period of time in each phase of the cycle, and rotational speed and load are changed every 20 ±1 s. Actually, certain measurement points were investigated due to the constrained architecture of our test bench, and the research scope was modified due to the measurements at each point with different electrical loads, i.e. 0.4 kW, 2.6 kW, 2.8 kW. The research results enabled us to define the amount of fuel that was used only to generate electricity.

To define the operating points, rotational speed was calculated according to the formulae [9, 15].

Figure 3 shows the measurement points and research results for urban conditions.

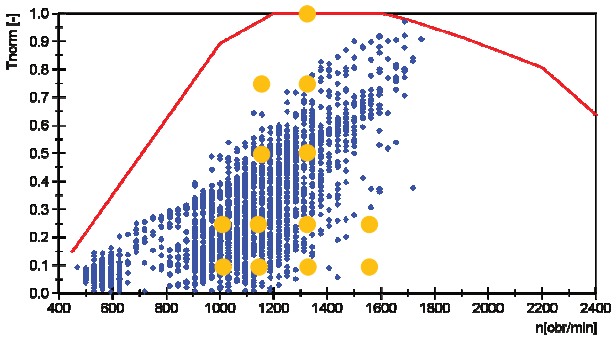


Fig. 3. Normalized torque as a function of crankshaft rotational speed and a series of measurement points

The following parameters were registered:

- power,
- torque,
- engine speed,
- accelerator pedal position (APP),
- fuel consumption per hour,
- carbon dioxide mass flow,
- voltage and electric current of the bus electrical installation.

4. Research results

This paper presents the research results for a single measurement point of n = 1,165 rpm, M_n = 0.1, see Fig. 4.

Our steady-state research allowed us to specify the amount of fuel consumed and carbon dioxide produced due

to the load generated by the on-board electrical devices. Our research examined engine power, electric power, fuel consumption per hour and CO_2 emission. The figure below depicts the results for the measurement point defined by crankshaft rotational speed and a standard torque. Modified by means of an extra receiver, i.e. light bulbs, the electrical load was 0.4 kW 1.6 kW and 2.8 kW. For each of these values, there were measurements for three positions of the accelerator pedal position, which corresponded changes in fuel consumption per hour and power on wheel. Registration time in each measurement point was at least 25 s.

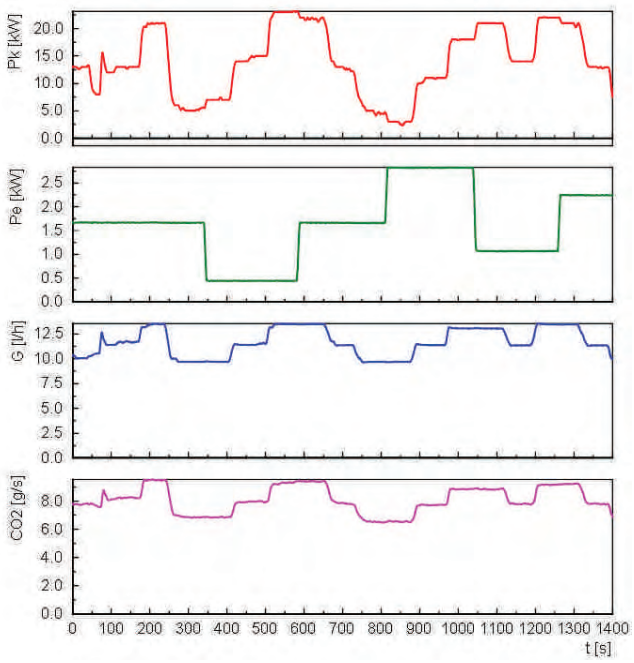


Fig. 4. Research results for the measurement point defined by n = 1,165 rpm, M_n = 0.1, P = 14 kW

The examination at the defined measurement point was as follows. The research results enabled us to correlate power on wheels and fuel consumption per hour. Accordingly, the wheel power for the same APP but varied electric power generated by the alternators was compared. Then, a horizontal straight line, corresponding to power required at a given measurement point, here 14 kW (Fig. 5), was marked. The points of intersection between horizontal straight line y = 14 and three straight lines to approximate the power at varied electrical loads indicate the amount of fuel to generate electricity. This method enables us to specify the amount of fuel to generate electrical energy. This difference results from the fact that for various electrical loads the same value of power on wheels, or desired speed requires fuel dosing to be modified. The research results in line with the methodology above are depicted in Fig. 5. The formulae to calculate the amount of fuel to generate 1 kWh of electricity can be as follows:

$$G_{kWh1} = ((G_2 - G_1)/P_2 - P_1) \quad (1)$$

and

$$G_{kWh2} = ((G_3 - G_2)/P_3 - P_2) \quad (2)$$

where: $G_{kWh1,2}$ – amount of fuel to generate 1 kWh of electrical energy, dm^3/kWh; $G_{1,2,3}$ – fuel consumption per hour, dm^3/h; $P_{1,2,3}$ – electric power, kW.

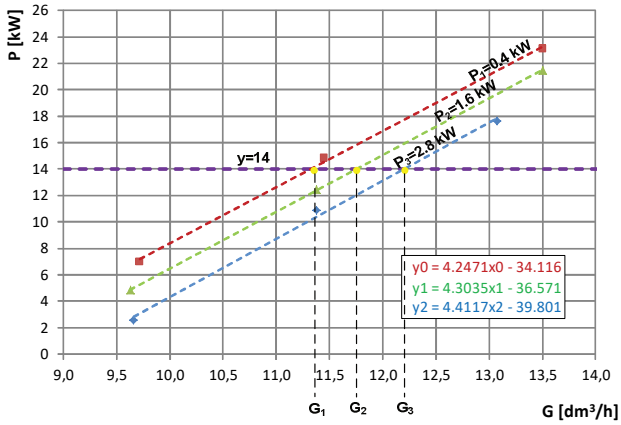


Fig. 5. Power on wheel vs. fuel consumption per hour for three options of electrical load

The following values were calculated: G_{kWh1} = 0.345 dm^3/kWh, G_{kWh2} = 0.383 litres/kWh. Our further analysis was based on the average value of GkWh = 0.364 dm^3/kWh.

Then, these results enabled us to specify the efficiency of electricity generation. It was assumed that a liter of diesel oil contains E_p = 9.7 kWh of chemical energy [8, 18]. Accordingly, it can be calculated that the obtained average value of G_{kWh} = 0.364 dm^3 contains E_{kWh} = 3.534 kWh of energy. Hence, the efficiency of electricity generation calculated as 1 kWh energy generated divided by E_{kWh} – the supplied chemical energy contained in the fuel reaches 28%.

5. Summary

The research discussed in this paper is preliminary and aims at presenting the methodology to specify the efficiency of on-board electricity generation based on the WHSC test. For the measurement point of n = 1,165 rpm, P = 14 kW, efficiency reaches 28%. This efficiency does not cover, however, the efficiency of in-battery energy storage. Our further research shall be done for other measurement points defined by the WHSC test.

Nomenclature

APP	accelerator pedal position
E_{kWh}	electric energy
$G_{kWh1,2}$	amount of fuel to generate 1 kWh of electrical energy
$G_{1,2,3}$	fuel consumption per hour
$P_{1,2,3}$	electric power
T_{norm}	normalized torque
WHSC	world harmonized stationary cycle

Bibliography

[1] BADRUDDIN, A., MEKHILEF, S., SILITONGA, A.S., ATABANI, A.E. A review on global fuel economy standards, labels and technologies in the transportation sector. *Renewable and Sustainable Energy Reviews Renewable and Sustainable Energy Reviews*. 2011, **15**, 4586-4610.

[2] BOSCH, R. Automotive handbook, fourth ed. *Bentley Publishers*, Cambridge, MA 1996.

[3] BRADFIELD, M. Improving alternator efficiency measurably reduces fuel costs. Remy, Inc.

[4] BRADFIELD, M. Improving alternator efficiency measurably reduces fuel costs. Delco Remy, 2008.

[5] Daimler Buses relying on intelligent steering systems. media.daimler.com.

[6] Emission factors for greenhouse gas inventories www.epa.gov.

[7] GONEN, E., GROSSMAN, G. Effect of variable mechanical resistance on electrodynamic alternator efficiency. *Energy Conversion and Management*. 2014, **88**, 894-906.

[8] GRABOWSKI, Ł., PIETRYKOWSKI, K., GĘCA, M., BARAŃSKI, G. The electric power generation efficiency in city bus. *SAE Technical Paper*. 2014, 2014-01-2898.

[9] HEINZ, S. Development of a world-wide harmonised heavy-duty engine emissions test cycle. Executive Summary Report. *ECE-GRPE WHDC Working Group*, 2001.

[10] IEA, Transport, Energy and CO_2. Paris. 2009.

[11] JANUSZ, P. Ropa naftowa – kierunki dostaw i struktura zużycia w Polsce w latach 1999-2011, *NAFTA-GAZ*. 2013, **1**.

[12] MA, Q., BRAHMA, A., RIZZONI, G. Idle speed control for automotive engines with an integrated starter alternator. *15th Triennial World Congress*. Barcelona, Spain.

[13] Materiały informacyjne firmy MAHA. www.maha.pl.

[14] POUDENXA, P., MERIDA, W. Energy demand and greenhouse gas emissions from urban passenger transportation versus availability of renewable energy: The example of the Canadian Lower Fraser Valley. *Energy*. 2007, **32**, 1-9.

[15] Regulamin nr 49 Europejskiej Komisji Gospodarczej Organizacji Narodów Zjednoczonych (EKGONZ).

[16] RIBEIRO, N.M., PINTO, A.C., QUINTELLA, C.M. et al. The role of additives for diesel and diesel blended (ethanol or biodiesel) fuels: a review. *Energy Fuels*. 2007, **21**, 2433-2445.

[17] ROZDMAN, K., REDUAN, M., MOHD, Z., ABDUL, H.A. Experimental study on the effect of alternator speed to the car charging system. *MATEC Web of Conferences* 90 01076.

[18] THOMAS, V.M., MEIER, A.K., GUNDA, S.G., WENZE, I.T.P. Cars are buildings: building-like energy use in automobiles. *Transportation Research Part D*. 2011, **16**, 341-345.

Łukasz Grabowski, DSc., DEng. – Faculty of Mechanical Engineering at the Lublin University of Technology.

e-mail: *L.Grabowski@pollub.pl*



Prof. Mirosław Wendeker, DSc., DEng. – Faculty of Mechanical Engineering at the Lublin University of Technology.

e-mail: *M.Wendeker@pollub.pl*



Grzegorz Barański, DSc., DEng. – Faculty of Mechanical Engineering at the Lublin University of Technology.

e-mail: *G.Baranski @pollub.pl*



Mariusz Duk, DSc., DEng. – Faculty of Electrical Engineering and Computer Science at the Lublin University of Technology.

e-mail: *M.Duk@pollub.pl*

Article citation info:
WYSOCKI, O., KROPIWNICKI, J., CZYŻEWICZ, J. Analysis of the possibility of determining the general characteristics using the operational data of a vehicle engine. *Combustion Engines*. 2017, **171**(4), 33-38. DOI: 10.19206/CE-2017-406

Oskar WYSOCKI
Jacek KROPIWNICKI
Jacek CZYŻEWICZ

CE-2017-406

Analysis of the possibility of determining the general characteristics using the operational data of a vehicle engine

The paper presents an analysis of the possibility of determining the general characteristics using the operational data of an engine of refuse collection vehicle. Data acquisition was done by reading information from the CAN network using FMS standard (Fleet Management System), which is widely used in heavy duty vehicles since year 2002. The paper presents the analysis of the expected measurement uncertainties resulting from the standard PN_ISO 15550-2009. The experimental data were filtered due to the established constraints that define the static states of the engine. On the basis of the obtained measurement data, corresponding to various defined static states, the general characteristics of the engine were made and discussed.

Key words: *combustion engine, general characteristics, fuel consumption, tests in dynamic states, CAN bus*

1. Introduction

The general characteristics of the engine include information about the regions of the engine's operating area that are most efficient, where specific fuel consumption reaches the smallest values. Economic operation based on those characteristics can contribute to a significant reduction of fuel consumption and consequently less pollutant emissions and lower costs. While the driver of a utility vehicle has a main impact on the fuel consumption during regular operation [6, 7, 10–12], the power take-off unit (PTO), such as the garbage truck's propulsion system, is determined by the characteristics of the driven machine. It has been shown in the paper [8] that an appropriate configuration of the drive system based on the general characteristics of the engine reduces the fuel consumption of the utility vehicle by up to 35%. Unfortunately, the information provided by the engine manufacturers contains only external characteristics and can not be used to determine the PTO performance, where the maximum received torque is several times lower then nominal. This introduces the need to determine the general characteristics using a chassis dynamometer for utility vehicles, what causes many problems and costs.

This paper presents the analysis of the possibility of determining the general characteristics using the operational data of a vehicle engine for the refuse collection vehicle. Data logging is possible by reading information from the FMS (Fleet Management System) standard, which has been widely used in heavy duty vehicles since 2002. It contains, among others: engine speed, torque, instantaneous fuel consumption. Data acquisition does not require interfering with the vehicle's onboard systems, just plug into a cab specially prepared by the manufacturer interface and record the data in real time to the storage it for later processing. By using this method, it is expected that the vast majority of data match the dynamic operation of the engine.

There are some differences in engine performance that work in dynamic states and those understood as static [13, 15]. Emerging operating conditions will be a consequence of long-term changes in the temperature of the engine components (e.g. warm-up after start-up) or engine operation at ambient temperatures significantly different from the average (e.g. winter operating conditions) and load and engine rapid changes [4, 9, 14]. For example, a spark ignition engine equipped with a typical three-function catalytic converter with oxygen sensor operating in a closed fuel delivery control loop emits more CO and HC during warm-up and cold start than in the operating phase when the thermal conditions are static. If the ambient temperature drops below 0°C, the above effect will be magnified.

Under such conditions it is necessary to enrich the air/fuel mixture due to the low efficiency of the evaporation process. This significantly diminishes or prevents the catalytic converter from working properly, resulting in increased CO and HC emissions. The low temperature of the engine components also lowers the engine's thermal efficiency due to increased heat exchange and reduced mechanical efficiency due to increased viscosity of the lubricating oil. Reduced engine operating temperature causes also difficulty with ignition of the mixture. The above described phenomena related to the thermal state of the engine and the parameters of its operation can be also applied to the compression ignition engines. In this case, the unfavorable phenomenon of excessive particulate matter emissions in the exhaust gases is also observed.

2. Static state of an engine operation

Static states are defined in theoretical way as conditions of engine operation, where the successive cycles in each cylinder are fully repeatable [1]. Those terms describe the following equations:

$$p(V) = \text{idem} \tag{1}$$

$$q(V) = \text{idem} \tag{2}$$

where: p − pressure in the cylinder, q − heat transfer between the working medium and the walls of the combustion chamber, V − instantaneous volume of the working medium.

The above conditions can not in fact be fulfilled due to the random conditions of engine cycles [16].

According to the Polish Standard [17] static states can be considered as torque and rotational speed changes within the permissible limits (Table 1). The range of permissible variations of engine performance such as particulate matter emissions, temperature and air pressure, exhaust gas, etc. are also specified.

Table 1. Acceptable deviations of the measured engine parameters acc. [17]

Parameter	Permissible deviation
Torque	±2%
Engine speed	±2%
Power	±3%
Fuel consumption	±3%
Specific fuel consumption	±3%

In addition, according to the Polish Standard [18], permissible fuel consumption deviations ΔG_e and engine power deviation ΔP should satisfy the following relation:

$$\sqrt{\Delta G_e{}^2 + \Delta P^2} \leq 3\% \tag{3}$$

However, the standard does not define the time, in which the specified deviations must be kept to conclude the engine is operating in the static state.

In his work [3, 5], Chłopek presented a detailed description of the concept of selection of operating conditions into static and dynamic, taking into account the real possibility of carrying out tests of internal combustion engines. The author considered that the measurement signal, before using it to classify the operating conditions of the engine, should be filtered using low pass filters with a prescribed stop frequency to remove from the recorded waveform measurement errors and accidental errors. The author pointed out that the classification of the operating conditions of the engine to static, when the derivative of the observed signal is equal to zero, in the real test conditions is too strict criteria. The author suggested for laboratory practice, as a criterion for qualifying operating conditions to static, that the derivative of observed signal is less than the assumed limit value. The operating state can then be specified as static with declared accuracy. Selection of limit values for such classification will be determined by the objectives set for the planned study.

3. Data logging using CAN bus

The engine speed is measured in the vehicle by an inductive sensor located at the flywheel, which records changes in the magnetic field generated by the teeth distributed around the edge of the flywheel. According to the FMS standard, the engine speed is measured every 20 ms with a resolution of 0.125 rpm. For a minimum engine speed of 600 rpm, a resolution of ±0.0625 rpm corresponds to a deviation of ±0.01% of the measuring instrument. The torque is read with an accuracy of 1% of the maximum torque of the motor. For the analyzed engine it is 1400 N·m, so the signal resolution is ±14 N·m. Therefore, only indications of over 700 N·m meet the measurement requirements of the Polish Standard [17] with a permissible measuring deviation of less than 2%. The fuel consumption is determined based on the injector opening time and is read with an accuracy of ±0.025 dm^3/h. Again, values greater than 0.833 dm^3/h should be taken into account in order not to exceed the deviations defined in [17]. This does not, however, introduce real boundaries, because fuel consumption during idle runs at 3 dm^3/h, so in the extreme cases the deviation is only ±0.83%. A summary of the measuring deviations of the instruments when recording CAN data is presented in Table 2.

Table 2. Measuring deviation values of the instruments when recording data from the CAN bus

Parameter	Deviation
n	≤ ±0.01%
M	≤ ±2% (for M > 700 N·m)
Ge	≤ ±0.83%

For such restrictions, the condition of formula (3) is satisfied:

$$\sqrt{0.83^2 + 2^2} = 2.17 \leq 3\%$$

It can be concluded, that using CAN bus data logging it is practically impossible to make measurements of engine performance according to Polish Standard [17] due to the low resolution of the recorded torque value in the full field of the engine operation. Consequently, in the further analysis, the limitation shown in Table 2 will be not applied, allowing the increase of torque measurement error.

4. Determination of the general characteristics of the engine

The data from 8 h 46 min of refuse vehicle's engine operation was taken into account [20]. The information about engine speed n, torque M and fuel consumption G_e was sampled every 20 ms. Due to high number of measuring points per second, a lowpass filter was applied. Torque and engine speed values was computed using MATLAB function cheby1, which is Chebyshev Type 1 filter. Function parameters such as Rp and Wp were set as 10 and 0.11 respectively, both for torque and engine speed. The result of filtration is shown in the Fig. 1.

Searching for static states during daily operation of truck's engine it is crucial to determine the length of time period T, in which the engine's parameters do not change, or at least do not change more than assumed values. As long as the specific value of time is neither defined by the norm [17] nor the literature, five T values were proposed (static state duration):

$$T = \{0.5, 1, 2, 3, 4\}\ [s] \tag{4}$$

Each measuring point i in time s_i were examined locally by defining a time period t with a span equal to the T value:

$$t \in \left(s_i - \frac{T}{2}; s_i + \frac{T}{2}\right) \tag{5}$$

With 50 Hz signal sampling each t period corresponds to N number of measuring points:

$$N = \{26, 50, 100, 150, 200\} \tag{6}$$

For further investigations it is needed to describe following quantities:

$$j \in \left(i - \frac{N}{2}; i + \frac{N}{2}\right) \tag{7}$$

$$M_j = \{M_{i-\frac{N}{2}}, M_{i-\frac{N}{2}+1}, \ldots, M_i, \ldots, M_{i+\frac{N}{2}-1}, M_{i+\frac{N}{2}}\} \tag{8}$$

$$n_j = \{n_{i-\frac{N}{2}}, n_{i-\frac{N}{2}+1}, \ldots, n_i, \ldots, n_{i+\frac{N}{2}-1}, n_{i+\frac{N}{2}},\} \tag{9}$$

where: M_i – value of torque in point i, n_i – value of engine speed in point i, M_j – value of torque in point j, n_j – value of engine speed in point j.

In terms of torque and engine speed values, to determine engine static state two conditions were proposed. First condition derives from norm [17] and specifies that any of M_j and n_j values within t period should not differ more than ±2% of values M_i and n_i:

$$\begin{cases} |M_i - M_j| \le 2\% \cdot M_i \\ |n_i - n_j| \le 2\% \cdot n_i \end{cases} \tag{10}$$

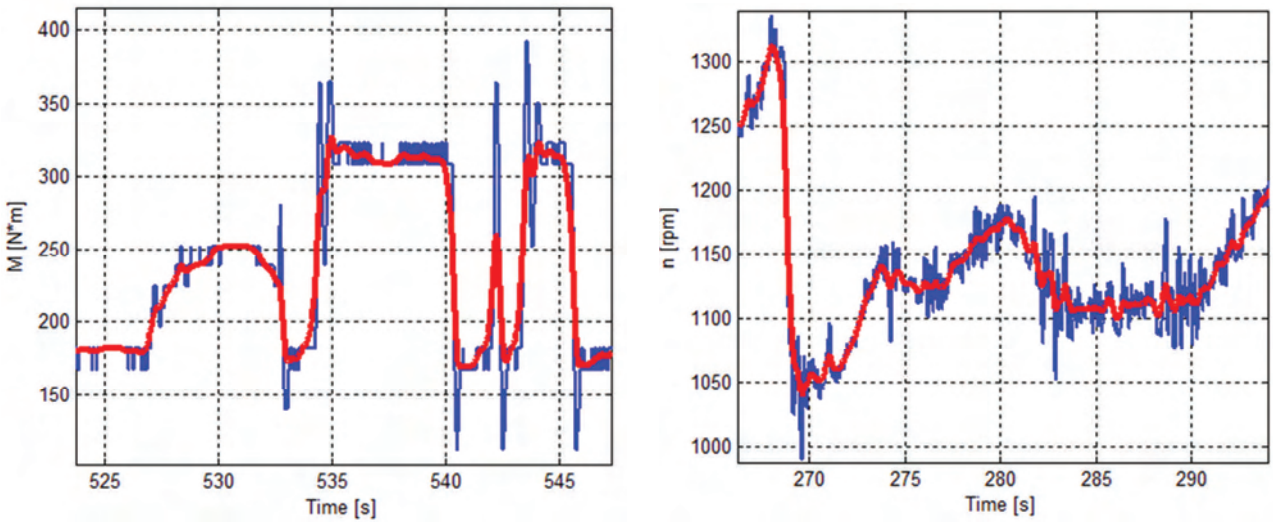


Fig. 1. Measuring points of engine speed (n) and torque (M) before (blue) and after filtration (red)

It is impossible to obtain constant values of parameters in real conditions, but their fluctuation can be examined. Second condition specifies the maximum derivatives of functions in examined point *i* [5]:

$$\begin{cases} \left|\frac{\delta M_i}{\delta t}\right| < M'_{max} \\ \left|\frac{\delta n_i}{\delta t}\right| < n'_{max} \end{cases} \tag{11}$$

Using the least square method, the linear functions were computed as approximations of M_j and n_j points. To fit the curves, the polyfit MATLAB function was used. As a results, two linear functions describing parameter's change in proximity of point i were obtained:

$$\begin{cases} M(t)|_i = a_1^M \cdot t + a_0^M \\ n(t)|_i = a_1^n \cdot t + a_0^n \end{cases} \tag{12}$$

The second condition for operation in steady state can be then expressed by the following relations:

$$\begin{cases} |a_1^M| < M'_{max} \\ |a_1^n| < n'_{max} \end{cases} \tag{13}$$

Four maximum derivative values were examined (derivative limits):

$$\begin{cases} M'_{max} = \{5, 10, 15, 20\} \left[\frac{N \cdot m}{s}\right] \\ n'_{max} = \{5, 10, 15, 20\} \left[\frac{rpm}{s}\right] \end{cases} \tag{14}$$

Graphical interpretation of the two conditions is shown in the Fig. 2.

Both conditions should be fulfilled simultaneously for engine speed and torque. First one examines the distribution of measuring points over the analyzed period T, the second defines tendency of the parameter change. It should be pointed that ±2% criterion is dependent on the value in specified point, which means the higher the value the wider limit's span. Measuring points, which do not fulfil the criteria were removed from data set. In Fig. 3 example of points selection corresponding to the static state has been shown. 5 values of T and 4 values of M'_{max} and n'_{max} were examined, which gives 20 combinations of analyzed criteria. As a result 20 sets of data with M, n and G_e were computed, each corresponding to assumed static state. Additionally, some of measuring points were removed from data sets. Minimum fuel consumption of examined engine while idling was calculated as 3.03 l/h. Thus, points for G_e less than 3 dm^3/h were not considered.

The next step of the analysis was to obtain fuel consumption and specific fuel consumption map. Due to the fact that measuring points distribution over the area of operation of the engine is not uniform, surface approximation was applied. Surface fitting was performed via MATLAB function fit, which creates a surface fit to the data in vectors M, n and G_e. Using the least square method, polynomial surface of degree 5 in M and n direction was assumed.

Computed polynomial coefficients allowed calculation of G_e value in each point in defined engine operation area A, which is a grid with uniformly distributed points in its range:

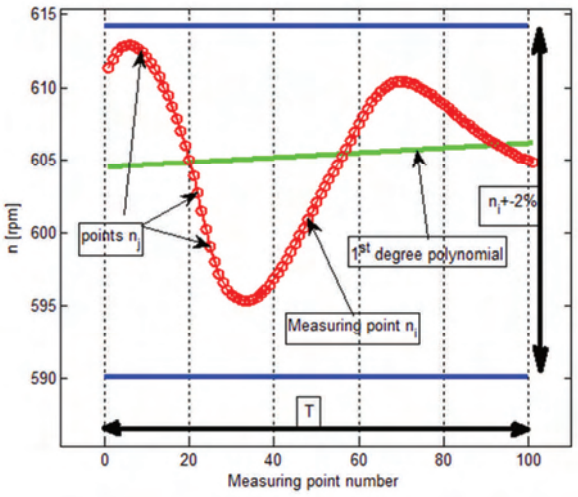


Fig. 2. Interpretation of two static state conditions for engine speed: blue lines – limit of 2% variation, green line – derivative of the approximation function

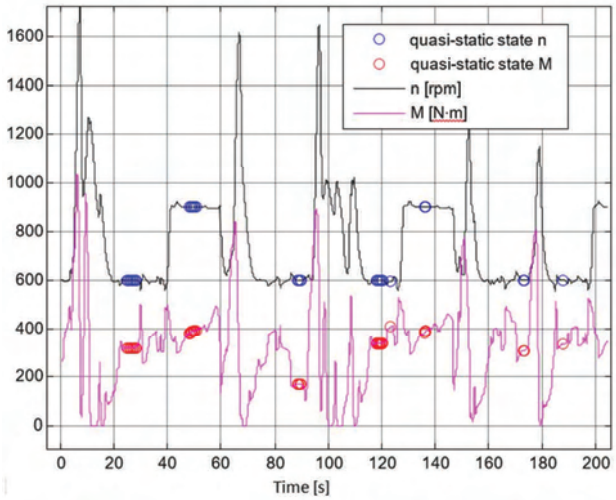


Fig. 3. Example of points selection corresponding to the static state; assumed minimum static state duration (T) 2 seconds

$$\{M, n\} \subset A \tag{15}$$

for:

$$M = \{M_{min},\ M_{min}+1,\ M_{min}+2, \ldots, M_{max}-2, M_{max}-1, M_{max}\}$$

$$n = \{n_{min},\ n_{min}+1,\ n_{min}+2, \ldots, n_{max}-2, n_{max}-1, n_{max}\}$$

where: $n_{min}, M_{min},\ n_{max},\ M_{max}$ – minimum and maximum of speed and torque values in analyzed data set.

Since maximum engine power equals 208 kW, the area above this value was removed from the map. Similarly, engine torque rises gradually from 700 N·m for 650 rpm to its maximum value 1400 N·m for 1000–1350 rpm. Thus, points above mentioned line were removed as well.

Calculated values of G_e over the area A were used to calculate specific fuel consumption g_e:

$$g_e = \frac{G_e}{M \cdot n} \tag{16}$$

As the lowest and highest value of g_e on the map was assumed 170 and 280 g/kWh respectively.

Finally applied algorithm for data selection and determining the general characteristics includes following steps:

- data filtering by lowpass cheby1 filter,
- definition of static state duration length T in point neighborhood,
- condition I: remove point if value in T domain differs more than 2% from value in point i,
- condition II: compute 1st degree polynomial curve in T domain. If its derivative is more than M'(or n') remove the i point,
- remove points where $G_e < 3$ dm^3/h,
- compute coefficients of polynomial fitting surface of 5th degree,
- compute G_e values for each point in uniformly distributed point grid in area A,
- remove points due to maximum power and torque constrains from the grid/map,
- compute g_e,
- remove points where $g_e < 170$ and $g_e > 280$ g/kWh,
- draw G_e and g_e map.

Results of described analysis are shown in Figs 4–10.

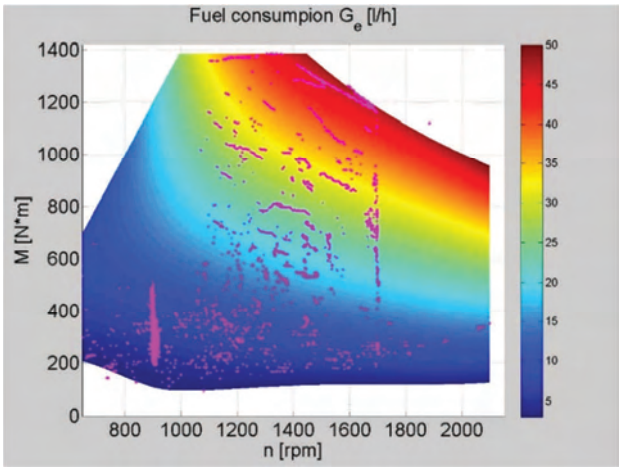


Fig. 4. Characteristics obtained from operational data: static state duration 0.5 s; derivative limits: 20 N·m/s, 20 rpm/s

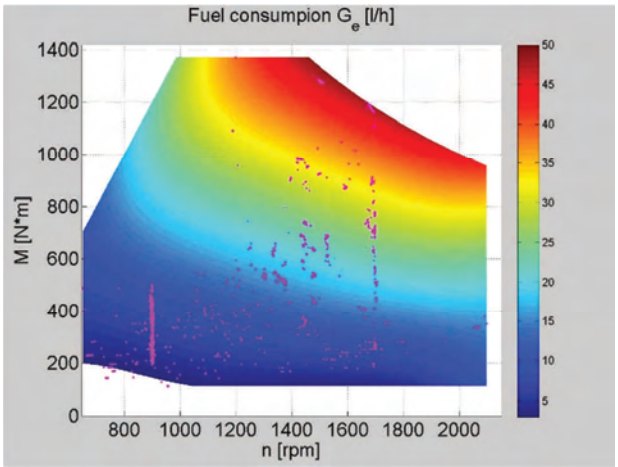


Fig. 5. Characteristics obtained from operational data: static state duration 0.5 s; derivative limits: 5 N·m/s, 5 rpm/s

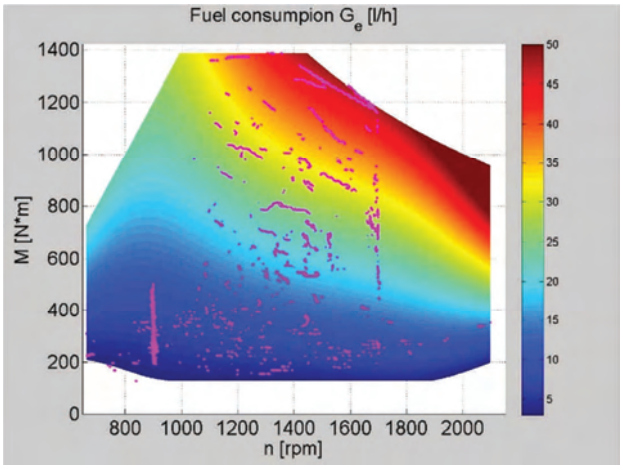


Fig. 6. Characteristics obtained from operational data: static state duration 1 s; derivative limits: 20 N·m/s, 20 rpm/s

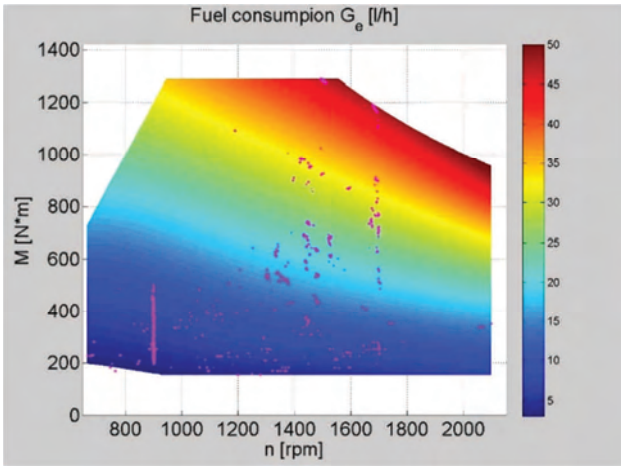


Fig. 7. Characteristics obtained from operational data: static state duration 1 s; derivative limits: 5 N·m/s, 5 rpm/s

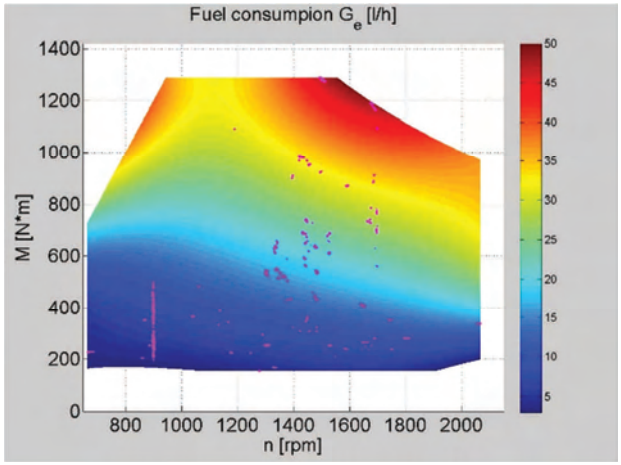


Fig. 8. Characteristics obtained from operational data: static state duration 2 s; derivative limits: 5 N·m/s, 5 rpm/s

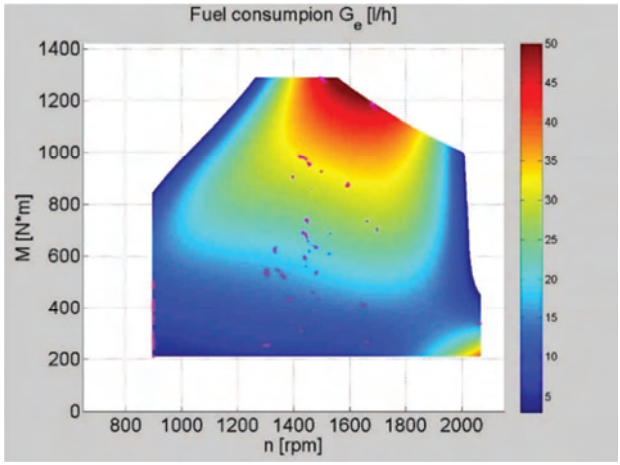


Fig. 9. Characteristics obtained from operational data: static state duration 4 s; derivative limits: 5 N·m/s, 5 rpm/s

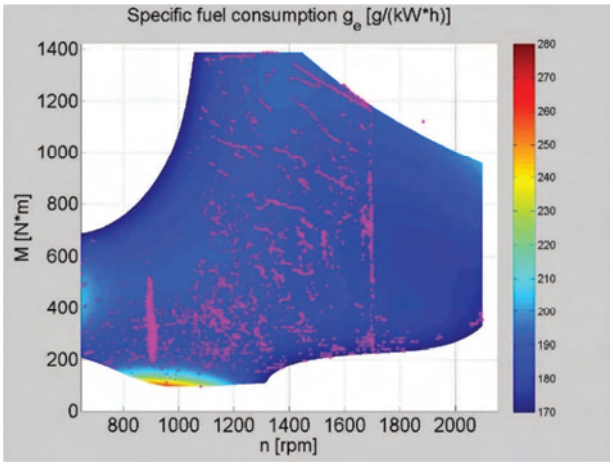


Fig. 10. General characteristics obtained from operational data: static state duration 0.5 s; derivative limits: 20 N·m/s, 20 rpm/s

Summary

The results shown in Figs 4–10 show a good similarity in monotonicity of functions in adequate regions of operation field. The noticeable divergence between extremes results from the accepted static state duration limits (4) and the acceptable value of the signal derivative limits in the interval under consideration (14). Reducing the static state duration limits, as well as increasing the allowed value of the derivative of the signal in the interval in question, results in increasing the number of measurement points. On the other hand, the repeatability of engine operating conditions, theoretically defined by the same coordinates: torque – engine speed, is worse. In some cases artificially generated extrema (outside the tested engine operation area) is observed, which is the result of the high degree approximation function usage. It may be expected that the use of low degree polynomial functions will reduce the quality of the projection of the measurement data, but will eliminate the development of artificial extremes. It can be observed that tightening the selection criteria reduces the available points mainly in the area of low engine speeds and high torque values. At the same time, it can be seen that the number of points that have passed the selection is more sensitive to the allowed value of the signal derivative.

The next stage of the work will be defining the quantitative criteria of the quality of map generation using data from road tests. This analysis can be performed using stationary tests done for the same engine as in road tests. It is expected some guidelines to improve the quality of the mapping, e.g. by increasing the length of the input data set, will be worked out.

Bibliography

[1] BERNHARDT, M., KRUCZYŃSKI, S. Praca silnika w warunkach nieustalonych, część I-VII. *Technika Motoryzacyjna*. 1982, 2-7.

[2] BIELACZYC, P., MERKISZ, J., SZCZOTKA, A. An Investigation of cold start and warm-up phases with a SI engine for meeting new European emissions regulations. *Archiwum Motoryzacji*. 1999, **1-2**, 67-84.

[3] CHŁOPEK, Z., SZCZEPAŃSKI, T. Research concept of the combustion engines properties in dynamic states. *Combustion Engines*. 2013, **154**(3), 168-174.

[4] CHŁOPEK, Z. Modelowanie procesów emisji spalin w warunkach eksploatacji trakcyjnej silników spalinowych. *Oficyna Wydawnicza Politechniki Warszawskiej*, Warszawa 1999.

[5] CHŁOPEK, Z. Some remarks on engine testing in dynamic states. *Combustion Engines*. 2010, **143**(4), 60-71.

[6] CICHY, M., KROPIWNICKI, J., MAKOWSKI, S. Model silnika spalinowego w formie grafów wiązań (GW). *Silniki Spalinowe*. 2004, **2**, 40-47.

[7] CICHY, M., KROPIWNICKI, J. Wykorzystanie metody rozbiegu do określania dynamicznego momentu obrotowego silnika. *Materiały konferencji I Forum Młodych*, ATR Bydgoszcz. 1998, 7-13.

[8] CZYŻEWICZ, J., KROPIWNICKI, J., WYSOCKI, O. Model of the hydraulic pump powertrain of refuse collection vehicle compaction mechanism. *Combustion Engines*. 2015, 626-630.

[9] DUARTE, G.O. et al. Establishing bonds between vehicle certification data and real-world vehicle fuel consumption – a vehicle specific power approach. *Energy Conversion and Management*. 2015, **92**, 251-265.

[10] FREY, H.C. et al. Comparing real-world fuel consumption for diesel- and hydrogen-fueled transit buses and implication for emissions. *Transportation Research Part D*. 2007, **12**, 281-291.

[11] GAO, Z. et al. Drive cycle simulation of high efficiency combustions on fuel economy and exhaust properties in light-duty vehicles. *Applied Energy*. 2015, **157**, 762-776.

[12] KROPIWNICKI, J., KNEBA, Z., ZIÓŁKOWSKI, M. Test for assessing the energy efficiency of vehicles with internal combustion engines. *International Journal of Automotive Technology*. 2013, **14**(3), 479-487.

[13] LONGWIC, R. Charakterystyka działania silnika o zapłonie samoczynnym w warunkach swobodnego rozpędzania. *Wydawnictwo Politechniki Lubelskiej*. Lublin 2011.

[14] MERKISZ, J., ANDRZEJEWSKI, M., PIELECHA, J. The effect of applying the eco-driving rules on the exhaust emissions. *Combustion Engines*. 2013, **155**(4), 66-74.

[15] OH, Y. et al. Modelling effect of vehicle specification on fuel economy based on engine fuel consumption map and vehicle dynamics. *Transportation Research Part D*. 2014, **32**, 287-302.

[16] PIĘTAK, A. Diagnozowanie silników o ZS na podstawie przebiegu procesu przejściowego. *Wydawnictwo Politechniki Poznańskiej* 1998.

[17] PN-ISO 15550-2009.

[18] PN-ISO 3046-3.

[19] SZCZEPAŃSKI, T. Metoda oceny użytkowych właściwości silnika spalinowego w stanach dynamicznych. *Rozprawa doktorska*. Politechnika Warszawska 2015.

[20] WYSOCKI, O. Rekonstrukcja charakterystyki jednostkowego zużycia paliwa na podstawie obserwacji wybranych parametrów pracy silnika spalinowego z zapłonem samoczynnym. *Praca dyplomowa magisterska*. Politechnika Gdańska 2016.

Oskar Wysocki, MEng. – Faculty of Mechanical Engineering at Gdańsk University of Technology.

e-mail: *OskWys@gmail.com*



Jacek Czyżewicz, PhD. – Faculty of Mechanical Engineering at Gdańsk University of Technology.

e-mail: *JacCzyze@pg.gda.pl*



Jacek Kropiwnicki, DSc., PhD. – Faculty of Mechanical Engineering at Gdańsk University of Technology.

e-mail: *JKropiwn@pg.gda.pl*



Article citation info:
RYBAK, A., HUNICZ, J., KRZACZEK, P. et al. Effect of different biofuels on common rail injector flow rate. *Combustion Engines*. 2017, **171**(4), 39-43. DOI: 10.19206/CE-2017-407

Arkadiusz RYBAK
Jacek HUNICZ
Paweł KRZACZEK
Wojciech GOLIMOWSKI
Damian MARCINKOWSKI

CE-2017-407

Effect of different biofuels on common rail injector flow rate

In this study dynamic flow rates of a common rail injector using diesel fuel and different biofuels were determined. As biofuels, fatty acid methyl esters originating from canola, poultry, cattle and used cooking oil were tested. The tested fuels exhibited different physical properties e.g. density and viscosity. Measurements of the injector delivery rates were performed on a test stand designed for determination of injectors and injection pumps characteristics. Each fuel was tested at temperatures between 30 and 60°C, under injection pressure in the range of 30–180 MPa and injection time in the range of 200–1600 microseconds. The results showed differences in injector flow rates depending on used fuel, however different fuel properties affected amount of fuel injected especially at short injection durations.

Key words: *oils & lubrication, engines, injector, diesel, biodiesel*

1. Introduction

Nowadays, there is a strong emphasis on reducing the negative impact of internal combustion engines on the environment and increasing the energy efficiency contained in the fuel. In diesel engines, the combustion efficiency and emission of toxic exhaust gas components are significantly influenced by the fuel injection process into the combustion chamber. The main parameters determining the fuel spray quality are the injection pressure and the amount, shape and size of the injector holes. Conducted research on the possibilities to increase injection pressure to 250 and even 300 MPa [1, 5, 20] and research towards reducing injector holes, primarily in the context of reducing NO_x and particulate emissions [26, 27]. However, increasing the pressure in the fuel system and reducing the size of the injector holes determines the rise of fuel flow velocity, which affects the appearance of turbulent flow and the occurrence of cavitation. This results in increased wear of the fuel system components during operation [5, 16]. Besides, the appearance of cavitation results in improvement of turbulence at the output of the injector, but may reduce the fuel flow [8, 18]. For this reason, the total amount of fuel injected into the combustion chamber and the level of fuel flow are the main factors characterizing the fuel injection process. Mainly dependent on fuel injection pressure, and the injector opening time. Determining the actual fuel flow rate allows to characterize the injector operation and comparison, especially in cases where the fuel is modified [11, 13].

Many factors affect the use of fuels other than diesel fuel in Diesel engine. For many years, the main reason given by the authors of scientific works are limited resources of fossil fuels. As an alternative to diesel, it is possible to use vegetable oils and their derivatives [22, 24]. On the one hand, pure vegetable oils are characterized by availability, low content of aromatic hydrocarbons and sulfur, and on the other hand have high viscosity and higher density, especially at low temperatures. As derivatives of oils, methyl esters of higher fatty acids, which are obtained by the transesterification of vegetable oils, are used [9]. The use of esters is currently the best way to use natural resources as a fuel to replace diesel. However, the production this type of fuel results in the use of edible oils for energy purposes and limiting their availability to comestible purpose. Therefore research is being undertaken in which the sources of biofuels are raw materials [21], plant [6] and animal [7]. This allows for diversification of raw materials for energy purposes, but also differentiates the chemical composition derived biofuels, which complicates their possible use in diesel engines [23].

Application of biofuels, especially second generation biofuels, necessitates the modification of the fuel systems due to different chemical composition and changed physicochemical properties [2, 3, 10]. Composition and properties are determined by the origin of raw materials or waste materials from which biofuels are produced [14]. A method of biofuel production, i.e. the type of catalyst used, or the presence of various contaminants from processing raw materials is also important [12]. Adaptation of diesel engines to chemical composition, density, viscosity, fractional composition, surface tension of diesel, makes the use of biofuel as an additive (e.g. B10, B20, B50) or as single fuel (B100) significantly changes fuel flow parameters, and consequently the process of combustion [19]. In many works, the authors point to the positive effect of the use biofuels on CO, HC, PM and CO_2 emissions value, however, the high oxygen content in biofuels can lead to increased NO_x emissions [25]. In addition, the use of biofuels, due to lower calorific value, results in lower engine performance and increased fuel consumption [4, 17]. However, today's common-rail systems can improve engine performance, reduce fuel consumption, and emissions of toxic compounds. It is important to properly select parameters such as injection pressure, injector opening time, so knowing the injection characteristics and fuel flow allows you to optimize these [17]. The purpose of the study was to investigate the fuel flow characteristics of injectors for biofuels produced from vegetable oils and waste fats (vegetable and animal origin).

2. Experimental conditions

The examinations were carried out using a six fuels. Table 1 shows the main parameters and table 2 shows main property of the tested fuels. All fuels were tested in temperature 30, 40, 50 and 60°C, under injection pressures, from range 30 to 180 MPa. The injection time for each tested pressure was changed between 200 and 1600 microseconds.

Table 1. Main parameters of the tested fuels

Common name of faty acide methyl ester	Carbon no.: double bond no.	BIO 1	BIO2	BIO3	BIO4	BIO5
Myristic	C14:0	–	–	–	2.65	0.23
Palmitic	C16:0	0.55	0.45	20.8	26.12	8.56
Palmitoleic	C16:1	4.6	4.57	–	3.21	0.42
Stearic	C18:0	1.63	1.65	6.3	21.33	2.11
Oleic	C18:1	61.96	61.82	44.6	37.4	61.72
Linoleic	C18:2	18.11	18.19	15.7	4.52	18.18
Linolenic	C18:3	9.6	9.75	0.85	0.58	6
Arachidic	C20:0	0.57	0.58	–		
Eicosenoic	C20:1	1.43	1.47	–		
Others		1.55	1.52	11.75	4.19	2.78

Table 2. Main property of the tested fuels

Fuel property	BIO 1	BIO2	BIO3	BIO4	BIO5	Diesel
Density @ 15°C (kg/m^3)	882.0	879.0	872.9	878.0	884.9	843.2
Density @ 30°C (kg/m^3)	871.9	868.9	862.8	867.9	875.0	832.3
Density @ 40°C (kg/m^3)	865.2	862.2	856.0	861.2	868.4	825.1
Density @ 50°C (kg/m^3)	858.4	855.4	849.3	854.5	861.8	817.8
Density @ 60°C (kg/m^3)	851.7	848.7	842.6	847.7	855.2	810.6
Viscosity @ 40°C (mm^2/s)	4.43	4.36	5.45	4.48	4.79	2.95

Were studied: Diesel available in retail and five biodiesel fuels, fatty acid methyl esters of rapeseed oil, marked as Bio1, of rapeseed oil with antioxidant, marked as Bio2, of beef fat, marked as Bio3, of poultry fat, marked as Bio4 and, of used cooking fat, marked as Bio5.The composition of the tested fuels were determined in accordance with PN-EN 14103 (Table 1). The density of fuels were determined by the hydrometer in accordance with PN-EN ISO 3675. Kinematic viscosity of studied fuels were determined by capillary according to PN-EN ISO 3104.

3. Experimental test stand

The test stand designed for determination of injectors and injection pumps characteristics occurring in the Common Rail system was used to carried out the research. Schema of the test stand shown in Fig. 1. consists of the CR fuel pump (1), which is driven by a toothed belt, by an asynchronous three-phase motor (2) inverter-controlled (19), connected with function control module (5) and drive control module (4). Buttons set (3) is used to turn on the power. Electric fuel pump (16) gives fuel from the tank (14) through the filter (15) to the CR pump. Fuel under high pressure goes, through the distributor (6), to the high-pressure rail (7) whence it gets to the injectors (20). The test stand is equipped with fuel dose burette (8), overflow burette (9) and pump efficiency burette (10). Pump tester (12) and injectors tester (13) allow automatic or manual work. Control wires are connected to the terminal block (11). Fuel conditioning is carried out in a system consisting of a heater (21), an electric pump (22) and a radiator (23). The test stand is made in the form of a metal frame on which all necessary supports and devices are attached [15].

Measurements were performed on a Common Rail system electromagnetic injector Bosch with number 044510135.

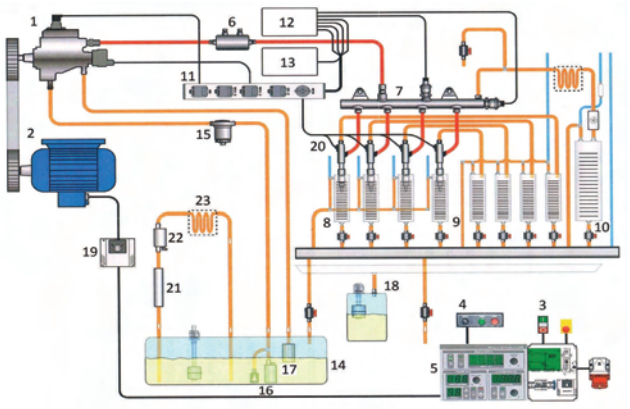


Fig. 1. Schema of test stand used in the experiment [15]

4. Experimental results and Identification of active flow cross section

The biofuels used in the research were of different origins, both vegetable and animal. All biofuels were obtained by transesterification using a homogeneous KOH catalyst. Bio1 and Bio2 fuels were made from rapeseed oil derived directly from the pressing process of raw materials from different sources and in two separate production facilities. The chemical composition is very similar, and the kinematic viscosity value is similar for both fuels (Table 1 and 2). The slight difference in fuel density results from the differences in chemical composition and the antioxidant added.

Other biofuels were made from waste materials. Fuel Bio5 has a similar composition to Bio1 and Bio2 as it is made from rapeseed oil. The differences in composition result from the thermal processes that the oil has undergone and from the biological substances with which the oil was in contact during the treatment. Fuel Bio5 is also characterized by slightly higher viscosity and density, which may have an effect on the fuel injection process.

Fuels Bio3 and Bio4, as opposed to the others, were made from animal waste fats. However, despite differences in origin, Bio4 fuel has a similar viscosity and density to Bio1 and Bio2 fuels. Instead, Bio3 has a lower density and a significantly higher kinematic viscosity at 40°C. These fuels have a different chemical composition and contain over 20% of C16 or lower esters. In addition, a high solidification temperature (14°C) of the Bio3 fuel was found, which may be significant for its potential use, especially under operating conditions.

Values of individual injections given in mm^3 for each inflicted parameters were received as a result of the measurements. Effective injection time, need to determine the volume flow rate as a ratio of the fuel volume injected on the test stand and mentioned effective time, has been calculated based on the values of individual injections as a difference between the time of injector coil supply and time designated by extrapolation of trend line of individual injection on the x axis. Identified active flow cross section is directly proportional to the volume flow rate of injected fuel and inversely proportional to the square root of the ratio between the value of twice the product of the differential pressure upstream and downstream of the injector and the value of density of the tested fuels. Determined values

of the active flow cross section were presented in Fig. 2, 3, 4, 5.

At 30°C (Fig. 2), the calculated active flow cross section increases to 80 MPa, in proportion to the pressure increase for all tested fuels. Afterwards, in the case of diesel, the coefficient is clearly reduced and reached the minimum at pressures of 100 to 140 MPa, at higher pressures it rises again to about 3 mm^2. For Bio1, Bio2, Bio4 and Bio5 biofuels, which have a similar density and viscosity, the active flow cross section receive a similar value and its course in pressure range from 80 to 180 MPa has a linear function. While the Bio3 active flow cross section obtained maximum (3.1 mm^2) at a pressure of 100MPa. With a pressure increase up to 180 MPa, the calculated active flow cross section is maintained at a range of 2.75 to 3.1 mm^2.The test at this temperature respond to the start-up and warm-up phase of the engine, therefore, in diesel engines, the dose and injection time should be corrected at pressures above 80 MPa.

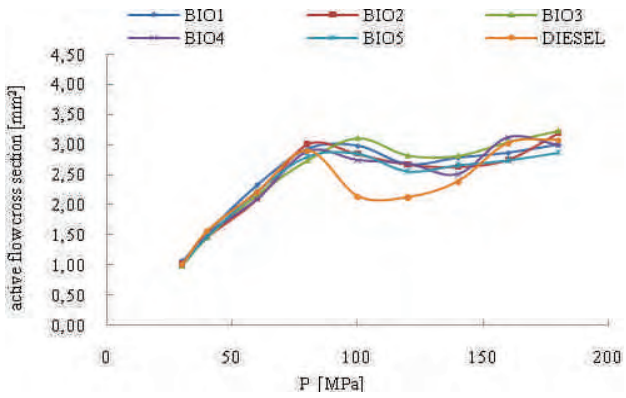


Fig. 2. Comparison of the active flow cross sections of tested fuels at 30°C

Increasing the fuel temperature to 40°C (Fig. 3) changes the course of the active flow cross section. Differences start already above 60 MPa. At a pressure of 80 MPa for all tested fuels, apart from Bio3, the active flow cross section achieves the maximum value. The value of the diesel coefficient is almost identical to that of 30°C. In the case of biofuels, higher active flow cross section values have biofuels produced from rapeseed oil, both raw and processed. However, the highest active flow cross section values for pressures above 60 MPa were found for Bio2 fuel. For other biofuels, the coefficient ranged between 2.4 and 2.7 mm^2. Temperature of 40°C occurs when the engine is running under normal conditions and at low loads, Therefore, adaptation of the control system of the fuel system should particularly concern a range above 60 MPa to 140 MPa.

An increase of the fuel temperature by another 10°C (Fig. 4) gives a clear change in the active flow cross section characteristics. In the range of 40 to 60 MPa the active flow cross section for diesel is slightly higher, it stabilizes in the range of 80 to 140 MPa and then increases significantly. For all biofuels, the flow rate increases proportionately to the pressure of 80 MPa and besides the fuel Bio3 reaches its maximum at this pressure. For Bio1 and Bio2 biofuels (1st generation biofuels), the coefficient value is clearly higher at 80 MPa. For Bio3 fuel the coefficient reached its highest value at 100 MPa. Then, in the pressure range of 100 to 160 MPa, the individual biofuels coefficients reach a similar value and above 120 MPa equate to the diesel factor. The differences reappear for the highest fuel pressure values, and the greatest increase can be seen for Bio2 and diesel fuel.

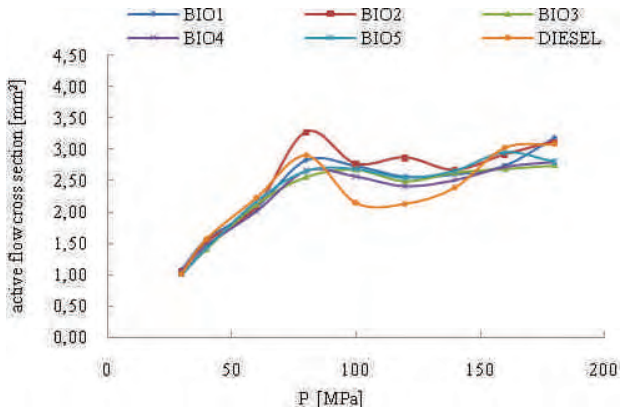


Fig. 3. Comparison of the active flow cross sections of tested fuels at 40°C

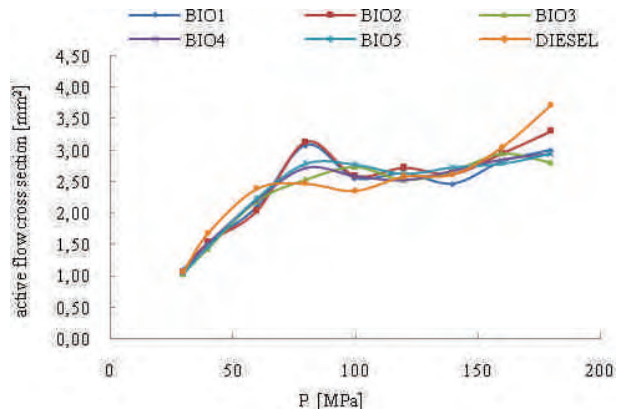


Fig. 4. Comparison of the active flow cross sections of tested fuels at 50°C

At a temperature of 50°C, which corresponds to the average engine load, correction of injection parameters should concern fuel doses for pressures from 40 MPa to 120 MPa and above 160 MPa due to the fuel used.

Raising the fuel temperature to 60°C (Fig. 5), which corresponds to the maximum thermal load of the engine, deepens the trends observed in the calculated fuel flow characteristics at 50°C. Again for biofuels proportional increase of the coefficient up to a pressure of 80 MPa, then slightly decreases at 100 MPa, then 120 MPa starts to grow slowly. For Bio3 biofuel, which has a higher viscosity and lower density, the maximum and minimum local active flow cross sections are offset by 20 MPa towards higher pressures. For diesel, the active flow cross section is clearly increasing at 60 MPa, the minimum is at 100 MPa, the same as biofuels. A continued increase of pressure results in a proportional increase in the active flow cross section, which, at pressures 160 and 180 MPa, is higher than for biofuels. In the case of fuels heated up to 60°C, the correction in the injection control system includes similar pressure ranges as for a temperature of 50°C.

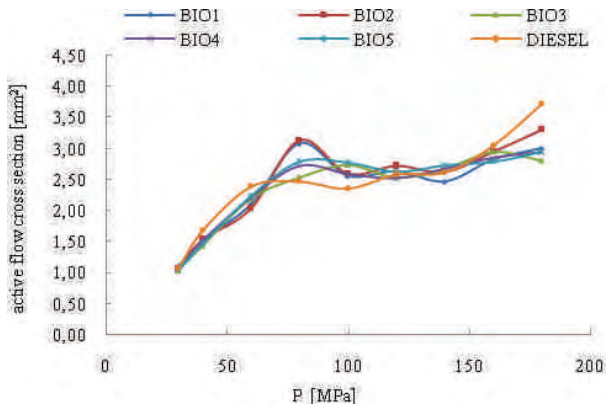


Fig. 5. Comparison of the active flow cross sections of tested fuels at 60°C

So far, the fuel flow through the injector has been analyzed at the same temperatures. Many authors point to differences in viscosity and density of diesel and biofuels [6, 9, 10, 24] indicating that heating of the fuel by 20 or 30°C relative to the diesel temperature results in a level of viscosity and density. A similar analysis was done at work Rybak et al. [19]. It has been shown that the active flow cross section for diesel at 40°C and for FAME at 60°C reach similar values over the range of utility pressures (30 to 180 MPa). Therefore, in Figure 6 comparison of the active flow cross sections of tested biofuels at 60°C and Diesel at 40°C was presented.

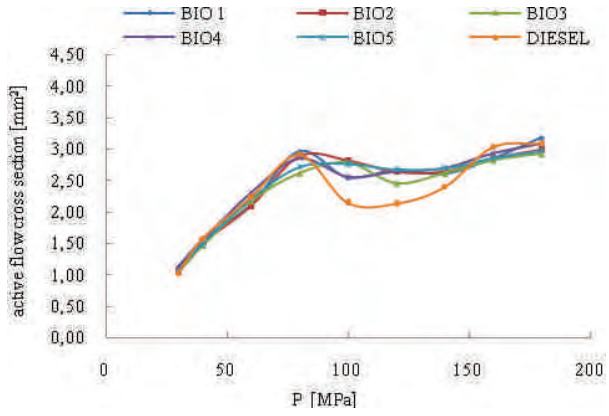


Fig. 6. Comparison of the active flow cross sections of tested biofuels at 60°C and Diesel at 40°C

As a result of this comparison, it can be noted that for both diesel and all biofuels, the active flow cross section increases proportionally between 30 and 80 MPa and beyond the Bio3 fuel, the maximum value is obtained. It can be expected that the fuel dosage in this range will be similar, the difference in engine control will be primarily due to the different chemical composition of each fuel and the thermal conditions of the engine. With a continued increase in pressure (100 to 140 MPa), there is a difference between the diesel and biofuel. The difference in fuel dose should be corrected in this interval by any change in the characteristics of the control system and the extension of the diesel injection time or the heating of the fuel by at least 10°C. The value of the active flow cross section is again equalized for all fuels tested at pressures above 140 MPa. The use of such high pressures corresponds to the operation of the engine with maximum loads and under high thermal stress conditions, which in practice is unlikely to keep the diesel temperature at 40°C. Constant fuel compression and heat transfer by the engine components will cause to heat up the diesel and change the active flow cross section, as can be seen in Figures 4 and 5.

5. Conclusions

Comparing the active flow cross section for individual fuels, there was a clear difference in the course of its characteristics as a function of the injection pressure. The coefficient values are also determined by the fuel temperature in common rail system.

At low temperatures (30 and 40°C) a proportional increase of coefficient independently to fuel for pressure up to 60–80 MPa can be observed. Then the coefficient for diesel is clearly decreasing(100–120 MPa), at higher pressures again equates to the active flow cross section values for biofuels.

Heating up fuel to 50 or 60°C significantly changes the flow rate characteristic, especially for diesel. The differences are already occurring at low pressures, where the biofuel factor is lower. Then the coefficient values are equal in the pressure range from 80 to 140 MPa. Above this range again the active flow cross section for diesel rapidly increases.

Conducted comparative analysis of the active flow cross section for different temperatures (Fig. 6) showed that its values for biofuels and diesel are close to in the range up to 80 MPa and above 140 MPa. At average pressures, there are still differences between fuels.

In research, fuels of different origins and chemical compositions were used. It can be stated that the active flow cross section for fuel produced from crude rapeseed oil (Bio1 and Bio2) is higher than for fuels from waste materials (Bio3, Bio4 and Bio5). It can be seen that the coefficient for animal derived fuels is lower in comparison with vegetable derived fuels. Significant differences were found for the Bio3 fuel, which had the lowest density among biofuels and the highest viscosity. The maximum flow rate for this fuel was shifted by about 20 MPa towards higher injection pressures, regardless of temperature. In conclusion, it can be stated that the chemical composition of fuels influences the value of the fuel active flow cross section because it determines the physical properties of the fuel (e.g. density, viscosity) and therefore changes the course of the flow rate characteristic as a function of the injection pressure.

Bibliography

[1] AGARWAL, A.K, DHAR, A., SRIVASTAVA, D.K., et al. Effect of fuel injection pressure on diesel particulate size and number distribution in a CRDI single cylinder research engine. *Fuel*. 2013, **107**, 84-89.

[2] BHUIYA, M.M.K., RASUL, M.G., KHAN, M.M.K. et al. Prospects of 2nd generation biodiesel as a sustainable fuel – Part 2: Properties, performance and emission characteristics. *Renewable and Sustainable Energy Reviews*. 2016, **55**, 1129-1146.

[3] BOHL, T., TIAN, G., SMALLBONE, A., ROSKILLY, A.P. Macroscopic spray characteristics of next-generation bio-derived diesel fuels in comparison to mineral diesel. *Applied Energy*. 2017, **186**, 562-573.
[4] CHOU CH, C., LIN, Y.-W., CHIANG, CH.-J., KU, Y.-Y. Experimental analysis of a turbo-charged common-rail diesel engine fueled with biodiesel. *Energy Procedia*. 2014, **61**, 1167-1170.
[5] DUAN, L., YUAN, S., HU, L. et al. Injection performance and cavitation analysis of an advanced 250 MPa common rail diesel injector. *International Journal of Heat and Mass Transfer*. 2015, **93**, 388-397.
[6] FADHIL, A.B. Evaluation of apricot (*Prunus armeniaca* L.) seed kernel as a potential feedstock for the production of liquid bio-fuels and activated carbons. *Energy Conversion and Management*. 2017, **133**, 307-317.
[7] FADHIL, A.B., AHMED, A.I., SALIH, H.A. Production of liquid fuels and activated carbons from fish waste. *Fuel.* 2017, **187**, 435-445.
[8] GAVAISES, M., PAPOULIAS, D., ANDRIOTIS, A., GIANNADAKIS, E. Link between cavitation development and erosion damage in diesel injector nozzles. *SAE Technical Paper*. 2007, 2007-01-0246.
[9] GOLIMOWSKI, W., BERGER, W.A., PASYNIUK, P. et al. Biofuel parameter dependence on waste fats' fatty acids profile. *Fuel*. 2017, **197**, 482-487.
[10] GÜLÜM, M., BILGIN, A. Measurements and empirical correlations in predicting biodiesel-diesel blends' viscosity and density. *Fuel*. 2017, **199**, 567-577.
[11] HWANG, J., QI, D., JUNG, Y., BAE, CH. Effect of injection parameters on the combustion and emission characteristics in a common-rail direct injection diesel engine fueled with waste cooking oil biodiesel. *Renewable Energy*. 2014, **63**, 9-17.
[12] KALARGARIS, I., TIAN, G., GU, S. Influence of advanced injection timing and fuel additive on combustion, performance, and emission characteristics of a DI diesel engine running on plastic pyrolysis oil. *Journal of Combustion.* **2017**, 3126342, 9.
[13] KUTI, O. A., ZHU, J., NISHIDA, K. et al. Characterization of spray and combustion processes of biodiesel fuel injected by diesel engine common rail system. *Fuel*. 2013, **104**, 838-846.
[14] MO, J., TANG, C., LI, J. et al. Experimental investigation on the effect of n-butanol blending on spray characteristics of soybean biodiesel in a common-rail fuel injection system. *Fuel*. 2016, **182**, 391-401.
[15] Opis techniczny stanowiska testowania pomp i wtryskiwaczy STPiW3. Centrum Szkolenia Motoryzacji "Autoelektronika Kędzia". Nr kat.: 1120. 2015.
[16] OSIPOWICZ, T., STOECK, T., GOŁĘBIEWSKI, W. Influence of fuel pollutants on operating parameters of contemporary fuel injector. *Journal of KONES Powertrain and Transport*. 2015, **22**(3), 169-174.
[17] PAYRI, R., SALVADOR, F. J., MARTÍ-ALDARAVÍ, P., MARTÍNEZ-LÓPEZ, J. Using one-dimensional modeling to analyse the influence of the use of biodiesels on the dynamic behavior of solenoid-operated injectors in common rail systems: Detailed injection system model. *Energy Conversion and Management*. 2012, **54**, 90-99.
[18] QIU, T., SONG, X., LEI, Y. et al. Effect of back pressure on nozzle inner flow in fuel injector. *Fuel*. 2016, **173**, 79-89.
[19] RYBAK, A., GĘCA, M., KRZACZEK, P., MAZANEK, A. Determination of common rail injector flow characteristics with the use of diesel and biodiesel fuels. *Journal of KONES*. 2016, **23**(4), 443-450.
[20] SALVADOR, F.J., DE LA MORENA J., MARTÍNEZ-LÓPEZ, J., JARAMILLO, D. Assessment of compressibility effects on internal nozzle flow in diesel injectors at very high injection pressures. *Energy Conversion and Management*. 2017, **132**, 221-230.
[21] SINGH, P.V., CHAUHAN, S.R. Carbonyl and aromatic hydrocarbon emissions from diesel engine exhaust using different feedstock: a review. *Renewable and Sustainable Energy Reviews*. 2016, **63**, 269-291.
[22] SLAVINSKAS, S., MICKEVICIUS, T. Experimental study on injection characteristics of diesel-bioethanol fuel blends. *Combustion Engines*. 2015, **161**(2), 28-32.
[23] SOMA, S., LONGMAN, D.E., RAMÍREZ A.I., AGGARWAL, S.K., A comparison of injector flow and spray characteristics of biodiesel with petrodiesel. *Fuel*. 2010, **89**, 4014-4024.
[24] TAKASE, M., ZHAO, T., ZHANG, M. et al. An expatiate review of neem, jatropha, rubber and karanja as multipurpose non-edible biodiesel resources and comparison of their fuel, engine and emission properties. *Renewable and Sustainable Energy Reviews*. 2015, **43**, 495-520.
[25] WASILEWSKI, J., KRZACZEK, P. Emission of toxic compounds from combustion of biodiesel: a report from studies. *Przemysł Chemiczny*. 2014, **93(3)**, 343-346.
[26] XANG, X., HUANG, Z., ZHANG, W.B, et al. Effects of ultra-high injection pressure and micro-hole nozzle on flame structure and soot formation of impinging diesel spray. *Applied Energy*. 2011, **88**, 1620-1628.
[27] YALIWAL, V.S., BANAPURMATH, N.R., GIREESH, N.M. et al. Effect of nozzle and combustion chamber geometry on the performance of a diesel engine operated on dual fuel mode using renewable fuels. *Renewable Energy*. 2016, **93**, 483-501.

Arkadiusz Rybak, MEng. – Faculty of Mechanical Engineering at Lublin University of Technology.

e-mail: *A.Rybak@pollub.pl*



Damian Marcinkowski, DEng. – Institute of Technology and Life Sciences in Poznań.

e-mail: *D.Marcinkowski@itp.edu.pl*



Paweł Krzaczek, DEng. – Faculty of Production Engineering at University of Life Sciences.

e-mail: *Pawel.Krzaczek@up.lublin.pl*



Article citation info:
ZADRĄG, R., KNIAZIEWICZ, T. Utilization of the zero unitarization method for the building of a ranking for diagnostic marine engine parameters. *Combustion Engines*. 2017, **171**(4), 44-50. DOI: 10.19206/CE-2017-408

Ryszard ZADRĄG
Tomasz KNIAZIEWICZ

CE-2017-408

Utilization of the zero unitarization method for the building of a ranking for diagnostic marine engine parameters

Changing some of the parameters of the engine structure affects the emission of harmful components in the exhaust gases This primarily concerns damage in the cargo exchange system as well as in the fuel system and engine boost system. Changes in emissions of harmful compounds are often ambiguous, depending largely on the parameters that shape the combustion process. An additional problem is that often simple but undesired interactions occur with the interaction of these parameters. It is therefore possible to speak of different diagnostic parameters' sensitivity to the same extractions from the engine structure, but implemented in other load states. In cases where the set of parameters is numerous and the values of these parameters are similar, there is a real problem with their proper classification, often based on the discretion of the researcher. In the paper the authors propose a methodology for classification of acquired diagnostic parameters. In previous papers [4, 5], Hellwig's method of information capacity index was proposed as a measure of diagnostic parameter sensitivity. This method can be used to build a diagnostic parameter ranking that divides the set of diagnostic variables into stimulators, destimulators and nominators. This normalization of the set seems to be helpful in making a diagnostic decision not influenced by the discretion of the researcher. The zero unitary method can also be helpful in creating diagnostic tests.

Key words: *diagnostic, theory of experiments, marine diesel engine, exhaust gas toxicity, multi-equation models*

1. Introduction

Transient states are particular states of the combustion engine operation. It should be explained by stating that the transient states disrupt the thermodynamic equilibrium of the cylinder which is present during the stationary loads. It disrupts the flow of the combustion process through momentary changes of the stream of fresh load delivered to the cylinder, as well as the amount of delivered fuel. As such, the ratio of fuel-air is temporarily changed, resulting in the shift of the combustion air factor, which leads to the increased emission of combustion products created through the local deficiency of oxygen. Further consequence of the increased amount of carbon oxide CO and unburned hydrocarbons HC is the decrease in the combustion temperature, which dictates the lowered emission of nitric oxide NO_x.

As such, the deciding factor for the value of toxic compound emissions originating from the transient states is, above all else, the value of excitations which trigger these states. It is not, however, the only factor. Another factor shaping the value of toxic compound emissions originating from the transient states which should be taken into consideration is the technical state of the engine. This state, described using the structure parameters, undergoes constant changes throughout the operation of the engine, which changes are responsible for the wear process. This intensifies the changes in the development of the toxic compounds during the transient states because the processes, while momentary, are dynamic enough to result in the CI concentrations by far exceed the values of the stationary states. Thus it should be expected that the engine with its structural parameters changed through wear will be more sensitive to the influence of transient states and determining its technical state will be easier. At the same time, a problem of unique identification arises, not for the diagnostic parameters, but for their sensitivity. It is especially vital in the cases with large quantities of the tested material as well as with large variations in the operation of the transient states. The aforementioned sensitivity of the diagnostic parameter can be defined as an information capacity and used further to specify the parameters that best describe the given phenomenon [1, 2].

One of the basic parameters deciding the correctness of the course of combustion inside of the CI engines is the angle of fuel injection. Even a small deviation of this angle results in substantial changes in the main indices of the engine operation, including the indices of exhaust emission. In the case of classic engine design, the "spontaneous" change in the angle of advance of fuel injection is unlikely. On the other hand, in the modern engine design, where the majority of the regulatory parameters is electronically controlled, it is possible for a situation to occur where it results in damage being done to the control system and the change of the angle of advance of fuel injection.

This paper is a continuation of the problem published by the authors in [4, 5]. Currently, the authors concentrate on defining and researching of the information capacity of the diagnostic parameter, which, as mentioned before, are the indices and characteristics of the exhaust gas compound emissions.

2. Research on capacity indicators of toxic compounds concentrations during dynamic processes

The tests were conducted on an engine fuel supply system (angle of advance of fuel injection) of a single cylinder test engine 1-SB, installed inside of the Laboratory of Marine Plant Exploitation of Polish Maritime Academy [3]. The experimental material was gathered using a developed trivalent complete plan. The realization of separate measurement systems (measurement points) of the aforementioned plan of experiment was achieved by using a programmable controller which allowed for getting a high repeatability of the dynamic processes. The duration of the dynamic process was assumed as the period between the introduction of the new injection system setting and the recurring stabilization of the output quantities. This time was chosen through experimentation and it amounts to about 106 s.

In order to identify the impact of the technical state of the fuel system on the power parameters of the engine during the dynamic processes, determined were ranges of input quantities (preset parameters) and output quantities (observed parameters).

To the needs of this paper, the size of the input quantities X was limited to three elements, i.e.: x_1 – engine speed n [r/min]; x_2 – engine torque T_{tq} [N·m]; x_3 – angle of advance of fuel injection α_{ww} [ºCA]. The research was conducted according to the adopted complete plan for the three engine speed values, i.e.: 850, 950, 1100 r/min. For each of the engine speed values the torque T_{tq} was increased, resulting in transient states for the following loads: 10, 20, 30, 50, 70 N·m. In the case of the rotational speed of 850 r/min, out of concern for overworking the engine, loads of 50 and 70 Nm were omitted. Similarly treated was the speed of 950 r/min with the load of 70 Nm. The angle of advancement of fuel injection was changed by ±5ºCA, resulting in three values, i.e.: nominal value – N, accelerated angle – W, delayed angle – P. Using this method resulted in 36 repeated transient states. The model scheme of the functional test subject was represented in Fig. 1.

Similarly treated was the range of output values Y, the number of its elements reduced to only the basic toxic compounds in the exhaust manifold: y_1 – condensation of carbon dioxide in the exhaust manifold C_{CO} [ppm]; y_2 – condensation of hydrocarbons in the exhaust manifold $C_{HC(k)}$ [ppm]; y_3 – condensation of nitric oxides in the exhaust manifold C_{NOx} [ppm]; y_4 – temperature of the exhaust gases t_{sp} [°C]; y_5 – excess air number λ.

As mentioned before, the observed data gathered during the active experiment, as well as the multiequation model [3–6] based off of it, were used for the detailed analysis of the dynamic processes.

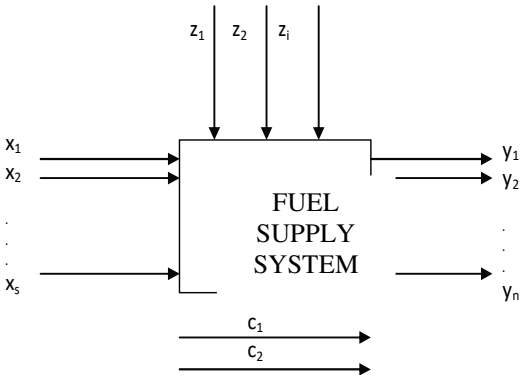


Fig. 1. Quantities characterizing the test subject x – input quantities, y – output quantities, z – disturbances, c – constant quantities

The statistical identification of both the empiric data and the model data was conducted using the GRETL software [1]. The estimation of the equation factors of the specific output variables was conducted with the help of the least squares method, and its purpose was the verification of the significance of its parameters and, in effect, the discarding of insubstantial values, which, consequently, helped to greatly simplify the models. As a measure of the strength and the direction of the correlation between the observed variables (Y, X), the linear correlation coefficient of Pearson was adopted.

Correlation coefficients r_{yx_k} between the variable Y and the variables X_k make up a vector of correlation coefficients $\mathbf{R_0}$, while, between individual illustrative variables, correlation coefficients $r_{y_k x_s}$ make up a matrix of correlation coefficients $\mathbf{R}$ (1) of the following form:

$$\boldsymbol{R_0} = \begin{bmatrix} r_{yx_1} \\ r_{yx_2} \\ \vdots \\ r_{yx_K} \end{bmatrix}_{K\times 1}, \boldsymbol{R} = \begin{bmatrix} r_{x_1x_1} & r_{x_1x_2} & \cdots & r_{x_1x_K} \\ r_{x_2x_1} & r_{x_1x_2} & \cdots & r_{x_2x_K} \\ \vdots & \vdots & \ddots & \vdots \\ r_{x_Kx_1} & r_{x_Kx_2} & \cdots & r_{x_Kx_K} \end{bmatrix}_{K\times K} \tag{1}$$

In the presented analysis of the test results, a substantial merit of the multiequation models comes into view – that is the possibility of a multi-criteria evaluation of the output quantities in the case where these quantities remain in a mutual correlation. Despite their unquestionable advantages, multiequation models do not directly provide the information on the quality of changes, which, in the given situation, are the changes in condensation of individual toxic compounds based on the shifts of the angle of fuel injection advance. Only after compiling the courses of the experiment, or analyzing the produced models, does the image of the phenomenon come into view. Individual correlations along with the fitting of the model to the values received from the experiments held on the engine are presented in further detail in works [5, 6].

As mentioned before, the values of condensations of individual condensations of toxic compounds derived from the transient states are characterized by a particular regularity and repeatability. In no way does it make the analysis easier, considering the notable similarity, independent from the values of the excitations of transient state courses. As such, a tool had to be found, which would be able to describe with relative accuracy and objectivity the character of the changes in the toxic compound concentrations. Using this method allows to describe the correlation of the researched transient state with the transient state adopted as the standard describing the given phenomenon. The analysis of the correlation function makes it possible to define the level of correlation as well as its character. Analyzing the components of a function lets us deduce the aforementioned character of the transient state, i.e. the involvement and intensity of its individual phases.

One of the selection methods for illustrative variables (input quantities of the plan of the experiment) for the model, based on the values of the correlation coefficients, is the information capacity index method of Hellwig [6]. This method relies on the choice of a combination of illustrative variables for which the information capacity is the biggest, and all of the potential illustrative variables are considered as information carriers. The experiment scheme itself imposes a suitable number of available combinations, which, in the given case, with the three input values being K = 3 (x_1 – engine speed n [r/min]; x_2 – engine torque T_{tq} [N·m]; x_3 – angle of fuel injection advance α_{ww} [ºOWK]), is as follows:

$$L(K) = 2^K - 1 \tag{2}$$

Thus created are (for each of the illustrated – output – variables) the following combinations:

- one-element: $C_1 = \{X_1\}$, $C_2 = \{X_2\}$, $C_3 = \{X_3\}$,
- two-element: $C_4 = \{X_1, X_2\}$, $C_5 = \{X_1, X_3\}$, $C_6 = \{X_2, X_3\}$,
- three-element: $C_7 = \{X_1, X_2, X_3\}$.

For each of the combinations mentioned above, an individual information capacity index h_{mx_k} for the variable X_k in the m[th] variable combination must be defined:

$$h_{mx_k} = \frac{r^2_{yx_k}}{1+\sum_{\substack{k,s\epsilon K_m \\ k\neq s}} |r_{x_k x_s}|} \tag{3}$$

where: r_{yx_k} – correlation coefficient between the illustrated variable Y and the illustrative variable X_k (correlation coefficient matrix $\mathbf{R_0}$), $r_{x_k x_s}$ – correlation coefficient between the illustrative variables (correlation coefficient matrix $\mathbf{R}$), m – number of combinations, k – number of illustrative variable X_k, for which the individual information capacity index h_{mx_k} is being calculated.

The next step in the Hellwig analysis is calculating for each of the combinations the integral information capacity index H_m

$$H_m = \sum_{k\epsilon K} h_{mx_k} \tag{4}$$

The highest value for this index makes up for the criterion for the choice of the suitable combination between the illustrative variables. Of course, taking into consideration the goal of this analysis, i.e.: the identification of the sensitivity of diagnostic parameters, which are the concentrations of the individual gas components of exhausts on the changes of parameters of the structure that was the angle of fuel injection advance, particular care was taken during the analysis of the input parameter combinations. These systems were C_3, C_5, C_6 and C_7.

Considering that the majority of the gathered empirical material and the limited form of this paper, the analysis of the information capacity index's variability was limited to one engine speed only, i.e.: n = 1100 r/min. Compounds which were the subject of this analysis were concentrations of HC, CO, NO_x. Analyzed were also the changes in excess air number λ.

The highest values of the H_m index were observed for the excess air number λ, followed by carbon oxide CO concentration and the unburned hydrocarbons HC. The lowest values of H_m were present for nitric oxides NO_x.

It should be noted that the observed regularity, namely the higher values of the H_m index were observed for the delayed fuel injection angle (22ºCA), which of course has a substantive justification, because the delayed angle of injection adversely affects the change in combustion conditions. In the first place, the value of the excess air ratio decreases, resulting in the formation of incomplete combustion products, thus increasing the concentration of CO and HC.

The correct estimation of the model is also shown through a negative correlation, both in the case of air abundance and NO_x concentration, as local oxygen deficiency is a factor reducing the concentration of this compound.

The highest values of the H_m index belong primarily to the C_5 combination, which involves the rotational speed (x_1) and the engine structure parameter, which was the fuel injection advance angle (x_3), for both accelerated and delayed fuel injection. Slightly lower H_m values are present for the C_7 combination which combines the three input values of the experiment plan (Figs 2–5).

The analysis of the integral information capacity index value H_m gives us not only the possibility of an accurate estimation of the model (which is its intended use) but also, thanks to this analysis, it is possible to define, from a vast pool of data, the conditions in which the impact on the researched subject is the greatest. Nevertheless, the values of the H_m index, relatively close to each other in numbers, are making difficult the deduction of which of the experiment plans wields the maximum information value, especially when they are only referring to one parameter or one combination of said parameters.

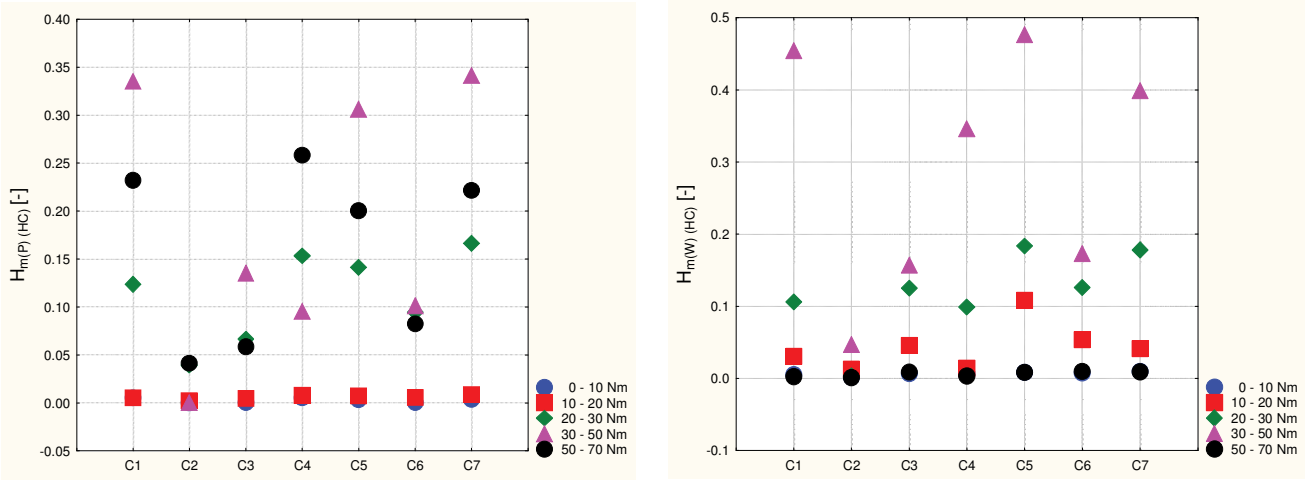


Fig. 2. Values of the information capacity index H_m for HC and the transient state at n = 1100 r/min and a change of load from T_{tq} = 0 Nm to T_{tq} = 70 Nm: P – delayed angle of injection advance; W – accelerated angle of injection advance; C_1 – C_7 – combinations of illustrative variables

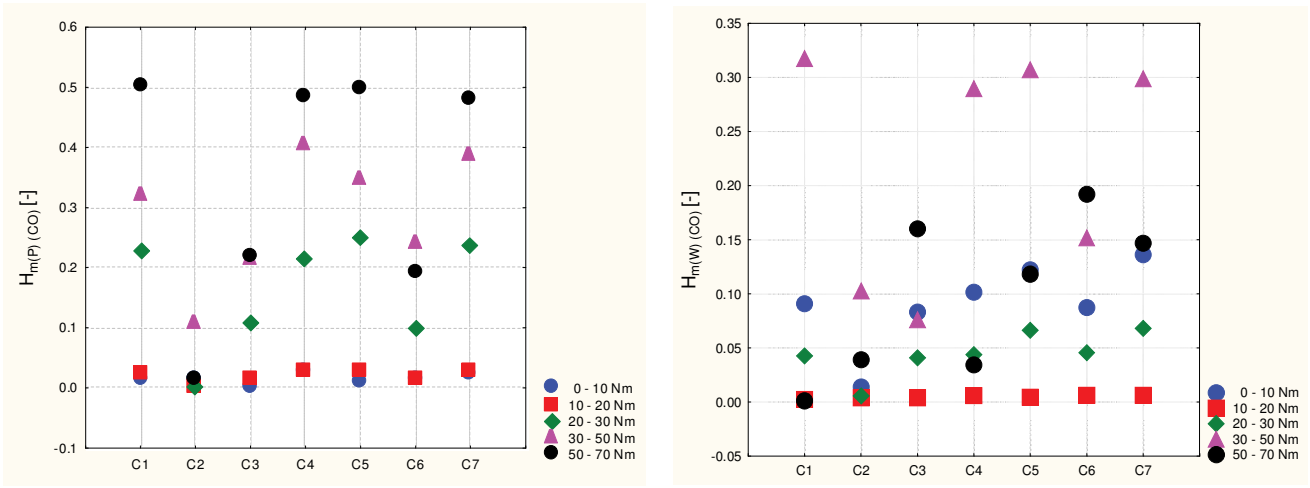


Fig. 3. Values of the information capacity index H_m for CO and the transient state at n = 1100 r/min and a change of load from T_{tq} = 0 Nm to T_{tq} = 70 Nm: P – delayed angle of injection advance; W – accelerated angle of injection advance; C_1 – C_7 – combinations of illustrative variables

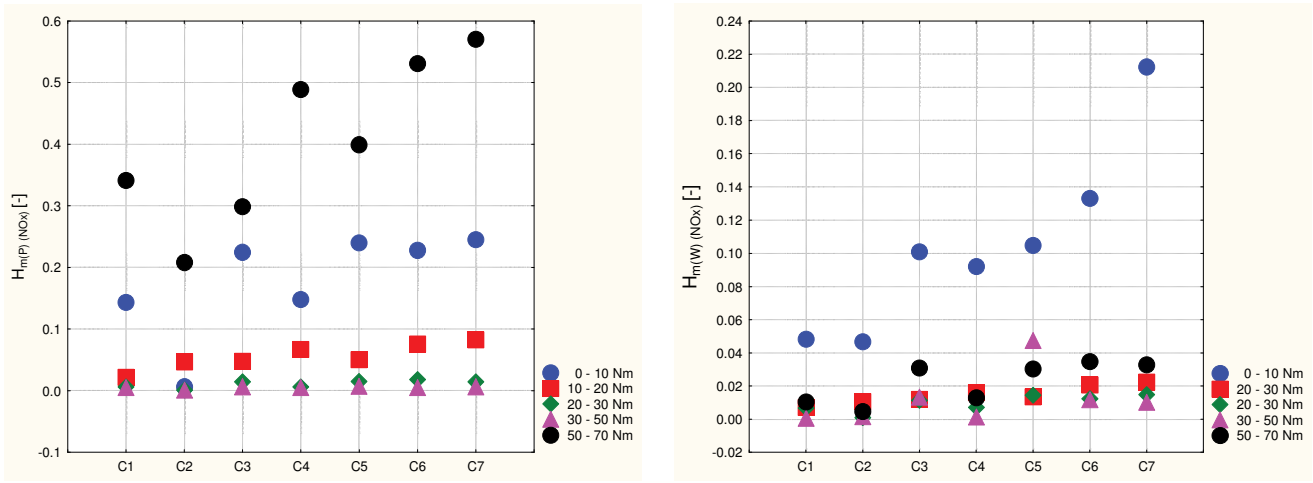


Fig. 4. Values of the information capacity index H_m for NO_x and the transient state at n = 1100 r/min and a change of load from T_{tq} = 0 Nm to T_{tq} = 70 Nm: P – delayed angle of injection advance; W – accelerated angle of injection advance; C_1 – C_7 – combinations of illustrative variables

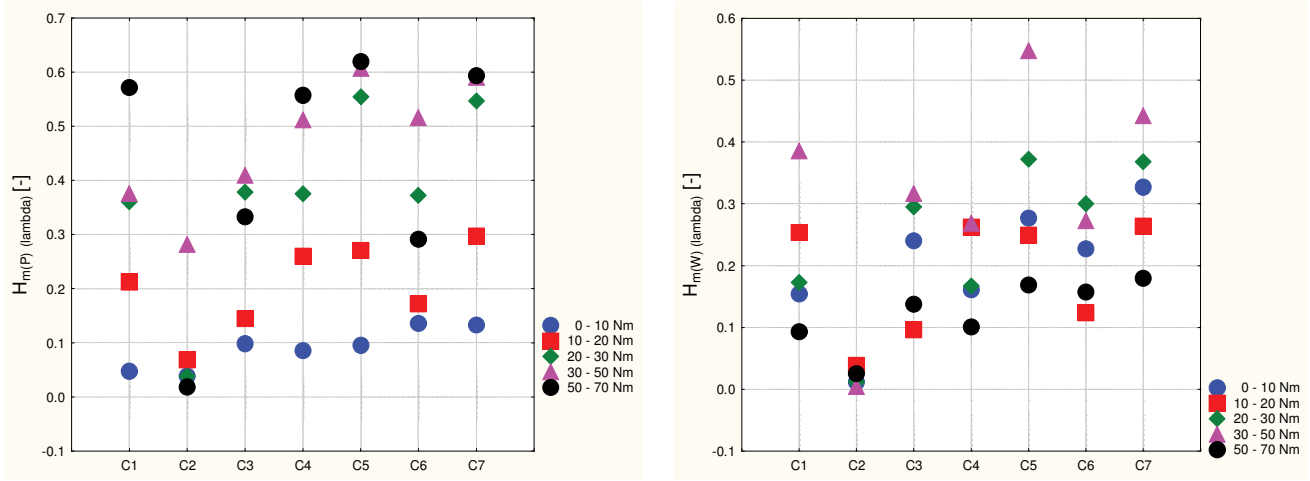


Fig. 5. Values of the information capacity index H_m for λ and the transient state at n = 1100 r/min and a change of load from T_{tq} = 0 Nm to T_{tq} = 70 Nm: P – delayed angle of injection advance; W – accelerated angle of injection advance; C_1 – C_7 – combinations of illustrative variables

In the above mentioned situation, using a parameter ranking seems to be a helpful option, as a ranking reflecting the multi-criteria evaluations (which includes all of the parameters and their combinations) is one of the main premises of making accurate diagnostic decisions.

3. Building a ranking

Taking into account the large quantities of the research material as well as the need of an objective indication of the most favourable diagnostic parameter, considering its sensitivity, a ranking was built on the basis of the zero unitization method. Because earlier each of the illustrative variables for the experiment scheme was run through the Hellwig's information capacity index method analysis, in the early stages of the creation of the ranking it was assumed that the diagnostic variables of the individual illustrative variables will be taken from the Hellwig's index values. These values, for the individual systems and input parameter combinations, are shown in Table 1.

The first step to building the ranking was the division of the diagnostic variable set into three subsets: S, D i N, i.e.:

$$X = S \cup D \cup N \tag{5}$$

where: S – subset of diagnostic variables called the stimulators, D – subset of diagnostic variables called the destimulators, N – subset of diagnostic variables called the nominants.

The transformation of stimulants into the normalized form was calculated using the correlation:

$$z_{ij} = \frac{x_{ij} - \min_i x_{ij}}{\max_i x_{ij} - \min_i x_{ij}}, \quad \begin{pmatrix} i = 1,2,\dots,r \\ j = 1,2,\dots,s \end{pmatrix}, \; X_i \in S, \tag{6}$$

respectively, the correlation used for destimulants:

$$z_{ij} = \frac{\max_i x_{ij} - x_{ij}}{\max_i x_{ij} - \min_i x_{ij}}, \quad \begin{pmatrix} i = 1,2,\dots,r \\ j = 1,2,\dots,s \end{pmatrix}, \; X_i \in D \tag{7}$$

Chosen as the stimulants, that is, the diagnostic variables whose growth should be associated with an increase, while the drop with a decrease of the evaluation of a complex phenomenon, were the combinations of illustrated variables C_1, C_3, C_4, C_5, C_7. While the chosen destimulants, that is, the diagnostic variables whose growth is associated with a decrease, while the drop with an increase of the complex phenomenon, were the combinations C_2 and C_6.

In the case of building a ranking which reflects the mutual interactions of individual exhaust components (which is the case presented in this paper) as well as a ranking which reflects the changes of the structure parameters (changed angle of fuel injection advance), the parameter should be added to the subset of nominants, whose normalization should proceed as follows:

$$z_{ij} = \begin{cases} \dfrac{x_{ij} - \min_i x_{ij}}{c_{0j} - \min_i x_{ij}}, & \text{when } x_{ij} < c_{0j}, \\ 1, & \text{when } x_{ij} = c_{0j}, \; X_i \in N, \\ \dfrac{x_{ij} - \max_i x_{ij}}{c_{0j} - \max_i x_{ij}}, & \text{when } x_{ij} > c_{0j} \end{cases} \tag{8}$$

The following step was the creation of the diagnostic characteristic normalization. This step is essential as it allows for receiving a linked multi-criteria evaluation of the analyzed subject. The linked evaluation is reached through aggregation, i.e., setting an aggregate (synthetic) variable Q_i.

$$Q_i = \frac{1}{s}\sum_{j=1}^{s} z_{ij} \qquad (i = 1, 2, \dots, r) \tag{9}$$

Knowledge of the variable Q allows building a ranking relative to the non-increasing Q_i values. As expected, the order of the ranking will be determined by the value of the synthetic variable Q_i, which is presented in Table 5–8.

By analyzing the tables containing the values of standardized diagnostic variables, it can be seen that the highest values are found for systems with a delayed fuel injection angle of 22ºCA, both for the concentrations of CO, NO_x and the excess air number λ. The characteristic layout of the experiment plan is the 1100P(50-70) system, which is implemented for a transient state at a rotational speed of 1100 r/min, with a load change of 50 to 70 Nm and for delayed fuel injection, which is 22ºCA (Table 6–8). Other systems in the ranking of information values (slightly lower), which are characterized by high values of standardized diagnostic variables, are intermediate load systems, i.e.: firstly when the load is changed from 20 to 30 Nm and secondly from 30 to 50 Nm. This mainly concerns the changes in CO concentration and the value of the excess air number λ. In the case of NO_x concentration (Table 7), systems are followed by other systems that are implemented for similar load changes but for an accelerated fuel injection advance angle (30°CA). This has its substantive justification stemming from the physics of creating individual toxic compounds in the cylinder. Thus, for nitrogen oxides, the dominant mode of their formation is primarily the high combustion pressure, with a significant excess air number, and the high combustion temperature associated with that pressure.

Table 1. Numerical values of the diagnostic variables for HC concentration

Plan system	C_1	C_2	C_3	C_4	C_5	C_6	C_7
1	2	3	4	5	6	7	8
1100P(50-70)	0.2318	0.0416	0.0586	0.2583	0.2001	0.0826	0.2217
1100P(30-50)	0.3350	0.0004	0.1351	0.0956	0.3060	0.1009	0.3412
1100P(20-30)	0.1236	0.0392	0.0665	0.1532	0.1412	0.0944	0.1664
1100P(10-20)	0.0053	0.0024	0.0049	0.0076	0.0075	0.0058	0.0087
1100W(50-70)	0.0027	0.0015	0.0087	0.0036	0.0084	0.0098	0.0092
1100W(30-50)	0.4545	0.0471	0.1570	0.3458	0.4768	0.1734	0.3988
1100W(20-30)	0.1059	0.0037	0.1252	0.0989	0.1835	0.1261	0.1784
1100W(10-20)	0.0304	0.0130	0.0456	0.0144	0.1086	0.0536	0.0414

Table 2. Numerical values of the diagnostic variables for CO concentration

Plan system	C_1	C_2	C_3	C_4	C_5	C_6	C_7
1	2	3	4	5	6	7	8
1100P(50-70)	0.5049	0.0169	0.2176	0.4859	0.4975	0.1947	0.4791
1100P(30-50)	0.3204	0.1096	0.2142	0.4067	0.3478	0.2413	0.3889
1100P(20-30)	0.2272	0.0008	0.1102	0.2146	0.2507	0.0995	0.2374
1100P(10-20)	0.0264	0.0021	0.0149	0.0280	0.0300	0.0136	0.0298
1100W(50-70)	0.0013	0.0390	0.1602	0.0343	0.1182	0.1919	0.1470
1100W(30-50)	0.3176	0.1028	0.0763	0.2898	0.3072	0.1521	0.2988
1100W(20-30)	0.0426	0.0056	0.0410	0.0440	0.0664	0.0456	0.0682
1100W(10-20)	0.0025	0.0042	0.0039	0.0060	0.0046	0.0064	0.0063

Table 3. Numerical values of the diagnostic variables for NO_x concentration

Plan system	C_1	C_2	C_3	C_4	C_5	C_6	C_7
1	2	3	4	5	6	7	8
1100P(50-70)	0.3412	0.2081	0.2986	0.4889	0.3488	0.5312	0.5705
1100P(30-50)	0.0048	0.0047	0.0062	0.0047	0.0071	0.0049	0.0065
1100P(20-30)	0.0059	0.0003	0.0140	0.0059	0.0148	0.0178	0.0141
1100P(10-20)	0.0213	0.0464	0.0477	0.0665	0.0501	0.0756	0.0826
1100W(50-70)	0.0106	0.0047	0.0309	0.0130	0.0304	0.0348	0.0328
1100W(30-50)	0.0006	0.0016	0.0133	0.0015	0.0476	0.0118	0.0103
1100W(20-30)	0.0069	0.0010	0.0115	0.0071	0.0146	0.0123	0.0148
1100W(10-20)	0.0071	0.0107	0.0119	0.0160	0.0136	00207	0.0224

Table 4. Numerical values of the diagnostic variables for λ

Plan system	C_1	C_2	C_3	C_4	C_5	C_6	C_7
1	2	3	4	5	6	7	8
1100P(50-70)	0.5714	0.0187	0.3324	0.6194	0.6194	0.2914	05938
1100P(30-50)	0.3761	0.2819	0.4101	0.5113	0.6073	0.5156	05906
1100P(20-30)	0.3608	0.0383	0.3781	0.3756	0.5544	0.3722	0.5468
1100P(10-20)	0.2628	0.0048	0.0982	0.2370	0.2389	0.2106	0.2367
1100W(50-70)	0.0934	0.0254	0.1381	0.1012	0.1693	0.1575	0.1799
1100W(30-50)	0.3859	0.0046	0.3167	0.2692	0.5478	0.2730	0.4426
1100W(20-30)	0.1738	0.0119	0.2954	0.1672	0.3722	0.3007	0.3679
1100W(10-20)	0.2538	0.0391	0.0963	0.2627	0.2501	0.1239	0.2642

Table 5. Normalized values of diagnostic variables and value of the synthetic variable for HC

Plan system	C_1	C_2	C_3	C_4	C_5	C_6	C_7	Q_i
1	2	3	4	5	6	7	8	9
1100P(50-70)	0.5071	0.1178	0.3531	0.7443	0.4104	0.5418	0.5460	3.2205
1100P(30-50)	0.7355	1	0.8560	0.2688	0.6361	0.4326	0.8523	4.7813
1100P(20-30)	0.2676	0.1692	0.4050	0.4372	0.2849	0.4714	0.4043	2.4396
1100P(10-20)	0.0058	0.9571	0	0.0117	0	1	0	1.9746
1100W(50-70)	0	0.9764	0.0250	0	0.0020	0.9761	0.0013	1.9808
1100W(30-50)	1	0	1	1	1	0	1	5.0
1100W(20-30)	0.2284	0.9293	0.7909	0.2785	0.3750	0.2822	0.4350	3.3193
1100W(10-20)	0.0613	0.7302	0.2676	0.0316	0.2154	0.7148	0.0838	2.1047

Table 6. Normalized values of diagnostic variables and value of the synthetic variable for CO

Plan system	C_1	C_2	C_3	C_4	C_5	C_6	C_7	Q_i
1	2	3	4	5	6	7	8	9
1100P(50-70)	1	0.8520	1	1	1	0.1983	1	6.0503
1100P(30-50)	0.6336	0	0.9841	0.8349	0.6928	0	0.3826	3.5280
1100P(20-30)	0.4485	1	0.4974	0.4346	0.4992	0.6036	0.4887	3.9720
1100P(10-20)	0.0498	0.9880	0.0515	0.0458	0.0515	0.9693	0.0497	2.2056
1100W(50-70)	0	0.6488	0.7314	0.0589	0.2304	0.2103	0.2975	2.1773
1100W(30-50)	0.6280	0.0625	0.3388	0.5913	0.6139	0.3797	0.6186	3.2328
1100W(20-30)	0.0820	0.9558	0.1736	0.0791	0.1253	0.8331	0.1309	2.3798
1100W(10-20)	0.0023	0.9687	0	0	0	0	0	0.9710

Table 7. Normalized values of diagnostic variables and value of the synthetic variable for NO_x

Plan system	C_1	C_2	C_3	C_4	C_5	C_6	C_7	Q_i
1	2	3	4	5	6	7	8	9
1100P(50-70)	1	0	1	1	1	0	1	5.0000
1100P(30-50)	0.0123	0.9995	0	0.0065	0	1	0	2.0183
1100P(20-30)	0.0146	1	0.0266	0.0090	0.0225	0.9754	0.0134	2.0615
1100P(10-20)	0.0607	0.2218	0.1419	0.1333	0.1258	0.8656	0.1349	1.6840
1100W(50-70)	0.0293	0.9788	0.0844	0.0236	0.0681	0.9431	0.0466	2.1739
1100W(30-50)	0	0.9937	0.0242	0	0.1185	0.9868	0.0067	2.1299
1100W(20-30)	0.0184	0.9951	0.0181	0.0114	0.0219	0.9859	0.0147	1.0339
1100W(10-20)	0.0191	0.9499	0.0194	0.0297	0.0190	0.9699	0.2819	2.2889

Table 8. Normalized values of diagnostic variables and value of the synthetic variable for λ

Plan system	C_1	C_2	C_3	C_4	C_5	C_6	C_7	Q_i
1	2	3	4	5	6	7	8	9
1100P(50-70)	1	0.2631	0.7524	1	1	0.5723	1	5.5878
1100P(30-50)	0.5914	0	1	0.9000	0.9731	0	0.9922	4.4567
1100P(20-30)	0.5594	0.8784	0.8980	0.6013	0.8556	0.3661	0.8864	5.0452
1100P(10-20)	0.3544	0.9992	0.0061	0.2976	0.0696	0.7786	0.1372	2.6427
1100W(50-70)	0	0.9249	0.1332	0	0	0.9142	0	1.9723
1100W(30-50)	0.6119	1	0.7024	0.3682	0.8409	0.6193	0.6347	4.7774
1100W(20-30)	0.1672	0.9736	0.6345	0.1446	0.4508	0.5486	0.4542	3.3735
1100W(10-20)	0.3356	0.8755	0	0.3539	0.1795	1	0.2037	2.9482

In the case of hydrocarbon concentration (Table 5), it can be seen, similarly to the NO_x concentration (except for the first system), that the highest values occur in the experiment plan of 1100W(30-50), that is transient state created at 1100 r/min, with a load change from 30 to 50 Nm and for accelerated fuel injection which was 3°CA. This may indicate that this system carries the greatest information value.

The 1100P(30-50) system will hold the next rank of the information value (slightly lower) due to changes in the fuel supply system structure. It should be noted that in both cases these are not the systems with the highest torque values. The conclusion is that intermediate test systems may play an important role in the design of diagnostic tests. Only the next, third system in the ranking, is one that is realized at the maximum torque load.

5. Summary

The numerically similar values of the H_m index do not provide answers as to which of the experiment plan systems carry the maximum information value, considering the changes in the test subject structure, especially when they only adhere to one parameter or one combination of said parameters. However, a ranking reflecting multi-criteria evaluations (encompassing all of the parameters and their combinations) is easily one of the fundamental premises of making accurate diagnostic decisions. Of course, it is viable to build a more in-depth ranking, taking into consideration, for example, a nominant diagnostic variable and its subset of nominal values, which will mirror the state of the engine in its full aptitude. It is also possible to create a more complex set of illustrative and illustrated variables so that the ranking could encompass all of the toxic compound parameters registered during the course of the testing, including the excess air number λ.

Directly regarding the results of the ranking, a regularity should be noted. The higher values of synthetic variable Q_i were observed, except for the very highest value, for the delayed angle of fuel injection (22°CA), which has its substantial justification, as the delayed angle of injection unfavourably influences the change in the combustion conditions. At first the value of the excess air number lowers, which causes the creation of incomplete combustion products, i.e., an increase of HC concentration, which comprised the main subject of this analysis.

Bibliography

[1] RUDNICKI, J., ZADRĄG, R. Problems of modelling toxic compounds emitted by a marine internal combustion engine in unsteady states. *Polish Maritime Research*. 2014, **21**, 57-65.

[2] ZADRĄG, R. Criteria for the selection of the diagnostic parameter for diagnosis of marine diesel engine. *Logistyka*. 2010, **4**.

[3] ZADRĄG, R., ZELLMA, M. Modelling of toxic compounds emission in marine diesel engine during transient states at variable pressure of fuel injection. *Journal of Polisch CIMAC*. 2014, **8**(1).

[4] ZADRĄG, R., KNIAZIEWICZ, T. The identification of toxic compound emission sensitivity as a diagnostic parameter during dynamic processes of the marine engine. *Journal of Polish CIMAC*. 2015, **10**(1), 161-170.

[5] ZADRĄG, R., KNIAZIEWICZ, T. Identification of diagnostic parameter sensitivity during dynamic processes of a marine engine. *The 6th International Congress on Combustion Engines*. PTNSS-2015-3507, 2015.

Ryszard Zadrąg, DEng. – Faculty of Ocean Engineering and Ship Technology at Gdansk University of Technology.

e-mail: *RysZadra@pg.edu.pl*



Tomasz Kniaziewicz, DSc., DEng. – Faculty of Mechanical and Electrical Engineering at the Polish Naval University.

e-mail: *T.Kniaziewicz@amw.gdynia.pl*



Article citation info:
WORSZTYNOWICZ, B. Influence of the method of implementing the forced air flow through the cooling system on the temperature of the coolant in heavy-duty engines. *Combustion Engines*. 2017, **171**(4), 51-55. DOI: 10.19206/CE-2017-409

Barbara WORSZTYNOWICZ

CE-2017-409

Influence of the method of implementing the forced air flow through the cooling system on the temperature of the coolant in heavy-duty engines

The article discusses the problem how forced air flow is implemented through the cooling module of heavy-duty engines. The kinematic connection between the coolant pump and the crankshaft of the engine, results in the fact that the pump performance often does not correspond to the engine demand at its part load. In conjunction with the fan drive method, the temperature of the coolant may be too low or too high for part load. The study was carried out in order to calculate the parameters of the cooling system in heavy-duty engines for maximum power and maximum torque, taking into account a mechanical fan drive, a hydraulic fan drive and an electric fan drive.

Key words: *heavy-duty engine, cooling system, heat transfer, coolant pump, fan*

1. Introduction

The performance of a coolant pump results from the kinematic connection with the crankshaft and, in most cases, does not correspond to the current engine demand for the parameters of the cooling system. According to [1], a coolant pump generates a flow that far exceeds the engine demand, even up to 95% of operating time. This is due to the fact that the components of the cooling system must be chosen in such a way that with high ambient temperature the conditions are met for the maximum load of the engine. On the other hand, the engine in the vehicle often works with low loads and at idle speed, especially when operating in the traffic [7]. Then, the loss of cooling heat in the thermal balance is much higher than during nominal load of the engine. As a result, the overall efficiency of the engine differs from the nominal one, so fuel consumption is increased, as well as the emission of harmful exhaust components [2, 4, 5, 9].

In order to improve the efficiency of converting energy included in the fuel, higher and higher temperatures of cooling liquid are used [4, 7, 9]. This practice aims at increasing the temperature of the engine work cycle by reducing the heat losses from the combustion chamber to the environment. To keep in the cooling system of higher and higher temperatures one needs to use higher and higher values of pressure.

Another way to optimize the engine's performance is to use two thermostats in the cooling circuit to provide a higher temperature of the liquid in cylinders and lower temperature in cylinder head [3, 13].

There is currently extensive research carried out into the use of coolant pumps driven by an electric motor and into control of thermostat opening using an electromagnetic valve [1–3, 10]. The electric drive of the pump eliminates the connection between the pump efficiency and the rotation speed of the engine so as to control the coolant flow depending on the instantaneous load on the engine. Besides that, immediately after the cold start of the engine, the pump may not be switched on until the coolant in the engine reaches the optimum temperature. This solution has already been used in VW's series produced engine (1.5 TSI evo).

In order to approximate the operating conditions of engines to adiabatic, the study is also being carried out concerning the use of ceramic coating on cylinder liners [6].

2. Heavy-duty engines

Heavy-duty compression ignition engines operate at a much lower rotational speed than in passenger vehicles, usually up to 2500 rpm. An example of an external speed characteristics of a heavy-duty engine is shown in Fig. 1.

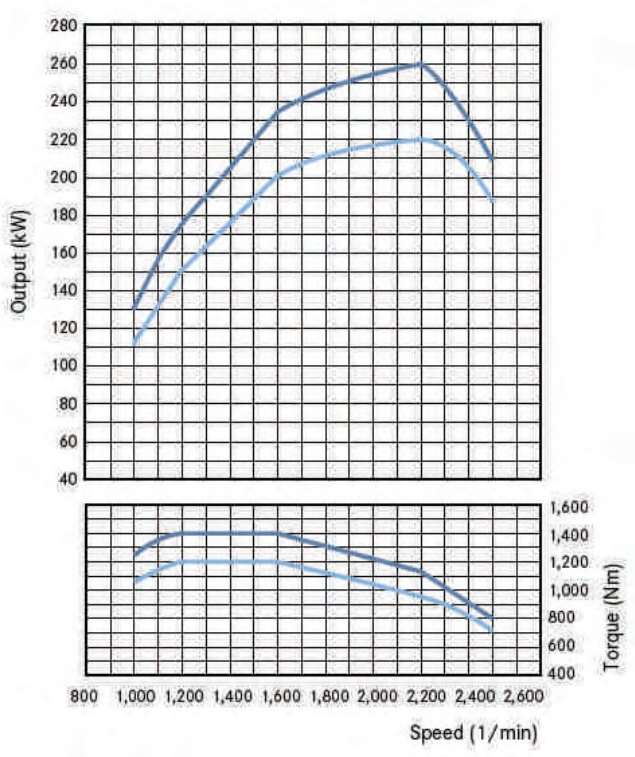


Fig. 1. External speed characteristics of a heavy-duty engine [14]

At the same time, they are more likely to work in stable heat conditions, as vehicles equipped with such engines cover long distances. Therefore, the kinematic connection between the crankshaft and the coolant pump is less unfavorable than that in a passenger vehicles. This does not mean, however, that the cooling parameters are optimal at each engine operating point. Apart from the appropriately

selected characteristics of a coolant pump, it is also important to implement forced cooling air flow through the cooling module. In trucks, the fan is most often driven directly from the crankshaft or through a gear (eg. a fan mounted on a coolant pump). The alternative solution may be a hydraulic fan drive, commonly used in buses and special vehicles. Another solution increasingly used in city buses is the replacement of systems with one, hydraulically driven fan, with systems consisting of several fans with electric motors of considerably smaller diameters [8].

The variety of vehicles with heavy-duty engines results in the fact that mentioned above ways of the forced air flow through the cooling module cannot be used interchangeably. However, for the purpose of analyzing the influence of the fan drive method on the cooling parameters in the various operating parameters of the engine, the calculation of a cooling module was performed, taking into account all three ways of fan drive.

3. Engines characteristics

The engines meeting the EURO VI norms were selected for the analysis. These are six cylinder engines in a straight configuration, turbocharged, as well as EGR cooling system. They are equipped with a direct fuel injection system based on the Common Rail system and an extensive exhaust aftertreatment system consisting of an oxidation catalytic converter, a diesel particular filter and a reduction catalytic converter with AdBlue system. Engines 1 and 2 have the same maximum power and maximum engine torque, while the engine 3 comes from the same series as the engine 2, however, it has higher values of maximum power and of torque. The basic data of the engines are given in Table 1.

Table 1. Engines data [11, 12]

Parameter	Unit	Engine 1	Engine 2	Engine 3
Rated power	kW	224	220	260
At speed	rpm	2100	2200	2200
Max torque	Nm	1200	1200	1400
At speed	rpm	1100–1700	1200–1600	1200–1600
Fuel Consumption at Rated Power	g/kWh	210	204	209

4. Calculations of the cooling system

4.1. Characteristics of the cooling system

The cooling module in vehicles containing heavy-duty engines consists of a radiator, a charge air cooler, a condenser of air-conditioning system and a fan or fans. If the fan drive is hydraulic, the cooling module also includes the oil cooler of the fan drive system. In addition, the cooling module can include an air cooler of the pneumatic system. As the analysis concerns the engine, the condenser and the pneumatic air cooler were not included in the calculation. In all studied cases of the fan drive the same heat exchangers with the same core systems and dimensions were used as shown in Table 2. The cooling system cover with a 60% clearance was also taken into consideration as it is an element on the path of air flow causing minor head loss.

Table 2. Heat exchangers dimensions

Radiator core		
height	mm	900
width	mm	700
depth	mm	52
Charge air cooler core		
height	mm	650
width	mm	600
depth	mm	68

Due to the range of data provided by heavy-duty engine manufacturers, the calculations were done for the parameters corresponding to the maximum engine power and the maximum torque. The cooling parameters that must be met for individual engines are shown in Table 3.

Table 3. Selected engine data at ambient temperature of 45°C [11, 12]

Parameter	Unit	Engine 1		Engine 2		Engine 3	
		Ne max	Mo max	Ne max	Mo max	Ne max	Mo max
Heat rejection to coolant	kW	133	102	152	105	167	122
Coolant flow	l/min	14 7	92	306	195	366	231
Coolant temp. max	°C	107	107	105	105	105	105
Temp. after turbocharger	°C	172	191	195	186	215	210
Charge air temp. before engine	°C	66	66	61	55	62	56
Charge air flow	kg/h	948	678	954	655	1098	792

The work of the cooling module is affected by other elements of engine compartment, whose impact is difficult to predict at the design stage. Therefore, an additional safety factor should be taken into consideration. It has been assumed that the amount of heat rejection to coolant will be 10% higher than stated by the engine manufacturers.

Taking into account the climatic conditions prevailing in Europe, an ambient temperature of 45°C was adopted for the calculations for which the acceptable value of the charge air temperature was increased by 20 K respectively.

Calculations were made in the GT-SUITE computational package, using the characteristics of BSPL core heat exchangers.

4.2. Fan drive from crankshaft

In the first case, the simplest solution was considered, namely, the fan drive directly from the engine. As a result, the cooling module will include a radiator, a charge air cooler and a 9 – blade sucker fan with 680 mm diameter. Both the installation of the fan, on a crankshaft (ratio 1:1) and on the coolant pump (ratio: 1:1.1 and 1:1.2), were considered, as well as slipping on the clutch. Figure 2 shows the calculation model 3D of a cooling module, Figure 3 the calculation model 1D, while tables 4, 5 and 6 show the results of the gear ratio between the engine and the fan respectively 1:1; 1:1.1; 1;1.2.

The kinematic connection of the fan with the engine is the cheapest option and is best suited for engines mounted on the front of the vehicle. However, very often it causes significant differences in coolant temperature values for maximum power and maximum torque. This is due to the amount of heat that must be transferred from the engine to the cooling system at maximum power and maximum torque and from the characteristics of the coolant pump and

the fan. This prevents optimal selection of engine cooling parameters in various operating conditions and may result in over-sizing of the cooling module, especially if it is not possible to apply different ratios between engine speed and fan speed. On the other hand, the higher the fan speed, the greater the heat loss of the engine on its drive.

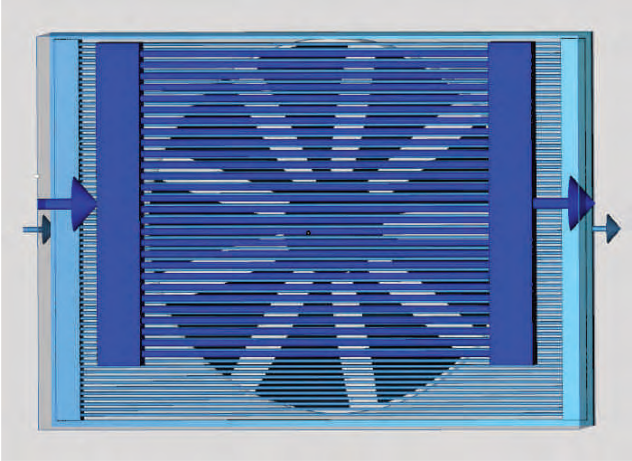


Fig. 2. Calculation model 3D of cooling module

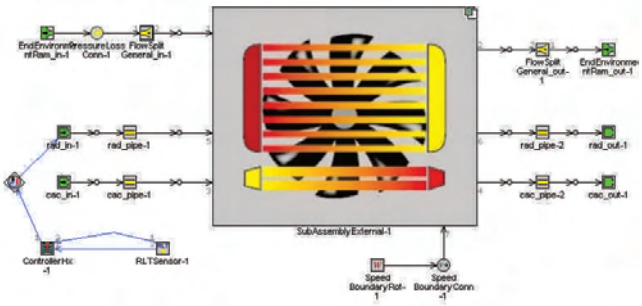


Fig. 3. Calculation model 1D of cooling module

Table 4. Calculation results, fan speed ratio 1:1

Parameter	Unit	Engine 1		Engine 2		Engine 3	
		Ne max	Mo max	Ne max	Mo max	Ne max	Mo max
Heat rejection to coolant	kW	146.3	112.9	167.2	116.7	183.7	135.2
Coolant temp. inlet engine	°C	96.2	106.5	96.1	97.5	102.1	107.8
Charge air temp. inlet engine	°C	50.4	50.5	51.2	49.3	54.6	53.1
Fan speed	rpm	1950	1240	2050	1330	2050	1330
Cooling air flow	kg/s	5.19	3.05	5.41	3.34	5.32	3.23
Fan power	kW	9.1	2.3	10.5	2.9	10.3	2.8

Table 5. Calculation results, fan speed ratio 1:1.1

Parameter	Unit	Engine 1		Engine 2		Engine 3	
		Ne max	Mo max	Ne max	Mo max	Ne max	Mo max
Heat rejection to coolant	kW	146.3	112.6	167.2	116.3	183.7	134.8
Coolant temp. inlet engine	°C	92.9	101.9	92.6	93.2	97.9	102.3
Charge air temp. inlet engine	°C	49.9	49.7	50.6	48.7	53.7	51.9
Fan speed	rpm	2150	1360	2250	1460	2250	1460
Cooling air flow	kg/s	5.81	3.44	6.03	3.76	5.94	3.66
Fan power	kW	12.4	3.0	14.1	3.8	13.9	3.7

Table 6. Calculation results, fan speed ratio 1:1.2

Parameter	Unit	Engine 1		Engine 2		Engine 3	
		Ne max	Mo max	Ne max	Mo max	Ne max	Mo max
Heat rejection to coolant	kW	146.3	112.5	167.2	116.0	183.7	134.6
Coolant temp. inlet engine	°C	90.4	98.3	89.7	89.5	94.5	97.6
Charge air temp. inlet engine	°C	49.5	49.0	50.1	48.2	53.0	51.0
Fan speed	rpm	2340	1480	2455	1600	2455	1600
Cooling air flow	kg/s	6.39	3.83	6.65	4.21	6.56	4.11
Fan power	kW	15.9	4.0	18.5	5.0	18.3	4.9

4.3. Fan drive with hydraulic system

The use of a hydraulic fan drive requires the expansion of the cooling module with a hydraulic pump and a hydraulic motor, as well as an oil tank and an oil cooler. This solution is much more expensive than the fan drive from the engine, but it allows the fan speed to be independent from the engine speed and the location of the cooling module from the engine mounting location.

It was assumed to use an external gear motor and two types of pumps: an external gear pump or axial piston pump. The type of pump was selected to provide optimum cooling parameters for both maximum engine power and maximum torque. The use of an axial piston pump results in the decrease of heat rejection by around 50 % which is generated by the oil to the cooling module, thus reducing the oil cooler. Figure 4 shows the cooling module calculation model 3D, Figure 5 the calculation model 1D, and Table 7 shows the calculation results.

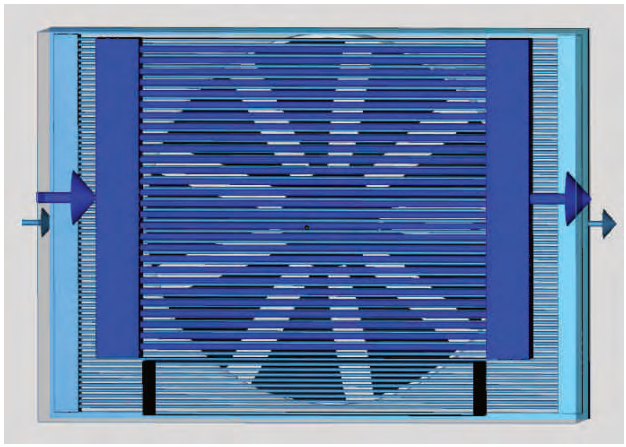


Fig. 4. Calculation model 3D of cooling module

The hydraulic fan drive allows for better adjustment of fan speed at various engine rotation speeds. However, the presence of certain types of hydraulic motors and hydraulic pumps results in the fact that the fan speed when running the engine with maximum torque will not always be optimal. During calculations, such a selection of fan operating parameters was assumed, that for maximum engine power the coolant temperature would be 3 K lower than the maximum temperature permitted by the engine manufacturer. This represents an additional safety factor in case of, for example, a greater major head loss in the coolant flow due to the greater distance between the engine and the radiator.

For engines 1 and 3, the coolant temperature during operation of the engine with a maximum torque is about 1–2 K smaller , and for the engine 2 it is greater by about 1.5 K. Keeping the coolant temperature close to maximum allowable values improves the efficiency of conversion of energy contained in the fuel.

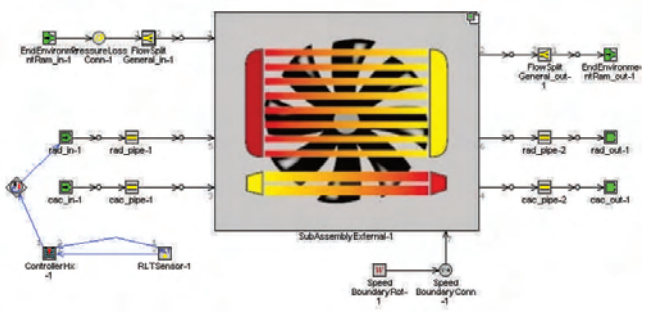


Fig. 5. Calculation model 1D of cooling module

Table 7. Calculation results, hydraulic fan drive

Parameter	Unit	Engine 1		Engine 2		Engine 3	
		Ne max	Mo max	Ne max	Mo max	Ne max	Mo max
Heat rejection to coolant	kW	146.4	112.6	167.2	116.7	183.7	134.7
Coolant temp. inlet engine	°C	103.9	102.3	102.1	103.6	102	100.9
Charge air temp. inlet engine	°C	51.4	49.3	52.0	49.9	54.4	51.4
Fan speed	rpm	1700	1430	1850	1240	2100	1540
Cooling air flow	kg/s	4.37	3.64	4.76	3.02	5.46	3.9
Fan power	kW	5.9	3.5	7.6	2.3	11.1	4.4
Heat rejection to oil	kW	9.0	9.0	6.3	6.3	5.0	5.0

4.4. Fan drive with electric motor

A 24 volt electrical installation on vehicles with heavy-duty engines excludes the use of a single large electric motor driven fan. Instead of that, several fans with a much smaller diameter are used, which operate at high rotation speed. These fans produce significantly lower pressure values. In addition, the control system is required so that, at part load and low ambient temperature, the fans would not working at maximum speed.

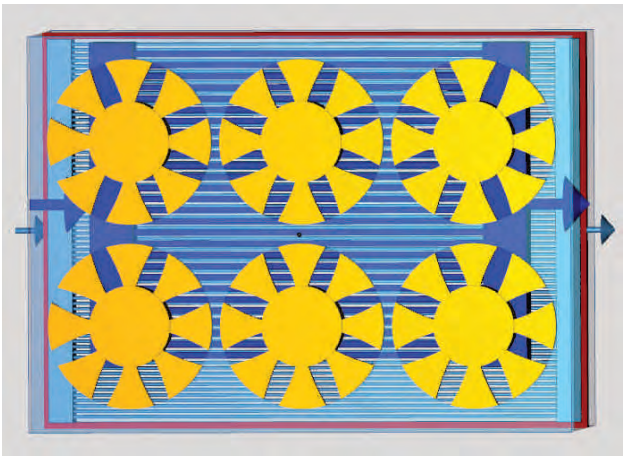


Fig. 6. Calculation model 3D of cooling module

For the calculation, six blower fans were used for these applications, with a diameter of 305 mm with brushless motors. The number of fans is the result of the amount of available space for their installation, namely, the frontal area of the cooling module. Figure 6 shows the calculation 3D model of the cooling module with electric motors, Figure 7 the cooling module calculation model 1D, and Table 8 shows the calculation results.

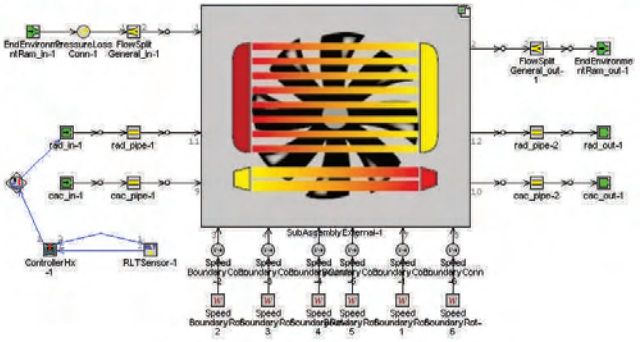


Fig. 7. Calculation model 1D of cooling module

The use of six 305 mm diameter fans with electric motors instead of one with diameter 680 mm with a mechanical drive, or a hydraulic drive, does not provide the right temperature of the coolant for engines 2 and 3 in operation with maximum power. Electric driven fans produce much less pressure, so they work better in side by side systems than in a sandwich one. The module with parallel arrangement of heat exchangers is usually larger, so it takes up more space in the vehicle. Electric driven fans running at maximum speed generate a large noise. Electric fan drive is a heavy load for the electrical installation of the engine.

Table 8. Calculation results, 6 fans with electric motor

Parameter	Unit	Engine 1		Engine 2		Engine 3	
		Ne max	Mo max	Ne max	Mo max	Ne max	Mo max
Heat rejection to coolant	kW	146.4	112.6	167.3	116.9	183.8	134.6
Coolant temp. inlet engine	°C	105.2	103.5	108.4	103.3	115.6	102.1
Charge air temp. inlet engine	°C	52.3	50.2	53.7	50.5	57.9	52.2
Fan speed	rpm	4750	4000	4750	3600	4750	4400
Cooling air flow	kg/s	4.05	3.32	4.02	2.9	3.99	3.69
Fan power	kW	4.5	3.8	4.5	3.3	4.5	4.1

5. Conclusions

The reduction of heat losses from the combustion chamber results in improved overall efficiency of the engine which, in turn, leads to lower fuel consumption and decrease of harmful exhaust components. This is accomplished, among others, by increasing the coolant temperature or by selecting a pump whose characteristics enables to reach the optimum coolant flow within the maximum possible range of rotation speed of the engine. Engine cooling

parameters are also influenced by non-engine cooling system components such as heat exchangers or fan characteristics.

Vehicles with heavy-duty engines use different fan drive methods, depending on the location of the engine in the vehicle. The mechanical fan drive is the simplest and cheapest solution, but it usually produces a significant difference in the coolant temperature between the maximum power and the maximum torque of the engine. This is due to the characteristics of the engine and the pump, but also to the resulting high difference in fan speed at the analyzed points of engine operation. The fan efficiency at low rotation speeds is considerably reduced. The alternative solution is a hydraulic fan drive, which is commonly used when placing the engine at the rear of the vehicle. The hydraulic system is much more expensive and more complicated, because it consists of more components. However, it allows for such a the selection of components that the coolant temperature can have an optimum value concerning a wide range of engine rotation speed. In city buses, besides the hydraulic fan drive, electric fans are also used, due to the lower cost. This system is suitable for low power engines, also it generates more noise and is a heavy load for the electrical installation of the vehicle.

Bibliography

[1] ZHOU, B., LAN, X., XU, X., LIANG, X. Numerical model and control strategies for the advanced thermal management system of diesel engine. *Applied Thermal Engineering*. 2015, **82**, 368-379.

[2] EID, S.M. Development and analysis of a variable position thermostat for smart cooling system of a light duty diesel vehicles and engine emissions assessment during NEDC. *Applied Thermal Engineering*. 2016, **99**, 358-372.

[3] KNEBA, Z. Development trends of automotive engine cooling systems. *Combustion Engines*. 2013, **154**(3), 291-296.

[4] KRAKOWSKI, R. Wpływ podwyższonej temperatury płynu chłodzącego na zwiększenie ekonomiczności pracy tłokowego silnika spalinowego. *Zeszyty naukowe Akademii Morskiej w Gdyni.* 2011, **71**.

[5] KRAKOWSKI, R. Model and experimental research of the pressure cooling system for the internal combustion engine. *Journal of KONES Powertrain and Transport*. 2014, **21**(4).

[6] MITIANIEC, W. Assessment of total efficiency in adiabatic engines. Scientific Conference on Automotive Vehicles and Combustion Engines. *IOP Conf. Series*: *Materials Science and Engineering*. 2016, **148**, 012080.

[7] WORSZTYNOWICZ, B. Bilans cieplny silników spalinowych typu heavy-duty w aspekcie norm emisji. *Silniki spalinowe i ekologia – opracowanie monograficzne*. Wydawnictwo Politechniki Krakowskiej. Kraków 2014.

[8] WORSZTYNOWICZ, B. The influence of fuel type on the cooling system heat exchanger parameters in heavy – duty engines. Scientific Conference on Automotive Vehicles and Combustion Engines, IOP Conf. Series: *Materials Science and Engineering*. 2016, **148**, 012080.

[9] WORSZTYNOWICZ, B., UHRYŃSKI, A. The analysis of heating process of catalytic converter using thermo-vision. *Combustion Engines*. 2015, **162**(3), 41-51.

[10] CHEN, X., YU, X., LU, Y. et al. Study of different cooling structures on the thermal status of an internal combustion engine. *Applied Thermal Engineering*. 2017, **116**, 419-432.

[11] Cummins – factory data.

[12] Mercedes-Benz – factory data.

[13] VW Self study programme 296.

[14] www.mercedes-benz.pl.

Barbara Worsztynowicz, DEng. – Faculty of Mechanical Engineering and Robotics at AGH University of Science and Technology.

e-mail: *Worsztyn@agh.edu.pl*



Article citation info:
KORCZEWSKI, Z., MARSZAŁKOWSKI, K., RUDNICKI, J. The concept of research on ecological, energy and reliability effects of modified marine fuel oils application to supply compression-ignition engines in real conditions. *Combustion Engines*. 2017, **171**(4), 56-61. DOI: 10.19206/CE-2017-410

Zbigniew KORCZEWSKI
Konrad MARSZAŁKOWSKI
Jacek RUDNICKI

CE-2017-410

The concept of research on ecological, energy and reliability effects of modified marine fuel oils application to supply compression-ignition engines in real conditions

Within the article, basic assumptions of the research project financed by Regional Fund for Environmental Protection and Water in Gdansk were described. The project concerns the experimental investigations carried out on laboratory compression-ignition engine in conditions of its supply with a non-standard marine fuel oil. Configuration and measuring capability of laboratory test bed presently being constructed were introduced. The concept of engine tests implementation as well as a general outline of research methodology was characterised. After being accepted by Polish Committee for Stardarization they could become an effective and efficient verification tool for various types of modified fuel oils introduced on the market, both for the maritime administration officies and shipyards as well as ship owners in operation.

Key words: *compression ignition engine, modified marine fuel oils, laboratory research test bed, concept of research implementation*

1. Introduction

A tightening the regulations that limit the emissions of pollutants emitted by ship engines imposes the necessity of new technologies development, which enable complying the requirements within this scope. It is in accordance with policy of Commission for Environmental Protection of International Maritime Organization, which sets the regulations for international shipping. This Organization, during its 70th Session organised in London on 24–28 October 2016, decided to radically decrease the permissible content of sulphur compounds in fuel oils applied in shipping from present maximum 3.5% to 0.5% per unit of mass. It was enacted that the new standard will be in force since 1 January 2020 and will apply to ships operating on all international waters (except for the SECA *Sulphur Emission Control Area*, where since 1 January 2015 sulphur content in fuel oil cannot exceed 0.1% per unit of mass) [1].

It is a long awaited decision of IMO, fundamental for natural environmental protection, not only for inshore areas, but also deep into the land. It is anticipated that limiting the emissions of sulphur oxides to the atmosphere will have immense impact on decrease of expenses on public health and only for the EU the savings are estimated on the level of 15–34 billion euros [IMO Report, 2016]. On the other hand, the considered decision of IMO is raising the justified anxiety of ship owners, who will be forced to bear additional costs of adjusting the owned ships to new law regulations in scope of sea transport. It can be expected that the average exploitation costs of ships can increase twice, what will intensify already experienced (after 1 January 2015) slowdown in the development of the widely considered maritime trade.

In this case, two ways of action are possible:

1. Equipment of exhaust gases systems of marine power plants with devices reducing the emissions of sulphur oxides to the atmosphere (wet methods – so called 'scrubbers' or dry methods – so called 'sorbers').
2. Applying modified low sulphur fuel oils or alternative fuel oils to supply marine engines.

In both cases it is necessary to conduct research works aimed an evaluation of technical and economical efficiency of the applied solution. However, wet and dry desulphurization of exhaust gases from the engine are quite well worked out and more and more often applied (despite considerable investment cost of 4–5 million euros), applying so called modified or alternative marine fuel oils is still stirring controversy and is putting a question mark for all ship owners interested in not only protection of sea environement, but also in high efficiency and reliability (durability) of engines installed on the board of already exploited as well as ordered ship.

It appears that there are not many research facilities conducting this kind of research on real objects, mainly because of its complex nature. Admittedly, producers of ship engines dispose of adequately equipped research engine test bed, but conducted programmes deal with only testing newly implemented construction solutions of produced engines, with applying standard fuel oils. Basic energy parameters of the given type of engine are then determined as well as the guaranteed time of its constructional subsystems operation. Another problem represents a considerable risk of undertaking trials to supply a serial ship engine, which can cost even up to several mln euros, with a non-standard fuel, having no knowledge on its actual impact on performance and efficiency of the engine, and on the constructional structure of its main functional elements. Moreover, long-lasting character of such research contributes to respectively high cost of their realisation. Due to this, the research is conducted on the specially adjusted laboratory test bed, performed in multiple times lower scale, though still with maintaining each constructional and process similarities with respect to the real object. This kind test beds must comply with specific requirements regarding safety of research implementation and protection of natural environment. This way, amount of fuel oil used for test is

being minimized (from several or several dozen tons to several kilos), together with the emissivity of harmful substances in exhaust gases (practically to 0) and costs of reconstruction of technical state of used elements and constructional subsystems (from tens thousands euros to several hundred euros). Confronting the problem, in the research project undertaken by the authors of the article, a specialised laboratory test bed of Diesel engine will be constructed, adjusted to burn modified marine fuel oils – Fig. 2. It will be equipped with measuring-diagnostic equipment enabling the evaluation of ecological, energy and reliability effects of applying other than standard types of fuel oils. A methodology of conducting engine tests with the use of modified marine fuel oils will also elaborated. Its implementation should contribute to the increase of the level of natural environment protection, increase of shipping safety and considerable reduction of exploitation costs of marine engines. It will constitute a significant supplement to ISO 8178 standard *„Combustion piston engines – measurements of exhaust gases emissions. Part 10: Cycles and research procedures of exploitation measurements of smoke of exhaust gases of compression-ignition engines operating in undetermined conditions"* [3], which is applied to research on engines operating in undetermined conditions, where rotational velocity of crankshaft of the engine or load, or both parameters change in time.

Constructed laboratory test bed will not require high expenditures for its maintenance, as it is in case of real objects, where every time after conducting verification tests it is necessary to rinse the fuel installation with large amount (several tons) of costly marine diesel oil and exchange of several times more expensive lubricant oil (even up to several hundred kilos).

2. Research test bed

A development (and competitiveness) of sea transport is strictly determined by numerous restrictions within applied marine fuel oils. On one hand, they need to be cheap enough, with maintaining high energy value, on the other – they need to comply with high ecological requirements, in the sense of permissible emissivity of exhaust gases of shipping machines, and reliability in scope of their readiness and durability guaranteed by producers. These restrictions are a challenge both for producers of fuel oils and ship engines, as well as for researchers conducting investigations on engine processes, considering the diagnostics and reliability aspects. It is even more significant and urgent problem, as recently business sector is sending numerous queries to Polish universities of technology to have the possibility to test new type of marine fuel oil on real objects, namely on adequately equipped laboratory test bed of combustion engines (last years mainly computer simulations of working processes were applied). In case of standard marine fuel oils, it is not an easy issue, as they are mainly so called residual fuel oils, of considerable density and viscosity, which in order to obtain liquid form, for transport and pulverisation, need to be heated up to the temperature in range between 35 and even up to 150ºC. However, the key technological element, determinative for the proper operation of the engine (and its technical condition), is continuous in time maintaining of required by the producer viscosity of the fuel oil injected to the combustion chamber, at the accuracy of 0.5 cSt. Especially critical process is the regulation of viscosity of the fuel oil in conditions of switching from supplying the engine with marine diesel oil fuel (start-up and lay-off) to heavy fuel oil (long-lasting operation) and reverse. Similar problems are connected with testing the biofuels e.g. methanol, more often applied in sea transport. Thus, most urgent metrological problem of constructed laboratory test bed was to select and properly assembly the viscometer, which would enable for the quick enough (several seconds) measurement of the kinematic viscosity of the fuel at the inlet of the injection pump of the engine. After analysis of the offers available on the Polish market, it was decided to select a portable rotational viscometer of VT1 Plus type, produced by HAAKE company, of measurement range 1.5–330 mPa·s – Fig. 1. In order to estimate the momentary kinematic viscosity of the fuel in place of the VT1 Plus viscometer installation, it is necessary to shut equally quick electronic thermometer.



Fig. 1. General view of portable rotational viscometer VT1 Plus type produced by HAAKE [4]

Liquid fuel oils applied in combustion power plants are to smaller or bigger extent contaminated with foreign bodies, as e.g.: sand, dust, rust, water etc., which get to the fuel oil during its transport and storage in containers. In order to reduce the consequences of the contaminants presence to the highest possible level, each fuel oil sample of minimum amount of 20 dm^3 requires special preparation for the research. The fuel oil is first filtrated by a reticular filter, and then heated up to the temperature 70–90ºC (heating temperature depends on nominal viscosity) in a settling tank of 30 dm^3 (Fig. 2) surrounded by a water jacket of 200 dm^3, temperature of which is stabilised by an electronic thermostat. Then, the fuel oil is centrifuged in a centrifugal separator type MAB104, operating first as a purifier, and then as a clarifier.

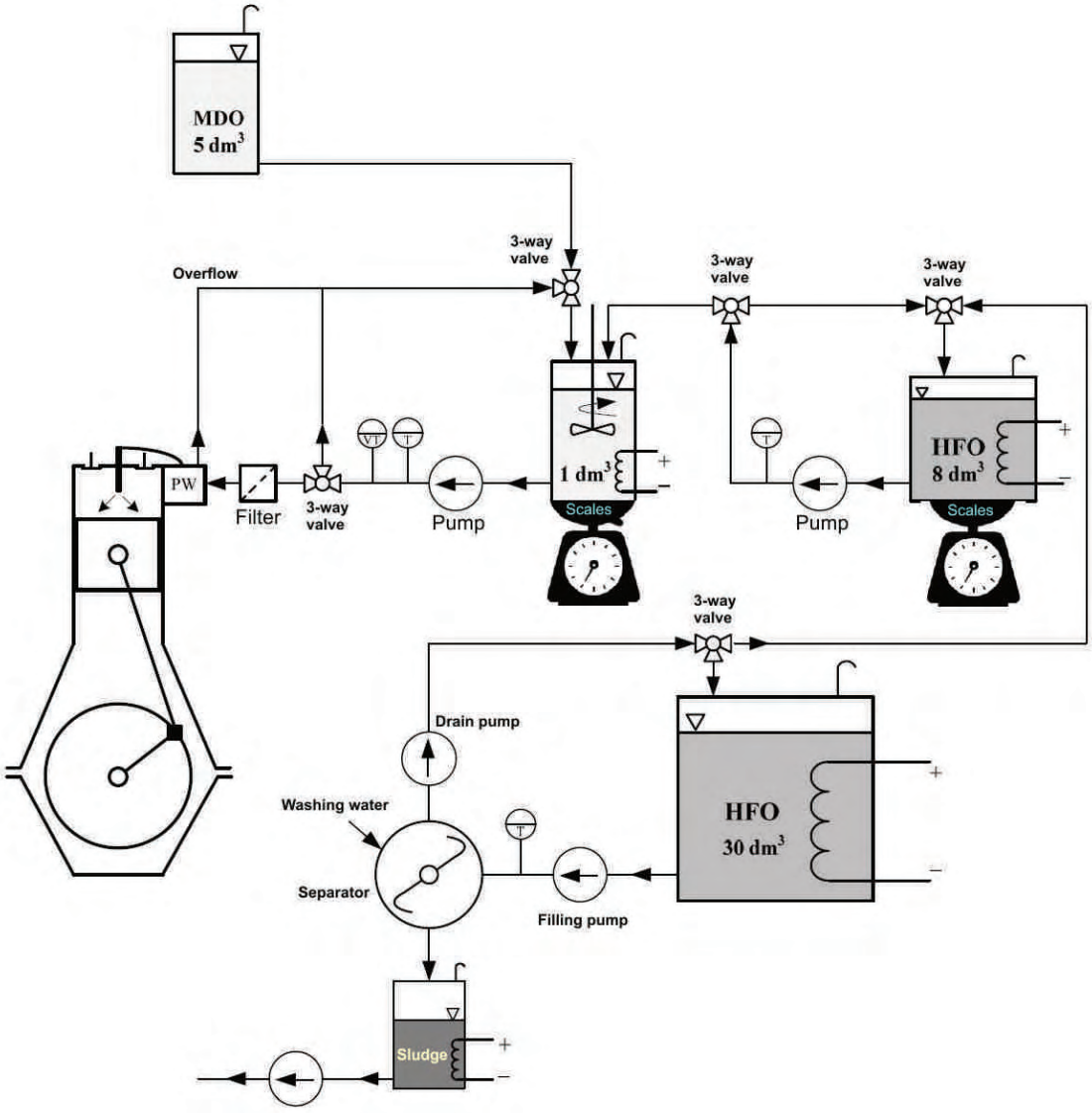


Fig. 2. Conceptual scheme of installation of supplying the laboratory engine Farymann Diesel type D10 with fuel oil: MDO – Marine Diesel Oil; HFO – Heavy Fuel Oil; PW – injection pump, VT – viscometer, T – thermometer

Single-cylinder, four-stroke compression-ignition engine applied in the laboratory test bed, is Farymann type D engine, at nominal power of 5.88 kW achieved at rotational velocity of crankshaft equal to 1500 rev/min. Hourly consumption of marine diesel oil at the engine load of 80% P_{nom} is equal to 0.86 kg/h, what corresponds to flow to injection pump equal to approx. 1 dm^3/h. Regarding the small amount of tested fuel oil and its low consumption by the engine, it is troublesome to select the circulating pump of such low efficiency and resistance to high operation temperature (temperature of the fuel oil can be even up to 150ºC). This is why, it was decided to apply gear pumps of type NSZ 10 in function of circulating pumps. These pumps induce the flow of the fuel oil in both service tanks, and can be characterised by nominal efficiency of 900 dm^3/h, at rotational velocity of 1500 rev/min. Due to the fact that fuel oil installation of the laboratory engine is supplied gravitationally, it was designed as low-pressure one. Assumed exchange of fuel oil in a preheater installation is relatively small, so the power needed for operation of pumps is not equal to its nominal power. For driving of the pumps moto reducers with DC engines were applied, with supplying voltage of 24 V and power of 0.45 kW. Such solution enables simple and effective regulation of rotational velocity, and so the efficiency of each of the pumps, with the use of DC pulse width modulation regulators.

Testing the fuel oil sample is every time initiated with the start-up of the engine on diesel oil. After reaching the constant temperature of ~100ºC by the engine (water evaporating cooling), it is loaded up to 80% of its nominal power, with the use of DC alternator. Simultaneously, the process of gradual heating up of the diesel oil is started. Given kinematic viscosity of the fuel during research is obtained in two stages, namely roughly and accurately. The sample of prepared fuel is being poured into the container of a centrifugal separator, to the main service tank of 8 dm^3, where it is heated up being constantly in flow, in a closed system of a fuel installation. Temperature, and indirectly also the viscosity of the fuel in this branch of the piping system, is stabilized by a precise electronic thermostat with PID (proportial – integral – derivative) regulation. When swithing to heavy fuel oil (the tested one), temporary mix-

ing of both fuel oils in a measure service tank of 1 $dm^3$is taking place, with increasing share of the tested fuel oil in the mixture. A this stage, dynamic viscosity and temperature of the fuel are measured. Depending on their values, the intensity of heating up of the fuel is regulated, additionally stabilised by an electronic thermostat. Switching to supply the engine with marine fuel oil (during its stoppage) takes place reversely, namely from the external container of 5 dm^3 the marine fuel oil is supplemented in the service tank (1 dm^3), the whole time controlling the viscosity and gradually decreasing the temperature of a service tank. The share of a tested fuel oil in a mixture of fuels in a measure service tank (1 dm^3) and consumption of the fuel by the engine is determined by measurement of fuels mass in both containers by electronic weights. Both service tanks are fully made of copper alloys, what enables their simultaneous heating up by electric heating elements of power 2 kW. Mixing of the fuels in a service tank is induced by circulating pumps, as well as mechanically – by paddle stirrer. Each container and piping system in the installation of supply the engine with fuel are carefully thermally isolated. In case of testing the fuels of higher viscosities, additional heating up of the piping system is foreseen.

3. Measuring equipment

The most relevant scientific problem in the considered issue is to determine the scope and programme of the required experimental research on the lab marine compression-ignition engine enabling the evaluation of ecological, energy and reliability effects of applying modified (alternative) marine fuel oils. It is thus necessary to elaborate the method of identification of working processes in combustion engine supplied with this type of fuel oils, and also identification of its constructional structure with highly specialised measuring (diagnostic) equipment. What is important, in case of conducting this kind of research by a team of specialists from the Department of Ship and Land Power Plants of the Faculty of Ocean Engineering and Ship Technology at Gdansk University of Technology, it won't be needed to construct the diagnostic system from scratch, as it already exists and is successfully applied in exploitational research on ship engines, contracted out by ship owners, both national and international ones. It will only be necessary to extend it and adapt it to the requirements of considered experiments methodology elaboration. At present, the diagnostic system consists of the following research equipment:

- electronic indicator of LEMAG PREMET® C type, produced by LEHMANN & MICHELS GmbH – determination of performance and efficiency of the compression ignition engine, based on the measurement of inner cylinder pressure and vibrations generated by work of mechanisms connected with cylinder system, transmitted to the measurement point at the surface of the head (determination of average indicated pressure, indicated power, maximum combustion pressure and pace of increase of pressure in the cylinder $d_p/d\alpha_{OWK,}$ as well as characteristic angles of crankshaft rotations, during which the fuel injector's opening and closing takes place, initiation of compression ignition in cylinders and cylinder valves' opening and closing);
- portable exhaust gases analyser of KIGAZ 300 type, produced by KIMO® – characteristics of harmful substances emissions within engine's exhaust gases, based on the measurement and analysis of the composition of exhaust gases in determined and undetermined conditions of engine's operation;
- digital recorder and analyser of vibrations of SVAN 956 type, produced by SVANTEK – evaluation of the mechanical system stability of the engine driving line, based on spectrum-correlation analysis of vibration signal generated by selected construction nodes of driving system;
- measuring videoendoscope of XLG3 type, produced by Everest, equipped with lens of *„ShadowProbe"* type – digital record an dimensional analysis of inner space of the engine (especially identification of damages and evaluation of the wear and tear process intensity of the constructional elements limiting the working space of the cylinder).

What is even more, the Department owns a research ship engine, which was supplied with the a test bed for desulphurisation with a dry method, perfectly adjusted to the analysis of exhaust gases and based on that evaluation of ecological effects of applying different heavy fuel oils. The test bed was designed and constructed within research project, co-financed from the Regional Fund for Environmental Protection and Water Management in Gdansk (project's number: RX-01/2015 + update).

4. Methodological assumptions

Elaborated methodology of engine research must respond to the following detailed questions:

1. Regarding the method of conducting experimental research:
   - what and where to measure? (which process: determined or undetermined? Where?)
   - how to measure? (which parameter? at which accuracy? how often?)
   - how to draw conclusions? (border conditions, categories of conditions)
   - when to measure? (either in full scope of energy processes or only in their particular stages)
2. Regarding the exploitational usage of the experimental research results:
   - how (in sense of quality and quantity) applying of modified marine fuel oil affects the energy measures of engine operation (its basic parameters)?
   - does the change of the fuel oil supplying the engine results in increase of intensity of wear and tear process of the engine's constructional structure or deterioration of rheological properties of lubricant oil?
   - what is the impact of modification of marine fuel oil on chemical composition of exhaust gases?

In order to accomplish the assumed aim of the research project, it is required to solve the following detailed issues:

- Design and building an external installation of the laboratory engine for the preparation of marine fuel oil (heavy fuel oil) for combustion. It should take into account the possibility of its heating up, purification and

precise regulation of viscosity before applying it to the combustion chamber of the engine;
- Modernisation of the engine's fuel fed system consisting in applying the gradual transition between fuel oils of big differences in viscosities (mixing the marine fuel oil and heavy fuel oil or methanol);
- Optimalisation of the adsorber injecting process in processing reactor, aimed at reduction of harmful substances emissions in exhaust gases;
- Design and constructing a stationary measuring system, enabling an observation of heat-flow processes within the engine's fuel fed and in the exhaust gases system;
- Elaboration of the research programme and conducting pilot tests with the application of the most representative marine fuel oils.

5. Results of pilot research

A separate part of the initial research covered the issue of the impact of basic indications of engine's work, on inclusion of the desulphurisation system of exhaust gases into engine's exhaust system [5].

Relatively big diameters and volumes of flow elements led to assumption that the expected impact would be infinitesimal, especially that in previous stages of research no alarming symptoms of engine operation could be observed (i.e. higher temperature or vibrations etc.).

Diagnostic device used to verify validility of these assumptions was the electronic indicator Lemag Premet C XL. The indicator was produced by Lehman&Michels GmbH. It complies with production requirements of ISO 9001 standard and is wired up to indicative valve of the engine via an adapter.

Indication was conducted twice, after obtaining the determined thermal condition of the engine – temperature of cooling agent was aprox. 95–98ºC – in the following conditions:

a) rotational velocity of the engine set at 1350 rev/min;
b) load of the engine – 5 kW (electric heating system, supplied with an alternator powered by the engine via belt);
c) indication I (I series) – exhaust system of the engine without modification (referential state);
d) indication II (II series) – process reactor of the desulpurisation system with the equipment in the exhaust system of the engine (modified exhaust system);
e) indication III (series III) – processing reactor of the desulpurisation system with the equipment in the exhaust system of the engine (modified exhaust system) and additionally supply of the engine with so called a vacuum diesel oil, at the sulphur content of 0.8%.

Obtained results of indication are presented in Fig. 3 and in Table 1.

Based on obtained results, general conclusion can be formulated, that from practical point of view inclusion of process reactor of desulpurisation system with the equipment, as the element of the exhaust gases system of considered engine, is not affecting significantly the initial indications of its operation parameters.

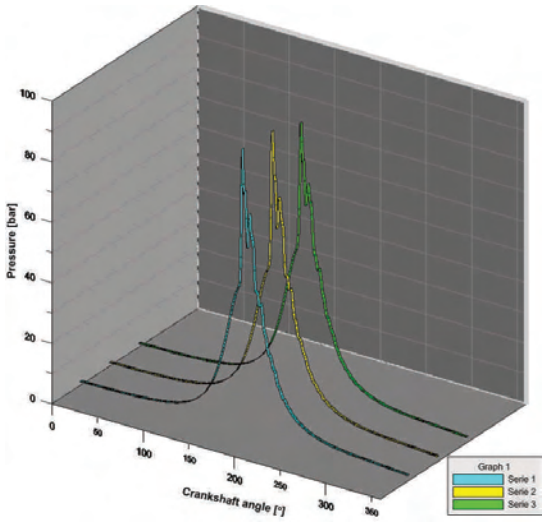


Fig. 3. Pressure changes in the cylinder – tests I, II and III

Table 1. Results of pilot research carried out on the engine with an application of the electronic indicator

No.	Engine performance indicators	Value			Change of value I-II [%]	Change of value I-III [%]
		Series I	Series II	Series III		
1.	Max combustion pressure – p_{max} [bar]	87.1	85.4	84.2	1.95 ⇓	3.3 ⇓
2.	Mean indicated pressure – p_i [bar]	3.7	4.0	3.8	8.1 ⇑	2.7 ⇑
3.	Indicated power – P_i [kW]	4.0	4.2	4.0	5.0 ⇑	0.0
4.	Max pressure angle [° after TDC]	0.5	0.5	0.25	-	-
5.	Exhaust pressure (36 ° after TDC) [bar]	21.5	22.5	21.0	4.6 ⇑	2.3 ⇓
6.	Max value of dp/dα [bar/° CA]	16.2	15.8	15.2	2.5 ⇓	6.2 ⇓

6. Remarks and final conclusions

It is anticipated that in results of project's realisation Polish producers of marine fuel oils. to whom it is primarily addressed. will have the possibility of complex and real evaluation of usability of their products to supply ship engines. This possibility could also be used by ship owners before making decisions on introducing new marine fuel oil for exploitation. Innovative aspect of proposed solution is to adjust the laboratory test bed of Diesel engine to conduct experimental research with an application of heavy fuel oils and alternative fuel oils. so that real conditions of ship engine operation can be simulated. with minimising the negative effects of applying heavy fuel oils on the natural environment.

The main aim of the project realization is to construct a laboratory test bed foreseen for research conduction on energy efficiency of newly produced fuel oils and evaluation of their impact on emissivity of exhaust gases and pollution of the atmosphere with toxic and harmful chemical substances. as well as the effects of their applying in the aspect of intensity of degradation of the engine's constructional elements.

Detailed aims: designing and realization of the laboratory position. which will make possible a realisation of objective investigations by means of complex. high-specialised measuring apparatus. as well as an elaboration

of the innovatory methodology of testing new kinds of marine fuels within real operation conditions of the engine work. keeping out the atmosphere pollution.

Except mentioned above cognitive and utilitarian aims of clean technical nature. an intention of authors of the undertaken project is the widest introduction of the suggested verification method for the newly produced and implemented marine fuels. in such a way their influence on natural environment as well as marine engines was earlier well-known and recognisable. An application to this aim computer simulation methods is definitely not sufficient at present.

Bibliography

[1] Emission Standards. International: IMO Marine Engine Regulations.
[2] Report of the Marine Environment Protection Committee. IMO MEPC 70th session. October 2016.
[3] ISO 8178-10:2013 Reciprocating internal combustion engines – Exhaust emission measurement – Part 10: Test cycles and test procedures for field measurement of exhaust gas smoke emissions from compression ignition engines operating under transient conditions.
[4] www.thermofisher.com/order/catalog/product/399-0100.
[5] KORCZEWSKI, Z., RUDNICKI, J., ZADRĄG, R. Budowa stanowiska laboratoryjnego do badania innowacyjnej metody suchej odsiarczania spalin silnika zasilanego paliwem pozostałościowym. Projekt dofinansowany ze środków Wojewódzkiego Funduszu Ochrony Środowiska i Gospodarki Wodnej (WFOŚiGW) w Gdańsku – sprawozdanie z realizacji zadania. Gdańsk 2016.

Zbigniew Korczewski, DSc., DEng. – Faculty of Ocean Engineering and Ship Technology at Gdansk University of Technology.

e-mail: *ZbiKorcz@pg.gda.pl*



Jacek Rudnicki, DEng. – Faculty of Ocean Engineering and Ship Technology at Gdansk University of Technology.

e-mail: *JacekRud@pg.gda.pl*



Konrad Marszałkowski, MSc. – Faculty of Ocean Engineering and Ship Technology at Gdansk University of Technology.

e-mail: *Konrad.Marszalkowski@pg.edu.pl*



Article citation info:
BEBKIEWICZ, K., CHŁOPEK, Z., SZCZEPAŃSKI, K, ZIMAKOWSKA-LASKOWSKA, M. Estimating pollutant emission from motor vehicles in the years 2000–2015. *Combustion Engines*. 2017, **171**(4), 62-67. DOI: 10.19206/CE-2017-411

Katarzyna BEBKIEWICZ
Zdzisław CHŁOPEK
Krystian SZCZEPAŃSKI
Magdalena ZIMAKOWSKA-LASKOWSKA

CE-2017-411

Estimating pollutant emission from motor vehicles in the years 2000–2015

National annual emission from motor vehicles were estimated with the use, for the first time in Poland, of the COPERT software programme developed in support of official reporting under the EU cooperation framework. The quantification of vehicular emission covered the period 2000–2015. The results were analysed for the following cumulated vehicle categories: passenger cars, light commercial vehicles, heavy duty vehicles, urban buses, coaches, motorcycles and mopeds. The national annual emission from motor vehicles in Poland was found to be markedly declining. The relative national annual emission of individual pollutants was balanced against the situation in the year 2000. Starting from 2006, a distinct decreasing trend was observed for the relative national annual emission of pollutants from a representative motor vehicle; this was valid for all the substances except for nitrous oxide alone.

Key words: *motor vehicles, inventory of pollutant emission, COPERT*

1. Introduction

Estimation of pollutant emission from motor vehicles can be done only if emission modelling is used [3, 4, 6].

Quantification of pollutant emission from motor vehicles entails the use of software programmes which assist in estimating emission. The software programmes are equipped with multiple tools that help to find the most appropriate factors for modelling pollutant emission from motor vehicles. The COPERT (Computer Programme for calculating Emissions from Road Traffic) is a widely preferred solution in the European Union, for inventorying pollutant emission from motor vehicles [7–9, 11]. The COPERT model was developed under the auspices of the European Environment Agency (EEA) for compiling national reports on GHG's and other pollutant emission from road transport due to the EU Member State reporting obligations. This paper presents the results of quantifying national emission of pollutants from motor vehicles with the use, for the first time in Poland, of the COPERT 4 programme dedicated to official reporting under the EU's cooperation [8, 11]. The estimation of pollutant emission from motor vehicles covers the years 2000–2015.

2. The COPERT Programme

The assumption underlying the COPERT model, likewise all models for estimating total emission of pollutants from motor vehicles, is that the total fuel consumption and the total energy consumption, as well as the total pollutant emission resulting from the use of motor vehicles with internal combustion engine, are sums of fuel consumption, energy consumption and pollutant emission, for the following states [3, 4, 6–10]:

– internal combustion engine heated up to a stable temperature,
– heating of internal combustion engine,
– fuel evaporation from the vehicle fuel system.

The COPERT 4 programme considers elementary categories of motor vehicles taking account of their [1, 3, 4, 6–10]:

– duty,
– conventional size,
– technical specification including, among others, the combustion system, cycle, fuel type as well as car technological level regarding pollutant emission.

The following categories of motor vehicles aggregated relative to their duties (including their original English names used by the COPERT programme, and abbreviations used in this publication) [1, 3, 7–9, 11] were considered:

1. Passenger cars – PC:
   – Gasoline passenger cars with spark ignition engine – PC-SI-G,
   – Liquefied petroleum gas passenger cars with spark ignition engine – PC-SI-LPG,
   – Passenger cars with compression ignition engine – PC-CI.
2. Light commercial vehicles (Light duty vehicles) – LCV:
   – Light commercial vehicles with spark ignition engine – LCV-SI,
   – Light commercial vehicles with compression ignition engine – LCV-CI.
3. Heavy duty trucks – HDT:
   – Heavy duty trucks – rigid (heavy duty container trucks) – HDT-R,
   – Heavy duty trucks – articulated (tractor units, ballast tractors) – HDT-A.
4. Urban buses – UB.
5. Coaches – C.
6. Motorcycles – Mc.
7. Mopeds – Mp.

Basic substances, for which emission can be quantified using models of pollutant emission include [1, 3, 7–9, 11]:

– carbon monoxide – CO,
– volatile organic compounds – VOC,
– non-methane volatile organic compounds – NMVOC,
– methane – CH_4,
– groups of organic compounds including, among others: alkanes, alkenes, alkines, furans, aldehydes, ketons, cycloalkanes, aromas, polycyclic aromatic hydrocarbons – PAHs.
– nitrogen oxides – NO_x,
– nitric oxide – NO,
– nitric dioxide – NO_2,

– nitrous oxide – N_2O,
– ammonia – NH_3,
– particulate matter PM from the exhaust system of an internal combustion engine,
– particulate matter PM10 from tribological elements of a vehicle,
– particulate matter PM2.5 from tribological elements of a vehicle,
– black carbon – BC,
– carbon dioxide – CO_2,
– lead and its compounds reduced to lead – Pb,
– sulphur oxides reduced to sulphur dioxide – SO_2,
– heavy metals: Cd, Cr, Cu, Ni, Se and Zn.

The most important input values in the COPERT programme cover [1, 3, 7–9, 11]:

– number of vehicles by elementary categories (vehicle type),
– vehicle use intensity by vehicle type – annual mileage,
– share of mileage by vehicle type and traffic conditions: in towns, outside towns, on highways and expressways in the total mileage,
– average vehicle velocity by vehicle type, under respective traffic conditions: in towns, outside towns, on motorways and on expressways,
– monthly temperature: minimum and maximum values in respective months,
– fuel sulphur content,
– fuel lead content,
– fuel element composition,
– fuel heavy metal content,
– fuel saturated vapour pressure,
– average after-start mileage by vehicle type,

Number of vehicles per cumulated category was estimated based on data contained in Poland in the Information System of the Central Register of Vehicles and Drivers (CEPiK) – Fig. 1.

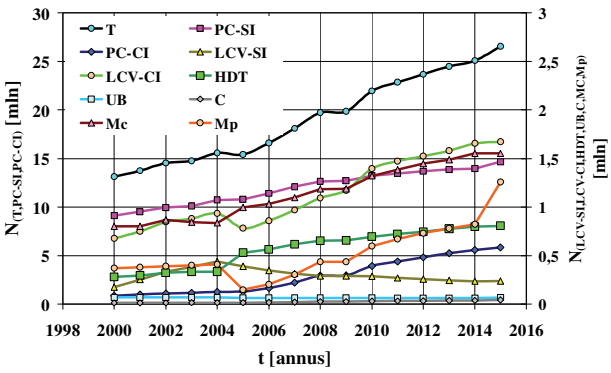


Fig. 1. Number of vehicles per cumulated category

The average mileage of vehicles by cumulated category was assessed taking into account [5]:

– transport performance,
– number of vehicles registered,
– average values of technical-operational characteristics of the road transport performance (e.g. average number of persons transported in a vehicle, average indicator of fleet utilisation, etc.).

Figure 2 illustrates the assumed annual mileage of vehicles by cumulated category.

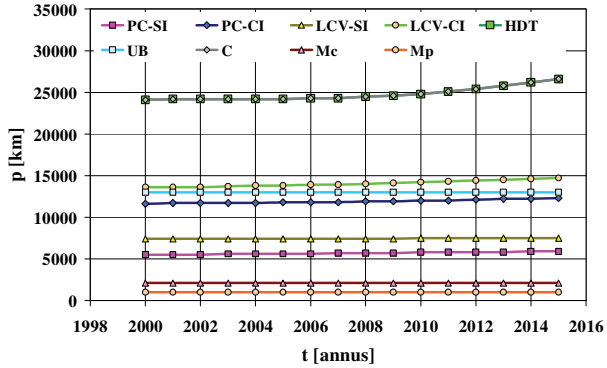


Fig. 2. Annual mileage of vehicles per cumulated category

To determine the annual mileage of motor vehicles per elementary, environmentally oriented, categories, which account for pollutant emission, the authors developed a model simulating vehicle use intensity. The model was built on the basis of functional likeness. Data on vehicle structure at the level of elementary categories were used to develop the model (data from the INFRAS software[10]).

Figures 3–5 show the assumed mileages covered by vehicles which enter the cumulated categories, under the following model traffic situations: urban, rural as well as on highways and expressways [5].

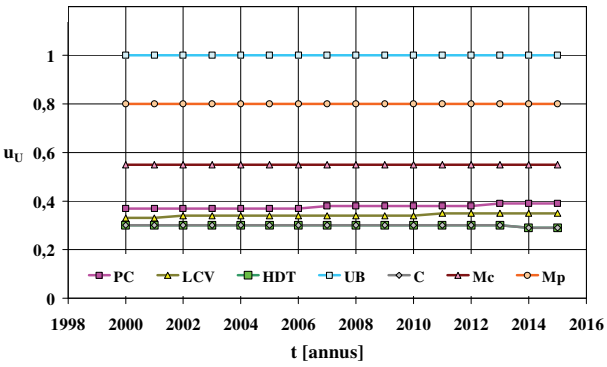


Fig. 3. Share of mileage by vehicles per cumulated category, under model traffic conditions: urban

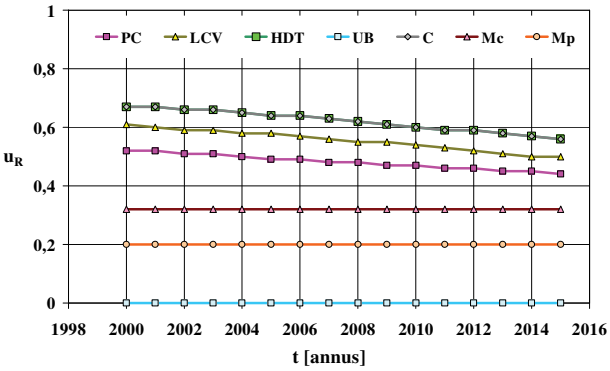


Fig. 4. Share of mileage by vehicles per cumulated category, under model traffic conditions: rural

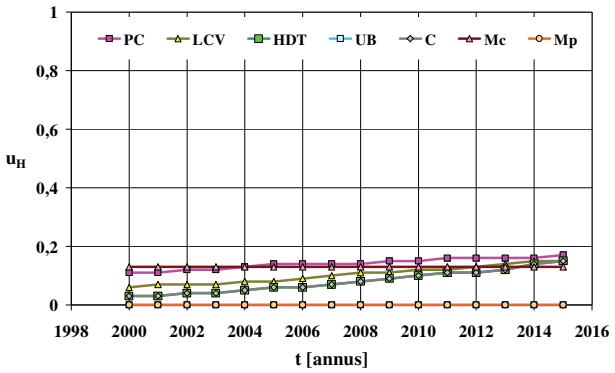


Fig. 5. Share of mileage by vehicles per cumulated category, under model traffic conditions: on highways and expressways

Figures 6–8 show the assumed average vehicle velocity per cumulated vehicle category, under the following model traffic conditions: in towns, outside towns as well as on highways and expressways [5].

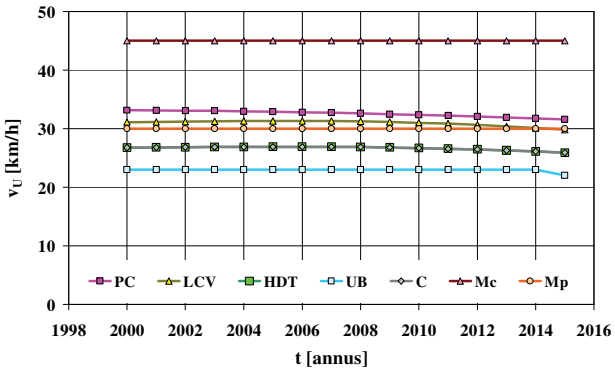


Fig. 6. Average vehicle velocity per cumulated vehicle category, under model traffic conditions: urban

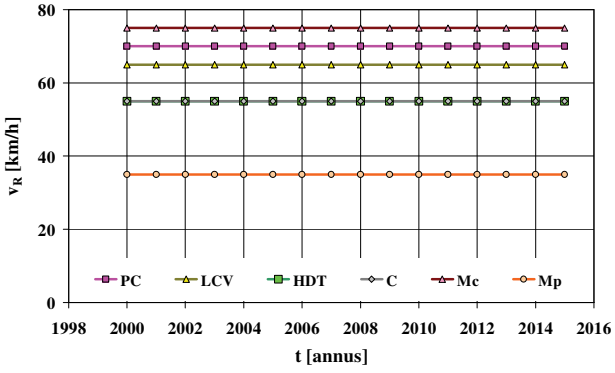


Fig. 7. Average vehicle velocity per cumulated vehicle category, under model traffic conditions: rural

The average mileage of vehicle after engine start was assumed to be 12 km [1].

Moreover, other data were also assumed following those addressed by the COPERT software, such as e.g.: parameters characterising fuel types and climate conditions in Poland.

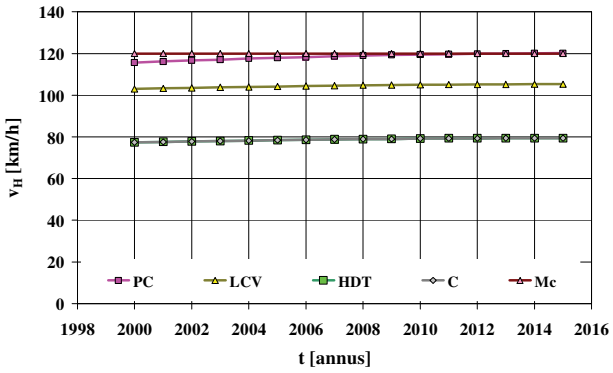


Fig. 8. Average vehicle velocity per cumulated vehicle category, under model traffic conditions: on highways and expressways

3. Estimating pollutant emission from motor vehicles in the years 2000–2015: the results

Figures 9–18 show the national annual emission of selected pollutants for respective cumulated categories of vehicles and for all motor vehicles – T.

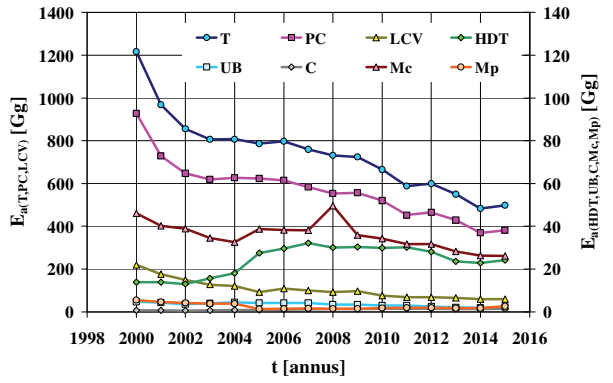


Fig. 9. National annual emission of carbon monoxide per cumulated vehicle category

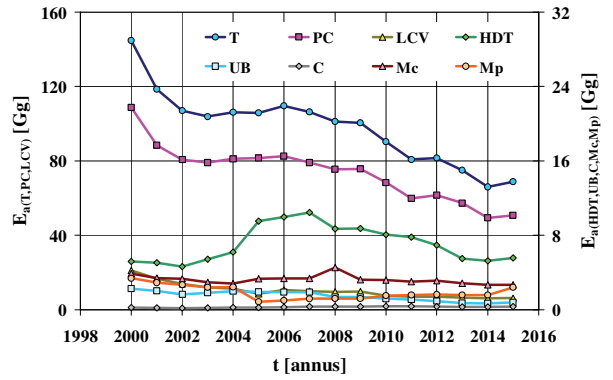


Fig. 10. National annual emission of volatile organic compounds per cumulated vehicle category

National annual emission is differentiated for different pollutants and cumulative vehicle categories. Generally for carbon monoxide and volatile organic compounds, there is a marked tendency of declining national annual emission.

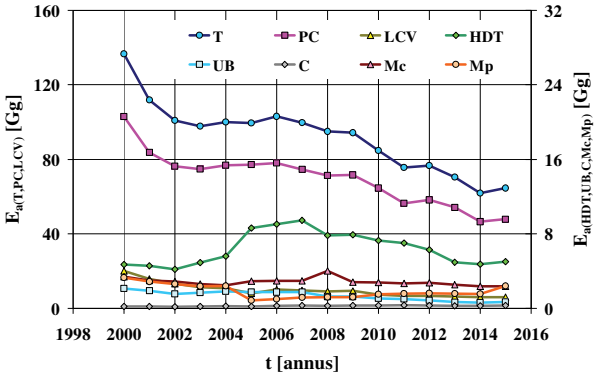


Fig. 11. National annual emission of non-methane volatile organic compounds per cumulated vehicle category

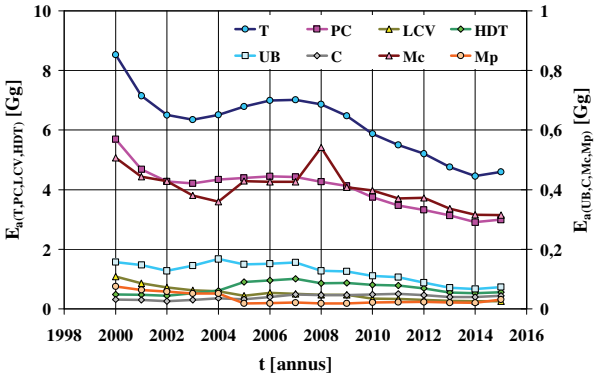


Fig. 12. National annual emission of methane per cumulated vehicle category

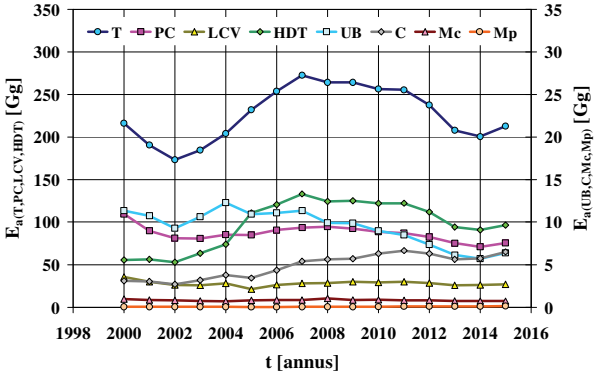


Fig. 13. National annual emission of nitrogen oxides per cumulated vehicle category

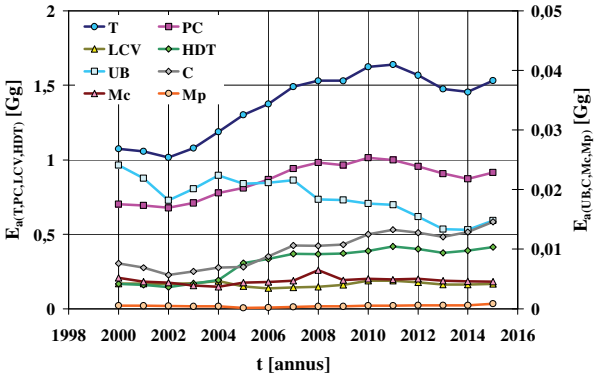


Fig. 14. National annual emission of nitrous oxide per cumulated vehicle category

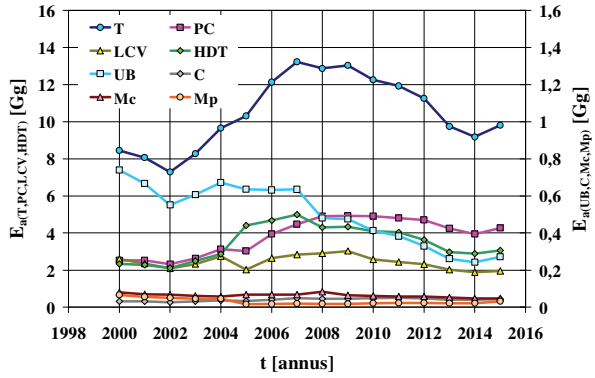


Fig. 15. National annual emission of particulate matter PM2.5 from tribological elements per cumulated vehicle category

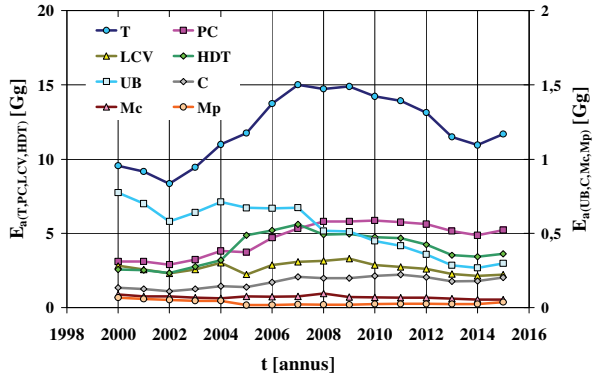


Fig. 16. National annual emission of particulate matter PM10 from tribological elements per cumulated vehicle category

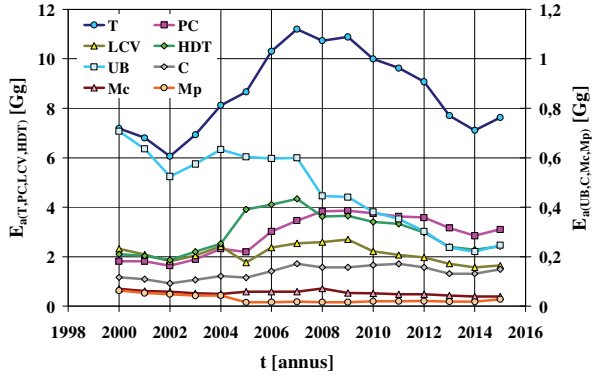


Fig. 17. National annual emission of particulate matter from the exhaust system of internal combustion engines per cumulated vehicle category

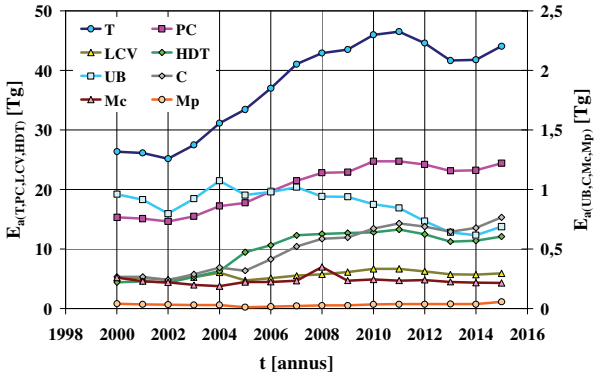


Fig. 18. National annual emission of carbon dioxide per cumulated vehicle category

Figure 19 shows the relative national annual emission of individual pollutants from all motor vehicles, versus the national annual emission in 2000.

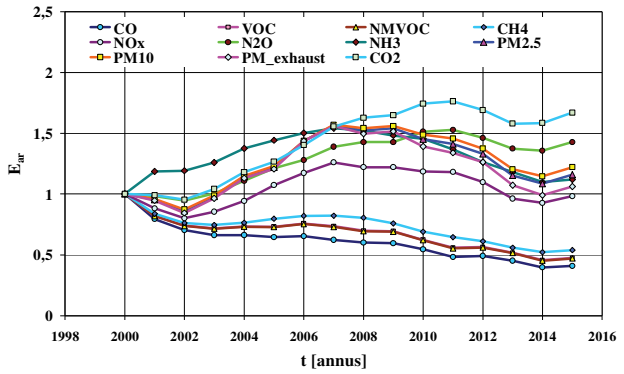


Fig. 19. Relative national annual emission of individual pollutants

In figure 20, there is presented the relative national annual emission of individual pollutants from one conventional motor vehicle, versus the national annual emission in 2000.

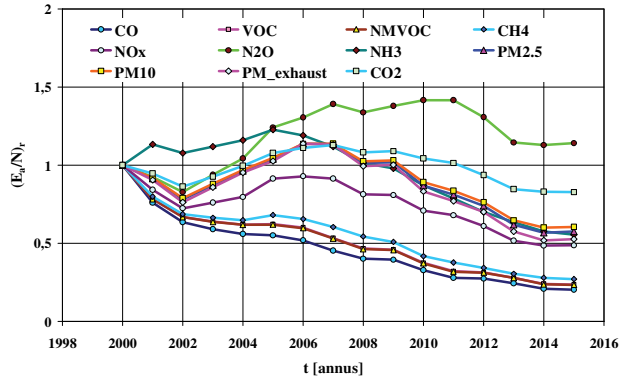


Fig. 20. Relative national annual emission of individual pollutants from one conventional motor vehicle

It is clear from Figures 19 and 20 how significant progress has been made in the field of automotive environmental protection. The greatest progress is for the emission of carbon monoxide and volatile organic compounds. It is also important to see a positive trend for carbon dioxide emissions.

4. Conclusions

Based on the study results presented above, the following conclusions can be drawn:

1. For the majority of harmful substances, the emission of which is limited by European regulations, there is a clear trend of decreasing national annual emission for subsequent years of inventory, although the number of vehicles and the intensity of their use have been considerably increasing. This trend is especially pronounced for carbon monoxide and volatile organic compounds. In the case of nitrogen oxides and particulate matter, the tendency for domestic annual emission to decline is from around 2007.
2. In the case of substances, the emission of which is not limited by European regulations, the increase in national annual emission is mainly attributed to nitrous oxide. In addition, the national annual carbon dioxide emission increased until 2011 and, since that time, there were minor changes. This emission is directly related to the consumption of motor fuels.
3. The relative national emission from one conventional motor vehicle shows a clear declining trend since 2006. This results from technological progress in the development of new constructions of motor vehicles.

On the basis of the experience gained with the inventory of pollutants from motor vehicles in Poland, in the years 2000–2015, the COPERT 4 software is an effective tool to support the study of pollutant emission from road transport. The most serious problem of modelling total emission from road transport is the determination of the intensity of use of motor vehicles classified to respective categories and the identification of their traffic patterns.

Nomenclature

C	coaches
CH_4	methane
CI	compression ignition
CO	carbon monoxide
E_a	national annual emission
H	highway
HDT	heavy duty trucks
HDT-A	heavy duty trucks – articulated
HDT-R	heavy duty trucks – rigid
LCV	light commercial vehicles
LCV-CI	light commercial vehicles – compression ignition (engine)
LCV-SI	light commercial vehicles – spark ignition (engine)
Mc	motorcycles
Mp	mopeds
N	number of vehicles per cumulated category
p	annual mileage of vehicles per cumulated category
PC-SI	passenger cars – spark ignition (engine)
PC-SI-G	passenger cars – spark ignition – gasoline
PC-SI-G	passenger cars – spark ignition – liquefied petroleum gas
R	rural
SI	spark ignition
T	total (vehicles)
t	time
u	share of mileage of vehicles per cumulated category under model traffic conditions
U	urban
UB	urban buses
v	average velocity of vehicles per cumulated category
VOC	volatile organic compounds

N	number of motor vehicles
N_2O	nitrous oxide
NH_3	ammonia
NMVOC	non-methane volatile organic compounds
NO_x	nitrogen oxides
PC	passenger cars
PC-CI	passenger cars – compression ignition (engine)
$PM_{exhaust}$	particular matter from exhaust system
PM10	particular matter PM10 from tribological elements of a vehicle
PM2.5	particular matter PM2.5 from tribological elements of a vehicle

Bibliography

[1] BEBKIEWICZ, K., CHŁOPEK, Z., SZCZEPAŃSKI, K., ZIMAKOWSKA-LASKOWSKA, M. Results of air emission inventory from road transport in Poland in 2014. *Proceedings of the Institute of Vehicles*. 2017, **1**(110), 77-88.

[2] BEBKIEWICZ, K., CHŁOPEK, Z., SZCZEPAŃSKI, K., ZIMAKOWSKA-LASKOWSKA, M. The influence of the properties of vehicles traffic on the total pollutant emission. *Proceedings of the Institute of Vehicles*. 2017, **1**(110), 89-102.

[3] BEBKIEWICZ, K., CHŁOPEK, Z., SZCZEPAŃSKI, K., ZIMAKOWSKA-LASKOWSKA, M. Issues of modeling the total pollutant emission from vehicles. *Proceedings of the Institute of Vehicles*. 2017, **1**(110), 103-118.

[4] BUWAL (Bundesamt für Umwelt, Wald und Landschaft), INFRAS AG (Infrastruktur-, Umwelt- und Wirtschaftsberatung). Luftschadstoffemissionen des Strassenverkehrs 1950–2010. BUWAL-Bericht Nr. **255**, 1995.

[5] CHŁOPEK, Z., WAŚKIEWICZ, J. The forecast of the pollutant emission from automotive internal combustion engines in Poland by 2030. *VI International Congress of Internal Engines*. Combustion Engines 2015.

[6] CHŁOPEK, Z. Zasady modelowania zużycia paliwa i energii oraz emisji zanieczyszczeń związanych z użytkowaniem pojazdów drogowych. *Technika Transportu Szynowego*. 2015, **12**, 262-267.

[7] COPERT Training 5. COPERT 5 vs COPERT 4. European Environment Agency. 2016. emisia.com/sites/default/files/COPERT_5_features.pdf (accessed 2016.12.06).

[8] EMEP/EEA air pollutant emission inventory guidebook – 2016. European Environment Agency. www.eea.europa.eu/publications/emep-eea-guidebook-2016 (accessed 2016.12.06).

[9] GKATZOFLIAS, D., KOURIDIS, CH., NTZIACHRISTOS, L., SAMARAS, Z. COPERT 4 Computer programme to calculate emissons from road transport User manual (version 9.0). European Environment Agency. Emisia SA. 2012. (accessed 2016.12.06).

[10] INFRAS AG. Handbook emission factors for road transport 3.2. Quick reference. Version 3.2. Bern, 2014.

[11] 2006 IPCC Guidelines for National Greenhouse Gas Inventories. www.ipcc-nggip.iges.or.jp/public/2006gl /vol2.html. (accessed 2016.12.06).

Katarzyna Bebkiewicz, MEng. – Institute of Environmental Protection – National Research Institute in Warsaw.

e-mail: *Katarzyna.Bebkiewicz@kobize.pl*



Krystian Szczepański, DSc., DEng. – Institute of Environmental Protection – National Research Institute in Warsaw.

e-mail: *Krystian.Szczepanski@ios.edu.pl*



Prof. Zdzisław Chłopek, DSc., DEng. – Institute of Environmental Protection – National Research Institute in Warsaw.

e-mail: *Zdzislaw.Chlopek@kobize.pl*



Magdalena Zimakowska-Laskowska, DSc., DEng. – Institute of Environmental Protection – National Research Institute in Warsaw.

e-mail: *Magdalena.Zimakowska-Laskowska @kobize.pl*



Article citation info:
SZRAMA, S., KADZIŃSKI, A. Hazard identification process in the selected analysis domain of the F100 turbofan engines maintenance system. *Combustion Engines*. 2017, **171**(4), 68-73. DOI: 10.19206/CE-2017-412

Sławomir SZRAMA
Adam KADZIŃSKI

CE-2017-412

Hazard identification process in the selected analysis domain of the F100 turbofan engines maintenance system

The multirole F-16 is the most advanced aircraft in the Polish Air Forces. It has been equipped with the very modern, sophisticated and advanced turbofan engine F100-PW-229. Due to the fact, that there is only one engine, its reliability, durability efficiency and performance are the crucial factors for the safety reasons. In the article authors researched maintenance system of the F100 turbofan engines, which are built on the multirole F-16 aircraft. For the study purposes F100 maintenance system model has been created. From this model, the main analysis domain was derived, comprising "Major engine objects discrepancies removal" process. Considering such an analysis domain, on the basis of the schematic diagram of the hazard identification process, authors presented the following procedures: tools preparation for the hazard sources identification, hazard sources identification, hazard sources grouping and hazards formulation. The main goal of this article was to provide hazard identification process results as hazard specifications, which include: a group of hazard sources, hazards formulation and the most probable/predictable consequences, severities and losses/harms of the hazard activation.

Key words: hazard source, hazard, hazard identification, risk management, F100 turbofan engine, maintenance system

1. Introduction

The F-16C/D Block 52 is powered by the Pratt & Whitney F100-PW-229 low-bypass, high compression ratio, fully ducted, twin–spool turbofan engine with an annular combustor and a mixed flow augmentor.

The F100-PW-229 engine general specifications are:

- Thrust
  - Maximum rating (augmented operation) = 29,100 lbs. (129.4 kN)
  - Intermediate rating (non-augmented operation) = 17,800 lbs. (79.2 kN)
- Weight
  - F-15; 3,784 lbs. (1,716 kg)
  - F-16; 3,819 lbs. (1,732 kg)
- Length
  - 208 in. (5.28 m)
- Diameter
  - Inlet diameter = 34.8 in. (0.88 m)
  - Maximum diameter = 46.5 in. (1.18 m)
- Bypass ratio = 0.36:1
- Overall pressure ratio = 32:1

The engine is also equipped with a full length annular duct and a variable convergent/divergent exhaust nozzle. It also incorporates variable vanes at the inlet of both compressors and a variable exhaust nozzle. The major rotating sections are supported by five main bearings.

The F100-PW-229 engine is designed to maximize its performance. Some features are:

- High thrust to weight ratio
  - 29,100 lbs./3,800 lbs. = 7.7:1
- Variable vanes
  - Compressor inlet variable vanes (CIVV)
  - Rear compressor variable vanes (RCVV)
- Fully ducted engine
- Mixed flow augmentor
  - Mixes core air flow with bypass air flow
- Variable exhaust nozzle

The engine is constructed using the modular concept, allowing the removal of functionally and physically associated parts as units, called modules.

The modular concept helps increase maintainability by:

- Allows removal of parts as units (modules).
- Allows replacement of unserviceable modules with serviceable modules.
- Allows rapid return of the engine and modules to service.

The modular concept does not prevent replacement of subassemblies or parts when replacement is the most effective repair method. Designed with the modular concept, the engine consists of the five modules (Fig. 1):

1. Inlet fan module
2. Core engine module
3. Fan drive turbine module
4. Augmentor duct and nozzle module
5. Gearbox module.

2. Engine maintenance system model as an aggregated analysis domain

The purpose of the engine maintenance system is to assess the F100-PW-229 engines powering the PLAF F-16 aircraft for serviceability and safety of flight.

The F100 family of engines has been designed to be maintained using three levels of maintenance explained in this section. Engine maintenance system is based on Modular Maintenance Concept.

F100 engine comprises of five major modules:

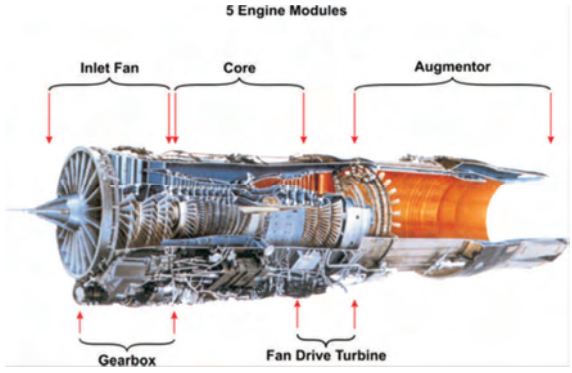


Fig. 1. F100 engine design structure [1]

The whole maintenance concept is organized in the way, which is based on the main idea that 97% of non-overhaul maintenance should be completed at the base – Fig. 2.

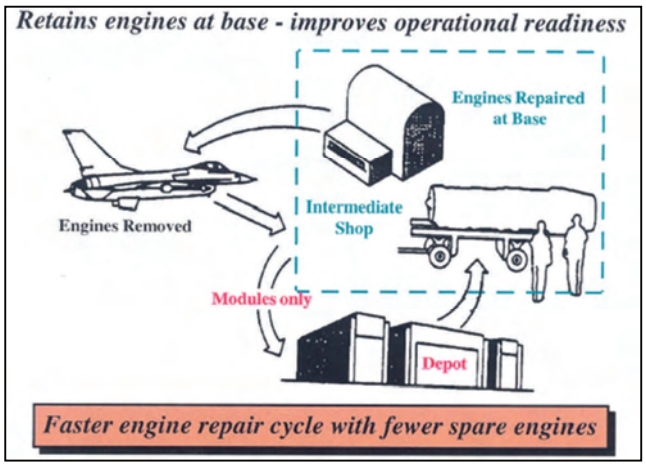


Fig. 2. Engine maintenance concept model

The main reason for such an arrangement is to keep as many engines and engine modules, as well as engine LRUs (Line replaceable units) on base, available for the fast discrepancy removal. Immediate removal and replacement of the engine broken object is the key element for the engine operational readiness and aircraft mission capability rate. To summarize, we are able to distinguish three different engine maintenance levels (Fig. 3).

I. Organizational (O) – Level, Flightline Maintenance

Maintenance repairs and inspections with engine installed in aircraft:

– Engine servicing
– Replacement of line replaceable units (LRU)

Main aspects of this level are:

– significant on-wing maintenance and troubleshooting
– easy access for routine maintenance
– Engine Maintenance & Monitoring System (EMMS) or Engine Maintenance & Tracking Systems (EMATS)
– fast line replaceable unit (LRU) replacement
– state of the art engine fault system identifies problems quickly to ensure operational safety

II. Intermediate (I) – Level, Base Engine Shop

Maintenance repair of engines and modules that cannot be repaired with engine installed in aircraft.

Main aspects of this level are:

– return to service by module replacement reduces engine down time
– simple and quick engine testing
– avionics shop and jet engine intermediate maintenance (JEIM) shop can maintain controls
– engine design maximizes base-level repair ability
– I-level maintenance arranged around horizontal repair and vertical (modular) maintenance.

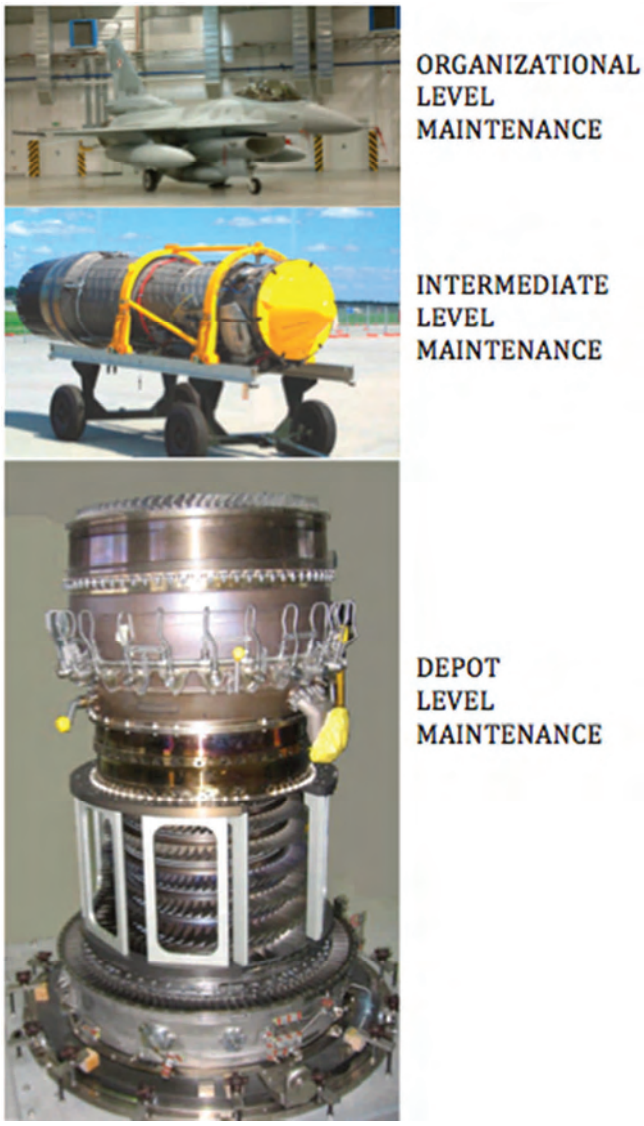


Fig. 3. Levels of maintenance

This type of maintenance could be divided into two sections:

1. Horizontal engine discrepancies removal (Fig. 4)
2. Vertical engine/module repair (Fig. 5)

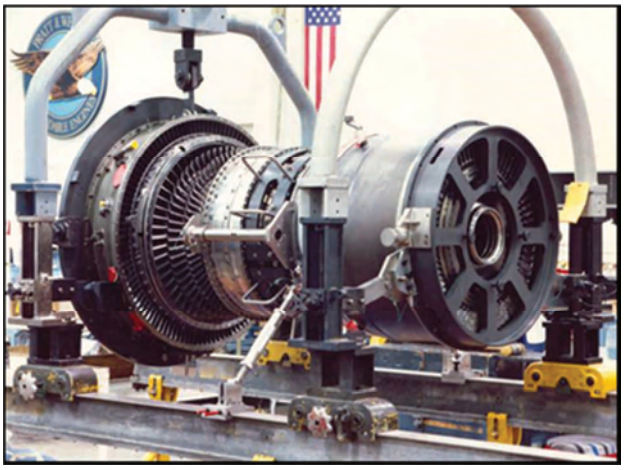


Fig. 4. Horizontal repair section



Fig. 5. Vertical repair section

III. Depot (D) – Level – Centralized Engine/Module Repair

Repairs that cannot be made at either Organizational or Intermediate maintenance levels. Specialized tools are required for component and parts repair.

Main aspects of this level are:

– comprehensive engine/module repair and overhaul beyond capability at I-level
– customer controls fleet maintenance and depot/repair options based on:
  - Flying/utilization trends
  - Fleet size
  - Annual budgets
  - Utilizing established depot & repair infrastructure
  - Applying Material Management Program
  - Leveraging in-country organic capabilities

3.Hazard identification

In order to identify hazards, hazard sources we should try to recognize what are the most common undesired events as far as the engine maintenance is concerned. The main events being tracked by all the international safety management personnel and engine manufacturers are:

1. F100 ENGINE RELATED LOSS OF AIRCRAFT (ERLOA)
2. NON-RECOVERABLE IN FLIGHT SHUTDOWN NRIFSD
3. IN FLIGHT SHUTDOWNS (IFSD)

Authors of this article researched F100-PW-229 engine maintenance system and analyzed this area of interest as a combination of three elements: human-hardware-environment. Considering all the relations between these elements we could identify single or multiple hazard sources. In this case the F100 engine maintenance system has been presented as an aggregated analysis domain model in order to implement procedures into the hazard identification process. This aggregated analysis domain is a combination of the three domains (Fig. 3), where hazards could be generated as a result of the maintenance processed performed at different levels of the F100 engine maintenance system.

For the study purposes, analysis domain 2 has been selected, representing second level of the engine maintenance system (engine intermediate level maintenance). One of the main maintenance processes performed at this level is major engine objects discrepancies removal. In this article this process is an area of the hazard identification. The selected process consists of the eleven following steps:

1. Engine receiving inspection
2. Pre-test cell engine mount
3. Engine/LRU preservation (engine run on TC)
4. Broken module removal (Gearbox, Augmentor, Fan, Core, LPT)
5. Modules/LRU inspections
6. Spare module installation
7. Engine Final assembly
8. Pre-test cell inspections
9. Pre-test cell engine mount
10. Test cell run
11. Engine Final Inspection

In this article, due to complexity of the F100 turbofan engine, authors considered only one process of the major engine object discrepancy removal. The main reason for the following research was that aircraft crew chief reported engine oil leakage during postflight inspection. After borescope inspection it was determined that this leakage is beyond acceptable limits.

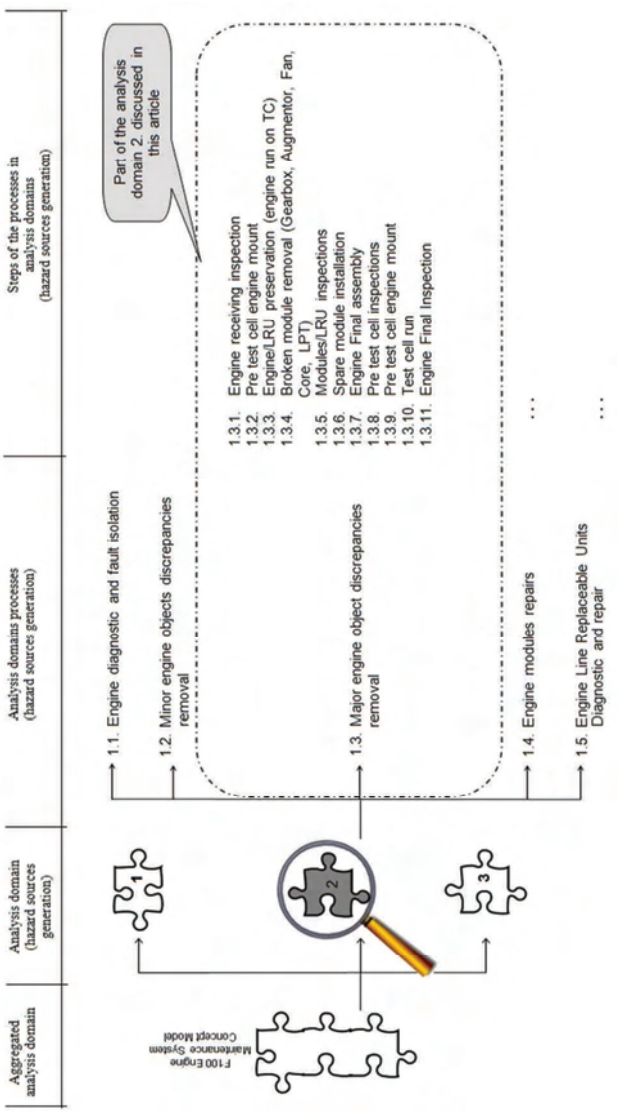


Fig. 6. Detailed schematic diagram of the aggregated analysis domain structure (detailed: Analysis domain 2. – Engine Intermediate level maintenance) being the model of the F100 engine maintenance system

4. Hazard sources identification

Hazard sources identification in the selected analysis domain is being conducted in accordance with the procedures of the forward hazard identification process. The list of the selected identified hazard sources within process 1.3 (major engine object discrepancies removal) is presented in Table 1.

Table 1. List of the selected identified hazard sources in the analysis domain (Engine Intermediate level maintenance) within process 1.3 (major engine objects discrepancies removal) – Fig. 3 and 6

No.	Identified hazard sources
-1-	-2-
1. HAZARD SOURCES LIST – STEP 1 OF THE PROCESS 1.3 (Fig. 6)	
<1.1>	Engine technician performing receiving inspection neglects other engine objects and does not identify other broken objects.
<1.2>	Engine technician performing inspection leaves tool in the engine nozzle.
<1.3>	Engine technician performing receiving inspection does not identify broken blades in the LPT (Low Pressure Turbine)
<1.4>	Engine technician uses broken light source during borescope inspection does not identify chaffing fuel tube in the combustion chamber.
<1.5>	Engine technician performs receiving inspection neglects chaffing clamps on the fuel tubes.
<1.6>	Engine technician using pliers accidentally cuts engine harness and damages signal wire to DEEC.
<1.7>	Engine technician uses outdated technical documentation without new safety and crucial inspections
<1.8>	Engine technician using broken borescope is unable to identify eroded turbine blades.
. . .	. . .
2. HAZARD SOURCES LIST – STEP 2 OF THE PROCESS 1.3 (Fig. 6)	
<2.1>	Engine technicians improperly mount engine on the T4000 trolley
<2.2>	Engine technician do not perform any safety position papers on engine
<2.3>	Engine technician leaves FOD inside engine
<2.4>	Engine technician does not torque fuel tube nut bolt
. . .	. . .
3. HAZARD SOURCES LIST – STEP 3 OF THE PROCESS 1.3 (Fig. 6)	
<3.1>	Engine technician neglect unusual noise from HPT
<3.2>	Fire suppression system in the test cell is not working
<3.3>	Engine technician does not notice fuel leak
<3.4>	Engine technician does not notice oil leak
<3.5>	Communication fail between test cell operator and engine technician
. . .	. . .
4. HAZARD SOURCES LIST – STEP 4 OF THE PROCESS 1.3 (Fig. 6)	
<4.1>	Engine technician uses broken crane to remove module
<4.2>	Engine technician is unable to operate crane
<4.3>	Engine technician uses broken hydraulic wrench to disassembly engine modules
<4.4>	Engine technician does not use IETM documentation while modules removing
<4.5>	Engine technician unable to use technical documentation properly
. . .	. . .
5. HAZARD SOURCES LIST – STEP 5 OF THE PROCESS 1.3 (Fig. 6)	
<5.1>	Engine technician roughly inspects augmentor liner
<5.2>	Engine technician does not notice No3 bearing seal damaged
<5.3>	Engine technician leaves nuts on MFC not safety wired
<5.4>	Engine technician is unable to identify augmentor burn through
<5.5>	Engine technician does not notice cracked LPT blade
. . .	. . .
6. HAZARD SOURCES LIST – STEP 6 OF THE PROCESS 1.3 (Fig. 6)	
<6.1>	Engine technician does not inspect spare core module assuming it is airworthy because returned from depot
<6.2>	Engine technician uses broken heating device to mount module
<6.3>	Engine technician neglects 4th stage vane turned installing spare module
. . .	. . .
7. HAZARD SOURCES LIST – STEP 7 OF THE PROCESS 1.3 (Fig. 6)	
<7.1>	Engine technician mount improper seal on the oil tube
<7.2>	Engine technician does not torque nuts on oil tubes.
<7.3>	Engine technician uses broken swine wrench to torque modules
<7.4>	Engine technician neglects improper air flow and vacuum checks due to lack of time
<7.5>	Engine supervisor does not verify proper engine final assembly
. . .	. . .
8. HAZARD SOURCES LIST – STEP 8 OF THE PROCESS 1.3 (Fig. 6)	
<8.1>	Engine pre test cell inspection performed quickly and roughly
. . .	. . .
9. HAZARD SOURCES LIST – STEP 9 OF THE PROCESS 1.3 (Fig. 6)	
<9.1>	Engine technician use broken test cell trolley T4000
<9.2>	Engine technician does not verify engine thrust pins and install old and cracked ones.
. . .	. . .
10. HAZARD SOURCES LIST – STEP 10 OF THE PROCESS 1.3 (Fig. 6)	
<10.1>	Engine operator does not verify engine performance parameters while engine test run
<10.2>	Engine technician neglects unusual noises from the engine core
<10.3>	Engine technician does not respect/follow safety rules during engine run
<10.4>	Engine technician does not notice fuel/oil leaks
. . .	. . .
11. HAZARD SOURCES LIST – STEP 11 OF THE PROCESS 1.3 (Fig. 6)	
<11.1>	Engine technician performs engine final inspection roughly and does not verify oil/fuel leaks
<11.2>	Engine supervisor does not verify engine status
<11.3>	Engine quality assurance verify paper work only without engine verification
. . .	. . .

5. Hazards specification

Hazards specification process is conducted in accordance with the following procedures: hazards sources grouping and hazards formulation.

Hazard sources grouping. This process is based on the previously created list of the hazards sources (Table 1). Not every selected source of the hazard from the list and not every combination of the other hazard sources, generates analysis domain status, where the developed scenario could

result into loss/harm (in this article – engine/aircraft damage, ERLOA, personnel injury, etc). The main goal of the hazard sources grouping procedure is creation of the groups of the hazard sources which could generate such an analysis domain status, where the developed scenario could result into the loos/harm. Results of this process are presented in Table 2 (segment "Hazard sources group H...").

Hazard formulation and predicted loss/harm during hazard activation. In order to formulate hazards, we select a group of the hazard sources which creates a certain analysis domain status might result into the loss/harm. Hazard formulation should express fear of the potential loss/harm (caused by undesired side effects) like for instance: NRIFSD, ENG Thrust Loss, Compressor STALL, Engine Exhaust Fire, FOD/DOD, Engine Throttle malfunction, etc.). Some proposed results of the hazard formulation procedure with the predicted loss caused by their activation are presented in Table 2, in the following segments: "Hazard formulation…", "Predicted loss/harm caused by hazard activation".

Table 2. Final results of the selected hazards specification process generated in analysis domain 2, within process 1.3 (major engine objects discrepancies removal) – own elaboration

Hazard H1
Hazard sources group H1 1. Engine technician uses broken light source during borescope inspection does not identify chaffing fuel tube in the combustion chamber. <1.4> 2. Engine technician performs receiving inspection neglects chaffing clamps on the fuel tubes. <1.5> 3. Engine technician does not notice fuel leak. <3.3> 4. Engine technician performs engine final inspection roughly and does not verify oil/fuel leaks. <11.1> 5. Engine supervisor does not verify engine status <11.2>
Hazard formulation H1 Hazard of loss resulting from fact, that engine fuel leak appears during flight and was not identified during engine discrepancy removal.
Predicted loss/harm during H1 hazard activation Loss resulting from engine inflight fire.
Hazard H2
Hazard sources group H2 1. Engine technician using broken borescope is unable to identify eroded turbine blades. <1.8> 2. Engine technician does not notice cracked LPT blade. <5.5> 3. Engine supervisor does not verify engine status
Hazard formulation H2 Hazard resulting from the fact that one of the Low Pressure Turbine blades cracks and tears off.
Predicted loss/harm during H2 hazard activation Loss resulting from the turbine damage.
Hazard H3
Hazard sources group H3 1. Engine technician does not notice oil leak. <3.4> 2. Engine technician does not torque nuts on oil tubes. <7.2> 3. Engine technician performs engine final inspection roughly and does not verify oil leaks <11.1> 4. Engine quality assurance verify paper work only without engine verification. <11.3>
Hazard formulation H3 Hazard of loss resulting from the fact that engine oil leak appears during flight and engine bearings lubrication system failure .
Predicted loss/harm during H3 hazard activation Loss resulting from the fact, that engine seizures up.
Hazard H4
Hazard sources group H4 1. Engine technician performs receiving inspection neglects chaffing clamps on the fuel tubes. <1.5> 2. Engine technician uses broken light source during borescope inspection does not identify chaffing fuel tube in the combustion chamber. <1.4> 3. Engine technician does not notice fuel leak. <3.3> 4. Engine technician performs engine final inspection roughly and does not verify oil/fuel leaks. <11.1> 5. Engine supervisor does not verify engine status <11.2> 6. Engine quality assurance verify paper work only without engine verification. <11.3>
Hazard formulation H4 Hazard of loss resulting from the fact that fuel leaks and does not reach combustion chamber.
Predicted loss/harm during H4 hazard activation Loss resulting from the NRIFSD
Hazard H5
Hazard sources group H5 1. Engine technician does not verify engine thrust pins and install old and cracked ones. <9.2> 2. Engine technician does not respect/follow safety rules during engine run. <10.3>
Hazard formulation H5 Hazard of loss resulting from the fact, that engine thrust pins were not inspected by engine technician and were cracked.
Predicted loss/harm during H5 hazard activation Loss resulting from the facts, that during engine high power tests in the test cell, engine liberated from the trolley and was severely damaged .
Hazard H6
Hazard sources group H6 1. Engine technician performing receiving inspection neglects other engine objects and does not identify other broken objects. <1.1> 2. Engine supervisor does not verify proper engine final assembly. <7.5> 3. Engine operator does not verify engine performance parameters while engine test run. <10.1> 4. Engine supervisor does not verify engine status. <11.2> 5. Engine quality assurance verify paper work only without engine verification. <11.3>
Hazard formulation H6 Hazard of loss resulting from the fact, that engine throttle malfunction was not identified.
Predicted loss/harm during H6 hazard activation Loss resulting from the engine throttle malfunction and ERLOA

6. Summary

Pratt&Whithey engine F100-PW-229 powering polish F-16Block 52+ is a very modern and advanced engine. However, due to its high power and very low intake, it is very vulnerable to the so-called FOD Foreign Object Damage. Engine and engine components repairs and overhauls on base level is the unprecedented situation in the Polish Air Forces. Military technicians responsible for this task must be aware of the hazards concerned with the engine maintenance processes. In this article authors selected intermediate level maintenance as an analysis domain and identified hazards generating such an analysis domain, which could result into the loss or harm. The main goal of this article was to show maintenance management personnel main hazards sources within engine maintenance processes. Elimination of these hazards sources directly affects F-16 safety system.

Nomenclature

DEEC	digital engine electronic controller
LRU	line replaceable unit
ERLOA	engine related loss of aircraft
TCTO	time compliance technical order
EMMS	engine maintenance & monitoring system
EMATS	engine maintenance & tracking systems
HPT	high pressure turbine
TC	engine test cell
IETM	interactive engine electronic technical manual
MFC	main fuel controller
FOD	foreign object damage
DOD	domestic object damage
LPT	low pressure turbine
NRIFSD	non-recoverable in flight shutdown
PEER	periodic engineering excellence review
MAP	maintenance awareness program

Bibliography

[1] LOCKHEED MARTIN STM 16-329PL (Poland Block 52) F100-PW-229 POWER PLANT.
[2] Biuletyn Eksploatacyjny, 2006, praca zbiorowa, Nr P/O/R/U/4901/E/2006, dotyczy: eksploatacji samolotu F-16.
[3] F100-PW-229 Periodic Engineering Excellence Reviev.
[4] KADZIŃSKI, A. Studium wybranych aspektów niezawodności systemów oraz obiektów pojazdów szynowych. *Wyd. Politechniki Poznańskiej*, seria Rozprawy. 2013, **511**.
[5] Szczegółowe zasady funkcjonowania służby inżynieryjno-lotniczej w JW1156.
[6] Technical Manual T.O.00-20-1 Aerospace Equipment Maintenance Inspections, Documentation, Policies and procedures.

Sławomir Szrama, MEng. – Squadron Commander at 31st Air Force Base Poznań-Krzesiny.

e-mail: *S.Szrama@ron.mil.pl*



Adam Kadziński, DSc., DEng. – Faculty of Mechanical and Transport Engineering at University of Technology.

e-mail: *Adam.Kadzinski@put.poznan.pl*



Article citation info:
KROPIWNICKI, J., DOMINICZAK, P., KNEBA, Z. et al. Analysis of the possibilities of using of DME fuel in motor boat drive systems. *Combustion Engines*. 2017, **171**(4), 74-80. DOI: 10.19206/CE-2017-413

Jacek KROPIWNICKI
Przemysław DOMINICZAK
Zbigniew KNEBA
Sławomir MAKOWSKI
Janusz T. CIEŚLIŃSKI
Maciej ZIÓŁKOWSKI

CE-2017-413

Analysis of the possibilities of using of DME fuel in motor boat drive systems

The characteristics of alternative fuel for diesel: dimethyl ether (DME) and an analysis of the potential to reduce emissions of toxic compounds by the engines when running on this fuel have been presented in this work. Basic types of design solutions of gas supply and control systems, possible for use in internal combustion engines with DME supply have been also presented. The paper presents a study of the legislation and an analysis of the feasibility of the system storage and fueling DME on board small vessels.

Key words: *internal combustion engines, dimethyl-ether (DME), alternative fuel, emission reduction, fuel storage on board small vessels*

1. DME properties as a potential alternative fuel for CI engines

Dimethyl ether (DME) is a chemical compound with a formula of $CH_3–O–CH_3$. Under standard atmospheric conditions (0.1 MPa at 298 K) DME is in gaseous state, it is invisible, non-toxic, odorless, environmentally benign and causes no negative health effects. When it is pressurized above 0.5 MPa or cooled under 248 K (–25°C), it condenses to the liquid phase. The key properties of DME, in comparison to the diesel fuel are shown in Table 1.

Table 1. The key properties of DME [1, 6, 11, 13]

Property (unit/condition)	Unit	DME	Diesel fuel
Chemical structure	–	$CH_3–O–CH_3$	–
Molar mass	g/mol	46	170
Carbon content mass	%	52.2	86
Hydrogen content mass	%	13	14
Oxygen content mass	%	34.8	0
Carbon-to-hydrogen ratio	–	0.337	0.516
Critical temperature	K	400	708
Critical pressure	MPa	5.37	3
Critical density	kg/m^3	259	–
Liquid density	kg/m^3	667	831
Relative gas density (air = 1)	–	1.59	–
Cetane number	–	> 55	40–50
Auto-ignition temperature	K	508	523
Stoichiometric air/fuel mass ratio	–	9	14.6
Boiling point at 1 atm	K	248.1	450–643
Enthalpy of vaporization	kJ/kg	467.13	300
Lower heating value	MJ/kg	27.6	42.5
Gaseous specific heat capacity	kJ/kgK	2.99	1.7
Ignition limits vol.	% in air	3.4–17	0.6–7.5
Minimum ignition energy	mJ	0.29	–
Kinematic viscosity of liquid	cSt	< 0.1	3
Vapour pressure (at 298 K)	kPa	530	10

Such properties as high cetane number and low auto-ignition temperature predestine DME to be an alternative fuel for CI engines (neat or mixed with other fuels). DME can be produced from natural gas, crude oil, residual oil, coal, waste products and biomass and may be considered as bio-fuel of second generation. There are two production methods of DME [7]:

- de-hydrogeneration of methanol,
- direct conversion from synthesis gas (syngas) which is a mixture of hydrogen (H_2), carbon monoxide (CO) and carbon dioxide (CO_2).

The well-to-wheels energy efficiency of DME fueled vehicles is projected to be in the interval (19–22.5)% [1]. This is comparable to compressed natural gas (CNG) fueled vehicles but less than in the case of direct injection (DI) diesels (26%). Due to the low carbon to hydrogen ratio of the DME, the well-to wheel carbon dioxide (CO_2) emissions of DME fueled vehicles are comparable to those using DI diesels.

Advantages of DME fuel

- High oxygen content: together with the absence of C–C bonds in the molecules it is a cause for its practically smokeless combustion which is one of the most important advantages of DME.
- Low boiling point temperature: leads to quick evaporation when liquid-phase DME spray is injected into the engine cylinder.
- High latent heat of vaporization: reduces the NO_x emissions due to the internal cooling of combustion chamber (injected liquid DME spray absorbs a lot of heat during evaporation process).
- High cetane number: results from the low auto-ignition temperature and almost instantaneous vaporization. The physical delay of DME is thus much shorter than in the case of conventional fuels. The chemical delay is also shorter, due to the smaller C–O bond energy (359.0 kJ/mol) than that of the C–H bond (410.4 kJ/mol) [13].
- The purity: DME doesn't consists contaminations like sulphur and vanadium.
- Major benefit from this fuel is the big reduction of CO_2 and NO_x and the absence of SO_x.
- The minor pressure that is needed to liquidize DME: 5 bars is needed to liquidize and there is no cooling required.

Disadvantages of DME fuel

- Low heating value: caused by the oxygen content in the molecules, it necessitates injected volume of DME be practically twice as large as in the case of diesel fuel (to deliver the same amount of energy).
- Low modulus of elasticity: the compressibility of DME is four to six time higher than that of diesel in a closed system (which means that the compression work of the high pressure fuel pump is 3.2 times greater [13]) and the compression work of the low pressure fuel pump for DME is greater by up to 10% in an open system [1].
- Lower viscosity than that of diesel fuel may cause leakage within the fuel supply system which relies on small clearances for sealing.
- Low lubricity can cause intensified surface wear of moving parts within the fuel injection system.
- High reactivity and corrosiveness: it is not compatible with most elastomers, the sealing can be achieved with inert material, such as teflon (PTFE).
- High vapor pressure: can be the cause of cavitation and erosion in the fuel system.
- DME can be toxic in great concentrations because it can block O_2 from reaching the lungs, just like CO_2.

2. Engine performance and emissions characteristics with DME fuel

2.1. Particulate matter (PM) emission

Soot is formed in fuel-rich regions (high equivalence ratio) under high temperature conditions (1500–2500 K). The precursors of soot are unsaturated hydrocarbons such as acetylene (C_2H_2), ethylene (C_2H_4) and propargyl (C_3H_3). These soot precursors decrease with an increase in oxygen content and a decrease in direct C–C bonds. It can be concluded that the soot formed in DME combustion should be almost zero at an oxygen content of 35% and no C–C bonds. This implies that DME-fuelled engines would not need a particulate filter in the exhaust aftertreatment system. However, very small amounts of PM emissions are sometimes detected due to fuel additives used to improve lubrication, impurities in the fuel, or the engine lubrication oil.

2.2. NO_x emission

Comparative values of NO_x emissions from DME CI engines and those from diesel fuel vary depending on the engine conditions and the fuel supply system. Some studies found that NO_x emissions are lower, while others reported the opposite [4, 17].

Lower NO_x emission

Some researches reported that DME combustion results in lower NO_x emissions [5, 10] than diesel combustion due to the lower heating value, the higher heat of vaporization, the shorter ignition delay, the smaller amount of fuel injected during the ignition delay period and the smaller amount of fuel burned during the premixed burning phase which results in the lower peak combustion temperature.

Higher NO_x emission

It is possible that higher amount of NO_x can be produced from DME than from diesel fuel for an early start of injection since the duration of the peak temperature would be longer in the initial combustion period due to shorter ignition delay of DME. When injection retardation is optimized for each fuel, NO_x from DME is lower than from diesel fuel [1].

2.3. HC and CO emission

HC emissions from DME are usually lower or equal to those from the combustion of diesel fuel [9, 12, 15]. The over-reach and over-lean mixture regions, which the main source of unburnt hydrocarbons, may be smaller because DME has a short ignition delay period and HC emission can be reduced. DME is an oxygenated fuel containing 35% by mass of oxygen, has good mixing characteristics and is a superheated vapor after entering the combustion chamber. The volume of fuel-reach regions could thus be less, resulting in reduced HC emissions.

The data of CO emissions show some contradictions depending on the engine system and operating conditions. The higher CO emissions sometimes associated with DME could result from the longer injection duration, lower injection pressure and larger spray holes. The lower emissions of CO are linked to the structure of the DME molecule. The low C/H ratio, the lack of C–C bonds and the high oxygen content of the fuel should give faster and more effective oxidation of intermediate species. The HC and CO emissions could easily treated with an oxidation catalyst in the aftertreatment system.

2.4. Non-regulated exhaust emissions

Similarly to other oxygenated fuels, it is likely that some formaldehyde (CH_2O) is formed during the combustion of DME in a CI engine. The formaldehyde emissions could be 1–10% of the non-methane hydrocarbon emissions, but can be reduced by oxidation catalyst to a negligible level.

2.5. Combustion noise

Since ignition delay is shorter for DME than for diesel, the pressure rise during the premixed burning stage is slower which results in reduced combustion noise.

3. Basic types of design solutions of gas supply and control systems

Closed pressurized fuel system are commonly in use: because of the low boiling point of DME (248 K = –25°C), it is a gas under standard atmospheric conditions and therefore must be pressurized in a fuel system, including a storage tank and it is sold like a liquefied gas. Thus, the low boiling point of DME necessitates a closed pressurized fuel system. The vapor pressure of DME, roughly the same as LPG, demands the same kind of handling and storage considerations as for LPG.

The high vapor pressure of DME means that cavitation can take place, which in turn impedes stable fuel-injection operation. It is unavoidable in the fuel-injection equipment using higher pressure.

Although DME is kept in the liquid phase under atmospheric temperature conditions, when pressurized to above 0.5 MPa the fuel-supply pressure (the feed pressure from the storage tank to the fuel pump) must be between 1.2 and 3 MPa to avoid cavitation in the fuel line. This is

not only because of the higher temperatures during engine operation, when the saturated vapor pressure of DME is higher, but also due to dynamic flow effects leading to the formation of vapor zones in the fuel line.

DME vaporizes immediately during injection, due to its low boiling point, even though it is injected as a liquid. Therefore, the high fuel injection pressures, such as 50–150 MPa, used in modern diesel injection systems are not required for DME and there is a consensus that 20–30 MPa is sufficient as long as the required amount of DME can be supplied during the corresponding injection period even at high engine speeds.

Because of its low viscosity, currently available fuel-injection systems are not suitable for DME due to leakage problems. Even at atmospheric conditions the leakage of DME can be significant in regions of small clearance. In heavy-duty engines, leakage along the plungers is more serious than in light-duty engines, where the drive mechanism is engine-oil lubricated. To prevent this, most sealing material made of conventional elastomers should be replaced with anticorrosive material such as Teflon-coated o-rings or PTFE based high-tension sealing components.

Lower DME lubrication than diesel fuel results in wear problems. Lubrication can be improved using up to 2000 ppm of lubricant, e.g. Lubrizol (1000 ppm), Hitec 560 (100 ppm) and Infineum R655 (500 ppm), diesel fuel, dimethyl carbonate (DMC) and fatty acids [1]. The DME injection system is expected to operate at injection pressures not exceeding 30 MPa, while current diesel common rail systems are fitted to DME with lubrication additives at injection pressures up to 55 MPa.

The low liquid density and low calorific value require a higher volume of DME to be injected into the cylinder, compared with that for diesel fuel, 1.8 times the volume of diesel fuel is needed (to supply the same amount of energy), which causes a longer injection period.

The physical properties of DME, in comparison with diesel fuel, causes different characteristics of the needle lift of the injector, flow cavitation in the nozzle orifice was found to play a crucial role in the formation of the emerging from the nozzle spray. Initial tests showed that there can be expected a high rate of leakage of fuel past the nozzle plunger. To avoid leakage to the atmosphere the connection via by-pass return line to the pressurized fuel inlet to the pump can be used. In this way, leakage of DME past the nozzle remained liquefied and is returned to the inlet of the injection pump. A common rail fuel injection system is probably the best solution for a DME powered engines. AVL has developed such a system, which has leakage control with double seals and a purge system.

Two examples of the experimental DME fuel systems with direct injection have been presented subsequently in Fig. 1 and 2. The DME split injection strategy was applied in system presented in Fig. 2. The first DME injection starts at 100 CA BTDC with a quantity of 2.5 mg/cycle. The start of second DME injection is varied around TDC and its quantity was fixed at 1.8 mg/cycle.

Two examples of the experimental DME fuel systems with indirect injection have been presented subsequently in Figs 3 and 4, subsequently with liquid injection before valves and vapor injection before valves. In system shown in Fig. 3 the intake air system should be to form an approximately homogeneous mixture of DME and air. DME would absorb much heat when it is gasified due to its high latent heat of evaporation. Thus an intake heating system must be used to maintain the intake temperature at a constant level.

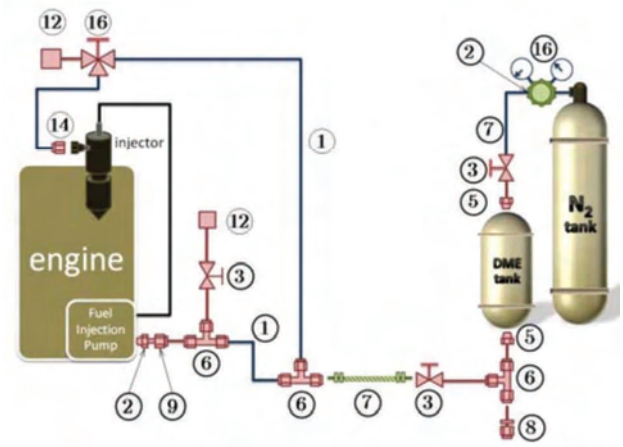


Fig. 1. High pressure direct injection engine test stand 1 – flexible Teflon hose tube adapter, 2 – male connector, 3 – ball valve, 5 – tube adapter, 7 – flexible teflon hose tube adapter [16]

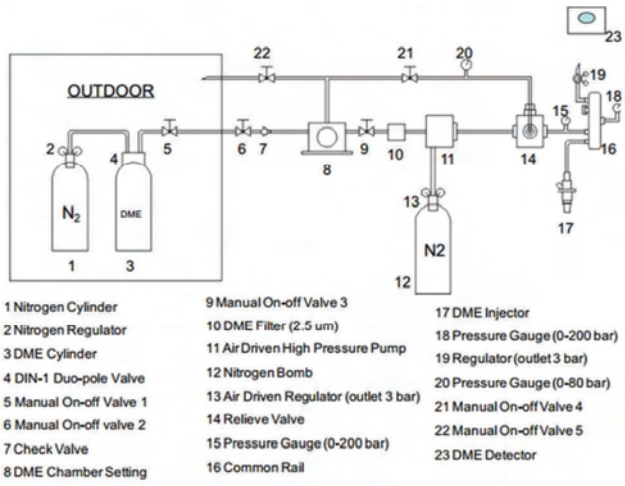


Fig. 2. Experimental test stand for DME direct injection [1]

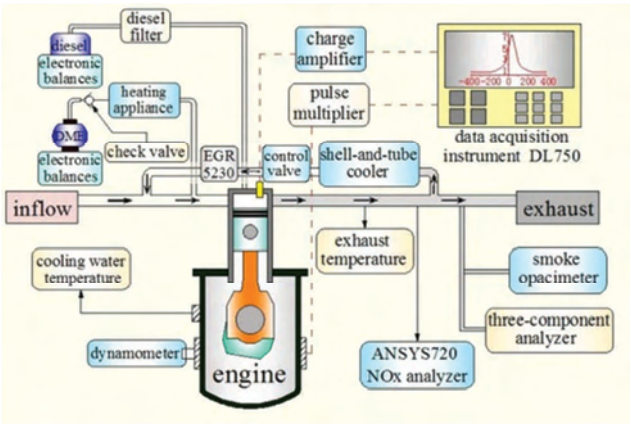


Fig. 3. Experimental DME fuel systems with indirect liquid injection before valves [18]

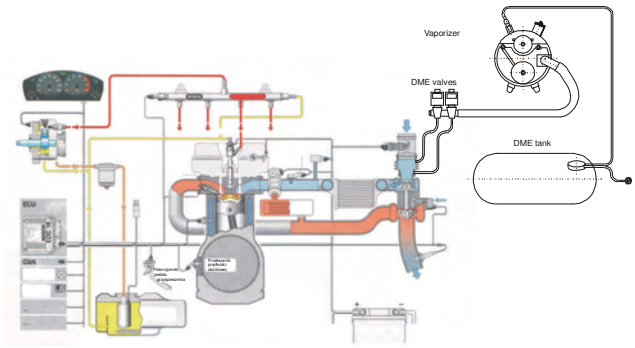


Fig. 4. DME vapor injection

4. Analysis of the requirements for DME safe storage and fueling for vessels

Ships and vessels are subject to the supervision of classification societies. From this reason all matters related to fuel storage and fueling (bunkering) are covered by appropriate rules published by classification societies. In Poland most of vessels, especially inland, are registered by Polish Ship Register. PRS has published following rules for small ships and vessels [14]:

- Rules for the Classification and Construction of Small Sea-going Ships;
- Rules for the Classification and Construction of High Speed Craft;
- Rules for the Classification and Construction of Inland Waterways Vessels;
- Rules for the Classification and Construction of Motor Boats.

Each of above publication include chapter related to Machinery and Piping Systems where all requirements related to fueling systems are described. Those are mainly general rules focused on marine fuels diesel and petroleum. For small ships and vessels gaseous fuels are still not popular, but for big cargo ships – especially gas carriers (LNG or CNG) technologies for engines fueling with gaseous fuels are very well known.

For those ships IMO, the International Maritime Organization which is the United Nations specialized agency with responsibility for the safety and security of shipping and the prevention of marine pollution by ships, has published International Code of Safety for Ship Using Gases or Other Low-flashpoint Fuels (IGF Code) [8]. This regulation is used as the base for all classification societies for new rules elaboration which cover all matters related to gaseous fuels on ships and vessels. IGF Code include all requirements related to usage both gaseous and liquefied gas fuels such as:

- ship/vessel design requirements,
- requirements for gas safe machinery space,
- requirements for ESD (Emergency Shut Down) protected machinery spaces,
- requirements for location and protection of fuel piping,
- liquefied gas fuel containment safety principles,
- design of barriers in relation to tank types,
- filling limit for liquefied gas fuel tanks,
- maintaining fuel storage condition.

The IGF Code is foreseen mostly for big marine ships and for small ships and boats can be used as reverence not as strict rules because the scale of fuel system complicity is quite different. Furthermore the IGF Code is mostly focused on CNG and LNG fuels whereas DME even if its theoretically covered by IGF but there is no strict rules for this particular fuel. That means that use IGF code for DME fueling systems, especially for small vessels, should be pointed mostly to maintain save conditions but some technical requirements could be not feasible for that kind of vessels.

DME is non-carcinogenic, degrades rapidly in the atmosphere and is not a global warming agent. Accidental spills cannot poison water. DME will not sink to the water and it is not absorbed by the soil. It is a gas in ambient conditions and requires a pressure of about 5 bar to stay liquefied, but does not require cryogenic storage. DME is not less safe than the conventional fuels like MGO and HFO. When a tank with DME catches fire, the pressure inside will rise. A safety valve will open and a flame will eject from the tank. The DME is instantly gas and is less harmful. When oil catches fire, it burns but it might explode also. Enough evidence can be found of cars that exploded during fire. This makes DME not necessarily less safe, despite the low flash temperature. This case is well known from automotive usage of LPG, which in case of storage is very similar to DME. Year of operation of cars fueled with LPG show that safe storage and engine fueling is technically well implemented and can be transferred for vessels and DME usage.

Properties of DME described in tab. 1 show that it behaves similar to propane. For that reason DME has more or less the same requirements for handling and storage precautions as LPG. It is stored and transported at ambient temperatures in tanks similar to those used in the propane industry. In terms of infrastructure availability, unlike CNG and LNG, the global propane infrastructure is robust, inexpensive and extensive. Hence, propane distributors can be used for transportation and storage of DME. Also form the point of view of small vessels on board DME fuel installation it will be more similar to propane handling fuel system (Fig. 5).

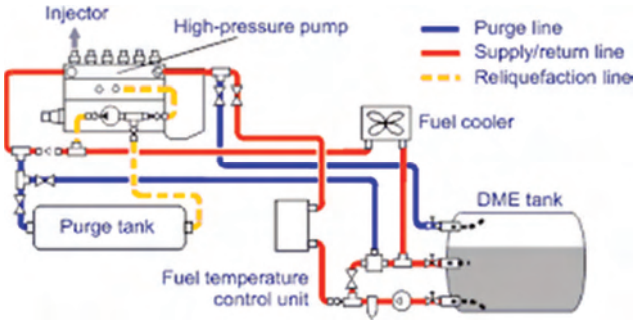


Fig. 5. Example of DME handling fuel system for small vessel [3]

LPG fuel which is very similar to DME is very well known from automotive industry. There are large number of installations for spark ignited engines and also for diesel engines (so called gasdiesel). So the technology is known and very well developed and it should not be very difficult

to transfer knowledge and experience from automotive to marine installations. The biggest difference and also challenges are as follows:

– engineering – in case of regasification, the process needs heat to prevent pressure regulator blocking by frost. In case of outboard engines it is required to deliver the engine heat for cooling system to the pressure regulator. It can be also covered by electric heating system;
– refueling – for bigger vessels with bigger tanks refueling can take lot of time. For this case there should be investigated two possible solutions:
  • development of high-speed filling equipment for DME with capacity of min. 80 L/min to be competitive against existing diesel oil filling speed,
  • development of exchangeable DME storage tanks system;
– safety – in case of automotive applications any leakage of fuel cannot enter inside car because of the natural parameters of liquefied gas and due to the fact that whole fueling installation is located outside of the compartment with the driver and passengers. In case of ships/boats it is impossible to have all fueling system outside the hull. For that reason there is need for more investigation in relation between the real safety, IGF Code requirements and reasonable technical capabilities.

Gas cylinders are designed to be stored and operated in an upright position with their 'on cylinder' valve uppermost. To help prevent damage and leaks they should be kept and used in this way. If cylinders and their associated pipework and fittings can move about too much, those fittings, valves or regulators can quickly become damaged and leak. To reduce the risk of this happening, cylinders and their lockers must be securely stowed. It's recommended that cylinders, cylinder lockers or cylinder housings do not obstruct people moving around the deck or walkway, or interfere with the normal and safe operation of the boat. Cylinders are designed to release excess pressure that can build up if they're exposed to extreme heat. Under these circumstances, gas can quickly find its way into the interior of the boat presenting a significant and immediate risk of fire or explosion (Fig. 6). To minimize the risk of this happening cylinders, cylinder lockers or cylinder housings must not be located near to heat sources. In the event of a fire on board, which causes the cylinders to overheat, an explosion could occur or the cylinder could jet gas onto a fire. To give crew, or the emergency services, a chance to get to the cylinders to remove them they must be readily accessible and movable.

All gas fittings and components between the cylinder and the input side of the gas regulator (which is there to reduce the output pressure of the bottled gas) are classified as the 'high pressure' side of the gas system. Damage here could cause a very rapid and significant burst of gas. To reduce the chances of this gas reaching the interior of the boat the high pressure components must be installed in one of the following locations:

– on the open deck,
– on the cabin top,
– outside the cockpit,
– in a cylinder housing.

If two or more cylinders are used, each high pressure connection must be protected by a non-return valve. This will prevent a high pressure leak occurring when one of the two cylinders is disconnected.

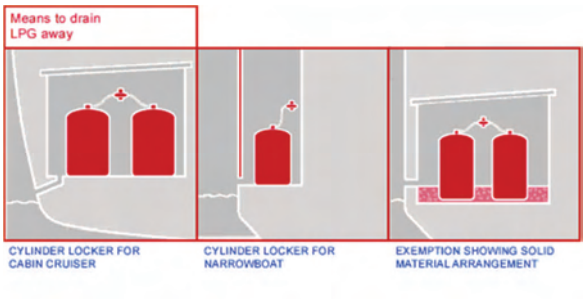


Fig. 6. Ways of draining of fuel leaks [2]

5. Simulation of gas leaking diffusion from installation

Using the computer program Fire Dynamics Simulator (FDS) ver. 6.5.3 the simulation of DME gas leaking diffusion from installation in a 15-meter sailing yacht the Voyager 495-2 has been made. The yacht is equipped with Diesel engine, placed in an engine compartment, which is ventilated by an exhaust fan with a capacity of 150 m^3/h. The scheme of the fuel supply system, in which the motor is equipped is shown in Fig. 4. In the simulation, two variants of leakage were assumed:

– variant I – small leakage due to imperfect installation assembly and faulty seals, leakage occurs in the form of gas, just after the reducer: 0.1 dm^3/h;
– variant II – large leakage due to failure of the fuel delivery system, liquid leakage: 4.8 dm^3/h.

Figure 7 shows a diagram of the engine compartment with the location of the leakage.

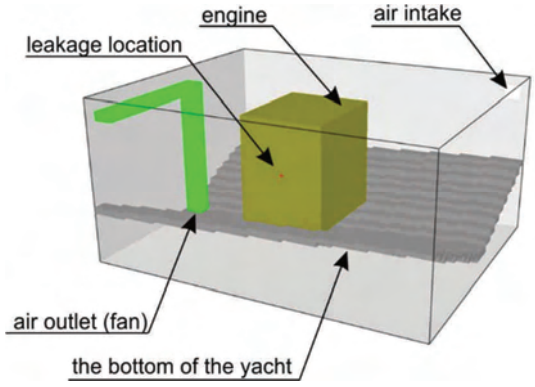


Fig. 7. Diagram of the engine compartment

The simulations concerned the first 120 seconds since gas leakage started. Figures 8 and 9 show the total mass of DME gas accumulated in the engine compartment, respectively for I and II leakage variant. For extrapolated results, the maximum average volumetric gas concentration in the air should not exceed, respectively for variant I and II: $1.90 \cdot 10^{-8}$ % and $2.51 \cdot 10^{-04}$ %, and they are well below the ignition limit.

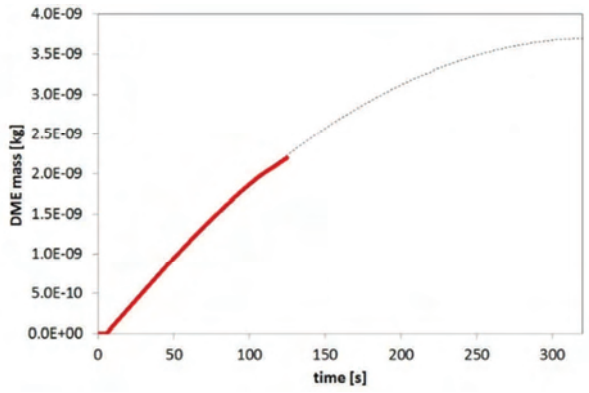


Fig. 8. DME gas accumulation in the engine compartment, leakage variant I

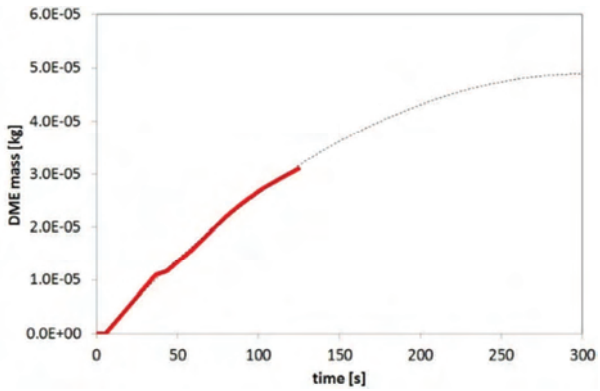


Fig. 9. DME gas accumulation in the engine compartment, leakage variant II

Locally, DME concentrations in the air can be significantly higher, but for the first 120 seconds of the test (Fig. 10 and 11), no dangerous levels were reached in any of the controlled sections.

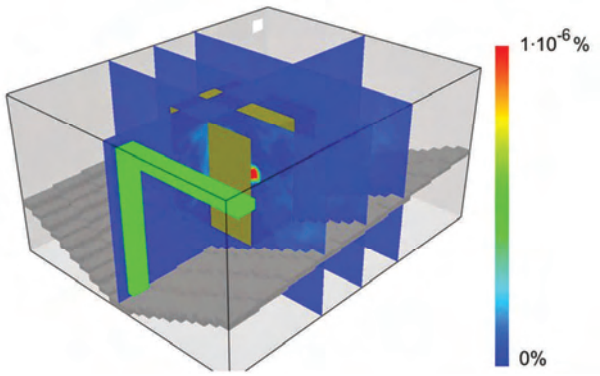


Fig. 10. DME volumetric concentration in the air, leakage variant I

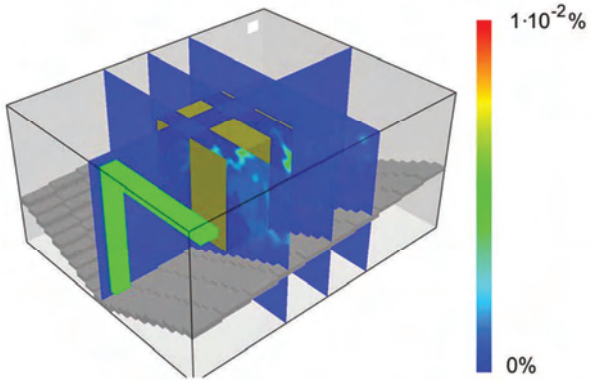


Fig. 11. DME volumetric concentration in the air, leakage variant II

Low concentrations of DME in the air result from the use of an efficient ventilation system for the engine compartment (Fig. 12).

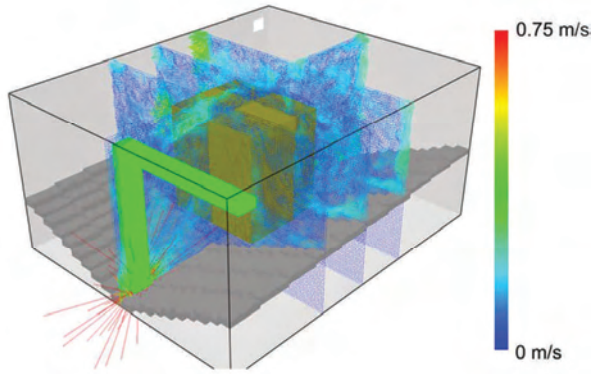


Fig. 12. Air velocity distribution in the engine compartment

Summary

From the environmental benefits point of view, DME is better than diesel fuel. The main advantage is a negligible level of PM emission. The HC and CO emissions are comparable to diesel-fueled engines. Unfortunately, the NO_x emissions are also comparable and have to be treated similarly, i.e. with such methods as exhaust gas recirculation (EGR), urea-selective catalytic reduction (SCR) or lean NO_x traps (LNT).

DME fueling systems for boats and vessels seems to be very perspective, especially from the environmental point of view. From technical point of view the fuel handling and storage system could be very similar to LPG systems very well-known from automotive industry.

Gas leakage simulations have shown that the use of a standard exhaust fan enables to keep low vacuum in the engine compartment. On the other hand, in case of leakage, the concentration of DME gas is kept much below the ignition limit.

Bibliography

[1] ARCOUMANIS, C. et al. The potential of di-methyl ether (DME) as an alternative fuel for compressed ignition engines: A review. *Fuel*. 2008, **87**, 1014-1030.

[2] Boat Safety Scheme, www.boatsafetyscheme.org.

[3] DieselNet Technology Guide » Alternative Diesel Fuels – Dimethyl Ether www.dieselnet.com/tech/fuel_dme. php.

[4] Dimethylether. Decreasing emissions caused by seagoing vessels. Maritime Symposium Rotterdam 2013 www.maritimesymposium-rotterdam.nl/uploads/Route/ Dimethylether.pdf.

[5] FLEISCH, T.H., MEURER, C. DME, the diesel fuel for the 21st century? In: *AVL conference engine and environment*. 1995.
[6] FLEKIEWICZ, M., FABIŚ, P. Ocena wpływu mieszaniny DME i LPG na osiągi silnika ZI. *Zeszyty Naukowe Politechniki Śląskiej, Seria: Transport*. 2013, **81 Z**, 31-44.
[7] IDZIOR, M., KARPIUK, W., SMOLEC, R. Eter dimetylowy jako nowoczesne paliwo alternatywne drugiej generacji do zasilania współczesnych silników o zapłonie samoczynnym. *Logistyka*. 2015, **3**, 1836-1845.
[8] IGF Code 2016 Edition Published by IMO, www.imo.org.
[9] ISHIDA, M., JUNG, S., UEKI, H., SAKAGUCHI, D. Combustion of premixed DME and natural gas in a HCCI engine. *Combustion Engines*. 2005, **121**(2), 20-29.
[10] KAPUS, P., OFNER, H. Development of fuel injection equipment and combustion system for DI diesels operated on di-methyl ether. *SAE Technical Paper*. 1995, 950062.
[11] MOIRANGTHEM, K. Alternative fuels for marine and inland waterways. *JRC Technical Reports*. 2016.
[12] PARK, S. Optimization of combustion chamber geometry and engine operating conditions for compression ignition engines fueled with dimethyl ether. *Fuel*. 2012, **97**, 61-71.
[13] PARK, S.H., LEE, C.S. Applicability of dimethyl ether (DME) in a compression ignition engine as an alternative fuel. *Energy Conversion and Management*. 2014, **86**, 848-863.
[14] PRS rules and publications – classification rules, www.prs.pl/prs-rules-and-publications/classification-rules.html.
[15] THOMAS, G., FENG, B., VEERARAGAVAN, A. et al. Emissions from DME combustion in diesel engines and their implications on meeting future emission norms: A review. *Fuel Processing Technology*. 2014, **119**, 286-304.
[16] WATTANAVICHIEN, K. Implementation of DME in a small direct injection diesel engine. *International Journal of Renewable Energy*. 2009, 4(2), 1-12.
[17] ZHANG, H.F., SEO, K., ZHAO, H. Combustion and emission analysis of the direct DME injection enabled and controlled auto-ignition gasoline combustion engine operation. *Fuel*. 2013, 107, 800-814.
[18] ZHAO, Y., WANG, Y., LI, D. et al. Combustion and emission characteristics of a DME (dimethyl ether)- diesel dual fuel premixed charge compression ignition engine with EGR (exhaust gas recirculation). *Energy*. 2014, **72**, 608-617.

Jacek Kropiwnicki, DSc., DEng. – Faculty of Mechanical Engineering at Gdańsk University of Technology.

e-mail: *JKropiwn@pg.gda.pl*



Przemysław Dominiczak, DEng. – e-engineer computer simulations, Gdańsk.

e-mail: *PDominiczak@e-engineer.eu*



Zbigniew Kneba, DSc., DEng. – Faculty of Mechanical Engineering at Gdańsk University of Technology.

e-mail: *ZKneba@pg.gda.pl*



Sławomir Makowski, DEng. – Faculty of Mechanical Engineering at Gdańsk University of Technology.

e-mail: *SMakow@pg.gda.pl*



Prof. Janusz T., Cieśliński, DSc., DEng. – Faculty of Mechanical Engineering at Gdańsk University of Technology.

e-mail: *JCieslin@pg.gda.pl*



Maciej Ziółkowski, DEng. – Faculty of Mechanical Engineering at Gdańsk University of Technology.

e-mail: *Maciej.Ziolkowski@pg.gda.pl*



Article citation info:
DOUSTDAR, O., WYSZYNSKI, M.L., TSOLAKIS, A., MAHMOUDI, H. Bio-ketones from lignocellulosic biomass: experimental investigation on fuel properties, combustion and emission characteristics of cyclopentanone blends with diesel in compression ignition engine. *Combustion Engines*. 2017, **171**(4), 81-86. DOI: 10.19206/PTNSS-2017-414

Omid DOUSTDAR
Miroslaw Lech WYSZYNSKI
Athanasios TSOLAKIS
Hamid MAHMOUDI

CE-2017-414

Bio-ketones from lignocellulosic biomass: experimental investigation on fuel properties, combustion and emissions characteristics of cyclopentanone blend with diesel in compression ignition engine

Use of alternative fuels in compression ignition engines is the topic for many studies. This paper presents the results of lubricity, calorific value, viscosity, surface tension and density of a ketone blend with diesel to use as a fuel in compression ignition engine. Analyses of fuel properties are vital due to their effect on fuel system. In addition, this study is related to the development of future biofuels and it indicates the effect of oxygen double bond in molecular structure of ketones on important fuel properties. Cyclopentanone which has cyclic molecular structure was used; it can be produced from lignocellulosic biomass through various processing ways. This ketone was blended with diesel fuel at 10% vol. Results from fuel properties tests were compared to the conventional diesel fuel. In the next step this blend was tested in a research diesel engine to analyse its combustion behaviour and emission characteristics of exhaust gases; these results were compared with ultra-low sulphur diesel fuel. Results showed that cyclopentanone, as an additive to diesel, improved surface tension and density of the fuel but in contrast had negative effect on viscosity, lubricity and calorific value of the fuel, but still in the standard range. Combustion behaviour of this fuel in the diesel engine also showed longer ignition delay of ketone blend and also that gaseous emission such as CO and THC are higher than from diesel fuel and NO_x emission is less than from conventional diesel fuel combustion.

Key words: *lubricity, viscosity, calorific value, diesel engine, cyclopentanone, emission*

1. Introduction

The increasing demand for oil in transportation and production of energy has envisaged a possible oil crunch and hence lent some urgency to the discovery of alternative fuels with biofuels being a promising substitute. Biofuels are hence required to overcome uncertainties with relation to energy insecurities, increase economic development in both developed and developing nations and to mitigate climate change and achieve lower greenhouse gas emissions and a lower carbon footprint. According to the World Energy Council's 2015 resources survey, 86% of all power was generated using fossil fuels (oil, coal and gas). This detrimental reliance on fossil fuels pushes the need for a diversity of energy production [1]. Bioenergy is the largest renewable energy source with 14% out of 18% renewables in the energy mix and supplying 10% of global energy supply. The World Energy Resources report in 2015 further determined that biofuels are the most viable and sustainable option in replacing oil dependency. Future demand will come from the need for renewables in transport, followed by heating and electricity sectors. Biodiesel is defined as a fuel comprised of mono-alkyl esters of long-chain fatty acids derived from vegetable oils or animal fats. Vegetable and animal derived feedstock used to produce biodiesel is known as triglycerides. The suitability of a vegetable oil for biodiesel ultimately depends on its fatty acid composition and many of the fuel properties. These fatty acid ester-influenced biodiesel fuel properties include cetane number (CN), calorific value, kinematic viscosity (KV) and lubricity [2].

However, it is vital that the advanced biofuels are produced from cellulosic or other non-food feedstocks [3]. Further, the fuels used in road transportation are subjected to increasingly stringent regulations [4, 5]. Biofuels can effectively reduce emissions in modern four-stroke compression ignition engines in comparison to petroleum diesel. Biofuels have been observed to reduce carbon monoxide (CO), unburnt hydrocarbons and particulate matter (soot) however, nitrogen oxide emissions (NO_x) has been observed to increase [6, 7]. Although biofuels have considerable advantages, numerous properties such as power output, calorific (heating) value and NO_x emissions are questionable.

In the quest for renewable energy sources, researchers have used various microbial organisms to transform lignocellulosic biomass into biofuels. Methyl Ketones are originally found in the fragrant evergreen plant, rue (*ruta graveolens*). Methyl Ketones are also found in tomatoes and other plants and insects and are usually used to provide the scent in essential oils. However, researchers are working on methods to produce them in large quantities using engineered E. coli bacteria to break down glucose [8].

Researchers found various methods to produce biofuels by endophytic fungal conversion of cellulose [9]. The present study investigates the physico-chemical properties, combustion and emission characteristics of one of the cyclic ketones i.e. Cyclopentanone compared with standard engine fuel characteristics. These bio ketone fuels are prototypes for biofuels which were produced by endophytic fungi. There are only a few results from researchers relevant to this work. Ketones behaviour in engine is not well understood and needs more investigation.

2. Experimental methods

2.1. Fuel molecules investigated

One cyclic ketone was investigated i.e. cyclopentanone (Fisher Scientific, Acros Organics, 99+%, pure, molecular

weight 84.118 g/mole) with molecular formula C_5H_8O. Additionally diesel fuel was tested to provide reference data for comparison with these oxygenated ketone fuels. The Ultra-Low Sulphur Diesel (ULSD) fuel was supplied from Shell Global Solutions UK. The Molecular structure of this ketone is shown in Figure 1. The C=O double bond represents a carbonyl functional group. The oxygen atom in ketone makes it more combustible due to its electronegative properties.



Fig. 1. Molecular Structure Cyclopentanone

The aim of the experiments was to investigate the effects on fuel properties, combustion and exhaust emissions of the following molecular features: blend of cyclic carbonyl group such as cyclopentanone with standard Ultra Low Sulphur diesel, which is a mixture of alkanes with approx. 20–25% aromatics.

2.2. Fuels characterization

For fuels characterization the proportion of ketone in blend with diesel blends was 10% vol. Lubricity, calorific value, viscosity, density and surface tension were measured by dedicated instruments and the effect is discussed. Other important properties were gathered from references and experimental studies summarized in Table 2.

2.2.1. Lubricity

Lubrication properties of Cyclopentanone were measured on a High Frequency Reciprocating Rig. This is shown schematically in Figure 2. The test specimens are 6mm dimeter steel ball and steel disc. All of the lubricity tests were conducted according to the EN ISO 12156-1:2006 (max 460 µm) [10–13].

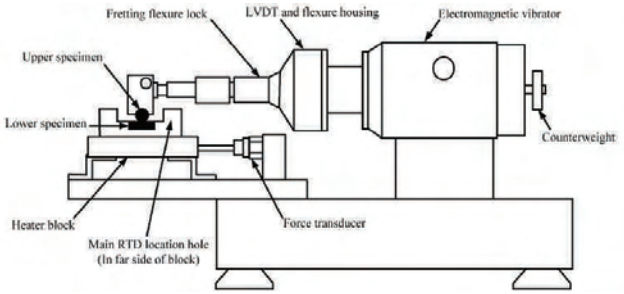


Fig. 2. Schematic diagram of the HFRR [10, 11]

The test conditions are: fuel temperature maintained at 60°C, humidity and temperature of test environment controlled in cabinet which is employed to provide the laboratory air conditions as shown in Figure 3. During the test the lower specimen (disc) is fully submerged in the fuel and the ball is pressed from above and subjected to reciprocating motion with frequency of 50 Hz lasting for 75 minutes. At the end of each test all the contacted components were cleaned by ethanol and acetone consecutively. All fuel samples were tested two times and repeatability was demonstrated to be less than 20µm in the scar diameter. In addition, friction coefficient μ and film concentration reported by the HFRR instrument computer. 100 x optical magnification microscope camera was used to measure the size of the wear scar on the ball in micrometres.

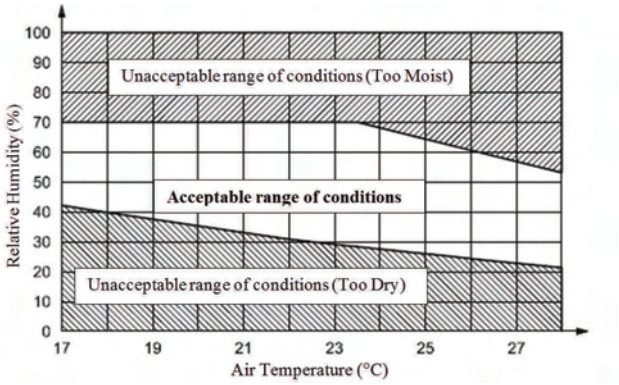


Fig. 3. Laboratory Air Conditions [10, 11]

2.2.2. Calorific value

Heat of combustion is determined in this test method by burning a fuel in an oxygen bomb calorimeter under controlled conditions [14]. The tests were carried out in IKA C200 calorimeter under the specific conditions and assumptions: temperature of 25°C for the fuel and its combustion products, decomposition vessel to be filled with 99.5% pure oxygen at a pressure of 30 bars to optimize the combustion process. The tests were done to adhere to the EN 14213 standard with minimum value of 35 MJ/kg. Gross (higher) calorific value (HCV) was measured and the Net (lower) calorific value (LCV) was then calculated based on the formula taking account of the hydrogen presence in fuel.

2.2.3. Surface tension

Surface tension values are essential in understanding fuel spray behavior and are an important fuel property which affects the stability of surface waves during the drop breakup process. A Sita Proline T15 tension meter system was used to obtain the surface tension measurements as it complies with the ASTM D971 standards. Maximum bubble pressure method was used to measure the surface tension of the sample fuels. Figure 4 shows the schematic

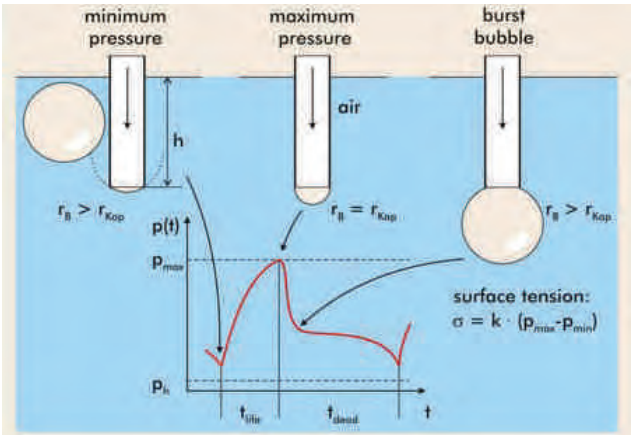


Fig. 4. Schematic diagram of tension meter structure [15]

diagram of the bubble pressure method. This method makes use of this bubble pressure which is higher than surrounding water environment, the gas which is pumped in to fluid creates some bubbles as shown in Figure 4 [15].

2.2.4. Viscosity

The automotive industry places a great deal of significance to the accurate measurement of dynamic viscosity at very high shear rates. The High Temperature High Shear (HTHS) viscosity at temperatures of 40°C, 60°C and shear rate 10^7 s^{-1} was measured using an Ultra Shear Viscometer. The USV can measure at high shear rates, it is connected to a DC servo motor capable of speeds of over 20000 rpm and an electromagnetic clutch which engages the rotor for only a very short period of time (100 ms) [16]. This brief shearing interval minimizes the shear heating in the lubricant. Schematic diagram of USV is shown in Figure 5. The process was fully automated with a simple to use software and a rapid turnaround. Results were analysed to adhere to the ASTM D6751-15a standard specifications where they are required it to be between 1.90 and 6.00 (mm²/s) [17].

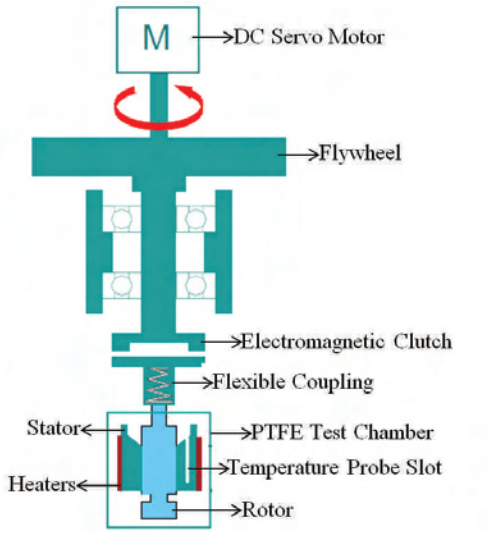


Fig. 5. Schematic diagram of the USV [16]

2.3. Engine and emissions

A modern single cylinder, water cooled, four stroke experimental diesel engine equipped with common rail fuel injection system was used in this paper. This engine is a single cylinder engine which was designed as one of the cylinder heads of V6 Jaguar Land Rover production engine. Full main specification of the engine is given in Table 1.

Table 1. Research engine specifications

Engine parameters	Specifications
Engine type	Diesel 1-cylinder, four stroke
Stroke type	four stroke
Bore	84 mm
Stroke	90 mm
Connecting rod length	160 mm
Compression ratio	16.1
Displacement	499 cc
Engine speed range	900–2000 rpm
IMEP range	< 7 bar
Fuel pressure range	500–1500 bar

Figure 6 indicates the schematic diagram of the experimental setup. This study in the engine was performed under a constant engine speed of 1500 rpm with an engine load of 2 bar IMEP (Indicated Mean Effective Pressure). An AVL GH13P pressure transducer mounted in the cylinder head and an AVL FlexiFEM 2P2 Charge Amplifier were used to record the in-cylinder pressure [18]. To measure the crank shaft position, a digital shaft encoder was used which produces 360 pulses per revolution. The data from the crank shaft position and pressure was combined to create an in-cylinder pressure trace. The fuel injection was split into pre- and main fuel injections with injection timing of 15 and 5 deg bTDC correspondingly, injection pressure of 500 bar and injection duration of 0.15 ms pre-injection and 0.250 ms to 0.500 ms for the main injection. A MKS MultiGas 2030 FTIR spectrometry based analyzer was employed for exhaust gaseous emissions measurement such as: Total Hydrocarbons (THC), carbon monoxide (CO), carbon dioxide (CO_2), nitrogen oxides (NO_x), nitrous oxide (N_2O), and individual hydrocarbons species such as methane (CH_4), ethane (C_2H_6), ethylene (C_2H_4).

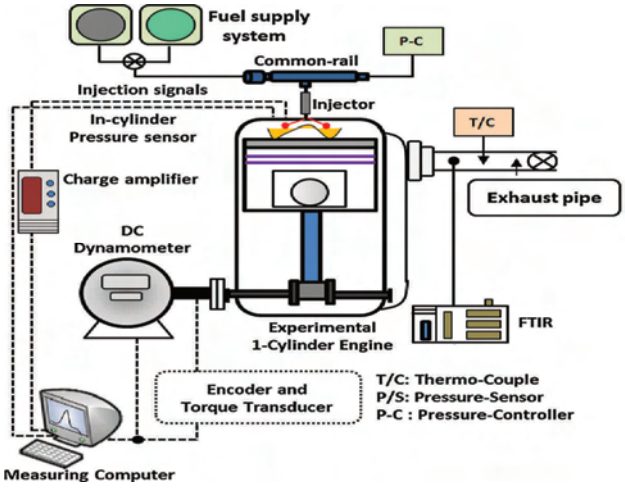


Fig. 6. Schematic diagram of test platform and sampling system

3. Result and discussion

3.1. Fuel characterization

The most critical properties of tested fuel are density, viscosity, lubricity, surface tension and calorific value. The results in Table 2 show that for a blend with approximately 10% by volume of cyclopentanone in ULSD. The density of cyclopentanone is higher than the maximum limit which is given in EN 590 (820−845 kg/m^3), blending of it with diesel make it more suitable for combustion.

As a result of lubricity tests, the average lubrication film concentration for ULSD was 49% and average friction coefficient is 0.203. However, the presence of oxygen in for pure cyclopentanone the average film concentration decreases to 28% with an increased average friction coefficient of 0.248. A positive effect is observed for the D90C10 blend where film concentration increases to 43% with a lower average friction of 0.197. EN590:2009 industry standards limit the wear scar for diesel fuels not to exceed 460 µm. ULSD which is provided by Shell company shows the lubricity result of 409µm, pure Cyclopentanone fuel is

recorded to produce a wear scar diameter of 585 μm making it an unfavourable alternative fuel to be used in CI engines. However, the D90C10 blend produces a wear scar diameter of 419 μm which is less than Cyclopentanone. This proves that the D90C10 is a favourable replacement to petroleum diesel in CI engines which would reduce wear due to sliding and scuffing resulting in reduced failures.

EN 14213 specifications require a minimum calorific value of 35.00 MJ/kg (LCV). ULSD is recorded to have the highest calorific value amongst the fuels tested with a value of 44.90 MJ/kg (LCV). This research also observes that the presence of a carbonyl functional group results in a lower calorific value as displayed by that of Cyclopentanone with a value of 35.67 MJ/kg (LCV). This results in lower thermal energy and less deliverable power by the fuel. The D90C10 fuel blend, however, displays a higher calorific value in comparison to Cyclopentanone with a value of 39.96 MJ/kg (LCV) presenting characteristics of higher power availability thereby higher performance.

Surface tension determines the quality and effective combustion of the fuel. Thereby it requires increased atomisation for complete combustion. ULSD, pure Cyclopentanone and D90C10 fuels display surface tensions of 25.5, 29.5 and 25.7 mN/m respectively. The D90C10 blend displays an almost same surface tension as Diesel.

Kinematic viscosity measures the resistance to motion and a higher viscosity suggests delays in combustion and poor fuel spray. ASTM D6751-15a specifies a standard between 1.90 and 6.00 (mm²/s or cSt). The results recorded for the D90C10 blend denotes an average value of 2.1077 mm²/s. This suggests that the blend fits well within the specification providing sufficient lubrication without inducing deposits or limiting fuel flow. Measurement of viscosity of pure cyclopentatone was not possible because its high volatility and danger of fire in the high-shear instrument. The effect of adding 10% volume of cyclopentanone in diesel on main fuel properties are summarized in Table 2.

Table 2. Physical and chemical properties of tested fuels

Abbreviation	% volumetric makeup		
ULSD	100 Ultra Low Sulfur Diesel		
CycN	100 Cyclopentanone		
D90C10	90 ULSD + 100 CycNone		
Properties	ULSD	CycN	D90C10
Chemical formula	$C_{14}H_{26}$	C_5H_8O	–
Cetane number	53.9 [19]	–	–
Density at 15ºC (kg/m^3)	813.8	950	837.8
Kinematic viscosity at 40ºC (cSt)	2.52	–	2.05
Lower calorific value (MJ/kg)	44.9	35.67	39.96
Lubricity at 60ºC (μm)	409	585	419
Surface tension at 25ºC (mN/m)	25.5	29.5	25.7
Carbon (wt%)	86.44 [19]	71.33	–
Hydrogen (wt%)	13.56 [19]	9.51	–
Oxygen (wt%)	0 [19]	19.16	–

3.2. Engine and emissions

Figure 7 shows the effect of the bio ketone blend with diesel on the in-cylinder pressure and the rate of heat release (ROHR) versus crank angle degree (CAD). The values of the peak pressure developed in the engine and the crank angle location for both ULSD and the D90C10 blend are displayed in Figure 7. It has to be noted that use of cyclopentanone as a blend affects the combustion behaviour; this is attributed to the presence of double bond oxygen in the ketone hydrocarbons. It was observed that peak in-cylinder pressure for both fuels occurred at 368^o with maximum pressures of 51.23 bar and 51.25 bar for ULSD and D90C10 respectively. Smooth readings were obtained for both ULSD and D90C10 with very little variation between the two lines. This further contributes to previous studies suggesting that there is no difference in in-cylinder pressure for diesel and moderate biodiesel percentage blends. It was observed that peak in-cylinder pressure for both fuels occurred at 368^o with maximum pressures of 51.23 bar and 51.25 bar for ULSD and D90C10 respectively. Smooth readings were obtained for both ULSD and D90C10 with very little variation between the two lines. This further contributes to previous studies suggesting that there is no difference in in-cylinder pressure for diesel and moderate biodiesel percentage blends. This further determines that the Cyclopentanone-Diesel blend is a worthy substitute for petroleum diesel in CI engines as it provides sufficient pressure to aid in a similar performance to ULSD. However, it should be noted that research should be carried out for additional blends at varying loads to identify the full capabilities of Cyclopentanone-Diesel blends.

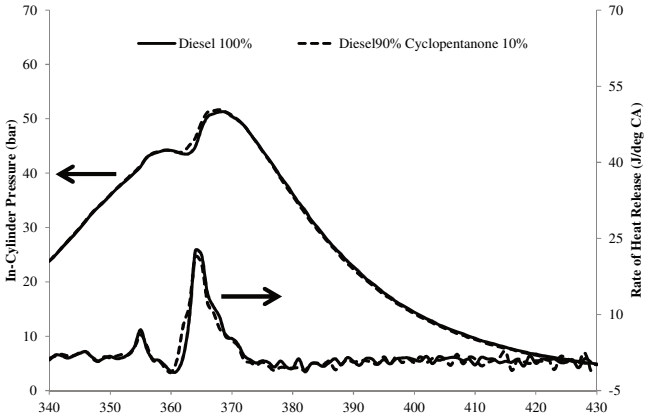


Fig. 7. Effect of tested fuels on combustion characteristics

Use of Cyclopentanone-Diesel blends as a fuel has effect on the gaseous emissions coming from the exhaust. Figure 8 show the CO and THC engine-out emissions for the investigated fuels. It can be concluded that both CO and THC for the tested cyclopentanone blend were higher compared with diesel combustion in engine. Also Figure 9 indicates that ethylene, ethane and methane emissions are higher than those from diesel fuel.

In contrast to all of these results, Figure 10 shows that NO_x concentrations from the tested fuel were lower than from diesel fuel. The carbonyl function group in cyclopentanone is thought to result in lower NO_x emissions which were tested at low loads. Slight increase of NO_2 can be due to the presence of oxygen content in cyclopentanone, so oxygen content and lower cetane number of the cyclopentanone affect the decrease of total NO_x species in the exhaust emissions [18].

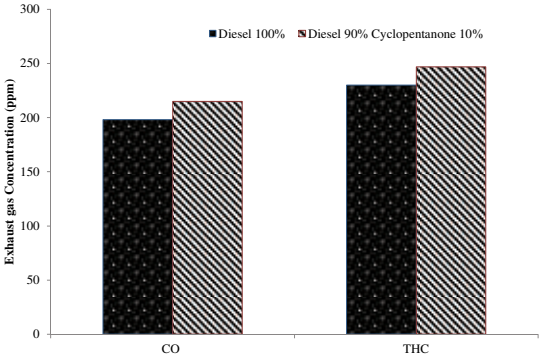


Fig. 8. Exhaust CO and THC species measured for each tested fuels

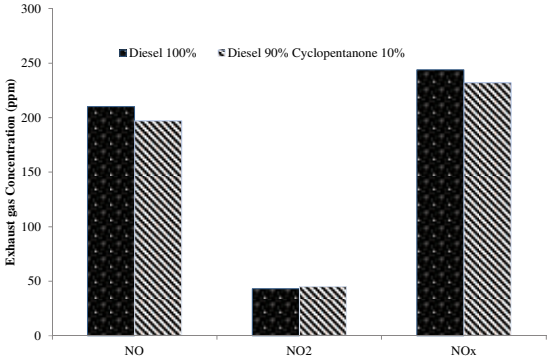


Fig. 10. Engine exhaust NO_x species concentration for each tested fuels

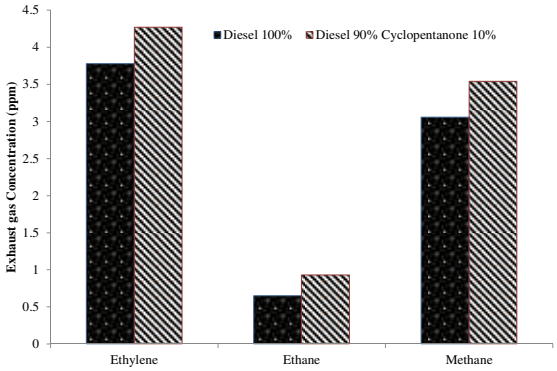


Fig. 9. Engine exhaust hydrocarbon species measured for each tested fuels

Uses of appropriate Diesel Oxidation Catalysts, Selective Catalytic Reduction and NO_x absorber catalyst were suggested for further investigation in different engine experiment conditions.

4. Conclusion

Use of alternative fuels such as biofuels in the last years becomes more interesting due to the scarcity of fossil fuels and their environmentally negative impact on human health. Bio-ketones which are produced from lignocellulose biomass are one of the new alternative fuels to use in the current engine without any modifications. Results show that ketone blends have proper fuel properties to use in the diesel engine without use of any additives or lubricant. This blend had slightly longer ignition delay than diesel because of carbonyl groups which make H-abstraction more difficult from ketone compared to diesel (Alkanes) [20]. NO_x emissions from combustion of this fuel is slightly lower that diesel fuel which make this fuel more interesting for further investigation. Increase of other gaseous emissions requires some more studies based on use of after treatment strategies in various engine conditions. From the literature, due to the presence of oxygen content in carbonyl groups a reduction in particulate mass can be expected; this will be studied in the future by using Scanning Mobility Particle Sizer Spectrometer.

Acknowledgement

Department of Mechanical Engineering at the University of Birmingham (UK) is greatly acknowledged for the provision of a PhD scholarship and maintenance grant.

Nomenclature

CI	compression ignition
ULSD	ultra low sulphur diesel
CycN	cyclopentanone
CN	cetane number
KV	kinemativ viscosity
LCV	lower calorific value
HCV	higher calorific value
HFRR	high frequency reciprocating rig
HTHS	high teperature high shear
USV	shear viscometer
WSD	wear scar diameter
FTIR	Fourier Transform Infrared Spectroscopy
IMEP	indicated mean effective pressure
CAD	crank angle degree
bTDC	before top dead centre
ROHR	rate of heat release
CO	carbon monoxide
CO_2	dioxide
NO_x	nitrogen oxides
N_2O	nitrous oxide
THC	total hydrocarbon
CH_4	methane
C_2H_6	ethane
C_2H_4	ethylene

Bibliography

[1] ARBAB, M.I., MASJUKI, H.H., VARMAN, M. et al. Fuel properties, engine performance and emission characteristic of common biodiesels as a renewable and sustainable source of fuel. *Renewable and Sustainable Energy Reviews*. 2013, **22**, 133-147.

[2] ISLAM, M.A., BROWN, R.J., BROOKS, P.R. et al. Investigation of the effects of the fatty acid profile on fuel properties using a multi-criteria decision analysis. *Energy Conversion and Management*. 2015, **98**, 340-347.

[3] SCHNEPF, R., YACOBUCCI, B.D. Renewable fuel standard (RFS): overview and issues. 2013. *Congressional Research Service*. www.fas.org/sgp/crs/misc/R40155.pdf.
[4] UNEEN-590, Automotive fuels–diesel-requirements and test methods. 2004.
[5] ASTMD975-06, Standard specification for diesel fuel oils.
[6] Lapuerta, M., Armas, O., Rodríguez-Fernández, J. Effect of biodiesel fuels on diesel engine emissions. *Progress in Energy and Combustion Science*. 2008, **34**(2), 198-223.
[7] GRABOSKI, M.S., MCCORMICK, R.L. Combustion of fat and vegetable oil derived fuels in diesel engines. *Progress in Energy and Combustion Science*. 1998, **24**(2), 125-164.
[8] DUFFIN, A. Methyl ketones, A sweeter smelling biofuel. 2012. earthtechling.com/2012/04/methyl-ketones-a-sweeter-smelling-biofuel.
[9] BARARI, G., SARATHY, S.M., VASU, S.S. Improved combustion kinetic model and HCCI engine simulations of di-isopropyl ketone ignition. *Fuel*. 2016, **164**, 141-150.
[10] DOUSTDAR, O., WYSZYNSKI, M.L., MAHMOUDI, H., TSOLAKIS, A. Enhancing the properties of Fischer-Tropsch fuel produced from syngas over Co/SiO_2 catalyst: lubricity and calorific value. *IOP Conference Series: Materials Science and Engineering*. 2016.
[11] SUKJIT, E., DEARN, K.D. Enhancing the lubricity of an environmentally friendly Swedish diesel fuel MK1. *Wear*. 2011, **271**(9–10), 1772-1777.
[12] BOGARRA-MACIAS, M., DOUSTDAR, O., FAYAD, M.A. et al. Performance of a drop-in biofuel emulsion on a single-cylinder research diesel engine. *Combustion Engines*. 2016, **166**, 9-16.
[13] BSI, BS EN ISO 12156-1:2006, Diesel fuel, assessment of lubricity using the high frequency reciprocationg rig (HFRR) Part 1. Test Method. 2006.
[14] Standard, A.N., Standard test method for heat of combustion of liquid hydrocarbon fuels by bomb calorimeter/ASTM D240-02. 2007. *ASTM International United States*.
[15] SITAlabSolutions. Bubble pressure method for measuring the dynamic surface tension. 2017. www.sita-lab.com/information-service/basics-about-sita-lab-solutions/surface-tension/bubble-pressure-method.
[16] PCS, USV Ultra shear viscometer brochure. 2016, *PCS Instruments*.
[17] PIASZYK, J., LEUNG, P., WYSZYNSKI, M.L. et al. Neat tallow combustion in a large diesel engine for electricity generation from waste. *Energy & Fuels*. 2012, **26**(12), 7288-7298.
[18] FAYAD, M.A., TSOLAKIS, A., FERNÁNDEZ-RODRÍGUEZ, D. et al. Manipulating modern diesel engine particulate emission characteristics through butanol fuel blending and fuel injection strategies for efficient diesel oxidation catalysts. *Applied Energy*. 2017, **190**, 490-500.
[19] SUKJIT, E., HERREROS, J.M., PIASZYK, J. et al. Finding synergies in fuels properties for the design of renewable fuels – hydroxylated biodiesel effects on butanol-diesel blends. *Environmental Science & Technology*. 2013, **47**(7), 3535-3542.
[20] KOIVISTO, E., LADOMMATOS, N., GOLD, M. Compression ignition and exhaust gas emissions of fuel molecules which can be produced from lignocellulosic biomass: levulinates, valeric esters, and ketones. *Energy & Fuels*. 2015, **29**(9), 5875-5884.

Omid Doustdar, MEng., AMIMechE – Department of Mechanical Engineering, University of Birmingham.

e-mail: *O.Doustdar@bham.ac.uk*



Miroslaw Lech Wyszynski, MEng., PhD, MIDGTE MSAE, MSIMP – Department of Mechanical Engineering, University of Birmingham.

e-mail: *M.L.Wyszynski@bham.ac.uk*



Athanasios (Thanos) Tsolakis, BEng., PhD. CEng., FIMechE, FHEA – Department of Mechanical Engineering, University of Birmingham.

e-mail: *A.Tsolakis@bham.ac.uk*



Hamid Mahmoudi, MEng, PhD – Department of Mechanical Engineering, University of Birmingham.

e-mail: *Msh.Mahmoudi@gmail.com*



Article citation info:
WIRKOWSKI, P.J., KNIAZIEWICZ, T. Evaluation of marine gas turbine engine parameters in terms of issue of emissions of exhaust toxic fumes. *Combustion Engines*. 2017, **171**(4), 87-91. DOI: 10.19206/CE-2017-415

Paweł WIRKOWSKI
Tomasz KNIAZIEWICZ

CE-2017-415

Evaluation of marine gas turbine engine parameters in terms of exhaust harmful emissions

The article presents an analysis of the use of gas turbine engine in the propulsion and marine power plant of vessels, taking into account environmental aspects. The preliminary results of emission tests of harmful exhaust emissions of the laboratory gas turbine engine were presented. Also an analysis was also undertaken on the possibility of carrying out measurements of concentrations of pollutants in the marine gas turbine engine propulsion systems in terms of its operation on the vessel.

Key words: *harmful compounds, emission, exhaust gases, marine gas turbine engine*

1. Introduction

Energy requirements of maritime transport arising from their operational needs related to the function of the movement of the vessel and their existential functions has long been carried out by using mainly internal combustion piston engines.

In the case of gas turbine engines, depending on the destination of the vessel and energy needs, power units and marine power plant with steam turbines are used in cases where nuclear power plants and systems with the so-called gas turbines in the form of gas turbine engines are used.

As a result of smaller energy efficiency and the resulting higher fuel consumption, gas turbine engines for marine use are being replaced by piston engines and represent only a few percent share in the total population of marine internal combustion engines. However, gas turbine engines have one significant advantage – they are characterized by a high concentration of power expressed as a ratio obtained under the terms of the weight of the engine. In comparison, the vessels power must take into account not only the weight but the mass of the entire engine propulsion unit, since the use of the gas turbine engine requires the use of additional reduction of gear rotational speed of the motor drive shaft to the desired speed of the vessel propulsion. The list compares power, economic and technical parameters conducted for piston and gas turbine engines used for main propulsion and the validity of the use of gas turbine engines for propulsion of warships is achieved.

In connection with a significant quantitative predominance of marine internal combustion piston engines of the vessel's gas turbine engines, legal regulations concerning the emission of harmful exhaust gases of marine engines are mainly with regard to piston engines (Table 1). One of these acts is the International Convention for the Prevention of Pollution from Ships of 1973, Signed in London on 2 November 1973 as amended by the Protocol compiled in London on 17 February 1978 (Journal of Laws of 1987 No. 17, item 101) and by the Protocol done at London on 26 September 1997 (Journal of Laws of 2000 No. 202, item 1679), hereinafter known as the „MARPOL Convention".

All engines used on warships are exempt from compliance with standards of emission of harmful exhaust gases. It should be noted that the percentage of the population of gas turbine engines installed on warships is several times higher in comparison to the civil fleet. However, governments with warship fleets seek to implement the provisions relating to the protection of the marine environment (e.g. MARPOL) on warships as far as it is possible.

Table 1. The emission limit unit values for NO_x for marine combustion-ignition engines with power over 130 kW according to Annex VI to the MARPOL Convention 73/78 [10]

Emission level	Year of validity	NO_x emission limits [g/(kWh)] depending on the nominal engine speed n [rpm]		
		Low Speed Engine n < 130	Medium Speed Engine n ≤ 130 < 2000	High Speed Engine n ≥ 2000
I	2000	17.0 *	$45.0 \cdot n^{-0.2}$ *	9.8 *
II	2011	14.4 **	$44.0 \cdot n^{-0.23}$ **	7.7 **
III	2016	3.4 ***	$9.0 \cdot n^{-0.2}$ ***	2.0 ***

* these values apply to vessels built or those that have undergone modernization after 1 January, 2000 and before 1 January, 2011,
** these values apply to any vessel built after 1 January, 2011,
*** these values apply to any vessel built after 1 January 2016. and sailing in the North American Emission Control Area or Area in the Caribbean Sea of the United States.

Ever increasing emission of exhaust gases from marine engines implemented have necessitated the development of new construction concepts of marine power plant of civilian ships and warships. Increasingly, it contemplates the use of gas turbine engines in marine power plant focused on the production of electricity used by electric motors vessel propulsions. In the case of gas turbine engines, the disadvantage is lower efficiency of electricity generation, as evidenced by the high value of the specific fuel consumption (Fig. 1), but the important advantage is the high concentration of generated energy in the unit occupied by the combustion power system volume. The advantage of using gas turbine systems is the ability to supply these motors with so-called light fuels with low sulfur compounds, alternate fuels such as vegetable oil esters, methanol, ethanol, methane and gaseous fuels such as natural gas and propane-butane.

The use of natural gas to supply the drive marine power plant may be particularly advantageous in LNG transportation ships with this type of fuel. The argument for the use of systems of turbine generators of electricity is the possibility to increase cargo space (Fig. 2) which improves the cost-effectiveness ratio of vessel shipment, eliminating the lower overall efficiency of gas turbine engines. It is especially the preferred solution of using light and alternative fuels such as natural gas, propane-butane, vegetable oil esters, methanol or ethanol.

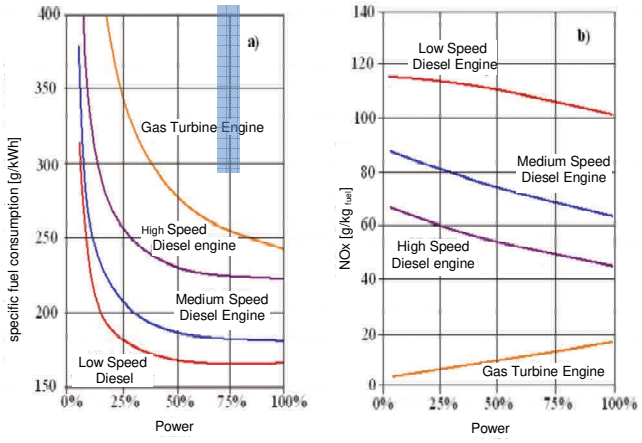


Fig. 1. Specific fuel consumption (a) and NO_x (b) as a function of the power used for the propulsion types of compression-ignition and gas turbine engines [7]

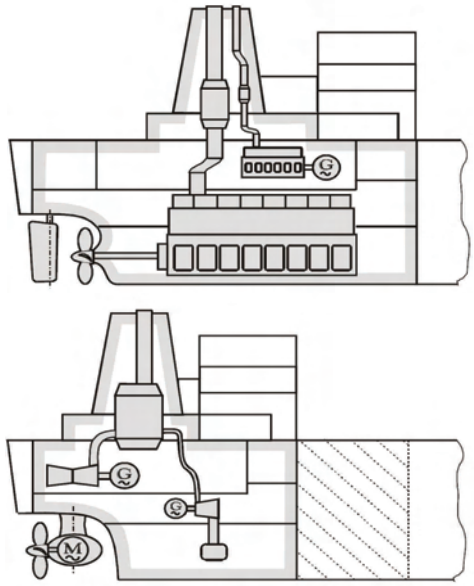


Fig. 2. Comparison of the drive system of the turbine generators of energy in the planned LNG tanker to the traditional direct drive of low-speed compression ignition engine [1]

The concepts of using gas turbine engines is associated with the necessity of accepting higher specific fuel consumption resulting from lower engine efficiency, but also to contribute to obtaining the improvement of ecological indicators in the form of lower emission of harmful fume emissions. Assessment of the real benefits of using gas turbine engines for marine propulsion, obtained under the operating and environmental parameters requires a number of studies and analyzes, some of which are presented in this article.

2. Characteristics of the unit

The authors therefore undertake to try to determine the emission of harmful exhaust gases in marine turbine engine, used in the drive system of guided missile frigate class of warship (Fig. 3).



Fig. 3. Oliver Hazard Perry class missile frigate [11]

The propulsion system unit consists of a power unit equipped with two gas turbine engines from General Electric LM 2500 (Fig. 4), a cumulative drive reduction gear ratio of 1/20, one line shaft and adjusting screw. The power of the drive is about 30 000 kW at a maximum turbine propulsion speed of n_{TN} = 3600 rpm.

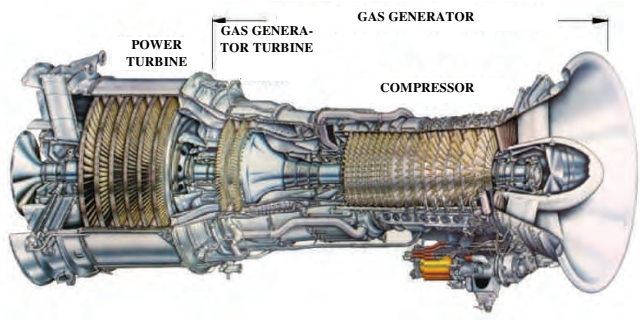


Fig. 4. LM 2500 marine gas turbine engine

Gas turbine engines used in the propulsion system of frigates consist of two rotor units. The basis of engine design is the exhaust gas generator in which the sixteen-axial compressor is driven by a two-stage high-pressure turbine. The first six stages of the compressor are equipped with an adjustable steering blades operating in the range of the -30^o – $+30^o$ angular position with an accuracy of 10'. Setting the steering is dependent on the pressure of fuel supplied to the injectors, the rotor speed of the gas generator and the air temperature in the inlet section of the engine. This solution enables the extension of the stable operation of the compressor, especially in transition processes. The continuous combustion process takes place in an annular combustion chamber supplied with fuel through the thirty-two injectors. Six level separate turbine propulsion co-operates with the exhaust gas generator which constitutes a source of mechanical energy for the vessel propulsion system. The engine is entirely located in a casing isolating it from the rest of the power system. This solution was adopted for reasons

of fire safety and for reducing noise propagation inside the power system. The exhaust system has a length of a several meter vertical channel with a diameter of two meters, ending in narrowing to a diameter of about a meter.

3. The operating parameters LM 2500 engine

Measurements of thermal gas-dynamic parameters of the working medium made in specific sections of the engine control are an important source of diagnostic information about the state of the structure of construction part of the flow. The schematic diagram of the LM 2500 engine (Fig. 5) presented with marked control flow sections enables visualization of the distribution points. The measured values and calculation of individual parameters of the engine and the measurement range expressed in units of force in the power system of vessels is summarized in Table 2.

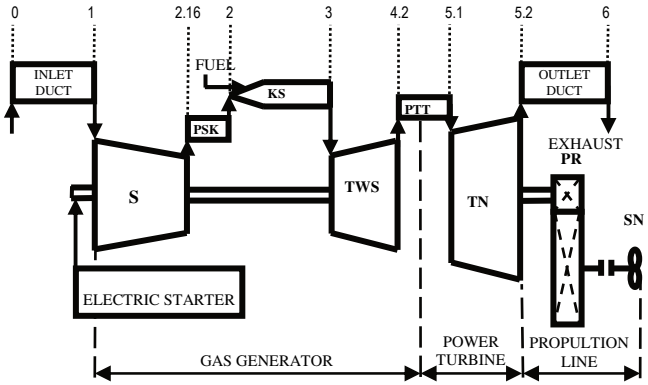


Fig. 5. Block diagram of LM 2500 gas turbine engine

Table 2. Operating parameters LM 2500 engine

Name parameter, designation, unit	Measurement range
Barometric pressure p_o [hPa]	800–1040
Ambient temperature t_o [°C]	-40 – +40
The rotational speed of the gas generator shaft n_{GG} [rpm]	0–12000
The rotational speed of the power turbine shaft n_{PT} [rpm]	0–5000
The inlet air temperature to the engine t_1 [°F]	–40 – +150
The inlet air total pressure to the engine p^*_1 [psig]	0–16
Air pressure on the outlet compressor p_2 [psig]	0–300
The temperature of the exhaust stream before the power turbine $t_{4.2}$ [°F]	0–2000
Total pressure of the exhaust stream before the power turbine $p^*_{4.2}$ [psig]	0–75
Temperature exhaust gas T_6 [°F]	0–1000
The fuel temperature before engine T_f [°F]	0–100
Pressure fuel injectors before p_f [psig]	0–1500
Torque (calculated) on the power turbine shaft M_{PT} [LB FT]	0–50000
Power on the power turbine shaft P_{TN} [KM]	0–25000

The location of the turbine engine in the engine room requires the assurance of supply to the inlet of the corresponding mass flow of air and exhaust mass derivation generated from the engine exhaust. Vertical air intake channels and exhaust gas outlet channels (Fig. 6) of about 15 m have been designed for Oliver Hazard Perry class missile frigate equipped with two LM 2500 turbine engines. The air from the manifold is directed mostly to the inlet of the engine. A small portion of air from the intake side channel is collected and is fed to the interior of the container assembly for the engine in order to ensure a proper temperature around the running engine. Air flowing from the outer parts of the engine in the container housing is ultimately directed into the exhaust duct to be mixed with the gases generated by the turbine engine. Depending on the need to ensure the appropriate parameters, air flowing from the outside of the engine is suitably prepared by an appropriate temperature using the cooling system and the heaters and the flow rate of the respective container inside the housing, controlled by using a fan.

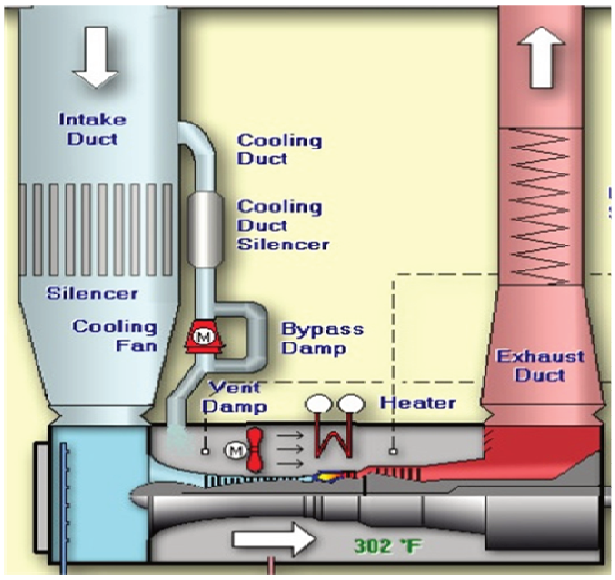


Fig. 6. Arrangement of air intake and LM 2500 engine exhaust outlet mounted on an Oliver Hazard Perry class missile frigate

4. The operating parameters and the emission of harmful compounds in the exhaust gas turbine engine

The idea of operating an internal combustion engine is directed in order to achieve the operational performance which translates into propulsion operation. The flow of the exhaust stream generating torque of the power turbine is important for the turbine shaft which eventually results in the drive shaft receiving power from the engine. Parameters values of exhaust gas generated by the so-called generator exhaust – part of the turbine engine – are responsible for the operating parameters obtained from the power turbine shaft. These parameters include mass flow of exhaust gases and the energy described by the temperature and the flow rate at various stages of the turbine. The resulting thermodynamic parameters of the exhaust gas as a working medium are directly dependent on the conditions in the combustion chamber, which are closely related to the operating parameters resulting from the energy requirements. Therefore, there is a relationship between the operating parameters and the conditions of the combustion process occurring in the combustion chamber and the emission of pollutants in the exhaust gas which was generated in order to obtain the required mechanical energy on the drive shaft of the motor.

According to these interdependencies, the emissions contaminants contained in the generated exhaust gases can be evaluated depending on engine load energy. For this

purpose, it is necessary to specify the mass flow of generated exhaust gases as a function of engine load and concentrations of harmful compounds contained in them. It is necessary to obtain emission characteristics of the engine as a function of load. The issue is familiar and is presented many more studies [3, 4, 6, 9]; however, studies of high power turbine engines require an individual approach, so much so that the issue of the assessment of gas emission from turbine engines is carried out under static conditions at a few selected points of the study and for certification purposes of the engine. In contrast, the evaluation of pollutant emissions, carried out by the authors, in the exhaust gases of the turbine engine shaft used at sea is focused on the evaluation of the operating conditions of the vessel during the voyage being undertaken.

In order to determine the characteristics of the LM 2500 engine emission, it is necessary to estimate the generated mass flow of exhaust gases. The mass flow of exhaust gases is the total flow of air and fuel supplied to the engine. Therefore, it is necessary to designate the mass flow of air and the mass flow of fuel. When available, the possible measured values of engine operating parameters LM 2500 can be troublesome. Therefore, the calculation of one of these values and measuring the excess air ratio for the engine carried out in the combustion process using a broadband oxygen sensor is a necessary condition. By knowing the ratio of the air-fuel consumption, the air or engine fuel according to which the value is obtained from the measurement can be established. Establishing the exhaust gas mass can be linked to the value of concentrations of harmful compounds, thus obtaining the emission of pollutants in the exhaust gases. In carrying out the emission characteristics of the engine as a function of load, it is necessary to obtain the dependent equation that can be used in the algorithm for determining the instantaneous emission engine operating conditions. Examples of the emission characteristics have been developed by the authors on the basis of the GTD-350 turbine engine shaft [7] and the resulting equations describe the changes of the concentration of the individual compounds as a function of load (Fig. 7). The distribution of received values and dependencies should be considered as an example of a distribution of received values of described equations are a feature of its own motor. Therefore, it is necessary to determine the emission for the engine, for which assessment of emission standards in operating conditions shall be undertaken in the subsequent stage. It is necessary to associate the obtained dependencies on the operating parameters of the engine in order to make such evaluation, i.e. the engine-generated power, the speed of rotation of the shaft gas generator, the rotational speed of the power turbine shaft, rotational speed and screw settings of the ship propeller, and the sailing speed of the vessel and the parameters of the course as a further step.

With the increase in engine power demand, the combustion temperature rises, thereby increasing the concentration of nitrogen oxides (NO_x) in the exhaust gas. As the engine power increases, the concentration of carbon monoxide (CO) decreases. Carbon monoxide is an incomplete combustion product, and therefore, when it comes to the lack of air for burning fuel, it occurs. Therefore, with increasing power of the engine carbon monoxide will be less and less. At higher temperatures carbon monoxide oxidizes to carbon dioxide (CO_2), which results in an increase in carbon dioxide emissions.

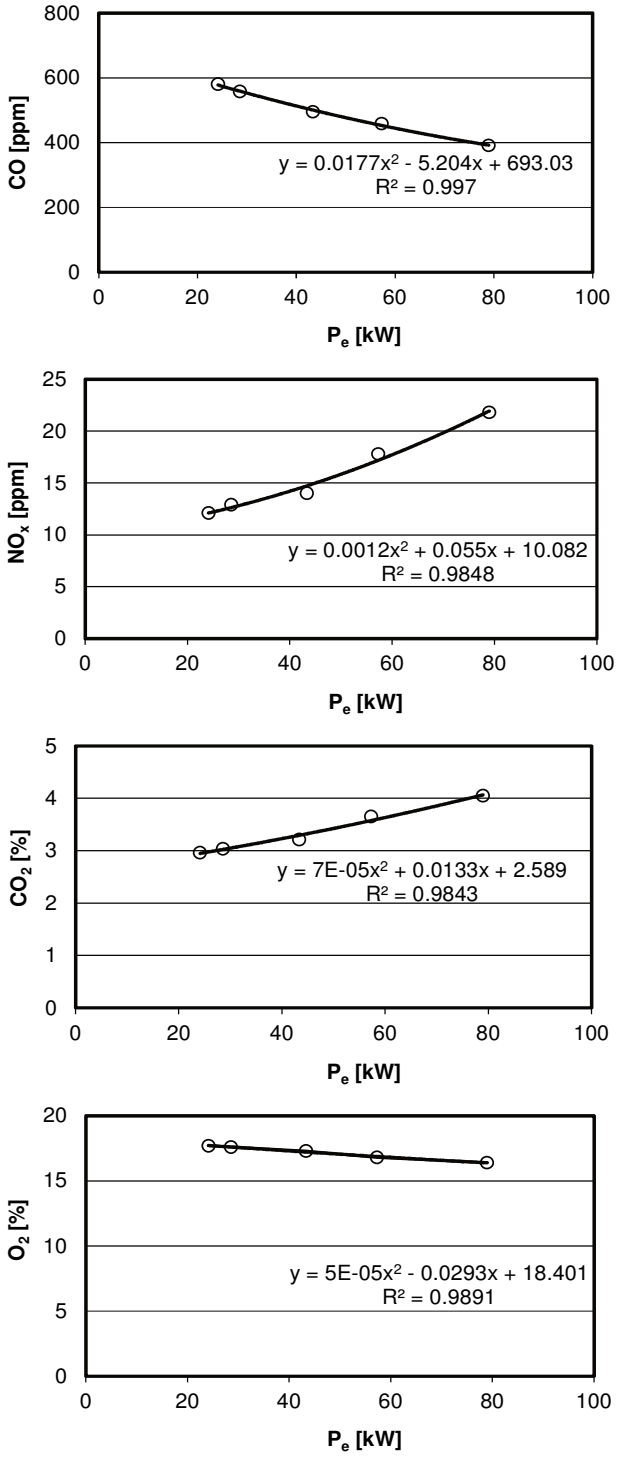


Fig. 7. Examples of the concentration of selected components of the exhaust gas as a function of the power of GTD-350 gas turbine engine

Taking into account available parameters monitored in the engine room, the following one can be used:

– rotor speed of gas generator,
– the rotational speed of the separate power turbine,

- the temperature of the inlet air to the engine,
- the total pressure of the inlet air to the engine,
- the temperature of the exhaust gas stream before the turbine engine,
- the total pressure of the exhaust gas stream upstream of the turbine engine,
- output torque of the power turbine,
- power on the power turbine shaft.

Other information should be obtained using the measurement system of excess air, and using apparatus for testing the concentration of pollutants in the exhaust gas.

5. Summary

The analysis of the monitored operating parameters in the engine room the Oliver Hazard Perry guided missile frigate class which is in the service of the Polish Navy, highlighting the need for additional equipment and mathematical algorithms to determine the level of performance necessary to assess pollutant exhaust gas generated by the turbine engine shaft of the main drive. This evaluation requires earlier studies related to obtaining emission characteristics of the engine for all of its operations. However, the supplemented characteristics of the algorithm determine the mass flow of exhaust allow it to derive the emission of harmful compounds in the operating conditions of the vessel.

Nomenclature

S	compressor
KS	combustor
TWS	gas generator turbine
TN	power turbine
PR	reduction gear
SN	propeller
PSK	space between S and KS
PTT	space between TWS and TN

Bibliography

[1] HOUNTALAS, D.T., KOUREMENOS, A.D. Development of fast and simple simulation model for the fuel injection system of diesel engines. *Advanced in Engineering Software*. 1998, **26**(1), 13-28.

[2] HOUNTALAS, D.T., KOUREMENOS, A.D. Development of fast and simple simulation model for the fuel injection system of diesel engines. *Advanced in Engineering Software*. 1998, **26**(1), 13-28.

[1] GIERNALCZYK, M., GÓRSKI, Z. Ship engine rooms, part I, fundamentals of drive and energy ship. *Publisher Gdynia Maritime University*. Gdynia 2011.

[2] GŁOWACKI, P., SZCZECIŃSKI, S. Turbine jet engine as a source of environmental threats. *The work of the Institute of Aviation*. 2011, **213**.

[3] KNIAZIEWICZ, T. Process modeling of ship emissions of internal combustion engines for main propulsion under real operating conditions. *Publisher Academic AMW*. Gdynia 2013.

[4] KOTLARZ, W. ed. Group work, turbine powertrains source of air pollution at military airports. *Publisher WSOSP*. Deblin 2003.

[5] KOWALEWICZ, A. Fundamentals of combustion processes. *Publisher Scientific-Technical*. Warszawa 2000.

[6] MARKOWSKI, J. Exhaust emission from aircraft piston engines. *Publisher Poznan University of Technology*. Poznan 2013.

[7] MARKOWSKI, J., PIELECHA, J., JASIŃSKI, R. et al. Evaluation of relations operating and ecological parameters of turbine engines. *Journal of Polish CIMEEAC*. 2015, **10**(1).

[8] MERKISZ, J., MARKOWSKI, J., ŚLUSARZ, G. et al. Comparative analysis of exhaust emission test for a turbine engine. *Combustion Engines*. 2015, **162**.

[9] MERKISZ, J., PIASECZNY, L., KNIAZIEWICZ, T. Issues emissions of marine engines. *Publisher Poznan University of Technology*. Poznan 2016.

[10] The International Convention for the Prevention of Pollution from Ships, 1973/1978 MARPOL. *Publisher PRS*. Gdansk 2015.

[11] www.google.pl/search?q=fregata+273.

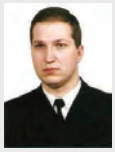
Paweł Wirkowski, MSc. – Faculty of Mechanical and Electrical Engineering at Polish Naval Academy.

e-mail: *P.Wirkowski@amw.gdynia.pl*



Tomasz Kniaziewicz, DSc., DEng. – Faculty of Mechanical and Electrical Engineering at Polish Naval Academy.

e-mail: *T.Kniaziewicz@amw.gdynia.pl*



Article citation info:
BEBKIEWICZ, K., CHŁOPEK, Z., SZCZEPAŃSKI, K, ZIMAKOWSKA-LASKOWSKA, M. Evolution of national annual pollutant emission from motor vehicles in Poland. *Combustion Engines*. 2017, **171**(4), 92-96. DOI: 10.19206/CE-2017-416

Katarzyna BEBKIEWICZ
Zdzisław CHŁOPEK
Krystian SZCZEPAŃSKI
Magdalena ZIMAKOWSKA-LASKOWSKA

CE-2017-416

Evolution of national annual pollutant emission from motor vehicles in Poland

The work analyses the national annual emission of pollutants from passenger cars in Poland, in the years 2000–2015, including the classification of combustion engines relative to the ignition system. The study was carried out in accordance with the methodology used in the COPERT 4 software. The vehicle traffic model was analysed under the following conditions: urban, rural and on motorways and expressways. The national annual pollutant emission was found to change substantially alongside the changes in vehicle properties over the period analysed; the effect varied due to the performance of respective substances. The relative annual national emission of the various pollutants compared to the situation in 2000 were determined. There was a clear declining trend, from 2008 onwards, in the relative annual emission of pollutants from a representative passenger car; this was valid for all substances.

Key words: *motor vehicles, inventory of pollutant emission, COPERT*

1. Introduction

Pollutant emission from internal combustion engines of passenger cars is by far more sensitive to engine parameters and operation conditions than the emission from engines of the other vehicles [5, 10]. This is particularly evident in the case of spark ignition engines [5, 10]. Consequently, the subject of the assessment of the national annual pollutant emission from passenger cars in Poland during the 2000-2015 balancing period was taken into account.

2. The COPERT software

The COPERT 4 software [1, 2, 7–9, 11] was used to determine the national emission of pollutants from passenger cars. This software accounts for a number of data, which can be used to solve a given task including, among others, fuel characteristics and climatic data for a particular country. However, there are also parameters that need to be provided by the user of the programme. These parameters concern elementary categories of cars due to, inter alia, type of engine cycle, type of combustion system, fuel type, engine displacement and ecological level, determined for pollutant emission. The number of passenger cars (Fig. 1) was determined with the use of data contained in the Information System of the Central Register of Vehicles and Drivers (CEPiK) [1].

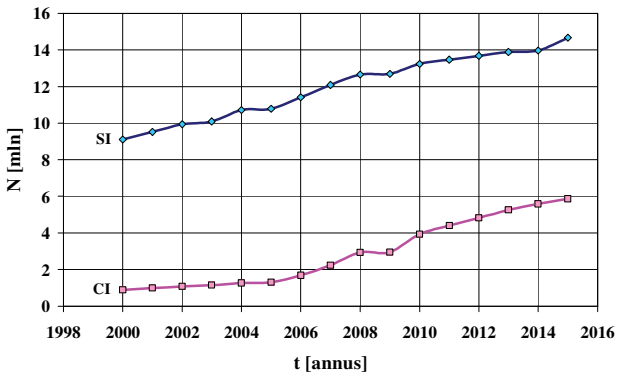


Fig. 1. Number of passenger cars with spark ignition- and compression ignition engines

The vehicle annual mileage provides the measure of the car-use intensity. This mileage was determined, taking into account, among other things [4]: the transport work and the value of technical and operational parameters characterising the work of road transport. Figure 2 shows the annual mileage of passenger cars with spark ignition- and compression ignition engines [4].

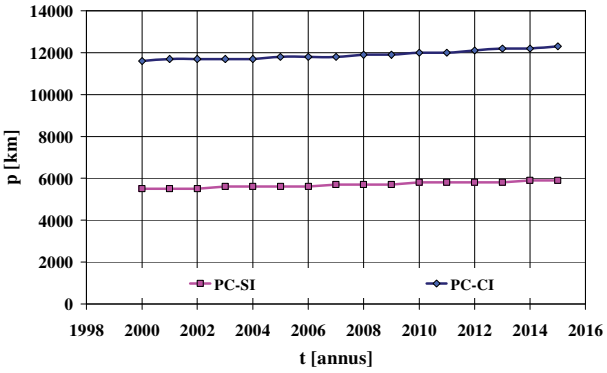


Fig. 2. Annual mileage of passenger cars with spark ignition- and compression ignition engines

A specially developed model of vehicle use intensity, build on the principle of functional similarity, was used to determine the annual mileage of motor vehicles, per elementary ecological categories which are related to pollutant emission. Data on motor vehicle structure at the level of elementary categories were used to identify the model [10].

The description of vehicle traffic [3, 6] was assumed in accordance with the data provided in [4].

Figure 3 shows the mileage of passenger cars under the following model traffic conditions: urban, rural and on highways and expressways; while Fig. 4 – the average vehicle velocity under the above mentioned conditions.

There is a large difference in national annual emission for compression ignition engines and spark ignition engines. Particularly significantly is the national annual emission for cars with spark ignition engines for carbon monoxide and volatile organic compounds. For nitrogen

oxides, there is a growing tendency for national annual emission. This is the result of the increasing number of cars with compression ignition engines. Of course, the national annual emission of particulate matter from cars with compression ignition engines is much higher.

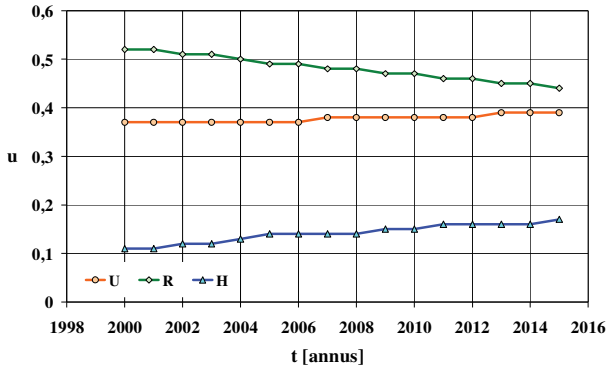


Fig. 3. Mileage of passenger cars under the following model traffic conditions: urban, rural and on highways and expressways

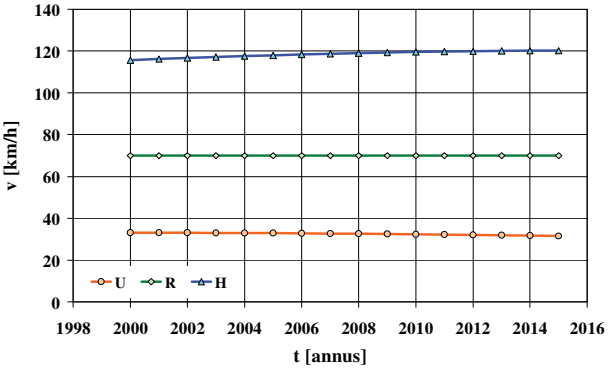


Fig. 4. Average velocity of passenger cars in towns, outside towns, on highways and expressways

The average mileage of a vehicle after engine start, used to determine the cold-start emission, was assumed to be 12 km [1].

3. The results of quantifying pollutant emission from passenger cars in the years 2000–2015

Figures 5–15 show the national annual pollutant emission, by selected pollutants, from passenger cars.

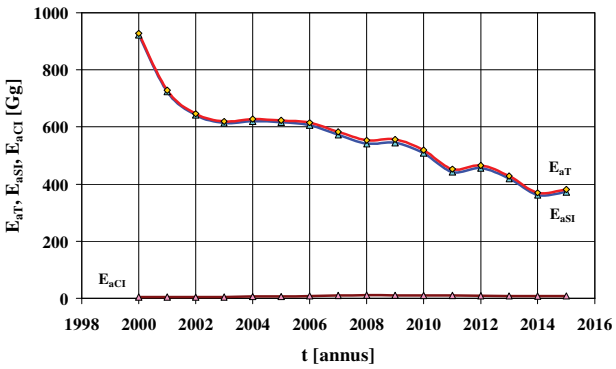


Fig. 5. National annual emission of carbon monoxide from passenger cars

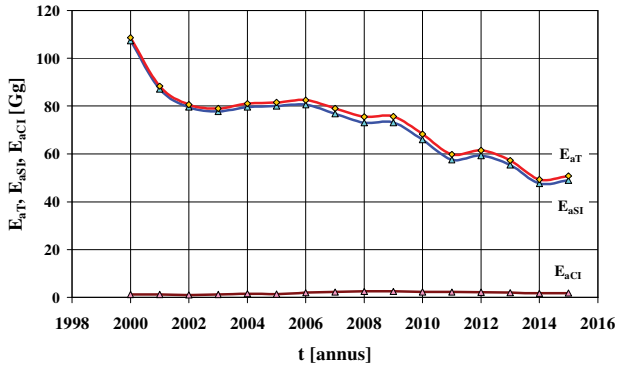


Fig. 6. National annual emission of volatile organic compounds from passenger cars

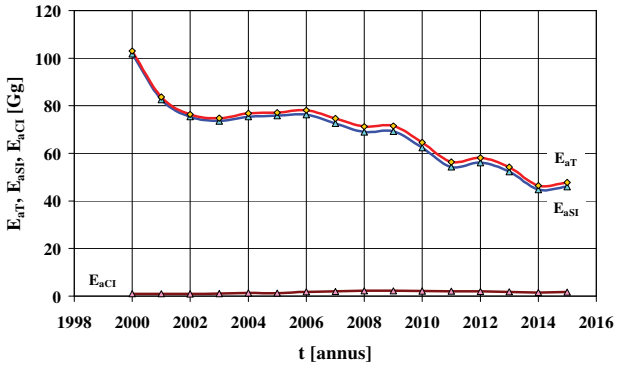


Fig. 7. National annual emission of non-methane organic compounds from passenger cars

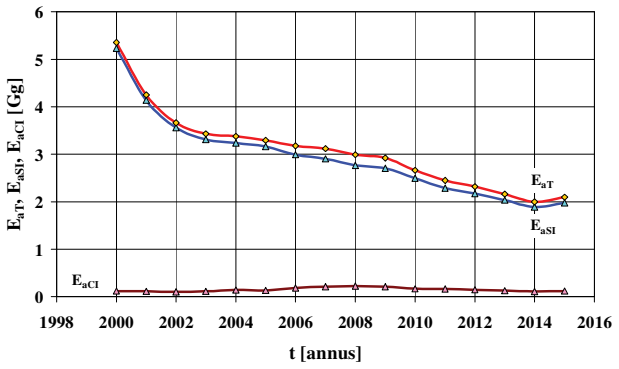


Fig. 8. National annual emission of methane from passenger cars

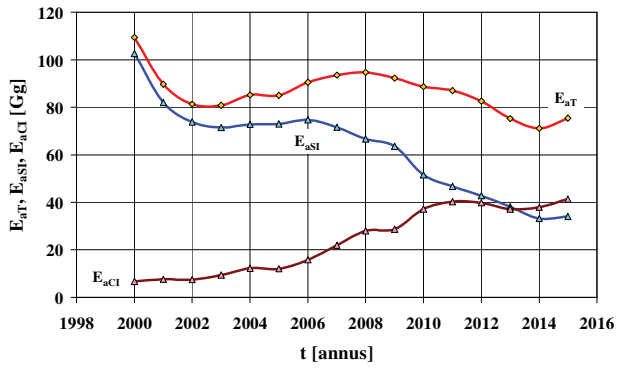


Fig. 9. National annual emission of nitrogen oxides from passenger cars

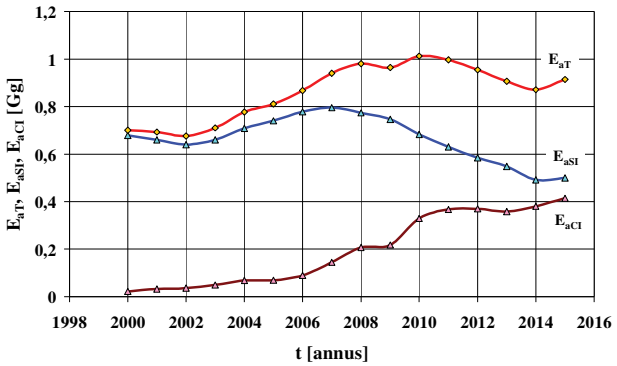


Fig. 10. National annual emission of nitrous oxide from passenger cars

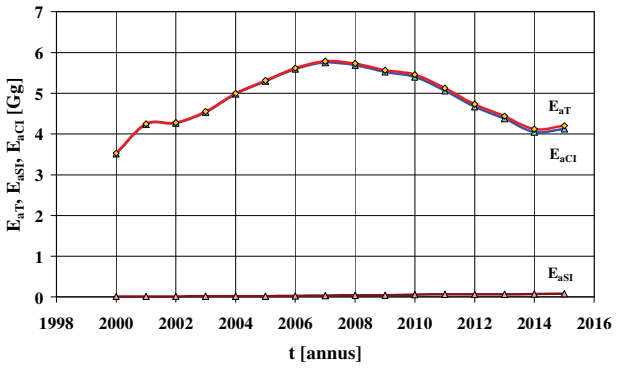


Fig. 11. National annual emission of ammonia from passenger cars

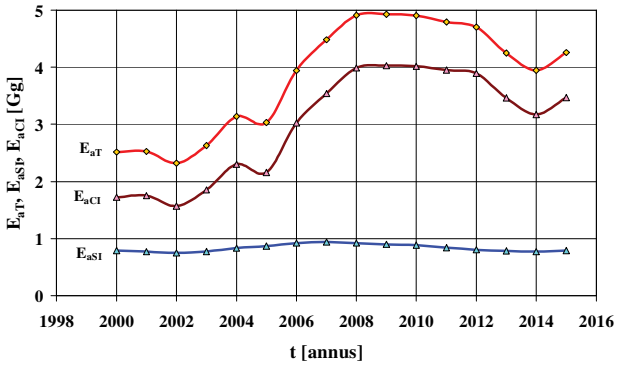


Fig. 12. National annual emission of particulate matter PM2.5 from tribological elements of passenger cars

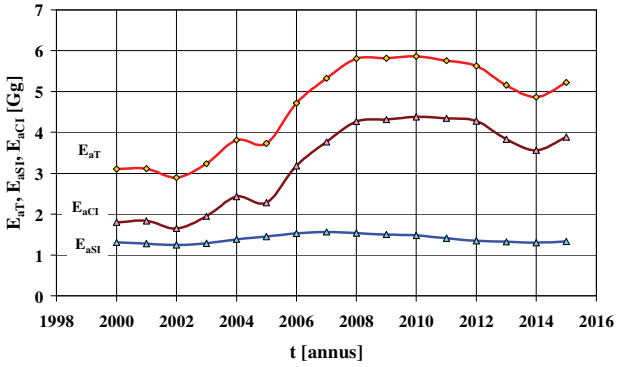


Fig. 13. National annual emission of particulate matter PM10 from tribological elements of passenger cars

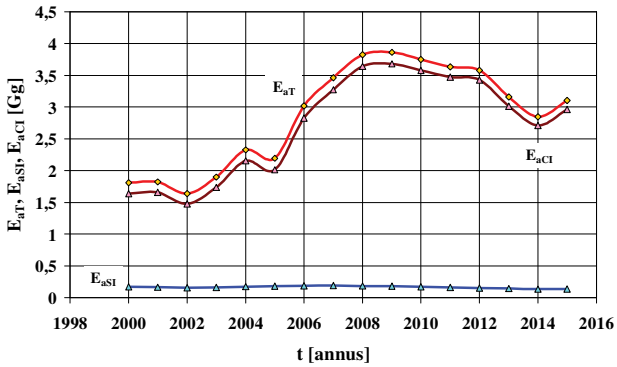


Fig. 14. National annual emission of particulate matter from the exhaust system of passenger car engines

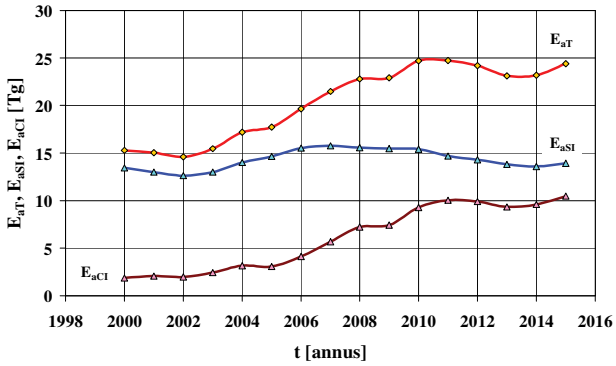


Fig. 15. National annual emission of carbon dioxide from passenger cars

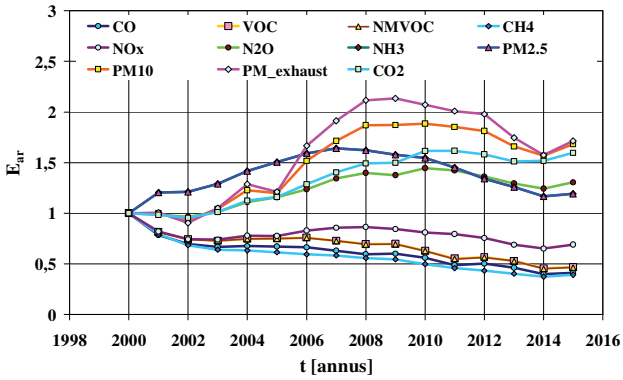


Fig. 16. Relative national annual emission of individual pollutants

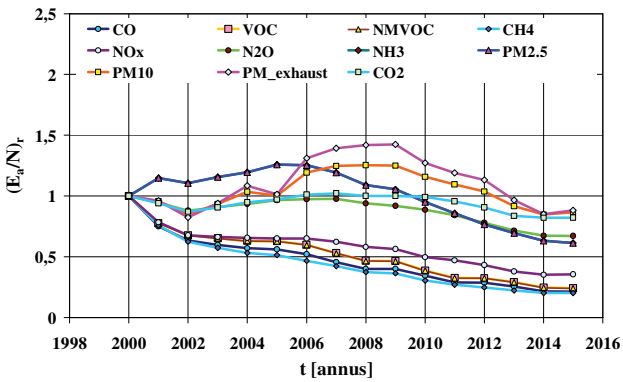


Fig. 17. Relative national annual emission of individual pollutants from a single passenger car

In Figure 16, the relative national annual emission of individual pollutants from passenger cars is presented, relative to the national annual emission in 2000. Whereas, Figure 17 shows the relative national annual emission of individual pollutants from a single conventional passenger car, as compared to the national annual emission in 2000.

4. Conclusions

The following conclusions can be drawn from the results of study carried out on the model of pollutant emission from passenger cars:

1. For the majority of harmful substances, the emission of which is limited by European regulations, there is a clear trend of decreasing national annual emission over the subsequent years of inventory, although the number of vehicles and the intensity of their use increase as the years go by. Apparently, this is evident in the case of carbon monoxide, volatile organic compounds, non-metallic volatile organic compounds and methane. Less evident is this tendency for nitrogen oxides: in the case of spark-ignition engines, there is a decrease in the national annual emission from 2006 onwards, while in the case of compression ignition engines, this emission is increasing, albeit national annual emission for all passenger cars decline since 2008. Annual emission of particulate matter increase until 2008 and then tend to stabilize or decline.
2. For carbon monoxide, volatile organic compounds, non-metallic volatile organic compounds and methane, the national annual emission from compression-ignition engines are considerably lower than those from spark-ignition engines. The opposite relationship is for solids.
3. The national annual carbon dioxide emission tend to increase, which is related to the increase in fuel consumption due to the increase in the number of vehicles and the intensity of their use.
4. The relative national emission from one conventional passenger car have been on a clear decreasing trend since 2008 for all substances, but for most pollutants since already 2005 – despite the rapid increase in the number of vehicles and the intensity of their use. This is the result of technical progress in the development of construction of new passenger cars.

Nomenclature

CH_4	methane
CI	compression ignition
CO	carbon monoxide
PC-SI	passenger cars – spark ignition (engine)
SI	spark ignition
T	total (vehicles)
VOC	volatile organic compounds
C	coaches
CH_4	methane
CI	compression ignition
CO	carbon monoxide
E_a	national annual emission
H	highway
LCV	light commercial vehicles
LCV-CI	light commercial vehicles – compression ignition (engine)
LCV-SI	light commercial vehicles – spark ignition (engine)
Mc	motorcycles
Mp	mopeds
N	number of vehicles per cumulated category
P	annual mileage of vehicles per cumulated category
PC-SI	passenger cars – spark ignition (engine)
R	rural
SI	spark ignition
T	total (vehicles)
t	time
u	share of mileage of vehicles, per cumulated category, under model traffic conditions
U	urban
UB	urban buses
v	average velocity of vehicles per cumulated category
VOC	volatile organic compounds
N	number of passenger cars
N_2O	nitrous oxide
NH_3	ammonia
NMVOC	non-methane volatile organic compounds
NO_x	nitrogen oxides
PC	passenger cars
PC-CI	passenger cars – compression ignition (engine)
PM exhaust	particular matter from exhaust system
PM10	particular matter PM10 from tribological elements of a vehicle
PM2.5	particular matter PM2.5 from tribological elements of a vehicle

Bibliography

[1] BEBKIEWICZ, K., CHŁOPEK, Z., SZCZEPAŃSKI, K., ZIMAKOWSKA-LASKOWSKA, M. Results of air emission inventory from road transport in Poland in 2014. *Proceedings of the Institute of Vehicles*. 2017, **1**(110), 77-88.

[2] BEBKIEWICZ, K., CHŁOPEK, Z., SZCZEPAŃSKI, K., ZIMAKOWSKA-LASKOWSKA, M. The influence of the properties of vehicles traffic on the total pollutant emission. *Proceedings of the Institute of Vehicles*. 2017, **1**(110), 89-102.

[3] BEBKIEWICZ, K., CHŁOPEK, Z., SZCZEPAŃSKI, K., ZIMAKOWSKA-LASKOWSKA, M. Issues of modeling the total pollutant emission from vehicles. *Proceedings of the Institute of Vehicles*. 2017, **1**(110), 103-118.

[4] CHŁOPEK, Z., WAŚKIEWICZ, J. The forecast of the pollutant emission from automotive internal combustion

engines in Poland by 2030. *VI International Congress of Internal Engines*. 2015.
[5] CHŁOPEK, Z. Modelowanie procesów emisji spalin w warunkach eksploatacji trakcyjnej silników spalinowych. *Prace Naukowe. Seria „Mechanika"*. 1999, **173**. Oficyna Wydawnicza Politechniki Warszawskiej. Warszawa.
[6] CHŁOPEK, Z. Zasady modelowania zużycia paliwa i energii oraz emisji zanieczyszczeń związanych z użytkowaniem pojazdów drogowych. *Technika Transportu Szynowego*. 2015, **12**, 262-267.
[7] COPERT Training 5. COPERT 5 vs COPERT 4. European Environment Agency. 2016. emisia.com/sites/default/files/COPERT_5_features.pdf. (accessed 2016.12.06).
[8] EMEP/EEA air pollutant emission inventory guidebook – 2016. European Environment Agency. www.eea. europa.eu/publications/emep-eea-guidebook-2016. (accessed 2016.12.06).
[9] GKATZOFLIAS, D., KOURIDIS, CH., NTZIACHRISTOS, L., SAMARAS, Z. COPERT 4 Computer programme to calculate emissions from road transport. User manual (version 9.0). European Environment Agency. Emisia SA. 2012. (accessed 2016.12.06).
[10] INFRAS AG. Handbook emission factors for road transport 3.2. Quick reference. Version 3.2. Bern, 2014.
[11] 2006 IPCC Guidelines for National Greenhouse Gas Inventories. www.ipcc-nggip.iges.or.jp/public/2006gl/vol2.html (accessed 2016.12.06).

Katarzyna Bebkiewicz, MEng. – Institute of Environmental Protection – National Research Institute in Warsaw.

e-mail: *Katarzyna.Bebkiewicz@kobize.pl*



Krystian Szczepański, DSc., DEng. – Institute of Environmental Protection – National Research Institute in Warsaw.

e-mail: *Krystian.Szczepanski@ios.edu.pl*



Prof. Zdzisław Chłopek, DSc., DEng. – Institute of Environmental Protection – National Research Institute in Warsaw.

e-mail: *Zdzislaw.Chlopek@kobize.pl*



Magdalena Zimakowska-Laskowska, DSc., DEng. – – Institute of Environmental Protection – National Research Institute in Warsaw.

e-mail: *Magdalena Zimakowska-Laskowska @kobize.pl*



Article citation info:
ALQAHTANI, A., WYSZYNSKI, M., MAZURO, P., XU, H. Evaluation of the effect of variable compression ratios performance on opposed piston 2-stroke engine. *Combustion Engines*. 2017, **171**(4), 97-106. DOI: 10.19206/CE-2017-417

Ali ALQAHTANI
Miroslaw WYSZYNSKI
Pawel MAZURO
Hongming XU

CE-2017-417

Evaluation of the effect of variable compression ratios performance on opposed piston 2-stroke engine

Numerous skills involving the introduction of (OP) opposed piston engine have been developed in the recent past. Indeed, novel techniques can help to improve the performance of the engine. The aim of this paper is to model and simulate a simple single-cylinder two-stroke opposed-piston engine and minimise fuel consumption and heat loss, using the software programme AVL BOOST™. AVL BOOST is an engine modelling software, which analyses the performance of a modelled single cylinder two-stroke opposed-piston engine by changing desired parameters. In order to meet this aim, experimental results from a unique engine are used to make a comparison with the results obtained from AVL BOOST model. Six combinations of compression ratios (12, 13.5, 15, 16.5, 18 and 19.5) are analysed in this study with the engine speed running at 420 rpm and 1500 rpm. In addition to the compression ratios, the effect of stroke-to-bore (S/B) ratios on OP2S performance is investigated. Various values of S/B ratios, whilst maintaining a constant swept volume, port geometry and combustion timing, and their effect on fuel consumption and heat loss are analysed in this study.

A comparison between the two engine speeds with increasing combinations of compression ratios, and the S/B ratios revealed minimal differences in peak pressure, peak temperature, IMEP, ISFC, indicated efficiency and total heat loss. Detailed analyses of these parameters are highlighted in discrete sections of this paper.

Key words*: opposed piston, AVL boost, VCR, compression ratio, numerical simulation*

1. Literature review

Witting engineered the first OP engine to have appeared for public use in Germany, in 1878. Although, it was only commercialised for land marine and aviation purposes in the 1900s. Pinault and Flint [2], interpret that Witting's OP engine has a classic three-throw crank with the centre throw linked to the inner piston, which operated on a four-stroke cycle. Prolific OP engines have typically functioned on a two-stroke cycle, as they were prominent in achieving high thermal efficiency as well as high power density. In 1888, Oechelhaeuser and Hugo Junkers revolutionised OP engines with the consideration of two-stroke operation. This OP2S engine produced some immense figures with a mechanical efficiency of 77% and a 40% reduction in fuel consumption in comparison to a modern day four-stroke engine. Between 1930 and 1945, Hugo Junkers developed and manufactured OP engines for use in German civil and military airplanes. In World War Two, Junkers 205 and 207 aviation engines were record-breaking, in terms of fuel efficiency and reaching altitudes of 20,000 feet [3]. The basic concept, of Hugo Junkers, has employed in many applications with a trend towards very large capacity installations.

During the early 1900s, only a few OP engines were developed with a varying degree of success. One of which was the Doxford engines. William Doxford and Sons Ltd, was a British shipbuilding and marine engineering company. Doxfords developed vertical, OP2S diesel engines for ships (up to 8000 bhp). This design became a standard unit for British flag-carriers. However, in the early 1960s, the licence-built Sulzer and B&W engines have been developed to overcome Doxfords pistons deficiencies. The single-crankshaft engines had connecting rods for both the lower and upper pistons, with two rods for the upper piston. The factor that differentiates Doxford's OP engine to Junkers' OP engine is that in Doxford's the upper pistons are connected to the single crankshaft by connecting rods each side of the main cylinder. One of the advantages of Doxford's OP engines, over the traditional four-stroke engine, were that the two-stroke running enables a low operating speed (115 rpm), which eliminates the requirement for a reduction gearbox between the engine and the propeller. In addition, no reverse gear was required since the engine was reversible. The Doxford engine was being predominant until its decline in 1980s. [4].

The Stelzer engine was proposed by Frank Stelzer. It uses conjoined pistons in a push-pull arrangement which allows for fewer moving parts and simplified manufacturing. Moreover, the engine fairly indestructible and almost maintenance-free. There are two combustion chambers and a central recompression chamber. Control of the air flow between the recompression chamber and the combustion chambers is made by stepped piston rods. In 1983, a prototype engine was demonstrated in Frankfurt. A prototype car with a Stelzer engine and electric transmission was shown at a German motor show in 1983 which thermodynamics efficiency of 56%.

An exhaustive thermodynamic investigation has been practised by Herold et al. [5] titled; "Thermodynamic Benefits of Opposed-Piston Two-Stroke Engines" demonstrate the fundamental efficiency advantages of OP2S engine over a four-stroke engine with noticeable power output and geometry. From the simulation results, it can be observed that a 10.4% reduction was noted in ISFC over the four-stroke engine. Along with the geometric advantage of reduced heat transfer of OP architecture, the double firing frequency of the two-stroke cycle allows linear operating conditions. This enables the two-stroke cycle to maintain high ratio of specific heats during combustion, and reduced energy release density. The OP2S

engine demonstrated an indicated thermal efficiency of 53%, which is 5.5% greater than its four-stroke counterpart.

Another intriguing piece of work was carried out by Rishikesh Venugopal, in 2013; utilising three-dimensional (3D) computational fluid dynamics (CFD) integrated with state-of-the-art spray, turbulence and combustion models. Venugopal [6] analysed the effects of injection pattern design on piston thermal management through combined experiment and analytical approach.

Achates Power is based in San Diego, California and was founded in 2004 by James Lemke. At Achates Power, modern analytical tools, materials, and engineering methods have been enforced to develop an OP2S compression ignition engine for use in commercial and passenger vehicles. According to the Achates Power Opposed-Piston Two-Stroke Engine: Performance and Emissions Results in a Medium-Duty Application [1], "the engine design has demonstrated a 15–21% BSFC improvement compared to a state-of-the-art 2010 medium-duty diesel engine at similar engine-out emissions levels". Moreover, "oil consumption has been measured to be less than 0.1% of fuel over the majority of the operating range". With the two-stroke cycle, each combustion event is shorter in duration thus closer to optimum timing as compared to the four-stroke engines. While development of historic OP engines ceased for use in on-road car and truck applications with the introduction of modern emissions standards, Achates Power says that it has patented many modifications to the original architecture in order to meet current standards. A detailed numerical simulation of the Achates Power 1.64L single cylinder research engine is executed and validated against existing experimental data.

Most recently, WUT is developing a new-type barrel engine called PAMAR-4 under a Polish-Norwegian research programme. This is an iteration from a successor of PAMAR-3, which was a 3.0L, 340 kW engine built for the purposes of aviation. PAMAR 3 was a huge success mainly due to an eight-cylinder barrel engine. Counter-rotating cylinder groups and crankshaft provide cancellation of torque reactions and gyroscopic forces during engine speed fluctuations and vehicle manoeuvres. Some of the advantages of a barrel engine are as follows: simple technology; less parts required hence low weight; axial symmetry; low vibration level; and high power concentration. PAMAR-3 accomplished a test bench efficiency of 44% and has successfully functioned on LPG, propane, alcohol, CNG, gasoline and diesel fuels. One of the many reasons for the great outputs of the PAMAR-3 engine was due to an OP2S engine which meant; unnecessary strokes were eliminated; uniflow scavenging; and no valvetrain. In addition, the elimination of a crankshaft reduced piston side thrust. All of these factors led to an increased ME, henceforth increased engine efficiency. Another reason for great outputs of the PAMAR-3 engine is due to its axial symmetry of cooling system – keeping a constant thermal condition in all cylinders – and inlet and exhaust axial symmetry – keeping a constant volumetric efficiency and equivalence ratio in all cylinders. Consequently, equal work of cylinders thus Homogeneous Charge Compression Ignition (HCCI) at whole range of loads. The manufacturing cost of PAMAR-3 engine was reduced by an incredible 40%. Opaliński et al. [7] refers to a comparison of gas-dynamics of this engine, which has been modelled and quantified using Ricardo WAVE (1D) and Ansys Fluent (3D CFD).

2. PAMAR engine

A research team at WUT in Poland have been developing a modern car engine, called PAMAR, under the management of dr Pawel Mazuro. Having collaborated with the research team, some experimental data from PAMAR series engine were obtained and used for the modelling process of this project.

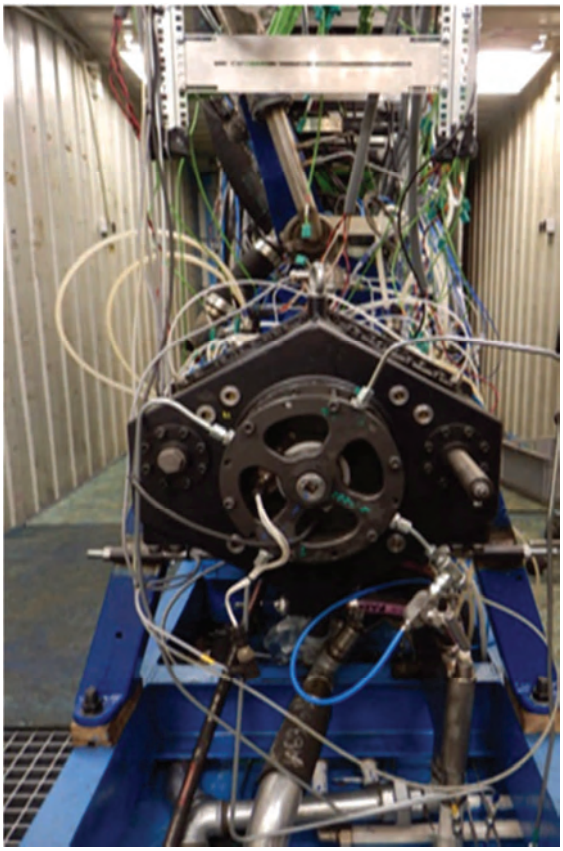
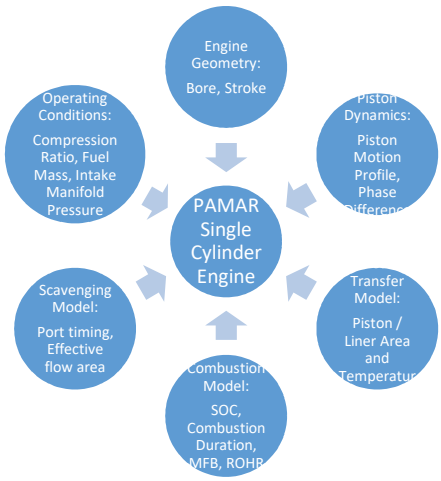


Fig. 1. PAMAR-4 Engine

2.1. Numerical methodology



2.2. PAMAR engine OP configuration

PAMAR engine is equipped with uniflow scavenging system with an injector on its cylinder liner. Gas ports are positioned on either ends of the cylinder, intake ports to deliver fresh charge into the cylinder from one side, and exhaust ports on the other side to get rid of the burnt gas as well as residuals. The piston motion controls the opening and closing of these ports. Two pistons are deployed at opposite ends of the cylinder liner, intake and exhaust pistons, respective to their effective control of port opening and closing during the scavenging process. A combustion chamber is formed at inner dead center (IDC), i.e. at the point of minimum distance between the pistons. Outer dead center (ODC) is defined when the distance between two pistons are at maximum.

The reciprocation movements of piston are driven by opposed crank-connecting rod mechanism. The reciprocating movement accomplishes air-exchanging by combining the position with gas ports. [8]

2.3. OP2S engine working cycle

The OP2S cycle is completed by every crankshaft revolution. The compression stroke begins when the pistons entirely cover the intake and exhaust ports, and ends once the piston reaches IDC. At the end of the compression stroke, fuel is injected at high pressure, just before the pistons reach IDC. Subsequently, fuel is atomized, evaporated and burned in the high pressure, high temperature environment produced by the in-cylinder air which is then followed by the expansion stroke.

The expansion stroke is induced due to the prompt increase in pressure and temperature as a result of fuel combustion, causing the pistons to move from IDC to ODC. Near the end of the expansion stroke, exhaust ports are open to allow burnt gases to discharge with the aid of residual gas pressure. Moments later, the intake ports are opened, allowing the fresh charge to enter the cylinder at the same time driving the exhaust gas out of the cylinder. At this instant the in-cylinder pressure is lower than atmospheric pressure.

Scavenging process is vital as it comprises of both forcing the exhaust gas out of, and consenting fresh charge into, the cylinder. Intake and exhaust ports remain open at the start of the compression stroke, therefore scavenging process begins from the instant the ports are uncovered during the expansion stroke, and continues until completely closed again.

3. Methodology

3.1. Numerical modelling of engines

There are three major 1D engine simulation computer programs when it comes to numerical modelling of ICEs, namely GT POWER, Ricardo WAVE, and AVL BOOST™. Unfortunately, since OP engines are unique, none of them has a built-in module capable of simulating an OP engine. Having said that, AVL BOOST is the favorite of the above-mentioned, due to its compatibility of defining relative piston motion profile, thus enabling to model the OP configuration. In addition, AVL BOOST provides the option of advanced engine simulations in terms of cycle simulation, design and predictive combustion models, in comparison to other industrial modelling platforms.

3.2. OP configuration in AVL BOOST

As mentioned before, AVL BOOST has no built-in module capable of simulating an OP engine. Thus, simulating a flawless model of OP engine proved challenging at the initial stages of this project and some difficulties were encountered during the process of modelling.

3.3. Engine cycle simulation

The main tool used in AVL BOOST software is Workspace (graphical user interface), which is composed of predefined elements that represent components of ICE. The 1D engine model is built within the workspace by selecting various elements from the element tree and are joined by pipe attachments to their desired connectors. Table 1 lists all the elements, as well as quantity, used to create an OP configuration in AVL BOOST.

Table 1. Elements used to create an OP configuration in AVL BOOST

Element	Symbol	Quantity
Engine	E	1
Cylinder	C	1
Plenum	PL	2
Measuring Point	MP	3
System Boundary	SB	2
Pipe	–	4

Since an OP is an unique engine, a cylinder with a plenum on either side of the cylinder was modelled to create an OP configuration in AVL Boost. The screenshot of the model in AVL BOOST is represented in Figure 2.

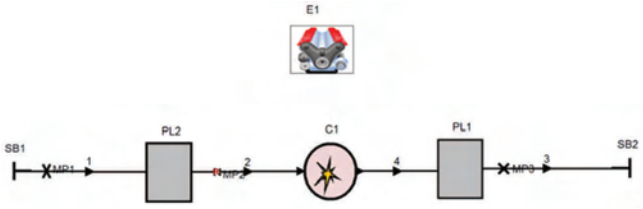


Fig. 2. Screenshot of the model in AVL Boost

3.4. Defining constraints in AVL Boost

Having designed the model in AVL BOOST, the data collected from PAMAR series engine were then entered into the computer software.

Certain constraints, such as crank radius, con-rod length, bore and stroke were collected from PAMAR. These values are listed in Table 2. Using these constraints, other parameters such as squareness, bore surface area and swept volume were calculated, which are also presented in Table 2. Although a piston stroke length of 150 mm was required, the con-rod length was defined as 300 mm (twice the stroke) in order for the software to assume it is an OP engine.

Phase difference was a vital variable in this investigation. It affects the minimum and maximum value of the cylinder volume. As the phase difference increases, the minimum distance between the pistons at IDC increases, thus reducing the maximum distance at ODC. Consequently, compression ratio is adversely affected.

Table 2. Engine geometry parameters used in AVL BOOST

Parameter	Value
Crank Radius (mm)	75
Con-rod length (mm)	300
Bore (mm)	55
Stroke (mm)	150
Squareness	0.367
Bore Surface Area (cm2)	23.76
Swept Volume (cm3)	356

According to Ma et al. [8], with increasing piston motion difference, from 0° to 18°, delivery ratio and scavenging efficiency increases progressively throughout. On the other hand, trapping efficiency initially increases and then decreases after it achieves optimum efficiency at 15°, so does indicated work. As a result, 15° was decided upon as phase difference. The intake port and exhaust port dimensions are listed in Table 3.

Table 3. Dimensions for intake port and exhaust port

	Intake port	Exhaust port
Height (mm)	20	25
Width (mm)	6.4	6.4
Number of holes	24	18
Maximum Flow Area (mm2)	3072	2880
Phase difference (°)	0	15

Since AVL BOOST has no built-in module capable of simulating an OP engine, the piston motion was user defined. Due to a phase difference in piston motion on both pistons, the two pistons are out of alignment, thus non-harmonic (i.e. do not reach IDC in harmony). Having decided upon a value for the phase difference (α), the piston displacements were calculated using the following equations [8]:

$$X_{in} = r(1 - \cos\left(\varphi - \frac{\alpha}{2}\right) + \frac{1}{2}\lambda\sin^2\left(\varphi - \frac{\alpha}{2}\right)) \quad (1)$$

$$X_{ex} = r(1 - \cos\left(\varphi + \frac{\alpha}{2}\right) + \frac{1}{2}\lambda\sin^2\left(\varphi + \frac{\alpha}{2}\right)) \quad (2)$$

where: X_{in} and X_{ex} are displacement of the intake and exhaust piston respectively; r is the crank radius; λ = r/l is the ratio of crank radius to connecting rod; l is the length of the connecting rod; φ is the equivalent crank angle.

Intake and exhaust pistons move towards each other face-to-face. One of the limitations observed whilst modelling an OP engine is that the option user defined piston motion in AVL BOOST only allows to input a relative position of the piston profile. Relative displacement is obtained by simply adding the displacements of each piston. This approach conserves the volume change rate of the engine, therefore avoiding possible discrepancies of work done in the thermodynamic cycle. The relative displacement of piston was determined by the following equation [8]:

$$X_{relative} = r(1 - \cos\left(\alpha - \frac{\varphi}{2}\right)) + r(1 - \cos\left(\alpha + \frac{\varphi}{2}\right)) \quad (3)$$

From the graph above, it is evident that the compression and expansion stroke of this OP2S engine is asymmetric about the IDC. The exhaust piston leads from 0˚CA to 180˚CA and the intake piston leads from 180˚CA to 360˚CA relative to each other.

The effect of variable compression ratio on OP2S engine performance was analysed. To investigate this effect, six different values for the compression ratio were selected upon ranging from 12 – 20. Using the compression ratios, clearance volume and clearance height were calculated which are presented in Table 4.

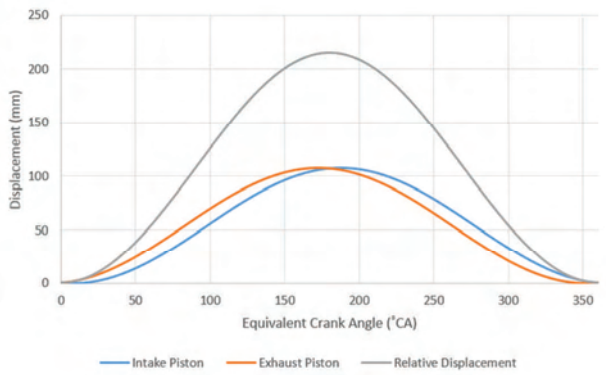


Fig. 3. Graph of piston motion profile

Table 4. Variables of the model

Compression ratio	12	13.5	15	16.5	18	19.5
Clearance volume [mm^3]	32398	28510	25455	22992	20963	19263
Clearance height [mm]	13.636	12	10.714	9.677	8.824	8.108

The heat release rate was calculated in Microsoft Excel using pressure obtained from experimental data of PAMAR series engine, and volume using the parameters in Table 2. The pressure and volume were obtained for one cycle (360°) with an increment of 0.5°. Pressure and volume against crank angle degree (CAD) are illustrated in Figures 4a and 4b respectively.

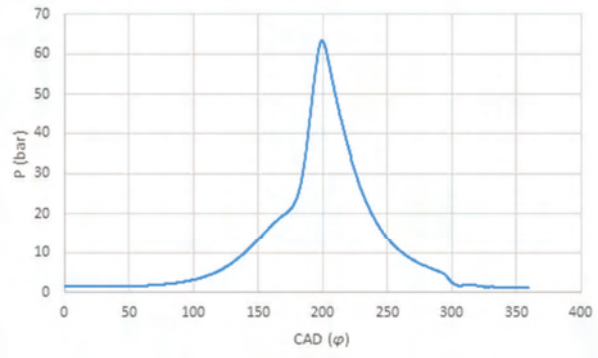


Fig. 4a. Graph of cylinder pressure against CAD

The change in cylinder volume with respect to CAD was calculated using Equation 4 from [9], where: A is bore area; r is crank radius; φ is crank angle; and λ is ratio of crank radius to con-rod length.

$$V = Ar[(1 - \cos\varphi) + \frac{\lambda}{4}(1 - \cos 2\varphi)] \quad (4)$$

A p-V diagram was plotted to visualise the changes in pressure with respect to volume in an opposed-piston system (see Fig. 4c). The graph also represents the amount of energy expended or received by the system as indicated work which can be determined by integrating the area within the curve.

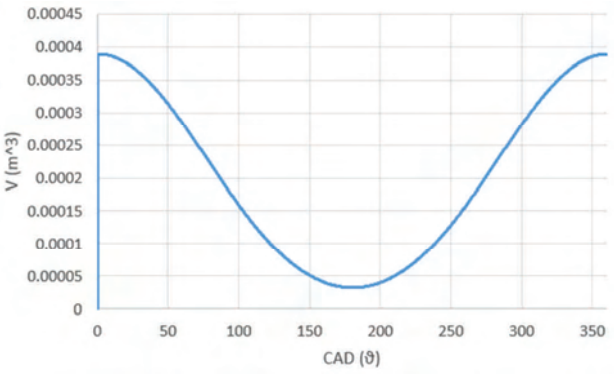


Fig. 4b. Graph of cylinder volume against CAD

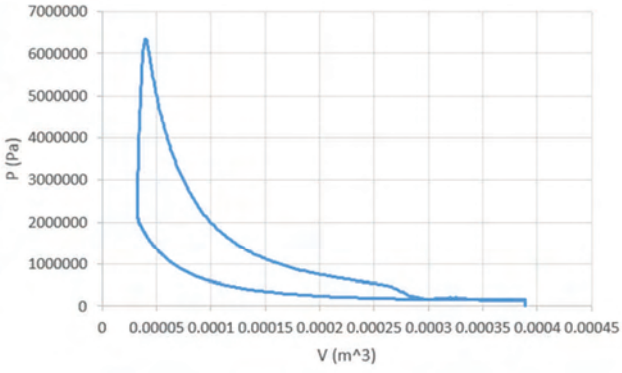


Fig. 4c. Graph of cylinder pressure against cylinder volume

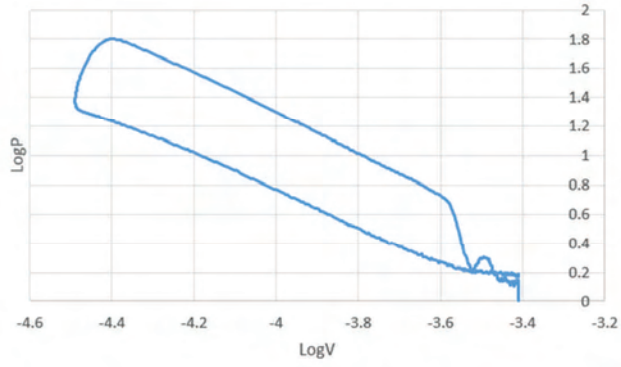


Fig. 4d. Graph of logP against logV

Figures 4c and 4d shows pressure-volume data on both a linear p-V and a log(p) versus log(V) diagram. In Figure 4d, the compression process is a straight line of slope 1.32, and the expansion stroke following combustion is essentially linear with slope 1.36. Since both the compression of the unburned mixture prior to combustion and the expansion of the burned gases following the end of combustion are close to adiabatic isentropic process (for which pV^k = constant; $k = c_p/c_v$), the observed behaviour is as expected [10]. More extensive studies [11, 12] show that the compression and expansion process are well fitted by a polytrophic relation:

$$pV^n = \text{const} \quad (5)$$

log(p) versus log(V) plots can be used to check the quality of cylinder pressure data [10]. Furthermore, log(p) versus log(V) plots approximately define the start and end of combustion, but do not provide a mass fraction burned profile.

Heat release calculations are an approach to acquire information about combustion processes. Heat release analysis is performed based on Cylinder Gas Pressure (CGP) data. The most widely used one was developed by Krieger and Borman [13].

Using the cylinder pressure (p), cylinder volume (V) and the obtained polytropic index (k), the heat release rate (HRR) was calculated with using Equation 6 [14].

$$HRR = \frac{k}{k-1} p \frac{dV}{d\varphi} + \frac{1}{k-1} V \frac{dP}{d\varphi} \quad (6)$$

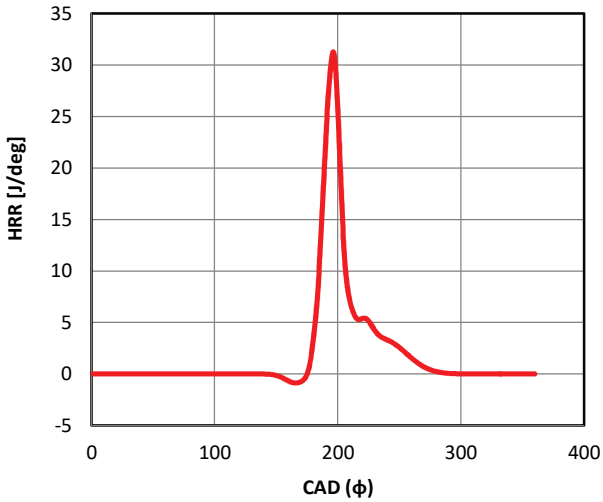


Fig. 5. Graph of heat release rate against CAD

The piston and cylinder head shapes and valve geometry influence the turbulence level in the engine and therefore the rate of heat release during combustion [15].

Having calculated the desired values and specified the range for compression ratio, the simulation was set to run at two engine speeds, 420 rpm and 1500 rpm, to make a comparison. In these, the rate of heat release was assumed as not changing between cases.

4. Effect of variable compression ratio (VCR)

VCR is a technology that allows to adjust the compression ratio of an engine while it is in operation to increase fuel efficiency while under varying loads. Thus, a VCR mode allow for the volume passed the piston at IDC to be changed. For automotive use this is achieved dynamically in response to the load and driving demands. VCR is a cost-effective method of achieving increased fuel

economy, reduced carbon dioxide emission about 30-40% in comparison to conventional motors.

The effect of variable compression ratio at two different engine speeds – 420 rpm (simulation 1) and 1500 rpm (simulation 2) – was investigated and discussed in this section. To do so, the following parameters were analysed: IMEP; peak pressure; peak temperature; ISFC; BSFC; volumetric efficiency; and mechanical efficiency. The results obtained from AVL Boost are presented in a tabular form below.

Table 5. Results obtained from AVL Boost

	420 rpm						1500 rpm					
Parameters	Compression Ratio						Compression Ratio					
	12	13.5	15	16.5	18	19.5	12	13.5	15	16.5	18	19.5
Peak Pressure (MPa)	5.02209	5.36196	5.67318	5.95697	6.21475	6.44725	5.10922	5.48479	5.81518	6.12601	6.41423	6.68478
Peak Temperature (K)	2490.22	2493.29	2496.08	2499.01	2500.41	2501.73	2560.58	2570.6	2576.03	2582.04	2585.18	2588.01
IMEP (Pa)	784179	785847	785967	784786	782716	779981	926046	941214	951718	962099	969500	976128
BMEP (Pa)	684179	685847	685967	684786	682716	678881	810046	825214	835718	846099	853500	860128
FMEP (Pa)	100000	100000	100000	100000	100000	100000	116000	116000	116000	116000	116000	116000
ISFC (kg/Ws) e-008	7.3713	7.3557	7.3546	7.3656	7.3851	7.4110	6.2421	6.1415	6.0737	6.0082	5.9623	5.9218
BSFC(kg/Ws) e-008	8.4487	8.4282	8.4267	8.4412	8.4668	8.5009	7.1359	7.0048	6.9167	6.8319	6.7726	6.7204
Indicated Efficiency	0.311864	0.312527	0.312575	0.312105	0.311282	0.310194	0.368284	0.374316	0.378493	0.382622	0.385565	0.388201
Pressure @SOC (Pa)	2.38144	2.67484	2.95111	3.22056	3.48481	3.73191	2.36844	2.66704	2.95881	3.24454	3.52245	3.79302
Temperature @SOC (K)	903.942	927.435	948.214	966.715	983.771	997.751	898.031	928.395	945.961	966.209	984.407	1000.98
Vomuetric effciency	0.880563	0.86811	0.857698	0.849614	0.842933	0.837365	0.855234	0.842658	0.832687	0.824669	0.818034	0.812466
Delivery ratio	91.5004	91.5061	91.5108	91.5156	91.5208	91.526	26.6925	26.6928	26.6935	26.6939	26.6945	26.6949
Heat loss - Piston (kJ)	0.0183031	0.0183128	0.0183113	0.0183125	0.0183145	0.0183136	0.014174	0.0141737	0.0141734	0.0141731	0.0141729	0.0141727
Heat loss - Liner (kJ)	0.105667	0.105763	0.105747	0.105758	0.105778	0.105768	0.0799471	0.0799402	0.0799343	0.0799293	0.0799251	0.0799215
Heat loss - Total (kJ)	0.123945	0.12405	0.124032	0.124044	0.124066	0.124055	0.0940821	0.0940792	0.0940763	0.094074	0.0940719	0.0940707
Indicated Power (kW)	1.96	1.96	1.96	1.96	1.96	1.96	8.25	8.39	8.48	8.57	8.64	8.7
Friction Power (kW)	0.25	0.25	0.25	0.25	0.25	0.25	1.03	1.03	1.03	1.03	1.03	1.03
Brake Power (kW)	1.71	1.71	1.71	1.71	1.71	1.71	7.22	7.35	7.45	7.54	7.61	7.68
Indicated Thermal Efficiency												
Mechanical Efficiency	0.87244898	0.87244898	0.87244898	0.87244898	0.87244898	0.87244898	0.875151515	0.876042908	0.878537736	0.879813302	0.880787037	0.882758621

Some parameters either remained constant with increasing CR or did not show a trend. This suggests that these parameters were independent of CR. Thus, Graphs of each parameter mentioned above against compression ratio were plotted for both simulations of the models to visualise values in Table 5 clearly.

4.1. Indicated mean effective pressure (IMEP)

IMEP is the ratio of indicated work to swept volume. IMEP is a fictitious constant pressure that would produce the same amount of work per cycle if it acted on the piston during the power stroke.

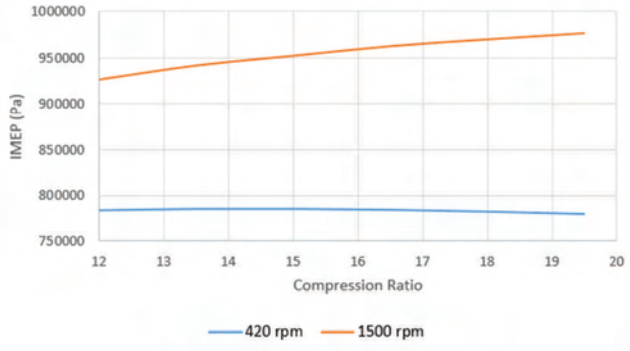


Fig. 6a. Graph of IMEP against compression ratio

The general trend is that a higher IMEP is achieved with increasing engine speed. In simulation 1, IMEP remains approximately around 780000 Pa where as in simulation 2, when the engine speed was increased from 420 rpm to 1500 rpm, IMEP starts to increase from 926046 Pa to 976128 Pa, with increasing CR. The IMEP is higher when the engine speed is set at 1500 rpm.

4.2. Peak pressure

The purpose of an engine is to generate internal pressure which can be used to do work. Therefore, high pressures are desirable. However, excessively high and erratic pressures are a source of potential damage and should be avoided.

Cylinder pressure is the pressure in the engine cylinder during the two strokes of engine operation. Cylinder pressure is constantly changing inside the cylinder for both strokes. There are certain characteristics of this pressure which can be analysed, for example peak (maximum) cylinder pressure near IDC.

During the combustion stroke, the air/fuel mixture is ignited, creating very high cylinder pressure which rise very quickly (also known as the peak pressure). This is where the engine's power comes from, as it forces the piston down. As the piston moves towards ODC, the cylinder volume increases which reduces the cylinder pressure. When the piston reaches ODC there will be a significant amount of reduction in cylinder pressure.

Peak pressures occurring during combustion are much higher and are more difficult to obtain by calculation. Thus, AVL BOOST was used to determine the peak pressure for each case. Figure 6c indicates the change in peak pressure with increasing CR.

For the 420 rpm simulation, at a compression ratio of 12 and 19.5 the peak pressures were 5.02 MPa and 6.45 MPa,

respectively. As for the 1500 rpm simulation, at a compression ratio of 12 and 19.5 the peak pressures were 5.11 MPa and 6.68 MPa, respectively.

The general trend is that peak pressure increases with increasing CR. Since, compression ratio is equal to the ratio of volume at ODC and volume at IDC, compression ratio is inversely proportional to the volume at IDC. Thus, a higher CR means a reduction in volume at IDC. A reduction in volume at IDC means that the piston can do more work and compress the air/fuel ratio further, hence increasing the cylinder pressure at IDC (i.e. peak pressure). Thus, an increase in CR means an increase in peak pressure.

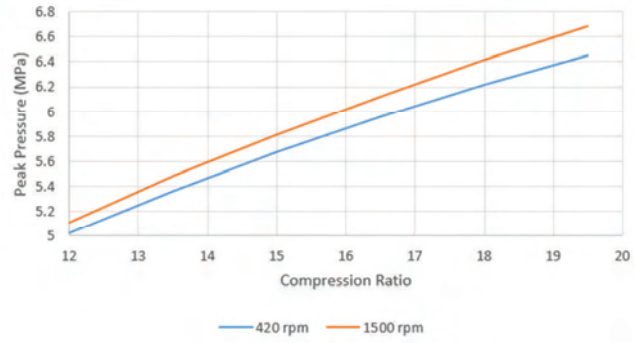


Fig. 6b. Graph of peak pressure against compression ratio

A more observed trend that can be obtained from Figure 6b is that a higher engine speed results in a higher peak pressure. At 420 rpm and 1500 rpm, the maximum peak pressure obtained were 6.45 MPa and 6.68 MPa (at a CR of 19.5), respectively. As the engine speed increases, the mixture in the combustion chamber must be ignited earlier as there is less time between spark and optimum peak pressure angle. In case the mixture density is changed due to higher compression ratio or boost, the spark has to be ignited later to achieve the same optimal point.

4.3. Peak temperature

During the combustion process, the cylinder gas temperature reaches a high value (known as the peak temperature). The maximum temperature was recorded at the IDC. A considerable amount of heat is transferred to the walls of the combustion chamber. Thus, it is vital to provide proper cooling to the walls of the combustion chamber. Chemical and physical changes in the lubricating oil are possible to occur due to the prevailing high temperature. Excessive cylinder wall temperatures will therefore cause the rise in the operating temperature of piston head, which can affect the strength of the piston severely.

Figure 6c suggests that for both simulations peak temperature increases with increasing CR. At an engine speed of 420 rpm peak temperature increases from 2490.22 K to 2501.73 K, and when the engine speed was set at 1500 rpm peak temperature increases from 2560.58 K to 2588.01 K. This suggests that at low engine speed, peak temperature increases with very small increments as the CR increases.

According to [15]: 'Peak temperatures may range from 2400 to 2800 K'. Thus, the peak temperatures obtained from AVL BOOST are acceptable.

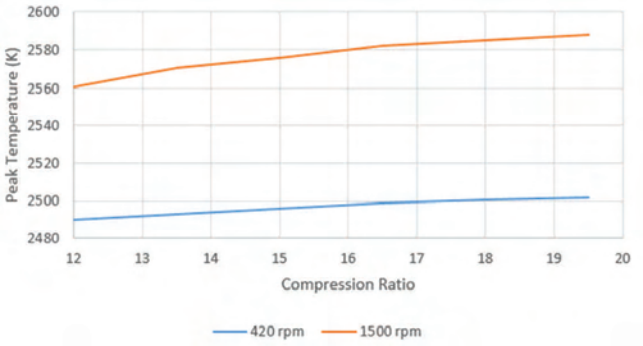


Fig. 6c. Graph of peak temperature against compression ratio

The compression due to piston motion and combustion in a confined volume leads to very high burned gas temperatures in reciprocating engines. The compression ratio determines the peak pressure and hence the peak temperature in the cycle. An increase in CR reduces clearance volume at IDC. As a result, cylinder pressure increases as it compresses air/fuel mixture further. Work done by the gas in the cylinder on the piston during the compression stroke heats the combustion products, thus increasing cylinder gas temperature. Therefore, increasing the CR, increases peak temperature.

Nitrogen oxides (NO_x) emissions result from the thermal fixation of atmospheric nitrogen, so control of these emissions can be achieved by reducing the peak flame temperatures. Therefore, in order to reduce lower peak temperature, the compression ratio must also be lower, thereby limiting NO_x formation. On the other hand, the NO_x, emission reductions achieved by reducing CR are smaller in comparison to those accumulated by retarding the spark. One other way of reducing peak temperature is by diluting the charge with cool combustion products. This process is known as exhaust gas recirculation (EGR). The benefits of cooling combustion products for dilution instead of excess air are as follows: 1) dilution of the air/fuel mixture without the addition of excess O_2 that aids in NO_x formation; and 2) an increase in the specific heat of the gas due to the presence of H_2O and CO_2, reducing the temperature somewhat more than would equivalent dilution with excess air. Another way of reducing peak temperature is through exhaust gas recirculation or retarding the injection timing. Injection timing delays cause the heat release to occur late in the cycle, after some expansion work has occurred, thereby lowering the peak temperature.

4.4. Engine efficiency

Engine efficiency is becoming a more prominent factor in automobile manufacturer's decision making. It is the relationship between the total energy contained in the fuel, and the amount of energy used to perform useful work. This makes engine efficiency one of the most vital factors to consider when modelling an internal combustion engine. Three efficiencies were discussed in this section of the report and these were: indicated, volumetric and mechanical.

4.4.1. Indicated efficiency

Thermal efficiency can be quoted as either brake or indicated. Indicated efficiency is derived from measurements taken at the flywheel.

Indicated efficiency is calculated as a result of indicated power. Since the indicated powers for the 420 rpm and 1500 rpm simulations remain constant (at 31%) and increase in small increments (from 36.8% to 38.8%) respectively, a similar observation can be noted for the indicated efficiencies also. Like the indicated power, the indicated efficiency is also higher when the engine speed is set at 1500 rpm, implying the power developed by combustion of fuel in the engine cylinder is greater with increased engine speed. This can be validated with the following equation

$$\mathrm{ip} = \mathrm{P} \cdot \mathrm{V} \cdot \mathrm{N} \cdot \mathrm{K} \tag{7}$$

where: ip is the indicated power; P is the mean pressure; V is the displacement volume; N is the rotational speed; and K is the number of cylinders.

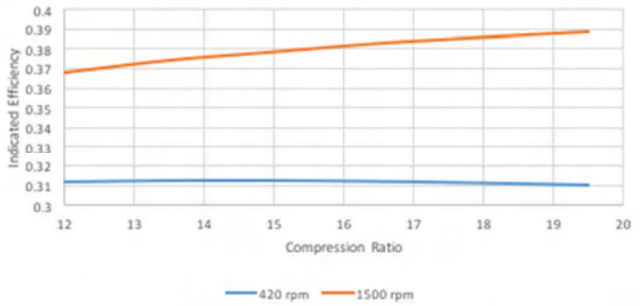


Fig. 6d: Graph of indicated efficiency against compression ratio

Thus, from Equation 7, indicated power is directly proportional to the rotational speed (i.e. engine speed).

4.4.2. Volumetric efficiency

The volumetric efficiency is probably one of the most variable efficiencies governing the performance of engines. Volumetric efficiency is the ratio of the actual volume of the air/fuel mixture drawn in during combustion to the swept volume of the piston. Volumetric efficiency determines how efficiently fuel is burnt thus affecting the power output, because the amount of air drawn inside the cylinder is dependent on the volumetric efficiency of an engine.

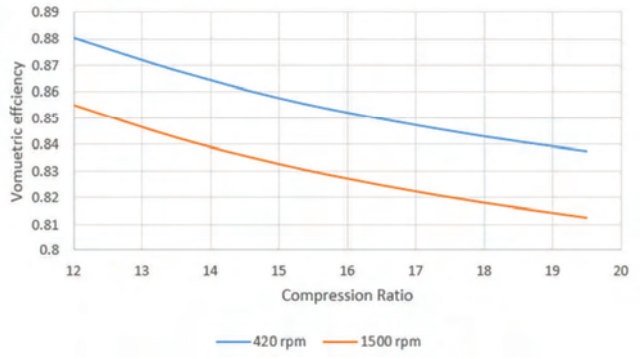


Fig. 6e. Graph of volumetric efficiency against compression ratio

The general trend is that volumetric efficiency decreases with increasing CR. When the engine speed was set at 420 rpm, the volumetric efficiency reduced from 88.1% to 83.7%. Similarly, the volumetric efficiency reduced from 85.5% to 81.2%, when the engine speed was set at 1500 rpm.

Typical values for WOT are in the range 75%–90%, and lower when the throttle is closed [16]. For both simulations, volumetric efficiency is within the typical range, thus the values obtained from AVL Boost are acceptable.

$$\mathrm{CR} = \frac{\mathrm{Vs+Vc}}{\mathrm{Vc}} \tag{8}$$

where: Vs is swept volume; and Vc is clearance volume.

$$\eta\mathrm{v} = \frac{\mathrm{Vair}}{\mathrm{Vs}} \tag{9}$$

where:ηv is volumetric efficiency; and Vair is volume of air drawn into cylinder.

Therefore, equating Equations 8 and 9 gives:

$$\mathrm{Vs} = \frac{\mathrm{Vair}}{\eta\mathrm{v}} = (\mathrm{CR} * \mathrm{Vc}) - \mathrm{Vc} \tag{10}$$

Compression ratio is inversely proportional to volumetric efficiency, thus results obtained from AVL Boost are acceptable.

The value of volumetric efficiency of a normal engine lies between 70 and 80% [16], and the values obtained from AVL Boost lies between 80 and 90 percent, proving an OP engine is volumetrically more efficient in burning fuel.

One way of increasing the engine volumetric efficiency in order to increase engine power would be forced induction. This can be achieved by using turbo or super-charger. This draws in more air into the cylinder thus increasing volumetric efficiency.

Another method of increasing volumetric efficiency is induction ram. However, this only occurs at high speed and is due to the inertia of the high-speed air. In part intake valves are left open after ODC to take advantage of this.

A third way of improving volumetric efficiency is intake tuning. The reflected pressure waves can be used to increase the air density at the inlet valve just prior to closing. This method is key to the success of naturally aspirated engines.

4.4.3. Mechanical Efficiency

The mechanical efficiency is how much of the power developed by the expanding of the gases in the cylinders is actually delivered as useful power.

Some of the power generated in the cylinder is used to overcome engine friction. The friction power (i.e. the power loss in the mechanical components of engine due to friction) is defined as the difference between the indicated power and brake power (i.e. difference between the moving parts and the energy taken to run the auxiliary equipment such as the fuel pump, water pump, oil pump and alternator). Thus, the mechanical efficiency is defined as the ratio of brake power to indicated power.

Friction losses in the engine come from friction between moving parts (such as the piston rings on the cylinder walls), the power required to run the valve gear and the pumps, and the pumping losses involved in getting the

gases in and out of the cylinder. A large part of the work appears as heat in the coolant and oil. The approximate breakdown of the contributions of each of the losses are as follows: pistons, rings, pins and rods (46%); valve train (23%); water pump and alternator (13%); crankshaft and seals (12%); and oil pump (6%).

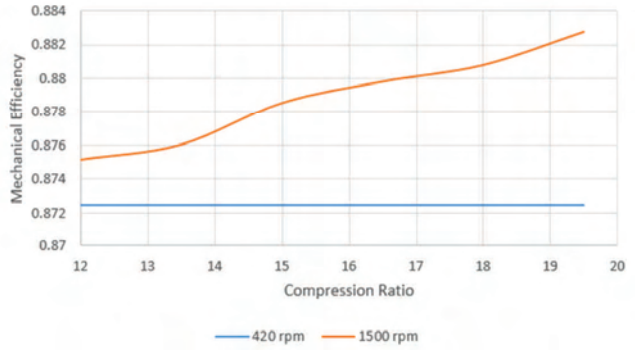


Fig. 6f. Graph of mechanical efficiency against compression ratio

For the 420 rpm simulation, an indicated power of 1.96 kW and a brake power of 1.71 kW were obtained, thus a mechanical power of 87.2% was obtained from AVL Boost for each CR. This suggests that at low engine speed the mechanical efficiency is independent of compression ratio.

Conversely, once the engine speed was set at 1500 rpm, the mechanical efficiency increases with respect to compression ratio, as do the indicated power and brake power. Therefore, a higher engine speed has an effect on mechanical efficiency.

5. Conclusion

This report discussed the effect of variable compression ratio on OP2S engine performance by modelling and simulating a simple single-cylinder two-stroke opposed-piston engine in AVL Boost. The aim was achieved by completing all the objectives. Results obtained from AVL Boost indicate a general trend between the analysed parameters and compression ratio.

In conclusion, the analysis of the results showed that some parameters, such as IMEP, peak pressure, peak temperature and volumetric efficiency, have an effect when increasing the compression ratio. Positive correlations were attained when analysing IMEP, peak pressure and peak temperature. On the other hand, volumetric efficiency decreased with increasing compression ratio.

In addition, certain parameters, such as mechanical efficiency, were only affected when the engine speed was set at 1500 rpm, and remained constant at an engine speed of 420 rpm. One of the reasons as to why the results remained constant or had very little effect when increasing the compression ratio for simulation 1 is because perhaps 420 rpm was too low of an engine speed to analyse engine performance. In future, a higher value of engine speed will be used and more simulations will be carried out to make a better comparison.

Finally, it is recommended to use AVL Boost to model and simulate an OP2S engine as it is easy and fast to setup model, and provide reliable and accurate simulation of steady and transient engine performance parameter.

Nomenclature

OP2S	opposed-piston two-stroke
OP	opposed-piston
CR	compression ratio
IMEP	indicated mean effective pressure
HCCI	homogeneous charge compression ignition
IDC	inner dead centre
ODC	outer dead centre
ICE	internal combustion engines
CAD	crank angle degree
VCR	variable compression ratio
BMEP	brake mean effective pressure
FMEP	friction mean effective pressure
SFC	specific fuel consumption

Bibliography

[1] REGNER, G., HEROLD, R., WAHL, M. et al. The Achates power opposed-piston two-stroke engine: performance and emissions results in a medium-duty application. *SAE Int. J. Engines*. 2011, **4**(3), 2726-2735.

[2] PIRAULT, J.-P., FLINT, M. Opposed piston engines: evolution, use, and future applications. *SAE International*. Warrendale, 2009.

[3] Achates. A Historical Look at Opposed-Piston Engines. 2011. (online) Available at: achatespower.com/opposed-piston-engine-history (accessed 19.10.2016).

[4] Tank and AFV News. Ukraine announces 1500 HP version of 6TD engine. 2016. (online) Available at: tankand-afvnews.com/2016/05/24/ukraine-announces-1500hp-version-of-6td-engine (accessed 20.10.2016).

[5] HEROLD, R., WAHL, M., REGNER, G. et al. Thermodynamic benefits of opposed-piston two-stroke engines. *SAE Technical Paper*. 2011, 2011-01-2216.

[6] VENUGOPAL, R., ABANI, N., MACKENZIE, R. Effects of injection pattern design on piston thermal management in an opposed-piston two-stroke engine. *SAE Technical Paper*. 2013, 2013-01-2423.

[7] OPALIŃSKI, M., MAZURO, P., WYSZYNSKI, M. Comparison of flow performance in one and three dimensional software for modelling of opposed piston engines. *Archivum Combustions*. 2015, **35**(1).

[8] MA, F., ZHAO, C., ZHANG, F. et al. An experimental investigation on the combustion and heat release characteristics of an opposed-piston folded-cranktrain diesel engine. *Energies*. 2015, **8**(7), 6365-6381.

[9] XU, H.M. Powertrain lectures: engine operating dynamics. University of Birmingham. 2017.

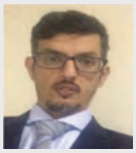
[10] HEYWOOD, J.B. Internal combustion engine fundamentals. *McGraw-Hill*, 1988.

[11] LANCASTER, D.R, KREIGER, R.B., LIENESCH, J.H. Measurement and analysis of engine pressure data. *SAE Technical Paper*. 1975, 750026.

[12] CARIS, D.F., NELSON, E.E. A new look at high compression engines. *SAE Trans*. 1959, **67**, 112-124.
[13] KRIEGER, R.B., BORMAN, G.L. The computation of applied heat release for internal combustion engines. ASME Paper 66-WA/DGP-4; *SAE Warrendale*. 1966.
[14] BRUNT, M.F.J., RAI, H., EMTAGE, A.L. The calculation of heat release energy from engine cylinder pressure data. *SAE Technical Paper*. 1998, 981052.
[15] FLAGAN, R.C. Internal combustion engines. 4th ed. 1988, 242, 248, 252, 274.
[16] RAJPUT, R.K. A text book of automobile engineering — Google Books. Books.google.co.in. 2007-01-01. (accessed 9.03.2017).

Ali Alqahtani, MEng. – School of Mechanical Engineering at University of Birmingham.

e-mail: *AMA374@student.bham.ac.uk*



Miroslaw L. Wyszynski,, MEng, PhD, MIDGTE, MSAE, MSIMP – Faculty of Mechanical Engineering at University of Birmingham.

e-mail: *M.L.Wyszynski@bham.ac.uk*



Paweł Mazuro, DEng. – Faculty of Power and Aeronautical Engineering at Warsaw University of Technology.

e-mail: *Pawel.Mazuro@itc.pw.edu.pl*



Hongming Xu, BEng, MEng, PhD, DIC, FSAE, CEng, FIMechE, FHEA – School of Mechanical Engineering at the University of Birmingham, UK

e-mail: *H.M.Xu@bham.ac.uk*



Article citation info:
WRÓBLEWSKI, P. The effect of the distribution of variable characteristics determining the asymmetry of the sealing rings sliding surfaces on the values of friction loss coefficients and other selected parameters of oil film. *Combustion Engines*. 2017, **171**(4), 107-116. DOI: 10.19206/CE-2017-418

Piotr WRÓBLEWSKI

CE-2017-418

The effect of the distribution of variable characteristics determining the asymmetry of the sealing rings sliding surfaces on the values of friction loss coefficients and other selected parameters of oil film

The article presents the results of research on the effect of the change in coordinates that determine the location of the common vertex of the parabolas and ellipses demonstrating the asymmetric shape of the rings sliding surfaces on the change in the thickness of oil film, the amount of scraped oil, and the oil left on the cylinder wall, once a set of selected sealing rings has passed, as well as the results concerning friction losses. Mathematical relationships of the asymmetric shapes of the rings sliding surfaces were presented, and the values of coefficients characterizing selected parameters of oil film and friction losses were determined. It was confirmed that there is a large dependence of the coordinate values of the vertices determining the asymmetric shapes of these surfaces on the condition and cooperation between piston rings and the cylinder bearing surface, and mainly on the amount of the oil scraped in the selected engine strokes.

Key words*: rings asymmetrical sliding surface, friction loss, oil film*

1. Introduction

Currently, sealing rings of a symmetrical barrel-shape sliding surface are most commonly used in the design of piston internal combustion engines [5, 6]. The continuous development of internal combustion engines aims at reducing the emission of toxic substances emitted into the environment by increasing the engine thermal and mechanical efficiency. In this case, it is important to reduce friction losses in the set of sealing rings, while ensuring the oil film continuity between the cooperating surfaces of kinematic pairs throughout the entire engine cycle [1]. An important structural factor for reducing friction loss in the piston ring set is the selection of the sliding surfaces of the lower and upper sealing rings [7]. The previous studies concerning modeling parameters for the piston-cylinder group have not paid major attention to modeling the shape of the sliding surface of a piston [2–5]. In most models, the authors accept a symmetrical shape of the sliding surfaces of sealing rings as the boundary condition. Therefore, there is then a justified need to examine the possibility of reducing friction loss by applying the asymmetric shape of these surfaces. The most important task is to determine the appropriate shape of the upper sealing ring, due to its specific working conditions, especially at the reduced thickness of the oil film just before TDC in the compression stroke and just after the TDC in the expansion stroke [7]. Each transition from the symmetrical shape of these surfaces to an asymmetric shape is related to a change in pressure distribution in the oil film throughout the entire engine cycle. The main purpose of this article is to present the influence of the distribution of variable characteristics determining the selected shapes of sealing rings on friction loss and the selected parameters of the oil film.

The pressure distribution in the oil film is also affected by the piston ring structural conditions, i.e. the force of elasticity, resulting from the type of material used, the geometrical parameters of the ring, the permeability and thermal expansion of the material, and the operating conditions of the engine, which results directly in the value of the gas force in a given period of engine work. Most of these parameters can be assumed theoretically, and then verified experimentally while designing the sealing rings. It is much more difficult to determine the distribution coverage of the sliding surfaces of sealing rings with the oil film in each engine stroke while taking into account the variable arrangement of the sealing rings and the scraper ring in the piston grooves, local changes in the temperatures of oil and materials, changes in oil viscosity and elasticity, and engine angular velocity [3, 4]. It is of particular importance to determine the oil film distribution between the sealing ring surfaces at low angular velocities and the low temperatures of lubricating oil [2]. Therefore, it is necessary to verify the influence of these parameters on the oil film coverage of the asymmetric shapes of the sealing rings sliding surfaces while taking into account the variable position of these surfaces due to the rings' rotation in the piston grooves. Such parameters strongly influence the pressure ratio resulting from extrusion and slip. Anticipating the effects of applying the asymmetry of the rings sliding surfaces for selected conditions of engine work and its design in terms of the functional needs of the lower and upper sealing rings may contribute to a significant reduction in friction losses. Unfortunately, the precise setting of all boundary conditions requires that a simulation be conducted for each selected engine design. However, the formation of a database or mathematical model determining the results of such adjustments in the ring shape under certain engine operating conditions and its structural parameters can greatly facilitate the engine design and construction work. The shape of sealing rings sliding surfaces directly influences the extrusion and slip effects, that is the amount of oil scraped into the next ring or the combustion chamber in the compression and exhaust strokes and the instantaneous thickness of the oil layer left on the cylinder bearing surface once the given ring has passed. In addition, the mathematical part of the author's model introduced to the model developed by A. Iskra can greatly accelerate the verification of the effects of the changes in the asymmetric shapes of the sealing rings on the distribution of the oil film on the cooperating surfaces, minimum thickness of oil film, friction loss and lubricant oil consumption.

2. Distribution of variable characteristics determining the asymmetry of parabolic and elliptical shapes of the sealing rings sliding surfaces

Expressing the effect of the changes in asymmetry of parabolic and elliptical shapes of the sealing rings sliding surfaces requires the formation of appropriate equations describing the distribution of variable features in the Cartesian coordinate system. Next, the coordinates of the points that are within specific ranges are introduced into the mathematical model. The ranges are sections of parabolas or ellipses with common coordinates of vertices or edge points coordinates. The mathematical presentation of relationships of shape asymmetry enables the expression of the effects of changes in the vertex coordinates of a set of parabolas or ellipses on the pressure distribution in oil film, and thus as a result of the friction loss, the parameters determining the oil film distribution on the cooperating surfaces and the lubricating oil consumption. An important feature of such mathematical presentation of these shapes and the adoption of certain coefficients for a given combination of shapes and their asymmetry is the ability to determine the influence of the change in coordinates of the common vertex on the most important parameters of the oil film distribution. Such modeling approach enables the selection of asymmetry of surface shapes for the required conditions of cooperating surfaces resulting from individual engine characteristics. It should be noted that the results of the illustrated simulations are unique for each given engine and are not a general indicator for all engines. By using the current model to approximate the results with polynomial functions of higher degrees or by interpolation, one can generate a significant error in certain engine areas, especially when there is a shift in the common peak of the parabola or ellipse expressing the given shape. In these areas of the engine cycle and for shapes with a large peak shift, an increased number of computational steps should be applied by generating a large number of co-ordinates describing the ring shape. Based on these assumptions, the change in friction loss and oil film parameters can be calculated for any engine design with a modified set of sealing rings.

Figure 1 shows the way of presenting asymmetric geometry of parabolic and elliptical shapes, and a diagram of velocity and pressure fields at the starting and separating points of oil film for two sealing rings.

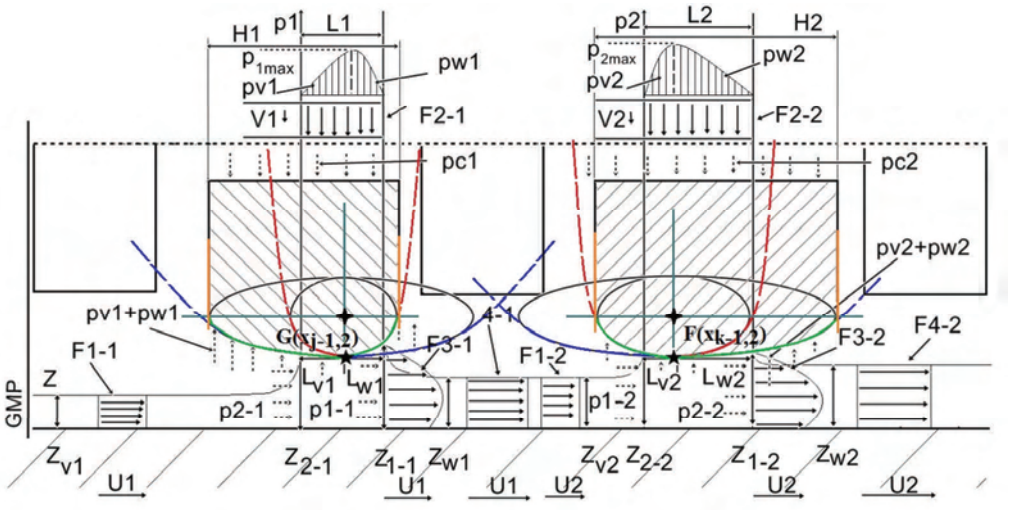


Fig. 1. Schematic representation of asymmetric geometry of parabolic and elliptical sliding surfaces, as well as velocity and pressure fields at the starting and separating points of the oil film for the lower and upper sealing rings where: ★ – $W_{j,k\,1-2}$ vertex coordinates of the parabolas and ellipses defining the given asymmetric shape of the sliding surface, ♦ – coordinates of the ellipses common center, green line – function expressing the asymmetrical shape of the sealing rings sliding surfaces

The presented mathematical model for which the corresponding mathematical relationships were selected and the results of the simulation do not take into account the changes in reference points coordinates, which represent the roughness and defects of the material structures existing on the sealing rings sliding surfaces and the cylinder walls. However, knowing the value of roughness Ra, which is determined experimentally for the given surfaces by approximating the coordinates of micro-roughness vertices, one can implement it into the current model. The implementation of the above consists in introducing a large number of coordinates of points representing the given roughness of the opposing surfaces. However, such action requires a considerable number of computational steps, up to over a dozen thousand of them, which is due to the number of coordinates of the two planes. It should be noted that by implementing only the coordinates of the points representing the roughness of the surface in an approximated manner, it is not possible to accurately represent the exact conditions that occur at the time of mixed or boundary friction. Then the current mathematical model for calculating selected oil film parameters and friction loss must be extended by additional blocks of mathematical equations expressing the co-operation conditions when the oil film thickness is reduced below the minimum value. Such a mathematical model should also take into account the distance criterion of the individual coordinate points describing the shape and directional position of the two planes and, in the case of

mixed friction conditions, it should implement mathematical equations describing the conditions of the contact of micro-roughness vertices while separating the necessary parameters.

The asymmetric shape of the sealing rings parabolic sliding surfaces is to be expressed by four functions: $g(x_{j1})$, $g(x_{j2})$, $f(x_{k1})$, $f(x_{k2})$ with common parabola vertices coordinates $\mathbf{W_{j1} = W_{j2}}$ and $\mathbf{W_{k1} = W_{k2}}$. The vertex coordinates W_{jn} and W_{kn} are the coordinates of the critical transition point of the experimental piston rings' actual shape, which affects the ratio of the extrusion and slip coefficients. The functions defining the character of asymmetrical parabolic shapes can be expressed by the following set of equations:

$$g(x_{j1}) = a_{1j1}(x_{j1} - p_{j1})^2 + q_{j1}$$

$$g(x_{j2}) = a_{2j2}(x_{j2} - p_{j2})^2 + q_{j2}$$

$$f(x_{k1}) = a_{1k1}(x_{k1} - p_{k1})^2 + q_{k1}$$

$$f(x_{k2}) = a_{2k2}(x_{k2} - p_{k2})^2 + q_{k2}$$

where: $(a_{1j1}, a_{2j2}, a_{1k1}, a_{2k2}) \neq 0$; $x_{j1}, x_{j2}, x_{k1}, x_{k2} \in \mathbf{R}$

$$\mathbf{W_{j1}} = (p_{j1}, q_{j1}); \mathbf{W_{j2}} = (p_{j2}, q_{j2})$$

$$\mathbf{W_{k1}} = (p_{k1}, q_{k1}); \mathbf{W_{k2}} = (p_{k1}, q_{k1})$$

where: $p_{j1} = p_{j2} \neq 0$; $p_{k1} = p_{k2} \neq 0$; $q_{j1} = q_{j2} \neq 0$; $q_{k1} = q_{k2} \neq 0$

$$x_{j1}, x_{j2} \in (m_{j1}, k_{j1}); x_{k1}, x_{k2} \in (m_{j2}, k_{j2})$$

thus

$$G(x_{j1,2}) = \begin{cases} a_{1j1}(x_{j1} - p_{j1})^2 + q_{j1} \text{ for } x_{j1} \in (m_{j1,2}, p_{j1,2}) \\ a_{2j2}(x_{j2} - p_{j2})^2 + q_{j2} \text{ for } x_{j2} \in (p_{j1,2},, k_{j1,2}) \end{cases}$$

$$F(x_{k1,2}) = \begin{cases} a_{1k1}(x_{k1} - p_{k1})^2 + q_{k1} \text{ for } x_{k1} \in (m_{k1,2}, p_{k1,2}) \\ a_{2k2}(x_{k2} - p_{k2})^2 + q_{k2} \text{ for } x_{k2} \in (p_{k1,2},, k_{k1,2}) \end{cases}$$

where: $G(x_{j1,2})$, $F(x_{k1,2})$ – trigonometric functions in canonical form, expressing the asymmetrical parabolic shapes of the sliding surfaces of the upper and lower sealing rings – the green parabola.

Presenting the shapes of the rings' sliding surfaces by means of two parabolas with a common vertex $W_{j1\text{-}2}$ enables to illustrate the influence of the vertex position on the friction loss and the selected oil film parameters. The selection of the number of coordinate points implemented into the simulation program from the two ranges of the set representing the selected shape of the sliding surface is of a unique character and depends on the required calculation accuracy. If one exclusively assumes the occurrence of liquid friction conditions, then a range of 50 to 200 coordinate points is considered sufficient for calculation. The number of coordinate calculation points depends on the complexity of the asymmetric shape of the sliding surfaces of the sealing rings and the axial height of the selected ring in the set. For the purpose of this simulation, it is assumed that $H_1 = 1.50$ mm and $H_2 = 2.00$ mm.

In order to determine the coordinates of any points defining a given shape, the following boundary conditions are assumed:

$$x_{j1-2} \in (m_{j1,2}, k_{j1,2}) \Leftrightarrow m_{j1,2} \leq x_{j1-2} \leq k_{j1,2}; m_{j1,2} = 1; k_{j1,2} = 50, x_{j1,2} \in \mathbb{N}_+$$

$$x_{k1-2} \in (m_{k1,2}, k_{k1,2}) \Leftrightarrow m_{k1,2} \leq x_{k1-2} \leq k_{k1,2}; m_{k1,2} = 1; k_{k1,2} = 50, x_{k1,2} \in \mathbb{N}_+$$

If $\mathbf{H_1 \neq H_2}$ then $|\mathbf{x_{j1,2}}| \neq |\mathbf{x_{k1,2}}|$

where:

$$|x_{j1,2(n+1)} x_{j1,2(n)}| = \sqrt{\left(x_{j1,2(n+1)} - x_{j1,2(n)}\right)^2 + \left(y_{j1,2(n+1)} - y_{j1,2(n)}\right)^2}$$

for $x_{j1} \in (m_{j1,2}, p_{j1,2}) \wedge x_{j2} \in (p_{j1,2}, k_{j1,2})$

$$|x_{k1,2(n+1)} x_{k1,2(n)}| = \sqrt{\left(x_{k1,2(n+1)} - x_{k1,2(n)}\right)^2 + \left(y_{k1,2(n+1)} - y_{k1,2(n)}\right)^2}$$

for $x_{k1} \in (m_{k1,2}, p_{k1,2}) \wedge x_{k2} \in (p_{k1,2}, k_{k1,2})$

On condition that: $H_1 \vee H_2 < 2.00$ mm, then $k_{j1,2} \wedge k_{k1,2} \geq 50$.

By accepting the specified vertex coordinates $W_{j1,2} \wedge W_{k1,2}$ and the values $m_{j1,2}, k_{j1,2} \wedge m_{k1,2}, k_{k1,2}$, one can map the actual asymmetric shape of the sliding surfaces of the rings. If $H_1 = 1.50$ mm, the actual vertex height $W_{j\text{-}k}$ is 10 µm, distance p_{j1-2} from the lateral side of the sliding surface conventionally defined as $m_{j1,2} = 60\%\ H_1$ and $k_{j1,2} = 50$, then one takes $p_{j1-2} = 30$ and $q_{j1-2} = -0.10$ as coordinates $W_{j1,2}$. Based on the accepted boundary conditions, the remaining coordinates of points from the range $x_{j1,2} \in (m_{j1,2}, k_{j1,2})$ can be calculated. For the calculation module of the simulation program, the obtained values $x_{j1,2-n}$ must be inserted into the equation:

$$Xsym_{j1,2-n} = (x_{j1,2-n} + |q_{j1-2}|) \times 0.0001$$

For the second set of functions $f(x_{k1}) \wedge f(x_{k2})$ representing the asymmetric parabolic shape of the lower sealing ring, all mathematical operations are identical and the final formula for these functions is equal to:

$$Xsym_{k1,2-n} = (x_{k1,2-n} + |q_{k1-2}|) \times 0.0001$$

Similar shapes of the asymmetric sliding surfaces of the sealing rings can also be expressed by using elliptical functions, i.e. several curves closed symmetrically with respect to their common center. One recommends expressing the selected asymmetric elliptic shapes by ellipses $E(x_{j1})$, $E(x_{j2})$, $E(x_{k1})$, $E(x_{k2})$. The eccentricity of the ellipses is called parameter e which constitutes the value expressing the ratio of the focal length to half the length of the transverse diameter. As a boundary condition, it is assumed that the common coordinates of the center of ellipse pairs are $E(x_{j1})$, $E(x_{j2})$, as well as $E(x_{k1})$, $E(x_{k2})$. Directional coordinates p_{j1} and p_{j2} determine the position of the common center of the two ellipses on the x axis. According

to the accepted assumptions, the ellipse data in canonical form can be described in the Cartesian coordinate system by the following equations:

$$E(x_{j1}) = \frac{(x_{j1}-p_{j1})^2}{a_{1j1}^2} + \frac{y_{j1}^2}{b_{1j1}^2} = 1; E(x_{j2}) = \frac{(x_{j2}-p_{j2})^2}{a_{2j2}^2} + \frac{y_{j2}^2}{b_{2j2}^2} = 1$$

$$E(x_{k1}) = \frac{(x_{k1}-p_{k1})^2}{a_{1k1}^2} + \frac{y_{k1}^2}{b_{1k1}^2} = 1;\ E(x_{k2}) = \frac{(x_{k2}-p_{k2})^2}{a_{2k2}^2} + \frac{y_{j2}^2}{b_{2k2}^2} = 1$$

where:

$$a_{1j1} \neq a_{2j2};\ b_{1j1} = b_{2j2};\ a_{1k1} \neq a_{2k2};\ b_{1k1} = b_{2k2}$$

$$G(x_{j1,2}) \text{ and } F(x_{j1,2}) \leq 0$$

hence:

$$\frac{y_{j1}^2}{b_{1j1}^2} = 1 - \frac{(x_{j1} - p_{j1})^2}{a_{1j1}^2}$$

$$y_{j1}^2 = b_{1j1}^2 - \frac{b_{1j1}^2 (x_{j1} - p_{j1})^2}{a_{1j1}^2}$$

where: $y_{j1}^2 = w \Leftrightarrow y_{j1} = \sqrt{w} \cup y_{j1} = -\sqrt{w}$ – the significant parameter is $-\sqrt{w} > 0$

$$y_{j1} = -\sqrt{b_{1j1}^2 - \frac{b_{1j1}^2 (x_{j1} - p_{j1})^2}{a_{1j1}^2}}$$

$$y_{j2} = -\sqrt{b_{2j2}^2 - \frac{b_{2j2}^2 (x_{j2} - p_{j2})^2}{a_{2j2}^2}}$$

$$G(x_{j1,2}) = \begin{cases} -\sqrt{b_{1j1}^2 - \frac{b_{1j1}^2 (x_{j1} - p_{j1})^2}{a_{1j1}^2}} \text{ for } x_{j1} \in (m_{j1,2}, p_{j1,2}) \\ -\sqrt{b_{2j2}^2 - \frac{b_{2j2}^2 (x_{j2} - p_{j2})^2}{a_{2j2}^2}} \text{ for } x_{j2} \in (p_{j1,2}, k_{j1,2}) \end{cases}$$

Similarly, an elliptical function $F(x_{k1,2})$ can be expressed as:

$$F(x_{k1,2}) = \begin{cases} -\sqrt{b_{1k1}^2 - \frac{b_{1k1}^2 (x_{k1} - p_{k1})^2}{a_{1k1}^2}} \text{ for } x_{k1} \in (m_{k1,2}, p_{k1,2}) \\ -\sqrt{b_{2k2}^2 - \frac{b_{2k2}^2 (x_{k2} - p_{k2})^2}{a_{2k2}^2}} \text{ for } x_{k2} \in (p_{k1,2}, k_{k1,2}) \end{cases}$$

On the basis of the above equations describing the relationships between two parabolas or ellipses, one can determine a specific number n of their coordinates expressing the given asymmetric shape of the rings sliding surface. By entering the above data into the mathematical model [1], it is possible to record the balance of velocity fields equivalent to the flow balance between the sliding surfaces of the sealing rings and the surface of the cylinder wall. Based on the accepted data, mathematical model and on the adoption of a certain number of broken curves depending on the complexity of the shape of these surfaces, it is possible to determine the tendency of change in friction loss and selected parameters of the oil film, depending on the displacement of the common peak of the given functions at the axial height of these rings.

3. Dimensional coefficients for friction losses and selected oil film parameters for parabolic asymmetric shapes of the sealing rings sliding surfaces

Based on the results of the simulation shown below, it can be observed that there is a close dependence of the location of the common point of the parabolas $\mathbf{W_{j1}} = (p_{j1}, q_{j1})$ and $\mathbf{W_{j2}} = (p_{j2}, q_{j2})$ on the friction power of the individual piston rings in the set. For the mathematical model in the simulation, it is assumed that the coordinates $p_{j1} = p_{j2}$ refer to the upper sealing ring. All simulation results were expressed for the change of parabolic coordinates p_{j1-2} and p_{k1-2} according to the above assumptions. This is justified by the positive results of the simulation which concern the shape formation of the sealing rings sliding surfaces. According to these assumptions, the shape of the upper sealing ring's sliding surface must favor the formation of the shape characterized by a high value of the slip effect coefficient and a low value of the extrusion effect coefficient. The contours with a high value of the slip effect coefficient should be located on the sliding surface of this ring from the crankcase side when the piston moves in the direction of the TDC in the compression and exhaust strokes. The contours with small values of extrusion effect coefficient should be implemented on the opposite side. Thus, changing the coordinate value p_{j1-2} for this ring denotes the displacement of the vertex $\mathbf{W_{j1-2}}$ in the crankcase direction at the axial height H_1. If $k_{j1-2} = 50$, then $p_{j1-2} = 25$ = the symmetrical ring, $p_{j1-2} = 30 = m_{j1,2}$ = 40% H_1, $p_{j1-2} = 35 = m_{j1,2}$ = 30% H_1, $p_{j1-2} = 40 = m_{j1,2}$ = 20% H_1 and $p_{j1-2} = 45 = m_{j1,2}$ = 10% H_1.

For the lower sealing ring, the relationship is expressed by the coordinates $p_{k1} = p_{k2}$, which, along with the increase in values, are shifted towards the crankcase. For this ring, the contours with high extrusion effect coefficient values must be located on the sliding surface from the combustion chamber side, and the contours of the low slip effect coefficient values – on the opposite side. Thus the relation can be denoted as: $p_{k1-2} = 30 = m_{k1,2}$ = 60% H_2, $p_{k1-2} = 35 = m_{k1,2}$ = 70% H_2, $p_{k1-2} = 40 = m_{k1,2}$ = 80% H_2 and $p_{k1-2} = 45 = m_{k1,2}$ = 90% H_2. Accurate simulation and experimental results are needed to show changes in selected friction and oil film parameters for the specified coordinates p_{j1-2} and p_{k1-2} for both sealing rings.

According to the presented results, it can be seen that the reduction of the friction power and the friction force at 20° on the crankshaft after the TDC in the expansion stroke for the sealing ring occurs only for the selected coordinates of p_{j1-2} and p_{k1-2} and always runs in a nonlinear manner.

Consequently, the effect of the change of vertex coordinates for both sealing rings must be expressed by additional factors whose direction of change can be represented by a polynomial of higher degrees or by approximation of the results through interpolation. However, this method is subject to a significant error, for some special cases of shapes, especially at high values of the vertex offset $p_{j,k\text{-}1\text{-}2}$. For this reason, a more convenient method for approximating such results is to provide a comprehensive database for various engine designs, dynamic oil viscosities, and engine angular velocities.

It is also important to determine the effect of the changes in the asymmetrical shape, depending on the value of the gas pressure in the combustion chamber, especially in the expansion stroke. Below, there are only examples of simulation results for changes in $p_{j,k\text{-}1\text{-}2}$, for the design and performance of Cinquecento 700 engine, three selected crankshaft rotational speeds and two 10W/30 oil dynamic viscosities. All engine design parameters are shown in the simulations concerning the circumferential grooves placed on the sealing rings sliding surfaces [7]. The design features of this engine were selected for simulations solely because of the possibility to verify the obtained results with the results of bench tests. The impact of the change in the $p_{j,k\text{-}1\text{-}2}$ coordinate values on the percentage change in friction loss values and on oil film parameters selected for uncharged engines of similar geometric dimensions is comparable to most engines. As it can be expected, the simulation end values for these parameters are unique for each engine. However, their percentage difference in value from the simulation results that express the symmetry of the shape of standard rings used in any engine is already very similar to the presented results. It should be noted that the results are for a two-cylinder engine, whereas the results for engines with more cylinders must be properly corrected.

Figure 2 indicates that the increase in the coordinate value of parabola $p_{j,k\text{-}1\text{-}2}$ for both sealing rings simultaneously causes a reduction in the upper sealing ring friction force of 1–2% as compared to the value $p_{j,k\text{-}1\text{-}2} = 40$. Further displacement of the parabola common peak above this value leads to a significant increase in friction power of the entire ring set. For this range of the vertex shift, in some areas of engine operation, there occurs a discontinuity in the oil film between the upper sealing ring and the cylinder wall.

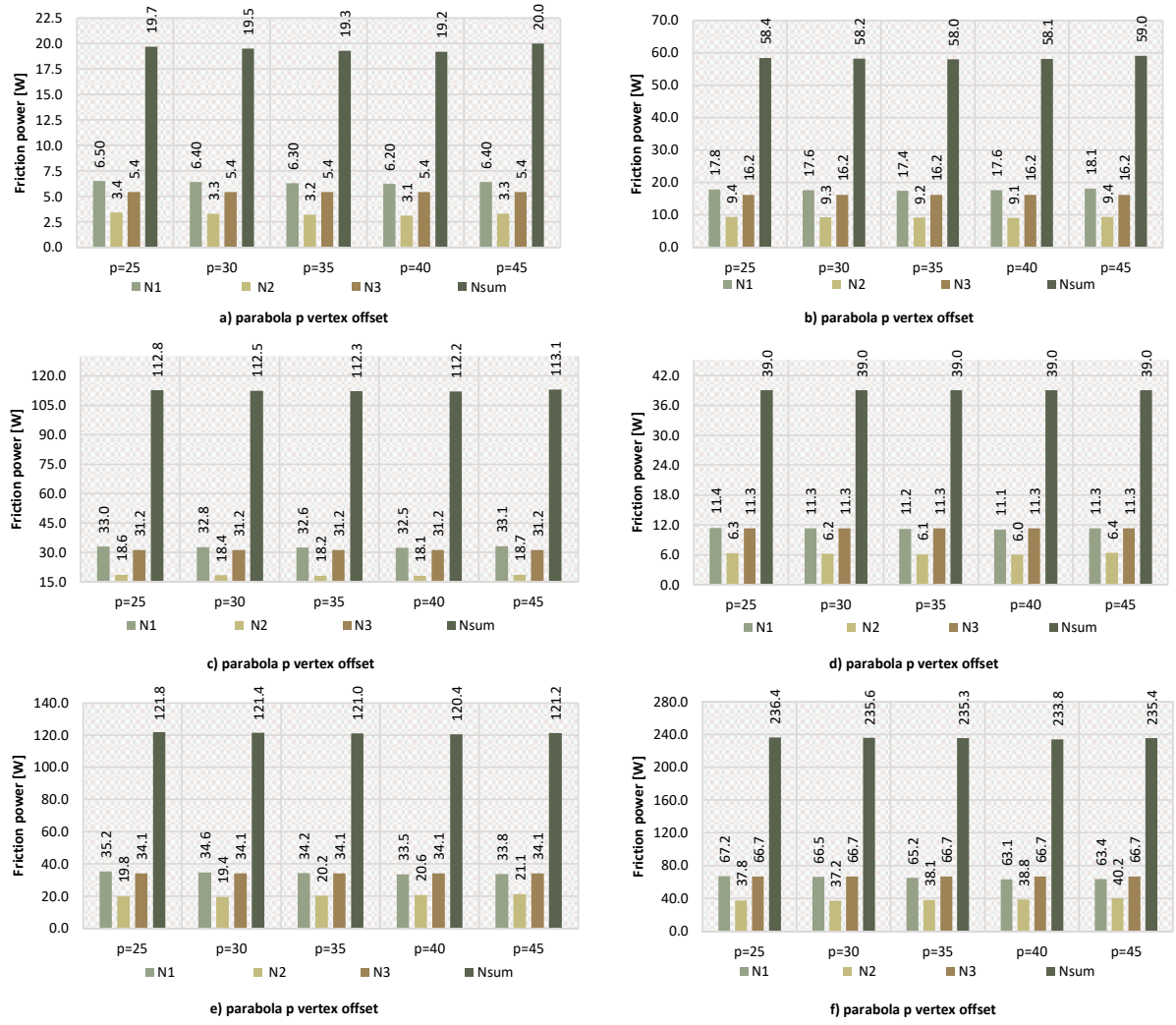


Fig. 2. Piston ring friction power for the engine velocity relative to the parabolic value of $p_{j,k\text{-}1\text{-}2}$, where: N_1 – Friction power of the upper sealing ring, N_2 – Friction power of the lower sealing ring, N_3 – Friction power of the scraper ring, N_{sum} – Friction power of a piston ring set, a) for 1000 rpm, b) for 2000 rpm, c) 3000 rpm – dynamic viscosity of lubricating oil 0.0120 Pa ×s, d) for 1000 rpm, e) for 2000 rpm, f) 3000 rpm – dynamic viscosity of lubricating oil 0.0386 Pa×s

As shown in Figure 2, for dynamic oil viscosity of 0.0386 Pa×s, a significant reduction of approximately 5% in the friction power of the upper sealing ring is observed, with the permissible vertex shift $p_{j,k-1-2,}$ and the increase in friction power of the lower sealing ring at the engine velocity of 3000 rpm. The increased friction power of the lower sealing ring is determined by the local increase in the oil film thickness between the sliding surface of the ring and the cylinder wall. Under favorable conditions, this may also be due to the rupture in the oil film continuity as a result of the reduction in thickness of the oil layer left on its return passage. On the basis of the data presented, it can be assumed that the most advantageous range for the sealing ring set, due to the reduction in friction power, is the offset of the vertex coordinates $p_{j,k-1-2}$ in the range 35 to 40, i.e. 70% to 80% of the ring axial height. It is highly probable that independently of the selection of the values $p_{j,k-1-2} \in$ <26;40> one can obtain a reduction in the friction force of a piston ring set with respect to the symmetrical shape of the sealing rings. It should be noted that the symmetrical sliding surface of the sealing rings $q_{j,k-1-2} = -0.10$ has been accepted for simulation studies, which is equivalent to the vertex offset of 10 µm extending from the outer edge of the ring. In the actual reference rings, the value of this extension does not, on average, exceed 5 µm for the molybdenum and chromium coatings after reaching the piston rings. The asymmetric shapes of the sealing rings, on the other hand, are produced with a vertex offest of about 20 µm, and after running-in it is within the range of 8 to 12 µm. This is of high importance due to the value of the sealing rings friction power because the rings with larger offsets have a significantly lower friction power. This is justified by the reduced axial oil film coating of the sliding surfaces of these rings. In this case, the minimum oil film thickness for the upper sealing ring is also reduced. This is, however, sufficient to ensure the conditions for liquid friction throughout the entire engine cycle. For the engine in question, the minimum oil film thickness is greater than 0.201 µm at a dynamic viscosity of 0.0120 Pa×s. With the required roughness of the sliding surfaces of both the rings and the cylinder wall there is a negligible risk of breaking the continuity of the oil film for such rings in a longer period of engine operation.

Figure 3 shows the change in the friction force at 20° on the crankshaft after TDC in the expansion stroke for the upper sealing ring, depending on the displacement of the vertex $p_{j,k-1-2.}$ On the basis of the data presented, it can be clearly stated that the shift of the vertex $p_{j,k-1-2,}$ results in a significant reduction in friction force in the most loaded engine area. The friction force in this engine cycle period decreases with each modification in engine velocity and oil viscosity. The force of friction is influenced by the velocity gradient caused by slip.

For symmetrical shapes of rings, velocity gradients generated by the extrusion and slip effects, as well as differential pressure under and above the ring slightly affect friction force. However, for asymmetric shapes with a significant vertex shift $p_{j,k-1-2}$ the effect of the velocity gradient caused by the extrusion coefficient is significant. The velocity gradient caused by the difference in pressures below and above the ring for asymmetric ring shapes in supercharged engines is also of great importance. Knowing the unit friction force tangential to the cylinder liner with respect to Newtonian liquids, one can determine the total sealing ring friction force and the power absorbed to overcome the internal friction resistance in the oil film.

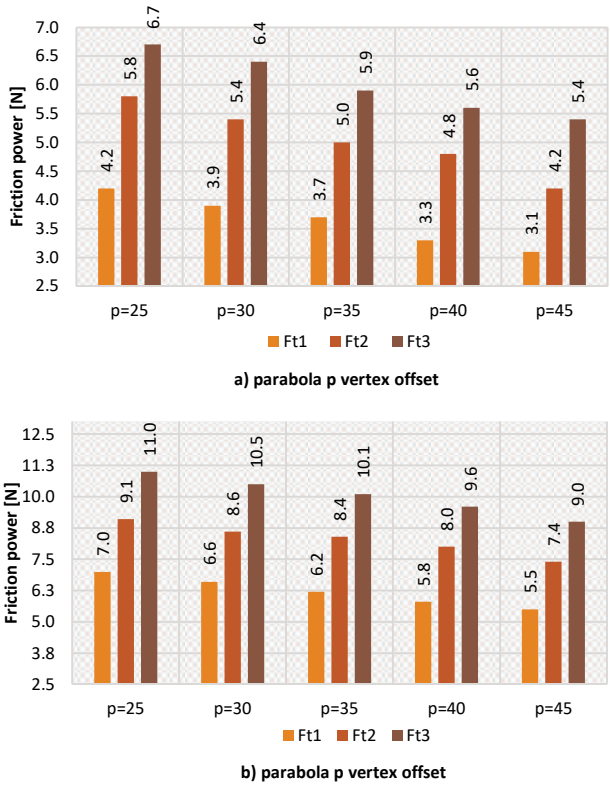


Fig. 3. Friction force at 380° on the crankshaft in the expansion stroke according to the parabolic vertex value of $p_{j,k-1-2}$ describing the sliding surface shape of the sealing rings, where: F_{t1} = 1000 rpm, F_{t2} = 2000 rpm, F_{t3} = 3000 rpm; a) for the dynamic viscosity of lubricating oil 0.0120 Pa×s, b) for the dynamic viscosity of lubricating oil 0.0386 Pa×s

By analyzing Figure 4, it is possible to observe the change in the oil film thickness depending on the vertex shift $p_{j,k-1-2.}$ Figures 4a and b indicate that for the oil dynamic viscosity of 0.0120 Pa×s the vertex shift $p_{j,k-1-2}$ causes variation in the oil film thickness. This is due to the change in crankshaft angle in the expansion stroke assigned to the minimum oil film thickness, depending on the vertex displacement $p_{j,k-1-2.}$ This means that the crankshaft angle, for which the oil film thickness between the ring's sliding surface and cylinder wall is minimal, depends on the dynamic viscosity of the oil. If $p_{j,k-1-2} = 25$, then $z_{min} = 364°$ on the crankshaft, $p_{j,k-1-2} = 30$, then $z_{min} = 366°$ on the crankshaft, $p_{j,k-1-2} = 35$, then $z_{min} = 370°$ on the crankshaft, $p_{j,k-1-2} = 40$, then $z_{min} = 372°$ on the crankshaft and $p_{j,k-1-2} = 45$, then $z_{min} = 374°$ on the crankshaft. For dynamic viscosity of oil at 0.0386 Pa×s, the oil film thickness can be reduced by increasing the value of $p_{j,k-1-2}$. This is especially noticeable for higher engine speeds – from 1000 rpm upwards. The change in the oil film thickness, depending on the change in the vertex position and dynamic viscosity of the oil, is determined by a variety of thickness of the scraped oil layers left by the ring on its return passage after the TDC and the

thickness of the oil film scraped by the lower sealing ring. It should also be noted that the displacement of the vertex $p_{j,k-1-2}$ for the upper sealing ring towards the engine crankcase results in its encounter with the scraped oil layers in the expansion stroke in the further angles of the crankshaft in this stroke. For the value of $p_{j,k-1-2} \in \langle 26;40 \rangle$ this is a beneficial effect that affects the reduction of the friction force and power in that ring. When the value of $p_{j,k-1-2} = 40$ is exceeded, a significant reduction in film thickness is achieved, which may not only form conditions for mixed friction, but also for boundary friction and irreversible engine damage. It should be mentioned here that the value of $p_{j,k-1-2} = 40$ = limit, may vary for each engine. Thus, the limit value of parameter $p_{j,k-1-2}$ depends on the engine geometry and especially on the thickness of the oil layers scraped by each ring in the set and on the thickness of the oil film scraped by the lateral surface of the piston.

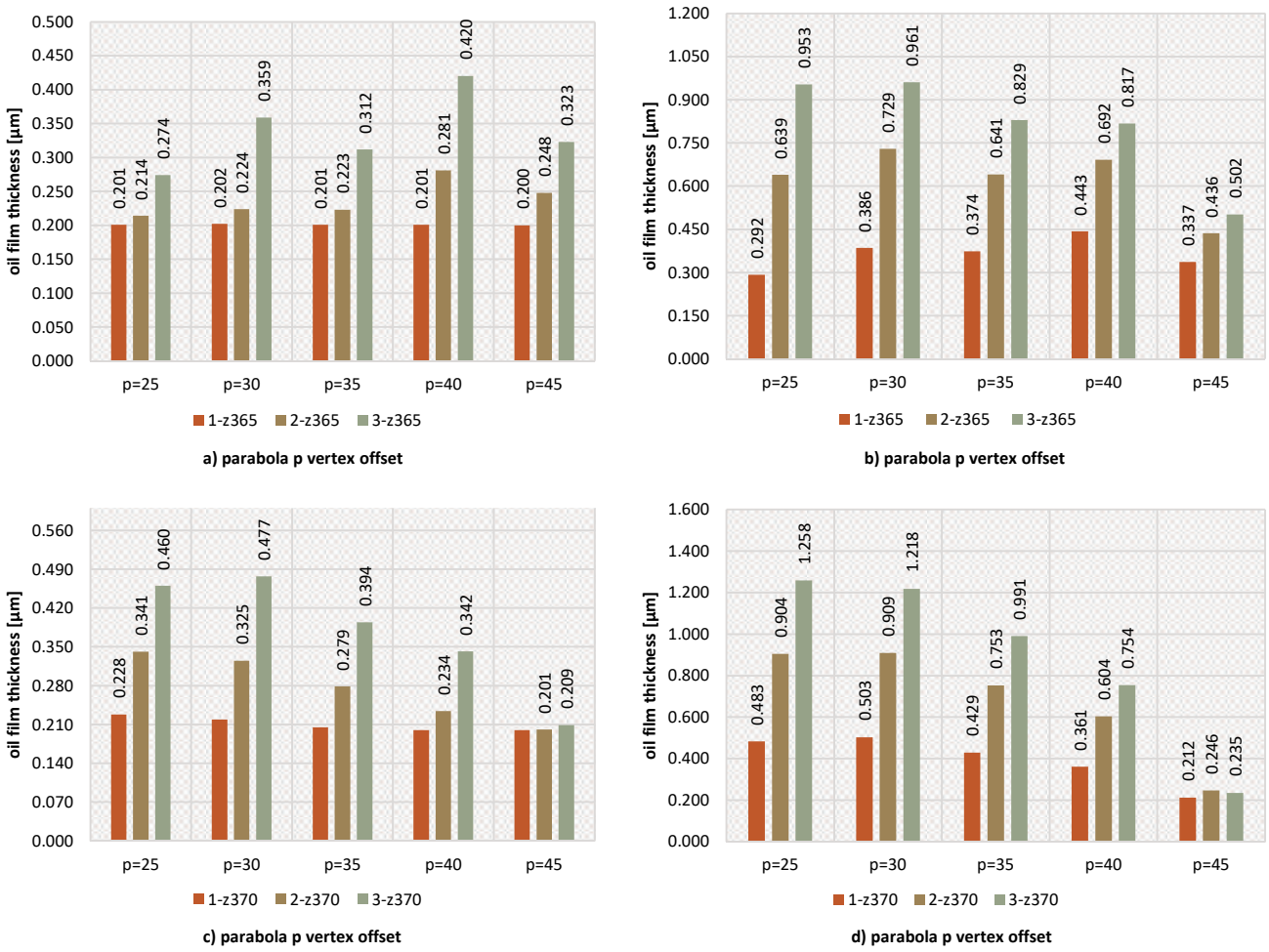


Fig. 4. Oil film thickness on the upper sealing ring slide surface depending on the parabolic vertex coordinate value $p_{j,k-1-2}$, where: 1 – 1000 rpm, 2 – 2000 rpm, 3 – 3000 rpm, z365 – the thickness of the oil film at 5° after TDC in the expansion stroke, z370 – the thickness of the oil film at 10° after TDC in the expansion stroke; a), c) for the dynamic viscosity of lubricating oil 0.0120 Pa×s, b), d) for the dynamic viscosity of lubricating oil 0.0386 Pa×s

4. Quantitative oil consumption analysis for parabolic asymmetric shapes of sealing rings sliding surfaces

The dynamic viscosity of the lubricating oil is one of the factors determining oil consumption. However, a multiple increase in the dynamic oil viscosity, which is due to the change in engine operating temperature and for the symmetrical sliding surfaces of the rings, does not significantly alter the quantitative oil consumption. As it is shown in Figure 5, the most important parameter determining oil consumption is the volume of oil scraped in the compression stroke V2 and the exhaust stroke V4 into the combustion chamber. The engine velocity also substantially influences the amount of scraped oil in the combustion chamber. Despite the large changes in both parameters for the symmetrical surfaces, volumes V2 and V4 are very similar. As can be seen in the graphs (Fig. 5), the displacement of the $p_{j,k-1-2}$. coordinates is quite significant for the volume of scraped oil in the combustion chamber throughout the entire engine cycle. An increase in this parameter to the value between 35 and 40 results in a very large reduction in the amount of consumed oil. When the value of parameter $p_{j,k-1-2} > 40$, there is a slight increase in the volume of oil scraped into the combustion chamber, with oil dynamic viscosity of 0.0120 Pa×s. For larger oil dynamic viscosities, the amount of oil scraped into the combustion chamber for this range of values also decreases.

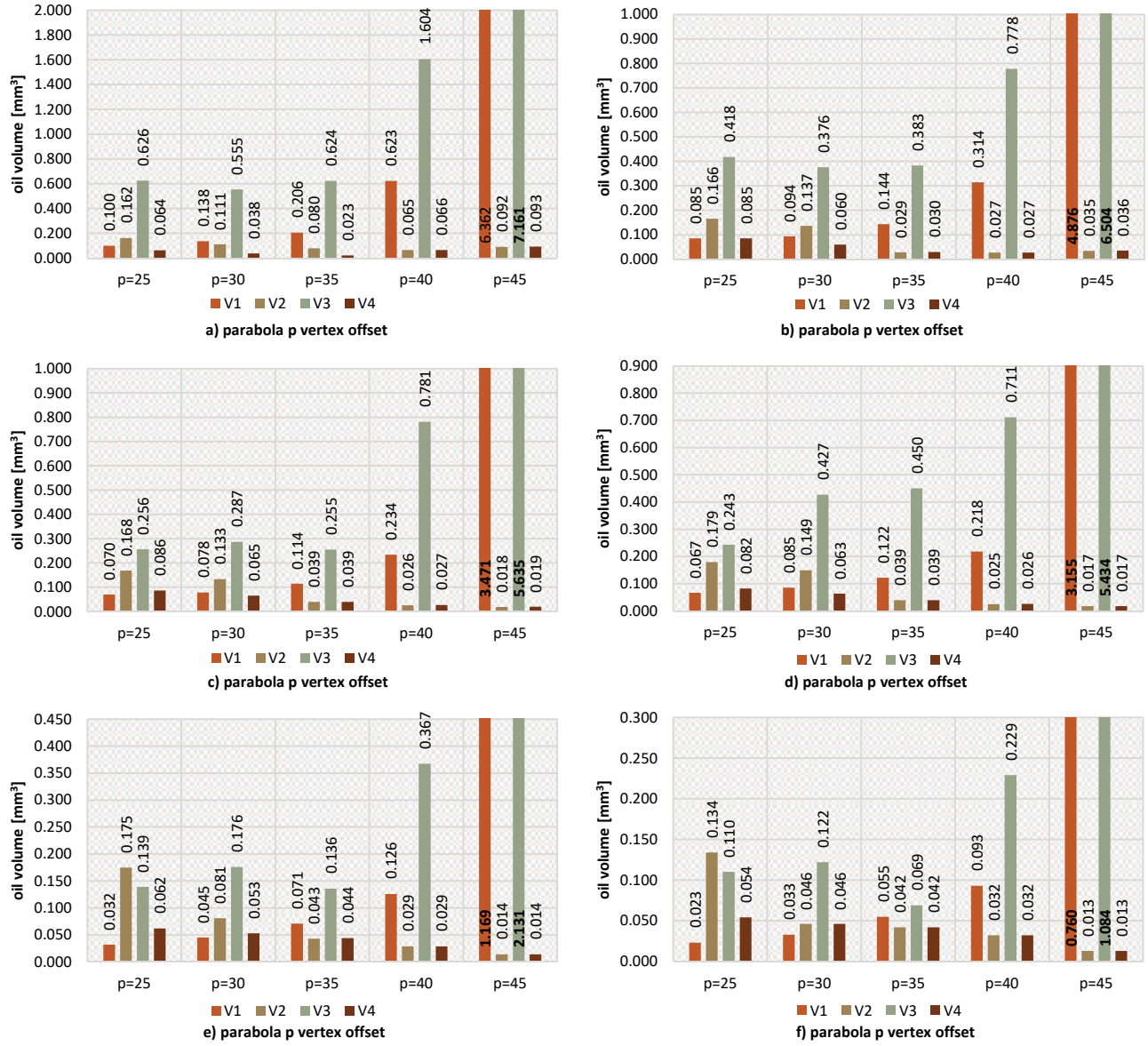


Fig. 5. The volume of lubricating oil scraped into the combustion chamber and crankcase in selected engine running strokes depending on the vertex offset value of the parabola $p_{j,k\text{-}1\text{-}2}$, where: V_1 – intake stroke, V_2 – compression stroke, V_3 – expansion stroke, V_4 – exhaust stroke; a) for 1000 rpm, b) for 2000 rpm, c) 3000 rpm – for the dynamic viscosity of lubricating oil 0.0120 Pa×s, d) for 1000 rpm, e) for 2000 rpm, f) 3000 rpm – for the dynamic viscosity of lubricating oil 0.0386 Pa×s

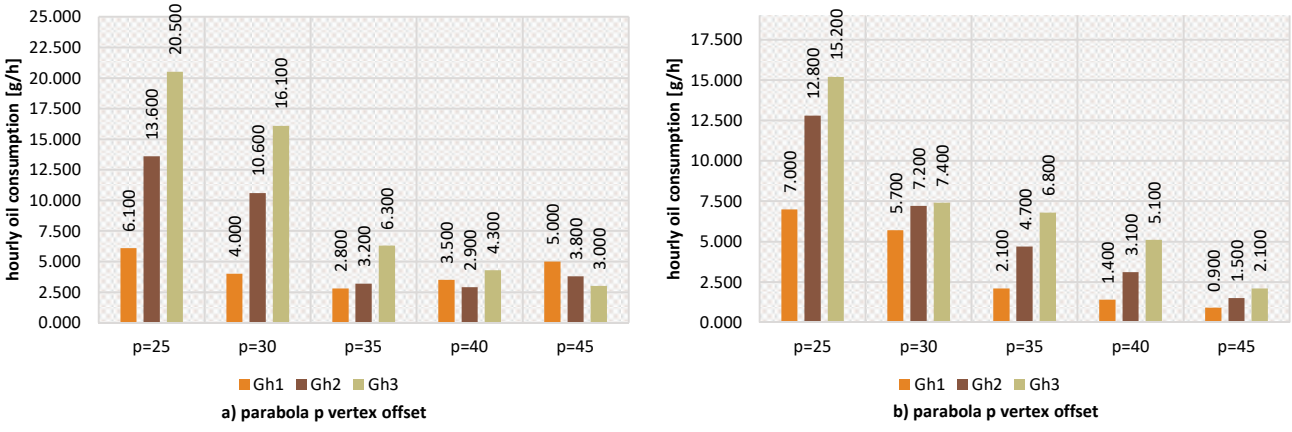


Fig. 6. The hourly consumption of lubricating oil according to the parabolic vertex value of $p_{j,k\text{-}1\text{-}2}$, where: Gh_1 = 1000 rpm, Gh_2 = 2000 rpm, Gh_3 = 3000 rpm; a) for the dynamic viscosity of lubricating oil 0.0120 Pa×s, b) for the dynamic viscosity of lubricating oil 0.0386 Pa×s

Table 1. Values of the coefficients determining the change in parameter $p_{j,k-1-2}$ expressing the asymmetric shape of the sealing rings sliding surfaces on the volume of scraped oil in the individual engine running strokes into the crankcase in strokes V1 and V3, and into the combustion chamber in strokes V2 and V4

$p_{j,k-1-2}$*	25	26	27	28	29	30	31	32	33	34	35
V1 [mm^3]	0.100	0.107	0.113	0.121	0.129	0.138	0.145	0.155	0.167	0.180	0.213
V1 [%]	100	107	113	121	129	138	145	155	167	180	213
V2 [mm^3]	0.162	0.146	0.134	0.125	0.117	0.111	0.104	0.098	0.092	0.086	0.080
V2 [%]	100	90.12	82.72	77.16	72.22	68.52	64.20	60.49	56.79	53.09	49.38
V3 [mm^3]	0.626	0.605	0.583	0.570	0.560	0.555	0.561	0.570	0.584	0.604	0.624
V3 [%]	100	96.65	93.13	91.05	89.46	88.66	89.62	91.05	93.29	96.49	99.68
V4 [mm^3]	0.064	0.057	0.051	0.046	0.042	0.038	0.034	0.030	0.027	0.025	0.023
V4 [%]	100	89.06	79.69	71.88	65.63	59.38	53.13	46.88	42.19	39.06	35.94
$p_{j,k-1-2}$*	------	36	37	38	39	40	41	42	43	44	45
V1 [mm^3]		0.259	0.311	0.382	0.491	0.623	0.934	1.560	2.765	4.430	6.362
V1 [%]		259	311	382	491	623	934	1560	2765	4430	6362
V2 [mm^3]		0.076	0.072	0.069	0.066	0.065	0.067	0.071	0.076	0.083	0.092
V2 [%]		46.91	44.44	42.59	40.74	40.12	41.36	43.83	46.91	51.23	56.79
V3 [mm^3]		0.687	0.802	0.978	1.234	1.604	2.130	2.801	3.750	5.102	7.161
V3 [%]		109.74	128.12	156.23	197.12	256.23	340.26	447.44	599.04	815.02	1143.93
V4 [mm^3]		0.026	0.033	0.041	0.053	0.066	0.074	0.081	0.086	0.089	0.093
V4 [%]		40.63	51.56	64.06	82.81	103.13	115.63	126.56	134.38	139.06	145.31

* for the lubricating oil dynamic viscosity value of 0.0120 Pa×s and engine speed 1000 rpm

As shown in Figure 5, the vertex shift $p_{j,k-1-2}$ for the upper sealing ring in the crankcase direction, and for the lower sealing ring towards the combustion chamber within the range of 51% to 80% results in a significant reduction in the volume of oil scraped into the combustion chamber. Similar conclusions can be reached following the analysis of Figure 6, concerning hourly oil consumption. It can be stated that the most advantageous reduction of oil consumption for 10W/30 oils can be obtained for the $p_{j,k-1-2}$ vertex coordinate shift to a maximum value of about 37. When the maximum value is exceeded at a normal engine running temperature of about 90°C, one observes an increase in the hourly oil consumption. At lower temperatures of this oil, the oil consumption is reduced at the higher values of the vertex coordinates $p_{j,k-1-2}$.

The reduction in the volume of oil scraped into the combustion chamber in strokes V2 and V4 and in the hourly oil consumption as the vertex position $p_{j,k-1-2}$ changes is determined by the lower thickness of the oil layer on which the return movement of the upper sealing ring is made. This is explained as follows: the higher the vertex offset of the $p_{j,k-1-2}$, the closer the turning point of the upper sealing ring is to the turning point of the lower sealing ring. The selected coefficients expressed as a percentage change in the volume of the scraped oil for the range of the vertex offests $p_{j,k-1-2} \in \langle 25;45 \rangle$ are summarized in Table 1. A similar comparison can be made for any engine design and any engine velocity and dynamic lubricating oil viscosity.

5. Conclusions

On the basis of the data obtained from the simulations, one can state that the simultaneous opposing offset of the vertex $p_{j,k-1-2}$ for the lower and upper sealing rings with parabolic and elliptical asymmetrical sliding surfaces results in:

– reduction in the lower and upper sealing ring friction power from 1% to 5% depending on the dynamic viscosity of the lubricating oil as the vertex coordinates $p_{j,k-1-2}$ increase
– reduction in the friction force at 20° crankshaft after the TDC in the expansion stroke from several to more than 20% for the range of $p_{j,k-1-2} \in \langle 26;45 \rangle$ depending on the engine velocity and oil dynamic viscosity,
– reduction in oil film thickness from 5 to 10° on the crankshaft after TDC in the expansion stroke whose value decreases with the increase of the vertex coordinates $p_{j,k-1-2}$,
– displacement of the crankshaft angle after TDC in the expansion stroke into higher values for which the minimum film thickness is recorded as the value of the vertex coordinates $p_{j,k-1-2}$ increases,
– significant reduction in the volume of oil scraped to the combustion chamber in the V2 compression stroke and V4 exhaust stroke and the reduction in hourly oil consumption for $p_{j,k-1-2} \in \langle 26;40 \rangle$. The percentage change in the value of these parameters affects the engine velocity and the dynamic viscosity of the oil. When $p_{j,k-1-2} > 40$, there is a rapid increase in the volume of oil scraped into the combustion chamber in each engine stroke.

Some additional conclusions can be drawn:

– determining the value of coefficients on the basis of simulation studies for individual oil film parameters and friction losses at different engine performance and different oil viscosities can contribute to a rapid verification of the effects of changes in symmetrical shapes of the reference rings into asymmetrical shapes adapted to individual engine geometric parameters.
– the asymmetric shapes of the sealing rings sliding surfaces make it possible to improve the engine mechanical efficiency while maintaining its durability and reducing oil consumption at the same time.

At present, the reduction in friction losses of a piston ring set is most frequently achieved by reducing their axial height and maintaining symmetrical shapes. Such actions result in serious consequences, i.e. a significant increase in the consumption of lubricating oil and a drastic reduction in the oil film thickness between the upper sealing ring's sliding surface and the cylinder wall. On the basis of the conducted simulations, the use of asymmetrically shaped sealing rings seems to be more advantageous. Their design does not significantly reduce the minimum thickness of the oil film between the cooperating surfaces but reduces the total thickness of the oil film and the total oil film coverage of these surfaces throughout the entire engine cycle. This is a very advantageous solution due to the fact that the only period of engine operation most prone to rupturing the oil film between cooperating kinematic pairs is in the range of 5 to 20° on the crankshaft after TDC in the expansion stroke for the upper sealing ring. In the remaining crankshaft angles throughout the engine cycle, outside the area just before the TDC, the thickness of the oil film in the compression stroke is several times higher, which means that there is no increased risk of oil film failure in the crankshaft angle range. This only occurs if the minimum oil film thickness at the beginning of the expansion stroke for the upper sealing ring is fulfilled. This means that the reduction in the thickness of the oil film in the remaining crankshaft angles throughout the whole engine cycle is a very desirable phenomenon. Such distribution of film thickness and oil film coverage of the sealing rings sliding surfaces can be achieved primarily by using the asymmetric shapes of those rings with a suitably selected individual displacement of the vertex $p_{j,k-1-2}$.

Nomenclature

F_1	oil film speed gradient at the oil film entrance point
F_2	oil velocity gradient due to mutual approach of the surfaces limiting the oil film
$F_3 = F_4$	oil speed gradient at the outlet from the lubricant slot
H_1, H_2	axial height of the sealing rings
L_x	the length of the lubrication gap covered with the oil film
p_1, p_2	external pressure acting on the oil film on the divergent and convergent side
p_v	pressure in the oil film caused by the extrusion effect
p_w	oil pressure caused by the slip effect
U_1, U_2	relative sliding speeds
Z_{1-x}, Z_{2-x}	distance of divergent and convergent oil boundaries
Z_v	thickness of oil film applied on the cylinder liner
Z_w	thickness of oil film left on cylinder surface after ring passage

Bibliography

[1] ISKRA, A. Rozkład filmu olejowego na gładzi cylindrowej silnika spalinowego, *Rozprawy nr 181*, Politechnika Poznańska 1987.

[2] KOSZAŁKA, G. Application of the piston-rings-cylinder kit model in the evaluation of operational changes in blowby flow rate. *Maintenance and Reliability*. 2010, **4**, 72-81.

[3] TIAN, T. Dynamic behaviors of piston rings and their practical impact – part ii: oil transport, friction, and wear of ring/liner interface and the effects of piston and ring dynamics. *Proc. Inst. Mech. Eng., Part J: Journal of Engineering Tribology*. 2002, **216**.

[4] WOLFF, A. Numerical analysis of piston ring pack operation. *Combustion Engines*. 2009, **2**, 128-141.

[5] WOLFF, A. Modelowanie i symulacja numeryczna funkcjonowania pakietu pierścieni tłokowych dwusu-wowego silnika okrętowego. *Zesz. Nauk. Inst. Pojazd., Wydz. Sam. i Masz. Robocz., Warsaw University of Technology*. 2011, **1**(82), 5-17.

[6] WOLFF, A. Numerical analysis of piston ring pack operation of a marine two-stroke engine. *Combustion Engines*. 2011, 146(**3**).

[7] WRÓBLEWSKI, P., ISKRA, A. Geometry of shape of profiles of the sliding surface of ring seals in the aspect of friction losses and oil film parameters. *Combustion Engines*. 2016, **167**(4), 24-38.

Piotr Wróblewski, MEng. – Faculty of Machines and Transport at Poznan University of Technology.

e-mail: *Piotr.Je.Wroblewski@doctorate.put.poznan.pl*



Article citation info:
MROZIK, M., DANILECKI, K. Environmental assessment of the production process of internal combustion engines. *Combustion Engines*. 2017, **171**(4), 117-120. DOI: 10.19206/CE-2017-419

Małgorzata MROZIK
Krzysztof DANILECKI

CE-2017-419

Environmental assessment of the production process of internal combustion engines

The aim of this article is to demonstrate using the LCA methodology the environmental effects of material composition changes on Volkswagen Golf passenger cars over the past 30 years. The simplified LCA model of the engine presented in the work shows the energy consumption and total CO_2 emissions based on the mass of materials. It was built to investigate general assumptions about material production and car recycling. The results of the research presented in the paper give an image of the modernity of a passenger car engine on the basis of consumption and the degree of recovery of materials used for its construction.

Key words: *car, combustion engine, LCA, eco-design, production*

1. Introduction

The most complex product of mass industrial production is a passenger car.It consists of thousands of parts made of almost all kinds of materials such as metals, aluminum and its alloys, plastics, glass and ceramics. Car production currently has a significant impact on the environment. The choice of more environmentally friendly construction materials from which it is manufactured can significantly reduce its environmental impact. The main component of each vehicle is the car engine. In the past, car engines were mainly designed for high performance, which caused that environmental pollution by motor vehicles became a significant problem in the second half of the 20th century and today. Since then, the development of environmental requirements has become a major factor stimulating the development of modern engine designs.

Currently the strategic goal of the European Union's energy policy in the transport sector is to reduce greenhouse gas emissions by 60% by 2050 compared to the levels from 1990. One way to achieve this is to strive for a more sustainable use of all means of transport due to the fact that this sector represents a major and still growing source of greenhouse gas emissions. That forces manufacturers to improve the energy efficiency of vehicles through the introduction of new technologies, especially in the field of drive systems. The effects of concern for the environment are visible – the unit emissions of pollutants in the exhaust fumes from new cars are reduced. Already at the beginning of the 1950s, Californian researchers for the first time linked environmental pollution to vehicle traffic. There, the first emission standards were introduced. Since then, the development of environmental requirements has become a majorfactor stimulating the development of modern engine designs [1, 2].

The traditional approach to environmental assessment of a car is first of all to determine pollutants and CO_2 emissions, which depend on the type and amount of fuel consumed. Research methods of the sizes are largely objectified, have a long tradition in the automotive industry and are based on extensive knowledge. The result of this approach are existing emission standards. The Life Cycle Method (LCA) described in ISO 14040 [3] and 14044 [4] expresses a contemporary approach to the problem of the impact of a car and its components on the environment. These standards define comprehensive, quantitative determination of an environmental load, based on the inventory of environmental factors associated with the object, process or other activity throughout the cycle from extracting raw materials to their final disposal [5–8]. The LCA method, introduced since the 1970s [9, 10], is one of the most effective and reliable eco-balance tools for assessing the amount of energy consumption and the volume of emissions of hazardous substances and materials in all phases of a product existence – from raw materials acquisition to liquidation of exploited products [11]. This is the basis for estimating the available options in order to reduce the load into the environment [5, 6].

2. Modeling of the engine life cycle

2.1. Purpose and scope of research

Current requirements for construction materials used in the automotive industry is primarily a tendency to use materials with lower density and greater strength and better performance. This makes it possible to reduce the weight of the vehicle and thus reduce fuel consumption so that the vehicle's carbon emissions to the environment are reduced. The use of new construction and operating materials, as well as a technology of a vehicle manufacturing and service, should help to increase the durability of vehicles and their components and extend the service intervals.

This reduces the environmental load of waste materials associated with the handling and disposal of end-of-life vehicles. The benefit is also the saving of raw materials and energy needed to process materials and produce parts and assemblies of vehicles. New construction materials and vehicle design itself should be adapted to the efficient recycling of vehicles. It is therefore necessary to optimize the design of cars, taking into account the issues of material selection and recycling at the design stage.

In the article, the LCA method was used to compare the environmental profiles of six spark-ignition internal combustion engines with similar operating characteristics produced in the last 30 years. The main objective of these studies was to assess the environmental effects of using different construction materials in engines [14, 15]. This assessment takes into account the use of recycled materials. A recycling scenario has been adopted in which materials recovered from end-of-life vehicles go back into the pro-

duction cycle of materials as a secondary raw material (closed loop recycling). In this way, recycling replaces primary raw materials and the impact of primary raw material production on the environment is avoided.

The research was conducted in accordance with the LCA method described in the Europe standards. Environmental impact is presented in the form of energy flows and total pollutant emissions with significant potential for global warming.

The results relate to six generations of the Volkswagen Golf petrol engine with similar exhaust gas operating characteristics, produced in the last 30 years (Table 1).

Table 1. Technical specifications of tested Volkswagen Golf cars

Model	Golf Mk1	Golf Mk2	Golf Mk3	Golf Mk4	Golf Mk5	Golf Mk6
Year of construction	1976-1983	1983-1987	1991-1997	1997-2003	2006-2008	2008-2012
Kerb weight [kg]	830	875	1030	1174	1153	1215
Engine capacity [cm^3]	1272	1272	1391	1390	1390	1390
Average fuel consumption NEDC [l/100 km]	7.8	6.1	6.8	6.4	6.8	6.4

2.2. Data sources

Material data of the VW Golf internal combustion engines was obtained during tests conducted at a certified vehicle dismantling station in Szczecin and using the most recent data from the literature. During the research, the cars were dismantled into assemblies and single parts.In order to draw up the list of materials used in the engine, the parts were weighed and the type of the material was determined. Many small parts were made from one material and in a similar technology. In this case, the list of parts was determined by the total weight in kilograms.

The list of the parts, along with information about the material weight, was used to build the LCA model of the car. As the parts are made from different materials, to simplify the model and facilitate the presentation of the life cycle assessment results, materials were assigned to five material groups:

- steel, cast steel, cast iron,
- aluminum and its alloys,
- plastics and rubber,
- non-ferrous metals,
- other materials.

The list of materials used in the Golf car engines is shown in Table 2.

Table 2. Percentage share of Volkswagen Golf engine materials

Model	Golf Mk1	Golf Mk2	Golf Mk3	Golf Mk4	Golf Mk5	Golf Mk6
Year of construction	1976-1983	1983-1987	1991-1997	1997-2003	2006-2008	2008-2012
Steel, cast steel, cast iron	58.4	59.4	53.3	52.7	50.0	49.8
Aluminum and its alloys	28.6	28.1	25.3	25.2	26.7	26.9
Plastics and rubber	2.6	3.0	7.8	8.2	8.6	10.2
Non-ferrous metals	2.2	2.1	4.9	5.9	6.3	6.3
Other materials	8.2	7.4	8.7	8.0	8.4	6.8

An inventory of the impact of the production processes of these materials is shown in Figure 1. Inputs include the streams of materials used in the engine that come from the natural environment (primary production) M_1, M_2, …, M_n and from recycling (secondary production) M_{R1}, M_{R2}, …, M_{Rn}. The system outputs include pollutant emissions P_1, P_2, …, P_n and energy consumption E_1, E_2, …, E_n associated with their generation.

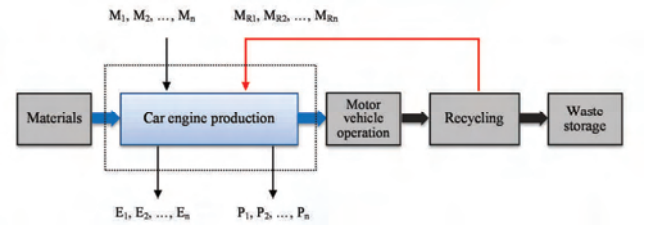


Fig. 1. Inventory of the car's life cycle

For each material stream, the volume of emissions of the substance was determined, i.e. CO, CO_2, CH_4, N_2O, NO_x, NMVOC, which accompany primary and secondary production of materials.Data regarding the size of these emissions was obtained from the Ecoinvent 2.1 database, which is widely used in life-cycle studies. The environmental impact of these variables was converted into CO_{2eq} carbon dioxide emissions.Eco-Indicator EI99 E/A Europe was used for the conversion. In the LCA studies, the total CO_{2eq} emission was treated as an environmental impact category. While the energy consumption in the production processes of materials was specified on the basis of Gemis and Raport LCA Plastics Europe and from the assisting calculation programs: SimaPro oraz Greet.

3. Evaluation results of engine production process

Material data obtained reflects changes in the design of the internal combustion engine of the car. It is therefore necessary to assess whether the presented tendencies of these changes are justified from the point of view of the impact of the materials on the environment.

3.1. Changes in the use of materials

The material data presented in Figure 2 reflects the general tendency to increase the mass of new cars.

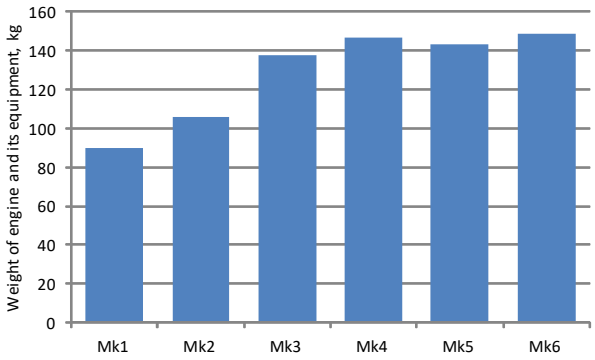


Fig. 2. Weight of Volkswagen Golf engine and its equipment

Weight of the engineand its equipment increased by over 65% between models Mk1and Mk6. Table 2 shows a decrease in the share of steel, cast steel and cast iron in the engine construction by 8.5% between Mk1 and Mk6, with an almost four-fold increase in the share of plastics and rubber and nearly three-fold increase in the share of non-ferrous metals.

3.2. Impact of primary production of materials

This chapter presents the results of the environmental assessment of engines based on the energy inputs and carbon dioxide (CO_2) emissions associated with the primary production of the materials.The comparison of environmental loads for the individual materials of the car engine is shown in Figures 3 and 4.

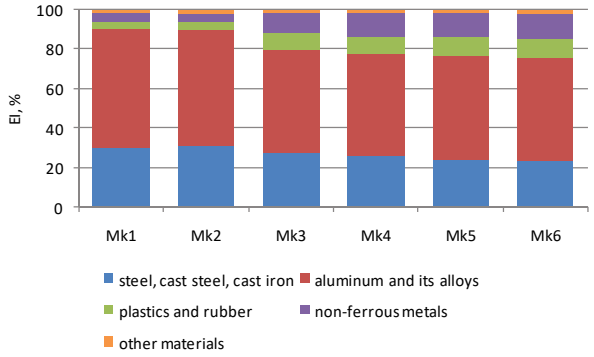


Fig. 3. Percentage share of energy inputs for the Volkswagen Golf engine and its equipment divided into materials

Based on the results of the assessment, the dominant share of aluminum and its alloys in total energy expenditure can be found. The higher energy consumption of these materials compared to steel results from a fourfold increase in the unit energy consumption index of the material primary production, which for aluminum is 166.169 MJ/kg, while for steel it is only 40.903 MJ/kg.

Compared to the Mk1 model, the percentage share of energy inputs for steel, cast steel and cast iron in the Mk6 model decreased by 6.6% and by 8.5% for aluminum and its alloys (Fig. 3). A systematic increase in the environmental load associated with the use of other materials can be observed. For non-ferrous metals, the share of energy inputs was over two and a half times higher, while for plastics and rubber it was a three-fold increase.

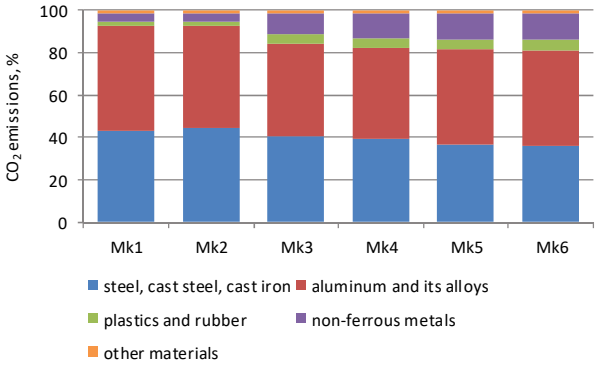


Fig. 4. Percentage share of CO_2 emissions for the Volkswagen Golf engine and its equipment divided into materials

Such changes in energy inputs correspond to changes in carbon dioxide emissions. Percentage share of CO_2 emissions between models Mk1 and Mk6 decreased by 7.4% for steel, cast steel and cast iron, and by 4.3% for aluminum and its alloys. For plastics and rubber there was more than two and half times increase in CO_2 emissions, and for non-ferrous metals – almost three-fold increase in CO_2 emissions.

3.3. Impact of secondary production of materials (recycling)

In the environmental assessment of materialssecondary production, a closed loop recycling scenario has been adopted where the size of the "environmental credit" of the se-condary production of the materials recovered from scrapped cars was determined as compared to the primary production of the materials. The amount of energy inputs (EI) and CO_2 emissions related to the production of recycled materials was determined for the reuse and recycling indicators, which have come into effect since 2015 for all engines of vehicles withdrawn from use (RRR Directive, 2005). The results of the comparative assessment are shown in Figures 5 and 6.

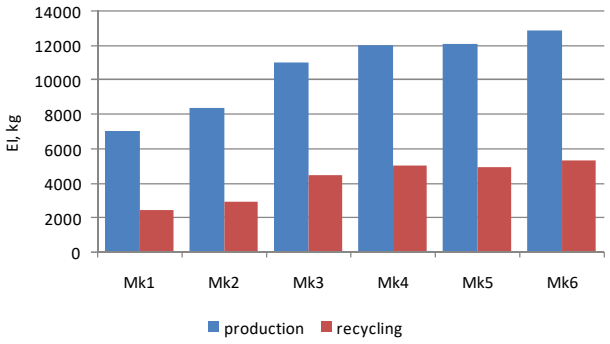


Fig. 5. Energy inputs for different scenarios of material production

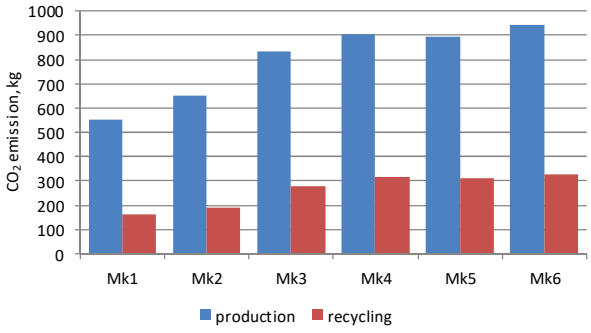


Fig. 6. CO_2emissions for secondary production

The results indicate the significant potential of recycling to reduce energy consumption and CO_2 emissions during the production process. Despite the systematic increase in energy consumption and CO_2 emissions for both primary and secondary production of materials, a noticeable reduction in environmental loads in the case of secondary production of materials is observed. At the same time, there is a reduction in the benefits of the use of recycled materials. This is the result of the growing use of plastics in

the construction of engines whose recycling creates the greatest environmental problems.

4. Conclusion

The results presented in the paper show the environmental effects of changes in the composition of the material in the engines of Volkswagen Golf passenger cars in the past 30 years. The simplified LCA model of the engine presented in the paper shows the energy consumption and total CO_2 emissions based on the mass of materials. Changes in the use of materials are a signal of the technological progress that has taken place in car construction in the past 30 years. The greatest progress was made with the introduction of the third-generation model. A number of changes to improve comfort and safety have been introduced. The price of these changes was to increase the weight of the whole car by about 18%. At the same time, lightweight materials such as aluminum, plastics and rubber and non-ferrous metals increased by about 4%. So clear, compared to the predecessors, the increased use of these materials indicates the beginning of the implementation of a car weight reduction strategy, aimed at offsetting the effects of the changes in the design of not only the whole car but also the engine.

The selection of construction materials used in the construction of internal combustion engines of the Volkswagen Golf car has a significant impact on the level of their environmental impact. There is a tendency to reduce the share of steel, cast steel and cast iron while increasing the share of other materials. Systematic increase in the environmental burden associated with the use of other materials can be observed.

Based on the analysis, it can also be said that the recycling of materials can be an effective way to reduce the negative impact of internal combustion engines on the environment. The results indicate significant recycling potential in reducing energy consumption and CO_2 emissions during the car engine production process. A significant reduction of environmental burden in the production of secondary materials from which the engine is built can be observed, despite the systematic increase of energy consumption and CO_2 emissions.

Nomenclature

LCA life cycle assessment
CO_2 carbon dioxide
EI energy inputs
Mk1 Volkswagen Golf I
Mk2 Volkswagen Golf II
Mk3 Volkswagen Golf III
Mk4 Volkswagen Golf IV
Mk5 Volkswagen Golf V
Mk6 Volkswagen Golf VI

Bibliography

[1] MERKISZ, J. Ekologiczne problemy silników spalinowych. *Wydawnictwo Politechniki Poznańskiej*. Poznań 1998.

[2] MERKISZ, J. Ekologiczne aspekty stosowania silników spalinowych. *Wydawnictwo Politechniki Poznańskiej*. Poznań 1995.

[3] International Organization for Standardization (ISO), 2006a. 14040–Environmental Management. Life Cycle Assessment. Principles and Framework.

[4] International Organization for Standardization (ISO), 2006a. 14040 – Environmental Management. Life Cycle Assessment. Requirements and Guidelines.

[5] KOWALSKI, Z., KĘDZIERSKA, D., NOWAK, A.K. et al. LCA analysis of processing of the zinc and lead ores in Trzebionka Mining Works. *10th Conference on Environment and Mineral Processing, VŠB-TU Ostrava, Czech Republic, Proceedings Part II*, 22-24.06.2006, 105-115.

[6] KULCZYCKA, J. Ekologiczna ocena cyklu życia (LCA) nową techniką zarządzania środowiskowego. *IGSMiE*. Kraków 2001.

[7] PN-EN ISO 14040. Zarządzanie środowiskowe – Ocena cyklu życia – Zasady i struktura. Polski Komitet Normalizacyjny, czerwiec 2006.

[8] PN-EN ISO 14040. Zarządzanie środowiskowe – Ocena cyklu życia – Wymagania i wytyczne. Polski Komitet Normalizacyjny, lipiec 2006.

[9] ELIASZ, J. Rozprawa habilitacyjna: Model całościowej, energetyczno-ekologicznej oceny technologii energetycznych. *Technische Universität Dresden*. Drezno 2002.

[10] GÓRALCZYK, M., KULCZYCKA, J. Ekologiczna ocena cyklu życia (LCA) – nową normą z rodziny ISO 14000. *ProblemyEkologii.* 2001, **4**.

[11] HOOFTMAN, N., OLIVEIRA, L., MESSAGIE, M. et al. Environmental analysis of petrol, diesel and electric passenger cars in a Belgian urban setting. *Energies*. 2016, **9**(2), 1-24.

[12] DOBROSZ, K., MATYSIAK, A. Tworzywa sztuczne w pojazdach samochodowych. *Wydawnictwa Komunikacji i Łączności*. Warszawa, 1982.

[13] IDZIOR, M. Kierunki zmian materiałowychw motoryzacji w świetlewymogów ekologii. *Motrol*. 2007, **9**.

[14] DANILECKI, K., MROZIK, M., SMURAWSKI, P. Changes in the environmental profile of a popular passenger car over the last 30 years – Results of a simplified LCA study. *Journal of Cleaner Production*. 2016, **141**, 208-218.

[15] BIRAT, J., GUERIN, V., ROCCHIA, L., TUCHMAN, M. Ecodesign of automobiles basedon the environmental properties of body materials. *SAE Technical Paper*. 2004, 2004-01-0250.

Małgorzata Mrozik, DSc., DEng. – Faculty of Mechanical Engineering and Mechatronicsat West Pomeranian University of Technology in Szczecin.

e-mail: *Malgorzata.Mrozik@zut.edu.pl*



Krzysztof Danilecki, DSc., DEng. – Faculty of Mechanical Engineering and Mechatronicsat West Pomeranian University of Technology in Szczecin.

e-mail: *Krzysztof.Danilecki@zut.edu.pl*



Article citation info:
BEBKIEWICZ, K., CHŁOPEK, Z., STOSIO, G. et al. Evolution of national annual pollutant emission from motor vehicles in Poland. *Combustion Engines*. 2017, **171**(4), 121-126. DOI: 10.19206/CE-2017-420

Katarzyna BEBKIEWICZ
Zdzisław CHŁOPEK
Grzegorz STOSIO
Krystian SZCZEPAŃSKI
Magdalena ZIMAKOWSKA-LASKOWSKA

CE-2017-420

Effect of average velocity of passenger cars on national annual emission of pollutants

The paper presents the results of the study on the sensitivity of the national annual emission of pollutants from passenger cars to their average velocity under the following traffic conditions: urban, rural, and on motorways and expressways. The study was carried out in accordance with the methodology used in the COPERT 4 software. The effect of traffic speed within cumulated categories of passenger cars on the national emission of pollutants was analyzed. The national annual pollutant emission of pollutants was found to be substantially affected by the average car velocity, this effect being largely differentiated due to the character of road traffic. The type of the dependence of the national annual pollutant emission on the average velocity is similar for all substances, especially under traffic conditions in rural areas as well as on highways and expressways. A distinct minimum of the national pollutant emission was found at a velocity of about 70 km/h under rural conditions.

Key words: *motor vehicles, inventory of pollutant emission, COPERT*

1. Introduction

It is well known, that the performance parameters of internal combustion engines are dependent, sometimes decidedly, on the operating conditions of engines [6, 7]. Emission of pollutants is particularly strongly dependent on engine operating conditions, due to both the values describing dynamic states, and the occurrence of dynamic states [6, 7]. The emission of pollutants is most sensitive to the engine operating conditions in the case of spark ignition engines [6]. In the case of compression ignition engines, the presence of dynamic states affects highly the emission of particulate matter, especially when fuel input is rapidly increasing [6, 14].

The values describing operating conditions of internal combustion engines include [6]:
– engine thermal state,
– parameters characterising the engine work intensity, such as: engine crankshaft speed and, usually, torque output.

The basic process, which determines vehicle engine operation in the stable thermal state, is the process of vehicle velocity [2, 6]. That is why, the qualitative pollutant emission testing is carried out in road tests, simulating the real world conditions of vehicle use [2, 15].

The process of vehicle velocity may vary greatly depending upon the traffic pattern. Typically, the following traffic patterns of vehicles have been distinguished [1–3, 6, 8–12, 16]:
– urban,
– rural,
– on highways and motorways.

Sometimes, the traffic pattern in the street congestion situation may be disengaged from the model of urban traffic [3].

Therefore, for the purpose of balancing pollutant emission as well as fuel and energy consumption, the state of vehicle engine operation under conditions of traction use can be characterized by the share of road travelled by vehicles under model traffic conditions, and by the value describing the velocity process under model traffic conditions. As this value, taken as a representative zero-dimensional characteristics of the process of driving velocity, the value of average velocity is most often adopted [2, 5, 6, 8–13]. Other zero-dimensional characteristics of velocity [6, 13] were also considered, including, first of all, the average value of the absolute value of the product of velocity and acceleration [2, 6, 13], albeit the above characteristic is applied solely in the cognitive studies, and not in the practical ones.

Practical tests of pollutant emission from vehicle engines, use characteristics which are dependencies of the specific distance emission of pollutants on the average velocity of vehicles [2, 4–6, 9–13]. These characteristics depend on the environmental characteristics of car engines, which relate to the emission of pollutants.

This paper presents the results of a simulation study on the national annual emission from passenger car engines, based on the average velocity under model traffic conditions: urban, rural and on highways and expressways.

The objective of the study – apart from a cognitive one – was also the practical one, as the selection of values of the average velocity of vehicles under model conditions is extremely difficult, owing to the lack of sufficiently systematic results of empirical study, which would allow for a reliable identification of the above mentioned values.

Consequently, it is advisable to estimate the sensitivity of the modelled national annual emission of pollutants emission from motor vehicles to the average vehicle velocity under model traffic conditions.

2. The COPERT software

The COPERT 4 [9–11], applied in this study, is the software of preference in the European Union, for inventorying emission from motor vehicles [16].

The study was performed for the automotive situation in 2015. Table 1 shows the values for passenger car traffic in 2015, based on data reported in [1].

Table 1. Values characterizing passenger car traffic in Poland in 2015

N_{PC}	[mln]	20.52
$N_{PC\text{-}SI}$		14.66
$N_{PC\text{-}CI}$		5.86
$p_{PC\text{-}SI}$	[km]	5900
$p_{PC\text{-}CI}$	[km]	12300
u_U		0.37
u_R		0.5
u_H		0.13
v_U	[km/h]	31.5
v_R	[km/h]	70
v_H	[km/h]	120

The remaining parameters of the model were assumed in accordance with those suggested by the COPERT 4 software.

3. Results of simulation study

In the paper, the results are presented of three simulations studies – schematic of the studies is given in Table 2.

Table 2. Schematic of studies Nos 1, 2 and 3

Study No 1			Study No 2			Study No 3		
v_U	v_R	v_H	v_U	v_R	v_H	v_U	v_R	v_H
[km/h]			[km/h]			[km/h]		
21.5	70	120	31.5	50	120	31.5	70	100
23	70	120	31.5	60	120	31.5	70	110
25	70	120	31.5	70	120	31.5	70	120
26.5	70	120	31.5	80	120	31.5	70	130
28	70	120	31.5	90	120	31.5	70	140
31.5	70	120	–	–	–	–	–	–
36.5	70	120	–	–	–	–	–	–
41.5	70	120	–	–	–	–	–	–

The average velocity of vehicles was assumed as a variable, respectively, under conditions of urban traffic in the study No 1, under rural traffic – in the study No 2, and under conditions of traffic on highways and expressways – in the study No 3.

The results of the simulation study for selected pollutants are illustrated in Figures 1–21.

There is a significant similarity between the characteristics of the vehicle traffic conditions. For urban traffic conditions, the sensitivity of national annual emission is insensitive to average velocity. For traffic rural conditions, there is a clear minimum national annual emission for average velocity of around 70 km/h. For traffic conditions on highways and expressways, national annual emission is an increasing function of average velocity.

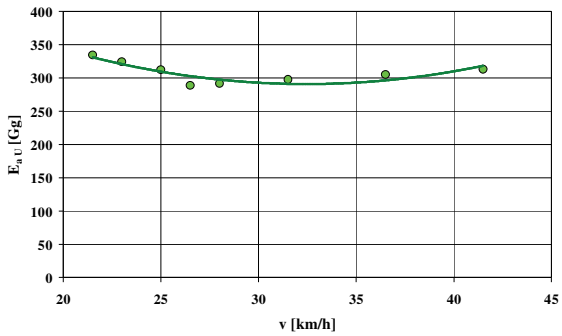


Fig. 1. Dependence of the national annual emission of carbon monoxide from passenger cars upon the average velocity, under model conditions of urban traffic

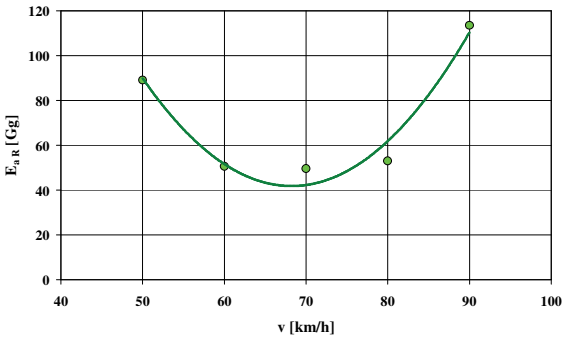


Fig. 2. Dependence of the national annual emission of carbon monoxide from passenger cars upon the average velocity, under model conditions of rural traffic

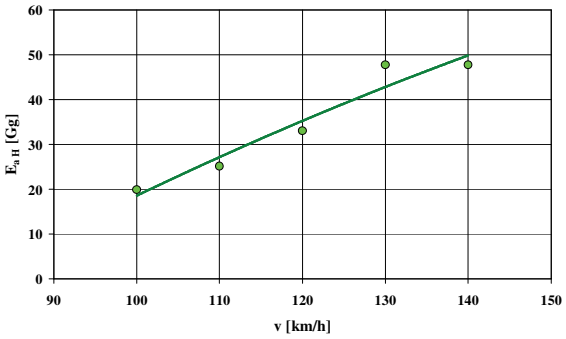


Fig. 3. Dependence of the national annual emission of carbon monoxide from passenger cars upon the average velocity, under model conditions of traffic on highways and expressways

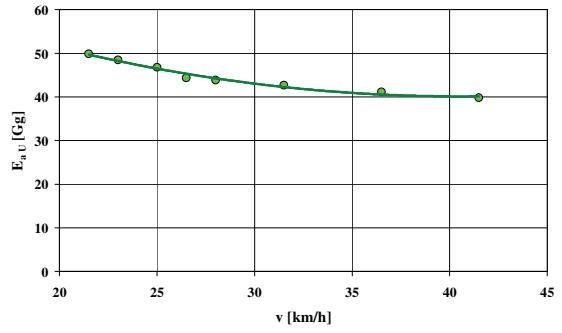


Fig. 4. Dependence of the national annual emission of volatile organic compounds from passenger cars upon the average velocity, under model conditions of urban traffic

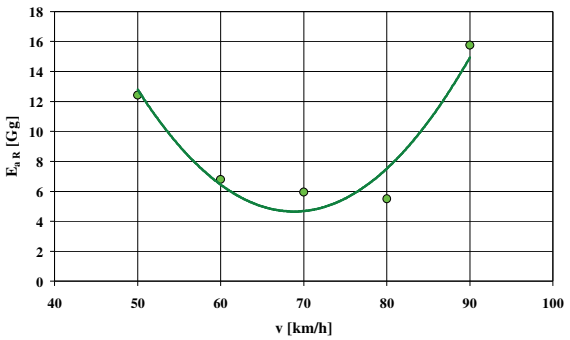


Fig. 5. Dependence of the national annual emission of volatile organic compounds from passenger cars upon the average velocity, under model conditions of rural traffic

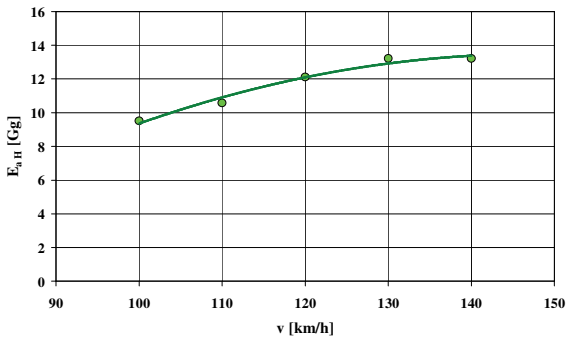


Fig. 9. Dependence of the national annual emission of nitrogen oxides from passenger cars upon the average velocity, under model conditions of traffic on highways and expressways

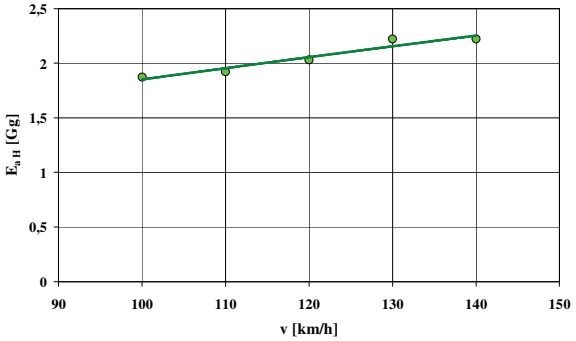


Fig. 6. Dependence of the national annual emission of volatile organic compounds from passenger cars upon the average velocity, under model conditions of traffic on highways and expressways

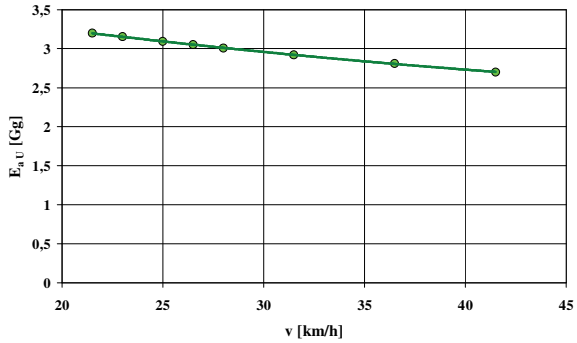


Fig. 10. Dependence of the national annual emission of particulate matter PM10 from tribological elements of passenger cars upon the average velocity, under model conditions of urban traffic

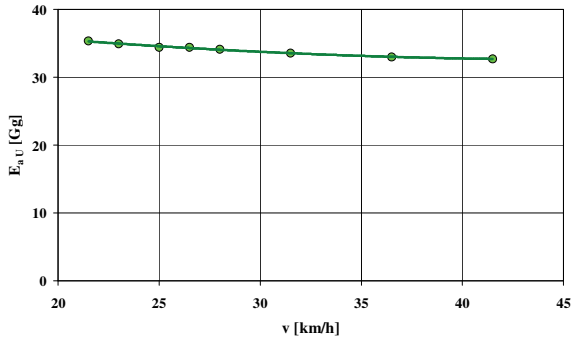


Fig. 7. Dependence of the national annual emission of nitrogen oxides from passenger cars upon the average velocity, under model conditions of urban traffic

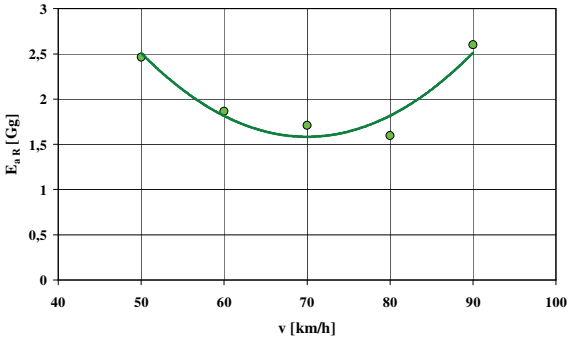


Fig. 11. Dependence of the national annual emission of particulate matter PM10 from tribological elements of passenger cars upon the average velocity, under model conditions of rural traffic

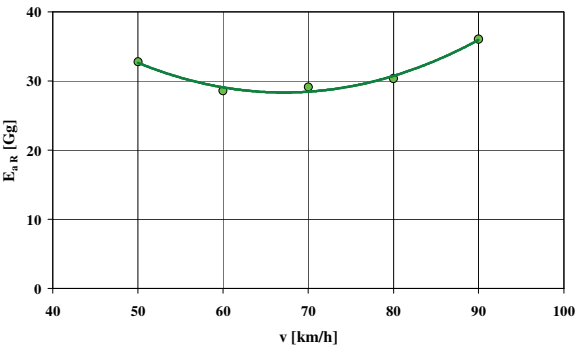


Fig. 8. Dependence of the national annual emission of nitrogen oxides from passenger cars upon the average velocity, under model conditions of rural traffic

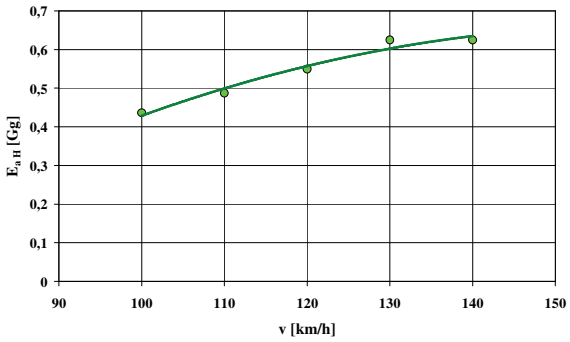


Fig. 12. Dependence of the national annual emission of particulate matter PM10 from tribological elements of passenger cars upon the average velocity, under model conditions of traffic on highways and expressways

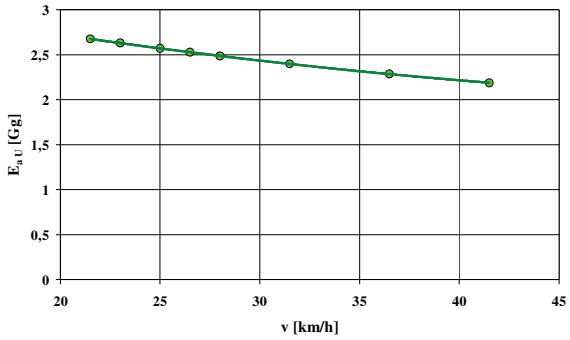


Fig. 13. Dependence of the national annual emission of particulate matter PM2.5 from tribological elements of passenger cars upon the average velocity, under model conditions of urban traffic

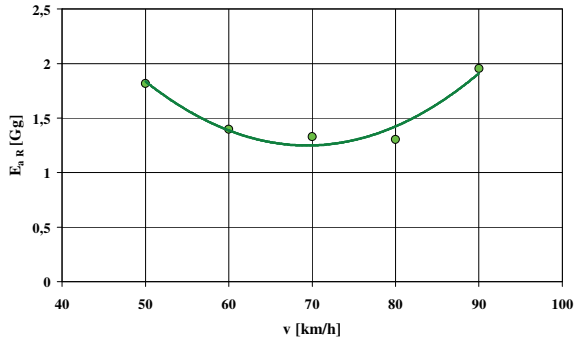


Fig. 14. Dependence of the national annual emission of particulate matter PM2.5 from tribological elements of passenger cars upon the average velocity, under model conditions of rural traffic

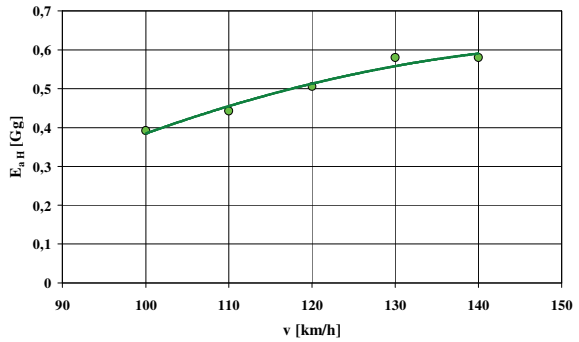


Fig. 15. Dependence of the national annual emission of particulate matter PM2.5 from tribological elements of passenger cars upon the average velocity, under model conditions of traffic on highways and expressways

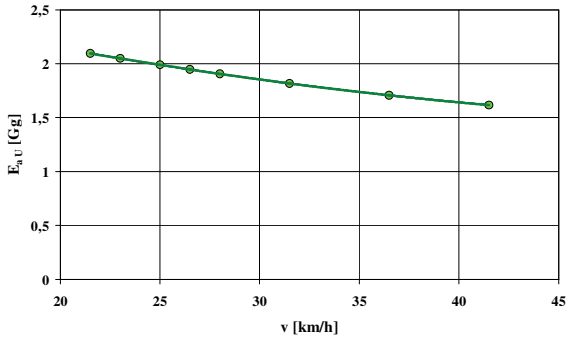


Fig. 16. Dependence of the national annual emission of particulate matter from the exhaust system of passenger car engines upon the average velocity, under model conditions of urban traffic

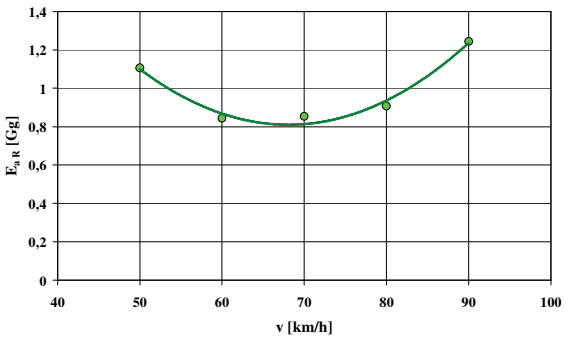


Fig. 17. Dependence of the national annual emission of particulate matter from the exhaust system of passenger car engines upon the average velocity, under model conditions of rural traffic

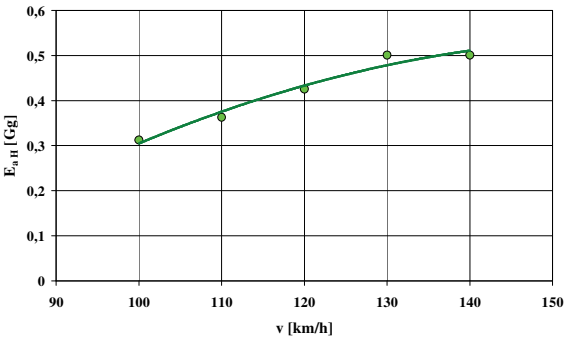


Fig. 18. Dependence of the national annual emission of particulate matter from the exhaust system of passenger car engines upon the average velocity, under model conditions of traffic on highways and expressways

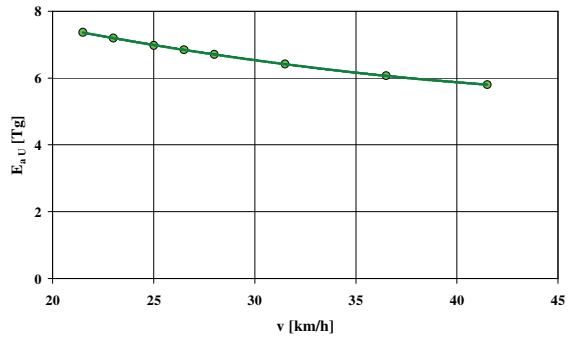


Fig. 19. Dependence of the national annual emission of carbon dioxide from passenger cars upon the average velocity, under model conditions of urban traffic

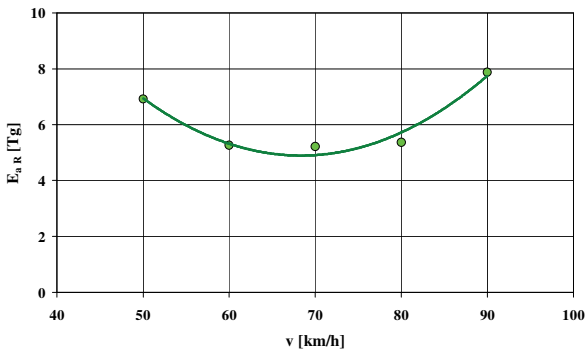


Fig. 20. Dependence of the national annual emission of carbon dioxide from passenger cars upon the average velocity, under model conditions of rural traffic

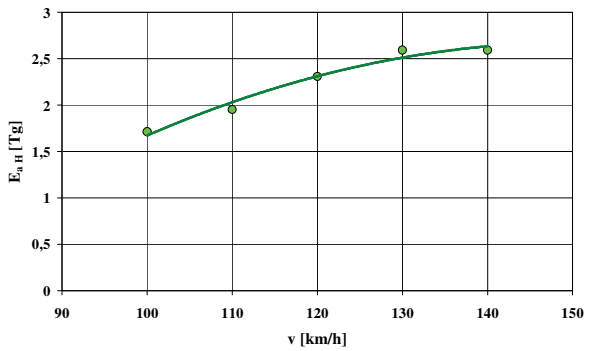


Fig. 21. Dependence of the national annual emission of carbon dioxide from passenger cars upon the average velocity, under model conditions of traffic on highways and expressways

4. Conclusions

The simulative study on the dependence of national annual pollutant emission from passenger cars on the average vehicle velocity under model traffic conditions authorize the following conclusions:

1. Despite the differences in the dependencies shown in Figures 1–21, some regularities can be stated. Much smaller differences exist in the characteristics of individual substances than in the conditions of vehicle traffic. There is a substantial similarity of dependence – irrespective of pollution type – for traffic conditions: urban, rural, and on motorways and expressways. The most differing dependencies, among the remaining characteristics, are those for the rural traffic.
2. The highest sensitivity of the national annual pollutant emission to the average velocity of road traffic was found for practically all substances under conditions of rural traffic, while – for some substances – under conditions of traffic on highways and expressways.
3. General conclusions based on the studies conducted show, that the estimation of average velocity values under model traffic conditions, for the purpose of quantifying emission from motor vehicles, can be a source of significant uncertainty in modeling results. This justifies the expediency of implementing an empirical research programme for vehicle traffic on a scale so that it is possible to formulate reliable conclusions about the representative characteristics of passenger car traffic.

Nomenclature

b	specific distance emission
CI	compression ignition
E_a	national annual emission
H	highway
N	number of vehicles per cumulated category skumulowanych
p	annual mileage of vehicles per cumulated category
PC	passenger cars
PC-CI	passenger cars – compression ignition (engine)
PC-SI	passenger cars – spark ignition (engine)
R	rural
T	total (vehicles)
u	share of road travelled by vehicles per cumulated category under model traffic conditions
U	urban
v	average velocity of vehicles per cumulated category

Bibliography

[1] BEBKIEWICZ, K., CHŁOPEK, Z., SZCZEPAŃSKI, K., ZIMAKOWSKA-LASKOWSKA, M. The influence of the properties of vehicles traffic on the total pollutant emission. *Proceedings of the Institute of Vehicles*. 2017, **1**(110), 89-102.

[2] BUWAL (Bundesamt für Umwelt, Wald und Landschaft), INFRAS AG (Infrastruktur-, Umwelt- und Wirtschaftsberatung). Luftschadstoffemissionen des Strassenverkehrs 1950-2010. BUWAL-Bericht Nr. 255, 1995.

[3] CHŁOPEK, Z., BIEDRZYCKI, J., LASOCKI, J., WÓJCIK, P. Comparative examination of pollutant emission from an Automotive internal combustion engine with the use of vehicle driving tests. *Combustion Engines*. 2016, 164(1), 56-64.

[4] CHŁOPEK, Z., LASKOWSKI P. Pollutant emission characteristics determined using the Monte Carlo method. *Eksploatacja i Niezawodnosc – Maintenance and Reliability*. 2009, **2**(42), 42-51.

[5] CHŁOPEK, Z., ZIMAKOWSKA, M. Charakterystyki emisji zanieczyszczeń z samochodowych silników spalinowych. Rozdział w monografii „Współczesne problemy inżynierii i ochrony środowiska". *Zeszyt „Inżynieria Środowiska"*. Oficyna Wydawnicza Politechniki Warszawskiej. 2009, **55**, 53-66.

[6] CHŁOPEK, Z. Modelowanie procesów emisji spalin w warunkach eksploatacji trakcyjnej silników spalinowych. Oficyna Wydawnicza Politechniki Warszawskiej. *Prace Naukowe. Seria „Mechanika"*. 1999, **173**.

[7] CHŁOPEK, Z. Some remarks on engine testing in dynamic states. *Combustion Engines*. 2010, **143**(4), 60-72.

[8] CHŁOPEK, Z. Zasady modelowania zużycia paliwa i energii oraz emisji zanieczyszczeń związanych z użytkowaniem pojazdów drogowych. *Technika Transportu Szynowego*. 2015, **12**, 262-267.

[9] COPERT Training 5. COPERT 5 vs COPERT 4. European Environment Agency. 2016. emisia.com/sites/default/files/COPERT_5_features.pdf (accessed 2016.12.06).

[10] EMEP/EEA air pollutant emission inventory guidebook – 2016. European Environment Agency. www.eea.europa.eu/publications/emep-eea-guidebook-2016 (accessed 2016.12.06).

[11] GKATZOFLIAS, D., KOURIDIS, CH., NTZIACHRISTOS, L., SAMARAS, Z. COPERT 4 Computer programme to calculate emissons from road transport. User manual (version 9.0). *European Environment Agency*. Emisia SA. 2012. (accessed 2016.12.06).

[12] INFRAS AG. Handbook emission factors for road transport 3.2. *Quick reference*. Version 3.2. Bern, 2014.
[13] LASKOWSKI, P. Wyznaczanie charakterystyk emisji zanieczyszczeń w przypadkowych stanach pracy samochodowych silników spalinowych. *Rozprawa doktorska*. Politechnika Warszawska. Wydział Samochodów i Maszyn Roboczych. Warszawa 2015.
[14] PIELECHA, J. Identyfikacja parametrów cząstek stałych z silników spalinowych. *Wydawnictwo Politechniki Poznańskiej*. Poznań 2012.
[15] Worldwide emission standards. Passenger cars and light duty vehicles. *Delphi*. Innovation for the real world. 2016/2017.
[16] 2006 IPCC Guidelines for National Greenhouse Gas Inventories. www.ipcc-nggip.iges.or.jp/public/2006gl/vol2.html (accessed 2016.12.06).

Katarzyna Bebkiewicz, MEng. – Institute of Environmental Protection – National Research Institute in Warsaw.

e-mail: *Katarzyna.Bebkiewicz@kobize.pl*



Krystian Szczepański, DSc., DEng. – Institute of Environmental Protection – National Research Institute in Warsaw.

e-mail: *Krystian.Szczepanski@ios.edu.pl*



Prof. Zdzisław Chłopek, DSc., DEng. – Institute of Environmental Protection – National Research Institute in Warsaw.

e-mail: *Zdzislaw.Chlopek@kobize.pl*



Magdalena Zimakowska-Laskowska, DSc., DEng. – Institute of Environmental Protection – National Research Institute in Warsaw.

e-mail: *Magdalena.Zimakowska-Laskowska@kobize.pl*



Grzegorz Stosio, Eng. – Faculty of Automotive and Construction Machinery Engineering in the Warsaw University of Technology.

e-mail: *GrzegorzStosio@gmail.com*



Article citation info:
KAŁUŻNY, J., MERKISZ, J., STEPANENKO, A. et al. Piston assembly in the most powerful 2.0l diesel engine – case study of the current tribological system and innovative concepts for the future. *Combustion Engines*. 2017, **171**(4), 127-133. DOI: 10.19206/CE-2017-421

Jarosław KAŁUŻNY
Jerzy MERKISZ
Aleksander STEPANENKO
Emil WRÓBLEWSKI
Bartosz GAPIŃSKI
Adam PIASECKI
Dawid GALLAS

CE-2017-421

Piston assembly in the most powerful 2.0l diesel engine – case study of the current tribological system and innovative concepts for the future

This article is a contribution to the ongoing debate on the scenario of the vehicle powertrains development. The directions of the internal combustion engines development in search of the possibility of effective economic and ecological indicators improvement have been indicated. It has been pointed out that this goal can be achieved through the use of nanotechnology in order to exceed the downsizing barriers resulting from the permissible mechanical loads for conventional materials. The article presents the study of the construction and materials used in the piston assembly of the most advanced four-cylinder, compression-ignition diesel engine currently in manufacture. Original concepts of nanotechnology have been proposed to reduce friction losses in major friction components of future engines with extremely high loads. The main idea is to verify the hypothesis that the sub-micron surface texture of the friction components obtained in the process of applying anti-wear outer layers can lead to an effective reduction of friction losses under real engine operating conditions. Computer simulations of the effects of introducing the surface texture in the upper sealing ring on friction loss confirm this hypothesis by showing friction value being reduced by 3-4% relative to the standard ring profile. In the summary, further advanced technologies designed to effectively utilize the unique properties of carbon nanotubes have been described.

Key words: *piston engine, powertrains development, tribological system*

1. Introduction

The production of the VW Golf with a diesel engine started in 1976. It was the first popular car with this type of engine. This construction was the response to the oil crisis after 1973. The 1.5 dm^3 displacement combustion engine with a swirl chamber was characterized by a limited power of 37 kW and a maximum torque of only 80 Nm, but it offered extremely low fuel consumption. In subsequent years, the engine was improved, increasing the displacement and introducing turbocharging, while other manufacturers began mass-producing competing cars with similar engine designs. A major breakthrough came in 1989 when a supercharged diesel engine and direct fuel injection system were successfully introduced into production. Subsequent generations of the CI engines were characterized by increasing unit power and torque indexes, while consuming much less fuel than comparable SI motors (Fig. 1).

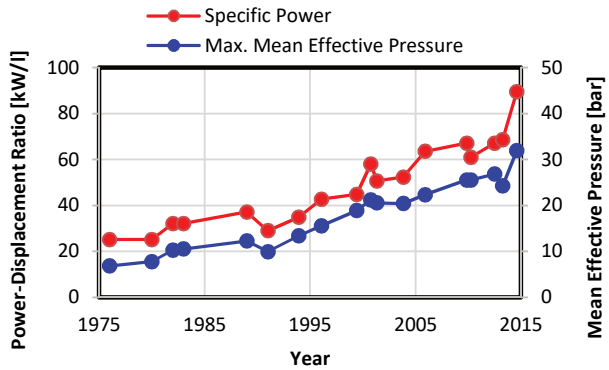


Fig. 1. Development of CI engines on the example of VW engines; mean effective pressure and specific power

CI engines have become an increasingly popular source of automobile propulsion. In some European countries more cars with CI engines were purchased than with SI engines.

At present, the share of CI engines in the market of new cars sold in Europe is somewhat limited, which is due to the cost of production of complex exhaust gas aftertreatment systems. However, such engines are still needed in order to meet the carbon dioxide reduction target, among other reasons.

1.1. The role of the IC engines in the future

Reciprocating internal combustion engines have been used in car drives for over a hundred years, but in recent years there has been a growing tendency to replace them with electric motors. These types of efforts are politically motivated or dictated by fashion – ecology and modernity, but are devoid of rational technical justification. It is also worth noting that neither the electric nor hybrid vehicles can be regarded as an invention of modern times.

Road transport is one of the main sources of carbon dioxide and toxic air pollutants emissions. Air pollution continues to be a problem, especially in large cities, demanding an urgent solution. In this case the elimination of vehicles with combustion engines from city centers and replacing them with electric drive buses and taxis is an effective solution that can be quickly implemented. Such actions make sense, if they are local in nature, but striving for global replacement of combustion engines with electric motors as quickly as possible makes no sense. Well-to-wheel analysis indicates that as long as electricity is produced mainly in power plants burning fossil fuels the replacement of automotive internal combustion engines with electric motors

will not bring a radical improvement in transport ecology. Currently about 67% of globally generated electricity is produced in power plants through the burning of fossil fuels. The development of renewable energy sources does not even compensate for the power lost due to nuclear power plants shut offs, as a result the share of energy derived from fossil fuels does not even decrease [20].

In the case of electric cars the unfavorable ratio of stored energy to the battery mass remains an unsolved problem. If coordinated action is planned and initiated the challenging technical task of dramatically increasing the battery energy concentration could be realized in the future; as in the past a clearly defined plan allowed building a vehicle in a few years that allows man to fly to the moon.

An alternative to the search for solutions to increase the energy concentration on board the electric vehicles is to improve the existing internal combustion engines. The authors believe that when determining further directions of automotive industry development the first consideration to take into account is the ratio of the expected benefits to the cost of a project and not its ambition. In this context, it is reasonable to strive for improvements to internal combustion engines; where the ecological and economic aspects play a special role. The environmental performance cannot, however, be seen as a formal meeting of the current tests requirements, but to ensure that the actual emission of toxic compounds is as small as possible in all operating conditions [14–16]. LCA analysis is an important issue [11].

1.2. Future requirements in the piston assembly of CI engines

At present, the downsizing trend is evident in the design of passenger car engines [9], Fig. 1. In the author's view, the downsizing limits will continue to shift in order to achieve the benefits of improved engine efficiency and reduced fuel consumption [12]. This is due to increased thermal and mechanical loads in the piston assembly. The constantly increasing power of the engines causes the piston's bottom to be heated to the limits of the aluminum alloy durability, thus replacing aluminum with steel is considered [1, 2, 4, 18].

Another important factor is meeting the requirements for toxic gas emissions. In order to reduce the emission of nitrogen oxides in CI engines, exhaust gas recirculation (EGR) and injection delay in high engine load conditions are common (Fig. 2). However, this action inevitably leads to delays in the combustion process, high cylinder pressure occurs when the piston is already far from the TDC in the stroke. The normal pressure of the piston pushing on the cylinder walls increases considerably as a result. Attention is increasingly paid to new materials capable of reducing friction in mixed lubricating regime, and to prevent seizure of the piston in the cylinder [4–7].

In this article, the authors wish to pay particular attention to the tribological benefits of applying texture on the surface of the piston assembly elements. In this context, the results of the work presented in [10, 21] are promising. Surface textures can be obtained as a side effect of applying standard top layers with proven beneficial tribological properties, such as chromium and magnesium phosphate.

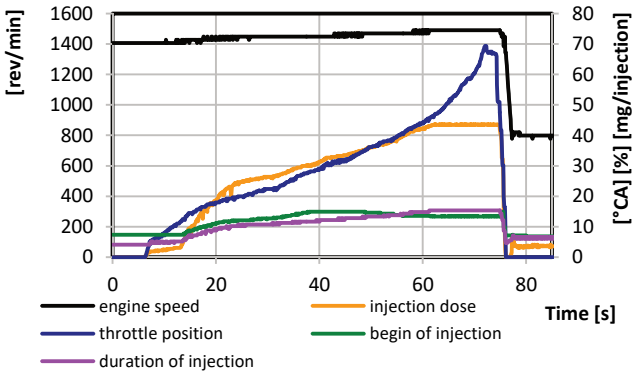


Fig. 2. Injection timing of the CI engine as a function of the engine load; engine type: Volkswagen AXD [12]

2. Piston design for the 2.0l Diesel engine with the highest specific power

All the research results presented in this article are only for the elements of the twin turbocharged 2.0l TDI BiTurbo engine from Volkswagen. With an output of 176 kW at 4,000 rpm and 500 Nm of torque from 1,750 to 2,500 rpm, it has a specific power of 88 kW/l. This means the new Volkswagen engine achieves the highest specific power of all four-cylinder series-production diesel engines. A compact charging assembly with two turbochargers enabling charge absolute pressures of up to 0.38 MPa is a characteristic aspect of this engine. A further major innovation with respect to extremely efficient combustion is the common-rail injection system with piezoelectric injectors for injection pressures of 250 MPa. The crankcase, crankshaft, conrods and pistons have been reinforced for the combustion pressure of 20 MPa. The general outline of the engine design was discussed by the manufacturer in [8], Figure 3 shows the cross section of the engine piston.

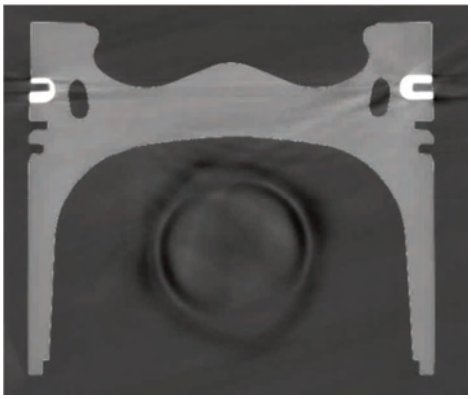


Fig. 3. Cross section of the VW TDI engine piston, with a displacement of approximately 2 dm3 and a maximum power of 176 kW, the picture obtained in a computer tomography

3. Piston assembly friction components – materials and surfaces

3.1. The piston

The crankcase of the engine is cast in GJL-250. Aluminum pistons were used in the engine (Fig. 4), on which bowl-rim remelting further increases hardness in the areas subject to highest loads [8]. As with the weaker versions of the engines, piston pins with a DLC layer are used in con-

junction with bronze sleeves embedded in the piston. There is a standard oil cooler in the piston and an insert around the upper ring (cf. Fig. 3). The lateral surfaces of the piston are covered with anti-friction lacquer, as in most modern engines. Topography of the lacquer surface is shown in Figure 5 as SEM images recorded with secondary electrons (SE) and back scattered electrons (BSE). The EDS analysis of this surface is shown in Fig. 6. Particularly the BSE image indicates that the lacquer has a composite structure with embedded particles ranging in size from a few to several micrometers.

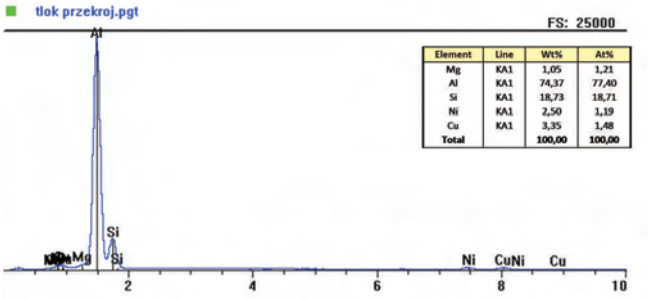


Fig. 4. EDS analysis of piston material

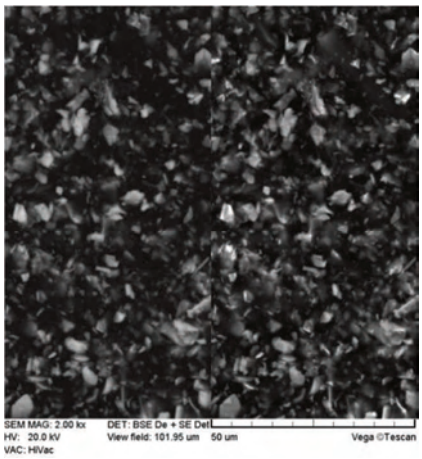


Fig. 5. Antifriction lacquer layer on the piston lateral surface in SEM image recorded by secondary electrons (left) and back scattered electrons (right); The sample was taken from a new piston that was washed with acetone in an ultrasonic bath

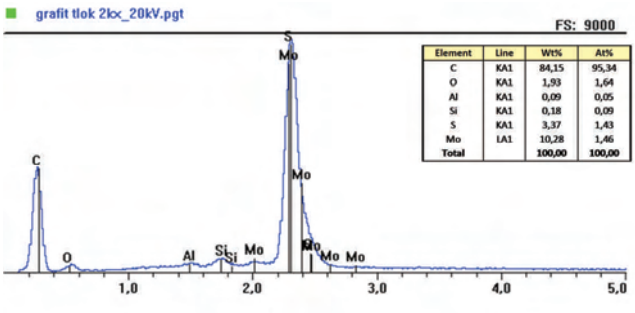


Fig. 6. EDS analysis of the sample shown in Fig. 5

3.2. Upper sealing ring

The upper sealing ring is covered with a chromium layer clearly visible on the SEM image and identified by EDS analysis (Fig. 7 and Fig. 8).

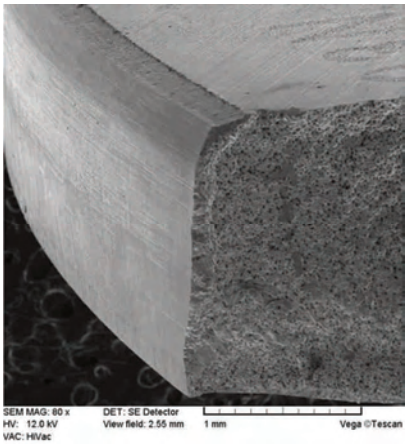


Fig. 7. Upper sealing ring cross section SEM image

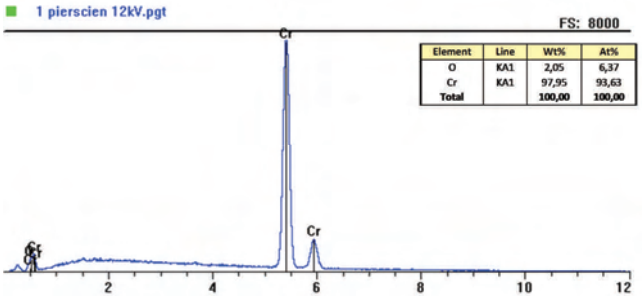


Fig. 8. EDS layer analysis on the upper sealing ring slide surface

3.3. The second piston ring

The second piston ring is shaped as a taper-faced Napier ring. The sliding surface of the ring is doped with zinc phosphate, forming characteristic structures exhibiting a certain degree of axial symmetry. Results of the tests using the electron microscope are shown in Figures 9 and 10.

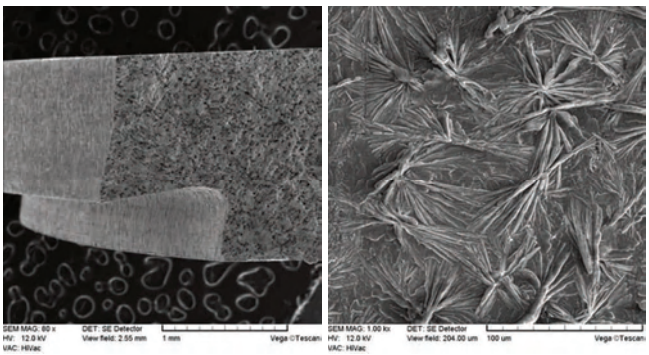


Fig. 9. Images of second ring recorded with SEM microscope; a cross-section view and a closeup on the sliding surface

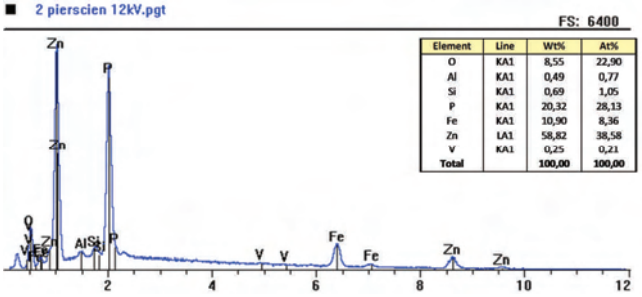


Fig. 10. EDS sliding surface analysis of the second ring

3.4. The third piston ring

The third piston ring is a double-beveled ring with spiral-type expander.

The SEM imaging results of the scraper ring are shown in Figures 11 and 12, same as previously. As in all other cases, new ring samples were used, that have never been installed in an engine; these samples were washed in acetone and sonicated.

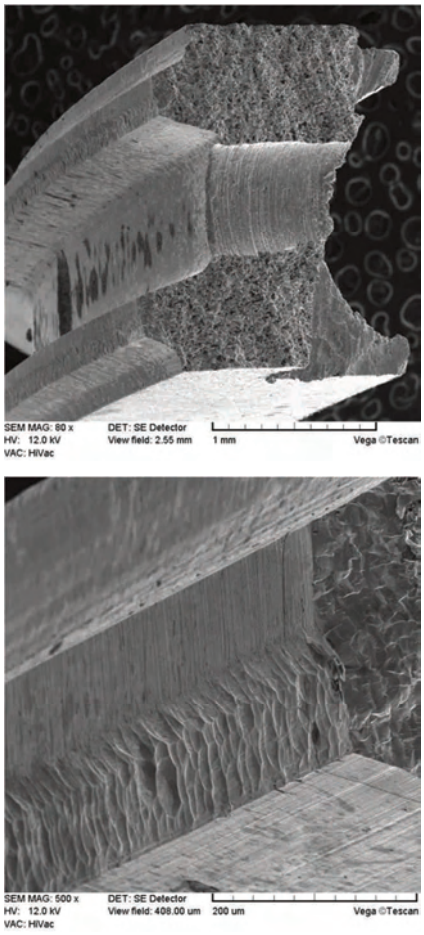


Fig. 11. The images of the third piston ring recorded with the SEM microscope; a cross-section view and a closeup on the sliding surface

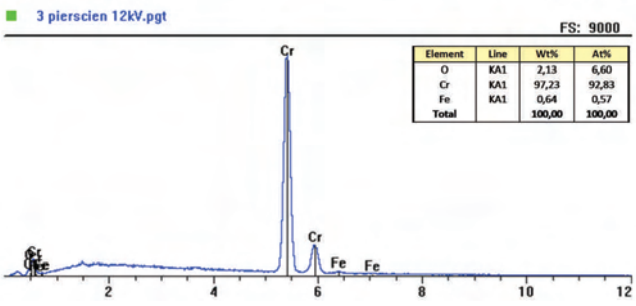


Fig. 12. EDS analysis of sliding surface of the third piston ring

4. Texturized surface – friction estimated by computer simulation

In order to investigate the use of the rings sliding surface textures for friction reduction in the main friction components of the piston engine, numerical simulations were performed using the MAHLE-VTL (Virtual Tribology Laboratory) program.

The principle of operation of the program uses a one-dimensional model of two friction surfaces, which allows to evaluate phenomena related to friction losses and oil film parameters. The program performs numerical calculations based on the classic Reynolds equation as well as the Greeenwood and Tripp equation. The mathematical model has been implemented in a program that enables numerical simulations. The simulation results include, among other things, the following parameters as a function of the crankshaft angle: minimum oil film thickness, friction coefficient and hydrodynamic pressure between the ring and the cylinder wall. Despite the constraints of a one-dimensional model, the program can be used as a virtual tool for analyzing the effects of changing ring profiles that affect mixed friction conditions [19].

Simulations were made for the spherical serial piston ring profile, then for an experimental surfaces with microgrooves providing favorable tribological properties. The inspiration for defining the shape of the microgrooves was the shape of the surface observed on the Volkswagen TDI engine piston ring, Fig. 13. (See also Fig. 11). Profiles adopted in the simulation program are shown in the Fig. 14.

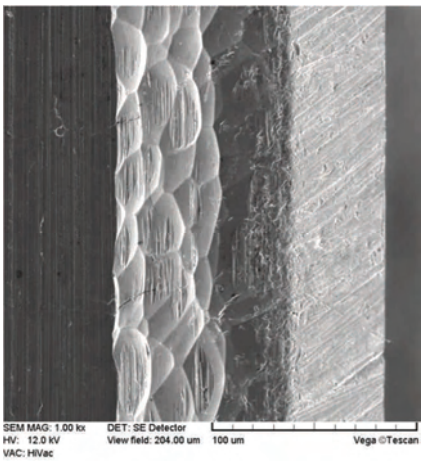


Fig. 13. Surface structure on the engine piston sealing ring of the Volkswagen TDI engine used as an inspiration for profiles adopted in numerical simulations; image recorded with SEM microscope,

Simulations were carried out for the characteristic dimensions and VW TDI engine top sealing ring operating conditions. The engine was discussed earlier in this article. To understand the effects of surface texture of the ring, the simulations were carried out for two characteristic engine operating points:

- engine idle,
- high load: (cylinder pressure 25 MPa, rotational speed 2000 rpm).

In Figures 15 and 16 the simulation results of the ring with microgrooves showed the greatest reduction in friction with respect to the serial ring.

The highest oil film capacity was obtained in the variant with the smallest microgroove width, i.e. the highest groove density (variant 2).

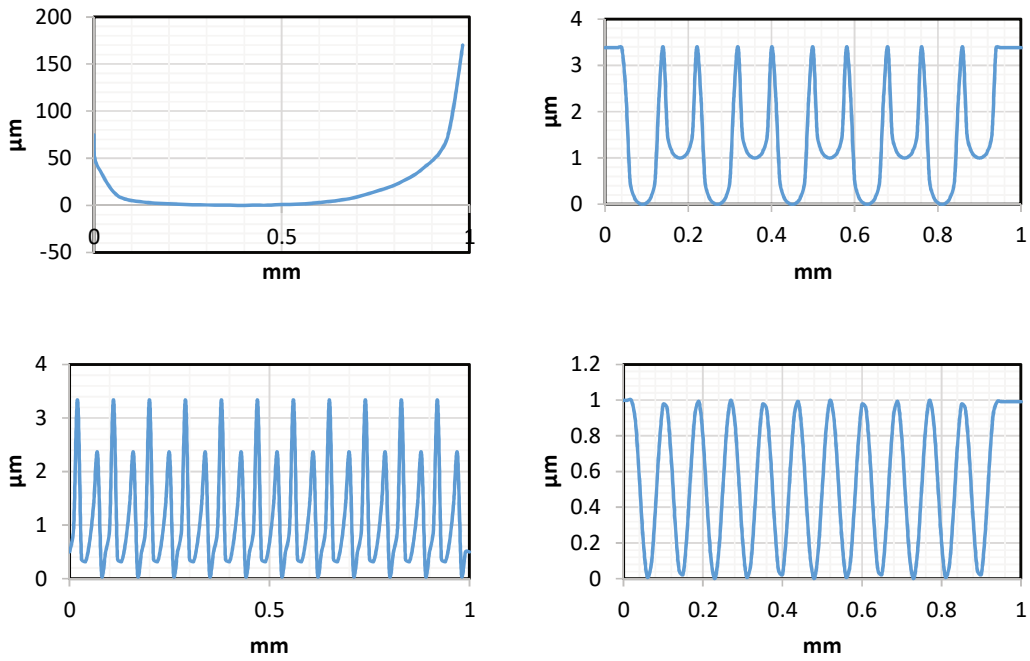


Fig. 14. Shape of sliding surface of rings adopted in the simulation program; standard ring profiles (top left – variant 1), and subsequent versions of profiles with microgrooves used in the simulations (top right – variant 2, bottom left – variant 3, bottom right – variant 4)

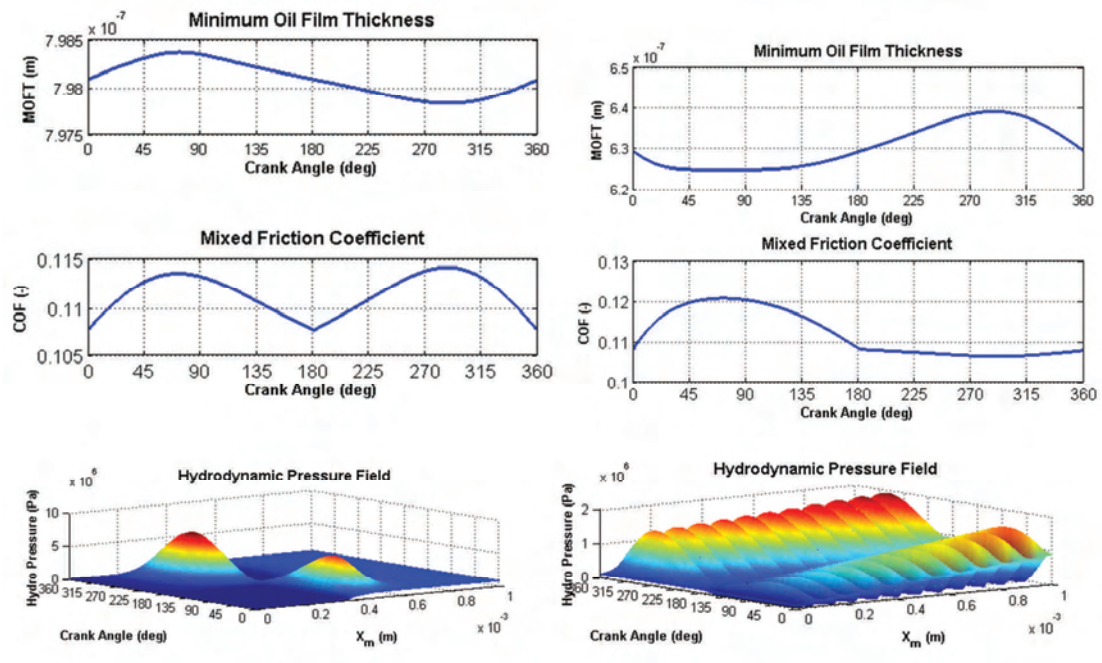


Fig. 15. Simulation results – selected engine idling parameters; serial profile ring (left), ring with added texture (right)

The existence of microgrooves results in a hydrodynamic load due to cavitation that occurs around the divergent portion of each groove. The formation of hydrodynamic pressure even in flat areas between each microgroove is particularly interesting. This effect is due to the non-zero pressure observed on each side of the groove, whereby the intermediate flat areas behave like linear pressure distribution bearings.

Applying textures on all experimental piston ring variants gave a higher hydrodynamic capacity of the oil film than the standard profile while reducing friction by about 3-4%. It is particularly important that these effects can be observed at high engine loads. The results show the need for further, extended research of the hydrodynamic effects obtained for more complex shapes of textured surfaces. In this case, however, it is necessary to use a calculation program equipped with additional functions, taking into account the effect of two dimensional flow, the effect of inertia and the effect of surface roughness on the lubricating oil flow.

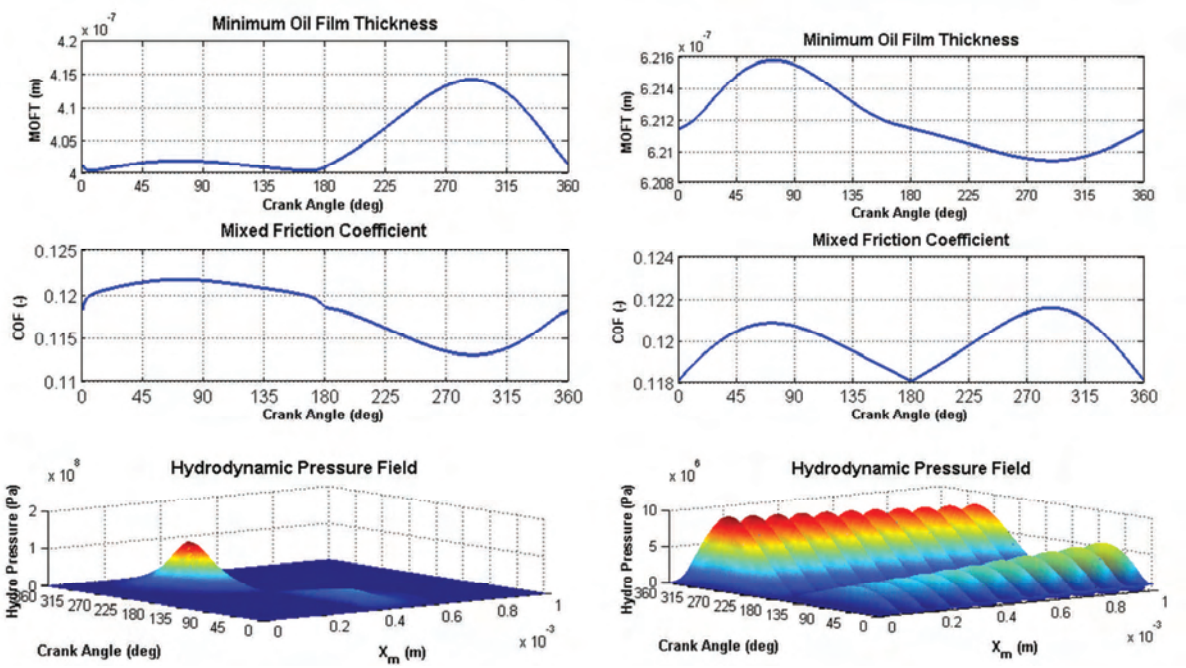


Fig. 16. Simulation results – selected maximum engine load parameters; serial profile ring (left), ring with added texture (right)

5. Summary and conclusions

1. The objective technical analysis validates the expectation that piston-type internal combustion engines will play a dominant role as a source of propulsion for cars. At the same time, potential for improving the environmental performance of subsequent generations of combustion engines is indicated. The use of new materials, in particular nanomaterials and nanotechnologies, is a particularly attractive area of improvements. Reducing the negative impact of car engines on the environment can be achieved by shifting the downsizing limits towards higher loads, while using new construction materials with properties superior to conventional materials.
2. For the future engines, it is particularly important to shape the friction layers in order to increase the thermal and mechanical loads. The coating layers on the friction surfaces of the piston assembly should effectively reduce friction, especially in the mixed friction regime.
3. The research allowed for a visualization of the different microstructures present on the piston assembly friction components surfaces of the four-cylinder CI engine with the highest power output among the mass-produced engines. The formation of such structures can be treated as a characteristic feature or even as a side effect of the applied technology of applying top layers. The authors propose a reverse approach assuming that the texture on the piston assembly friction surfaces can contribute to the reduction of engine friction losses.
4. The preliminary simulations of the piston assembly friction conditions have confirmed the validity of the accepted hypothesis. It has been shown that by replacing the smooth surface of the piston ring with a defined texture surface, a reduction in friction loss of 3–4% can be achieved.
5. The conducted computer simulations can be considered as an introduction to a broader program of finding optimal surface configurations.
6. The use of hierarchical nanostructures, described in [17, 22], can be extended to the conceptual design of the microtexture. In previous investigations, the authors have shown that the addition of carbon nanotubes dispersed in oil reduces friction losses [13]. In the context of earlier results, it may also be interesting to look for a synergistic texture effect on the nanoparticle oil lubricated sliding surfaces.

Nomenclature

DLC	diamond-like-carbon
EDS	electron dispersive spectroscopy
LCA	life cycle assessment
SEM	scanning electron microscope

Bibliography

[1] BABERG, A., FREIDHAGER, M., MERGLER, H., SCHMIDT, K. Aspekte der Kolbenmaterialwahl bei Dieselmotoren. *MTZ*. 2012, **12**.

[2] BACKHAUS, R. Kolben aus Stahl für Pkw-Dieselmotoren. *MTZ*. 2009, **12**.

[3] BLÜMM, M. et al. Innovative Schaftbeschichtungen für Otto- und Dieselmotorkolben. *MTZ*. 2016, **2**.

[4] BUSCHBECK, R. et al. Innovative Kolbensystemlösungen für Verbrennungsmotoren. *MTZ extra*.

[5] DEUSS, T., EHNIS, H., BASSET, M., BISORDI, A. Reibleistungsmessungen am Befeuerten Dieselmotor – Zyklusrelevante CO_2-Ersparnis. *MTZ*. 2011, **12**.

[6] DEUSS, T., EHNIS, H., FREIER, R., KÜNZEL, R. Reibleistungsmessungen am Befeuerten Dieselmotor – Potenziale der Kolbengruppe. *MTZ*, 2010, **5**.
[7] DEUSS, T., EHNIS, H., ROSE, R., KÜNZEL, R. Reibleistungsmessungen am Befeuerten Dieselmotor – Einfluss von Kolbenschaftbeschichtungen. *MTZ*. 2011, **4**.
[8] EICHLER F. et al. The New 2.0l 4-Cylinder BiTurbo TDI® Engine from Volkswagen. 23. Aachener Kolloquium Fahrzeug- und Motorentechnik, 23th Aachen Colloquium Automobile and Engine Technology, Aachen, DE, 6.-8. Okt, 2014.
[9] GOLLOCH, R. Downsizing bei Verbrennungsmotoren; Ein wirkungsvolles Konzept zur Kraftstoffverbrauchssenkung. *Springer-Verlag, Berlin-Heidelberg*, 2005.
[10] GROPPER, D., WANG, L., HARVEY, T.J. Hydrodynamic lubrication of textured surfaces: A review of modeling techniques and key findings. *Journal of Engineering Tribology*.
[11] KAŁUŻNY, J., MERKISZ, J., GALLAS, D. et al. An innovative system for piston engine combustion with laser-induced ignition of the hydrocarbon fuel consisting carbon nanotubes. *Combustion Engines*. 2017, **168**(1), 3-14.
[12] KAŁUŻNY, J. Eksperymentalne zastosowania nanorurek węglowych w konstrukcji tłokowego silnika spalinowego. *Wydawnictwo Politechniki Poznańskiej*. 2013.
[13] KAŁUŻNY, J., MERKISZ-GURANOWSKA, A., GIERSIG, M., KEMPA, K. Lubricating performance of carbon nanotubes in internal combustion engines – engine test results for cnt enriched oil. *IJAT*. 2017
[14] MERKISZ, J., PIELECHA, J., BIELACZYC, P., WOODBURN, J. Analysis of emission factors in RDE tests as well as in NEDC and WLTC chassis dynamometer tests. *SAE Technical Paper*. 2016, 2016-01-0980.
[15] MERKISZ, J., PIELECHA, J. Selected experiences in RDE in Polish reality for different combustion engine applications. *4rd International Conference "Real Driving Emissions"*, Berlin 25-27.10.2016.
[16] MERKISZ, J., PIELECHA, J. Selected remarks about RDE test. *Combustion Engines*. 2016, **166**(3), 54-61.
[17] NOORDUIN W.L. et al. Rationally designed complex, hierarchical microarchitectures. *Science*. 2013, **5**.
[18] OTTLICZKY, E., VOIGT, M., WEIMAR, H.J., WEISS, E. Stahlkolben für PKW-Dieselmotoren. *MTZ*. 2011, **10**.
[19] PROFITO, F.J., ZACHARIADIS, D.C., TOMANIK, E. One dimensional mixed lubrication regime model for textured piston rings. *Proceedings of COBEM*. 2011.
[20] RAMACHANDRAN, S., STIMMING, U. Well to wheel analysis of low carbon alternatives for road traffic. *Energy & Environmental Science*. 2015, **8**, 3313-3324.
[21] USMAN, A., PARK, C.W. Modeling and simulation of frictional energy loss in mixed lubrication of a textured piston compression ring during warm-up of spark ignition engine. *International Journal of Engine Research*. 2017, **18**(4), 293-307.
[22] REN, Z. et al. Hierarchically nanostructured materials for sustainable environmental applications. *Frontiers in Chemistry*. 2013, **1**(18), 1-22.

Jarosław Kałużny, DSc., DEng. – Faculty of Machines and Transport at Poznan University of Technology.

e-mail: *Jaroslaw.Kaluzny@put.poznan.pl*



Prof. Jerzy Merkisz, DSc., DEng. – Faculty of Mechanical Engineering at University of Technology.

e-mail: *Jerzy.Merkisz@put.poznan.pl*



Aleksander Stepanenko, MEng. – Faculty of Machines and Transport at Poznan University of Technology.

e-mail: *Stepanenko@wp.pl.*



Emil Wróblewski, MEng. – Faculty of Machines and Transport at Poznan University of Technology.

e-mail: *Emil.Z.Wroblewski@doctorate.put.poznan.pl*



Bartosz Gapiński, DEng. – Faculty of Mechanical Engineering and Management at Poznan University of Technology.

e-mail: *Bartosz.Gapinski@put.poznan.pl*



Adam Piasecki, DEng. – Faculty of Mechanical Engineering and Management at Poznan University of Technology.

e-mail: *Adam.Piasecki@put.poznan.pl*



Dawid Gallas, MSc. – Faculty of Machines and Transport at Poznan University of Technology.

e-mail: *Dawid.P.Gallas@doctorate.put.poznan.pl*



Article citation info:
CHŁOPEK, Z., SAMSON-BRĘK, I. Analysis of the ecological effects of biogas use of to supply the internal combustion engine in the electricity generation process – result of LCA analysis. *Combustion Engines*. 2017, **171**(4), 134-139. DOI: 10.19206/CE-2017-422

Zdzisław CHŁOPEK
Izabela SAMSON-BRĘK

CE-2017-422

Ecological effects of use biogas to supply the internal combustion engine in the electricity generation process – results of LCA analysis

Environmental life cycle assessment (LCA) in Poland is still a relatively new method of estimating the environmental impact of production processes. It enables the assessment of the environmental risks associated with the product system or activity, either through the identification and quantification of materials and energy used and waste introduced into the environment, as well as assess their impact on the environment. LCA method application also enables the calculation of greenhouse gas emissions in accordance with Directive 2009/28/EC on the promotion of energy from renewable sources.

This paper presents the results of the simplified life cycle analysis of electricity production process from agricultural biogas used as an engine fuel. LCA analysis was conducted based on data from one of the national biogas plants. The selection criterion was based on the availability of substrates (maize silage, distillery slop and sugar beet pulp) and the possibility of obtaining high quality data for analysis (actual data based on the existing biogas plant). In addition, the environmental impact of the biogas power generation technology obtained through the methane fermentation process only of waste materials (distillery slop, sugar beet pulp) and co-processing of waste and maize silage was compared.

Key words: *LCA*, *biogas, waste, combustion, electricity production*

1. Why LCA?

One of the most popular definitions of LCA available in the literature is the definition proposed by Fava et al. According to this author environmental Life Cycle Assessment (LCA) is a technique designed to assess the environmental risks associated with the product system or activity, either by identifying and quantifying energy and materials used and wastes introduced into the environment, as well as the impact of those materials, energy and waste on the environment. The assessment relates to the whole life cycle of the product or the activity from the mining and mineral processing, product manufacturing process, distribution, use, re-use, maintenance, recycling up to the final use and transportation. LCA directs the study of environmental impact of the product system to the area of the ecosystem, human health and resources used [1–6].

The main advantage of this method is its complexity. It covers the whole life cycle of a product ("*cradle to grave*"). [6]. Depending on the level of detail of the analysis, it is possible to link all individual processes and estimate their impact on the environment. The method enable also for quantitative identification of all materials and energy consumed to produce the product, as well as particulate and gaseous emissions, noise and radiation emissions and waste generation, allowing efficient management of the production process and reducing economic and environmental costs. By using life cycle assessment it is possible to identify those processes, which generate the greatest environmental burden and their modification to reduce those burdens. The LCA also allows for economic costs reduction by optimizing LCC (*Life Cycle Cost*) [7–9]. Thanks to such a comprehensive and systematic approach to production processes, LCA has become such a popular and widely used management technique.

One of the most important advantage of LCA is it's versatility. LCA has been widely used in research for years, but an increasing role is also being played in industrial analysis.

2. The aim and scope of the analysis

This paper presents the results of the environmental life cycle analysis of electricity production from agricultural biogas used as an engine fuel. The biogas is obtain through WtE (*waste-to-energy*) processes. For the LCA analysis has been selected one of the existing national plant. In this biogas plant electricity and heat are produces in cogeneration. As a substrate for biogas production are use corn silage and wastes from food industry (distillery slop, sugar beet pulp). Additionally, a comparison of the environmental impact of electricity production from biogas produced through anaerobic digestion only waste materials (distillery slop, sugar beet pulp) and co-digestion of waste materials and silage corn was performed.

In the frame of analysis were identified two main stage:

- raw material stage – corn cultivation for silage production;
- technological stage taking into account all processes take place in biogas plant.

2.1. Feedstock procurement

For raw material stage LCA analysis was covered by the corn cultivation (the establishment of plantation, fertilization, plant protection and harvest), and the process of corn ensiling in order to creation of corn silage (Fig. 1). So prepared corn is a proper feedstock for biogas plant. In addition to the raw material stage transport of corn silage to biogas plant was also included. Other substrates, such as distillery slop or sugar beet pulp is treated as waste in other manufacturing processes, and therefore (according to the methodology), it is assumed that their production is not an additional burden on the environment.

In the case of dedicated crops it is necessary to incur adequate material and energy expenditure. At the stage of maize cultivation, the following sub-stages were included in the calculations: treatments related to establishment of plantation, fertilization, plant protection and harvesting, as well as transport of maize to biogas and silage preparation.

All treatments and their unit processes are within the scope of the LCA analysis system.

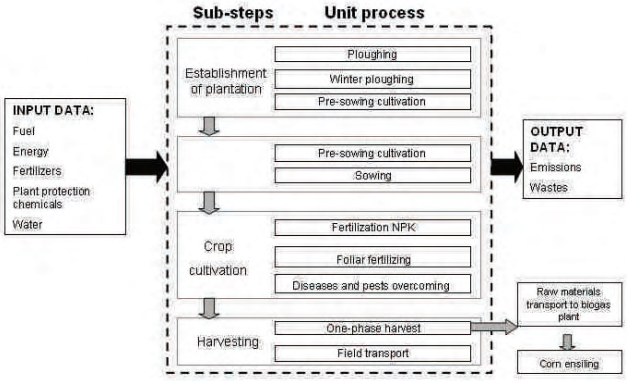


Fig. 1. The general scheme taking into account the system boundaries and functional unit of corn cultivation process and the silage formation

In the case of dedicated crops, the use of fertilizers and plant protection products is very important, as well as the inclusion in the system boundaries their production as extremely energy-consuming and causing high emissions.

Transport of maize to biogas plant is linked to fuel consumption in the form of diesel fuel.

In addition to the above-mentioned unit processes within the system boundaries was include the production of fertilizers and fuel (ON) used in field operations because on their significant impact of these components on the outcome of the environmental analysis and associated greenhouse gas emissions.

Outside the system borders were processes such as the production of plant protection products, the manufacture of agricultural machinery and the transport of seeds to the field.

Production of plant protection products, although it may affect the to the final result of the analysis, was not included in the system boundaries because of the lack of input data. The production of agricultural machinery has been excluded from the system boundaries as recommended in Annex V of 2009/28 / EC Directive, which contains guidelines for calculating the impact of biofuels, bioliquids and their fossil fuels equivalent on greenhouse gas emissions. In addition, it was considered that the determination of the assumptions underlying the magnitude of the impact of the mentioned processes was associated with too high recurrence.

For the raw material stage, a functional unit in the form of 1 Mg maize silage (1 Mg silage) was adopted.

2.2. Technological stage

In the case of technological step scope of the analysis included the technology of electricity production from biogas used as an engine fuel. This stage consists of the following sub-stages (Fig. 2):

1. Transport of raw materials for biogas plant and their storage.
2. Raw materials preparation (corn ensiling, grinding, maceration, mixing).
3. Loading of raw materials for digester.
4. Methane fermentation (hydrolysis, acetogenesis, octanogenesis, methanogenesis).
5. Storage of biogas.
6. Biogas purification.
7. Electricity and heat production.
8. Storage of digestate.
9. Management of digestate.

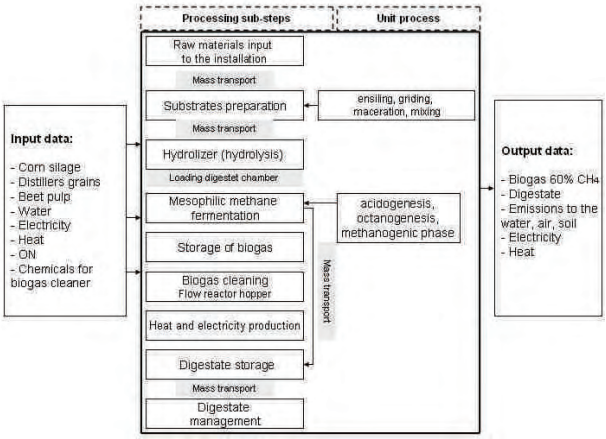


Fig. 2. The general scheme of biogas and electricity production

For technology stage in the scope of analysis was include also transport of slop grains from Krasnystaw distillery at the distance of 98 km (both 196 km in total) and sugar beet pulp from the sugar factory in Suchowola at a distance of 19.2 km (38.4 km).

Outside the system boundaries were treatments related to the application of digestive sludge in the field. At the same time, in the analysis was included so called avoided emissions associated with the production of mineral fertilizers, which are substitutes for biogas digesters.

For the technological stage, 1 MWh of electricity generated from biogas was used as a functional unit.

3. Method of environmental life cycle assessment

The SimaPro software, one of the widely used and common tools to perform the LCA analysis, developed by the Dutch company Pré Consultants was used in the research [10].

In SimaPro programme several methods, to assess the product life cycle impact, is available. They differ significantly, so it is necessary to determine the priorities of the LCA analysis. When choosing a method for performing the life cycle impact assessment (LCIA) as well as the impact categories, it is essential to take into consideration the goal and scope of the analysis [5]. Aspects that should be taken into consideration when choosing the appropriate method are as follows: the way of presentation of the final results, a method of weighting, timeframe outlined, geographical coverage, the degree of accuracy and impact categories considered.

Consequently, after analyzing the methods available in the SimaPro program, the Eco-Indicator 99 (e-indicator method) was considered the most appropriate. This method is aimed at assessing damage both to the environment as

well as to the human This method gives three endpoints defined as ecological impact results (Table 1) [10, 11]:

- human health expressed in DALY unit (*Disability Adjusted Life Years*) used by the WHO and the World Bank in health statistics;
- ecosystem quality (in categories: acidification, eutrophication and land use) – the value of the damage is given in PDF unit (*Potentially Dissapeard Fraction*); for ecotoxicity damage is expressed in PAF × m^2 × year unit, showing the percentage of species living in the environment under the toxic stress);
- depletion of natural resources (unit: MJ/t).

Each of the endpoints contains the corresponding categories of impact assigned to it. Those particularly important in the life cycle assessment of the electricity production from agriculture biogas are given in bold in Table 1.

Table 1. Endpoints and assigned them impact categories and indicators in Eco-Indicator 99 method [10]

Endpoints	Impact categories	Indicator
HUMAN HEALTH	**Climate change, ozone layer depletion**, carcinogens, respiratory organics and inorganics, radiation	DALY
BIODIVERSITY	**Acidification, eutrophisation, land use**, ecotoxitity	PDF (eutrophisation, acidification and land use) PAF × m^2 × year (ecotoxitity)
RESOURCE AVAILABILITY	**Reducing the amount of minerals and fossil fuels**	MJ/t

3.1. Environmental impact categories of

In the Eco-Indicator 99 method in the SimaPro program are available a lot of impact categories (Table 2) [10]. To show the impact of maize cultivation and the production of electricity from biogas on the environment, it is necessary to select some of the most important impact category, from taking into account the purpose of analysis. The following influence categories were selected:

- climate change,
- ozone layer depletion,
- eutrophisation/acidification,
- land use,
- reducing the amount of minerals and fossil fuels.

Table 2. The impact categories in the Eco-Indicator 99 method [10]

Impact category	Inputs and outputs (LCI)
climate change	carbon dioxide (CO_2), nitrogen dioxide (NO_2), mathane (CH_4), chlorofluorocarbon (CFC), hydrochlorofluorocarbon (HCFC)
ozone layer depletion	chlorofluorocarbon (CFC), hydrochlorofluorocarbon (HCFC), halons
acidification	Sulfur oxides (SO_x), nitrogen oxides (NO_x), ammonia (NH_4)
eutrophication	nitrogen oxides (NO_x), ammonia (NH_4), phosphate (PO_4), nitrates
fossil fuel depletion	the amount of fossil fuels and minerals used
land use	area of the land used for crops as well as its transformation and degree of transformation

Climate change. This impact category is characterized by an index defined by the sum of the greenhouse effect values for the substance over the years, including the pollutant (in kg). This indicator is therefore a development of the popular Global Warming Potential indicator(GWP). This indicates strong, and sometimes direct, connection to the amount of greenhouse gases emitted to the atmosphere, mainly CO_2 and CH_4.

The indicators for the global warming group are carbon dioxide (CO_2), nitrogen dioxide (NO_2), methane (CH_4), chlorofluorocarbons (CFC), hydrochlorofluorocarbons (HCFC), and methyl bromide (CH3Br). Each of the indiindicators is transformed into Eco-Indicator 99 to a characterization factor, which is equivalent to carbon dioxide (CO_2) [5, 10].

The ozone layer depletion is described as a indicator defined as the equivalent of the potential reduction of the ozone layer in the case of the disintegrated substance, together with the amount of pollution it cause (its quantity in kg). This indicator also define as indicator of stratospheric ozone depletion. Stratospheric ozone is a direct "barrier" to ultraviolet radiation reaching the surface of the Earth. Increasing the intensity of ultraviolet radiation cause harmful effects on humans, animals and plants. The emission of greenhouse gases by industry and agriculture is very significant for the reduction of the ozone layer. Energy-intensive technologies in agriculture and the frequent use of plant growth substances contribute to the depletion of the ozone layer in the final analysis. The effects of depletion of the ozone layer affect entire aquatic and terrestrial ecosystems, biochemical cycles, and indirectly on crop growth and productivity decline.

Ozone-depleting indicators are chlorofluorocarbons (CFCs), hydrochlorofluorocarbons (HCFCs), halons and methyl bromide (CH_3Br). Each of the above ratios is converted into a characterization factor, the equivalent of trichlorofluoromethane (CFC-11).

Eutrophication is the process of enriching natural water body into nutrients (nutrients, biogens) resulting in trophic growth or water fertility. This process also applies to natural watercourses. The main cause of eutrophication is the increasing load of biogenic elements, primarily nitrogen and phosphorus. Large amounts of phosphorus are associated with intensification of fertilization and increased erosion in the catchments. The increase in nitrogen supply is connected whereas with the increasing emission of nitrogen oxides into the atmosphere and thus their high content in atmospheric precipitation. Fertilizing the soil under cultivation also contributes to the growth of the nitrogen load. Heavy rainfall can easily wash out nitrogen from the surface layer of the soil and from fertilizers, while large amounts of phosphorus can also be brought into the tank. The main source of these compounds in the environment are fertilizers used in agriculture [5]. Considering the impact of production lines on eutrophication is therefore justified because of the use of energy crops.

Acidification is a phenomenon caused by excessive emissions of sulfur dioxide (SO_2), nitrogen oxides (NO_x) and ammonia (NH_3). Due to the fact that the combustion of fossil fuels contributes to high emissions especially of sul-

fur compounds, it is proposed to include the acidification category in environmental analysis. In addition, the use of fertilizers in agriculture is associated with NH_3 emissions. The excess of acidic compounds has a negative effect, among others. For surface and ground waters, soil, flora and fauna [12].

Reduce mineral resources and reduce fossil fuel resources. The natural resource reduction index is considered in the LCA method both globally and regionally and locally.

The use of land should be understood both to occupy land for crops and to transpose it from one type of use to another. The increase in the number of people contributing to the increase in the demand for food brings with it the inevitable need for the development of agriculture and the extractive industries in order to meet the needs of food and energy. It involves a great deal of the necessity of managing the ever larger area of the earth and its continuous transformation. The characterization index for the land use category is the development and degree of land conversion expressed in m^2.

4. Results

The results of the LCA analysis concern the environmental impact of the impact categories identified in the LCA analysis of the Eco-Indicator 99 method. They are presented in two variants: characterization and normalization. For a fuller picture of the results obtained, Sankey's graphs of material and energy flow for the biogas power generation process from different substrates are also included. Results are expressed in units assigned to each impact category. On the basis of these values it is possible to determine whether the advantage of the process of generating electricity from biogas derived from waste materials over the process of generating electricity from biogas obtained from maize silage expressed in much lower values of environmental indicators is unequivocal at the level of particular categories influence. Due to the fact that the categories are expressed in different units, they can not be compared to each other. The results below are expressed as a percentage of the highest result in a given benchmark category and are considered as a 100%.

In the Figure 3 we can see results of comparison life cycle assessment of 1 MWh of electricity production from biogas obtain from corn silage, distillery slop and sugar beet pulp as well as pig manure distillery slop and sugar beet pulp for each impact category in EI-99 method.

As the following figure shows the categories that have the greatest negative impact on the environment is climate change and land use. This result is related to the necessity of intending land for corn cultivation and the use of mineral fertilizers and plant protection products, which production and application of the plantation is energy-intensive and results in significant emissions of particulate matter and gases into the air. For result of the analysis significant influence has also the fuel combustion, mainly diesel fuel, during field work and raw material transport to the biogas plant. In the case of other impact categories, both for electricity from biogas produced from waste materials, such as corn silage the results are positive, which is connected with taking into account in the analysis so-called avoided production of ammonium nitrate, thanks to use post-fermentation digestate as fertilizer, and the replacement of heat from coal, through the use of waste heat producing in a biogas plant.

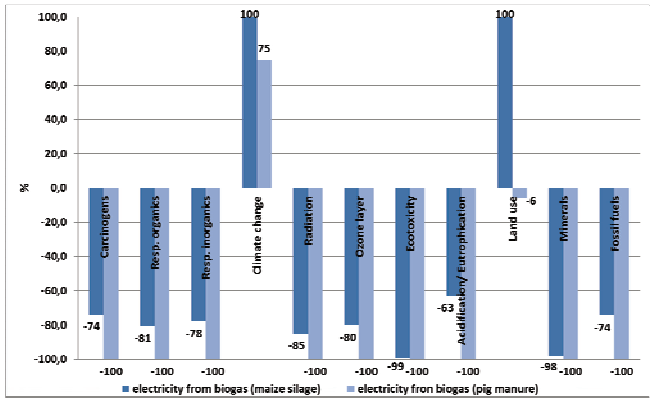


Fig. 3. Results of comparison life cycle assessment of 1 MWh of electricity production from biogas obtain from corn silage, distillery slop and sugar beet pulp ale well as pig manure distillery slop and sugar beet pulp for each impact category in EI-99 method (characterization)

In the climate change category the result is related to the use of diesel fuel to power agricultural machinery at different stages of corn cultivation for silage, starting from field work to prepare the land for cultivation, by planting, treatments associated with fertilization and application of plant protection products, harvesting, as well as raw materials transport (with fields, from sugar refinery and distilleries) to the plant. In this category is also very important production and use of mineral fertilizers and plant protection products.

In the land use category the result is significantly higher for electricity produced from biogas produced from corn silage. It is associated with the necessity of intending land for corn cultivation.

In addition, the previously mentioned impact categories, such as ozone layer depletion, eutrophication/acidification and depletion of minerals and fossil fuel resources should be also taking into account.

Ozone layer depletion category is closely related to greenhouse gas emissions arising from the combustion of diesel fuel during field work and raw material transport to the biogas plant, as well as extremely energy-intensive manufacturing of fertilizers and plant protection products, and their use in the field.

For the eutrophication / acidification impact category and the reduction of mineral resources the greatest impact has production and use of mineral fertilizers and plant protection products, which application is required during corn cultivation. Part of the dose of fertilizers and plant protection products is not absorbed by the plants and gets into the groundwater or is leached from the soil by rainfall and runoff goes into rivers, lakes and seas.

The assumptions show that category, which has a significant impact on the environment is a “reduction of fossil fuels”. It is connected witch the use of diesel fuel to power agricultural machinery at different stages of corn cultivation for silage and its transport to the biogas plant at a distance of 12 km in both directions. Founded transport distance for distillery slop and sugar beet pulp is significant and

amounts to 196 and 38.4 km in both directions. In order to use of diesel fuel it is necessity of obtaining fossil fuels needed to produce the fuel. Taking into account the aggregate fuel consumption during field work and transport of corn silage to biogas plant and comparing them with the fuel consumption during transportation of sugar beet pulp and distillery slop, we obtain the value of the index for the category at a similar level.

Sankey graph (Fig. 4) generated based on material and energy balance of the electricity production process from biogas produced from corn silage, distillery slop and sugar beet pulp shows the percentage of individual processes and emissions in overall effect associated with the environmental impact of mentioned process. As the following graph shows the greatest impact on the environment have material and energy inputs and emissions from the cultivation of maize for silage and its transport from the field to the biogas plant (it is 55.5% of the total environmental impact of electricity production from biogas). The graph also shows that the positive environmental impact is associated with the consideration in the analysis of avoided production of ammonium nitrate and heat from coal.

Sankey graph is presented with regard to the processes / factors which impact is not less than 9% (cut-off 9%).

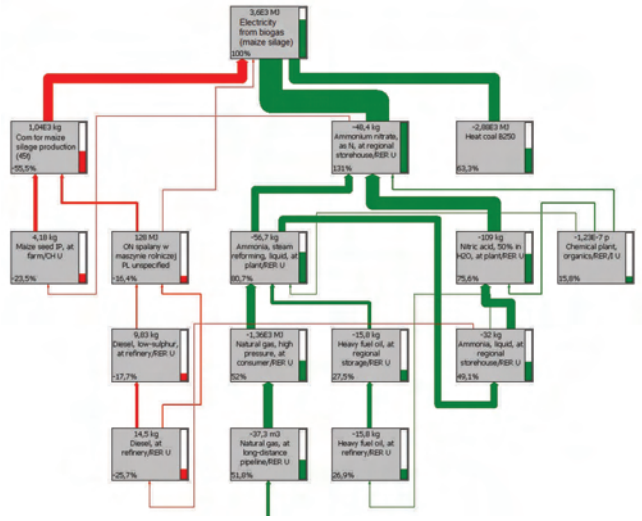


Fig. 4. Sankey graph for 1 MWh of electricity production from biogas obtain from corn silage, distillery slop and sugar beet pulp (material-energy balance fragment)

From the Sankey graph (Fig. 5), for the process of electricity production from biogas used as an engine fuel, where maize silage was replaced with pig slurry, it is clear that the most significant environmental impacts are material and energy inputs and emissions associated with the burning of diesel during transport of sugar beet pulp to the biogas plant (it is 7.58% of the total environmental impact of the biogas power generation process). This graph also shows that the positive impact on the environment associated with avoiding the ammonium nitrate production and the avoidance of heat generation from hard coal.

Sankey graph is presented with regard to the processes / factors which impact is not less than 5% (cut-off 5%).

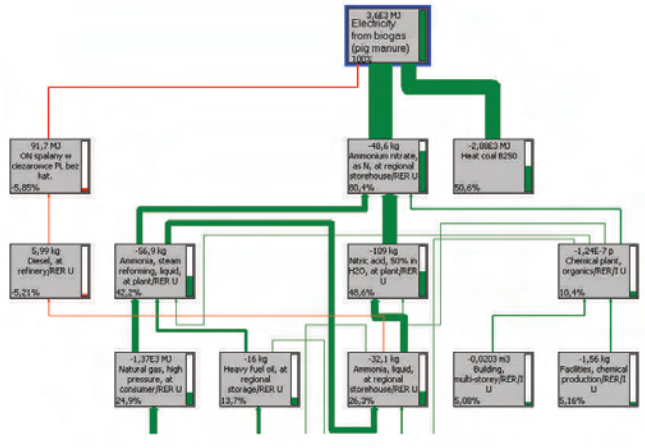


Fig. 5. Sankeya graph for 1 MWh of electricity production biogas obtain from pig slurry, distillery slop and sugar beet pulp ((material-energy balance fragment)

Figure 6 presents LCA results for endpoints within the used Eco-Indicator 99 method, such as human health, ecosystem quality and reduced natural resources. The obtained values of the ecoindicator [Pkt] are expressed in the general unit – the points determining the size of the impact on the environment. Changing the results expressed in different units [DALY, PDF, PAF or MJ] is done after the normalization process [4].

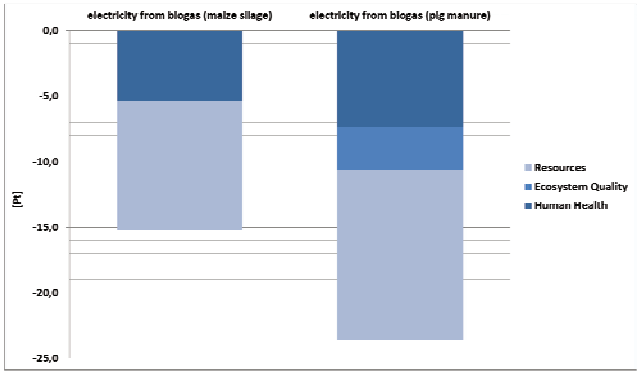


Fig. 6. Results of a comparative analysis of a 1 MWh of electricity production from biogas obtain from corn silage, distillery slop and sugar beet pulp as well as from pig slurry, distillery slop and sugar pulp for individual EI – 99 impact categories (normalization)

As is evident from the graph below, the environmental impact of individual endpoints, especially human health and resources, is positive for both type of biogas (from corn and from wastes). This result is conditioned by taking into account in the analysis of the avoided production of ammonium nitrate and heat from hard coal using the digestate sludge as a fertilizer and the management of waste heat.

5. Conclusions

In this publication the results of simplified life cycle assessment analysis for electricity production from agricultural biogas obtain through WtE processes was presented. The main stages and unit processes of the technology were also defined, as well as system boundaries, material and energy inputs and emissions to water, soil and air.

The results show that the greatest impact on the environment have two unit processes connected with the cultivation of corn for ensiling purposes. This result is related to the necessity of intending land for corn cultivation and the use of mineral fertilizers and plant protection products, which production and application of the plantation is energy-intensive and results in significant emissions of particulate matter and gases into the air. For result of the analysis significant influence has also the fuel combustion, mainly diesel fuel, during field work and raw material transport to the biogas plant.

It is also worth to underline that the positive impact on the environment of electricity producing process from biogas obtained from both type of substrate is determined by taking into account on the analysis the avoided production of ammonium nitrate and heat from hard coal thanks to Use of post-fermentation sludge as a fertilizer and management of waste heat generated in biogas plants. It shows how important it is from an environmental point of view to manage all possible waste and by-products generated during this process. It also draws attention to waste as a valuable source of energy and recyclable substrates, which in relation to sustainable development is particularly important, because it combines all the key elements of the sustainable development concept.

Nomenclature

LCC	life cycle cost
LCIA	life cycle inventory analysis
WtE	waste to energy
DALY	disability adjusted life years
PDF	potentially dissapeard fraction
ODP	ozone layer depletion
GWP	global warming potential
ON	diesel fuel
CO_2	carbon dioxide
NO_x	nitrogen oxides
NO_2	nitrogen dioxide
SO_2	sulphur dioxide
CH_4	methane
CFC	chlorofluorocarbon)
HCFC	hydrocholorofluorocarbon
CH_3Br	methyl bromide
NH_3	ammonia

Bibliography

[1] SAMSON-BRĘK, I. Zastosowanie metody oceny cyklu życia LCA do oszacowania wpływu na środowisko wytwarzania paliwa biogazowego do silników spalinowych. *Archiwum Motoryzacji*. 2011, **2**(53), 69-79.

[2] BIERNAT, K., GIS, W., SAMSON-BRĘK, I. Application of the life cycle assessment (LCA) method to the estimation of environmental impact of the engine biofuels generation for example of biogas fuel. *Combustion Engines*. 2012, **148**(1), 25-32.

[3] GÓRZYŃSKI, J. Podstawy analizy środowiskowej wyborów i obiektów. *Wydawnictwa Naukowo-Techniczne*. Warszawa 2007.

[4] LEWANDOWSKA, A. Środowiskowa Ocena Cyklu Życia Produktu na przykładzie wybranych typów pomp przemysłowych. *Wydawnictwo Akademii Ekonomicznej*. Poznań 2006.

[5] GÓRALCZYK, M., KOWALSKI, Z., KULCZYCKA, J. Ekologiczna ocena cyklu istnienia procesów wytwórczych (LCA). *Wydawnictwo Naukowe PWN*. Warszawa 2007.

[6] FAVA, J. A technical framework for life-cycle assessment. In: SETAC and SETAC Foundation for Environmental Education, Washington1991.

[7] SZKODA, M. Analiza kosztu cyklu trwałości (LCC) w ocenie efektywności środków transportu szynowego. *Logistyka*. 2011, **3**.

[8] PN-EN 60300-3-3:2006 – Zarządzanie niezawodnością – Część 3-3: Przewodnik zastosowań – Szacowanie kosztu cyklu życia.

[9] Life cycle cost handbook – guidance for life cycle cost estimation and analysis, office of acquisition and project management. *U.S. Department of Energy*. Washington, 2014.

[10] GOEDKOP, M., SPRIENSMA, R. The eco-indicator 99. A damage oriented method for life cycle assessment. Methodology report, *PRé Consultants B.V*. Netherlands 2000.

[11] LINDFORS, L.G. Nordic guidelines on life-cycle assessment. *Nordic Council of Minister*. Copenhagen 1995.

[12] SENSI, A. Eurostat, agriculture and acidification. *European Commission*. ec.europa.eu/agriculture/envir/report/en/acid_en/report.htm#Foot3a.

Prof. Zdzisław Chłopek, DSc., DEng. – Faculty of Automotive and Construction Machinery Engineering at Warsaw University of Technology.

e-mail: *Z.Chlopek@pimot.eu*



Izabela Samson-Bręk, MSc. – Department of Liquids Fuels and Bioeconomy in Automotive Industry Institute in Warsaw.

e-mail: *I.Samson@pimot.eu*



Article citation info:
FABER, J., BRODZIK, K. Elemental analysis as an important tool for fuels and biofuels quality control. *Combustion Engines*. 2017, **171**(4), 140-144. DOI: 10.19206/CE-2017-423

Joanna FABER
Krzysztof BRODZIK

CE-2017-423

Elemental analysis as an important tool for fuels and biofuels quality control

Article presents normalized analytical methods for determination of elements in fuels and biofuels with emphasis on inductively coupled plasma emission spectrometry (ICP-OES) and their advantages and disadvantages. Analytical procedure applied for determination of 20 elements (Al, B, Ba, Ca, Cr, Cu, Fe, K, Mg, Mn, Mo, Na, Ni, P, Pb, Si, Sn, Ti, V and Zn) is described with elements of validation. Broad range of elemental analysis results of fuels (B0, B7 and B10) and pure FAME samples are described. Typical contents of selected elements are presented which allows discussion on the domestic fuel quality in regard to non-standardized parameters and their potential effect on combustion engines performance.

Key words: *fuels, biofuels, FAME, elemental composition, ICP-OES*

1. Introduction

Analysis of liquid petroleum products characteristics is a challenge for every chemist due to variety of these products (petroleum, diesel fuel, biofuels, engine oils, gear oils, hydraulic oils, coolants etc.). Conclusion regarding these products quality are usually based on numerous laboratory analyses.

In order to determine diesel fuel quality analyses are required such as cetane number and cetane index, distillation characteristics, density, viscosity, fatty acid methyl esters (FAME) content, water content, polycyclic aromatic hydrocarbons content, flash point, carbon residue, total contamination, copper strip corrosion, oxidation stability, lubricity and climate dependent cold filter plugging point and cloud point. Within the analyzed range of properties are also concentration of manganese and sulfur which content is checked and verified against EN 590 standard's requirements, as the only elements in diesel fuel which concentration need to be indicated directly [1]. In case of petrol concentration of three elements need to be verified against EN 228 [2] requirements namely: lead, sulfur and manganese. Other parameters which has to be checked to control fuel quality are: distillation characteristics, vapour pressure, density, research and motor octane number, oxidation stability, existent gum content, copper strip corrosion, aromatics and olefins hydrocarbons content, oxygen and oxygenates content and benzene content. More detailed elements analysis is required in case of fatty acids methyl esters [3], in which sulfur, phosphorus, sodium, potassium, calcium and magnesium concentrations need to be checked in order to verify this component quality. In fact, normative requirements regarding these elements concentration are only ones allowing estimation of some guideline values for discussion on elemental concentration in regular fuels. These should be free from any adulterant or contaminant that may render the fuel unacceptable for use in engine vehicles as it is described in both EN 228 and EN 590 standards [1, 2].

Determination of concentration of wide variety of elements requires proper sample preparation before measurement, as well as application of suitable measurement technique which would allow reaching very low limits of determination (LOD) leading to precise and repeatable results despite the demanding organic matrix.

This paper discusses trace elements analysis in liquid fuels: diesel and biodiesel fuels. In BOSMAL Automotive Research and Development Institute Ltd fuel quality check includes routine determination of 20 elements (Al, B, Ba, Ca, Cr, Cu, Fe, K, Mg, Mn, Mo, Na, Ni, P, Pb, Si, Sn, Ti, V and Zn) concentration in case of diesel and biodiesel. In case of fuels without biocomponents concentration of these elements are usually below 1 mg/kg.

2. Elemental analysis of fuels and biofuels

2.1. Legal requirements

As it was mentioned above, only limited number of elements is an object of normative regulation. In case of sulfur and manganese 10 and 2 mg/kg, respectively, is upper allowed concentration in petrol and diesel, and additionaly in case of petrol lead content is limited to max 5 mg/kg. In case of FAME used as a 100 % biofuel or blending component in diesel fuel, six elements content is limited namely: sulfur (max 10 mg/kg), phosphorous (max 4 mg/kg), summary content of sodium and potassium content limited to max 5 mg/kg, exactly the same as summary content of calcium and magnesium. On the other hand sodium, zinc and silicon content above 2 mg/kg may have negative impact on injectors performance of modern diesel engines, furthermore increased concentration of some elements may result in engine components corrosion and formation of deposits at elevated temperatures [4, 5]. Taking into account these negative aspects of trace elements presence, their concentrations in fuels should be monitored, especially during the demanding process of engine testing.

2.2. Methods of trace elements determination

Trace elements concentration is usually measured by spectroscopic methods, mainly inductively coupled plasma optical/atomic emission spectrometry (ICP-OES, ICP-AES) and wavelength or energy dispersive X-ray fluorescence (WD-XRF, ED-XRF). Comparison of standardized methods with description of sample preparation, measurement parameters for different petroleum products and concentration ranges is presented in Table 1 and 2.

Table 1. List of standardized ICP-OES/AES measurement methods for determination of elements in fuels, biofuels and biocomponents

Sample type	Sample preparation	Analyzed elements	Measurement range [mg/kg]*	Bibl.
Inductively coupled plasma optical emission spectrometry ICP-OES				
Ethanol	Direct measurement	P Cu S	0.13–1.90 0.050–0.300 2–15	[6]
FAME	Dilution with naphtha (mas. 1:2)	Ca, K, Mg, Na	1–10	[7]
Unleaded petrol	Dilution 20x with naphtha	Mn	2–8 [mg/l]	[8]
FAME	Dilution 4x with naphtha, IS: Co, Sc, Y	P	2.5–8.0	[9]
Diesel (up to 30%vol. of FAME)	Dilution with kerosene (mas. 1:1) IS: Co, Sc,Y	Na K, P Ca Cu,Zn	1.2–2.5 0.9–2.5 0.3–2.5 0.2–2.5	[10]
Liquid petroleum products: fuels, crude petroleum fuel	Dilution 10x with organic solvent (naphtha, xylene) IS: Co, Sc, Y	Ni V	4–55 4–150	[11]
FAME	Dilution 10x min. with xylene or other organic solvent	P	4–20	[12]
Diesel (up to 10%vol. of FAME)	Dilution with kerosene (1:1) IS: Co, Sc, Y	Fe, Mn	0.5–7.0	[13]
Inductively coupled plasma atomic emission spectrometry ICP-AES				
Fuels (boiling range 150 ÷ 390 ºC	Direct measurement	Ag, Al, Ba, Ca, Co, Cr, Cu, Fe, K, Li, Mg, Mn, Mo, Na, Ni, P, Pb, Pd, Pt, Si, Sr, Sn, Ti, V, Zn	0.1–2.0	[4]
Liquid fuels: naphtha, diesel and similar	Direct measurement or dilution with organic solvent	Ba, B, Cr, Ag, Al, Cu, Ca, Fe, K, Mg, Mn, Mo, Na, Ni, P, Pb, S, Si, Sn, Ti, V, Zn	0.1–5.0 (for direct measurements)	[14]
Fresh oils and fuels	Method A – dilution 10x mas. with organic solvent Method B – mineralization with H_2SO_4 and combustion in 525 ºC, residue dissolved in HNO_3	Fe Ni V	1–10 10–100 50–500	[15]

* – other units indicated below, IS – Internal Standard

Table 2. List of standardized other measurement methods for determination of elements in fuels, biofuels and biocomponents

Sample type	Measurement parameters	Analyzed elements	Measurement range [mg/kg]*	Bibl.
Wavelength dispersive X-Ray fluorescence WD-XRF				
Liquid, solid or semi-solid petroleum products	30-50 kV, 30–70 mA crystal: Ge, PET, graphite film: polyester or polypropylene IS: Zr	S	0.001–2.5 [%mas.]	[16]
Petroleum products	Crystal: LiF or other IS: Mn	Ni V	5–100 5–1000	[17]
Ethanol	> 30 kV, > 50 mA, crystal: Ge, PET, graphite Film: polyester	S	7–20	[18]
Liquid fuels (cont. ≤3.7%mas. of oxygen)	> 30 kV, > 50 mA, crystal: Ge, PET, graphite Film: polyester	S	5–500	[19]
Petrol	50 kV, 25-45 mA, crystal: LiF IS: Bi (met. A)	Pb	2.6–1 320 [mg/l]	[20]
Energy dispersive X-Ray fluorescence ED-XRF				
Petrol (cont. ≤3.7%mas. of oxygen) Petrol (cont. ≤10%vol. of ethanol) Diesel cont. ≤10%vol. of FAME)	-	S	8–50	[21]
Unleaded petrol	-	S	48–1 000	[22]
Atomic absorption spectrometry AAS				
FAME	Dilution 25x with xylene or cyclohexane	Na	≥ 1	[23]
FAME	Dilution 25x with xylene or cyclohexane	K	≥ 0.5	[24]
Ultra violet fluorescence UV-F				
Petrol (cont. ≤3.7%mas. of oxygen) Petrol (cont. ≤10%vol. of ethanol) Diesel (cont. ≤10%vol. of FAME)	Burning in 1000-1100 ºC Measurement of SO_2, direct measurement or dilution with toluene or isooctane	S	3–500	[25]
Biodiesel, fuels, light hydrocarbons, engine oils	Burning in 1075 ºC Measurement of SO_2, direct measurement or dilution with xylenes or isooctane	S	1–8 000	[26]

* – other units indicated below, IS – Internal Standard

2.3. Sample preparation for ICP-OES/AES measurements

One of most important stages, in each analytical procedure is sample preparation. Improper sample preparation may lead to enrichment or impoverishment of analitu, for example due to contamination. That is why the sample preparation procedure should be as simple as

possible to minimalize possibility of error. Sampled fuel should be homogenous and usually requires placing in water bath [6], homogenization by intensive mixing [7–10, 14, 21], heating up to 60–100ºC and intensive shaking [4, 11] or by mechanical homogenization [14].

After homogenization, in case of ICP-OES or ICP-AES, usually sample is diluted with pure solvent with viscosity and boiling point similar to the sample. Alternatively direct measurements of undiluted samples are also possible. However it is important to bear in mind that both of this approaches are improper if insoluble particles are to be taken into account in elemental analysis, and may lead to underestimation of results [4, 14]. It is of high importance that standards solutions and samples have very similar viscosity as this is the critical parameter influencing spraying efficiency in spray chamber of spectrometer. That is why both, samples and standards solutions, should be prepared with the use of the same solvent. Additionally, in order to increase accuracy of the results internal standards (IS) are used and their role is to correct matrix effects and slight differences between viscosities of the samples and standards solutions. Internal standards are used in form of metalorganic compounds of usually: Sc, Y or Co, which are not present in the sample. In case of highly volatile samples as ethanol or petrol measurements may be performed on undiluted samples however, it may result in unstable plasma work and cooled spray chamber may be required.

3. Experimental

Elements concentration was measured by inductively coupled plasma optical emission spectrometer Perkin Elmer Optima 8300 with horizontal plasma and binary, radial and axial, observation system.

Due to low concentration of elements, below 1 mg/kg, samples after homogenization were analyzed undiluted. International standards recommends minimum 10x dilution what significantly deteriorate determination limits which in result makes accurate determination of trace elements difficult. Such approach is relatively easy for petrol and diesel containing up to 10%vol. of FAME (B10), however in case of pure FAME its viscosity is too high and sample dilution was required. For dilution of high viscosity samples V-solv (VHG Labs, Manchester, USA) solvent was used (declared concentration of elements below 0.25 µg/g).

Before measurements optimization of spectrometer parameters was done for each analyzed element, in order to achieve limit of determination as low as possible, signal to background ratio as high as possible, repeatable measurements and stable plasma work. Selected working conditions are presented in Table 3. For each analyzed element plasma gas flowrate, auxiliary gas flowrate, nebulizer gas flowrate, plasma power and observation direction were optimized. For most of analyzed elements, except Al, B, Cr, K and Na, 2 or 3 analytical lines were chosen and applied. In case of potassium and phosphorous binary plasma observation, radial and axial, was applied. Obtained limits of quantification (LOQ) were: 0.1 mg/kg for Al, Ba, Ca, Cu, Fe, Mg, Mn, Pb, Si, Ti, V and Zn; 0.3 mg/kg for Cr and 0.5 mg/kg for B, K, Mo, Na, Ni, P and Sn.

Four point calibration curves were prepared for each analyzed element and were based on multielemental standard solutions obtained by dilution of basic standard solution of elemnts in metalorganic form and concentration of 100 mg/kg each (WM-22-10x-100, AccuStandard, New Heaven, USA). Correlation coefficient for most elements was above 0,9995, except: Na (r^2 = 0.9991) and P (r^2 = 0.9979). Correctness of developed method was checked by testing of measurement repeatability (relative variation coefficient for 1.0 mg/kg concentration level was from 2.1 to 11.4% depending on measured element), recovery by standard addition method (90.2–114.4%, except B: 80.4%) and correctness of calibration curves preparation (98.7–108.4%).

Table 3. ICP-OES Optima 8300 work parameters

Parameter	Working conditions
RF generator power	1 500 W
Plasma gas flowrate	18 L/min
Auxiliary gas flowrate	1.0 L/min
Nebulizer gas flowrate	0.35–0.45 L/min
Nebulizer	Parallel (V-groove type)
Spray chamber	Glass cyclonic Baffled-type
Central torch pipe	Quartz, i.d. 0.8 mm

4. Results and discussion

The aim of conducted research was quality check of fuels from Polish market. Over 370 samples of fuels: diesel without FAME (B0), diesel with up to 7 %vol. FAME (B7), diesel with up to 10 %vol. FAME (B10) and FAME (B100) were tested within four years between 2013 and 2017. Within these samples there were 96 samples of B0, 207 samples of B7, 66 samples of B10 and 10 samples of B100.

Average elements contents in tested fuels are presented in Figs 1–3. Comparison of measured elements concentrations including minimum and maximum values is presented in Table 4, and these are the typical elements contents in tested fuels.

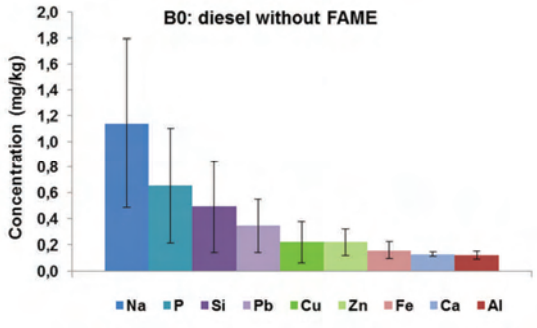


Fig. 1. Concentration of main elements in B0 diesel fuels

Elements most frequently present in B0, B7 and B10 fuel samples were: Al, Ca, Cu, Na, P, Pb, Si and Zn. Within these elements sodium was predominant taking into account both: its concentration in fuels and its presence frequency. Average sodium content in B0, B7 and B10 was ca. 1,0 mg/kg, and it was present in 90% of tested B0 samples and 78% of B7 and B10 fuel samples. In case of pure FAME, B100 samples sodium content was significantly higher (6.3 ± 1.3 mg/kg), however only 10 samples of B100 were tested. In case of silicon, average concentration in B0 samples was 0.5 mg/kg with maximum of 1.6 mg/kg (presence in 81% of B0 samples), in B7 average concentration was 0.3 mg/kg with maximum at 1.0 mg/kg (presence in 57% of samples) and in case

of B10 average content of silicon was 0.2 mg/kg with maximum of 0.6 mg/kg (presence in 68% analyzed samples). It was noticed that average silicon content was decreasing with increasing of FAME content in diesel fuel.

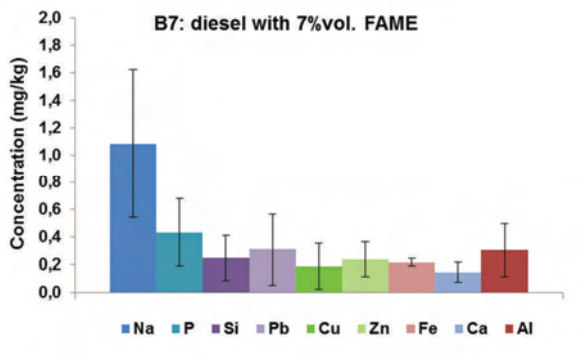


Fig. 2. Concentration of main elements in B7 diesel fuels

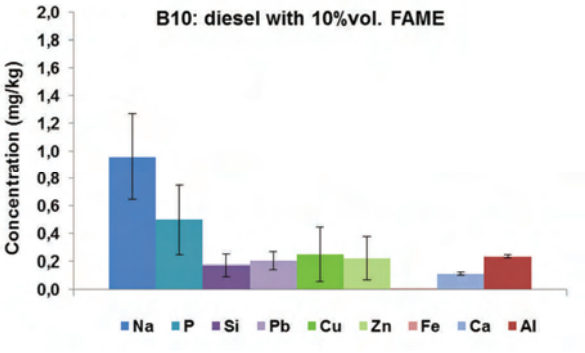


Fig. 3. Concentration of main elements in B10 diesel fuels

Zinc was present in tested fuels samples at average level of 0.22 ±0.13 mg/kg and no relation to biocomponent content in fuel was noticed. In case of pure FAME average concentration of this element was 0.76 mg/kg.

The highest phosphorous content was noticed in FAME samples (average of 2.8 mg/kg) while in fuels samples it was on average level of 0.5 mg/kg, in the range of minimum 0.1 and maximum 1.7 mg/kg. Similar dispersion of results was observed in case of silicon, average value of 0.3 mg/kg with dispersion of results from 0.1 to 1.6 mg/kg and in case of lead, average value of 0.3 mg/kg with dispersion from 0.1 to 1.4 mg/kg. Phosphorous presence was noticed in case of 31% of B0 samples, 51% of B7 samples and 62% of B10 samples, while lead was present in 44% of B0 samples, 41% of B7 and 32% of B10 samples.

There was no B, Ba, Cr, K, Mn, Sn, Ti, and V presence noticed in case of any of tested samples. Other elements than these mentioned above were present in relatively small number of samples, like magnesium, which presence was noticed only in 4 from 90 tested B0 samples. Moreover, its concentration was 0.1 mg/kg which was also the limit of quantification. Iron and nickel were present in some individual cases ie. Fe was present in 12 samples of B0 and only in 4 samples of B7, while Ni in 5 samples of B7 and 2 samples of B10. There were no iron presence noticed in any of B10 and B100 samples as well as no Ni presence in B0 and B100 samples. Molybdenum concentration in most of the samples was below limit of quantification (0.5 mg/kg) and was estimated in the range of 0.15–0.30 mg/kg. Molybdenum concentration was higher than LOQ only in three cases of B7 fuels.

Table 4. Elements content in fuels and biofuels mg/kg

Element	B0 (n = 96)	B7 (n = 207)	B10 (n = 66)	B100 (n = 10)
	min–max [mg/kg]			[mg/kg]
Zn	0.10–0.47	0.10–0.64	0.10–0.58	0.76 ±0.27
Al	0.10–0.20	0.10–0.58	0.24	< 0.1
B	< 0.1	< 0.1	< 0.1	< 0.1
Ba	< 0.5	< 0.5	< 0.5	< 0.5
Ca	0.11–0.15	0.10–0.43	0.10–0.13	0.17 ±0.09
Cr	< 0.3	< 0.3	< 0.3	< 0.3
Cu	0.10–0.81	0.10–0.72	0.10–0.74	0.13 ±0.04
Fe	0.11–0.32	0.19–0.25	< 0.1	< 0.1
K	< 0.5	< 0.5	< 0.5	< 0.5
Mg	0.10	< 0.1	< 0.1	< 0.1
Mn	< 0.1	< 0.1	< 0.1	< 0.1
Mo	< 0.5	< 0.5–0.75	< 0.5	< 0.5
Na	0.42–2.8	0.16–2.4	0.29–1.7	6.3 ±1.3
Ni	< 0.5	< 0.5–0.59	0.56	< 0.5
P	0.10–1.7	0.11–1.5	0.14–1.3	2.8 ±1.0
Pb	0.13–0.94	0.10–1.4	0.13–0.33	< 0.1
Si	0.12–1.6	0.10–1.0	0.11–0.57	< 0.1
Sn	< 0.5	< 0.5	< 0.5	< 0.5
Ti	< 0.1	< 0.1	< 0.1	< 0.1
V	< 0.1	< 0.1	< 0.1	< 0.1

The lowest results dispersion was observed in case of calcium. This element was present in 8% of total samples number and its average concentration was 0.13 ±0.03 mg/kg. Copper, which was present in 26% of total samples, results dispersion was significantly higher with average concentration for this element 0.22 ±0.16 mg/kg.

5. Conclusions

Negative effect of some elements presence, especially Zn, Na and Si, on engine performance is well known [5]. In some cases relatively small increase in some elements concentration may lead to significant engine performance drop. This is particularly true in case of soap formatting elements like Na, which responsibility for injector cooking is of great importance. The effects of other elements than mentioned above on engine performance is not that well known, mainly due to their trace level presence in most of diesel fuels. However, while dynamic development of combustion engines is taken into account with the accompanying development of alternative fuels production processes, it is possible that some of the elements which presence is not of that great importance, like the ones mentioned earlier, may become more important in the future.

Inductively coupled plasma emission spectrometry is a well-known and mature technique allowing measurements of broad range elements in the limits usually do not achievable for other spectrometry techniques, like X-Ray fluorescence or atomic absorption spectrometry. Different possibilities relating to sample preparation and control of versatile measurement parameters by ICP-OES techniques allows reaching very low LOQ values what is necessary for monitoring of trace elements. Despite the fact that, in case of diesel fuels, only sulfur and manganese content is limited by the standards there is need to other elements monitoring, especially in case of engine testing or vehicle testing activities as their presence may have significant effect on engine

performance. The effect of fuel contamination with trace elements in regular car usage will have presumably less dynamic nature and the engine performance drop will be less noticeable.

Nomenclature

AAS	atomic absorption spectrometry
ED-XRF	energy disppersive X-Ray fluorescence
IS	internal standard
ICP-OES	inductively coupled plasma optical emission spectrommetry
ICP-AES	inductively plasma coupled atomic emission spectrometry
LOQ	limit of quantification
LOD	limit of determiantion
UV-F	ultra-violet fluorescence
WD-XRF	wavelenght disppersive X-Ray fluorescence

Bibliography

[1] PN-EN 590:2013 Automotive fuels – diesel – requirements and test methods.

[2] PN-EN 228:2013 Automotive fuels – unleaded petrol – requirements and test methods.

[3] PN-EN 14214:2012 Fatty acid methyl esters (FAME) for use in diesel engines and heating applications – requirements and test methods.

[4] ASTM D7111-16 Standard test method for determination of trace elements in middle distillate fuels by inductively coupled plasma atomic emission spectrometry (ICP-AES).

[5] BARKER, J., COOK, S., RICHARDS, P. Sodium contamination of diesel fuel, its interaction with fuel additives and the resultant effects on filter plugging and injector fouling, *SAE International Journal of Fuels and Lubrication*. 2013, **6**(3), 826-838.

[6] PN-EN 15837: 2011 Ethanol as a blending component for petrol. Determination of phosphorous, copper and sulfur content. Direct method by inductively coupled plasma optical emission spectrometry (ICP OES).

[7] PN-EN 14538:2008 Fat and oil derivatives. Fatty acid methyl ester (FAME). Determination of Ca, K, Mg and Na content by optical emission spectral analysis with inductively coupled plasma (ICP OES).

[8] PN-EN 16136:2015-03 Automotive fuels. Determination of manganese and iron content in unleaded petrol. Inductively coupled plasma optical emission spectrometry (ICP OES) method.

[9] PN-EN 16294:2013-05 Petroleum products and fat and oil derivatives. Determination of phosphorus content in fatty acid methyl esters (FAME). Optical emission spectral analysis with inductively coupled plasma (ICP OES).

[10] PN-EN 16476:2014-07 Liquid petroleum products. Determination of sodium, potassium, calcium, phosphorus, copper and zinc contents in diesel fuel. Method via inductively coupled plasma optical emission spectrometry (ICP OES).

[11] PN-EN 15944:2011 Liquid petroleum products. Determination of nickel and vanadium content. Inductively coupled plasma optical emission spectrometry method (ICP OES).

[12] PN-EN 14107:2004 Fat and oil derivatives. Fatty acid methyl esters (FAME). Determination of phosphorous content by inductively coupled plasma (ICP) emission spectrometry.

[13] PN-EN 16576:2014-12 Automotive fuels. Determination of manganese and iron content in diesel. Inductively coupled plasma optical emission spectrometry (ICP OES) method.

[14] PN-V-04030:2000 Oznaczanie zawartości pierwiastków w paliwach płynnych i produktach podobnych metodą emisyjnej spektrometrii atomowej z plazmą indukcyjnie wzbudzoną (ICP AES).

[15] ASTM D 5708-12 Standard test methods for determination of nickel, vanadium, and iron in crude oils and residual fuels by inductively coupled plasma (ICP) atomic emission spectrometry.

[16] PN-EN ISO 14596:2009 Petroleum products. Determination of sulfur content. Wavelength-dispersive X-ray fluorescence spectrometry.

[17] PN-EN ISO 14597:2005 Petroleum products. Determination of vanadium and nickel content. Wavelength-dispersive X-ray fluorescence spectrometry.

[18] PN-EN 15485:2009 Ethanol as a blending component for petrol. Determination of sulfur content. Wavelength dispersive X-ray fluorescence spectrometric method.

[19] PN-EN ISO 20884:2012 Petroleum products. Determination of sulfur content of automotive fuels. Wavelength-dispersive X-ray fluorescence spectrometry.

[20] ASTM D 5059-14: Standard test methods for lead in gasoline by X-ray spectroscopy.

[21] PN-EN ISO 13032:2012 Petroleum products. Determination of low concentration of sulfur in automotive fuels. Energy-dispersive X-ray fluorescence spectrometric method.

[22] ASTM D 6445-99: Standard test method for sulfur in gasoline by energy-dispersive X-ray fluorescence spectrometry.

[23] PN-EN 14108:2004 Fat and oil derivatives. Fatty acid methyl esters (FAME). Determination of sodium content by atomic absorption spectrometry.

[24] PN-EN 14109:2004 Fat and oil derivatives. Fatty acid methyl esters (FAME). Determination of potassium content by atomic absorption spectrometry.

[25] PN-EN ISO 20846:2012 Petroleum products. Determination of sulfur content of automotive fuels. Ultraviolet fluorescence method.

[26] ASTM D 5453-16e: Standard test method for determination of total sulfur in light hydrocarbons, spark ignition engine fuel, diesel engine fuel, and engine oil by ultraviolet fluorescence.

Joanna Faber, DEng. – BOSMAL Automotive Research and Development Institute Ltd.

e-mail: *Joanna.Faber@bosmal.com.pl*



Krzysztof Brodzik, DEng. – BOSMAL Automotive Research and Development Institute Ltd.

e-mail: *Krzysztof.Brodzik@bosmal.com.pl*



Article citation info:
STAWECKI, W., MERKISZ, J., BAJERLEIN, M., DASZKIEWICZ, P. New technologies of enhanced plastic for use in rail vehicles to reduce noise emissions. *Combustion Engines*. 2017, **171**(4), 145-149. DOI: 10.19206/CE-2017-424

Włodzimierz STAWECKI
Jerzy MERKISZ
Maciej BAJERLEIN
Pawel DASZKIEWICZ

CE-2017-424

New technologies of enhanced plastic for use in rail vehicles to reduce noise emissions

The article presents an overview of modern plastics for use in rail vehicles. The analysis of plastics and composites in the constructional aspect was analyzed. The trends in the development of polymer materials, technologies and constructions used in the manufacture of vehicles, on the one hand, are determined by the technical and economic requirements of industry and, on the other, by the continued emphasis on reducing fuel consumption and CO_2 emissions. Further development will be subject to pre-impregnation techniques, particularly in the form of different types of reinforcement. Full use of the advantages of reinforced polymer materials in vehicle production will only be achieved when further optimization of the resin properties and development of automation will result in the widespread use of composite components in series production. Observing the trends and pace of development, it is possible to predict that there are still restrictions on the use of polymeric materials in the transport sector, such as relatively high prices, technological constraints and the hindering automation of large-scale production. Modern construction and material solutions, in particular those using reinforced plastics, are primarily designed to reduce vehicle weight and have better noise and vibration damping properties. Rail vehicles are becoming more environmentally friendly at the time and travel comfort is higher.

Key words: *rail vehicles, new materials, plastics and composites, CO_2 emissions*

1. Introduction

Plastics consists of individual elements – molecules. After these small elements are linked into chains, large or very large molecules are formed and make up macromolecules. Thermoplastics and plastomers are the main types of plastics that consist of linear or branched macromolecular chains that are not connected to one another (fig. 1b). Due to their many beneficial properties, thermoplastics have a significant contribution in the process of designing vehicles. Thermoplastics can be melted and dissolved many times. This has a very high significance, particularly with regard to environmental protection. If individual types are not mixed with one another, thermoplastics are ideally suited for recycling, since new parts can theoretically made from used ones [4]. Another benefit they offer is that they can be heat-sealed, so it is possible to remove cracks and scratches. Elastomers are the next group, where both stronger and weaker bonds between macromolecules are possible, resulting in diverse cross-linking. In the case where a small number of neighboring molecular chains are joined by bonds, plastics – i.e. elastomers – are formed (fig. 1c). Elastomers neither melt nor dissolve, however they have good stretch properties, with qualities similar to rubber. Elastomers are frequently present in rail vehicles as seals, but thermoplastic elastomers (fig. 1d) are most commonly used to make spoilers, as their structure is made up of co-polymers consisting of hard and soft blocks or a mixture of thermoplastics with (non-cross-linked or partially cross-linked) rubber. Duroplastics are the third group, in which a greater number of cross-links makes the material harder but also more brittle. A large number of molecular chains form one large cross-linked network. Such a strongly cross-linked plastic is called a duroplastic, or hardening plastic. Duroplastics can neither be melted nor dissolved. The capacity for stretching, present in elastomers, also disappears. However duroplastics are resistant to heat. For this reason, they are used to make engine chamber body parts, for example. Innovative design and materials solutions, particularly those applying reinforced plastics, mainly lead to reduction of vehicle weight and attenuation of noise and vibrations. Thus, the vehicle is more environment-friendly and comfortable.

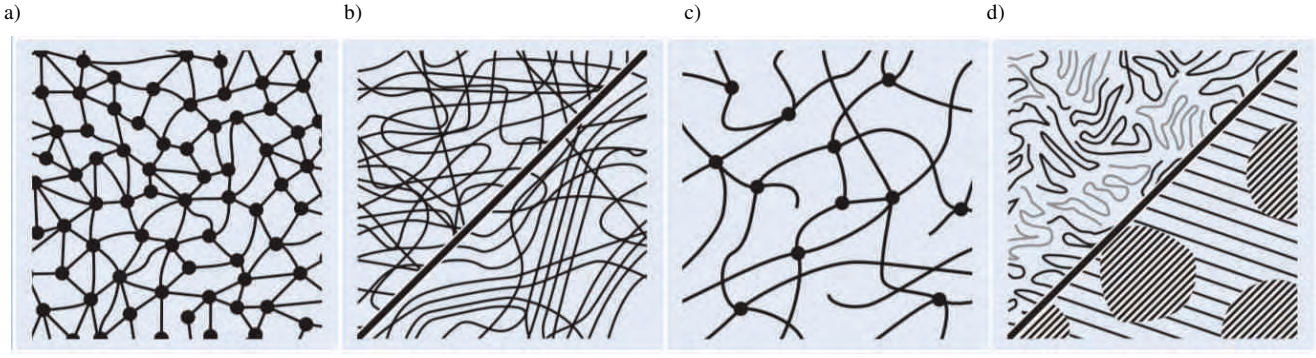


Fig. 1. Structure: a) duroplastic, b) termoplastic, c) elastomer, d) thermoplastic elastomer

The next group consists of laminates (composites), made up of at least 2 materials. They exhibit different properties than their individual components. A reinforcing substance is a material that significantly improves the properties of laminates or makes it possible to obtain certain composites. The remaining material, ensuring cohesion between the components, is the matrix. Laminates can be divided into the following categories:

- layered laminate composites,
- fibrous composites,
- particle composites,
- infiltrated composites.

Multi-layered composites (Fig. 2) are also being used increasingly frequently, and these are composites where the matrix is made up of a polymer or plastic. Fibrous composites (FVK) are particularly important in this case. The reinforcing material consists of natural or synthetic fibers (organic and/or non-organic). These fibers can be short, long and unterminated, or they may be present in the form of products like unwoven fabric, mats, woven fabric or knitted fabric. By combining the fibers with the matrix (in an oriented or unoriented manner), mechanical and thermal properties are improved, such as tensile strength, breaking strength, thermal resistance and modulus of elasticity.



Fig. 2. Composites reinforced with amide fibers with a macromolecular structure

The application of plastics in vehicle design is an expression of energy savings in comparison to steel and aluminum. This is not only due to lower operating costs but also lower costs of producing, processing and machining the material itself. Eliminating plastics in vehicle design would increase energy demand by 26%. Plastics will be a necessity in mass-scale industry in the foreseeable future, and one should also account for the fact that reducing a vehicle's weight by 100 kg reduces fuel consumption by up to 0.6 dm^3/100 km, thus reducing CO_2 emissions by 13 g/km [1, 2].

Currently, plastics have a 23% share in vehicles, and by 2030, this percentage is expected to grow to approx. 70%. According to the current trend, plastics are applied on the exterior of a vehicle (approx. 50%), e.g. sheathing, bodywork. In a vehicle's interior, plastics (approx. 30%) mainly serve to improve comfort and reduce noise. Parts and assemblies in the drive chamber are applications of plastics (approx. 20%) in which there are heavy working conditions. Thermoplastics and hardening plastics find broad applications in vehicle design due to their properties. Reinforced plastics from both groups are dominant in these applications. The chemicals industry is engaged in intensive cooperation with vehicle manufacturers, offering materials fit to purpose more and more frequently. This does not just involve the proper mechanical properties but also other qualities, e.g. enabling the application of plastic parts in elevated temperatures, suitability for industrial lacquering. Although it is generally recognized that metals are characterized by higher strength than plastics, this is often not the case when reinforced plastics enter into the comparison. Specific strength, or the ratio of strength to density $\sigma\ \gamma$ is particularly interesting, because for many plastics (particularly reinforced plastics), this strength exceeds values determined for metals, as illustrated in Fig. 3.

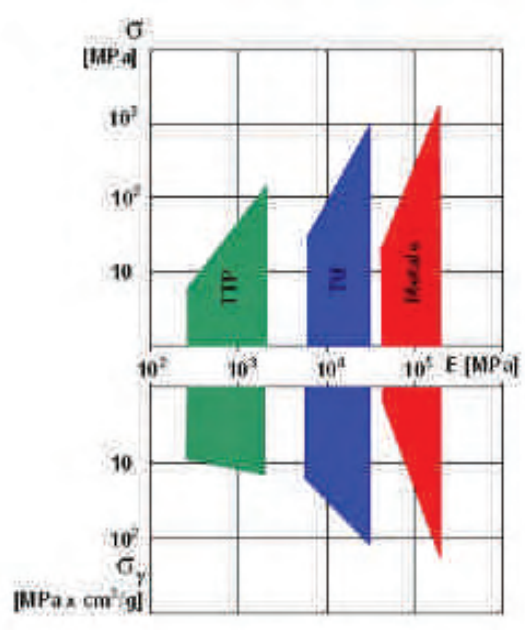


Fig. 3. Selected mechanical properties of plastics in comparison with metals (TTP – thermoplastics, TU – hardening plastics)

Linear thermal expansion α is an important property of plastics that is accounted for in vehicle design. Plastics exhibit linear thermal expansion 10 times that of metals. However, this does not apply to polymer composites, which have thermal expansion that is twice as high (glass reinforcement) or sometimes even lower (carbon reinforcement) compared to steel. In the case where plastics are applied as parts located near a heat source, their resistance to elevated temperatures is particularly important. As working temperature increases, the material's strength and rigidity decrease significantly. The chemicals industry currently offers polymers that can be used at temperatures up to 300ºC. The acoustic features of polymer materials provide greater comfort and also have a pro-environmental impact. Sound waves propagate much more slowly in plastics than in metals, so they are perfect noise-damping materials. Sound wave absorption is greater the less elastic the plastic is. Plastic vehicle parts themselves also emit less noise.

2. Modern materials and technologies

The properties of plastics used in transport are generally the effect of modifications, including the addition of rein-

forcing agents. The resultant polymer material (granulate, resin) is an inhomogeneous material composed of at least two phases: the matrix and the reinforcing agents embedded in it (i.e. carriers, reinforcement). The latter particularly include fibers in various forms (cut, long, continuous) made from various materials. The carriers introduced into the matrix affect most properties: strength grows, as does maximum working temperature, the thermal expansion coefficient decreases, etc. Among the various carriers, organic and non-organic materials of natural origin are being used more and more frequently. Although jute, sisal, hemp and other fibers do not increase the material's strength and Young's modulus significantly, they may meet essential requirements posed towards certain vehicle subassemblies while being well-perceived for environmental reasons. Examples of applications of natural fibers for reinforcement of polypropylene (PP) vehicle parts are:

- shelves, door guard, soffit ceiling finishing – curaua, kenaf, sisal or jute fibers,
- noiseproofing and insulating elements for doors, floor, etc. – cotton, linen, hemp and sisal fibers.

In recent years, nanomaterials have been introduced as an additive to polymers in order to reinforce them or endow parts with specific properties. Particles based on montmorillonite are most commonly used to reinforce polyamides and polypropylene. Nanoparticle-containing polyamides are used to manufacture covers, parts of the fuel system while polypropylene is used to make dashboards with increased resistance to scratches and dirt. Synthetic materials are used decidedly more often as carriers than natural materials. Certain organic materials can be distinguished in this group, such as oriented polyethylene fibers, aramid fibers, as well as non-organic materials – glass, mineral fibers, e.g. wollastonite (calcium metasilicate with aciform structure) and others.

The following reinforcements can be differentiated according to form:

- particles and dispersions, e.g. powders, micro-spheres, flakes, etc.,
- fibers, rowing, wires, whiskers, nanotubes, etc.,
- mats, unwoven fabric, tapes, etc.,
- plaited fabric, etc.

Most of the aforementioned carriers are used to reinforce plastics applied in parts manufacturing. Parts reinforced with short glass fibers are dominant among those manufactured from thermoplastics, although carbon fiber reinforcement is being applied with increasing frequency despite high materials and technological costs. This is due to the material's high static and fatigue strength as well as its pleasing aesthetic even without additional coatings, even on parts installed outdoors. The reduced weight of parts with carbon reinforcement in comparison to steel parts (60% lighter) and aluminum parts (25% lighter) is also not without significance. Hybrid parts, structural assemblies, load-bearing structures and complete vehicle bodies are all potential applications of the aforementioned materials. Polyamides are the thermoplastics most commonly used as load-bearing parts of vehicles, particularly PA66, reinforced by up to 60 glass fibers. PA6 and PA66 with glass fibers (GF30, GF35) are used to make collectors, and with the addition of 15% mineral fillers and glass fibers (GF25) - also covers. PA66 (GF35) is also applied in the drive system, pneumatic springs, etc. In the motorization industry, polyamides are also applied in the form of mixtures with other thermoplastics. The polyamide + polyphenyl ether mixture (PA + PPE) is a material characterized by significantly greater thermal resistance and thermal shape and dimensional stability. Polyamides for bodywork applications are the effect of cooperation between the chemicals and motorization industries. Cathode Dip Painting (CDP) followed by the drying operation at up to 200°C does not result in loss of the part's shape and dimensional stability [5, 7, 8]. Similarly to other thermoplastics, reinforced polyamides are generally processed by means of conventional methods. In typical cases, granulate containing a specific quantity of fibers cut to a certain length (within the 0.3–10 mm range) is used. Fibers may also be introduced into the plastic via processing, and mixing occurs in the plasticizing system of the injection molder. It is also possible to mix the plastic with fibers in a separate process by means of compounding machines, where fibers are introduced in the form of roving or cut, or by continuously saturating fiber bands with melted polyamide (pultrusion method) and cutting them into granulate (the fibers are oriented). Introducing long fibers to a polymer matrix improves the material's directional reinforcement even further. The production technology for thermoplastics was recently mastered, although it was already known for parts made from hardened resins. Polyamides (PA66, PA6), PP, polybutyl terephthalate (PBT) and polyacetal (POM) are the polymers reinforced most often. Parts of the bodywork and load-bearing structures for fastening headlights, etc. are made using the method of pressing plasticized thermoplastic reinforced with long glass fiber (LFT – Long Fiber Thermoplastics).

Another technology for manufacturing structural elements from plastics reinforced with long fibers, delivered in the form of roving, is realized by means of a process line consisting of a compounding machine (machine used to prepare the plastic and additives for processing), double-worm injection molder and high-speed press (Fig. 4).

Another technology is also used to process polyamides, PP, polyethylene terephthalate (PET), which are reinforced with fibers about 25 mm in length. In such cases, IMC (Injection Molding Compounder) technology, combining the continuous compounding process and the cyclic injection process, is applied. Polyurethanes (PUR) are another type of plastic commonly used in vehicle design. Depending on the components, modifiers and molding technology, the properties of manufactured parts differ significantly. On one hand, the material in foamed form is capable for significant energy absorption and attenuation of vibrations, which is why it is used in bumpers and parts with insulating-noiseproofing properties, and on the other hand, in bulk form, it is resistant to elevated temperatures.

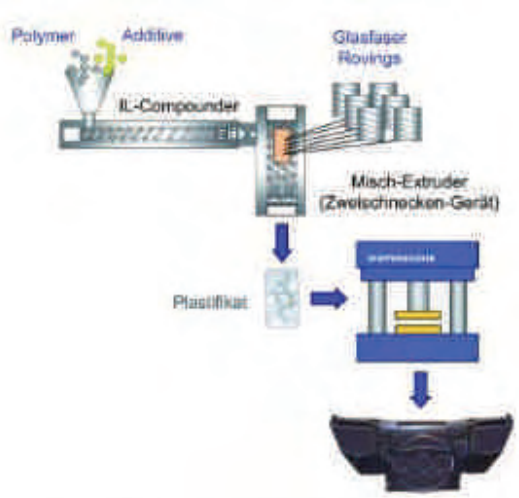


Fig. 4. Technology of molding parts made from plastic reinforced with long fibers

The plastic is characterized by high impact resistance at low temperatures, low thermal expansion (after reinforcement), low moisture absorption, and it meets requirements posed towards bodywork elements, even in a warm and humid climate. The technology of injecting reactive ingredients (polyol and isocyanate) with the addition of cut fiber – R-RIM (Reinforced Reaction Injection Molding) has been used in parts manufacturing for many years. Pressing techniques are also applied to manufacture bodywork elements from thermoplastics reinforced with continuous fiber [5, 6]. Reinforcing fibers form structures formed by textile techniques (woven fabrics, knitted fabrics) in this case. In this manner, the so-called "organic sheets" are created, whose final shape is endowed by forming in the pressing tool. Another technique for manufacturing sheathing elements is to polymerize the plastic (e.g. casting polyamide) in a mold filled with continuous fibers. For several years now, hybrid designs combining a metal part and plastic have been applied in vehicle design. The metal part is most often shaped by plastic working and mounted in the socket of the mold, into which thermoplastic is injected. This technology reduces the weight of manufactured parts while simultaneously increasing their strength and rigidity. Production costs are generally lower, and designers gain greater freedom in shaping the body. The technology described above has successfully been applied to manufacture the front belt, rear cover and other structural elements. Long or continuous fibers are applied to reinforce the structure in certain cases. Significant improvement of a part's strength is achieved in the case where "hybrid plus" technology is applied, in which ribbing made from fiber-reinforced PP is injected onto steel drawpieces.

Hardened plastic parts are most often molded from plastics obtained using BMC technology (Bulk Molding Compounds), containing reinforcements like glass fiber and others. The injection and pressing process is used to manufacture even large-sized window frames for the motorization industry. Numerous examples of applications of polymer composite parts can be seen in vehicles that are currently being manufactured. These are mainly parts of the exterior sheathing and shaped parts made from composites with glass and carbon reinforcement. Polyester resins (UP) and epoxide resins (EP), others less often, are most commonly used as the matrix. Because continuous fibers exhibit very high tensile strength, reinforcement of the structure should also ensure fiber orientation so that they are stretched during work. Polyester or epoxide body elements reinforced with layers of mat or fabric are pressed under low pressure. The process is usually performed using the RTM (Resin Transfer Molding) method, in which dosed resin saturates layers of reinforcement properly arranged in layers, and at the same time, the excess is drained off by the vacuum generated. In serial production, the industry relies on pre-impregnates obtained using SMC (Sheet Molding Compounds) technology. Depending on design requirements, semi-products with a random or oriented arrangement of cut fibers, or with unidirectionally oriented continuous fibers, can be applied. Successive versions of pre-impregnates are characterized by increasingly high strength and Young's modulus. After the required outline is cut out and placed in the mold, preimpregnates are hardened in the low-pressure pressing process under the proper temperature and pressure conditions.

Hardened plastics are also used in combination with other plastics. Roofs consisting of an exterior epoxide layer, an insulating/noiseproofing layer made of foamed PUR and epoxide-glass laminate, are an example of such a solution. The entirety is made in three steps using the RTM method.

3. Conclusions

The directions of development of polymer materials, technology and designs with applications in vehicle manufacturing are defined by technical and economic requirements posed by the industry on one hand, and on the other, by the constant pressure from environmentalists to limit fuel consumption and CO_2. This generates innovation in the scope of the applications of modern materials, methods of processing them, as well as new design solutions, and results in reduction of the vehicle's weight as well as a series of benefits in comparison to metal, which include:

- low density,
- good attenuation of sound and vibrations,
- electric insulation or regulated conductivity,
- good resistance to the action of chemicals,

– high degree of freedom in shaping,
– permeable to electromagnetic waves,
– very good corrosion resistance,
– thermal insulation,
– possibility of modifying specific parts for specific cases of application.

Even today, the boldest forecasts show that at the current rate of technical development, a vehicle's weight will be reduced by 30% on average in the near future thanks to these materials. In the scope of materials, trends of broader applications are being outlined for modern plastics reinforced with materials such as:

– nanocomposites,
– composites reinforced with carbon fibers,
– biopolymer composites (green polymers),
– reinforced with nanotubes, carbon fibers and natural fibers,
– thermoplastic multi-material composites or multi-material systems, e.g. laminate rein-forced with nanotubes,
– high-quality recyclates,
– modern films and coating materials.

Techniques of preparing pre-impregnates will continue to be developed, particularly with respect to the forms of various types of reinforcement. Plaited, knitted and sown parts have found industrial applications. However, complete utilization of the advantages afforded by reinforced polymers in vehicle manufacturing will only take place when the possibility of broad application of composite parts in serial production arises as a result of further optimization of the properties of resins and the development of automation. Observing trends and the rate of development, it can be predicted that the limitations to the applications of polymers in the motorization industry that still exist, such as relatively high prices, technological conditions and difficult automation of large-series manufacturing will soon be surmounted. Modern design and materials solutions, particularly those that utilize reinforced plastics, mainly serve to reduce vehicle weight, in addition to having better noise and vibration attenuation properties. Thanks to such solutions, rail vehicles become more environment-friendly, and the comfort of travel is greater. The application of plastics at the designing stage of vehicles of this type is an expression of energy savings in comparison to steel and aluminum. This is not only due to lower operating costs but also lower costs of producing, processing and machining the material itself. Abandoning plastics used in passenger vehicle design would cause a 26% increase in energy demand [2].

Bibliography

[1] ENGELMANN, H.-J., GŁUSZEWSKI, W. Kompozyty polimer-metal w ochronie radiologicznej. *Journal: Tworzywa Sztuczne w Przemyśle*. 2016, **4**.

[2] FELDMANN, J. Kunststoffe – Werkstoffe der Energieeffizienz. Kunststoffe im Automobilbau. *VDI-Verlag* 2015.

[3] GESELLA, G., SZELEZIŃSKI, A., MURAWSKI, L., MUC, A. Wykorzystanie tworzyw sztucznych w sektorze motoryzacyjnym. Wpływ temperatury pracy wytłaczarek na jakość wyrobu. *Autobusy. Technika, Eksploatacja, Systemy Transportowe*. 2015, **6**.

[4] HINZ, T., LEWKOWICZ, R. Wpływ kształtu elementów konstrukcyjnych nadwozi samochodowych wykonanych z tworzywa sztucznego na ich wytrzymałość. *Mechanik.* 2015, **5-6**(05).

[5] KEUERLEBER, M. Kunststoff-Trends im Powertrain, Kunststoffe im Automobilbau. *VDI-Verlag*. 2014.

[5] KOETH, C.-P. Leichtbau – die Zweite, *Automobilindustrie*. 2016, **3**.

[6]. KRÓLIKOWSKI, W. Tworzywa wzmocnione i włókna wzmacniające. *Wydawnictwo Naukowo-Techniczne.* 2010.

[7] POCHWAŁA, T., ŚLIWA, A., WALA, T. Wpływ procesu impregnacji na mikrostrukturę tworzywa ogniotrwałego. *Szkło i Ceramika*. 2016, **4**.

Włodzimierz Stawecki, Ph.D. – Rail Vehicles Institute TABOR in Poznan.

e-mail: *Sekretariat@tabor.com.pl*



Maciej Bajerlein, DSc., DEng. – Faculty of Machines and Transport at Poznan University of Technology.

e-mail: *Maciej.Bajerlein@put.poznan.pl*



Prof. Jerzy Merkisz, DSc., DEng. – Faculty of Mechanical Engineering at University of Technology.

e-mail: *Jerzy.Merkisz@put.poznan.pl*



Pawel Daszkiewicz, DEng. – Rail Vehicles Institute "TABOR" in Poznan.

e-mail: *P.Daszkiewicz@tabor.com.pl*



Article citation info:
FLEKIEWICZ, M., KUBICA, G., MARZEC, P. The possibilities of using DME (BioDME), as an additive to conventional gaseous fuels in SI engine. *Combustion Engines*. 2017, **171**(4), 150-155. DOI: 10.19206/CE-2017-425

Marek FLEKIEWICZ
Grzegorz KUBICA
Paweł MARZEC

CE-2017-425

The possibilities of using DME (BioDME), as an additive to conventional gaseous fuels in SI engine

The results of SI engine fueled with blends of LPG and DME are presented in the paper. The range studies submitted includes measurements at varying engine loads, at selected values of speed. The research was conducted on a chassis dynamometer, specifying the engine load by the degree of throttle opening. Value of the mass fraction of DME in the blend with LPG was determined based on previous analyzes. The selected fuel blends containing from 7 to 17% DME (mass fraction). During the study was also performed a series of comparative measurements with pure LPG. Analyses show that of DME can be used as a partial substitute for LPG in SI engines. Its presence does not a negative impact on performance and emissions of the engine. The obtained results indicate that the amount of addition of DME should be varied depending on the engine load. Moreover, the use of this fuel does not require changes to the design fueling system and storage of LPG.

Key words: *dimethyl ether, DME+LPG, fuel blend, SI engine*

1. Introduction

The use of DME as fuel also in SI engines is becoming more frequently considered. Economic and ecological benefits combined with very favorable physicochemical properties are the direct cause of these interests [5, 6]. The most important aspect to mention is the possibility of obtaining DME as a renewable fuel produced from biomass. As a result, there is the possibility of significant reduction of CO_2 emissions, compared with LPG, 30–80% [1] and NO_x reduction: 5–15% [1], in the total balance. On the other hand, similar LPG properties allow to use the infrastructure and fueling systems commonly used for LPG.

Among the methods of obtaining DME on an industrial scale, the most effective are gas-based technologies (e.g. the formation of DME from synthesis gas). DME is characterized by a high CN, of over 55 (for a comparison diesel has about 53), which can also be used in CI engines. In SI engines is used in combination with LPG [7, 8]. In the previous studies, carried out at the Faculty of Transport of Silesian University of Technology [2, 3], the changes that occur in the combustion process, depending on the amount of DME's participation, were determined. These tests were conducted at idle and at full engine load for selected speeds. In those preliminary studies, the range of changes in participation of DME in the blend with LPG, which ensures proper combustion process has been determined. The results showed that a limited DME additive, in the range of approximately 7–15% by weight, increased engine performance. On the other hand, increasing the DME's share over this gives the opposite effect (Fig. 1). These conclusions were formulated on the basis of the results obtained at full engine load (full throttle opening). Interpretation of these changes is the result of the analysis of the function of the heat release rate during the combustion process (Fig. 2). Too large amount of DME in the fuel causes a reduction in combustion rate and prolongs the process. The engine management during the test was performed according to the settings developed by the manufacturer.

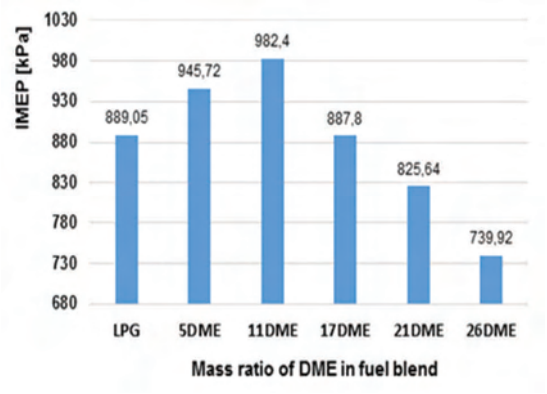


Fig. 1. IMEP for engine fueled by LPG-DME mixtures, at 2500 rpm; WOT and λ = 1.0 [2]

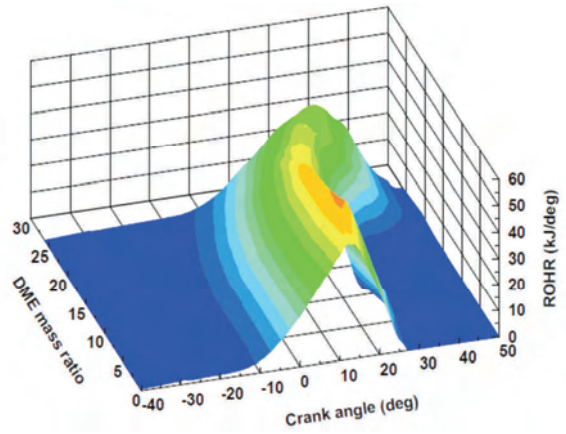


Fig. 2. ROHR as a function of DME ratio, at 2500 rpm; WOT and λ = 1.0 [3]

Current research was aimed at determining the basic values of the engine's performance, depending on the load. The main objective of this study is to determine the share of LPG/DME fuel components providing the highest efficiency, as a function of engine load. The equivalent of the engine load in the tests is degree of throttle opening.

2. Research of engine partial load

2.1. Measurement set-up

The popular passenger car powered by 1.6 liter engine, naturally aspirated with a compression ratio of 9.6, port fuel injection, two valves per cylinder, flat pistons and without external EGR was used in the experiments. The experiments were performed on a BOSCH FLA 203 chassis dynamometer as presented on Fig. 3. Main features characterizing the engine installed on the tested vehicle have been listed in the Table 1. Engine performance has been estimated on the basis of acquired dynamic characteristics, defining the power on wheels in function of vehicle speed. Test stand has been equipped with various transducers and sensors allowing the identification of engine operating conditions. Basic measurements and control systems allowed continuous acquisition of engine operating conditions, through registrations of:

- in-cylinder pressures, crank angle, with the TDC identification,
- power on wheels,
- manifold pressure,
- inlet air temperature,
- exhaust gases temperature,
- fuel mass flow to the engine.

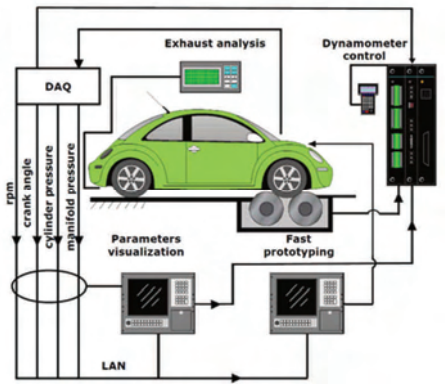


Fig. 3. Diagram of experimental stand [2]

The in-cylinder pressure was measured by Kistler 6121 piezoelectric pressure transducers and a charge amplifier, Kistler 5011A. The signals were processed in type NI PCI-6143 board in a computer for online pressure measurements. The pressure recording system was also connected to the Kistler 2613B crank angle encoder giving the temporal resolution of the pressure recordings of 0.5 CA. The pressure measurements were recorded and stored on a computer, with recordings performed for 200 subsequent cycles in each test, and were further processed with the help of a script debugged in LabView 7.1 environment.

Table 1. Engine specifications

Engine code	X16SZR
Cylinder number and layout	4 R
Maximum power	55 kW@ 5200 rpm
Maximum torque	128 N·m @ 2800 rpm
Displacement	1598 ccm
Bore x stroke	79.0 x 81.5 mm
Compression ratio	9.6

2.2. Methodology of research

The scope of the tests included determining the external characteristics of the engine, its maximum power and torque depending on the load. The tests were carried out according to the BOSCH FLA203 dynamometer producer's procedure, which consists in accelerating the vehicle in direct gear to the maximum engine speed and slowing down at idle speed. Taking into account the results obtained in the previous step [3], for testing were prepared 6 fuels containing: 0, 7, 9, 11, 14, 17% mass DME mixed with LPG. Parameters of prepared fuels are presented in Table 2.

The test was performed for the following engine loads 21, 33, 48, 60, 75, 90 and 100%. The engine load was determined based on the degree of throttle opening. Repeatable test conditions were provided by use of the accelerator pedal limiter, with different heights (Fig. 4).

Based on the experimental results, the combustion process was calculated using a verified simulation program EnComAn [4].



Fig. 4. View of accelerator pedal limiter

3. Results and discussion

3.1. Vehicle performance

The results of power and torque measurements of the engine in full range of speed, with constant throttle position, for one of tested fuel are shown in the graphs (Fig. 5 and 7). These results indicate that when the throttle is opened above 70%, the achieved values are very close. By contrast, reducing the load below this limit reduces the value of power, torque and maximum speed.

Table 2. The parameters of fuels prepared for test

Fuel composition [% by mass]		Molecular mass of fuel [kg/kmol]	Stoichiometric air fuel ratio A/F [kg/kg]	Lower heating value [MJ/kg]
LPG	DME			
100	0	51	15.76	45.95
93	7	50.615	15.30	44.67
91	9	50.506	15.17	44.26
89	11	50.397	15.04	43.88
86	14	50.236	14.84	43.33
83	17	50.080	14.64	42.78

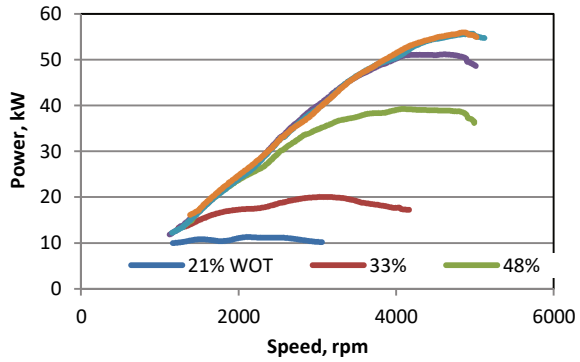


Fig. 5. Engine power for different WOT. Fuel LPG/DME: 91/9%

The chart showing the maximum values of the measured engine power (Fig. 6) indicates that with the engine load drop, the fuel composition changes to give the maximum power (red line in the graph). The change in fuel composition consists in increasing DME's share. For the analysis of maximum torque values (Fig. 8), there is a similar tendency, although not so pronounced. The power and torque measured on the wheels of the vehicle (Fig. 9 and 10) also show that, with less engine load, an increase of the DME share has a beneficial effect to the performance of the vehicle. This area is marked on the chart.

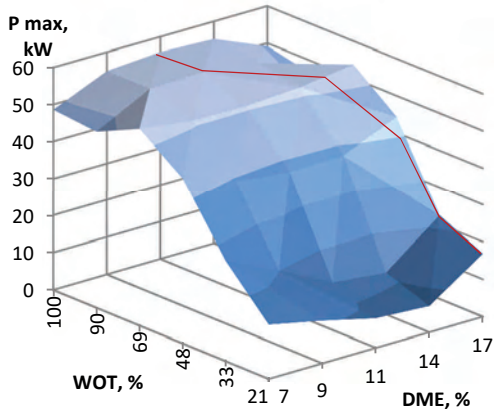


Fig. 6. Values of engine maximum power in depend of DME share & engine load, λ = 1.0

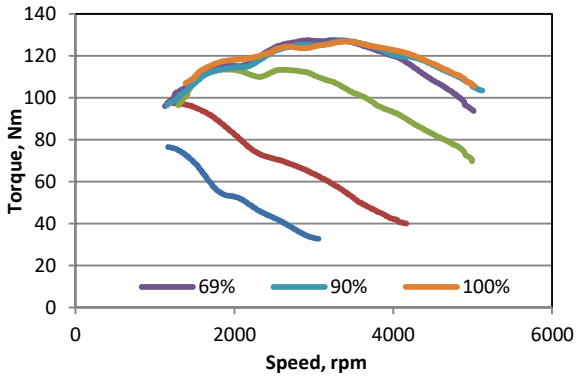


Fig. 7. Engine torque for different WOT. Fuel LPG/DME: 91/9%

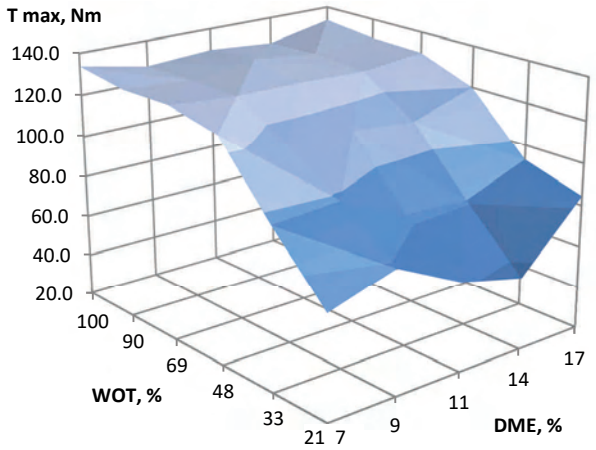


Fig. 8. Values of engine maximum torque in depend of DME share & engine load, λ = 1.0

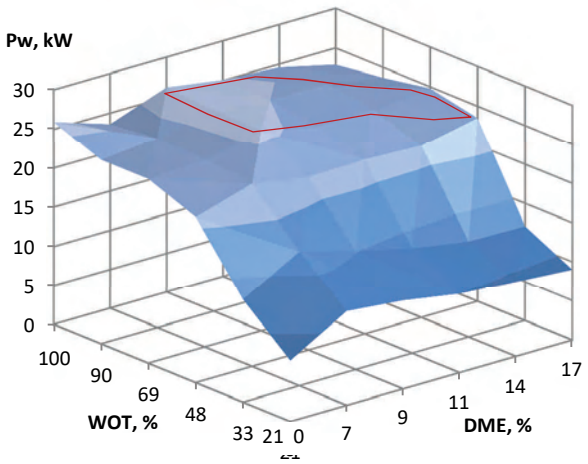


Fig. 9. The results of power on wheel measured during experimental test; n = 2500 rpm

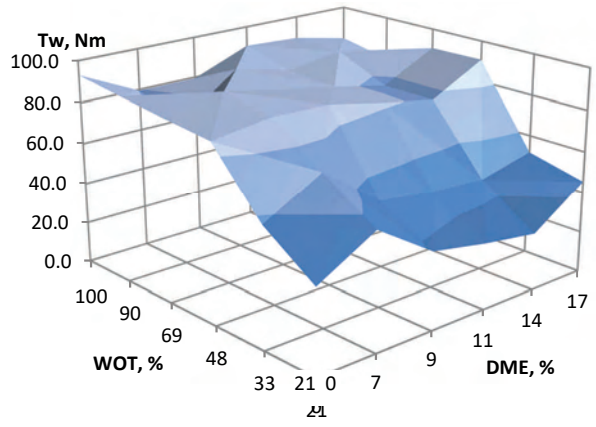


Fig. 10. The results of torque on wheel measured during experimental test; n = 2500 rpm

3.2. In-cylinder pressure and combustion process

The observed changes are apparently evident in the analysis of the phenomena occurring in the combustion chamber. In the graph showing the maximum values of the indicated pressure (Fig. 11), it can be seen that at the full engine load the highest pressure values were obtained with

DME = 9%. Increasing the share of DME reduces the value of obtained maximum pressure. On the other hand, with the reduction in engine load, the maximum pressure is observed for an ever greater share of DME.

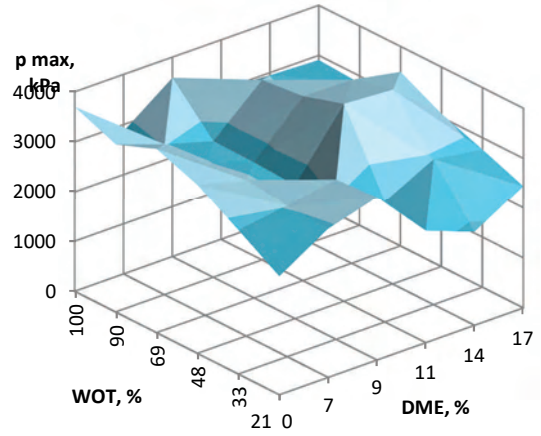


Fig. 11. Maximum in-cylinder pressure in depend of DME share & engine load, n = 2500 rpm

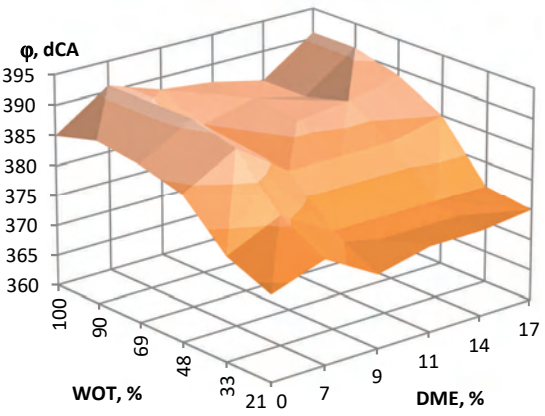


Fig. 12. A point of occurrence p_{max} in working cycle, n = 2500 rpm

Completion of this observation is a graph showing the angle of crank position, at which the maximum pressure is indicated (Fig. 12). The results presented on it, are information about the speed of the combustion process, among others. First of all, it is evident that a small DME addition exacerbates the course of the changes, which results in a deterioration of the engine performance parameters shown in the previous charts. In addition, there is also a delay in the occurrence of the maximum pressure point at full engine load and at several percent DME.

The following graphs (Fig. 13 and 14) show the angle of the crankshaft position corresponding to the characteristic points of the combustion process, 10 and 50% of the mass fraction burned MFB. In both cases, there is a strong relationship between the share of DME in the fuel and the rate of heat release. In the conditions which prevail in the combustion chamber at a load of 90-100%, only a small addition DME allows to keep appropriate combustion velocity. Increasing DME share over 11% slows down the process under these conditions. But with decreasing engine load moves this limit, making it possible to gradually increase the addition of DME. The load change is also associated with a change in the ignition advance angle. That was determined by the original driver.

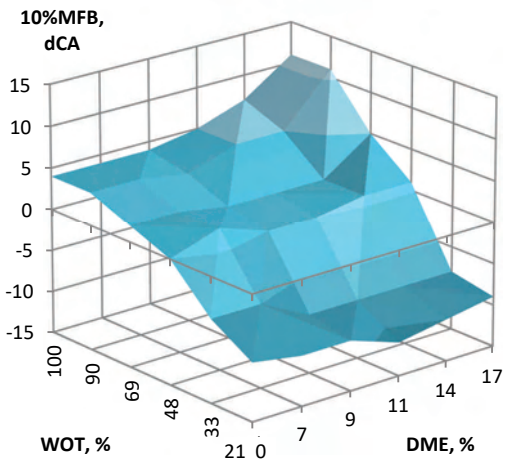


Fig. 13. A point of 10% MFB during combustion process, n = 2500 rpm

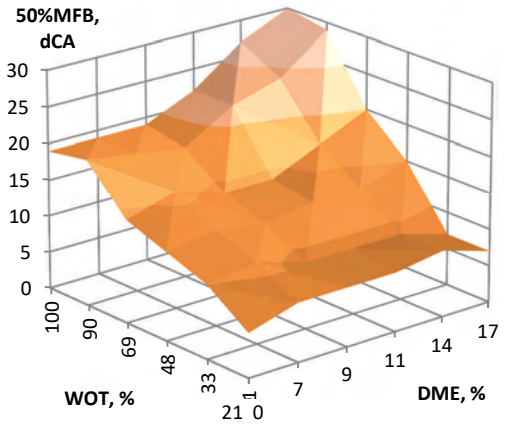


Fig. 14. A point of 50% MFB during combustion process, n = 2500 rpm

3.2. Temperature and exhaust gas component

The model simulation enabled the determination of temperature changes in the cylinder on the basis of experimental results. The results of the calculations are presented in graphs. Figure 15 shows the change in the maximum in-cylinder temperature, and Figure 16, the temperature of the exhaust gases leaving the combustion chamber. These parameters are presented in the function of the fuel composition and the load of tested engine.

In the graph of the maximum temperature can be observed that despite the drop in engine load, maximum temperature remained at a similar level to that part of the area where was tested the fuel with increased share of DME (over 11%). In contrast, the temperature of the exhaust gas leaving the combustion chamber (the exhaust valve opening) in this area of the graph is significantly lower. The reason for these changes can be good flammability of DME (high CN), which at partial load of the engine (30 to 60% WOT) can maintain the appropriate combustion velocity.

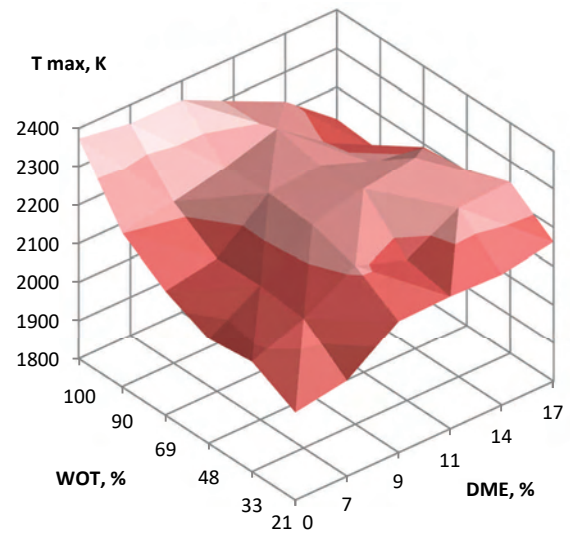


Fig. 15. Maximum in-cylinder temperature in depend of DME share & engine load, n = 2500 rpm

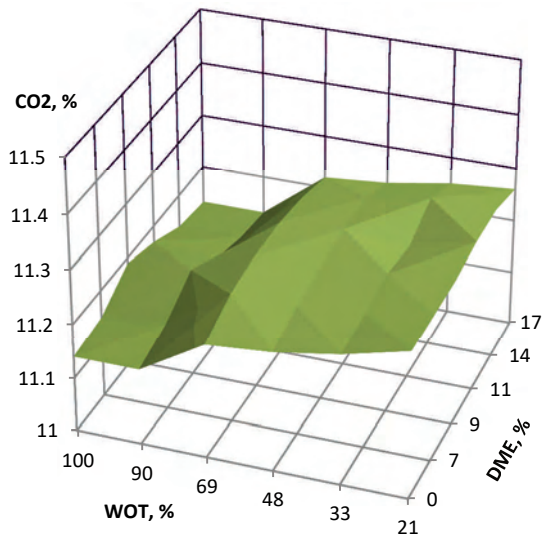


Fig. 17. An influence of DME share & engine load on emission CO_2, λ = 1.0, n = 2500 rpm

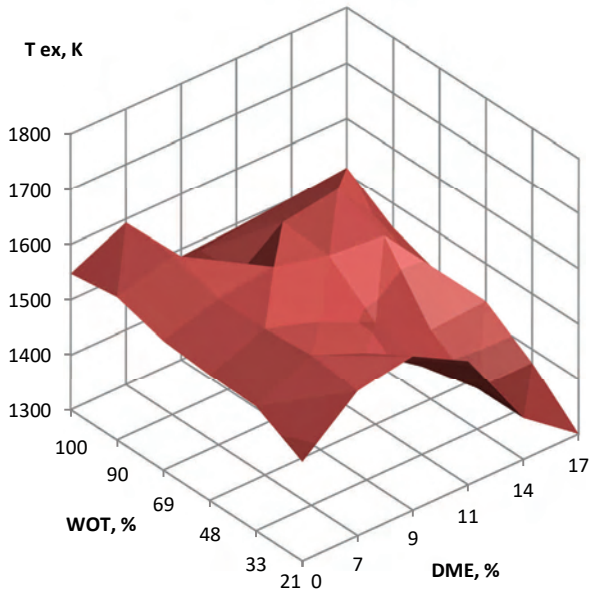


Fig. 16. An influence of DME share & engine load on temperature of raw exhaust gases, n = 2500 rpm

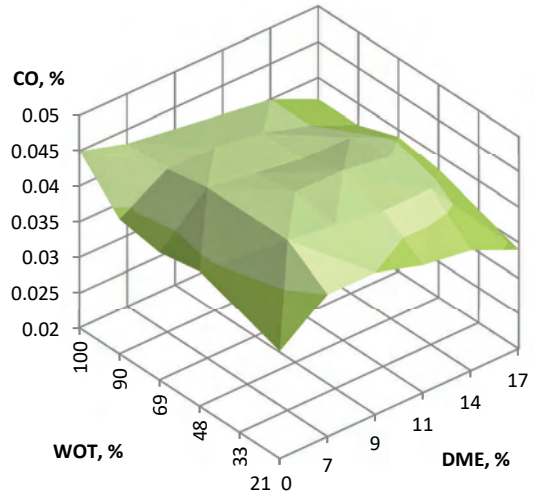


Fig. 18. An influence of DME share & engine load on emission CO, λ = 1.0, n = 2500 rpm

Another aspect of the analysis is the composition and emission of combustion products. The changes in the concentration of selected exhaust components are shown in the following graphs.

Emissions of carbon-containing compounds: CO_2 (Fig. 17) and CO (Fig. 18) are not subject to major changes. The influence of the type of fuel is not noticeable, because in the group of the studied fuels the total share of the C-component in the stoichiometric mixture is similar, from 2.83 to 2.86%. CO emissions are maintained at a constant level of 0.045–0.035%, indicating the correct course of the combustion process. The NO_x concentration (Fig. 19) decreases with the decrease in engine load.

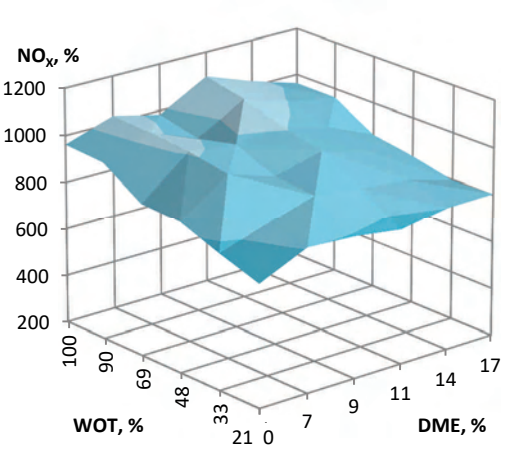
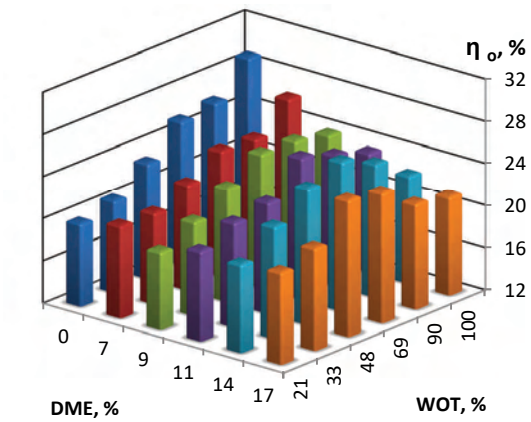


Fig. 19. An influence of DME share & engine load on emission NO_x, λ = 1.0, n = 2500 rpm



	100	90	69	48	33	21
0	29.07	26.1	25.65	22.95	20.7	19.8
7	26.28	23.76	23.94	22.05	20.61	20.7
9	23.94	24.66	24.75	22.77	20.88	19.35
11	23.31	24.39	25.47	22.5	21.87	20.52
14	22.23	24.66	26.19	24.93	22.59	20.34
17	21.33	21.96	24.3	24.93	21.69	20.7

Fig. 20. Efficiency of tested engine in depend of DME share & engine load, n = 2500 rpm

4. Conclusion

Based on the research and analyzes carried out, the following conclusions can be drawn:

1. DME (BioDME) can be used as a component of fuel blend with LPG in certain proportions, as it ensures maintenance of the engine performance level. Too high DME content causes changes in the combustion process, which leads to a deterioration of the energy conversion efficiency of the SI engine
2. At full engine load an additive of DME should be limited to approx. 10% (by weight). In the partial load range, of 50–70%, its share can be increased to about 17%.
3. The use of the DME additive does not increase the temperature and thermal stresses of the engine compared to feeding only with LPG. The presence of DME in the indicated amounts, does not adversely affect the emission of toxic exhaust gas components
4. Because of the general efficiency of the engine (Fig. 20), the range of partial loads is most advantageous because the highest values (LPG-like) are obtained there. This is the most common operating range of the engine.
5. The observed effect of DME share on the combustion velocity requires further investigation taking into account the ignition advance angle correction.

Nomenclature

CI compression ignition
CN cetane number
CNG compressed natural gas
DME dimethyl ether
LPG liquified petrolum gas
MFB mass fraction burned
SI spark ignition

Bibliography

[1] IDA Fact Sheet DME/LPG Blends 2010 v1.
[2] FLEKIEWICZ, M., KUBICA, G., FLEKIEWICZ, B. The analysis of energy conversion efficiency in SI engines for selected gaseous fuels. *SAE Technical Paper*. 2014, 2014-01-2692.
[3] FLEKIEWICZ, M., KUBICA, G., The effects of blending dimethyl ether with LPG on the engine operation and its efficiency. *Combustion Engines*. 2013, **154**(3), 86-95.
[4] KUBICA, G. Efektywność konwersji energii w silniku o zapłonie iskrowym zasilanym paliwami gazowymi o obniżonym udziale węgla. *Publishing House of the Institute for Sustainable Technologies-National Research Institute in Radom*. 2013.
[5] LEE, S., OH, S., CHOI, Y., KANG, K. Effect of n-butane and propane on performance and emission characteristics of an SI engine operated with DME-blended LPG fuel. Fuel. 2011, **90**, 1674-1680.
[6] NAKAZONO, T., RAIHAN, K.A., NISHIMURA, A. A study of application DME-LPG blended fuel to gas engine for micro cogeneration (2nd Report, Engine Control). *JSME*. 2010, **76/763**, 397-399.
[7] SORENSON, S.C. Dimethyl ether in diesel engines: Progress and perspectives. *J. Eng. Gas Turbines Power*. 2001, **123**(3), 652-658.
[8] WEIDOU, N., LIJAN, T., DEWEI, F. Rational cognition of DME market in China. *Proceedings of 3rd Asian DME conference*. 2006, 21-38.

Marek Flekiewicz, DEng. – Faculty of Transport at Silesian University of Technology.
e-mail: *Marek.Flekiewicz@polsl.pl*



Paweł Marzec, MEng. – Faculty of Transport at Silesian University of Technology.
e-mail: *Pawel.Marzec@polsl.pl*



Grzegorz Kubica, DSc., DEng. – Faculty of Transport at Silesian University of Technology.
e-mail: *Grzegorz.Kubica@polsl.pl*



Article citation info:
CHŁOPEK, Z., BIEDRZYCKI, J., LASOCKI, J. et al. Modelling of motor vehicle operation for the evaluation of pollutant emission and fuel consumption. *Combustion Engines*. 2017, **171**(4), 156-163. DOI: 10.19206/CE-2017-426

Zdzisław CHŁOPEK
Jacek BIEDRZYCKI
Jakub LASOCKI
Piotr WÓJCIK
Izabela SAMSON-BRĘK

CE-2017-426

Modelling of motor vehicle operation for the evaluation of pollutant emission and fuel consumption

A novel approach to modelling of motor vehicle operation by employing special test cycles threated as realizations of the stochastic process of vehicle velocity is presented. The families of test cycles were designed to simulate driving conditions in street congestion, urban, extra-urban, and high-speed traffic. The data necessary for the development of test cycles was obtained in the empirical investigations conducted in real road traffic. The recorded velocity time-histories were analysed in the time, frequency, and process value domains. Fragments of the velocity vs. time curves, representative for the considered driving conditions, were selected to design test cycles. The statistical examination of those test cycles demonstrated that individual process realizations are similar to each other and to all the process realizations recorded during the empirical tests.

Key words: *vehicle driving test cycles, pollutant emission, fuel consumption*

1. Introduction

To acquire knowledge of the operational properties of automotive engines, in particular their economic performance in terms of fuel consumption and their ecological characteristics related to pollutant emission, vehicle driving test cycles are designed for the simulation of actual vehicle drive conditions. This stems from the fact that for similar characteristics of the power transmission systems in motor vehicles designed for comparable applications (e.g. motor cars), the process that determines the state of operation of an internal combustion (IC) engine during vehicle drive is the vehicle velocity, while the engine operation state is the main factor the operational properties of IC engines depend upon. The IC engine operation state is characterized by the quantities that define the intensity of engine operation, the measure of which is the effective power, and by the thermal state of the engine. The thermal state of an IC engine is defined by the set of temperatures of engine parts and operating fluids (engine oil and coolant, in most cases). The intensity of engine operation is described by the rotational speed of the engine crankshaft and a quantity characterizing the engine load, predominantly torque or mean effective pressure [7].

The earliest vehicle driving test cycles were developed for the purposes of pollutant emission and fuel consumption evaluation within type-approval testing of motor cars and light trucks (delivery vehicles). It was natural then that the vehicle driving test cycles used in the procedures of type approval of motor cars, light trucks, motorcycles, and mopeds have become standards, chiefly in the EU, USA, and Japan [13]. However, there was a need to acquire knowledge of the properties of vehicles operated in conditions other than those adopted in the type-approval procedures. Therefore, vehicle driving test cycles were developed at many research centers to simulate vehicle drives in various traffic conditions, ranging from street congestions to motorway traffic.

For the purposes of determining pollutant emission characteristics in the INFRAS AG software [17], numerous test cycles were prepared, applicable to motor cars, light trucks, motorcycles, and mopeds, as well as to motor trucks and buses [6]. Works on the tests for the simulation of various conditions of vehicle drive were also carried out in connection with the works on the inventory of pollutant emission within the CORINAIR (Core Inventory of Air Emissions) program [14]. Within the implementation of the European Artemis program, a system of Common Artemis Driving Cycles has been prepared, which consists of test cycles that simulate motor car drives in various traffic conditions [1, 3]. Another example of the vehicle driving test cycles is the system of test cycles developed at a French institute INRETS (Institut National de Recherche sur les Transports et leur Sécurité, i.e. National Institute of Transport and Safety) [23].

Many attempts were also made to undertake research works on the conditions of motor vehicle drive. The problem of modelling the motor vehicle drive in street congestions has been considered in publications by Bando et al. [2], Barth, Scora, and Younglove [4], Treiber, Hennecke, and Helbing [29]. In publications by Gong et al. [15], Souffran, Miègeville, and Guérin [27] the use of Markov chains for modelling the motor vehicle drive has been presented. In the works described by Lyons et al. [20], Schwarz [26], Tong, Hung, and Cheung [28] characteristics of pollutant emission from IC engines in static states were used for the simulation of pollutant emission in the conditions of vehicle drive on fast traffic roads. Studies by Jacobs [16], Lee and Filipi [18], Lin and Niemeier [19], Miller [22] have been devoted to the methods of modelling motor vehicle drive with the use of the theory of stochastic processes.

A definite majority of the vehicle driving test cycles having been developed are causal (deterministic) time histories of vehicle velocity (i.e. when applied as a test input, they determine the quantities measured as the test output). Publication by Barlow et al. [3] contains a set of most of the cycles having been published, including a summary of their zero-dimensional characteristics (such as test time, distance travelled, average velocity, standard deviation of the velocity, etc.) that make it possible to make comparisons between the properties of individual test cycles.

The aim of this paper is to present an authorial concept of motor vehicle driving test cycles treated as a set of realizations of the stochastic process of vehicle velocity. Such an approach enables not only the investigation of motor vehicle properties in conditions simulating its operation in real road traffic but also the evaluation of the uncertainty of measurements carried out in random vehicle operation conditions [9]. The paper makes a substantial extension of the paper by Chłopek et al. [10] and widens the scope of the analysis, creating a more detailed picture of modelling of motor vehicle operation for the evaluation of pollutant emission and fuel consumption.

2. Design of driving test cycles

Several different methods can be adopted to design driving test cycles. They can be assigned into three general groups:

– methods based on the assumption of a predefined time history of the relative vehicle velocity, which refers to the maximum velocity;
– methods based on the principle of faithful time-domain simulation of the time history of the vehicle velocity;
– other methods, based on the analysis of the velocity process characteristics in other domains, such as time, frequency, or process values.

The criterion for assessing the adequacy of the driving cycles is the similarity between zero-dimensional characteristics of the velocity processes in the driving cycles and during actual vehicle operation [1, 7, 23]. Those characteristics may be determined in the domains of: time, independent variable of the integral transformation of a time history of the vehicle velocity (usually frequency), or process values [7]. The most commonly used zero-dimensional characteristics in the time domain are the following [5, 7, 24]: average value, root-mean-square (RMS) value, variance, standard deviation, median, extreme values, proportions (distribution) of values in specific intervals. In the frequency domain, the amplitude and phase characteristics are predominantly determined. Their values for specific frequencies of their averaged values for specific frequency intervals are taken as representative point characteristics [7]. In the domain of process values, the most important characteristic is the probability density function and its zero-dimensional characteristics. The latter include: average value, most probable value, variance, or parameters of the standard probability density functions that approximate the probability function under analysis, in accordance with the criterion adopted [7].

The design of the test cycles in accordance with the principle of faithful time-domain simulation of the time history of the vehicle velocity can be performed in two ways. The first is the selection of fragments of the velocity vs. time curves that are representative for the velocity process under analysis. The other is the synthesis of selected fragments, considered representative for the velocity process under analysis.

The method of designing vehicle driving test cycles by assuming a predefined time history of the relative vehicle velocity referred to the maximum vehicle velocity has been employed in the preparation of numerous test cycles. The examples are the European type-approval test NEDC (New European Driving Cycle), consisting of the UDC (Urban Driving Cycle) and EUDC (Extra Urban Driving Cycle), or the Japanese type-approval test Japan 10-15 Mode [13].

Many of the tests designed in accordance with the principle of faithful time-domain simulation of the time history of the vehicle velocity were built by synthesizing selected fragments of such a time history that are considered representative for the velocity process under analysis. Examples of the test cycles of this kind are those developed in the USA for the testing of both motor vehicles (such as FTP-75, i.e. Federal Test Procedure) and IC engines (such as HDDTC, i.e. Heavy Duty Diesel Transient Cycle) [13]. Similarly, motor vehicle test procedures have been developed in order to determine pollutant emission and fuel consumption characteristics, utilized then for the preparation of a database for the INFRAS AG software [17]. The methods of building such tests have been presented in publication of BUWAL and INFRAS [6]. To select the fragments that would be representative for the vehicle velocity process under analysis from the recorded velocity vs. time curves, the method of cluster analysis was used [30]. As the criteria for comparisons, more than ten zero-dimensional characteristics of the velocity process were adopted, including the average velocity value and the average value of the product of absolute values of vehicle velocity and acceleration. Then, the selected fragments, found to be representative for the vehicle velocity process under analysis, were used to compile vehicle driving test cycles, which would be consistent with the vehicle velocity processes under consideration in accordance with the comparison criteria adopted, with the use of the Monte Carlo method [8, 21]. Thus, vehicle driving test cycles were set up, which represented motor vehicle drives in various traffic conditions, including street congestions and motorway traffic, as well as the traffic in streets with specific vehicle traffic intensities, with or without traffic lights.

A novel approach to modelling of motor vehicle operation by employing special test cycles threated as realizations of the stochastic process of vehicle velocity was developed at Automotive Industry Institute (PIMOT). Families of vehicle driving test cycles have been prepared within research project [10], to simulate the conditions of motor car drives in street congestion, urban, extra-urban, and high-speed (motorway and expressway) traffic.

3. Materials and methods

The data necessary for the preparation of the vehicle driving test cycles was obtained in empirical investigation conducted in real road traffic with the use of Honda Civic passenger car (Fig. 1). It was manufactured in 2000 and provided with a four-cylinder in-line spark-ignition engine of 1400 cm^3 capacity, meeting the requirements of the Euro 3 exhaust emission standard.



Fig. 1. Vehicle used in the empirical investigation

The empirical investigation included real-time measurements and recording of vehicle velocity, engine speed, engine steering, and vehicle location, with 10 Hz sampling frequency. The signals were recorded from On-Board Diagnostics system (OBD II) of the car, using OBD II reader Automex AMX530, and by GPS positioning device Racelogic Performance Box. For further processing of the signals obtained, the Golay-Savitzky smoothing filter [25] was adopted, with approximation to a polynomial of degree 2 for nine measuring points.

The vehicle operation was modelled to represent four categories of driving conditions:

– urban traffic congestions (denoted as CT),
– urban traffic (without congestions) (denoted as UT),
– extra-urban traffic (denoted as RT),
– high-speed (motorway and expressway) traffic (denoted as HT).

Vehicle velocity samples collected in empirical investigation were divided into those four categories, giving sets of the following cardinality: 19, 34, 16, and 8, respectively.

For each category of vehicle operation four driving test cycles were designed, in accordance with the criterion of faithful time-domain simulation. With this objective in view, the fragments of the velocity vs. time curves recorded during vehicle drives in real road traffic were chosen for which the values of the selected characteristics were close to the values of the characteristics corresponding to all the sets. As the top priority criterion, the average value was taken. The next criterion in was the standard deviation.

The designed driving test cycles were further analyzed in the time domain, frequency domain, and process value domain, with determining, *inter alia*, extreme values, average value, variance, median, and quartile deviation [5, 24]. The power spectral density of vehicle velocity vs. frequency curve was also plotted.

4. Driving test cycles designed at Automotive Industry Institute

The time histories of the vehicle velocity for individual vehicle operation models (CT, UT, RT, and HT) is presented in Figure 2. They are treated as realizations of stochastic processes of velocity for the said models.

The properties of the designed driving test cycles, representing vehicle operation models, are summarized in Table 1, showing selected zero-dimensional characteristics of the vehicle velocity process, i.e. average value and extreme values of the vehicle velocity.

The driving cycles for each vehicle operation model have close values of the considered zero-dimensional characteristics (Ch): maximum value (MAX), average value (AV), median (M), standard deviation (D), and quartile deviation (DQ). Figure 3 shows a comparison of those characteristics for individual driving test cycles (CT1–4, UT1–4, RT1–4, and HT1–4), for four test cycles of the same category (CT_{AV}, UT_{AV}, RT_{AV}, and HT_{AV}), and for all velocity samples collected in empirical investigation in real road traffic of the same category (AS_{AV}).

It can be clearly seen that the characteristics under assessment are similar to each other. With respect to the assessment criteria adopted, a significant similarity exists between the average values as well as the standard deviation values. The median and quartile deviation values are also close in individual tests, which is of considerable importance because the distributions of the processes under investigation are markedly asymmetric. Minor differences occur only in the case of the maximum value of the velocity. However, taking into account the randomness of the velocity processes, the maximum value for the whole set may be randomly high.

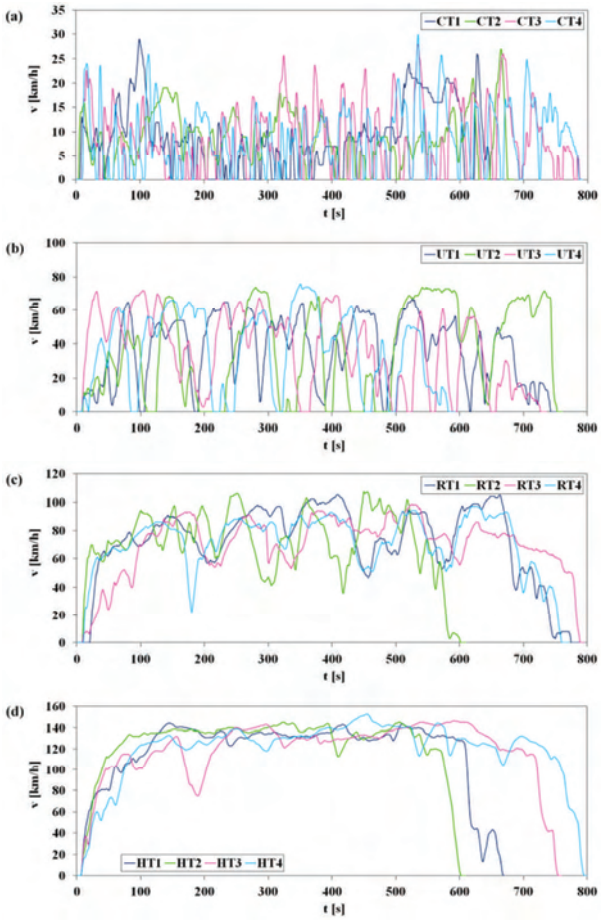


Fig. 2. Realizations of the vehicle velocity vs. time process for: a) urban traffic congestions (CT); b) urban traffic (UT); c) extra-urban traffic (RT); d) high-speed traffic (HT)

Further analysis of the vehicle velocity processes indicated certain diversity of the conditions of vehicle motion in individual driving cycles. It was based on the comparison between the coefficient of variation (CV) and the coefficient of interquartile range (CIQR, see (1)) determined for individual driving test cycles, for four test cycles of the same category, and for all the velocity samples collected in empirical investigation in real road traffic of the same category. The results of the analysis is shown in Figure 4.

$$\mathrm{CIQR} = \frac{\mathrm{DQ}}{\mathrm{M}} \tag{1}$$

As it was in the case of the results of examination of the maximum value, average value, median, standard deviation, and quartile deviation, a significant similarity was found to exist between the results of examination of the relative coefficients of variation and interquartile range.

Table 1. Summary of basic characteristics of the designed vehicle driving test cycles

Vehicle operation model	Test realization symbol	Distance travelled during the test [km]	Test duration time [s]	Share of time when vehicle velocity equals 0 [%]	Average vehicle velocity in the test [km/h]	Minimum vehicle velocity in the test [km/h]	Maximum vehicle velocity in the test [km/h]
Urban traffic congestions (CT)	CT1	1.583	662	20	8.59	0	29.0
	CT2	1.620	684	13	8.51	0	27.0
	CT3	1.881	792	21	8.54	0	28.0
	CT4	1.862	792	19	8.45	0	29.9
Urban traffic (UT)	UT1	7.528	751	5	36.04	0	67.0
	UT2	7.621	761	19	36.00	0	74.0
	UT3	7.366	736	9	35.98	0	72.0
	UT4	5.943	593	14	36.02	0	75.9
Extra-urban traffic (RT)	RT1	15.640	795	5	70.73	0	105.0
	RT2	11.981	610	3	70.59	0	107.3
	RT3	15.383	795	2	69.57	0	98.6
	RT4	15.172	772	3	70.66	0	97.0
High-speed traffic (HT)	HT1	21.745	672	2	116.32	0	144.0
	HT2	20.900	609	2	123.34	0	145.2
	HT3	24.865	760	2	117.63	0	146.4
	HT4	26.291	800	2	118.16	0	152.9

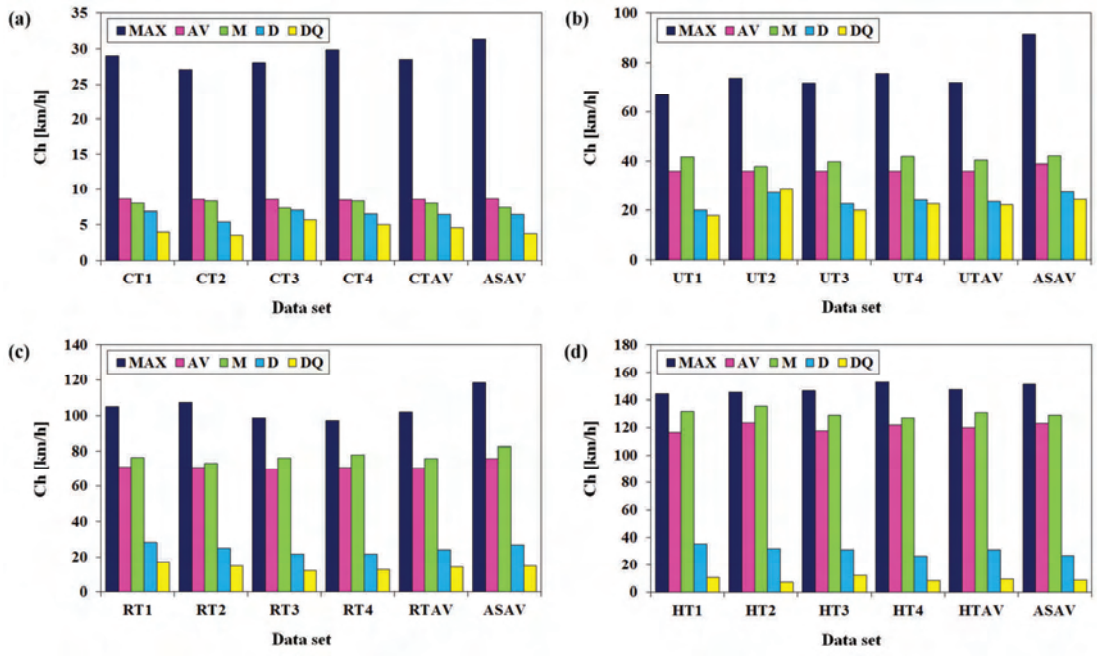


Fig. 3. Characteristics of the velocity process realizations in individual driving cycles, in sets of four cycles of the same category, and in all the velocity samples collected: a) urban traffic congestions (CT); b) urban traffic (UT); c) extra-urban traffic (RT); d) high-speed traffic (HT)

Figure 5 shows results of the analysis of vehicle driving test cycles at individual vehicle drive modes in the frequency domain. The analysis was carried out on standardized process values [5]. The standardized power spectral density was estimated with the use of the fast Fourier transform method. To improve the consistency of the power spectral density estimator, the Hamming window [5, 31] and frequency smoothing [5] techniques were applied in the data processing.

A comparison between individual vehicle driving test cycles in the frequency domain for all the vehicle drive conditions being modelled is presented in Figure 6. An analysis of the frequency characteristics of the vehicle velocity processes confirms that the vehicle operation conditions are most dynamic in the case of urban traffic congestions and the least dynamic in the case of high-speed traffic. According to this criterion, urban traffic without congestions and extra-urban traffic fall somewhere in between. It should be noted that high uniformity of the curves plotted for extra-urban traffic can be observed, in contrast to the curves plotted for high-speed traffic, which power spectral density is clearly divided into two ranges, especially for large frequency values.

The test analyses in the process value domain have been illustrated by investigations on the distribution of probability of the vehicle velocity. Figure 7 shows the discrete probability density (g[v]) of vehicle velocity (v) in the individual driving test cycles for four categories of driving conditions.

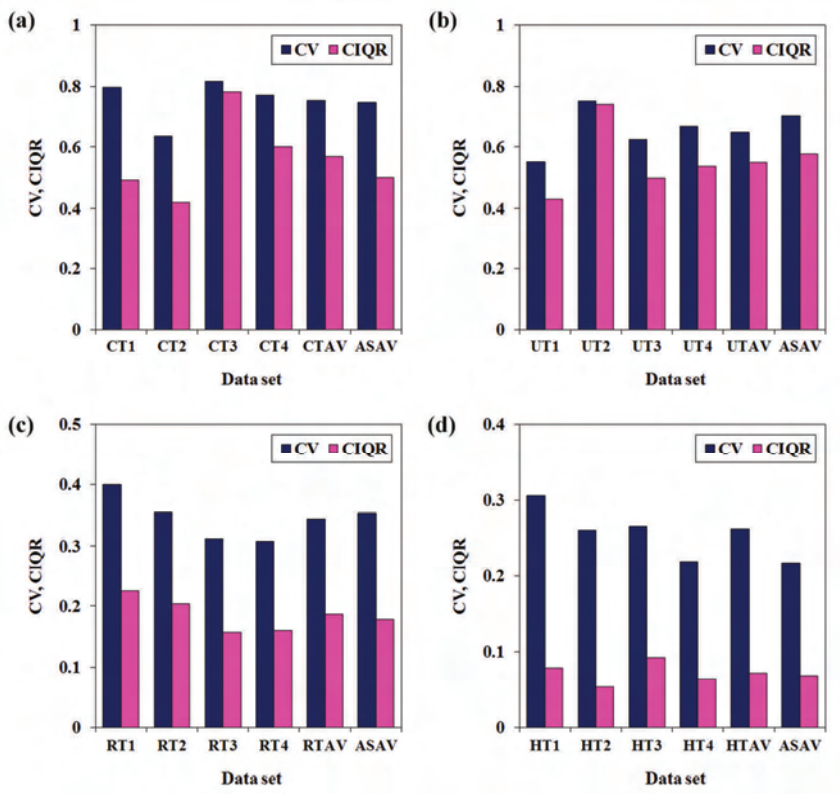


Fig. 4. Coefficient of variation (CV) and the coefficient of interquartile range (CIQR) for the velocity process realizations in individual driving test cycles, in sets of four test cycles of the same category, and in all the velocity samples collected: a) urban traffic congestions (CT); b) urban traffic (UT); c) extra-urban traffic (RT); d) high-speed traffic (HT)

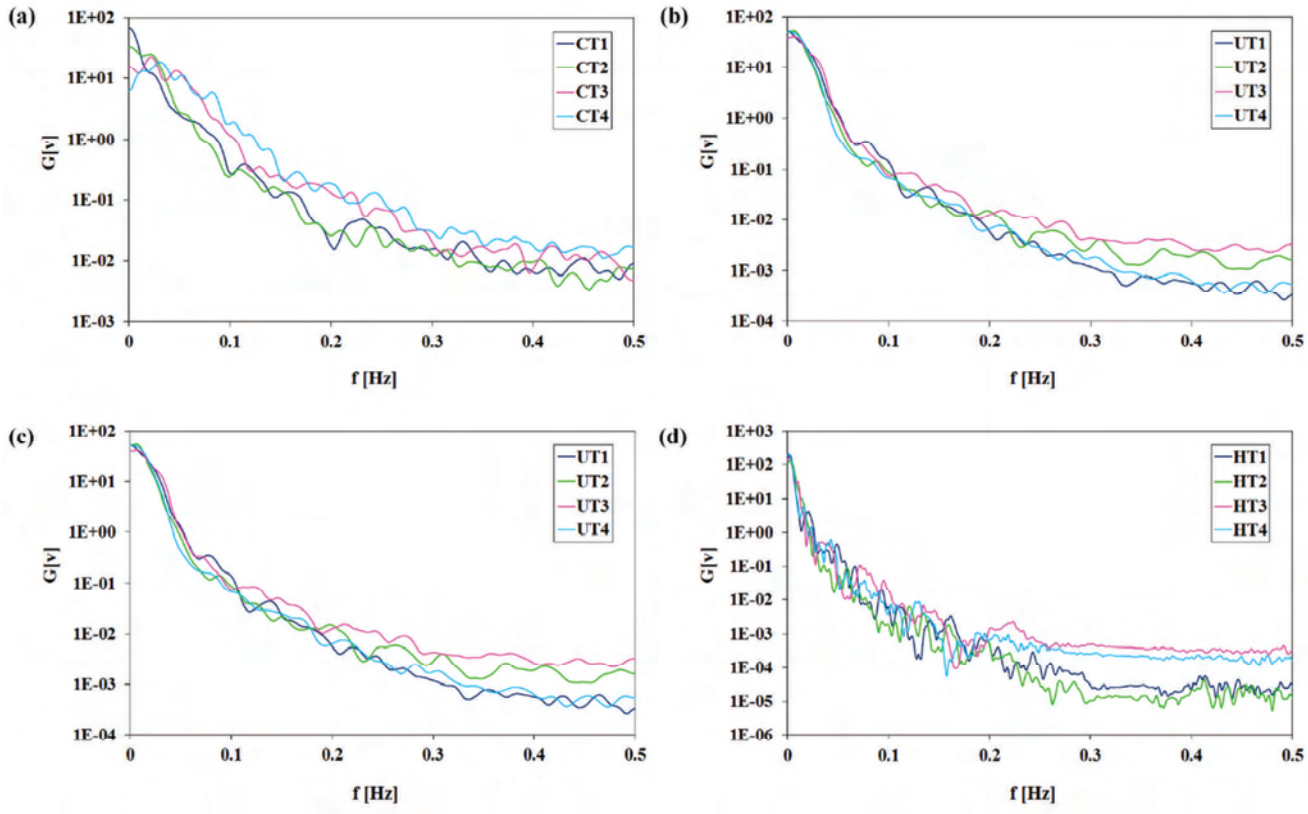


Fig. 5. The power spectral density of standardized velocity (G[v]) in the frequency domain (f) in the vehicle driving test cycles for: a) urban traffic congestions (CT); b) urban traffic (UT); c) extra-urban traffic (RT); d) high-speed traffic (HT)

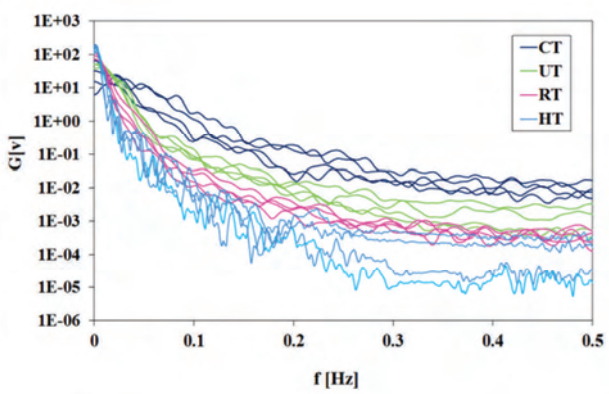


Fig. 6. Comparison between the curves representing the power spectral density of standardized velocity (G[v]) in the frequency domain (f) for all the vehicle operation conditions being modelled

The results of examination of the developed driving cycles in the process value domain confirm a significant similarity to exist between the properties of individual realizations of the tests. In spite of differences in the values of probability density in individual test realizations, the characteristics having been determined are similar to each other to a considerable degree.

An analysis of properties of the special vehicle driving test cycles developed has provided grounds for a statement that the tests for a specific vehicle drive model correspond to vehicle drives in comparable vehicle operation conditions. Simultaneously, and in accordance with expectations, substantial differences exist between tests representing different vehicle drive modes. In respect of the average value and the maximum value of vehicle velocity, the vehicle drive models may be arranged as follows, in a growing order of the said values: street congestions, urban traffic, extra-urban traffic, and high-speed traffic. Apart from that, an analysis of the frequency characteristics of the vehicle velocity processes confirms that the vehicle drive properties are most dynamic in the case of drives in street congestions. The second most dynamic vehicle drive properties occur when the vehicle is driven in urban traffic. In the third and fourth positions in this ranking, the extra-urban traffic and high-speed traffic should be mentioned, respectively.

An important unique feature of the method of designing vehicle driving test cycles as proposed herein is the treatment of such tests as realizations of stochastic processes, thanks to which conclusions can be drawn about the sensitivity of functional properties of internal combustion engines not only to dynamic but also to random conditions of engine operation.

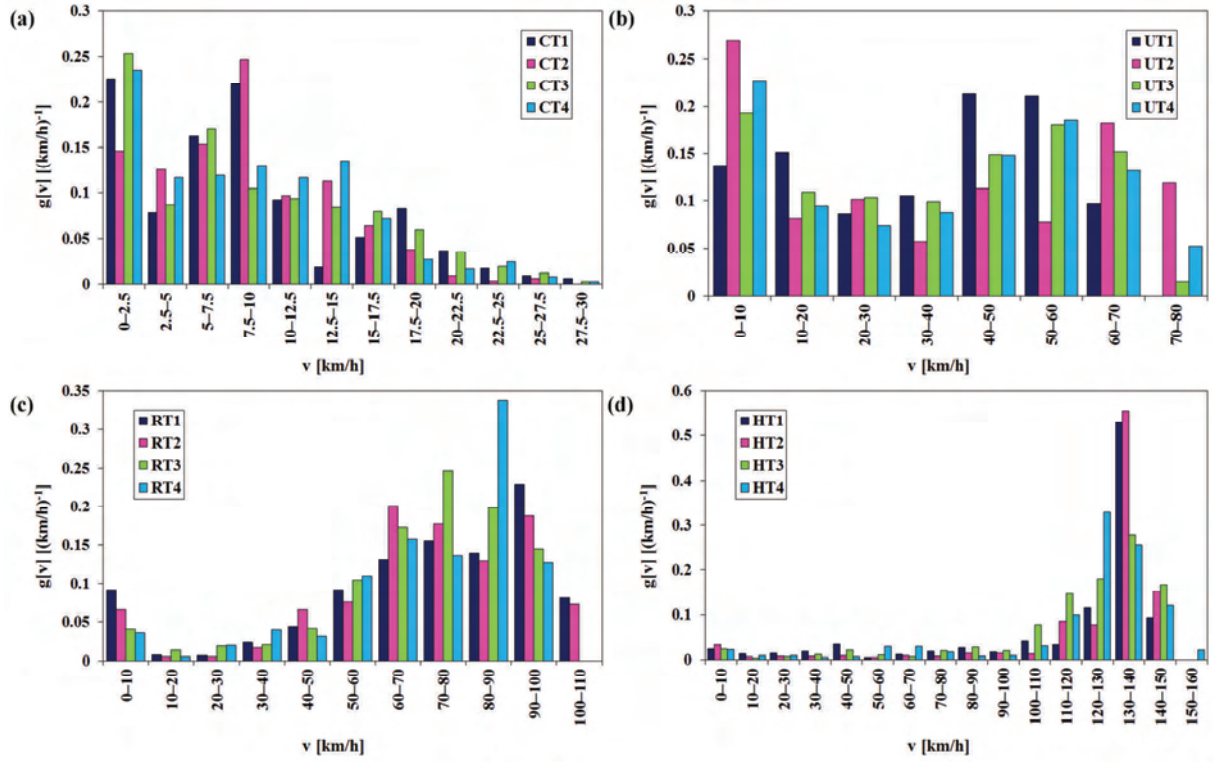


Fig. 7. Comparison between the discrete probability density (g[v]) of vehicle velocity (v) in the vehicle driving test cycles for: a) urban traffic congestions (CT); b) urban traffic (UT); c) extra-urban traffic (RT); d) high-speed traffic (HT)

5. Conclusions

The examination of motor vehicles by subjecting them to vehicle driving test cycles is the basic method of acquiring knowledge of the vehicle properties in conditions corresponding to the real vehicle operation. The examination of motor vehicles in vehicle driving test cycles is chiefly aimed at the evaluation of ecological vehicles' properties related to pollutant emission and their economic performance in terms of fuel consumption. Therefore, numerous works are undertaken on tests simulating various conditions of operation of motor vehicles, especially motor cars and light trucks, but also heavier trucks and buses [6]. Some of

such tests have been given the status of criteria of evaluation of pollutant emission and fuel consumption in type-approval procedures [13].

An overwhelming majority of the vehicle driving test cycles having been developed at numerous research and development centres have a causal (deterministic) nature (i.e. when applied as a test input, they determine the quantities measured as the test output). In this study, a concept has been presented where vehicle driving test cycles are treated as a set of realizations of stochastic processes, corresponding to motor car drives in the conditions of street congestions, urban traffic without congestions, extra-urban traffic, and high-speed (motorway and expressway) traffic. The tests have been prepared in the form of vehicle velocity process realizations, generated as faithful time-domain simulations with the use of results of empirical vehicle velocity measurements, recorded during typical vehicle operation. As the basic similarity criteria to be taken into account at the preparation of process realizations, the average value and standard deviation of vehicle velocity have been adopted.

The examination of the tests prepared, carried out in the time, frequency, and process value domains, has confirmed that individual process realizations are similar to each other and to all the process realizations recorded during the empirical tests.

The examination of motor vehicles with the use of vehicle driving test cycles treated as stochastic processes represented by process realizations provides a possibility of significant widening of the scope of the knowledge thus acquired, especially by enabling the evaluation of the uncertainty of results of measurements carried out in random vehicle drive conditions typical for the simulated vehicle operation mode. Example results of such investigations have been published [11, 12].

Acknowledgements

This paper is based on results of tests carried out within research grant No. N N509556440 entitled 'Sensitivity of pollutant emission and fuel consumption to the conditions of operation of a spark-ignition engine', sponsored by the National Science Centre of Poland.

Nomenclature

AV	average value
BUWAL	Bundesamt für Umwelt, Wald und Landschaft
Ch	zero-dimensional characteristic
CIQR	coefficient of inter-quartile range
CORINAIR	Core Inventory of Air Emissions
CT	urban traffic congestions
CV	coefficient of variation
D	standard deviation
DQ	quartile deviation
EUDC	extra urban driving cycle
FTP-75	federal test procedure
HDDTC	heavy duty diesel transient cycle
HT	high-speed traffic
IC	internal combustion
INFRAS	Infrastruktur- Umwelt- und Wirtschaftsberatung
INRETS	Institut National de Recherche sur les Transports et leur Sécurité
M	median
MAX	maximum value
NEDC	New European Driving Cycle
OBD II	on-board diagnostics system, II generation
PIMOT	Przemysłowy Instytut Motoryzacji (Automotive Industry Institute)
RT	extra-urban (rural) traffic
UDC	urban driving cycle
UT	urban traffic (without congestions)

Bibliography

[1] ANDRÉ, M. The ARTEMIS European driving cycles for measuring car pollutant emissions. *Science of the Total Environment*. 2004, **334-335**, 73-84.

[2] BANDO, M., HASEBE, K., NAKAYAMA, A. et al. Dynamical model of traffic congestion and numerical simulation. *Physical Review E*. 1995, **51**(2), 1035-1042.

[3] BARLOW, T.J., LATHAM, S., MCCRAE, I.S., BOUTLER, P.G. *A reference book of driving cycles for use in the measurement of road vehicle emission: version 3*. TRL, United Kingdom 2009.

[4] BARTH, M., SCORA, G., YOUNGLOVE, T. Estimating emissions and fuel consumption for different levels of freeway congestion. *Transportation Research Record: Journal of the Transportation Research Board*. 1999, **1664**, 47-57.

[5] BENDAT, J.S., PIERSOL, A.G. Random data: analysis & measurement procedures. *Wiley*, New York 1966.

[6] BUWAL, INFRAS. *Luftschadstoffemissionen des Strassenverkehrs 1950-2010*: BUWAL-Bericht Nr. 255. BUWAL, Bern 1995.

[7] CHŁOPEK, Z. Modelling of exhaust emission processes in the conditions of operation of combustion engines in mobile applications. *Publishing House of the Warsaw University of Technology*. Warszawa 1999.

[8] CHŁOPEK, Z. The cognitive interpretation of the Monte Carlo method for the technical applications. *Eksploatacja i Niezawodnosc – Maintenance and Reliability*. 2009, **43**(3), 38-46.

[9] CHŁOPEK, Z. The research of the probabilistic characteristics of exhaust emissions from vehicle engines. *Combustion Engines*. 2011, **144**(1), 49-56.

[10] CHŁOPEK, Z., BIEDRZYCKI, J., LASOCKI, J., WÓJCIK, P. Investigation of the motion of motor vehicles in Polish conditions. *The Archives of Automotive Engineering – – Archiwum Motoryzacji*. 2013, **60**(2), 3-20.

[11] CHŁOPEK, Z., BIEDRZYCKI, J., LASOCKI, J., WÓJCIK, P. Investigation of pollutant emissions from a motor vehicle engine in tests simulating real vehicle use in road traffic conditions. *Combustion Engines*. 2013, **154**(3), 202-207.

[12] CHŁOPEK, Z., BIEDRZYCKI, J., LASOCKI, J., WÓJCIK, P. Pollutant emissions from combustion engine of motor vehicle tested in driving cycles simulating real-world driving

conditions. *Proceedings of the Institute of Vehicles*. 2013 **92**(1), 65-74.
[13] DELPHI. 2016/2017 Worldwide Emission Standards: Passenger Cars and Light Duty. 2016.
[14] EEA. EMEP/CORINAIR Emission Inventory Guidebook – 2007.
[15] GONG, Q., MIDLAM-MOHLER, S., MARANO, V., RIZZONI, G. An iterative markov chain approach for generating vehicle driving cycles. *SAE International Journal of Engines*. 2011, **4**(1), 1035-1045.
[16] JACOBS, P.A. A random measure model for the emission of pollutants by vehicles on a highway. *Stochastic Processes and their Applications*. 1974, **2**(2), 163-176.
[17] KELLER, M., WÜTHRICH, P. Handbook emission factors for road transport 3.1/3.2: Quick Reference. *INFRAS AG*, Bern 2014.
[18] LEE, T.-K., FILIPI, Z.S. Synthesis of real-world driving cycles using stochastic process and statistical methodology. *International Journal of Vehicle Design*. 2011, **57**(1), 17-36.
[19] LIN, J., NIEMEIER, D.A. An exploratory analysis comparing a stochastic driving cycle to California's regulatory cycle. *Atmospheric Environment*. 2002, **36**(38), 5759-5770.
[20] LYONS, T.J., KENWORTHY, J.R., AUSTIN, P.I., NEWMAN, P.W.G. The development of a driving cycle for fuel consumption and emissions evaluation. *Transportation Research Part A: General*. 1986, **20**(6), 447-462.
[21] METROPOLIS, N., ULAM, S. The Monte Carlo method. *Journal of the American Statistical Association*. 1949, **247**(44), 335-341.
[22] MILLER, A.J. Road traffic flow considered as a stochastic process. *Mathematical Proceedings of the Cambridge Philosophical Society*. 1962, **58**(2), 312-325.
[23] NOLLET, V., SCHADKOWSKI, C., HUE, S. et al. Elaboration d'un cadastre d'émissions de polluants primaires dans la region Nord-Pas-de-Calais: Les transports automobiles. *Pollution atmosphérique*. 2000, **165**, 109-119.
[24] PAPOULIS, A., PILLAI, S.U. Probability, random variables and stochastic processes. *McGraw-Hill*, New York 2002.
[25] SAVITZKY, A., GOLAY, M.J.E. Smoothing and differentiation of data by simplified least squares procedures. *Analytical Chemistry*. 1964, **36**(8), 1627-1639.
[26] SCHWARZ, W. Consistent engine and vehicle modeling for real life fuel consumption and emission predictions. Paper presented at the AVL Sweden Seminar, Göteborg, November 7th 2012.
[27] SOUFFRAN, G., MIÈGEVILLE, L., GUÉRIN, P. Simulation of real-world vehicle missions using a stochastic Markov model for optimal design purposes. *IEEE Transactions on Vehicular Technology*. 2011, **61**(8), 1-6.
[28] TONG, H.Y., HUNG, W.T., CHEUNG, C.S. Development of a driving cycle for Hong Kong. *Atmospheric Environment*. 1999, **33**(15), 2323-2335.
[29] TREIBER, M., HENNECKE, A., HELBING, D. Congested traffic states in empirical observations and microscopic simulations. *Physical Review E*. 2000, **62**, 1805-824.
[30] TRYON, R.C. Cluster analysis: correlation profile and orthometric (factor) analysis for the isolation of unities in mind and personality. *Edwards Brothers*, Ann Arbor 1939.
[31] TUKEY, J.W. An introduction to the calculations of numerical spectrum analysis. In: Spectral Analysis of Time Series, edited by B. Harris, 25-46. *Wiley*, New York 1967.

Prof. Zdzisław Chłopek, DSc., DEng. – Automotive Industry Institute in Warsaw.

e-mail: *Zdzislaw.Chlopek@pimot.eu*



Jacek Biedrzycki, MEng. – Engine and Chassis Laboratory at Automotive Industry Institute in Warsaw.

e-mail: *J.Biedrzycki@pimot.eu*



Jakub Lasocki, DEng. – Faculty of Automotive and Construction Machinery Engineering at Warsaw University of Technology.

e-mail: *J.Lasocki@simr.pw.edu.pl*



Piotr Wójcik, MEng. – Engine and Chassis Laboratory at Automotive Industry Institute in Warsaw.

e-mail: *P.Wojcik@pimot.eu*



Izabela Samson-Bręk, MEng. – Liquid Fuels and Bio-economy Department at Automotive Industry Institute in Warsaw.

e-mail: *I.Samson@pimot.eu*



Article citation info:
KOLODZIEJ, C., WALLNER, T. Combustion characteristics of various fuels during research octane number testing on an instrumented CFR F1/F2 engine. *Combustion Engines*. 2017, **171**(4), 164-169. DOI: 10.19206/CE-2017-427

Christopher P. KOLODZIEJ
Thomas WALLNER

CE-2017-427

Combustion characteristics of various fuels during research octane number testing on an instrumented CFR F1/F2 engine

The Cooperative Fuels Research (CFR) engine is the long-established standard for characterization of fuel knock resistance in spark-ignition internal combustion engines. Despite its measurements of RON and MON being widely used, there is little understanding of what governs the CFR octane rating for fuels of various chemical compositions compared to primary reference fuels (iso-octane and n-heptane). Detailed combustion characteristics were measured on a highly instrumented CFR F1/F2 engine during RON testing of fuels with significantly different chemical composition. The results revealed differences in the cylinder pressure and temperature conditions, as well as knocking characteristics.

Key words: *octane, gasoline, fuel, auto-ignition, knock*

1. Introduction

The Waukesha CFR F1/F2 octane rating engine is the international testing standard for measuring fuel octane number. Two octane rating methods are commonly used for automotive spark-ignition engine fuels, namely the research method and motor method (ASTM D2699 and ASTM D2700, respectively) [1, 2]. Research octane number (RON) is the test measurement most commonly reported in the sale of automotive gasolines around the world, although most countries also regulate a minimum motor octane number (MON). In North America, gasoline fuels are marketed and sold based on the average of the RON and MON, giving rise to the terms pump octane number (PON) or anti-knock index (AKI), as seen in Equation 1.

$$AKI = (RON + MON) / 2 \quad (1)$$

The engine operating conditions of these two ASTM test methods can be found in Table 1.

Table 1. Engine operating conditions of RON and MON tests [1, 2]

Test	RON	MON
ASTM method	D2699	D2700
Engine speed (rpm)	600	900
Intake air temperature (°C)	Based on barometric pressure	38
Mixture temperature (°C)	Not controlled	149
Spark timing (°aTDC)	–13	Based on compression ratio
Coolant temperature (°C)	100	100

Initially the MON condition, with higher mixture temperature entering the engine and higher engine speed, was designed to be more representative of "higher severity" engine operation when compared to early vehicle road octane number testing. However, with the current trend of engine down-sizing and boosting, the cylinder pressures and temperatures common of modern turbocharged gasoline direct injection (GDI) engines are more similar to, if not beyond, the relatively lower temperature and higher pressure RON conditions [3, 4]. For this reason, and because of its more widely accepted use, the current study will focus on the cylinder combustion and engine operation conditions of the RON test method (ASTM D2699).

2. Experimental setup

2.1. Argonne CFR F1/F2 engine

In this work, several gasoline-like fuel blends were tested under the standard ASTM D2699 RON method test conditions on a Waukesha CFR F1/F2 octane rating engine. The RON method engine operating conditions were shown in Table 1 and the geometry of this engine can be found in Table 2.

Table 2. Waukesha CFR F1/F2 engine geometry

Combustion chamber	Cast iron, flat "pancake"
Compression ratio (-)	Adjustable 4:1 – 18:1
Bore x Stroke (inches)	3.25 x 4.5
Displacement (inch^3)	37.33
Intake valve	180° shroud, no rotation
Exhaust valve	No shroud, rotating
Valve overlap	Positive 5 CAD
Piston rings	Top: Chrome-plated, straight-sided Middle (3): Ferrous, straight-sided Oil (1): Cast iron, one-piece, slotted
Fuel system	Carbureted, adjustable level float chamber A/F control
Ignition	Capacitive discharge coil to spark

The typical CFR engine setup consists of several engine controls and basically two measurements: carburetor sight glass fuel level and knockmeter knock units. These controls and measurements can be seen in Table 3.

Table 3. Waukesha CFR F1/F2 engine controls and measurements

Controls	
Engine speed	Pulley drive ratio
Intake air rel. humidity	Refrigerated intake air conditioner
Intake air temperature	Air heater upstream of carburetor
Mixture temperature (MON only)	Mixture heater downstream of carburetor
Compression ratio	Worm gear around cylinder to adjust cylinder head height
Spark timing	Mechanically adjusted
Air-fuel ratio	Carburetor bowl height
Measurements	
Relative air-fuel ratio	Sight glass fuel level
Relative knock	Knockmeter system knock units (KU)

As shown in Table 3, the measurements obtained from standard ASTM RON (or MON) testing is limited to a

relative air-fuel ratio (dependent on carburetor jet sizes) and a relative measurement of combustion knock (measurement scale is tuned based on ±1 octane number of the test fuel). In order to get more detailed and absolute measurements of engine combustion characteristics and operating conditions, several instrumentation upgrades common for modern engine combustion research have been add to the CFR engine at Argonne National Laboratory. Important to note is that all of these measurement upgrades have taken place without affecting the geometry or performance of the CFR engine during standard octane testing. A list of the upgraded measurements and instrumentation are provided in Table 4.

Table 4. Modern engine combustion research measurement and instrumentation upgrades to the Argonne CFR F1/F2 engine

Crankshaft angle-based measurements	
Crank-angle based DAQ	AVL IndiCom & crankshaft encoder
Spark timing	Coil wire current clamp
Intake pressure	Kulite high-speed 2.0 bara pressure transducer
Exhaust pressure	Kulite water-cooled high-speed 3.5 bara pressure transducer
Cylinder pressure	Spark plug pressure transducer
Time-based measurements	
Time-based DAQ	LabVIEW
Intake pressure	Low-speed pressure transducer
Exhaust pressure	Low-speed pressure transducer
Intake, mixture, exhaust, coolant, and oil temperature	K-type thermocouples
Fuel rate	Coriolis meter
Lambda	Wide-band exhaust lambda sensor
Emissions	AVL SESAM FT-IR AVL i60 emissions bench
ASTM knock units	Data-logged knockmeter signal

To measure absolute air-fuel ratio, a wide-band lambda sensor was installed in the standard ASTM exhaust line between the exhaust port and the exhaust surge tank. In conjunction with the Coriolis fuel rate meter or emissions measurements, an air flow rate can be estimated. The lambda sensor will also be used to analyze the knockmeter response to lambda changes above and below that of peak knock. In addition to the ASTM knockmeter, which is a relative measurement based on the knocking characteristics of primary reference fuels (PRF) within one octane number of the test fuel, it is possible to measure absolute characteristics of the knocking combustion using a cylinder pressure transducer. While the spark plug pressure transducer is not as accurate of ringing combustion, it allows for some general analyses of the cylinder pressure and combustion characteristics between fuels while still measuring with the ASTM standard knockmeter simultaneously. In this paper, measurements and analyses will be discussed from the wide-band lambda sensor, Coriolis fuel rate meter, ASTM knockmeter, and simultaneously with the spark plug cylinder pressure transducer.

2.2. Test fuels

In this work, four fuels all having approximately 98 RON have been analyzed during standard RON test conditions. Two fuels are mostly iso-paraffinic with no ethanol. The "PRF98" fuel is simply a primary reference fuel (PRF) of 98%v iso-octane and 2%v n-heptane, while the "RON98Alk" fuel is an alkylate gasoline of approximately 75%v iso-octane, 20%v other iso-paraffins, 3%v n-butane, and a mixture of other families of hydrocarbons at lower concentrations. Two fuels were also tested with 30%v ethanol (E30). The "PRF71E30" fuel is composed of 70%v PRF 71 (71% iso-octane, 29% n-heptane) and 30%v ethanol, while the "RON98E30" is a 30%v ethanol full-boiling range gasoline containing paraffins (12.9%v), iso-paraffins (27.6%v), aromatics (13.8%v), naphthenes (7%v), and olefins (5.6%v). In this way, two non-ethanol highly iso-paraffinic fuels could be compared to two fuels with 30%v ethanol with blendstocks from either a highly iso-paraffinic fuel (PRF71) or a full-boiling range gasoline. The RON98Alk and RON98E30 fuels were prepared by Gage Products Company, while the PRF98 and PRF71E30 fuels were blended within the Argonne CFR engine test cell using a gravimetric method. The details of the test fuels can be found in Table 5.

Table 5. Properties of test fuels examined

Fuel	PRF98	RON98Alk	PRF71E30	RON98E30
RON (–)	98.0	97.8	97.8	97.4
MON (–)	98.0	96.6	–	86.6
Sensitivity (–)	0	1.4	–	10.8
HoV (kJ/kg)	308	309	519	536
LHV (MJ/kg)	43.3	44.5	39.3	38.2
A/F_{st} (–)	15.1	15.1	13.1	12.9
Paraffin (%v)	2	3	20	12.9
I-Paraffin (%v)	98	95.8	50	27.6
Aromatics (%v)	–	0.7	–	13.8
Naphthenes (%v)	–	0.02	–	7.0
Olefins (%v)	–	0.08	–	5.6
Oxygenates (%v)	–	–	30	30.4

The testing methodology for each fuel followed ASTM D2699 for determination of fuel RON. The engine was initially warmed up for an hour under knocking conditions typical of a RON 98 test fuel. This means the compression ratio and intake air temperature (upstream of the carburetor) was set based on ASTM D2699 to compensate for that day's barometric pressure and a fuel octane rating of 98. After one hour of warm-up at standard knocking conditions, intake and exhaust valve lash was verified or adjusted and the "Model 501-C Detonation Meter" (in this paper referred to simply as "knockmeter") was calibrated for standard knock on a PRF 98 fuel and spread of 12 to 15 knock units (KU) higher and lower than standard knock (50 KU) for the corresponding decrease or increase of PRF test fuel by one octane number (ON).

After proper engine warmup and knockmeter calibration for a range of 97 to 99 RON fuels, the peak knocking lambda condition was found for each fuel by performing a lambda sweep from 0.8 to 1.0. Crankshaft angle-based and time-based measurements were recorded and are compared in this work.

3. Results and discussion

3.1. Lambda sweeps

Fig. 1 shows the knockmeter measurements during lambda sweeps from 0.8 to 1.0 lambda with each fuel. The peak knocking lambda was approximately 0.89 for the non-ethanol highly iso-paraffinic fuels and approximately 0.93 for both the E30 fuels. This sort of detailed peak knocking

lambda information is not available in standard RON or MON rating tests because standard CFR engine installations do not have a lambda sensor installed. Despite the differences in the pre-ethanol blendstocks, both E30 fuels had a similar peak knocking lambda. The effect of ethanol to increase the peak knocking lambda (less rich) is not completely clear at this time. However variations in fuel blend properties that could influence this result, which will be examined in future work, with increased ethanol include the following possibilities: adiabatic flame temperature, laminar flame speed, stoichiometric air-fuel ratio, engine load, damköhler number, and Rayleigh number.

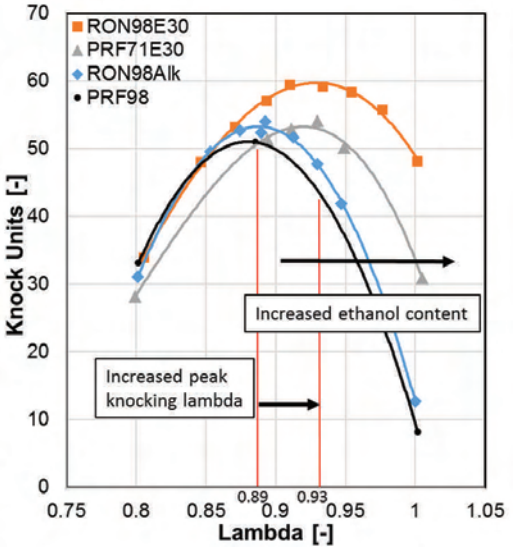


Fig. 1. ASTM knockmeter readings for lambda sweep from 0.8 to 1.0 for each fuel

The RON98E30 fuel, with a full boiling-range gasoline blendstock, measured slightly higher knock units at peak knocking lambda than the other three fuels. This resulted in an actual RON rating of 97.4. The RON98Alk and PRF71E30 fuels also produced slightly higher knocking than the PRF98, thus producing a RON rating of 97.8. However, this is within the ASTM 2699 standard deviation of ±0.25 ON from the 98.0 RON target (for RON 90 to 100).

It is interesting to see that the fuels had knockmeter measurements which were more similar at 0.8 lambda than at less-rich conditions closer to stoichiometry. The highly iso-paraffinic PRF98 and RON98Alk fuels produced very similar knockmeter response to lambda across the sweep, while the level of knock did not decrease as fast for the E30 fuels at stoichiometry. Future tests will add a small amount of ethanol to the RON98E30 fuel in order to obtain RON levels more similar to the others. As discussed in ASTM D2699, it should also be noted that the Meter 501-C Detonation Meter loses linearity for < 20 KU or > 80 KU.

3.2. Engine operation at RON rating conditions

As shown in Fig. 1, the lambda of peak knocking was higher for the E30 fuels. In Fig. 2, the engine fueling rate (FR) is shown along with each fuel's peak knocking lambda. Despite the less-rich lambda for the E30 fuels, they actually had higher fuel rate. Looking back to Table 5, it is observed that it was because of the significantly reduce stoichiometric air-fuel ratio (A/F_{st}) that the fuel rate for the E30 fuels was actually increased.

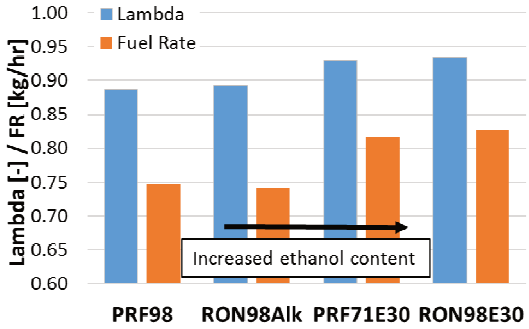


Fig. 2. Lambda and fuel rate (FR) at RON rating conditions for each fuel

Due to a combination of increased fuel rate and higher heat of vaporization (HoV), the E30 fuels had a significantly reduced mixture temperature entering the intake port (downstream of the carburetor) during RON rating. Fig. 3 shows the reduction in mixture temperature by 8 to 13°C, from the iso-paraffinic fuels to the E30 fuels. While the HoV of the RON98E30 was higher than the PRF71E30, it is likely that the differences in the pre-ethanol fuel blends did not allow for all of the fuel components to be completely evaporated before entering the intake port. This can also be observed in the lower temperature reduction between upstream and downstream of the carburetor (Carb. ΔT) for the RON98E30 fuel. Work by Foong has gone into greater detail in analyzing the effects of increased ethanol and HoV on the RON rating method because of this reduction to the mixture temperature entering the engine [5–7].

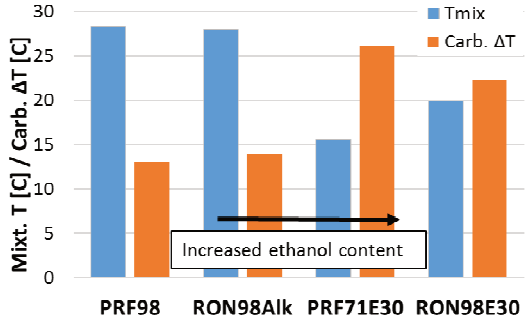


Fig. 3. Mixture temperature after the carburetor and corresponding temperature drop across the carburetor

Focusing on the engine operating conditions of peak knock for each fuel, the gross indicated mean effective pressure (IMEPg) is shown in Fig. 4. As shown in Fig. 5, the less-rich peak knocking lambdas of the E30 fuels allowed for more efficient engine operation and higher engine load during RON test conditions. The increased fuel rates with the E30 fuels does not seem to be the cause of increased load, being that the total fuel energy rate being supplied to the engine actually decreased when considering the reduction in fuel lower heating value (LHV) observed in Table 5. It is not clear whether this increase in engine load might have an effect on the knockmeter measurements, and in the end of the RON rating of these fuels.

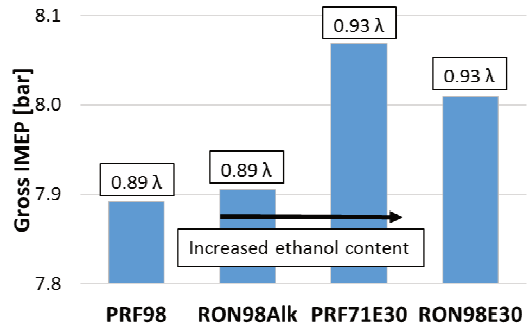


Fig. 4. Effect of fuel properties on engine load during RON testing

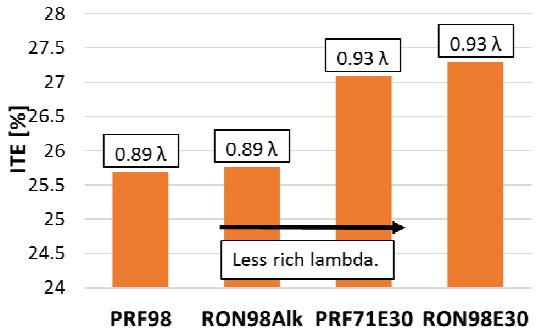


Fig. 5. Indicated thermal efficiency of each fuel at RON test conditions

As a result of the E30 fuels operating at peak knock closer to stoichiometry, the exhaust gas temperatures were also approximately 10°C higher, as can be seen in Fig. 6. It is likely that higher exhaust gas temperatures also caused a slight increase in cylinder residual gas temperature. Future work will look closer at how the combined effects of increased engine load and potentially increased residual gas temperatures may be possibly causing the E30 fuels to have their RON rating measured at more severe engine operating conditions than iso-paraffinic fuels with the same RON rating.

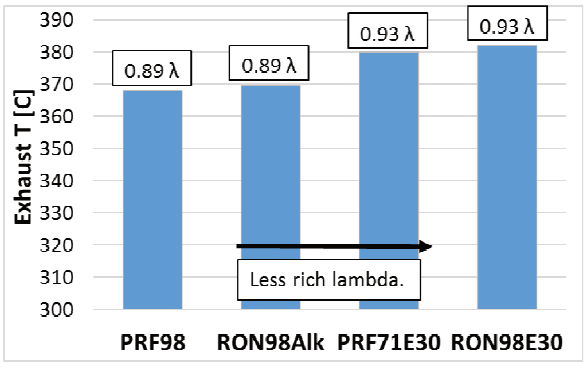


Fig. 6. Measured exhaust gas temperatures at RON conditions for each fuel

3.3. Combustion characteristics at RON rating conditions

Fig. 7 shows the different pressure-temperature trajectory cylinder conditions of each fuel from intake valve closing (IVC) to spark timing (ST). This plot was made using cylinder pressure data and an ideal gas law calculation of bulk gas temperature in AVL Concerto. Among the four fuels, the cylinder pressure from IVC to ST was very similar. However, variations in charge cooling from the increased HoV of the E30 fuels caused them to have lower cylinder temperatures during compression. This difference in temperature between the fuels increased during compression, likely due to mixture gamma effects. This would suggest that during normal flame propagating combustion, prior to the onset of knock auto-ignition, the end gas temperatures of the E30 fuels would remain slightly lower than the iso-paraffinic fuels.

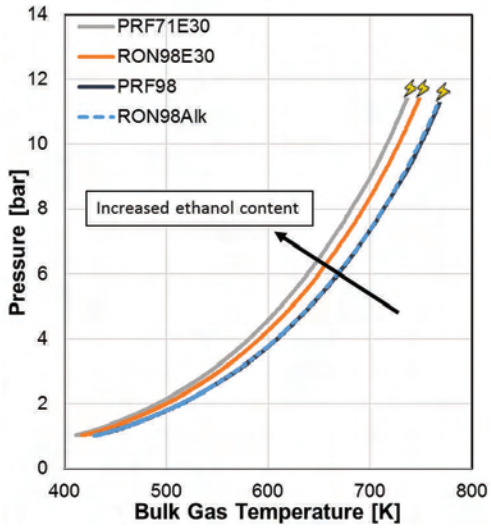


Fig. 7. Pressure-temperature trajectory from IVC to spark timing for each fuel at RON rating conditions

Fig. 8 shows cylinder pressure traces of each fuel under RON rating conditions from ST until shortly after the start of knocking combustion ringing. At the standard RON ST of -13 °aTDC, all fuels had roughly the same cylinder pressure near the end of compression. As seen in

Fig. 9, the start of combustion, denoted by the location of 10% mass fraction burned (CA10), is similarly just after firing top dead center (TDC) for all the fuels. The RON98E30 fuel achieved CA10 just slightly earlier than the other fuels. It has been shown that ethanol has a tendency to reduce the kernel development duration between ST and CA10 because of increased laminar flame speed [8, 9]. It is not clear why the PRD71E30 did not have a similarly early CA10. One possible reason is that PRF71E30 had lower bulk gas temperatures at spark timing than RON98E30, as seen in Fig. 7.

Despite the similar CA10 timing of PRF71E30 as the iso-paraffinic fuels, the increased fuel laminar flame speed did cause its CA50 time to advance slightly. However, still not as advanced as the CA50 time of the RON98E30 fuel, which had the assistance of an earlier CA10 time.

The “knock-point” is a term developed by Swartz and is used to describe the location in the cylinder pressure trace where there is a sudden increase due to the auto-ignition of the fuel-air mixture in the end-gas. The timing of the knock-point was similar between the iso-paraffinic fuels, slightly advanced for the PRF71E30 (0.2–0.3 CAD), and even more advanced for the RON98E30 (another 0.6 CAD). It likely that the significant advance of the knock-point for the RON98E30 is correlated with its lower RON

rating. Additional testing with a small increase in ethanol content to match RON rating with the other fuels would likely provide similar combustion characteristics as the PRF71E30.

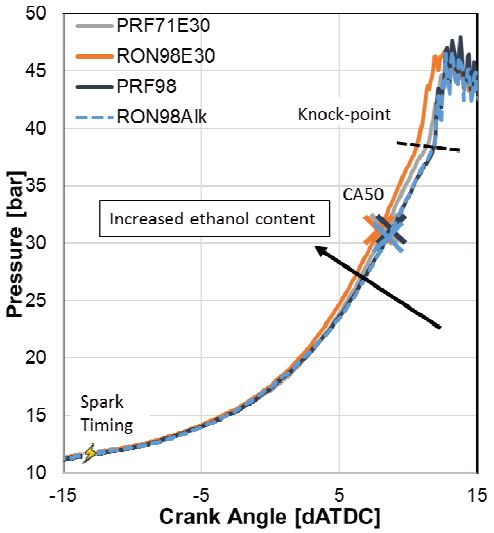


Fig. 8. Cylinder pressure from spark timing to combustion knock for each test fuel at RON rating conditions

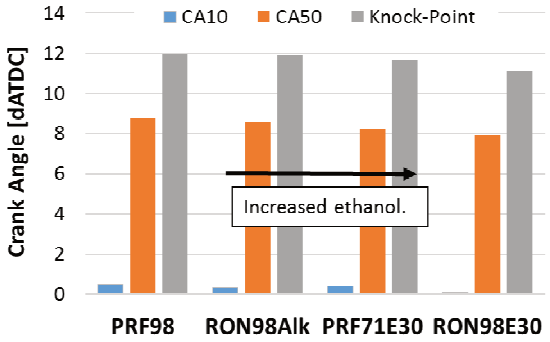


Fig. 9. Crankshaft angle position at 10% mass fraction burned (CA10), 50% (CA50), and the knock-point for all fuels at RON rating conditions

It is also observed in Fig. 8 that the rate of pressure rise after the knock-point was higher for the iso-paraffinic fuels despite a later knock-point timing than the E30 fuels. Fig. 10 shows a closer look at the cylinder pressure data just after the knock-point. It is observed that not only do the E30 fuels have a weaker pressure rise rate, but they also had a lower peak to peak ringing intensity than the iso-paraffinic fuels.

Fig. 11 shows a comparison of the ASTM knockmeter measurement against simultaneously measured peak pressure rise rates (PPRR) and knocking pressure peaks (KP_PK) using the spark plug cylinder pressure transducer. The advantage of the spark plug pressure transducer is that it allows simultaneous cylinder pressure measurement along with the ASTM knockmeter without any modifications to the cylinder head. The disadvantage is that it is not as accurate as a higher precision pressure transducer, such as the Kistler 6125C, which has been used in lieu of the knockmeter pickup. A future study will look at comparing the cylinder pressure measurements between these two pressure transducers and perform measurements with these fuels and the higher resolution pressure transducer instead of the knockmeter pickup under RON rating conditions.

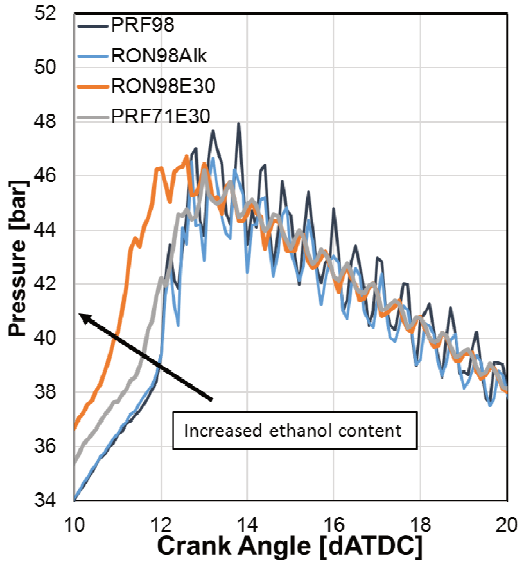


Fig. 10. Closer examination of the cylinder pressure behavior just after the knock-point

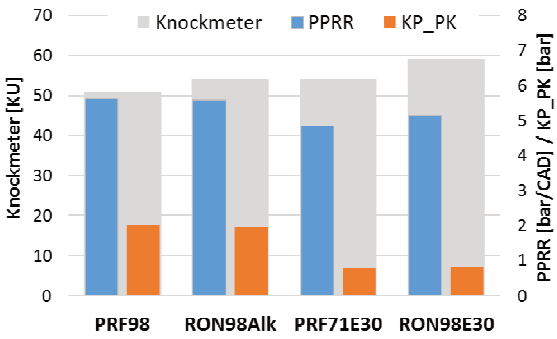


Fig. 11. Comparison of ASTM knockmeter measurement, peak pressure rise rate (PPRR), and knocking pressure peak (KP_PK)

Given that the modern knockmeter pickup is designed to replicate the older measurement of the bouncing pin, Swartz calculated that the knockmeter pickup measurement was mostly affected by the low frequency pressure rises, such as just after the knock-point [10, 11]. The peak pressure rise rate was investigated as a proxy for the amplitude in the low frequency pressure oscillations expected to be best measured by the knockmeter pickup. As seen in Fig. 10 and Fig. 11, the E30 fuels had lower pressure rise after autoignition, but the knockmeter measurement was the same as the iso-paraffinic fuels, if not higher (RON98E30). In normal spark-ignition engines, it is the pressure ringing after the onset of knock that causes a reduction of the boundary layer and increased heat transfer to the combustion chamber surfaces [12]. This aspect of the pressure trace was analyzed by KP_PK. However there was not a correlation of KP_PK with knockmeter readings either. Therefore it is likely that the knockmeter pickup measurement is more complicated than the rate of pressure rise after the knock-point or the ringing intensity.

4. Summary

In this work, a highly instrumented Waukesha CFR F1/F2 engine was used to measure the effects of fuel property effects on engine operating conditions and combustion characteristics. Between two iso-paraffinic fuels of similar RON, there were few differences in the engine operating and cylinder conditions. However, significant differences were observed between the engine operating and cylinder conditions of the iso-paraffinic and fuel blends with 30%v ethanol (E30) at the same (or similar) RON rating. The increased heat of vaporization (HoV) of the E30 fuels caused a reduction in mixture temperature entering the engine and the cylinder temperatures at intake valve closing. These temperature reductions initially due to HoV were increased during compression, likely due to gamma differences between the mixtures. Most notably, the peak knocking lambda, where RON is measured, occurred at less rich conditions for the E30 fuels. This caused the RON rating of the E30 fuels to be performed at a more efficient engine operating condition with higher load and exhaust temperature. While the auto-ignition timing (knock-point) of the E30 fuels occurred earlier, the rate of pressure rise and the ringing intensity was much lower than for the iso-paraffinic fuels. Given that all of these fuels had a similar RON rating, it is not clear what characteristics of the cylinder pressure trace would best represent the ASTM knockmeter measurement.

Acknowledgements

This research was conducted as part of the Co-Optimization of Fuels & Engines (Co-Optima) project sponsored by the U.S. Department of Energy (DOE) Office of Energy Efficiency and Renewable Energy (EERE), Bioenergy Technologies and Vehicle Technologies Offices.

Nomenclature

°aTDC	crank-angle degrees after firing top dead center
AKI	anti-knock index
CA10	crank-angle of 10% mass fraction burned
CA50	crank-angle of 50% mass fraction burned
CAD	crank-angle degree
E30	30%v ethanol
FR	fuel rate
GDI	gasoline direct injection
HoV	heat of vaporization
IMEPg	gross indicated mean effective pressure
IVC	intake valve closing
KP_PK	knock pressure peak
KU	knock unit
LHV	lower heating value
MON	motor octane number
ON	octane number
PON	pump octane number
PPRR	peak pressure rise rate
PRF	primary reference fuel
RON	research octane number
rpm	revolutions per minute
SI	spark ignition
ST	spark timing
TDC	top dead center

Bibliography

[1] ASTM D2699 – 15a, Designation: 237/87, Standard test method for research octane number of spark-ignition engine fuel.

[2] ASTM D2700 – 16, Designation 236/87, Standard test method for motor octane number of spark-ignition engine fuel.

[3] RICHARDS, P. Automotive fuels reference book: third edition. *SAE International* ISBN 978-0-7680-0638-4, 2014.

[4] SPLITTER, D., PAWLOWSKI, A., WAGNER, R. A historical analysis of the co-evolution of gasoline octane number and spark-ignition engines. *Front. Mech. Eng*. 2016, 1:16.

[5] FOONG, T., MORGANTI, K., BREAR, M. et al. The effect of charge cooling on the RON of ethanol/gasoline blends. *SAE Int. J. Fuels Lubr.* 2013, **6**(1).

[6] FOONG, T.M. et al. The octane numbers of ethanol blended with gasoline and its surrogates. *Fuel*. 2014, **115**, 727-739.

[7] FOONG, T.M., et al. Modeling end-gas autoignition of ethanol/gasoline surrogate blends in the cooperative fuel research engine. *Energy Fuels*. 2016.

[8] SZYBIST, J., SPLITTER, D. Effects of fuel composition on EGR dilution tolerance in spark ignited engines. *SAE Int. J. Engines*. 2016, **9**(2).

[9] KOLODZIEJ, C., PAMMINGER, M., SEVIK, J. et al. Effects of fuel laminar flame speed compared to engine tumble ratio, ignition energy, and injection strategy on lean and EGR dilute spark ignition combustion. *SAE Int. J. Fuels Lubr*. 2017, **10**(1), 2017-01-0671.

[10] YATES, A. et al. Insights relating to the autoignition characteristics of alcohol fuels *Fuel*. 2010, **89**, 89-93.

[11] SWARTS, A. Insights relating to octane rating and the underlying role of autoignition. *PhD thesis*. Univ. of Cape Town, 2006.

[12] HEYWOOD, J.B. Internal combustion engine fundamentals. *McGraw-Hill*. NewYork 1988.

Christopher P. Kolodziej – Argonne National Laboratory, USA.

Thomas Wallner – Argonne National Laboratory, USA.

Article citation info:
BEBKIEWICZ, K., CHŁOPEK, Z., STOSIO, G. et al. Study on sensitivity of national annual pollutant emission from passenger cars to traffic patterns. Combustion Engines. 2017, **171**(4), 170-174. DOI: 10.19206/CE-2017-428

Katarzyna BEBKIEWICZ
Zdzisław CHŁOPEK
Grzegorz STOSIO
Krystian SZCZEPAŃSKI
Magdalena ZIMAKOWSKA-LASKOWSKA

CE-2017-428

Study on sensitivity of national annual pollutant emission from passenger cars to traffic patterns

The paper presents the results of the study on the sensitivity of the national annual pollutant emission from passenger cars to traffic patterns. The study was carried out in accordance with the methodology applied in the COPERT 4 software. The traffic pattern was modelled as the share of road lengths under various traffic conditions: urban, rural and on motorways and expressways, in the total length of trips covered by vehicles. A relatively small and less varied sensitivity of the national annual pollutant emission from passenger cars to the traffic pattern was found due to the substance emitted. This was considered to be a valuable proposal for the selection of parameters for the total emission model of vehicular pollutants, in view of the difficulty of estimating the share of road lengths under model traffic conditions.

Key words: *motor vehicles, inventory of pollutant emission, COPERT*

1. Introduction

The performance parameters of internal combustion engines are highly sensitive to the operating conditions of the engines [7, 8]. Particularly sensitive to engine operating conditions is the emission of pollutants [1, 7, 8].

The sensitivity of operational properties of internal combustion engines to their operation conditions is related not only to values describing these conditions but also to the occurrence of dynamic states [7, 8]. Particularly in the dynamic states whose diversity is endless, the engine performance parameters may vary considerably from that of static states [7, 8].

The operating conditions of internal combustion engines can be described in terms of the engine thermal state and its work intensity [7, 8]. Under thermally stabilized conditions, the engine performance is usually described by torque output and engine crankshaft speed [7, 8]. Under traction use of an internal combustion engine, the latter values are determined primarily by the vehicle velocity [7].

The engine operating conditions may vary substantially between various models of road traffic. At the same time, the road traffic modelling encounters difficulties in identifying model parameters, thus, it is purposeful to investigate the sensitivity of the performance properties of internal combustion engines to these parameters.

The parameters of operating conditions of the internal combustion engine, determined by the process of vehicle velocity, include [1–6, 9–14]:

– share of vehicle mileage under model traffic conditions,
– average velocity of vehicles under model traffic conditions.

The following model traffic conditions have been assumed in the studies on the total emission from motor vehicles [1–6, 9–14]:

– urban,
– rural,
– on highways and expressways.

Particularly significant differences in the engine operating conditions occur in the case of passenger cars [1, 7]. For this reason, a study was undertaken to assess the sensitivity of the national annual pollutant emission from passenger cars to the traffic patterns. In this paper, we focused on the mileage of cars under model traffic conditions.

2. COPERT 4 software applied in this work

The COPERT 4 software [10–12, 14] was used for the simulation study. This is the preferred software in the European Union, for the inventory of pollutants from motor vehicles [14].

The study was conducted for the state of the automotive industry in Poland in 2015.The values entered as software data are given in table 1.

Table 1. Values characterising the traffic of passenger cars in Poland in 2015

N_{PC}	[mln]	20.52
$N_{PC\text{-}SI}$		14.66
$N_{PC\text{-}CI}$		5.86
$p_{PC\text{-}SI}$	[km]	5900
$p_{PC\text{-}CI}$	[km]	12300
u_U		0.37
u_R		0.5
u_H		0.13
v_U	[km/h]	31.5
v_R	[km/h]	70
v_H	[km/h]	120

The number of passenger cars was estimated based on data of the Central Statistical Office of 2015. The number of passenger cars applies to all vehicles – N_{PC} and to cars with spark ignition engine – $N_{PC\text{-}SI}$ as well as to those with compression ignition engine – $N_{PC\text{-}SI}$.

The annual mileage of passenger cars with spark ignition engine – $p_{PC\text{-}SI}$ as well as of those with compression ignition engine – $p_{PC\text{-}SI}$ was determined on the basis of data contained in [6].

The model simulating vehicle use intensity, developed specifically by the authors and built on the basis of functional likeness, was applied to elementary categories of cars relating to pollutant emission.

Data on vehicle structure at the level of elementary category were used to identify the model ([13]). The

definition of traffic patterns [4, 9] was assumed in accordance with data contained in [6].

The average distance travelled by the vehicle after start-up, which is used to determine the pollutant emission attributable to engine warming, was assumed to be 12 km [2].

The remaining parameters of the COPERT 4 model were assumed in accordance with the parameters suggested by the software equipment. Those parameters refer to, among others, fuel characteristics as well as to climatic data for a particular country.

3. Results of simulation study

Two types of simulation studies were performed (Table 2).

In the first study, the share of traffic on highways and motorways – u_H in the model traffic conditions, was assumed to be constant, while the shares of urban traffic – u_U and rural traffic – u_R were used as variables.

Table 2. Schematic of studies Nos 1 and 2

Study No 1			Study No 2		
u_U	u_R	u_H	u_U	u_R	u_H
0.29	0.58	0.13	0.39	0.58	0.03
0.34	0.53	0.13	0.39	0.53	0.08
0.39	0.48	0.13	0.39	0.48	0.13
0.44	0.43	0.13	0.39	0.43	0.18
0.49	0.38	0.13	0.39	0.38	0.23

In Figures 1–7, the results are presented of the simulation study No 1: the dependence of the annual national emission of selected pollutants from passenger cars upon the share of road length under the following model traffic conditions: U – in towns, R – outside towns, H – on highways and expressways and T – under all conditions.

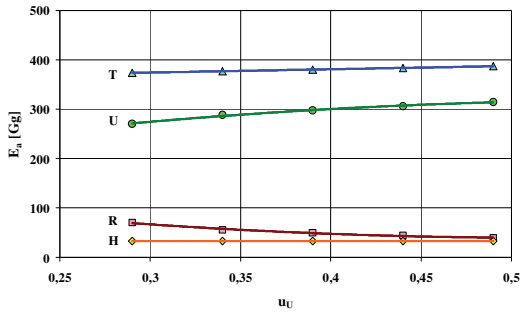


Fig. 1. Dependence of the national annual emission of carbon monoxide from passenger cars upon the road length travelled under the following model traffic conditions: U – urban, R – rural, H – on highways and expressways and T – under all conditions

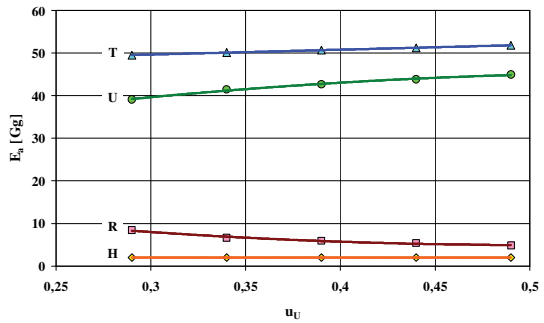


Fig. 2. Dependence of the national annual emission of volatile organic compounds from passenger cars upon the road length travelled under the following model traffic conditions: U – urban, R – rural, H – on highways and expressways and T – under all conditions

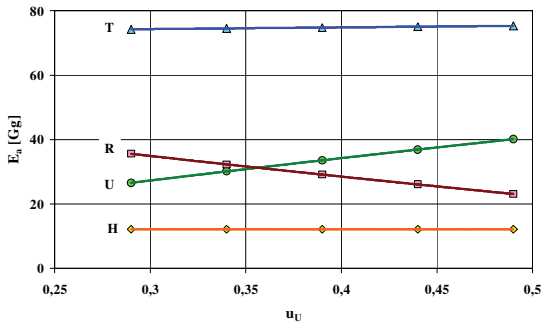


Fig. 3. Dependence of the national annual emission of nitrogen oxides from passenger cars upon the road length travelled under the following model traffic conditions: U – urban, R – rural, H – on highways and expressways and T – under all conditions

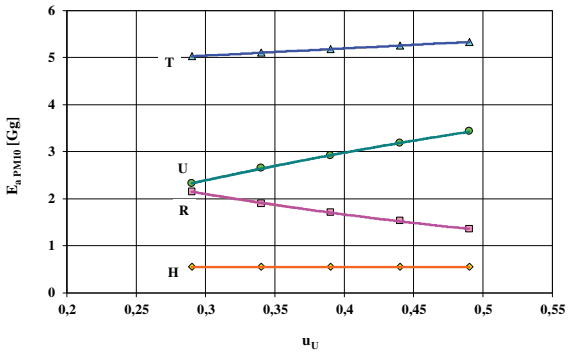


Fig. 4. Dependence of the national annual emission of particulate matter PM10 from tribological elements of passenger cars upon the road length travelled under the following model traffic conditions: U – urban, R – rural, H – on highways and expressways and T – under all conditions

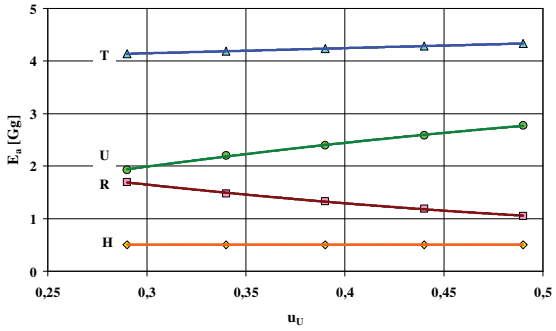


Fig. 5. Dependence of the national annual emission of particulate matter PM2.5 from tribological elements of passenger cars upon the road length travelled under the following model traffic conditions: U – urban, R – rural, H – on highways and expressways and T – under all conditions

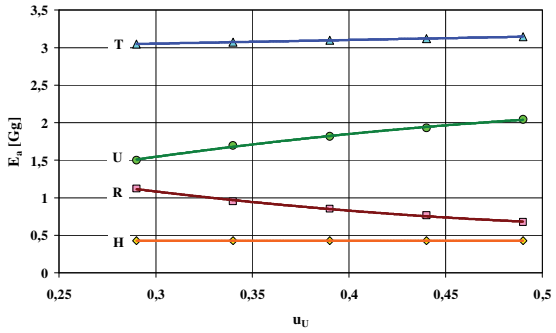


Fig. 6. Dependence of the national annual emission of particulate matter from the exhaust system of passenger cars engines upon the road length travelled under the following model traffic conditions: U – urban, R – rural, H – on highways and expressways and T – under all conditions

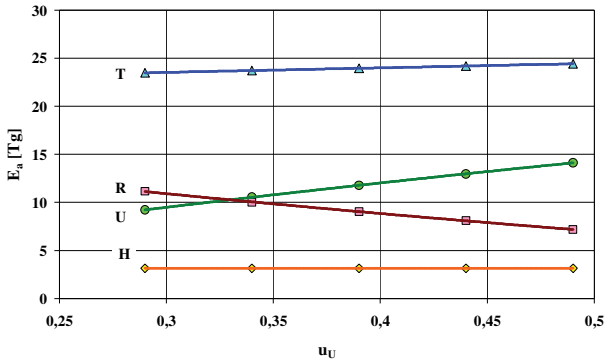


Fig. 7. Dependence of the national annual emission of carbon dioxide from passenger cars upon the road length travelled under the following model traffic conditions: U – urban, R – rural, H – on highways and expressways and T – under all conditions

In Figures 8–15, the results are presented of the simulation study No 2: the dependence of the national annual emission of selected pollutants upon the share of road length under the following model traffic conditions: U – urban, R – rural, H – on highways and expressways and T – under all conditions.

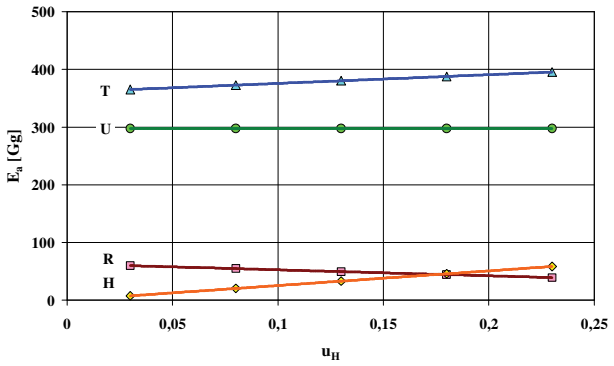


Fig. 8. Dependence of the national annual emission of carbon monoxide from passenger cars upon the road length travelled under the following model traffic conditions: U – urban, R – rural, H – on highways and expressways as well as T – under all conditions

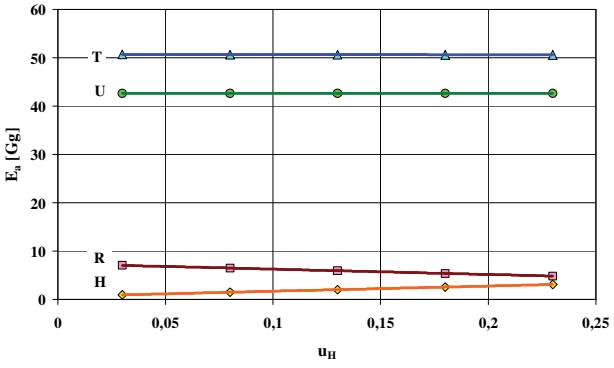


Fig. 9. Dependence of the national annual emission of volatile organic compounds from passenger cars upon the road length travelled under the following model traffic conditions: U – urban, R – rural, H – on highways and expressways as well as T – under all conditions

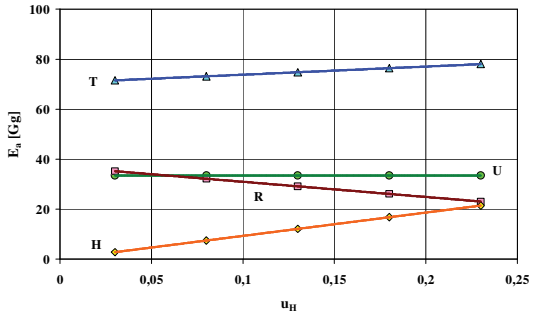


Fig. 10. Dependence of the national annual emission of nitrogen oxides from passenger cars upon the road length travelled under the following model traffic conditions: U – urban, R – rural, H – on highways and expressways as well as T – under all conditions

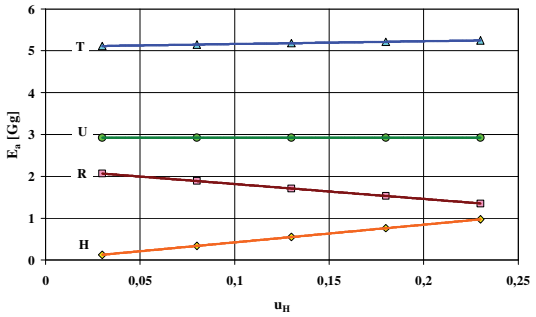


Fig. 11. Dependence of the national annual emission of particulate matter PM10 from tribological elements of passenger cars upon the road length travelled under the following model traffic conditions: U – urban, R– rural, H – on highways and expressways as well as T – under all conditions

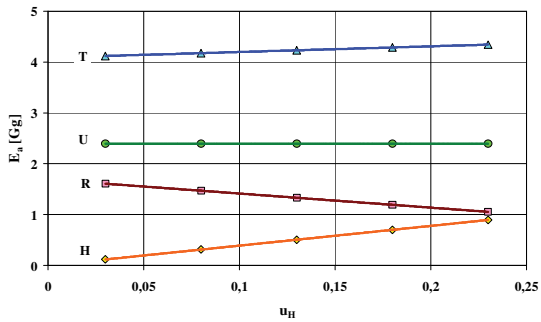


Fig. 12. Dependence of the national annual emission of particulate matter PM2.5 from tribological elements of passenger cars upon the road length travelled under the following model traffic conditions: U – urban, R – rural, H – on highways and expressways as well as T – under all conditions

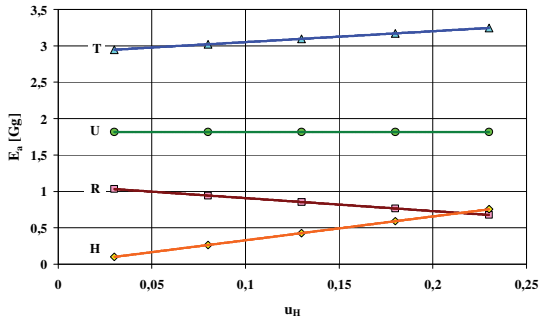


Fig. 13. Dependence of the national annual emission of particulate matter from the exhaust system of passenger cars engines cars upon the road length travelled under the following model traffic conditions: U – urban, R – rural, H – on highways and expressways as well as T – under all conditions

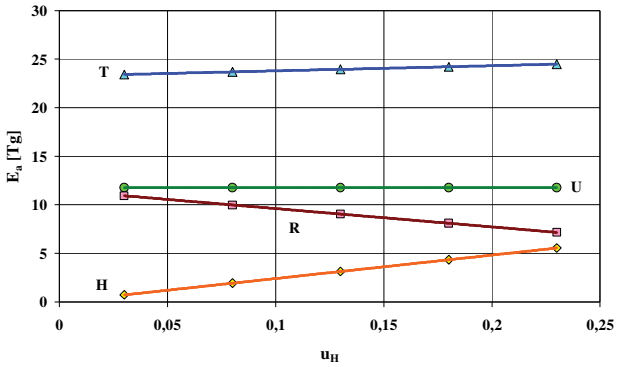


Fig. 14. Dependence of the national annual emission of carbon dioxide from passenger cars upon the share of road length travelled under the following model traffic conditions: U – urban, R – rural, H – on highways and expressways as well as T – under all conditions

For both types of simulation tests, there is a clear similarity between national annual emission of pollutants from road shares in model traffic conditions. In all cases, the low sensitivity to road shares in model traffic conditions is national annual emission of pollutants under all traffic conditions. There is no clear sensitivity of the characteristics to the specific pollution.

4. Conclusions

Based on the simulations, the following conclusions can be drawn:

1. The sensitivity of the national annual emission of all pollutants was found to be relatively low to the share of road travelled by cars under model traffic conditions.
2. The national annual emission under all traffic conditions was least sensitive to the share of roads travelled by cars under model traffic conditions. This constitutes an important practical finding, since identifying the parameters that characterize vehicle movement belongs to the most difficult tasks.
3. The conclusions made on the basis of the study conducted apply to passenger cars. Based on the research carried out by the authors, it can be stated, that the sensitivity of the national annual pollutant emission to the share of road travelled by vehicles under model traffic conditions is lower for other cumulated vehicle categories than for passenger cars. However, reporting the results of the latter study exceeds the volume of the present work.

Nomenclature

CI	compression ignition
E_a	national annual emission
H	highway
N	number of vehicles per cumulated category
p	mileage covered by vehicles per cumulated category
PC	passenger cars
PC-CI	passenger cars – compression ignition (engine)
PC-SI	passenger cars – spark ignition (engine)
R	rural
SI	spark ignition
T	total (vehicles)
u	share of road travelled by vehicles per cumulated category under model traffic conditions
U	urban
v	average velocity of vehicles per cumulated category

Bibliography

[1] ARREGLE, J. et al. Procedure for engine transient cycle emissions testing in real time. Experimental *Thermal and Fluid Science*. 2006. Volume 30, no5. 485–496.

[2] BEBKIEWICZ, K., CHŁOPEK, Z., SZCZEPAŃSKI, K., ZIMAKOWSKA-LASKOWSKA, M. Results of air emission inventory from road transport in Poland in 2014. *Proceedings of the Institute of Vehicles*. 1(110)/2017. 77–88.

[3] BEBKIEWICZ, K., CHŁOPEK, Z., SZCZEPAŃSKI, K., ZIMAKOWSKA-LASKOWSKA, M. The influence of the properties of vehicles traffic on the total pollutant emission. *Proceedings of the Institute of Vehicles*. 1(110)/2017. 89–102.

[4] BEBKIEWICZ, K., CHŁOPEK, Z., SZCZEPAŃSKI, K., ZIMAKOWSKA-LASKOWSKA, M. Issues of modeling the total pollutant emission from vehicles. *Proceedings of the Institute of Vehicles*. 1(110)/2017. 103–118.

[5] BUWAL (Bundesamt für Umwelt, Wald und Landschaft), INFRAS AG (Infrastruktur-, Umwelt- und Wirtschaftsberatung). Luftschadstoffemissionen des Strassenverkehrs 1950–2010. BUWAL-Bericht Nr. 255, 1995.

[6] CHŁOPEK Z., WAŚKIEWICZ J. The forecast of the pollutant emission from automotive internal combustion engines in Poland by 2030. *VI International Congress of Internal Engines. 2015*. Combustion Engines 2015.

[7] CHŁOPEK Z. Modelowanie procesów emisji spalin w warunkach eksploatacji trakcyjnej silników spalinowych. Prace Naukowe. Seria „Mechanika" z. 173. Oficyna Wydawnicza Politechniki Warszawskiej. Warszawa 1999.

[8] CHŁOPEK Z. Some remarks on engine testing in dynamic states. *Combustion Engines* 4/2010(143). 60–72.

[9] CHŁOPEK Z. Zasady modelowania zużycia paliwa i energii oraz emisji zanieczyszczeń związanych z użytkowaniem pojazdów drogowych. *Technika Transportu Szynowego* 12/15. 262–267.

[10] COPERT Training 5. COPERT 5 vs COPERT 4. European Environment Agency. 2016. http://emisia.com/sites/default/files/COPERT_5_features.pdf. (2016–12–06).

[11] EMEP/EEA air pollutant emission inventory guidebook – 2016. European Environment Agency. http://www.eea.europa.eu/publications/emep-eea-guidebook-2016. (2016–12–06).

[12] GKATZOFLIAS D., KOURIDIS CH., NTZIACHRISTOS L., SAMARAS Z. COPERT 4 Computer programme to calculate emissons from road transport User manual (version 9.0). European Environment Agency. Emisia SA. 2012. (2016–12–06).

[13] INFRAS AG. Handbook emission factors for road transport 3.2. Quick reference. Version 3.2. Bern, 2014.

[14] 2006 IPCC Guidelines for National Greenhouse Gas Inventories. http://www.ipcc-nggip.iges.or.jp/public/2006gl/vol2.html. (2016–12–06).

Katarzyna Bebkiewicz, MEng. – Institute of Environmental Protection – National Research Institute in Warsaw.

e-mail: *Katarzyna.Bebkiewicz@kobize.pl*



Krystian Szczepański, DSc., DEng. – Institute of Environmental Protection – National Research Institute in Warsaw.

e-mail: *Krystian.Szczepanski@ios.edu.pl*



Prof. Zdzisław Chłopek, DSc., DEng. – Institute of Environmental Protection – National Research Institute in Warsaw.

e-mail: *Zdzislaw.Chlopek@kobize.pl*



Magdalena Zimakowska-Laskowska, DSc., DEng. – Institute of Environmental Protection – National Research Institute in Warsaw.

e-mail: *Magdalena.Zimakowska-Laskowska@kobize.pl*



Grzegorz Stosio, Eng. – Faculty of Automotive and Construction Machinery Engineering in the Warsaw University of Technology.

e-mail: *GrzegorzStosio@gmail.com*



Article citation info:
BERA, P. Torque characteristic of SI engine in dynamic operating states. *Combustion Engines*. 2017, **171**(4), 175-180. DOI: 10.19206/CE-2017-429

Piotr BERA

CE-2017-429

Torque characteristic of SI engine in dynamic operating states

The article presents torque characteristic of the engine in dynamic operating conditions as a function of engine speed and throttle opening angle. All mentioned parameters are analyzed as independent variables over time. To develop such a characteristic an artificial neural network is used. The training data were obtained from measurements carried out on the test bench on SI engine. The operating states reflect all possible configurations of these parameters, which may occur during use of the vehicle in real traffic conditions. The article shows design of an artificial neural network that allows to designate the required dependences. Moreover, it describes the fit of the model to the measurement data, which clearly indicates its correctness. Then the developed characteristic in dynamic states is compared with the characteristic in static working states. The differences between them for selected cases of engine operation states are presented. It shows the versatility of the presented method.

Key words: *engine torque, dynamic states, engine characteristic, artificial neural network*

1. Introduction

Internal combustion engines used to propel automotive vehicles work mainly under dynamic working states. Static working states occur very rarely, primarily on idle or during extra-urban driving with constant speed. Therefore all engine characteristics should be based on measurements in dynamic working states. Currently manufactured measurement equipment enables such measurements but the problem is in data analysis. It is due to the fact that in dynamic working states engine parameters cannot be considered as a function of state. It is necessary to take into account engine parameters from previous time intervals. It leads to the situation where several values of few parameters affect another parameter.

Hence measurements in static states are commonly performed. On a basis of such measurements engine characteristics are determined and then saved in ECU. One of such characteristics is engine torque characteristic that in static states is a function of engine speed and throttle opening angle.

There are many methods that allow to designate engine torque characteristic. Except the one described above, there are also other ways. Some of them are as follows:

– the use of ANN to obtain a mathematical model of engine [4, 6–8],
– the use of nonlinear models based on mean-values algorithms [4, 5].

Dynamic states in combustion engines are very difficult to analyze because engine torque is strongly influenced by several factors: changes in kinetic energy in moving parts (e. g. crankshaft, camshafts or flywheel), unstable airflow in manifold or changes in linear speed of coolant or oil.

Due to the above problems, that are impossible to include, it was assumed in the article, that the engine is a black box. Thus only input (throttle angle and engine speed) and output (engine torque) parameters were measured in dynamic and static states and then analyzed in time intervals.

The tests were performed on SI engine with a displacement of 899 cm^3 and nominal power of 29 kW at 5500 rpm. In the performed tests both dynamic and static characteristics were collected. Measurement methodology was described in details by the author in works [2, 3]. Then these data are analyzed with use on ANN trained in supervised mode.

2. Engine torque characteristic in static states

2.1. Engine test bed measurements

In case of standard characteristic in static states measurements are performed on conventional eddy current engine dynamometer that ensures proper accuracy. Parameters such as engine speed, engine torque, throttle opening angle, air-fuel ratio etc. are constant. Engine inertial elements have then no influence because angular acceleration equals zero and throttle position is constant what ensures stable airflow in manifold.

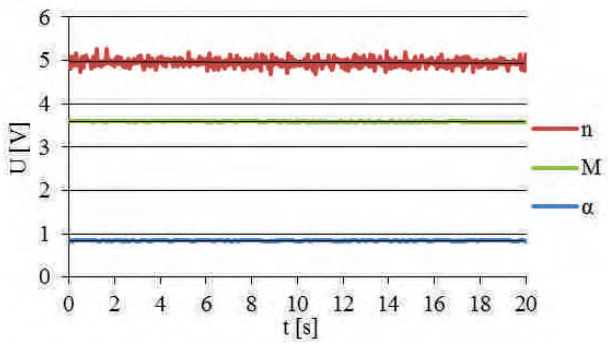


Fig. 1. A single measurement in static state

A single exemplary measurement, lasting 20 s, is shown in Fig. 1. Engine parameters are presented as originally measured – in Volts.

2.2. Data analysis

In case of characteristic based on static states data analysis is easy. To create such a 3d characteristic, where:

$$M = f(n, \alpha) \tag{1}$$

only basic computational tools are needed e.g. 3d graph in Excel or cftool in Matlab. In this study the second method was used. A characteristic obtained for an engine, that tests were performed on, is shown in Fig. 2. It was created based on 80 measurements in static states.

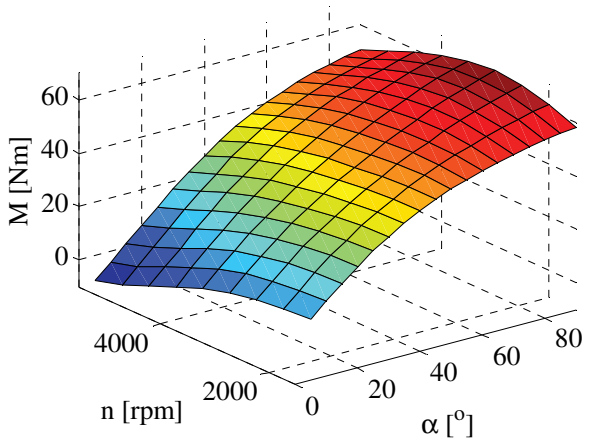


Fig. 2. Engine torque characteristic in static states

It can be noticed that for throttle angle of 90° the characteristic is the same as external speed characteristic provided by the manufacturer.

2.3. Conclusions

Although such an engine torque characteristic is easy to designate, it gives only a rough dependency between engine torque vs rotational speed and throttle opening angle. It cannot be used in accurate calculations of dynamic transitions between two points on characteristic.

3. Engine torque characteristic in dynamic states

3.1. Engine test bed measurements

Measurements in dynamic states must be performed on the engine test bed that ensures rapid changes of both drag torque and throttle opening angle. In case of presented characteristic 3 engine parameters must be constantly measured: rotational speed, throttle opening angle and engine torque. A single measurement is shown in Fig. 3.

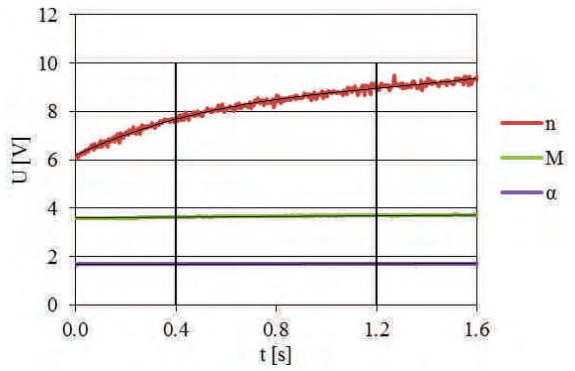


Fig. 3. Engine parameters in dynamic states

The graph clearly shows that in dynamic working states engine torque cannot be considered as a state function of engine torque and throttle opening angle because in this case:

$$M(t_1) = M(t_2) \tag{2}$$

but:

$$n(t_1) \neq n(t_2) \tag{3}$$

As results from this example in dynamic states the engine torque cannot be considered as a state function of rotational speed and throttle opening angle:

$$M \neq f(n, \alpha) \tag{4}$$

Parameters must be analyzed in time interval of specified length. ANN allows for such an analysis, what is described below.

3.2. Data analysis with use of ANN

Pursuant to information mentioned in the introduction, the analysis requires multidimensional attempt. Such an approach is possible with use of ANN method. Network can have many inputs that represent subsequent values of parameters in determined time interval because only then inertia phenomena can be included. It requires detailed analysis of time intervals. Moreover, it is impossible to determine up front which ANN architecture is the best for this particular problem. Therefore several configurations were examined before final choice.

All the data described in a previous point create a training sets for ANN. Before training, data were mixed, like described in [3], which improves training process significantly. Training set was constructed based on 220 measurements in dynamic states and 80 measurements in static states.

The first step is to decide which ANN architecture is the best for this particular problem. To do this, several network configurations were checked. In order to obtain relevant results each of 8 networks was trained with the same algorithm and the number of hidden neurons was always the same. According to recommendations included in [1–3] Lavenberg-Marquardt training algorithm and 10 hidden neurons were implemented.

Fig. 4 presents a representative dynamic state with described engine parameters that are later used in Table 1.

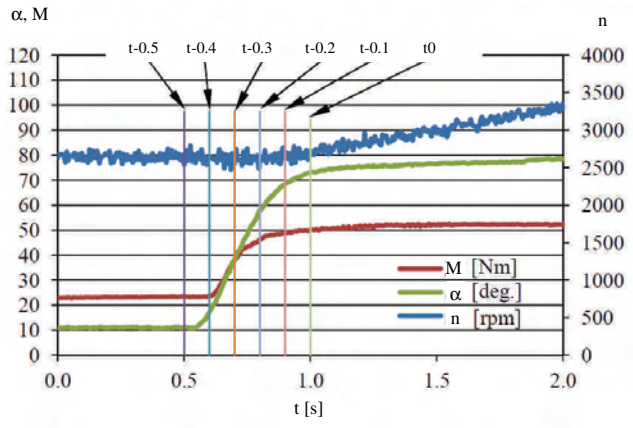
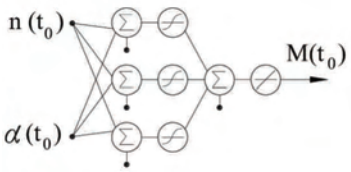
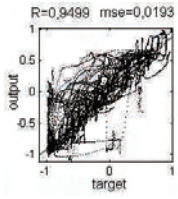
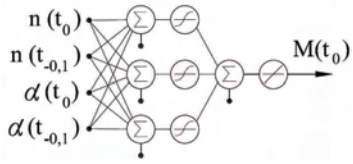
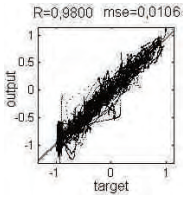
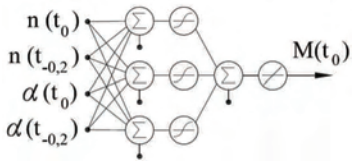
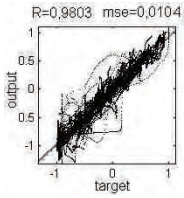
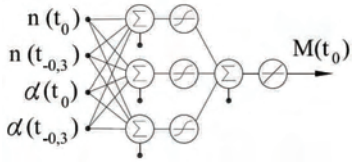
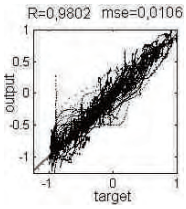
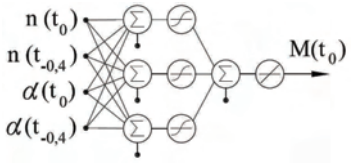
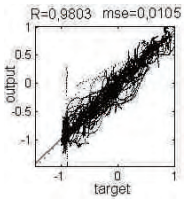
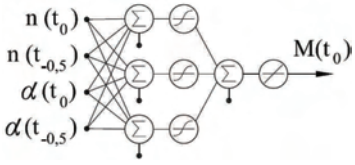
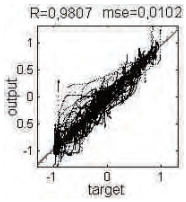
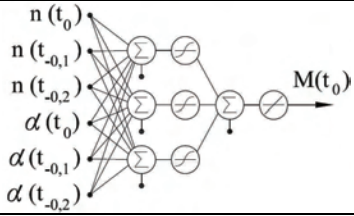
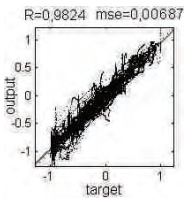
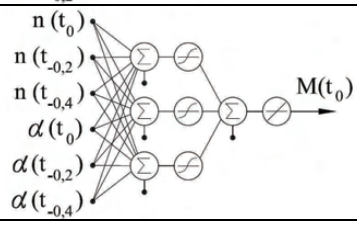
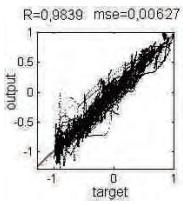


Fig. 4. Designation of time moments during engine operation

Author considered 8 ANN configurations (Table 1). The first one is in fact a static characteristic due to only one input of engine speed and one input of throttle opening angle. The next ones (2–8) ANNs take into account inertia phenomena and differ with number of inputs and time intervals, which are in the range 0–0.5 s.

Table 1. Considered configurations of ANN architectures and corresponding *mse* and *R* values

No	ANN configuration	Data fit after training process *x* axis – target *y* axis – net output
1		
2		
3		
4		
5		
6		
7		
8		

The best results (the smallest values of *mse* and *R*) are obtained with ANN number 8 from Table 1. It turns out that the best solution is obtained when there are 6 network inputs: three engine speeds and three throttle angles in time intervals of 0.2 second. The chosen network is shown in Fig. 5.

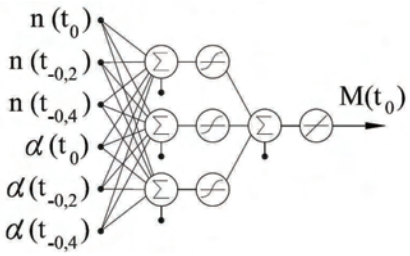


Fig. 5. ANN architecture that ensures best data approximation

The choice of proper ANN architecture is the first step. Then accurate number of hidden layers, number of hidden neurons and training algorithm must be chosen.

The number of hidden layers was set to one. According to [1] one layer with adequate number of neurons is capable of approximating any nonlinear problem with expected accuracy. Because training set consist of 210 000 columns, Levenberg-Marquardt method was implemented [1, 3]. As a result from performed calculations it turned out that 6 neurons is the best in this case. Further increase of neurons does not give any positive effect and the risk of overfitting raises.

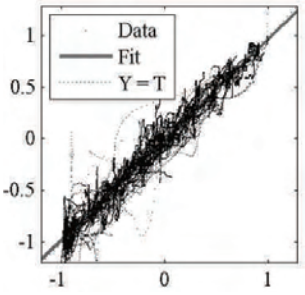


Fig. 6. ANN data fit after training process

Finally obtained results are presented in Fig. 6 and Fig. 7. The graphs clearly show that ANN model adequately approximates measurement data. R value equals 0.98 and the mse = 0.00625.

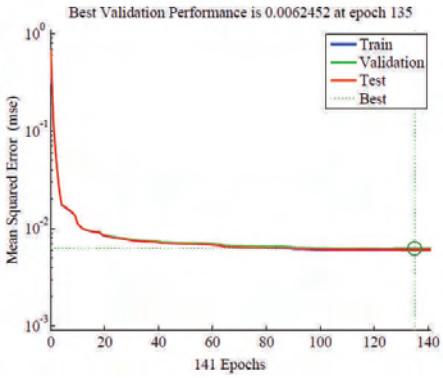


Fig. 7. Graph of errors for each subset during the ANN training

3.3. Conclusions

Calculations performed with ANN show that this method can be used to analyze measurement data from dynamic states to design engine torque characteristic. ANN model fits measurement data very well, what is supported by values of mse, R parameter and correctness of obtained graphs from simulations shown in the next points. Engine torque is supposed to change in a predictable way. Some training processes generated such a model that was, because of this reason, obviously judged as improper. Such a situation is due to the fact, that initial values of weights and biases are random and even with the same ANN parameters, reasonable network is obtained only after series of training processes.

4. Comparison of characteristic in dynamic states with characteristic in static states

4.1. Error definition

In this chapter the engine torque characteristic designated with use of ANN will be compared to the static characteristic. The difference between values calculated by these characteristics is defined as follows:

$$\delta = \frac{M_{stat} - M_{dyn}}{M_{stat}} \cdot 100\% \tag{5}$$

where: M_{stat} – engine torque calculated with use of characteristic in static states [Nm] (Fig. 2), M_{dyn} – engine torque calculated with use of characteristic in dynamic states [Nm] (designated with use of ANN).

In the article only situations with increasing engine speed will be considered therefore the error δ will always be positive.

4.2. Increase of both engine speed and torque

This simulation describes typical situation, when during driving with constant speed throttle is suddenly opened, engine torque raises rapidly and the vehicle begins to accelerate. In such case engine crankshaft angular acceleration depends on gear selected, slope of the road and vehicle speed. The bigger the transmission ratio (the lowest gear) the greater the engine angular acceleration.

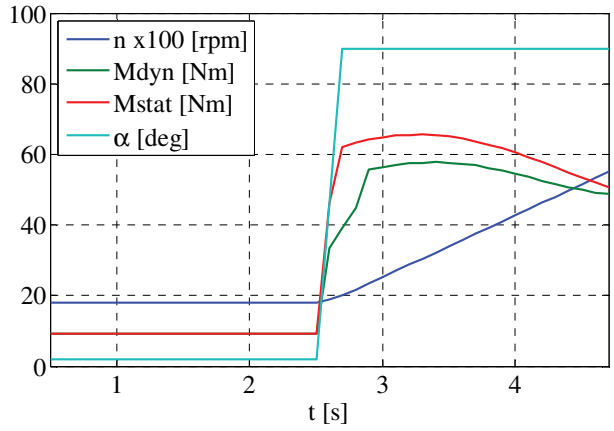


Fig. 8. Engine parameters in time of 2 seconds after full throttle opening

For the extreme case shown in Fig. 8 the difference in engine torque while increasing rotational speed is almost 15%. What is also important, the torque increase while throttle opening is noticeably slower in comparison to static characteristic. As it can be resulted from Fig. 9 that the largest error is in range that is mostly often used in a real traffic (2000–3000 rpm) and decreases with engine speed raise. The difference between two characteristics becomes negligible with angular acceleration of about 20 rad/s^2.

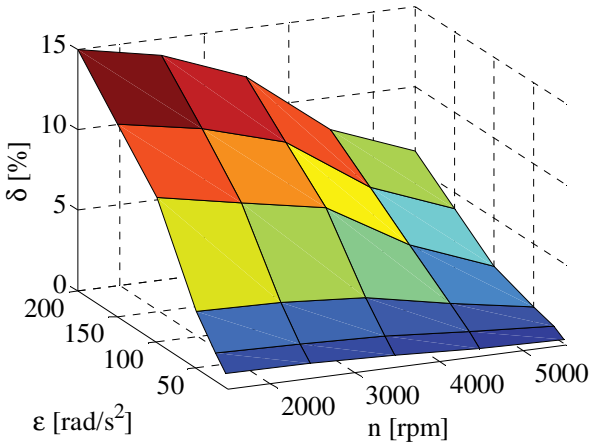


Fig. 9. Error δ in function of engine speed n and angular acceleration ε for throttle opening 90º

Fig. 10 shows similar situation but in this case throttle angle is only 30º. Maximum difference is for crankshaft angular acceleration of 200 rad/s^2 and equals 10%. It means that the difference δ decreases with decreasing throttle opening and is the largest at full throttle operation.

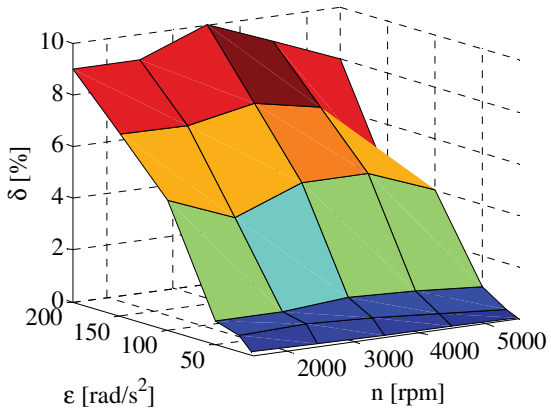


Fig. 10. Error δ in function of engine speed n and angular acceleration ε for throttle opening 30º

When angular acceleration is about 50 rad/s^2 the difference becomes negligible.

4.3. Increase in torque with constant speed

Another situation that might occur on the road is the need to maintain constant speed while traffic resistances are growing up. In such cases throttle openings are usually much slower than in case of sudden acceleration.

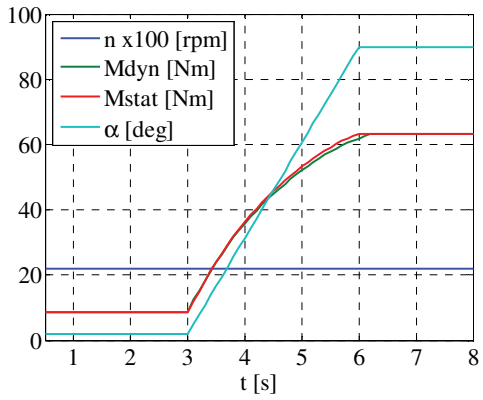


Fig. 11. Increase in engine torque with constant speed while full throttle opening

Fig. 11 clearly shows that there is a very small difference between values calculated by characteristics in static and dynamic states. Fig. 12 shows that the difference δ is the largest in the range of small engine speed and equals about 4%. Then decreases with increasing engine speed.

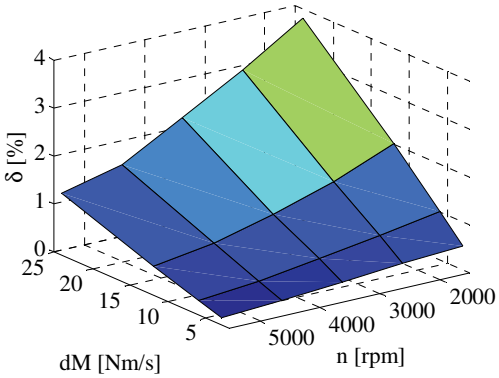


Fig. 12. Error δ in function of constant engine speed n and torque increase dM

4.4. Influence of throttle opening time on engine torque

Another problem that occurs in dynamic operating states is delay in engine response to a control signal.

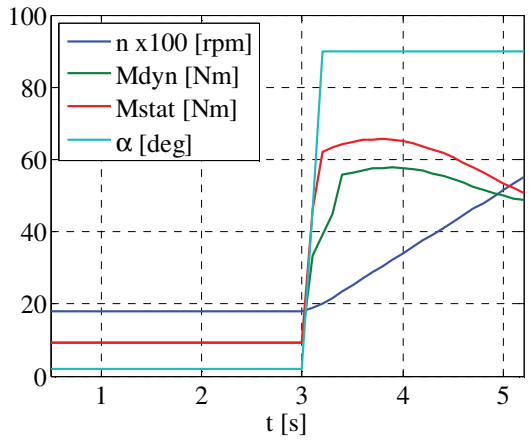


Fig. 13. Engine parameters during full throttle opening lasting 0.2 s

It can be noticed (Fig. 13) that throttle opening lasts 0.2 s whereas engine torque reaches top value after 0.4 s. So in this case delay is 100%. It would be even more noticeable in turbocharged engines. During this time engine torque is even 30% smaller than it would result from static characteristic.

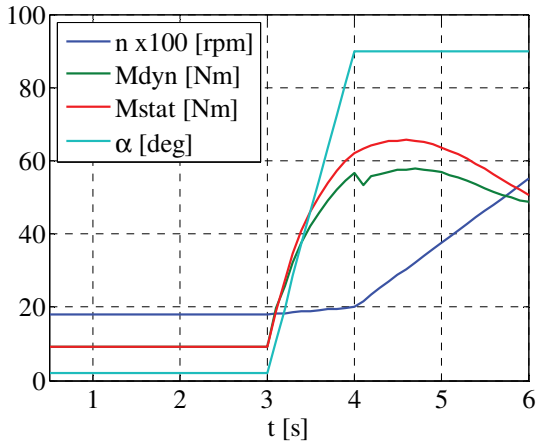


Fig. 14. Engine parameters during full throttle opening lasting 1 s

In Fig. 14 full throttle opening is realized in 1 s. Engine torque rises more slowly and the difference between two characteristics is smaller and equals 11%. So the conclusion is that the more sudden throttle openings are the bigger differences between characteristics become. Because in a city traffic throttle operation is usually realized in a very short time, only characteristic in dynamic states should be used to obtain reliable results e.g. in simulations.

5. Summary and conclusions

The article shows that combustion engine torque characteristic in dynamic working states can be successfully designated with use of proper approach to the problem and with use of proper mathematical analysis. The ANN method allows for taking into consideration few following engine parameters in consecutive moments. Obtained model was verified in three ways: mse error, R parameter and simulations in point 4.

Conducted simulations show that the greatest influence on differences between torque values calculated with use of static and dynamic characteristic has crankshaft angular acceleration. When engine speed raises rapidly, with angular acceleration of about 200 rad/s^2, the engine torque is up to 15% smaller, than it would result from static torque characteristic. The difference between two characteristics decreases both with decreasing angular acceleration and throttle opening angle and becomes negligible with crankshaft acceleration of about 20 rad/s^2.

The next conclusion is that in case of torque changes that occur at constant engine speed there is a very small difference between two characteristics. In such cases, regardless of throttle opening angle and engine speed the difference is smaller than 4%.

Another conclusion from performed simulations is that in case of rapid full throttle opening lasting 0.2 s engine torque raises to top value in time of 0.4 s. Which is quite

much delay in a naturally aspirated engine. In such transient states the use of static characteristic instead of characteristic in dynamic states would result in a very big error up to 30%.

Nomenclature

α	throttle opening angle
ANN	artificial neural network
n	engine speed
M	engine torque
mse	mean square error
v	vehicle speed
SI	spark ignition
ε	crankshaft angular acceleration

Bibliography

[1] BEALE, M.H., HAGAN, M.T., DEMUTH, H.B. Neural network toolbox. For use with Matlab. Release 2012b. *www.mathworks.com*. 2012.

[2] BERA, P. Fuel consumption analysis in dynamic states of the engine with use of artificial neural network. *Combustion Engines*. 2013, **162**(4), 726-731.

[3] BERA, P. The use of artificial neural networks trained in supervised mode to the analysis of measurement data of combustion engines and automotive vehicles. *Silniki Spalinowe i Ekologia*. 2014, Cracow University of Technology Press, 193-204.

[4] ISERMANN, R. Engine modeling and control. Modeling and Electronic Management of Internal Combustion Engines. *Springer*. 2014.

[5] KANG, M., ALAMIR, M., SHEN, T. Nonlinear constrained torque control for gasoline engines. *IFAC-PapersOnLine*. 2016, **49-18**, 784-789.

[6] SERIKOV, S.A. Neural network model of internal combustion engine. *Cybernetics and System Analysis*. 2010, **46**(6), 998-1007.

[7] TOGUN, N.K., BAYSEC, S. Prediction of torque and specific fuel consumption of a gasoline engine by using artificial neural networks. *Applied Energy*. 2010, **87**, 349-355.

[8] YIN, X., GE, A. A dynamic model of engine using neural network description. *Vehicle Electronics Conference*. 2001.

Piotr Bera, DEng. – AGH University of Science and Technology, Faculty of Mechanical Engineering and Robotics.

e-mail: *PBera@agh.edu.pl*



Article citation info:
GIS, W., WAŚKIEWICZ, J. Development of the international freight transport sector in Poland against the background of the EU market. *Combustion Engines*. 2017, **171**(4), 181-184. DOI: 10.19206/CE-2017-430

Wojciech GIS
Jerzy WAŚKIEWICZ

CE-2017-430

Development of the international freight transport sector in Poland against the background of the EU market

Development of Polish international road transport of goods after Poland's accession to the EU. Haulage work carried out between 2005 and 2015. International transport in the context of haulage carried out by the remaining EU transport. Transport arranged by types of haulage in 2005 and in 2015. Development of the number of Polish enterprises and their transport potential measured by the numerousness of the car fleet. Changing structure of the trucks fleet according to the pollutants emission standards in the years 2010–2015. Shaping of the average efficiency of the haulage work by the statistical vehicle. Factors influencing the future demand for international transport performed by Polish carriers. Trends for introducing high-volume lorries to run on the EU roads. Prospects for the development of Polish international freight transport until 2030.

Key words: road transport, international transport

1. Introduction

Growing competitiveness of the Polish international road hauliers as well as the competitiveness of companies from other Central and Eastern Europe as well as Southern European countries has become one of the reasons for some countries from so called "old Union" to try to circumvent the fundamental principle of European Union economic law, that is regarding the internal market as an "area without internal frontiers, where free movement of goods, persons, services and capital is ensured" (Article 26 (2) of the Treaty on European Union) [10]. Such EU countries as Germany, France, Austria, the Netherlands, and Italy are trying to defend their markets against competition from road transport companies from Central and Eastern as well as Southern Europe using the slogans on the need to protect the social rights of all European workers [7]. We are witnessing protectionist actions which are an attempt to restrict access to national markets for the carriers from other EU countries [6]. This is reflected, for example, by the facts of subjective law creation under the Minimum Wage Act, set in Germany in 2015 (MiLoG) and in France (Loi Macron) in 2016. These phenomena are a threat, among the others, to the significant position attained by the Polish carriers in the international market in the recent years [3]. The article presents measurable results of development after 2004 of the Polish international freight transport operating on the competitive transport market.

2. International transport haulage in the context of total haulage of the road transport and other modes of transport

The road transport has for many years been dominating the transport structure in Poland. Its share in volume of the freight transported by land transport in 2015 was about 84%, and its share in haulage work was about 79% [5]. The dynamics haulage by this branch of transport is high. In the years 2005–2015, with an increase in transport by land transport by about 177%, the dynamics of haulage work by the freight transport was 228%.

Following Poland's accession to the EU, obtaining the Community license gave the Polish road haulers more opportunity to operate on the markets of the member states. This was one of the driving factors of the dynamic development of the international transport sector. Other important factors contributing to the development of the sector were, among the others. [9]:

- dynamic development of Polish foreign trade,
- globalization of the market,
- generally good (despite the crisis since 2008), economic climate in Europe,
- easy access to the transport means,
- lower own costs of the Polish carriers compared to the Western carriers' costs,
- expansiveness of the Polish carriers supported by the skills of acquiring and operating on new shipping markets.

Since 2005, the transport conducted by the fleet of Polish-registered international freight transport companies has increased almost four times (204.7 million Mg in 2015) and the haulage work has tripled to 156 billion tkm in 2015 (Fig. 1)

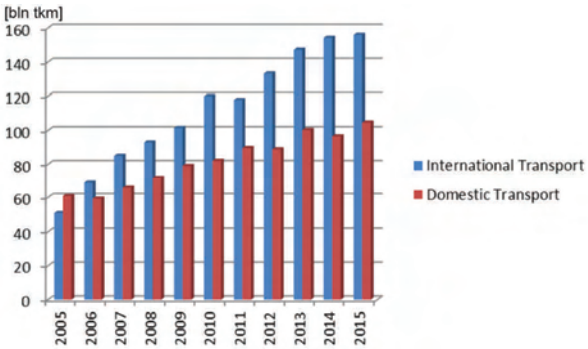


Fig. 1. Haulage work of the Polish freight road transport carried out in the years 2005–2015 by the vehicles exceeding 3.5 Mg GVW [bln tkm] (diagram based on CSO data [5])

Between 2005 and 2015, the average distance travelled by 1 ton of cargo in international freight transport fell from 968 km to 762 km. This decrease was related both to transport from Poland and to Poland and to transport between foreign countries. The average transport distance by 1 ton in cabotage has increased.

In the structure of types of carriage of goods by international road transport in recent years, exports and imports of bulk cargo to Poland has increased almost threefold in the recent years. On the other hand, the haulage carried out by Polish companies between foreign countries increased significantly (six times according to the tonnage transported) and cabotage (less than 11 times) (Table 1).

Table 1. Carriage and haulage work of the Polish international road transport in 2005 and in 2015 by the types of carriage [5]

	2005		2015	
	[thou. t]	[thou. tkm]	[thou. t]	[thou. tkm]
International Transport including:	52551	50886000	204660	156034000
export	21286	20570000	61075	53594000
import	19531	19018000	55756	48864000
Transp. between foreign countries	9314	106450000	56981	44386000
cabotage	2420	653000	26055	8634000

Out of the cabotage transport carried out in 2010 by the Polish companies, ¾ of the shipment was carried out in Germany and France [8].

Polish carriers have dominated the EU's international transport market (Fig. 2). Their market share in 2014 (calculated with respect to haulage work) has already exceeded 25% (Fig. 3) (in 2005 – 8.2%).

For example, the share of German carriers was less than 8%, and French carriers was slightly above 2% (Fig. 3). This fact demonstrates high competitiveness of the Polish road carriers on the international market.

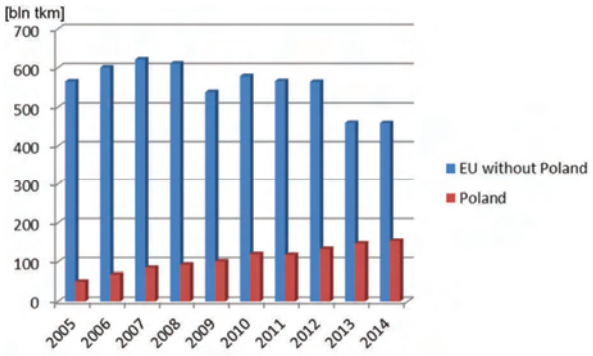


Fig. 2. Haulage work performed by the Polish international freight road transport against the background of international transport haulage work in other EU countries [bln tkm] (diagram based on CSO data [5])

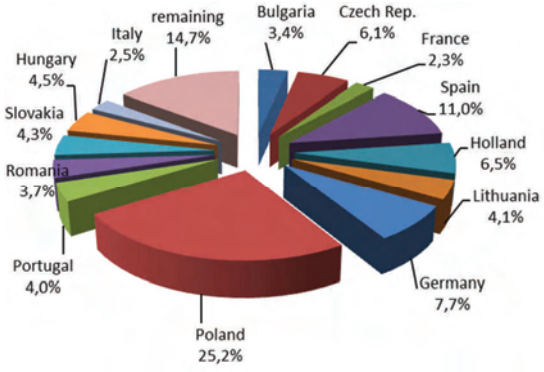


Fig. 3. Structure of international freight transport's haulage work of the EU countries in 2014 (diagram based on CSO data [5])

The goods that are transported mainly by the Polish road transport are (according to the share of haulage work): food, beverages and tobacco products (13.6%), chemicals, chemical products, synthetic fibres, rubber and plastic products (12.6%), metals, metal products (excluding machinery and equipment) (11.9%), wood, wood and cork products (without furniture), straw products, paper and paper products, printing products and sound recordings (10.3%) [5].

3. Structure of the Polish international road transport market

Particularly after 2004, the number of enterprises authorized to conduct international transport of goods, increased. As of the end of 2015 in Poland there were 29 thousand companies holding valid licenses, i.e. operating trucks for profit [4] (Fig. 4).

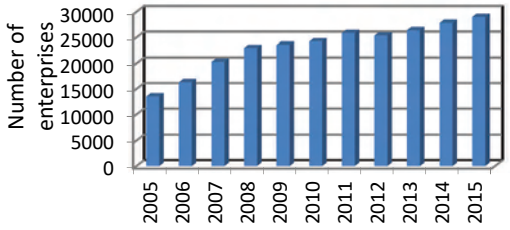


Fig. 4. Number of enterprises authorized to perform international road transport of goods (with valid licenses) between 2005 and 2015 (as of 31 December) (diagram based on GITD data [4])

Between 2005 and 2015, the number of trucks at the companies in question increased 2.5 fold and reached 185.4 thousand at the end of 2015 [4] (Fig. 5).

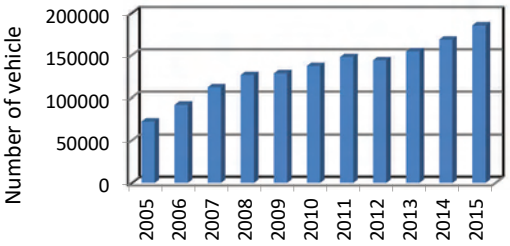


Fig. 5. Number of license excerpts (number of vehicles) of the international freight transport enterprises in the years 2005–2015 (as at 31 December) (diagram based on GITD data [4])

Small, often family-owned businesses dominate the structure of Polish international road freight transport. Companies with up to 4 vehicles account for 2/3 of the total number of companies (Table 2). There is an increase in the size of the statistical enterprise measured by the average number of trucks.

By the end of 2015, the average number of heavy goods vehicles in the international transport company was 6.2 (in 2005 statistically 5.4 in the past years, significant changes in the quality of the car fleet operated by international transport companies have occurred. The vehicles that meet Euro 5 and Euro 6 pollutants emission standards accounted for about 60% of the total fleet at these companies in 2015 (Fig. 6).

Table 2. Number of enterprises and trucks in the international transport in Poland arranged by the size of enterprises (as at the end of 2015) [4]

Number of vehicle at the enterprises	Number of enterprises	Number of vehicle	Avarage number vehicles in the enterprise
1	7038	7038	1
2 to 4	12531	34724	2,8
5 to 10	6618	44776	6,8
11 to 20	2219	31501	14,2
21 to 50	1051	32097	30,5
51 to 100	239	16444	68,8
Above 100	107	18820	175,9
Total	29803	185400	6,2

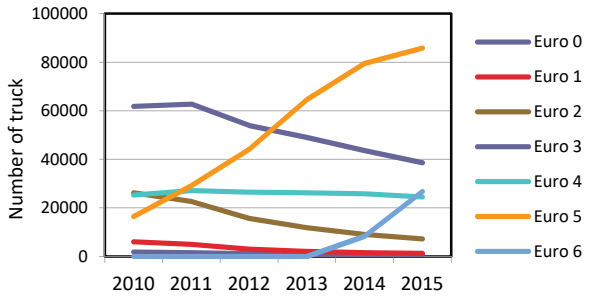


Fig. 6. Number of trucks at the international transport companies according to the pollutants emission standards in 2010 and in 2015 in Poland [4]

At the same time, the share of heavy goods vehicles meeting the requirements of Euro 2 and earlier standards is significantly decreasing.

4. Use of the fleet in the international transport

Since 2005 the international traffic has been witnessing an increase in the average annual productivity of the haulage work of a heavy goods vehicle. In 2005 it amounted to about 701 thousand tkm/vehicle and in 2015 it amounted to about 841 thousand tkm/vehicle (Fig. 7).

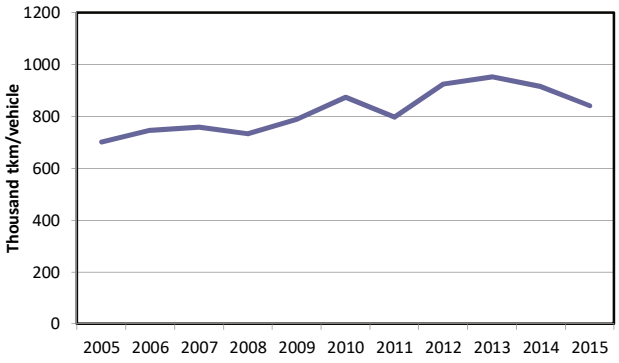


Fig. 7. Average efficiency of haulage work by the statistical vehicle at the Polish international freight transport in the years 2005–2015 [thousand tkm/vehicle] (diagram based on [4] and [5] data)

In 2006–2013 this increase was mainly due to the dynamic development of demand for transport because of the development of international goods exchange, increasing competitiveness of the Polish carriers on the international transport market (cabotage and third country transport). Some decrease in the average annual productivity of the haulage work by the statistical truck after 2013 is due to the growing competition on the international road haulage market caused by strong expansion of carriers of such countries as: Lithuania, Estonia and Slovakia. The competitiveness of road transport from these countries has influenced the decrease in rates for transport services on the European market, observed in the last two years and has led to a decrease in freight rates of Polish carriers, resulting in a decrease in their profitability.

For example, according to the ITS studies [9], average profitability of the Polish international freight transport companies operating usually along the routes to the markets of other EU countries amounted to around 6% in 2015.

In addition, the deterioration in profitability of the international freight transport in the years to come, as compared to 2013, could have been due to the situation on the market following the Russian embargo on some cargoes. This resulted in a temporary surplus of the market capacity supply in the international freight transport, which in turn has led to a decrease in freight rates on the competitive market.

5. Prospects for the international road transport market

The volume of demand for future international road haulage by Polish companies will generally be affected by two groups of factors, including:

- factors that characterize the overall volume of demand including e.g.:
  - Poland's economic potential
  - consumption potential of the society
  - international commodity cooperation
- factors affecting the service supply side by the Polish international road carriers dependent on:
  - services supply potential of the international freight transport in Poland
  - competitiveness of the international freight transport of other countries
  - Polish government policy towards its own road hauliers
  - other countries' policies towards competitiveness of their own international carriers
- effectiveness of the EU policy towards liberalization of the competitiveness rules of the international road hauliers
- effectiveness of the EU policies in terms of shaping changes in modal structure of shipments.

According to some forecasts, the demand for transport services in Europe will double by the 2050, and transport logistics will be covered by the European Union regulations [8]. Expectations on the development of intermodal transport should be expected, both at medium and long distances. In the longer term, the importance of rail transport is likely to increase as a substitute for road transport, although the practice of recent years has led to different trends.

At the same time as regards freight transport, the topic is discussed of allowing to operate, on the roads between the EU countries, the road sets of total weight of up to 44 Mg (instead of 40 Mg). Additionally, after permitting to operate on the roads of Sweden and Finland of the 25.25 m long road trains instead of the currently standardized 18.85 m (semi-trailer with a tractor) [8], the European politicians will have to consider this option, which would have an

impact on the haulage efficiency of the trucks fleet and a decrease in freight rates.

According to one of the latest forecasts prepared by Polish experts [2], the haulage work performed by trucks of Polish international carriers in the year 2030 will amount to 211–231 billion tkm (increase from 169% to 186% in the years 2010–2030).

During the forecast period the dominance of haulage work performed by heavy trucks fleet will be maintained. These are optimistic forecasts for the Polish carriers, signifying great development potential of the international road transport market.

It is predicted that in 2030 about 95% of the haulage work of the entire Polish freight road transport will be carried out with a fleet of above 3.5 Mg GVW.

6. Conclusion

Haulage work of the Polish freight road transport carried out in the years 2005–2015 by the vehicles exceeding 3.5 Mg GVW for international transport is greater than domestic transport.

Haulage work performed by the Polish international freight road transport against the background of international transport haulage work in other EU countries is relatively very large.

Number of enterprises authorized to perform international road transport of goods (with valid licenses) between 2005 and 2015 has increased significantly. Also number of license excerpts (number of vehicles) of the international freight transport enterprises in the years 2005–2015 has increased significantly too.

The numbers of vehicles meeting the requirements of Euro V and Euro VI is also increasing.

The Government of the Republic of Poland takes an unambiguously critical stance on the EC decisions such as the Posting of Workers Directive and on the attempts to regulate national markets through a very broad interpretation of EU regulations by governments of different EU countries (e.g. MiLoG, Loi Macron). These decisions may turn out to be unfavourable for the current significant market position of the Polish international road haulers. The Government of the Republic of Poland argues that "in the face of" emerging changes in the international geo-economic setting that creates a global threat..." the present EU's response should not be practices "... monopolizing markets and regulating isolation under the banner of harmonization, but political and economic consensus". It is emphasized that "reconciling various contradictions of the EU Member States is a necessary condition. The nature of these economic contradictions is rooted in another purchasing power parity as well as the competitive position of the states"[8].

Similar position to that of Poland's also represent governments, among the others of such countries as the Czech Republic, Slovakia, Hungary, Lithuania, Latvia, Estonia, Bulgaria, Romania.

The work on these issues related to the so-called "road package" that is to promote market harmonization whose one of the pillars are "social rules", is continuing in the EC.

Nomenclature

CSO	Central Statistical Office
EU	European Union
GITD	Main Inspectorate of Road Transport
GVW	gross vehicle weight
ITS	Motor Transport Institute
MiLoG	Minimum Wage Act

Bibliography

[1] BENTKOWSKA-SENATOR, K., KORDEL, Z., WAŚKIEWICZ, J. Freight Road Transportation; *ITS*. Warsaw, 2009.

[2] BURNEWICZ, J. Forecasts of the demand for transport in Poland by the 2020 and 2030 (base year 2010)"; Annex 2 to "Transport Development Strategy"; Ministry of Infrastructure; February 2012.

[3] GAWEŁCZYK, P. Who is not in Brussels, that does not count. *Przewoźnik*. 2017, **6**, 8-11.

[4] Main Road Transport Inspectorate; Report – Documents issued by GITD – important in legal proceedings. Status as at 31.12.2015; Warsaw, 28.01.2016, www.gitd.gov.pl.

[5]] CSO "Transport – Results of Operations" for the years 2005–2015.

[6] MAŁYSZKO, T. Carriers fight on the EU ring. *Przewoźnik*. 2015, **5**, 12-13.

[7] Proposal of the Commissioner for Employment, Social Affairs, Skills and Mobility of the Workers concerning the amendment of the basic act on posting of workers (96/71/EC) March 8, 2016.

[8] RACZKOWSKI, K., SCHNEIDER, F., LAROCHE, F. The impact of regulation of the road transport sector on entrepreneurship and economic growth in the European Union" Report. *Motor Transport Institute*. Warsaw–Linz–Lyon, February 2017, p. 57.

[9] WAŚKIEWICZ, J., KORDEL, Z., BALKE, I. Monitoring selected road transport market areas. Task No. 2 entitled: Studying average unit costs and transport rates at the international freight transport companies. *ITS*. Work No. 6501/2/ZBE; Warsaw 2016, p. 12.

[10] Concise version of the Treaty on European Union and the Treaty on the Functioning of the European Union; Official Journal of the European Union 2012/C 326/01.

Wojciech Gis, DSc., DEng. – Motor Transport Institute.

e-mail: *Wojciech.Gis@its.waw.pl*



Jerzy Waśkiewicz, DEng. – Motor Transport Institute.

e-mail: *Jerzy.Waskiewicz@its.waw.pl*



Article citation info:
SKOWRON, M., PIELECHA, I., WISŁOCKI, K. Optical tests as the basis for creating mathematical models to delay opening of CIDI injectors. *Combustion Engines*. 2017, **171**(4), 185-192. DOI: 10.19206/CE-2017-431

Maciej SKOWRON
Ireneusz PIELECHA
Krzysztof WISŁOCKI

CE-2017-431

Optical tests as the basis for formulating mathematical models of the opening delay of CIDI injectors

The main objective of this research was an attempt to evaluate the delay times of the actual needle opening of the diesel injectors in relation to the time of triggering the current control signals opening the solenoid and piezoelectric high-pressure injectors of diesel engines. The conducted tests take into account the variability of fuel injection pressure and backpressure prevailing in the operational chamber of the engine. To determine accurately the time of actual injection start, the optical tests analysing the image of the injector tip were used. Such high resolution images were obtained by high-speed recording with a frequency of 250 kHz (Δt = 0.004 ms). Based on a comparison of the results obtained, it was found that the maximum delay time of fuel injection for a piezoelectric diesel injector is about 12% shorter than for a solenoid injector.

Experimentally obtained results of the injection time delay were used as a basis to formulate mathematical models describing the delay of the real fuel injection in relation to the signal controlling the opening of the diesel injectors. These models take into account the dependence of the injector reaction from the injection pressure and the backpressure in the operational chamber of the engine. The correctness of the obtained models is confirmed by acceptable values of the determination coefficient (for solenoid injector – 0.6, for piezoelectric injector – above 0.8 – for correlation of injection delay and backpressure).

Key words: *diesel fuel, direct injection, injection delay, optical research, solenoid and piezoelectric injector*

1. Introduction

High pressure liquid fuel injection used in common rail system requires precise dosing of fuel through the injectors. Currently solenoid or piezoelectric injectors are used both in spark-ignition and diesel engines. Petrol injection systems operate at lower values of injected fuel pressure than CI engine systems, but fuel injection times are similar. This tendency causes that the requirements of engine injectors with SI and CI are similar. They should demonstrate short response time to input signals (controlling signals) and, at the same time, short closing times of injectors with high repeatability of the voltage-current signals.

The studies on the two types of injectors were conducted by Yu et al. [7], where the base fuels were kerosene and diesel. Using only electrical signals triggering injector (control signal) and changes in the flow of fuel from the injector, the fuel flow delay was specified. Permanent delay values regardless of the fuel injection pressure (were obtained 60 or 100 MPa). For piezoinjectors this time amounted to 0.45 ms, while for electromagnetic injectors to 0.55 ms. In addition, a significantly higher fuel flow rate at lower pressures of injected fuel were observed. It was stated that such an increase in the rate of the fuel flow brings tangible benefits in actual engines in the form of better atomization and evaporation of the fuel. Optical studies of the authors concerned only observation of the development of fuel spray planes and not delay assessment of fuel flow from the injector.

Research carried out by Zhou et al. [8] concerned the possibility of determining fuel flow rate for each of the little openings in the injector. The studies used a conventional injection system with a serial pump used in CI engines of the off-road vehicles. Based on the results of the fuel flow, the diversity of the fuel flow time for individual openings can be determined. Those differences amount to 2 degrees of rotation of the pump shaft at the speed range for this pump of 800–1000 rpm.

In research conducted by Salvador et al. [3] the opening delay was specified as the difference of the time of injector triggering (start of energizing) and the flow of fuel from the injector was determined in the system for measuring fuel flow rate (start of injection). The tests were conducted for fuel pressures ranging from 30 to 180 MPa and at different fuel temperatures. It was shown that with increasing fuel pressure the injection delay decreases. It amounts to 0.24-0.28 ms. This delay increases with decreasing fuel temperature. At fuel temperature of 253 K and P_{inj} = 40 MPa it is about 0.35 ms.

Optical studies on piezoelectric injectors were conducted by Magno and et al. [2]. These studies focused on the analysis of the difference in the rate of fuel flow from a new injector and an injector contaminated by long-lasting operation. Injection rate measurements have proven to be a useful tool to demonstrate that a contaminated injector operates with a delay in relation to the new injector. It was also found that both injectors inject a similar amount of fuel, but with altered characteristics of the injection. In fact, contaminated injector injects a bigger amount of fuel as a pilot dose, but smaller as the main dose. The studies didn't analyze, however, the delay of the fuel flow from the injectors.

Duan et al. [1] while conducting test on the new type of electromagnetic injectors obtained a hydraulic delay of 0.406 ms (at P_{inj} = 250 MPa, and energizing time = 1.5 ms). Compared to currently produced injectors, the hydraulic delay values were reduced by 11.5% (Cummins injector) and 24.8% in relation to the Bosch injector (for which the studies with the same values of configurable parameters were conducted).

Analysis of the literature showed a large number of publications concerning the determination of:

1) electrical signals parameters,
2) hydraulic parameters of piezo- and solenoid injectors; however, there is a lack of works indicating the assessment of the actual beginning of the flow from the injector while taking into account the electric and hydraulic delay in relation to the emergence of electrical signals controlling the beginning of the injection.

Previous works of the authors of this article [4–6] concerned the initial research to this problem. Optical tests conducted within these studies on the delay of hydraulic flow of fuel were carried out at the filming speed of 50 kfps (thousands of images per second). They confirmed the applicability of optical testing to determine the time of the start of fuel flow from the injector; it is recommended, however, to use a higher time resolution. More accurate research with an increased rate of filming for injectors in CI engines were partly completed in the current studies, in which the speed of filming has been greatly increased up to 250 kfps.

2. The research problem

The aim of this publication is the elemental analysis of the impact of injection parameters on the fuel injection delay (fuel pressure and air backpressure). On the basis of this analysis the mathematical description of the fuel injection delay relating to high-pressure electromagnetic and piezoelectric diesel injectors was developed. The acquisition of such a model is crucial in terms of issues concerning controlling combustion engine with the CIDI.

3. Research methodology

It was decided that the above formulated task would be resolved with the use of experiment involving optical methods. A constant volume chamber (CVC) was used to simulate the backpressure in the cylinder during fuel injection, as well as the combination of the system for measuring fast-varying process and the high-speed camera for fast registration of photos. Such a combination of apparatus for the acquisition allowed conducting synchronized measurements of the electrical signals at the injector and the observation of the physical appearance of drops in the measuring chamber. So prepared test bench is shown in Fig. 1. Parameters of the tested injectors are shown in Table 1, and the technical specifications of the recording apparatus are shown in Tables 2 and 3. For the purpose of these tests the frequency of 250 kHz ($\Delta t = 4$ μs) was used for recording optical tests and of 500 kHz ($\Delta t = 2$ μs) for recording electrical signals. To connect and synchronize both data types a flash light of diode was used.

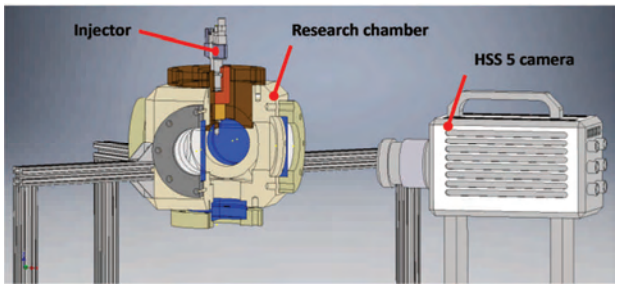


Fig. 1. Diagram of the test bench for optical analysis of the delay of fuel injection

As a control apparatus a sequencer was used generating a TTL signal (0–5 V) on the basis of which the systems triggering injection, the camera and the diode are controlled. For the tests were used two different injector common rail systems: the first was the piezoelectric injector, the other – solenoid injector (both by Bosch). Parameters of the injectors tested are presented in Table 1.

Table 1. Characteristics of the injectors

Parameter	Solenoid	Piezoelectric
Static flow	520 cm^3/min	705 cm^3/min
Angle of the cone of fuel spray	162 deg	–
Number of orifices	9	8
Fuel injection pressure	25–180 MPa	up to 200 MPa

Table 2. Details of the optical setup and devices employed to evaluate the fuel injection delay

Camera	LaVision High Speed Star 5
Light source	Halogen lamp – 2 × 500 W
Camera lens	Nikon Nikkor
Lens features	50 mm – f/1. 4
Image size (pix)	128 × 16
Frame rate (fps)	250,000
Test repetitions	2

Table 3. Details of the fast-varying setup and devices employed to evaluate the fuel injection delay

System	AVL Indimodule
Analog input channels	8 (0–10 V)
Maximum sampling rate	800 kHz
Software	AVL Indicom – recording system AVL Concerto – data analysis system
On board memory	64 MB

For such configured test bench test points that corresponded to the operation points of the injector during supplying the combustion engine were selected. The injection pressure, injector opening time (due to the difference of injector parameters, it was decided to use the longer opening times of opening for electromagnetic injector) and backpressure of the medium into which fuel was injected were subjected to analysis. The range of variation of these parameters is shown in Table 4. Each test point was repeated to confirm the result obtained.

Table 4. Points of measurements

Parameter	Value
Injection pressure P_{inj}	30–120 MPa; $\Delta P = 30$ MPa
Back-pressure in the CVC P_b	2.5–4 MPa; $\Delta P = 0.5$ MPa
Energizing time ET	0.2; 0.4; 0.6 ms for piezo-injector 0.3; 0;5; 0.7 ms for solenoid injector
No. of iterations	2 for each point

Delay for these tests was defined as a component of two factors. The first was the time of current rise in the system (defined as electrical delay – t_e, Fig. 2) and the other – the appearance of drops in the chamber, called a hydraulic delay – t_h. Only the sum of these two delays gives a complete picture of the entire delay between the injection request signal and its physical realization (according to Eq. 1).

$$t_d = t_e + t_h \quad (1)$$

Synchronization of the tests (optical and electrical) made it possible to determine the total time of delay in operation of injectors (t_d): electrical delay is defined as the time between the appearance of the TTL control signal, and the beginning of the current rise (I_{inj}) in the system (Fig. 2). The hydraulic delay is defined as the time from the moment of the current rise to the appearance of the first drops in the measuring chamber. So defined hydraulic delay time, due to the need of the use of two separate methods of recording (electric signal and photos) is described by Eq. 2.

$$t_h = t_1 + t_2 \quad (2)$$

The course of the current-voltage characteristics of the investigated piezoelectric injector of diesel is shown in Fig. 3.

The time from the moment of current rise until the moment the diode flash was defined as t_1. This interpretation made it possible to combine optical tests and registration of electrical signals.

The method of processing the results of optical tests is illustrated in Fig.4. First, the background image was subtracted in order to remove random reflections. Then the frame with a lit diode was found – from this frame the time in optical tests was measured. The other important recorded frame is the moment of fuel flow from the injector (100 µs in Fig. 4). The time between these frames is marked as t_2. The sequence showing the determination of the time t_2 is presented in Fig. 4.

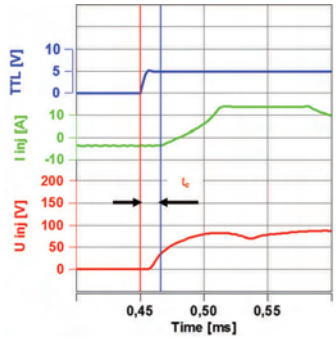


Fig. 2. A method for determining the electric delay for solenoid injector (based on data from solenoid injector: ET = 0.5 ms, P_{inj} = 120 MPa, P_b = 40 MPa)

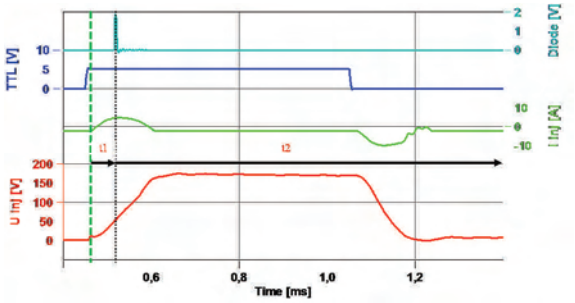


Fig. 3. A method for determining the time t_1 for the hydraulic delay (based on data from piezoelectric injector: ET = 0.6 ms, P_{inj} = 30 MPa, P_b = 25 MPa)

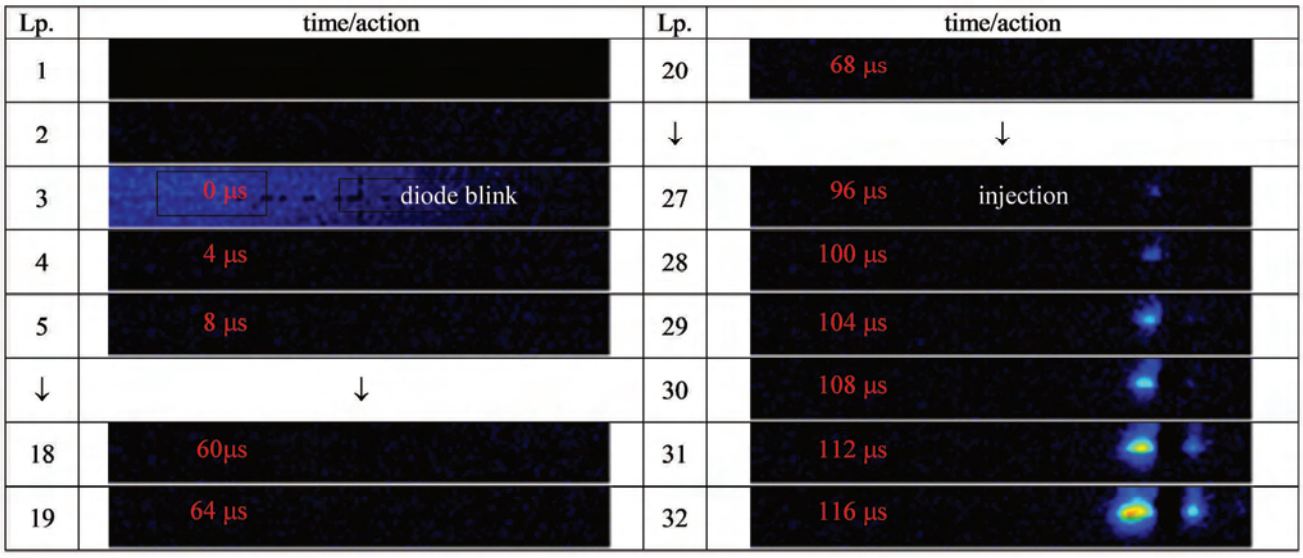


Fig. 4. Optical research algorithm to achieve time t_2 (based on data from solenoid injector: ET = 0.5 ms, P_{inj} = 120 MPa, P_b = 40 MPa)

4. Investigation of injection delay for piezo- and solenoid injectors

The tests carried out indicated the difference in the delay of both electromagnetic and piezoelectric injectors. Basing on the analysis of the obtained results, the factors were defined and their influence on the delay of injection. In the analysis the difference of the results at a level of 4 µs (resulting from the frequency of recording) should be treated as the same result due to the measurement uncertainty. The effect of such assumptions is demonstration of actual trends arising from the phenomena taking place during injection. A summary of the results obtained is shown in Fig. 5 for the solenoid injector and in Fig. 6 for piezoelectric injector. In the summary, the points with the same energizing time of the injection were located in one chart, allowing analysis the influence of injection pressure and back pressure (Fig. 7, Fig. 8).

Based on the results obtained, the operation of the electromagnetic injector can be assessed showing higher repeatability in relation to the piezoelectric injector. The

increase of the injection pressure was indicated as the main value determining an injection delay for electromagnetic injector. Comparing the test points it can be concluded that there is a significant randomness in operation of the piezoelectric injector. The analysis failed to show a trend for the impact of the triggering signal duration on the injection delay. It is possible to characterize the results for both injectors at injection pressure of 30 MPa – for this scope in both cases the increasing backpressure has influence on reduction of the delays.

The above-presented methodology of analysis was considered inadequate; therefore, it was decided to complement it with additional assessment tools based on mathematical statistics in order to obtain a more comprehensive assessment of the results obtained.

It was decided to use, subsequently:

– a mean value,
– medium value,
– dominant value.

After complementing the analysis with the indicated statistical options, again the summary of the results was carried out, but in this case adopting different criteria for the presentation of data. Summary to verify the impact of the injection time on the delay is shown in Figs 7 and 8, respectively, for solenoid and piezoelectric injector.

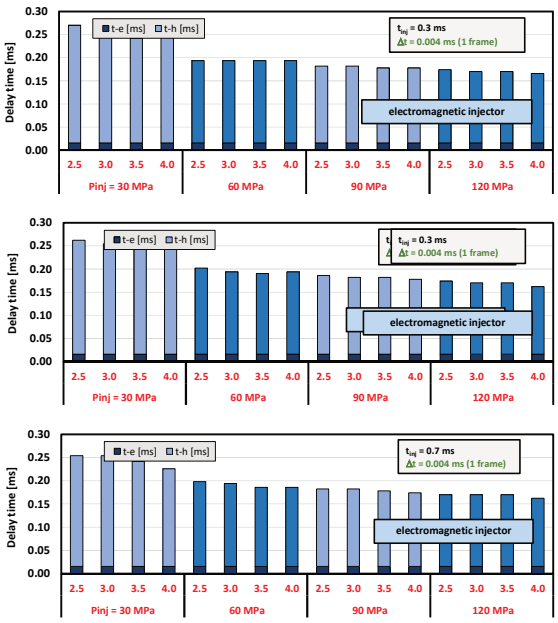


Fig. 5. Analysis of the times of injection delay at variable pressure of fuel injection and backpressure of air during solenoid injector operation

The summary for electromagnetic injector does not show any higher impact of the time of input signal of injection opening on the injection delay, which is a problem while defining the relationships. Overlapping of statistical values marked on the graphs with horizontal lines (Figs 7 and 8) confirms the inability to indicate the specific dependencies. However, a tendency for the lowest and highest injection pressure is visible, indicating that the increase of the backpressure in the chamber causes the acceleration of the injector opening. Two middle pressure injection settings, however, do not confirm this dependency.

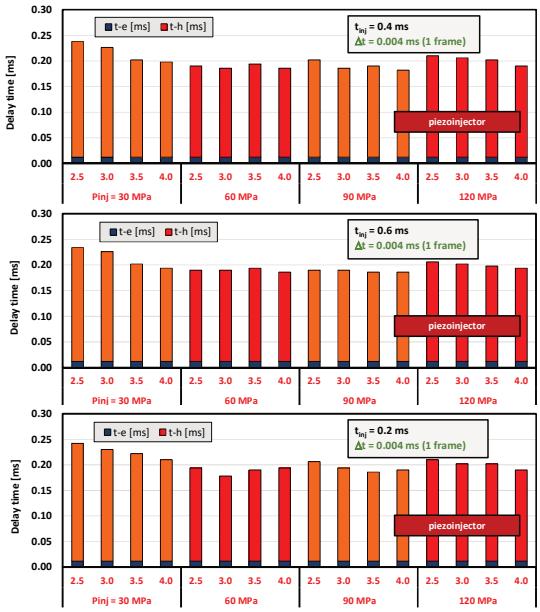


Fig. 6. Analysis of the times of injection delay at variable pressure of fuel injection and backpressure of air during piezoelectric injector operation

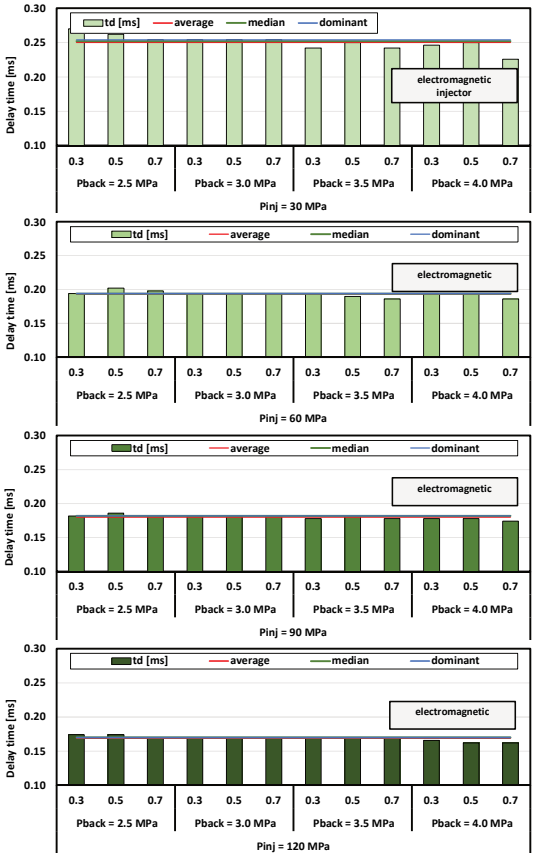


Fig. 7. Comparison of the times of fuel injection delays for electromagnetic injector for constant fuel injection pressure at variable backpressure and different energizing time

For a piezoelectric injector there is also no clear trend indicating the impact of input signal time on the injector response. This type of data presentation (Figs 7, 8) indicates the trends mentioned earlier in the positive influence of backpressure on the value of injection delay.

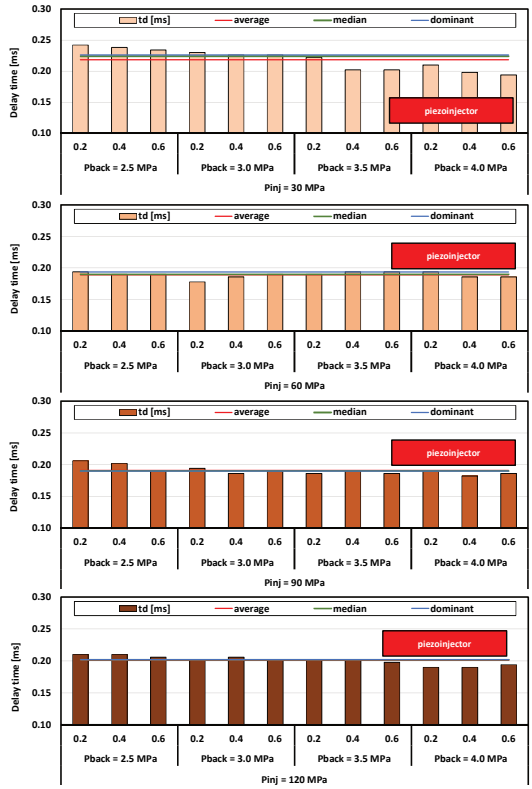


Fig. 8. Comparison of the times of fuel injection delays for piezoinjector for the constant fuel injection pressure at variable backpressure and different energizing times

5. An attempt to describe in mathematical terms the fuel flow delay

5.1. The impact of the fuel pressure on the delay of fuel outflow

The next stage of the study was an attempt at a mathematical description enabling obtaining the estimated value of the injection delay without the necessity to conduct tests. For this purpose the results were summarized and an attempt was made to assign the function best reflecting a trend that occurs between the fuel outflow delay and injection control parameters.

The first selected value, in relation to which the analysis was performed, was the injection pressure (for constant energizing time and backpressure) shown in Figs 9 and 10, for electromagnetic and piezoelectric injector, respectively. This analysis was presented for the mean, dominant and median value of injection delay time obtained from investigations. As the describing dependencies of this relation were selected linear, power and polynomial functions. For so selected functions the coefficient of determination was determined and, on this basis, the correctness of the description of this phenomenon with the use of indicated functions was estimated.

In all cases of results achieved for an electromagnetic injector, the power and polynomial functions produce a similar value of the coefficient of determination. The highest value was obtained for mean values described by the polynomial function of degree 2 and it amounted to R^2 = 0.977. Matching at this level is satisfactory for polynomial and exponential functions.

The same analysis procedure was performed for piezoinjectors. In this case, the descriptions of the linear and power functions were characterized by a coefficient of determination the values of which pointed out to insufficient the phenomenon description using these functions. Again, as in the case of electromagnetic injector, the best match was obtained using a polynomial function, however, the best match was obtained on the basis of the dominant, where R^2 = 1. For piezoelectric injectors, the analysis using various statistical measures indicates different characteristics of the dependency, which confirms the previous conclusion indicating the randomness of the injector operation.

The data analysis indicated the trend of changes for the electromagnetic injector was shown in Fig. 11. For the lowest injection pressure, the greatest differences were found for points with extreme backpressure values in the test chamber. This area alone has a clear tendency to show dependence on the backpressure.

It was assumed that the fuel injection time does not affect the opening delay of the electromagnetic injector. In this aspect, the opening delay of the injector t_d was related to the fuel pressure P_{inj} and the back pressure of the medium P_b (Fig. 11).

Due to the specificity of injection delay time, analysis was divided into two stages:

1) for injection pressure of 30 MPa – within this scope only the dependence on the back pressure of the medium was shown;

2) for injection pressure above 30 MPa: within this scope the mathematical relationship between both, the fuel pressure and the pressure of the medium was determined. The results of these tests are presented in the following sections.

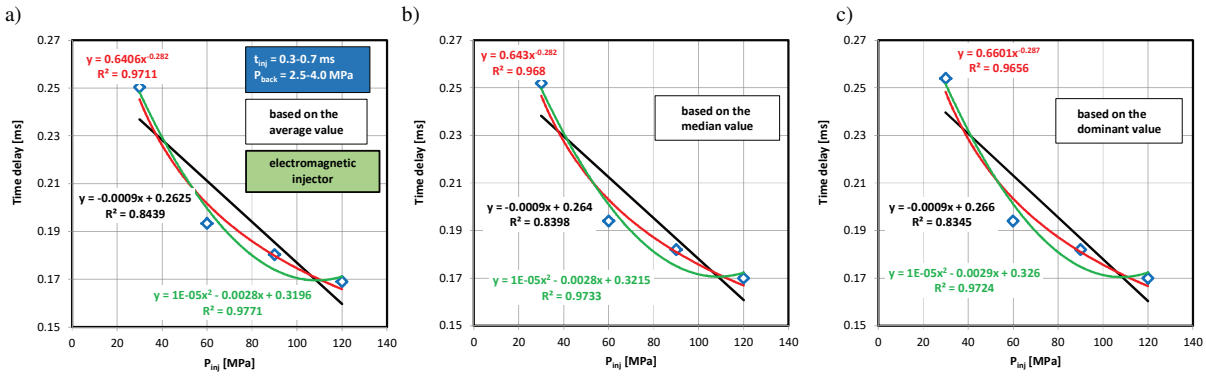


Fig. 9. Determination of mathematical models for electromagnetic injectors flow delay based on: a) mean values, b) values of the median, c) values of dominant, assuming independence of delay time from the time of the injection and backpressure

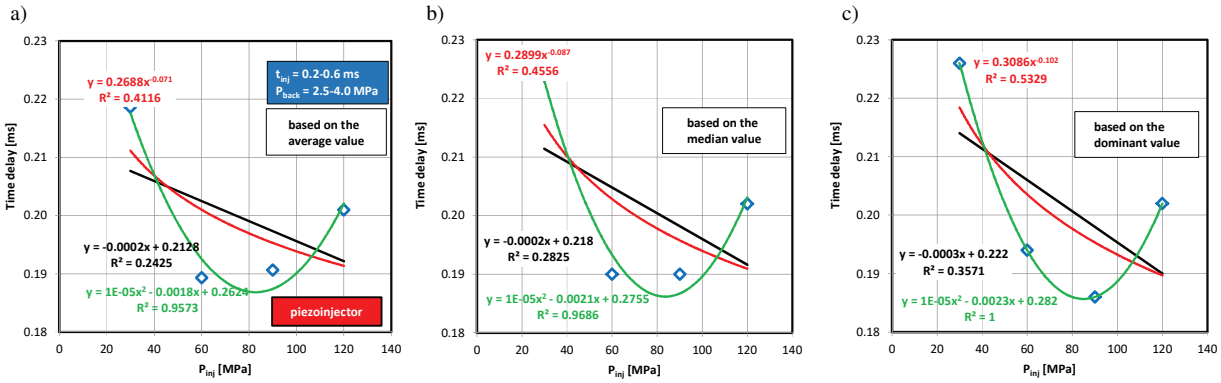


Fig. 10. Determination of mathematical models for piezoelectric injectors flow delay based on: a) mean values, b) values of the median, c) values of dominant, assuming independence of delay time from the time of the injection and backpressure

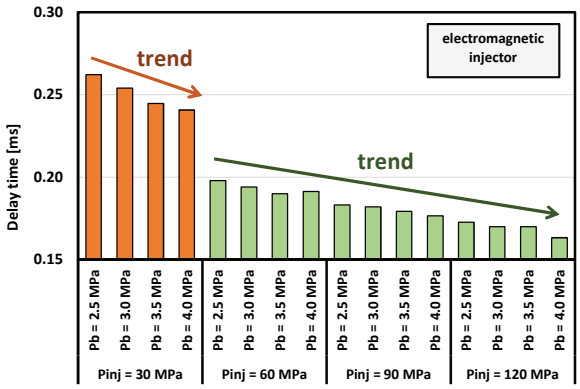


Fig. 11. Dependency of the delay time of opening of the electromagnetic injector from the injection time and backpressure of the medium

5.2. The impact of the backpressure of the medium on the delay of fuel outflow

The earlier assumptions about the parameters in relation to which a mathematical dependency is to be constructed require an initial estimate of the average step of change. Figure 12 shows a summary that provides information about the average change of the injection delay in relation to backpressure. A linear relationship was used to describe the mean change in injector response and the coefficient of determination was checked, which for both electromagnetic and piezoelectric injectors obtained a value of 0.98. The description of such a relationship was considered to be sufficient and further analysis was carried out to obtain an empirical equation describing the injection delay for the indicated area of operation of the injector.

5.3. A mathematical formula of the of fuel outflow dependency from the injector

Based on the previous analyzes performed within the study and the information that delay at low pressure values mainly depends on the value of backpressure of the medium, its mathematical form was determined.

For both types of injectors one type of equation was adopted, taking into account the value of backpressure of the medium (at a constant fuel pressure P_{inj} = 30 MPa) supplemented with the following coefficients: slope of line 'a' and exponent 'b'. The general equation is proposed arbitrary in the following form:

$$t_{d(Pinj = 30\ MPa)} = a \cdot P_b^{\ b} \qquad (3)$$

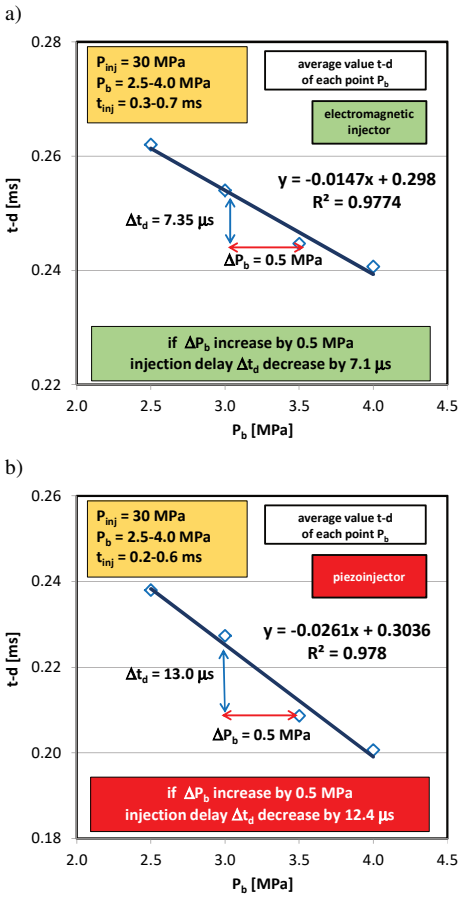


Fig. 12. Analysis of the change of fuel injection delay during changing the backpressure of the medium (P_{inj} = 30 MPa) on the basis of the average values of fuel injection using injectors: a) solenoid, b) piezoelectric

Determination of 'a' and 'b' coefficients requires the use of pseudo-optimization methods (which are here accepted as searching for proper function form and determination as the function's parameters). The optimization criteria are presented in the form of a decision to be minimized f(U), expressed as the sum of squares of differences of the individual values of delays of fuel flow dependent only on the backpressure of air, designated experimentally and based on equation (3).

A mathematical model contains the decision variables, constraints, and decision-making function:

– decision variables: a, b – coefficients of the equation (3),

– constraint (designating the range of acceptable solutions): a, b ≠ 0, values can be negative and positive, excluding zero (such value eliminates the equation),
– decision-making function: U(a, b) fulfils the constraint, for which the decision-making function f(U) reaches a minimum:

$$f(U)=\sum_{i=1}^{n}\left((t_d)_{ci}-(t_d)_i\right)^2 \rightarrow \min \qquad (3)$$

where (t_d) – is the calculated delay value for given data of the parameters P_b, $(t_d)_i$ – means a test value of the delay for the same values of P_b; i – is a subsequent value.

Using a solver implemented in MS Excel, a nonlinear solution to the task with nonlinear constraints was obtained. As mentioned earlier for this case only data used for injection pressure 30 MPa were used.

This procedure is presented in Fig. 13, where the dependence (3) is considered as the optimization criterion of the equation. The coefficient of determination value for the piezo-injector was found to be satisfactory for the result obtained. In case of the electromagnetic injector, the result is unsatisfactory even to estimate the injection delay. After obtaining the results and their qualitative assessment, it was decided to move on to the next stage in which the empirical equation was extended by the injection pressure parameter.

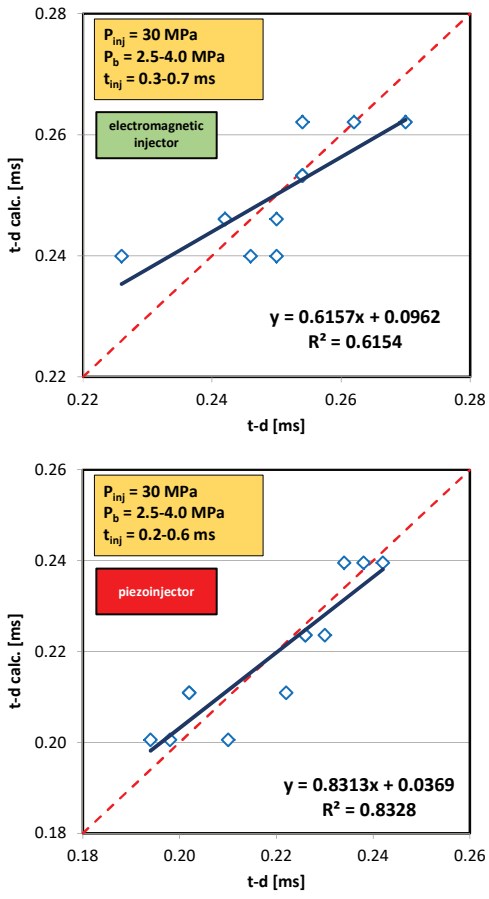


Fig. 13. The dependency of the fuel injection delay determined experimentally and analytically (conditions of the analysis are given in the figure; equation for electromagnetic injector: $t_d = 0.3112 \cdot P_b^{-0.187}$; equation for piezoinjector: $t_d = 0.3387 \cdot P_b^{-0.378}$)

Analysis of fuel injection delay at higher pressure values (Fig. 14) of fuel makes it possible to make the delay time dependent on two parameters: fuel pressure and backpressure of the medium. Using function:

$$t_{d(Pinj > 30\ MPa)} = a \cdot P_b^{\ b} \cdot P_{inj}^{\ c} \qquad (5)$$

and the optimization criterion given in equation (4), the coefficients "a" "b" and "c" were determined making it possible to determine the correlation between experimental and calculated delay values. Coefficient of determination is $R^2 = 0.94$, indicating a good match of the obtained coefficients with the experimental fuel injection delay.

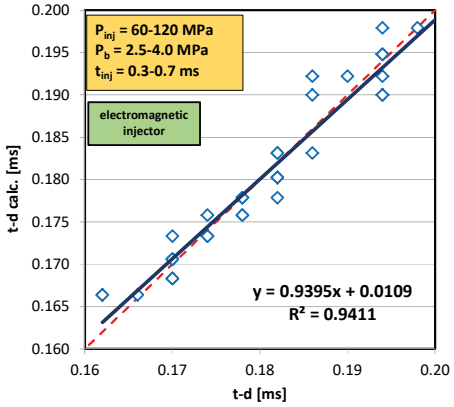


Fig. 14. Dependency of experimentally and analytically determined delay of fuel injection from electromagnetic injectors from fuel pressure and backpressure of the medium (conditions of analysis are given in the figure)

Table 5. The parameters characterizing fuel injection delay for diesel engines: piezo- and solenoid injectors

	Electromagnetic injector	Piezoinjector
Maximum injection delay	0.27 ms	0.24 ms
Delay ratio EM/P (P/EM)	1.125 (1)	1 (0.888)
Increase Δt_d if ΔP_b increase by 0.5 MPa	–7.35 µs	–13.0 µs
Equation of injection delay (only for P_{inj} = 30 MPa)	$t_d = 0.3112 \cdot P_b^{-0.187}$	$t_d = 0.3387 \cdot P_b^{-0.378}$
Coefficient of determination, R^2	0.6154	0.8328
Equation of injection delay (for P_{inj}> 30 MPa)	$t_d = 0.469 \cdot P_b^{-0.0869} \cdot P_{inj}^{-0.191}$	no correlation
Coefficient of determination, R^2	0.9411	–

Full analysis of the parameters of fuel injection delay and the process of optimization are presented in Table 5. A higher coefficient of determination was obtained when mathematical dependence was created for piezo-injectors, with the dependency of injection delay time only from backpressure (at injection pressure of 30 MPa).

The dependency describing the injection delay from the fuel pressure and the backpressure of the medium was determined only for electromagnetic injectors for the fuel pressure range above 30 MPa.

6. Summary

An electric and optical analysis of the gasoline injection delay makes it possible to determine the parameters characterizing the process. The use of averaged data indicates that any increase in air pressure ΔP_b by 0.5 MPa results in an

increase in the operating delay of the electromagnetic injector by 5.65 μs. Using experimental research, the mathematical dependence of the delay in injector operation time from the air backpressure was determined, as shown in Table 5. These equations were obtained for relatively high values of coefficients of determination, which means a large convergence with the results of experimental research.

As the results of experimental studies different times of fuel injection delay relating to electromagnetic and piezoelectric injectors were obtained.

Experimental studies allowed some observations and conclusions to be made regarding diesel fuel injectors:

1. A delay in opening the injectors can be described with the use of mathematical models in which the fuel pressure and backpressure of the medium are taken into account. The operation analysis of the solenoid injectors supplying diesel fuel indicates the reduction of the fuel flow delay time from the injector with the increasing fuel pressure (within the range from 30 to 120 MPa). Delay of diesel fuel flow from piezoelectric injectors is reduced only in the range of 30–60 MPa. For further increasing fuel pressure, the delay is constant or slightly increased.
2. At a pressure of 30 MPa the delay time for solenoid injectors of diesel fuel is proportional to the backpressure of air. Any increase in the backpressure of the air ΔP_b by 0.5 MPa decreases the time of fuel flow delay by 7.35 μs.
3. At low values of fuel pressure (30 MPa) the delay time for piezoelectric injectors of diesel fuel is proportional to the backpressure of air. Any increase in the backpressure of the air ΔP_b by 0.5 MPa decreases the time of fuel flow delay by 13.0 μs.
4. Delay of fuel flow from diesel fuel injectors at fuel supply pressure above 30 MPa is described by the dependence using P_{inj} and P_b and as a result the high compatibility of the equation with the experimental results was obtained. Unfortunately, this dependence could only be determined for electromagnetic injectors.

Nomenclature

CI	compression ignition
CNG	compressed natural gas
CVC	constant volume chamber
DI	direct injection
ET	energizing time (= t_{inj})
LPG	liquefied petroleum gas
P_b	back pressure
P_{inj}	injection pressure
SI	spark ignition
t_d	total time of delay
t_e	electrical time delay
t_h	hydraulic delay time

Bibliography

[1] DUAN, L., YUAN, S., HU, L. et al. Injection performance and cavitation analysis of an advanced 250 MPa common rail diesel injector. *International Journal of Heat and Mass Transfer*. 2016, **93**, 388-397.

[2] MAGNO, A., MANCARUSO, E., VAGLIECO, B.M. Experimental investigation in an optically accessible diesel engine of a fouled piezoelectric injector. *Energy*. 2014, **64**, 842-852.

[3] SALVADOR, F.J., GIMENO, J., CARRERES, M., CRIALESI-ESPOSITO, M. Fuel temperature influence on the performance of a last generation common-rail diesel ballistic injector. Part I: Experimental mass flow rate measurements and discussion. *Energy Conversion and Management*. 2016, **114**, 364-375.

[4] SKOWRON, M., PIELECHA, I. Analysis of injectors reaction on the external signals in direct injection systems. *Journal of Mechanical and Transport Engineering*. 2016, **68**(3), 39-51.

[5] SKOWRON, M., PIELECHA, I. Evaluation of difference between controling signal and injector response time in liquid fuel direct injection systems. *Combustion Engines*. 2015, **162**(3), 327-334.

[6] SKOWRON, M., PIELECHA, I., WISŁOCKI, K. Transient states analysis of CI engine injectors with the use of optical methods. *Publishing IOP Conf. Series: Materials Science and Engineering*. 2016, **148**, 1-8.

[7] YU, W., YANG, W., TAY, K. et al. Macroscopic spray characteristics of kerosene and diesel based on two different piezoelectric and solenoid injectors. *Experimental Thermal and Fluid Science*. 2016, **76**, 12-23.

[8] ZHOU, L.Y., DONG, S.F., CUI, H.F. et al. Measurements and analyses on the transient discharge coefficient of each nozzle hole of multi-hole diesel injector. *Sensors and Actuators A: Physical*. 2016, **244**, 198-205.

Maciej Skowron, MEng. – Faculty of Machines and Transport at Poznan University of Technology.

e-mail: *Maciej.Skowron@put.poznan.pl*



Ireneusz Pielecha, DSc., DEng. – Faculty of Machines and Transport at Poznan University of Technology.

e-mail: *Ireneusz.Pielecha@put.poznan.pl*



Prof. Krzysztof Wisłocki, DSc., DEng. – Faculty of Machines and Transport at Poznan University of Technology.

e-mail: *Krzysztof.Wisłocki@put.poznan.pl*



Article citation info:
SKARBEK-ŻABKIN, A. Effect of the addition of synthetic fuel on the selected physico-chemical properties of the fuel for the diesel engines. *Combustion Engines*. 2017, **171**(4), 193-195. DOI: 10.19206/CE-2017-432

Anna SKARBEK-ŻABKIN

CE-2017-432

Effect of the addition of synthetic fuel on the selected physico-chemical properties of the fuel for the diesel engines

Plastics present a major threat to today's society and environment. Though mankind has awoken to this threat and responded with developments in creating degradable bio plastics, there is still no conclusive effort done to repair the damage already caused. In this regard, the catalytic depolymerization studied here presents an efficient, clean and very effective means of removing the debris that we have left behind over the last several decades. By converting plastics to fuel, we solve two issues, one of the large plastic seas, and the other of the fuel shortage. This dual benefit, though will exist only as long as the waste plastics last, but will surely provide a strong platform for us to build on a sustainable, clean and green future. The paper presents results of density, viscosity, cetane number, ignition temperature of 100% synthetic fuel and this fuel's mixture with the diesel oil. The quality of the fuel-air mixture formation is best characterized by the SMD parameter – Sauter's average diameter of spray drops, and its value in analytical studies depends on the physical parameters of the fuel (density, viscosity, surface tension). The results of laboratory tests will be developed in terms of the use of the measured parameters of a synthetic fuel mixture to calculate SMD values and to correct analytical equations taking into account the actual SMD values measured by laser diffraction laboratory tests.

Key words: *alternative fuels, polymer materials, synthetic fuel, diesel engines*

1. Introduction

Over the past 150 years, plastics have enabled innovation and contributed to the development of society and the growth of its prosperity. Thanks to plastics, the society can meet challenges of the 21st century. Only 4 to 6% of the world oil production is consumed for its production. Plastics are the material commonly used for the production of a wide variety of products that are applicable in practically all areas of life. As a consequence, the share of these wastes in the municipal waste stream is increasing, which is a serious environmental problem. Due to the value of the raw material, all plastics waste should be recovered – either by recycling or by energy recovery. One way to utilize and use them is to convert them into liquid synthetic fuel.

2. Alternative fuels

Selected physicochemical properties of the fuel have been determined, which have a decisive influence on the correct operation of the internal combustion engine, its performance and the cleanliness of the exhaust gases emitted into the environment. The primary raw material for the production of engine fuels is crude oil, whose consumption has steadily increased over the recent years. Increasing demand for liquid fuels with scarce resources, rising oil prices and tougher environmental regulations has led to the need for new alternative energy sources.

Alternative fuels are divided into gaseous and liquid fuels. Synthetic fuel is classified as liquid fuel and obtained by chemical synthesis [1].

The fuel used to supply the internal combustion engines should be characterized by specific parameters that determine the proper operation of the engine. Values of these parameters are given in the relevant normative documents: specifications, technical conditions, industry standards for compliance with the given state standards, common standards for associated countries (e.g. EU), international organizations' directives (e.g. World Fuel Charter).

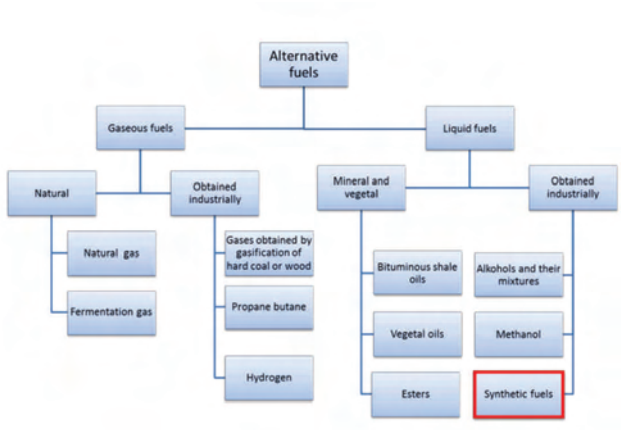


Fig. 1. Division of alternative fuels [3]

3. Polymer materials

Thanks to polymer materials we have the opportunity to create new products. They allow greater technological progress than any other material. Plastics thanks to the economy of raw materials and materials are one of the most efficient products. Only small part of the world's crude oil resources is used for their production.

More than 50 years ago the potential of these materials was discovered, but their era is only now beginning. Thanks to their properties, plastics are used in packaging, construction, automotive industry, aerospace industry, agriculture, sport, medicine. In 2015, the demand for plastics in Europe amounted to 49 million tons [6].

However, when plastic products cease to fulfill their utility functions and their life cycle ends, they must be appropriately recovered.

Plastic waste is dominated by polyolefins, i.e. polymers containing carbon and hydrogen, which are extracted directly from crude oil. Polyolefins are durable, rigid and abrasion-resistant. In addition, they have good dielectric properties, are resistant to water, have high gas permeability and low for water vapor. On the other hand, they are not

resistant to strongly oxidizing substances and atmospheric conditions cause their aging. Polymers include: polyethylene (PE), polypropylene (PP), polystyrene (PS), and acrylonitrile-butadiene-styrene (ABS). The first one is odorless and physiologically indifferent, but easy to burn. We can distinguish high density polyethylene (PEHD) and low density (PELD). PEHD is more mechanically resistant, has higher melting points and hardness and degree of crystallinity. Polypropylene allows to obtain transparent products with low absorbency and water permeability, and also impervious to gases [2].

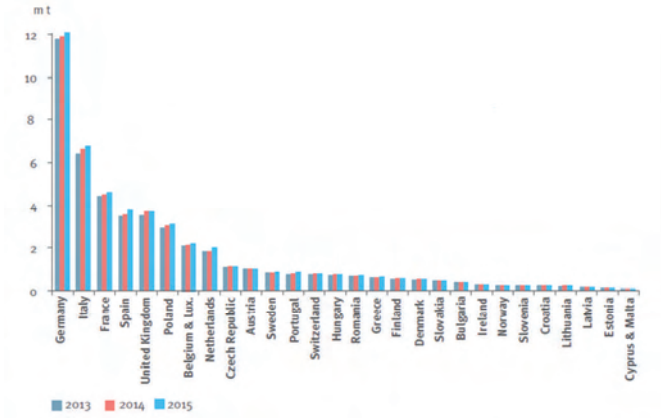


Fig. 2. Demand for Polymeric Plastics in Europe 2013-2015 [6]

Plastics account for about 10% by weight and 40% by volume of the household waste. The main source of plastic waste is packaging, which accounts for 55% of post consumer waste from plastics.

Waste from polymeric plastics can be utilized by:

– mechanical recycling,
– raw material recycling,
– energy recovery,
– processing into liquid synthetic fuel.

According to the National Alternative Fuel Infrastructure Development Plan, synthetic fuels are fuels obtained by chemical synthesis using various methods and raw materials. Synthetic fuels can be divided by the raw material used: 1. Fuel obtained from natural gas, so called, Gas to Liquid (GTL), 2. Fuel from coal, so called, Coal to Liquid (CTL), 3. Fuel obtained from biomass, 4. Fuel obtained from plastics (municipal waste) [4].

As a result of chemical processes, synthetic gasoline or synthetic diesel is produced. As a rule, the use of synthetic fuels does not entail the need to build new fueling facilities for vehicles powered by synthetic fuels, these fuels can be used by vehicles running on traditional fuels.

4. Research

The tests of physicochemical properties of synthetic fuel and its mixtures have been carried out at the research laboratory of the Research Center for Fuels, Working Fluids and Environmental Protection of the Faculty of Mechanical Maritime Academy.

The tests used:

– DMA 4500/5000 for density determination
– TV 2000 viscometer for determining kinematic viscosity
– Cetane ID 510 for determining a cetane number
– Device for determining the flash point

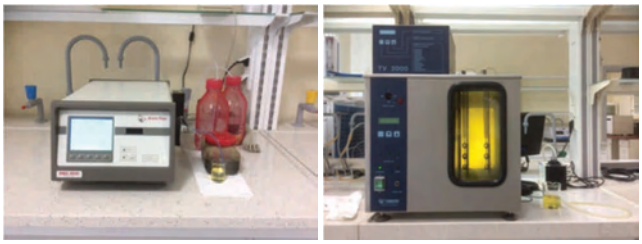


Fig. 3. DMA 4500/5000 for density determination and TV 2000 viscometer for determining kinematic viscosity



Fig. 4. Cetane ID 510 for determining a cetane number and Device for determining the flash point

Selected physicochemical properties of the fuel have been determined, which have a decisive influence on the proper operation of the internal combustion engine, its performance and the cleanliness of the exhaust gases emitted into the environment.

For studying physico-chemical properties, the liquid fuel was used, which is a mixture of waste made of PE and PP plastics and is produced in an installation that enables to recycle the largest group of plastic waste, i.e. polyethylenes (PE), polypropylenes (PP) and polystyrenes (PS).

The installation processes plastic waste mixed in any proportions of PP to PE or PS, which can come directly from landfills or waste sorting plants.

The plastic waste can be dirty and damp with a different texture and thickness, and may have different colored prints. The recycling process involves catalytic depolymerization. The waste that goes into the plant is converted into a gaseous form which, after cooling and filtration, is the final product of liquid fuel.

One of the main parameters determining the suitability of fuel for the supplying diesel compression engines is the cetane number. The CN determination is based on a comparison of the ignition properties of the test fuel with the analogous properties of standard fuel mixtures with known cetane numbers.

When using fuel in the engine, the effects of incomplete combustion appear in the form of deposits on the atomizers (injectors) and their amount depends on the fuel contents.

However, the cetane number is not a sufficient criterion for the correct combustion process (complete and total combustion). With both synthetic and fossil fuels, the incomplete combustion can occur, despite the cetane number appropriate for the given ignition engine, and despite the fact that all the parameters of the combustion formation (injection pressure, compression pressure) are correct.

Additionally, the process of creating a combustible mixture is closely related to the spraying process affected by other physical parameters of the fuel. The density, viscosity, and surface tension of the fuel play a decisive role in the formation of turbulent flow in the spray nozzles, providing proper atomization. The initial phase of supplying fuel to the combustion chamber, consisting of spraying the fuel, is crucial for further processes of preparing the fuel-air mixture, its ignition and combustion. The quality of the fuel-air mixture formation is best characterized by the SMD parameter – Sauter's average diameter of spray drops, and its value in analytical studies depends on the physical parameters of the fuel (density, viscosity, surface tension).

Table 1. Calculation formulas for determining the mean diametre of a drop [5]

Equation	Author
$SMD = 3330 d_o^{0.3} \eta_L^{0,07} \rho_L^{-0.648} \sigma^{-0.15} w_L^{-0.55} \eta_A^{0.78} \rho_A^{-0.052}$	Harmon
$SMD = 3.98 \cdot 10^7 d_o w_F^{-1} \sigma^{0.25} \rho_A^{-0.25} g^{0.5} [1 + 3.34 \cdot 10^{-2} \eta g^{0.5} (\sigma \rho_F d_o)^{-0.5}]$	Tanaswa and Toyoda
$SMD = 6156 \nu_L^{0.385} (\sigma \rho_L)^{0.737} \rho_A^{0.06} \Delta p_L^{-0.54}$	Elkotb
$SMD = 0.38 d_o Re^{0.25} We_F^{-0.32} \left(\frac{\eta_F}{\eta_A}\right)^{0.37} \left(\frac{\rho_F}{\rho_A}\right)^{-0.47}$	Hiroyasu and Arai
$SMD = 2362 d_o^{0.262} \varrho_A^{0.121} \varrho_F^{-0.0665} \Delta p_F^{-0.0695}$	Hiroyasu and Kadota

5. Conclusions

The results obtained of testing selected physico-chemical properties were related to the requirements set by PN-EN 590+A1:2011 standard. Fuels for motor-vehicles – Diesel oils – Requirements and test methods [7].

Firstly, pure synthetic polymer fuel and pure diesel were tested and the results compared. Pure synthetic fuel meets the standard only for the cetane number. The parameter that most differs from the norm is the flash point (Table 2). It was therefore reasonable to carry out a fuel mixtures tests with 7% and 20% share of synthetic fuel.

In the case of mixtures, we see that the 20% addition of synthetic fuel slightly changes the density, viscosity and cetane number. However, the flash point is still incompatible with the standard requirements for ON to supply internal combustion engines. By analyzing the results of the 7% mixture, we find that all the parameters tested are similar to the ON fuel parameters and meet the requirements set by the standard.

Table 2. Selected physico-chemical parameters of synthetic fuel and diesel oil

Test parameter	Unit	Synthetic fuel	Diesel	Requirements for diesel
density	[kg/m^3]	795	834	820–845
viscosity	[mm^2/s]	1.76	2.768	2.00–4.5
cetane number	[–]	64.4	55.8	min 51
ignition temperature	[°C]	30	65	< 55

Table 3. Selected physico-chemical parameters 7% and 20% synthetic fuel mixture and diesel oil

Test parameter	Unit	7% synthetic fuel	20% synthetic fuel	Requirements for diesel
density	[kg/m^3]	831	828	820–845
viscosity	[mm^2/s]	2.672	2.456	2.00–4.5
cetane number	[–]	56.9	57.4	min 51
ignition temperature	[°C]	55	45	< 55

The studies of physicochemical properties conducted will allow to develop a methodology for determining the possibility of using liquid synthetic fuels in compression ignition engines.

In the current standards, the only property of distillation fuels for diesel engines, directly referring to combustion, and reflecting their ignition characteristics, is the cetane number (CN). However, as shown by the analysis of scientific literature on fuels other than petroleum oils, the CN is not a sufficient parameter to evaluate its usefulness in diesel engines.

As a result of the studies, it was found that both, 100% synthetic fuel and its 20% share in diesel fuel did not meet the minimum ignition temperature limit, while the limit value of this parameter is met by the mixture of diesel oil with 7% synthetic fuel. Currently, the laboratory tests are being developed with regard to the use of measured viscosity, density and surface tension values for a mixture of synthetic fuels (up to 7% and petroleum oils), SMD calculation and analytical equations corrections taking into account the actual SMD values measured by laser diffraction method during the laboratory tests. The further direction of research is related to the definition of the operating and environmental parameters of a diesel engine fuelled with diesel oil with 7% synthetic fuel.

Bibliography

[1] BALAWENDER, K., JAKUBOWSKI, M., KUSZEWSKI, H. Parametry fizykochemiczne paliwa syntetycznego przeznaczonego do zasilania silników o ZS. *Вісник Національного транспортного університету*. 2014, **30**(1).

[2] CICHY, J., SOBCZYK, W. Odpady z tworzyw sztucznych i ich recykling. *Edukacja-Technika-Informatyka*. 2014, **5**(1).

[3] GRONOWICZ, J. Ochrona środowiska w transporcie lądowym. Poznań-Radom 2004.

[4] Krajowy plan rozwoju infrastruktury paliw alternatywnych.

[5] LIU, H. Science and Engineering of Droplets – Fundamentals and Applications, Noyes Publications, Park Ridge, New Jersey, U.S., *William Andrew Publishing*, LLC Norwich, New York 2000.

[6] Plastics Europe, Raport 2016.

[7] PN-EN 590+A1:2011 Paliwa do pojazdów samochodowych – Oleje napędowe – Wymagania i metody badań.

Anna Skarbek-Żabkin, MEng. – Motor Transport Institute.

e-mail: *Anna.Skarbek@its.waw.pl*



Article citation info:
FIEDKIEWICZ, Ł., PIELECHA, I., WISŁOCKI, K. Use of the gas ionization signal for combustion process diagnostics in the cylinder of a spark ignition engine. *Combustion Engines*. 2017, **171**(4), 196-200. DOI: 10.19206/CE-2017-433

Łukasz FIEDKIEWICZ
Ireneusz PIELECHA
Krzysztof WISŁOCKI

CE-2017-433

Use of the gas ionization signal for combustion process diagnostics in the cylinder of a spark ignition engine

The running diagnostics of the combustion process in an internal combustion engine is essential for increasing its efficiency and to improving its performance indicators. The modern diagnostics of this process no longer concerns only measurements of fast-changing thermodynamic variables, but also measurements of other parameters allowing for its evaluation. The use of electrical or optical methods in diagnostics enables the evaluation of local process parameters, such as occurrence of the flame and its temperature distribution. Actually, there are some new methods under investigation which are proposed for this kind of diagnostic.

This article focuses on demonstrating the potential for using an electric signal from the gas ionization to estimate the maximum combustion pressure in a cylinder of an SI engine. This is a comparative analysis of the gas ionization current signal in the cylinder and the fast-changing pressure at fixed operating points of a 4-stroke natural gas powered engine. The study was carried out on a one-cylinder 4-stroke SI engine equipped with a cylinder pressure recording system and monitoring of the cylinder ionization current using appropriate measuring systems. The influence of engine operating conditions on the ability to determine cylinder pressure based on the ionization current signal was analyzed. This impact assessment was analyzed statistically and a strong correlation was found between the analyzed signals. The obtained results point in the potential direction of development of this type of measuring system.

Key words: *gas engine, ionization sensor, pressure sensor, engine control, lean fuel mixture*

1. Introduction

Modern fast-changing pressure sensors used in diesel engine diagnostics allow high-frequency combustion pressure measurement under extreme operating conditions at high temperatures and in-cylinder pressures. The pressure profile inside the combustion chamber may be an important component of the procedure used to control the internal combustion engine, allowing continuous thermodynamic analysis of the process in real time and thereby enabling improved energy conversion efficiency and reduction of harmful substance emissions.

Due to the relatively high cost of manufacturing piezoelectric sensors, their usefulness is limited only to laboratory tests or to more expensive units used in motor vehicles. However, there are signs that optical methods of evaluating thermodynamic indicators and measuring the gas ionization degree may be a viable alternative. Optical methods rely on the analysis of light waves, but they require alterations in the engine design and the use of appropriate measured signal processing equipment [1]. Measurement of the so-called ionization current, i.e. the current flowing through the medium after ignition, enables the use of a standard spark plug in spark ignition engines, significantly reducing the cost of using a measuring system [2].

The ionization current signal has already been used for many motor applications. Byttner and Holmberg [3], by analyzing the ionizing current signal, showed a large effect of the recirculated exhaust gas on its amplitude and its nature while proving the possibility of using such a signal as a EGR content percentage sensor in the medium. With exhaust gas recirculation, combustion is slower and the temperature is lowered, resulting in smaller, time-shifted amplitude.

The ionization signal allows to determine the time when the maximum pressure in the combustion chamber is reached – this feature was used by Eriksson et al. [4] and Hellring et al. [9] when designing ignition feedback systems that control the position of the maximum combustion pressure point.

Mehresh et al. [5] analyzed the use of the HCCI spark plug as an ionization sensor, an alternative to expensive pressure transducers. The ionization current was measured when the engine was running on a lean fuel mixture. A small amount of the so-called chemical ionization has been found due to low-temperature combustion processes in this type of an engine.

Successful ionization current measurement can also be used in compression ignition engines, but most often it involves significant modifications to the engine [6].

The very high dependence of the ionization signal on the excess air ratio was demonstrated by Filipek et al. [2] and Abhijit et al. [7]. They have been able to control the fuel injection using an ionization signal. They further noticed that the ionization sensor showed a much faster response to changes in the fuel composition from the commonly used oxygen sensor, but unfortunately, its signal is highly unrepeatable.

The most common use of the ionizing current signal is knock detection and ignition detection [8, 10, 11]. Prominent manufacturers (Mazda, Harley-Davidson) use this type of system as a standard. The ionization current is used in a very limited range, but its efficiency and response time are incomparably shorter than conventional sensors, and the use of such a sensor significantly reduces costs by reducing the number of components required.

2. Ionization signal characteristics

In a short time after the discharge on the electrodes of the spark plug an intensive propagation of the flame in the mixture takes place – from the spark plug towards the cylinder walls, this is due to the intense chemical reactions

sustaining the combustion process. As a result of these reactions, free ions and electrons are produced in the so-called chemical ionization process. The stage of thermal ionization is associated with the formation of ions and electrons due to the effects of temperature and pressure.

Measurement of the degree of ionization in the combustion chamber – for the purposes of this article – was carried out using the system shown in Figure 1. At the time when the electric arc disappears, a constant voltage of about 80 volts was applied to the spark plug electrodes. The presence of free ions and electrons in the burning gas, causes a small current in the circuit (ionization current) of the order of several dozen microamps. According to Ohm's Law, a potential difference (ionization voltage) measured directly in the circuit is generated on the resistor connected to the circuit.

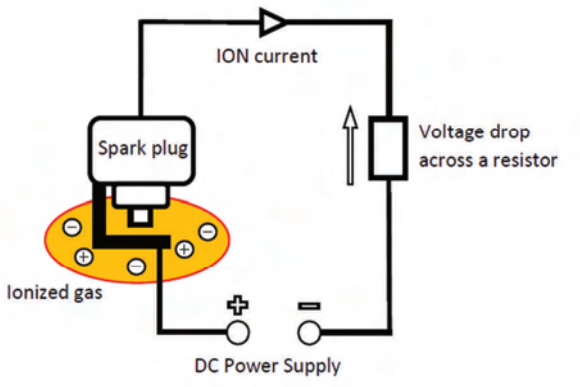


Fig. 1. Diagram of the ionization signal measurement circuit

Figure 2 shows an example of ionization voltage signal measurement along with the identified process steps [4, 7]. There are three main phases in this process:

a) ignition phase I – strong electromagnetic radiation from the ignition system – it causes interference in the ionization signal, making it difficult to analyze,

b) chemical ionization phase II – strongly associated with the formation of the flame front,

c) thermal ionization phase III – has a high correlation with maximum cylinder pressure and temperature.

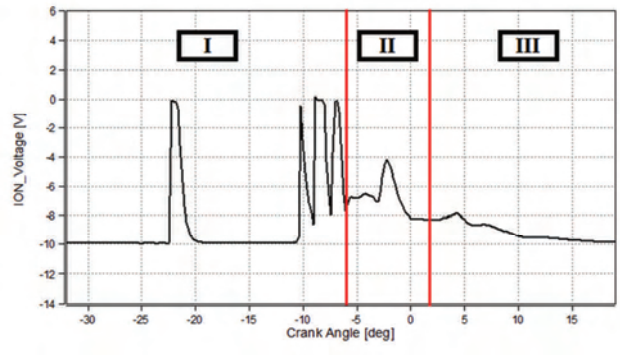


Fig. 2. Ionization voltage signal with defined phases

3. Motivation

Ionization current signal applications – presented in Chapter 1, mainly refer to engines powered using a stoichiometric gasoline mixture. There is little information in the literature on the use of this signal when burning gas mixtures.

The aim of this article is to try and determine the potential utilization of a diagnostic signal, such as the ionization voltage, for the combustion process diagnostics of an SI combustion engine powered by natural gas. Because of the strong association of the thermal ionization signal to the combustion pressure and the electromagnetic interference that limits the analysis of the chemical ionization signal, the authors focused on the third phase of the ionization signal – the thermal ionization.

Analysis of the results of such studies will allow to supplement information on the potential applications of the ionization voltage signal in the combustion of gaseous fuels in enclosed chambers.

4. Methodology

4.1. Test engine

The study was conducted on a one-cylinder, four-stroke AVL 5804 spark ignition engine. The basic compression ignition engine unit was adapted for the use of natural gas (Table 1). The compression ratio was reduced and the drive system was modified. An indirect injection of natural gas was applied to the intake manifold. The choice of fuel has provided a quite wide ignition range and the use of rich and lean fuel blends to increase the versatility of the results.

Table 1. Characteristics of the research engine

Parameter	Unit	Value
Engine	–	1-cylinder, 4-valve, SI
Cylinder volume	dm^3	0.5107
Bore x stroke	mm	85 x 90
Compression ratio	–	15.5
Fuel system	–	Indirect gas-injection (electromagnetic injector)
Air system	–	Supercharging

4.2. Research station

Ionization currents were measured at a constant engine speed of 1500 rpm. To maintain constant thermodynamic conditions, the station is equipped with a liquid and oil conditioning system. The natural gas supply system contained a high pressure tank with a reducer, a Bronkhorst 111B flow meter, and an additional volume of 2 dm^3 to reduce the wave phenomena present in the system (Fig.3, Table 2). The Bosch gas injector was placed in a spiral inlet duct.

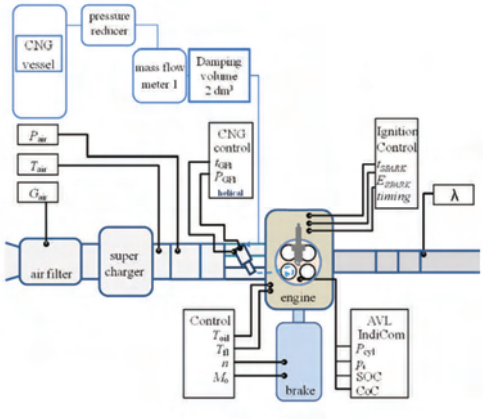


Fig. 3. Test rig for natural gas supply through indirect injection

Table 2. Measuring apparatus used in the tests

Parameter	Producer/name	Description
Engine brake	AVL AMK DW13-170	–50–300 Nm
Air system	Sensycon Sensyflow	0–720 kg/h
Fuel system	Bronkhorst 111B	0.1–100 g/h
Oil system	AVL 577	0–150 deg C
Water system	AVL 577	0-150 deg C
Fast-varying processes	AVL IndiSmart	8-channel acquisition (±10 V)
	AVL Concerto	Post-processing
Lambda sensor	Bosch LSU 4.9	$\lambda > 0.5$

In order to ensure high combustion pressures, the engine was supercharged with an external engine boost system. The air mass supplied to the cylinder was determined on the basis of the air flow meter. The gas dose – with adjustable timing and angle of injection – was delivered to the injector at a pressure of 9 bar. The ignition controller (from Mechatronics Comp./Poznan) enabled setting the ignition angle and the discharge energy value determined by the coil charging time. In order to control the quality of the air-fuel mixture supplied to the cylinder, a Bosch LSU 4.9 wideband probe was installed at the exhaust outlet. Measurement signals were sent to the AVL IndiSmart Data Acquisition System, which is compatible with AVL Concerto software, enabling real-time analysis of data.

4.3. Scope of the research

The scope of the research was based on the motivation to undertake the research problem presented in Chapter 3. The authors wanted to demonstrate that:

1) there is a dependence of the ionization current signal amplitude on the maximum cylinder pressure (Pmax),

2) it is possible to associate the angle of the maximum thermal ionization signal value occurring and the angle of the maximum cylinder pressure (α_Pmax).

The desire to demonstrate the above relationships has forced the use of certain engine settings. They were adopted as reference conditions and are presented in Table 3.

Table 3. Reference conditions for conducted research

Reference parameters	
Engine speed	1500 rpm
Oil/coolant temperature	80°C
Maximum pressure	66–98 bar
Angle of Pmax	0–10 deg
λ	1.0
Coil current	3 A

5. Influence of maximum cylinder pressure on the thermal ionization voltage value

Determining the dependence of the ionization voltage on the maximum combustion pressure required a constant value of the maximum pressure angle (α_Pmax) in order to eliminate the additional disturbance factor (that the change in this angle would be). This value was set at 5 degrees after TDC at constant charging coil current value – 3A and constant excess air ratio – $\lambda = 1$. The increase in maximum combustion pressure was achieved in part through adjusting the air supply by increasing the throttle opening angle as well as increasing the supercharging gas pressure along with an increase in the fuel dose (adjusted with λ = const). Achieving the required operating points required adjusting the ignition angle using a dedicated controller. In-cylinder pressure and ionization voltages were averaged (out of 100 measurement cycles) and then analyzed further (Fig. 4).

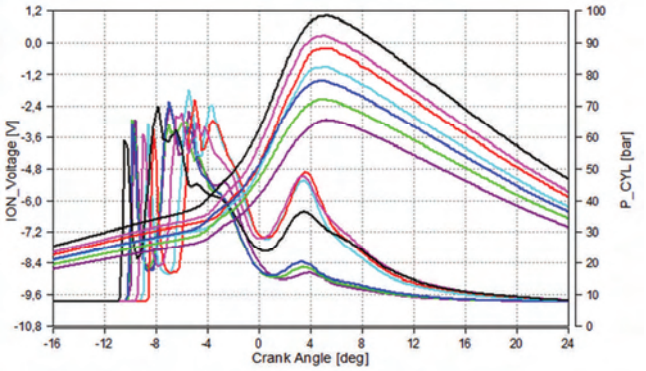


Fig. 4. Effect of the maximum combustion pressure on the thermal ionization signal value

As a result of the high non-repetitiveness and variation of the recorded signal (Figure 4), the chemical ionization phase was averaged together with the first ignition phase part, which made it impossible to analyze further. The thermal ionization voltage was then used to analyze the relationship between this signal and the maximum cylinder pressure. The results of this research test are shown in Figure 5.

The relation shown here is a partial correlation of maximum combustion pressure and ionization voltage (within one setpoint of supercharging pressure). The first three points were recorded by adjusting the throttle opening, while the remaining points by increasing the supercharge pressure and adjusting the throttle opening angle. It is probably the pressure increase in the intake system, and thus the increase in the temperature of the supercharged air, that affects the thermal ionization voltage value.

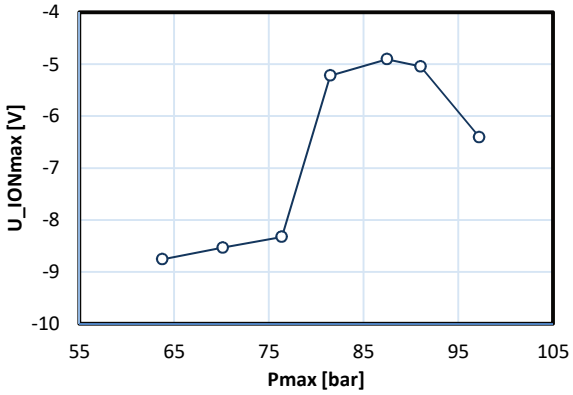


Fig. 5. Graph of the relation between maximum combustion pressure and ionization voltage value

6. Effect of the maximum combustion pressure angle on the thermal ionization voltage signal

In order to relation between the maximum combustion pressure angle and the ionizing current signal, changes in the maximum combustion pressure angle in the range of 0-

10 degrees on the crankshaft after TDC were recorded. These adjustments were made by changing the ignition advance angle setting in the range of 6-19 degrees on the crankshaft before TCD. Other parameters, such as air excess ratio (λ) and coil charging current were assumed as reference values. The results were averaged and further analyzed (Figure 6).

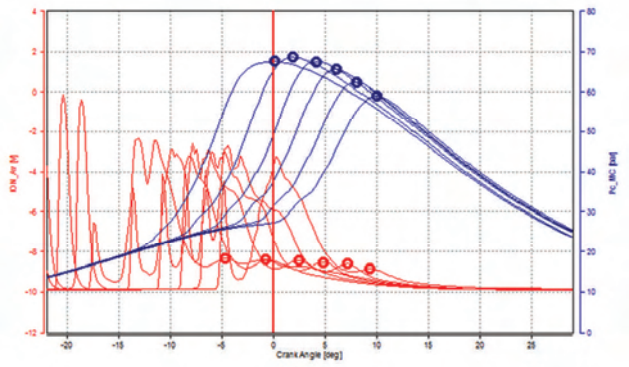


Fig. 6. The effect of the maximum combustion pressure angle (blue line) on the thermal ionization signal (red line)

For analysis aiming to determine the relationship between the maximum cylinder pressure angle and the ionization signal, thermal ionization values were used. The dependence of the angle of the maximum combustion pressure (α_Pmax) on the amplitude of the thermal ionization signal is shown in Fig. 7.

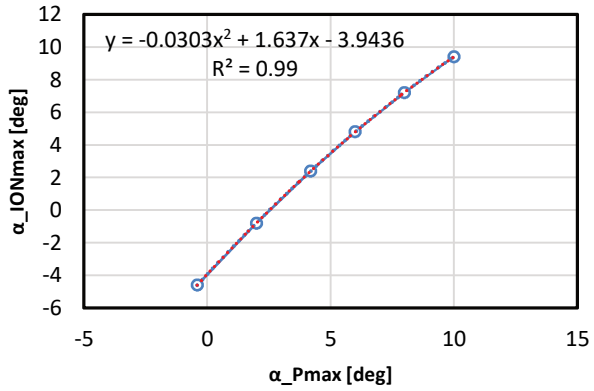


Fig. 7. The function of the angle of the thermal ionization signal amplitude relative to the angle of maximum combustion pressure

These points are described by a second degree polynomial with a determination coefficient $R^2 = 0.99$:

$$\alpha_ION = -0.0303 \cdot (\alpha_Pmax)^2 + 1.637 \cdot (\alpha_Pmax) - 3.9436$$

The above function has shown that there is a large correlation between the angles of both signals, which enables the reproduction of the angle of the thermal ionization amplitude based on the angle of maximum combustion pressure. The phase shift of the signals may be related to the local nature of the measurement or to a greater impact of the combustion temperature effect on the thermal ionization signal. Nevertheless, a thermal ionization signal can successfully be used to manage and control the ignition or, more generally, to control the combustion process.

The signals shown are average values from 100 engine cycles, which is too general (too many cycles) for ignition timing control or combustion control. The mean angle of maximum combustion pressure determined by the average angle of incidence of the thermal ionization amplitude (from 5 successive work cycles) indicates an error of ±0.25 degrees on the crankshaft. This is an acceptable value for engine control. It is more difficult to analyze the fast-changing analog signal with high variability that is the result of the stochastic nature of the engine. It is necessary to use complex algorithms and to eliminate interference from high-voltage discharges to obtain the desired maximum ionization voltage signal and the angle of its occurrence.

Conclusions

Analysis of the test results indicates the possibility of using an ionization voltage signal to diagnose the combustion process of a spark ignition engine.

The conducted research and analysis lead to the conclusions that:

1. A partial correlation between the maximum combustion pressure and the ionization voltage has been found. As the maximum combustion pressure increases, the ionization signal voltage increases, but there is no clear dependence.
2. There is a strong relation between the angle of the thermal ionization signal amplitude and the angle of the maximum combustion pressure. This relationship enables the reproduction of the maximum combustion pressure angle from the recorded ionization signal values.

Further research in this field will be conducted with respect to changes in the air excess ratio and the possibility of eliminating the information noise associated with the electric discharge on the spark plug.

Nomenclature

CI	compression ignition
CNG	compressed natural gas
DI	direct injection
HCCI	homogeneous charge compression ignition
ION_AV	average value of ionization signal
ION_voltage	ionization voltage
Pmax	maximum pressure
SI	spark ignition
TDC	top dead center
U_IONmax	maximum ionization voltage
α_IONmax	angle of maximum ionization current/voltage
α_Pmax	angle of maximum pressure

Bibliography

[1] WENDEKER, M., Sterowanie wtryskiem w silniku samochodowym. *Lubelskie Towarzystwo Naukowe*. 1999.

[2] FILIPEK, P.,WENDEKER, M. Opinion of ionization signal to estimating composition of mixture in combustion process about engine SI. *Journal of KONES Powertrain and Transport*. 2008, 15(3).

[3] BYTTNER, S., HOLMBERG, U. Closed-loop control of EGR using ion currents. *Proceedings of the 27th IASTED International Conference modelling, identification and control*. 2008, 978-0-88986-711-6.

[4] ERIKSSON, L, NIELSEN, L, GLAVENIUS, M. Closed loop ignition control by ionization current interpretation. *SAE Technical Paper*. 1997, 970854.

[5] MEHRESH, P., SOUDER, J., FLOWERS, D. et al. Combustion timing in HCCI engines determined by ion-sensor: experimental and kinetic modeling. *Proceedings of the Combustion Institute*.2005, 2701-2709.

[6] KOWALSKI, D. Analiza nierównomierności pracy silnika o zapłonie samoczynnym z wtryskiem wielofazowym. *Rozprawa doktorska*. Opole 2014.

[7] ABHIJIT, A., GEORGE, G., NABER, J. Correlation of air fuel ratio with ionization signal metrics in a multicylinder spark ignited engine. *SAE Technical Paper*. 2009; 2248, 45-62.

[8] ABHIJIT, A., NABER, J. Ionization signal response during combustion knock and comparison to cylinder pressure for SI engines. *SAE Technical Paper*. 2009; 2159, 25-40.

[9] HELLRING, M., HOLMBERG, U. A comparison of ion-current-based algorithms for peak pressure position control. *SAE Technical Paper*. 2001, 2001-01-1920.

[10] HUNG, D., ZHU, G., DANNE, N., MCKOSKEY, J. Knock detection for a large displacement air-cooled V-twin motorcycle engine using in-cylinder ionization signals. *SAE Technical Paper*. 2008, 2008-32-0028.

[11] LUNDSTROM, D., SCHAGERBERG, S. Misfire detection for prechamber SI engines using ion sensing and rotational speed measurements. *SAE Technical Paper*. 2001, 2001-01-0993.

Łukasz Fiedkiewicz, Eng. – Faculty of Machines and Transport at Poznan University of Technology.

e-mail: *Lukasz.Fiedkiewicz@put.poznan.pl*



Prof. Krzysztof Wisłocki, DSc., DEng. – Faculty of Machines and Transport at Poznan University of Technology.

e-mail: *Krzysztof.Wisłocki@put.poznan.pl*



Ireneusz Pielecha, DSc., DEng. – Faculty of Machines and Transport at Poznan University of Technology.

e-mail: *Ireneusz.Pielecha@put.poznan.pl*



Article citation info:
PIĄTKOWSKI, P., LEWKOWICZ, R., ŚCIEGIENKA, R., MYSŁOWSKI, J. The impact of intake channel geometry on in-cylinder swirl. *Combustion Engines*. 2017, **171**(4), 201-206. DOI: 10.19206/CE-2017-434

Piotr PIĄTKOWSKI
Ryszard LEWKOWICZ
Ryszard ŚCIEGIENKA
Janusz MYSŁOWSKI

CE-2017-434

The impact of inlet channel geometry on in-cylinder swirl

A few chosen methods of swirl generation inside the cylinder were presented in this article. There were presented the results of impact of intake channel geometry on chosen charge movement parameters related to the air-flow inside the cylinder. Moreover, there was presented an authors own conception of flexible and steerable element applied inside the inlet channel. This element influenced on kinematics of airflow through the inlet manifold. The result of this influence was observed as a swirl inside the inlet channel and inside the cylinder. There were also presented the results of experiment related to the own conception of swirl generation. The results of experimental research were compared with results of numerical calculation of air flow prepared on basis of ANSYS CFD. As final result it was stated that proponed flexible element inside the inlet channel have a significant impact on charge kinematics and it easy can controlled by engine control unit.

Key words: *intake system, swirl, ANSYS, CFD*

1. Introduction

The modern engines are being equipped with different kinds of technical solutions related to achievement of low fuel consumption and ultra-low emission [1]. These solutions are mainly connected with the engine control system, engine mechanicals, mixture formation and combustion [2]. It is caused by an increase in engine efficiency (torque, power, specific fuel consumption, emission, etc.).

The high efficiency of energy conversion process is strongly depended on proper air-fuel mixture formation. Additionally, this mixture must be combusted in practically optimal for each engine work conditions. Thus, there is a strong need to prepare proper air-fuel mixture with the kinematics parameters (kinematics parameters of mixture?) flow related to engine's operating conditions. Among the methods which influenced kinematics of in-cylinder flow we can mention about: variable valve timing system, variable volume inlet manifold system, specially shaped geometry of intake canal, location of intake canal in relation to cylinder axis, inlet valve equipped with deflector (mainly laboratory engines), installment of additional element which is able to change flux of air flow through the inlet valve (for example by a wing throttle) and specially shaped combustion chamber (mainly direct injection engines – DI).

Currently many engines (SI and CI) are equipped with one or more of these solutions which really help to obtain more effective combustion process and decrease exhaust gas emissions – especially related to their toxic compounds.

In every expansion stroke the combustion process is patchy and unrepeatable. Thus, the measurement and controlling of kinematics of charge flow is hard to achieve at the same level. The measurement of in-cylinder flow is realized with the usage of very quick and specific measurement devices (for example – Laser Doppler Velocimeter – LDV). However, not every type of engine can be used because in most cases the view for combustion chamber is needed. Only laboratory engines equipped with specially designed optical system allows to conduct in-cylinder flow measurement. Because of this, currently mainly numerical models of combustion chambers are used for analysis of in-cylinder flow motion.

2. In-cylinder flow motion

The main type of in-cylinder flow motions are defined in literature as: tumble, squish and swirl. The chosen examples of in-cylinder flow motion were presented in Figure 1. Type of flow motion dependent on their location towards cylinder axis and scale but each represents the type of rotary motion or split rotary and forward charge motion.

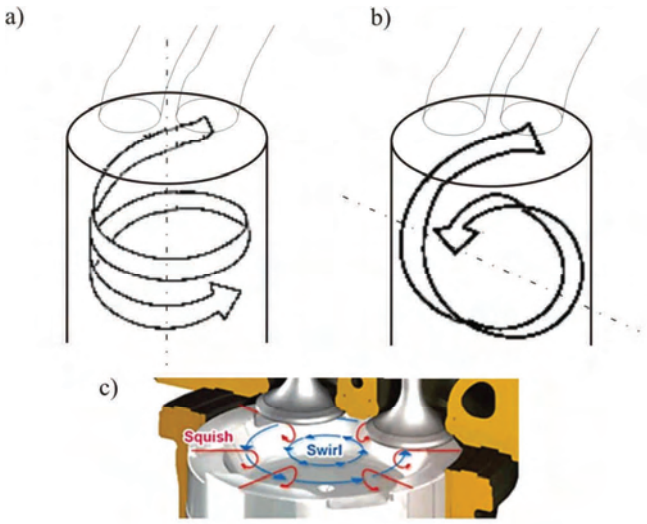


Fig. 1. Types of in-cylinder flow motion: a) swirl, b) tumble, c) squish and swirl [3]

The different type of charge motion are used for preparation of air-fuel mixture [4, 5] and flame propagation [6–8]. It is related to engine type, engine load and type of fuel (its properties). The experimental data available in literature [9–11] let us state, that currently very important for efficient fuel combustion is an achievement of swirl according to engine load [12]. Generally, swirl is defined as organized rotation of charge around the cylinder axis. Swirl is also characterized by swirl ratio (SR) and for real engine is usually defined by equation [4]:

$$SR = \frac{\varpi_s}{2\pi n} \text{ [-]}, \quad (1)$$

where: ω_s – angular velocity of solid-body rotating flow [s^{-1}], n – engine crankshaft rotational speed [rps].

This type of swirl ratio definition is also used during numerical research related to analysis of in-cylinder flow motion. However, the most of computer applications concerned simulation on engine charge exchange and combustion process are able to calculate many charge kinematic parameters (for example: Turbulence Kinetic Energy, Velocity, fuel drops mass distribution, etc.). One of these parameters directly characterise swirling load – Swirl Velocity. This parameter describes what is load rotation level refer to engine speed (this is Swirl Ratio).

3. The review of methods of swirl generation

3.1. Swirl generated by flow

Goto and Narusawa have been conducted research of impact of swirl on value of brake effective pressure and pressure change during combustion process [13]. The schematic view on intake channel with swirl generation system applied by them was presented in Fig. 2.

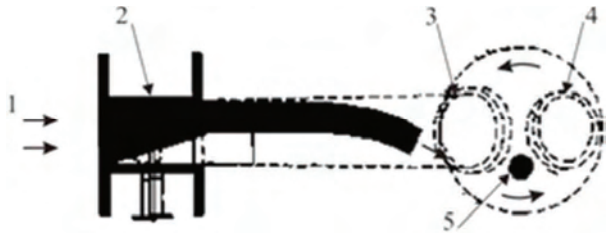


Fig. 2. The schematic view of swirl generation system [13]: 1 – direction of air-fuel mixture inlet, 2 – swirl regulation valve, 3 – inlet valve, 4 – exhaust valve, 5 – spark plug

This method of swirl generation is based on change of contribution of flow flux load through intake channel and swirl generation valve (part no. 2 – Fig. 2). If the air fully flows by the inlet channel then the obtained swirl is minimalized. If contribution of flux flow through swirl valve is raising, then the swirl is maximized. Moreover, the appeared swirl inside cylinder is caused by the curvature of cylinder wall. The examples of impact of the SR on changes in mean effective pressure were presented in Fig. 3 [13].

The results of research presented in Fig. 3 indicate that the swirl ratio (SR) is significantly affected by the increase in maximal pressure. Furthermore, the pressure changes which depend on crankshaft position are more stable. These results let us state, that the swirl helps to achieve the higher value of engine operation parameters as torque and effective power with decrease of fuel consumption and toxic gases emission.

Some current engine manufacturers equip their engines (especially CI engines) with special intake system. This system is responsible for swirl generation inside the cylinder during intake stroke. The main element of this system is a wing throttle fixed near one of intake valves. The scheme of this system is presented in Fig. 4. The main disadvantage of this system is swirl generation by closing flux flow through one of inlet channels. The swirl is generated by curvature of cylinder wall connected with flow of inlet flux (no. 2 – Fig. 4).

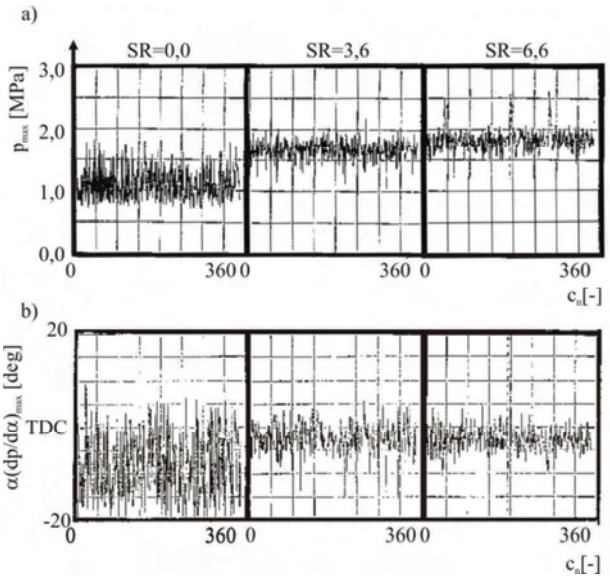


Fig. 3. The examples of impact swirl ration (SR) on [13]: a) – maximal value (p_{max}) of in-cylinder pressure, b) – pressure's change ($dp/d\alpha$) by engine's crankshaft position, α – the angle of crankshaft position, c_n – engine cycle subsequent no., engine's operation conditions: engine speed n = 1000 min^{-1}, engine fueled by CNG and MPI system, TWO – throttle wide open

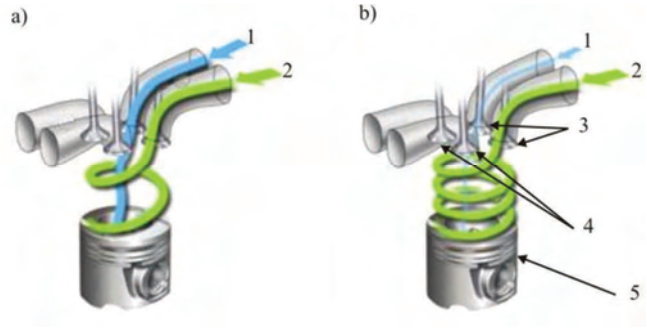


Fig. 4. The examples of swirl generation system by flow regulation [14]: a) – low swirl condition, b) – high swirl condition, 1 – flux flow by inlet canal, 2 – flux flow by inlet swirling canal, 3 – inlet valves, 4 – exhaust valves, 5 – piston

This type of swirl generation system leads to decrease in volumetric efficiency caused by a throttle wing fixed inside inlet channel. In practice, this system is used in turbocharged engines where decrease in volumetric efficiency is only partially redeemed by charging system. However, this system allows to achieve swirl parameters compatible with real time engine's load.

3.2. Swirl generated by intake channel geometry

The other results of research connected with assessment of impact of intake canal shape on swirl generation were presented in [10]. These research were based on swirl generation system caused by the inner wall of intake canal close to combustion chamber. The research was focused on the level of swirl (swirl ratio) and volumetric efficiency. The examples of analysed types of intake canals were presented in Fig. 5.

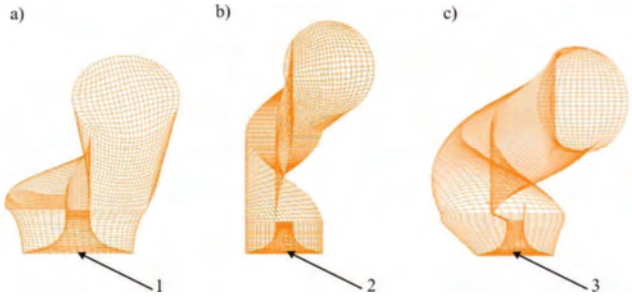


Fig. 5. The examples of discretion net of analysed type of intake channels [10]: a) – spiral type, b) – helical type, c) spirally-helical type, 1–3 – localisation of inlet valve heads

For calculation of intake stroke and volumetric efficiency and swirl ratio a numerical analysis were used. As it was shown in Figure 6, the highest volumetric efficiency was achieved for helical canal. It is connected with low level of flow resistance caused by the internal wall (shape) of inlet channel. However, the highest swirl ratio was observed for spiral type on inlet channel [10].

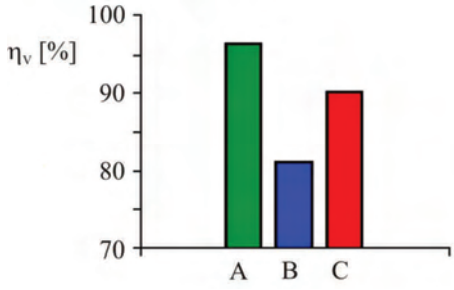


Fig. 6. The volumetric efficiency (η_v) by the type of inlet channel [10]: A – helical, B – spiral, C – spirally-helical (comp. Fig. 5)

The analysis of the results of numerical simulation presented in Figure 6 and conclusions formulated in work [10] let us state that, if one wants to achieve the higher volumetric efficiency than the engine should be equipped with inlet channel of helical shape. This conclusion is not sufficient for achievement high value of engine's operation parameters like torque or power. It is connected with process of air-fuel mixture preparation. For increase in efficiency of combustion process there is a need to prepare mixture with fully vaporised fuel and fully mixed with the air for good oxygen access. Mixture formation process requires proper charge motion inside the intake channel and inside engine's cylinder. It should be obtained during: intake stroke, compression stroke and combustion.

4. Experimental results

4.1. Theoretical background

On the basis of literature analysis there was prepared the new proposition of the technical method of swirl generation. By this method it is possible to generate a different level of swirl speed inside the inlet channel and inside the cylinder. For this conception an element with flexible geometry was used. The idea of influence by flexible element on air-flow and distribution and direction of the main charge flux velocities were presented in Fig. 7.

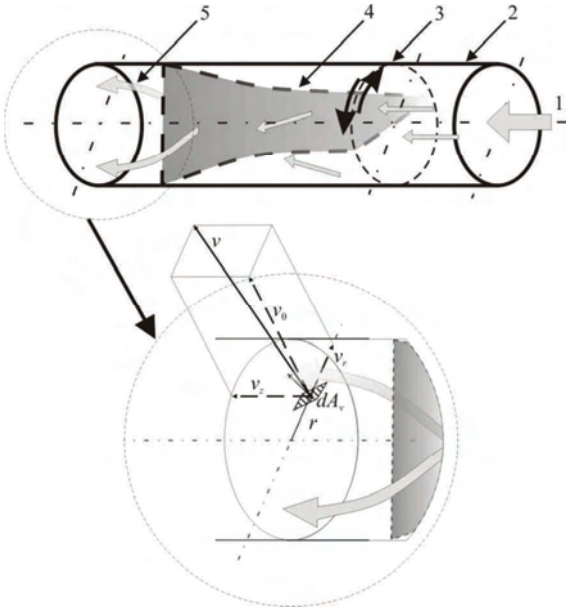


Fig. 7. Schematic of the flexible geometry element of inlet channel and velocity's distribution for each point of swirling flux (dA_v) during intake process: r – inlet channel inner radius, v_r – radial velocity, v_z – axis velocity, v_0 – normal velocity, v – mean velocity, 1 – inlet of air flux, 2 – wall, 3 – twisted the end of the flexible element (rotatable), 4 – flexible element, 5 – swirling air flux

Over flow of air-flux through the inlet channel, there is air-flow impact on the twisted shape of the flexible tape (part no. 4 – Fig. 7). It results in dividing of air-flux flow into two parts. Next twisted shape of flexible element has an impact on these two fluxes. It results in swirling of the airflow. After that the swirling charge motion is transported to cylinder through open inlet valve. The angular momentum of the air which leaves inlet channel and enters the cylinder is decreased by the friction between charge and cylinder wall. For each crank angle during induction an angular momentum of airflow decrease throughout the rest of the intake stroke and during the compression stroke due to the friction at the walls and turbulent energy dissipation within the fluid. The airflows angular momentum of the cylinder charge Γ_c is changing with time according to the momentum conservation equation. It can be expressed as [13]:

$$\frac{d\Gamma_c}{dt} = J_i - T_f \, , \, [kgm^2] \tag{2}$$

where: J_i – is the flux of angular momentum into the cylinder, T_f – is the torque due to wall friction.

The flux angular momentum for each point of intake process might be assessed as:

$$J_i = \int_{A_v} \rho r v_0 v dA_v \, , \, [\, kgm^2] \tag{3}$$

where: ρ – air density, r – cylinder radius.

Friction forces due to the cylinder wall can be estimated from:

$$\tau = 0.185\rho\left(\frac{\varpi_s D}{2}\right)^2 \lambda (Re_D)^{-0.2} \ [Pa] \tag{4}$$

where: D – cylinder bore, ω_s – equivalent rotational velocity (swirl), λ – empirical constant ($\lambda \approx 1.5$), Re_D – equivalent of the flat plate Reynolds number.

Moreover, described swirl example of this phenomenon occurs with the bowl-in-piston type of combustion chamber designed for medium- and high direct-injection diesel engines. However, in spark-ignition engines spherical swirl is used to increase the burning rate, the shape of the combustion chamber which is closing to top dead centre (TDC) can also force radially inward motion of the charge.

In order to reveal the effect of flexible element of inlet channel (Fig. 7) on kinematics of air-flux flow, the new numerical model was developed. A view of numerical model is presented in Fig. 8.

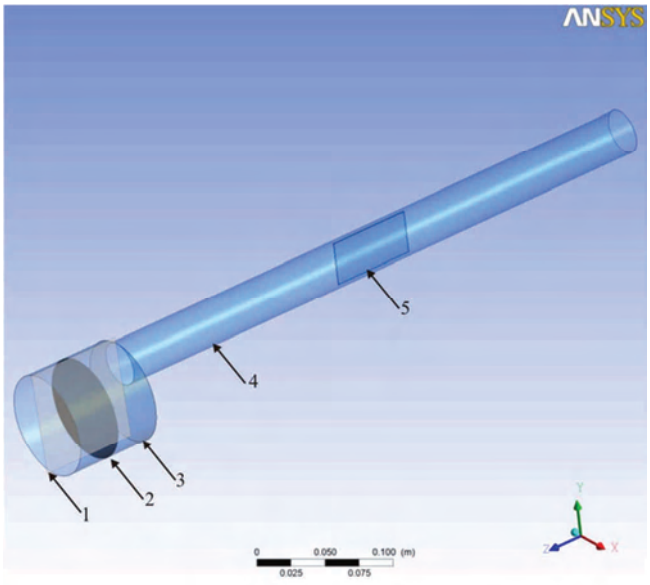


Fig. 8. Location of the planes for numerical analysis: 1 – the cylinder axis plane, 2 – the cylinder cross-section plane, 3 – cylinder wall, 4 – inlet canal, 5 – flexible tape

The main dimensions of flow system were based on intake system of real SI engine. The characteristic dimensions of experimental stand-up were:

– inner diameter of pipe-line – 32 mm,
– overall length – 465 mm,
– length of flexible tape – 65 mm,
– steel tape thickness – 0.4 mm.

To create the geometry of the system, the commercial CFD package ANSYS Workbench was used. Used mesh was a structural mesh that was inflated near the walls. The entire mesh consists of:

– 281 534 nodes,
– 16 038 quad-type elements, and
– 273 256 hexagonal-type elements.

Further modification (smoothing) of the mesh significantly elongated the numerical calculation without changing of obtained results. The analysed parameters were:

– swirl velocity (S_v),
– Turbulent Kinetic Energy (TKE),
– airflow velocity (V_a).

4.2. Turbulence kinetic energy

The example of the obtained numerical analysis results of the distribution of turbulence kinetic energy on the plane of the cylinder axis, which depends on the tape-twisting angle, was presented in Fig. 9. This result shows the case when the initial air flow velocity at the inlet to the flow system was w = 8 m/s.

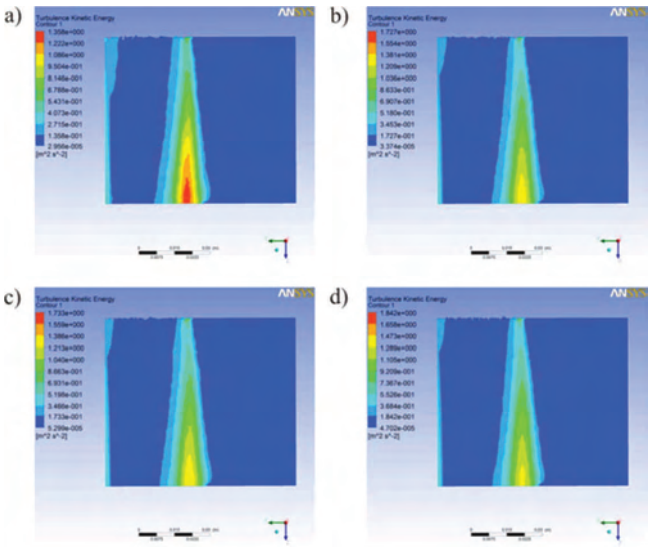


Fig. 9. The distribution of TKE inside of cylinder by the twisting angle (θ) for w = 8 m/s: a) θ = 6 deg, b) θ = 12 deg, c) θ = 18 deg, d) θ = 24 deg

When the tape-twisting angle increased, the gradient of the turbulent kinetic energy decreased. Similar relations were observed for the other analysed initial air-flux flow velocities. The smaller TKE gradients confirm that the flexible element strongly affect the charge motion and their flow through the inlet system to the cylinder. In addition, the dynamic forces of molecular interaction of the swirling air flux decay the trend of the air flow to become a turbulent.

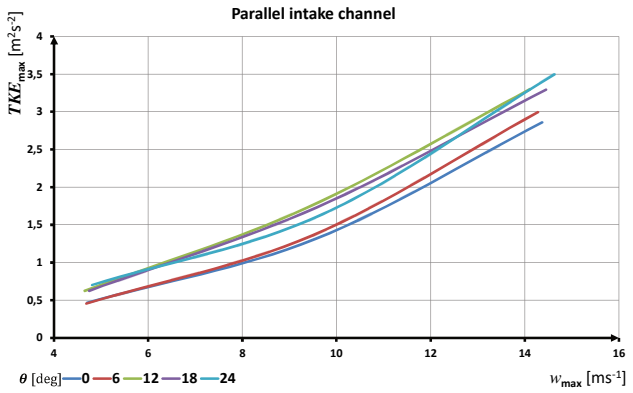


Fig. 10. The maximal turbulent kinetic energy dependence of the average air flow velocity w and an angle of twisting tape

These interactions stabilise the air flux flow. The flow stability does not help to prepare the optimal air-fuel mixture because air turbulence mixes the air and the level of fuel drops. Moreover, the airflow turbulences decrease of diameter of the fuel drops and significantly effect on a fuel vaporisation. Thus, the air turbulence should appear where the mixture forms and during combustion, but it should not cause flame dissipation. As it was shown in Fig. 10, the

turbulent kinetic energy is related to the tape-twisting angle and the air flow velocity.

The analysis of the numerical results being shown in figure 6 let us state that the TKE is directly proportional to increases in flow velocity. Moreover, the highest turbulent kinetic energy TKE_{max} was achieved when the tape-twisting angle was θ = 12 deg. This maximal value was 20% higher than those in the other analysed examples. The more intensive tape-twisting angles do not increase turbulent kinetic energy but reduce the airflow.

4.2. Swirl velocity

One of the most important effects of the air flux flow through the intake channel with the flexible element is the air flux swirling. As a result, the swirl transfers to the cylinder.

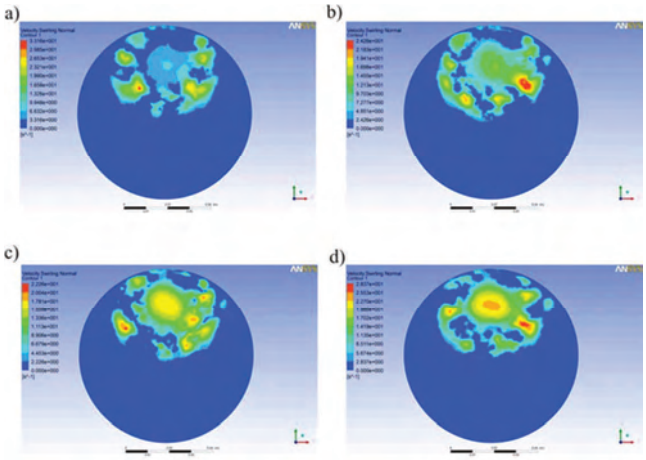


Fig. 11. The distribution of swirl inside the cylinder for charge's flow velocity w = 4 m/s; a) θ = 6 deg, b) θ = 12 deg, c) θ = 18 deg, d) θ = 24 deg

By changing the tape-twisting angle, one can control the in-cylinder charge motion. Examples of the numerical results of the swirl velocity and the tape-twisting angle were presented in Figs 11–13.

The analysis of the numerical results (Figs 11–13) of the swirl velocity showed a relation between the swirl velocity and the tape-twisting angle.

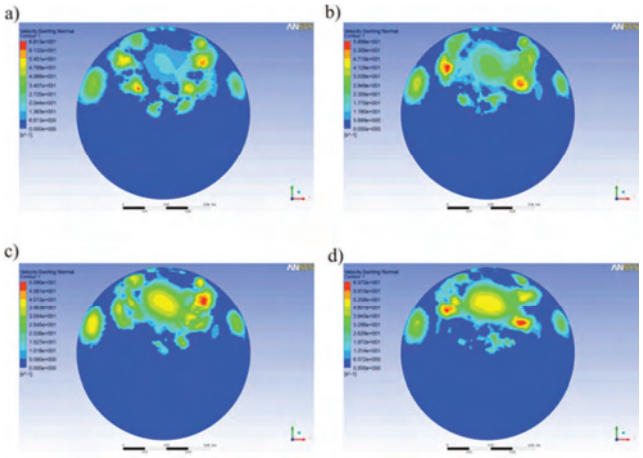


Fig. 12. The distribution of swirl inside the cylinder for charge's flow velocity w = 8 m/s; a) θ = 6 deg, b) θ = 12 deg, c) θ = 18 deg, d) θ = 24 deg

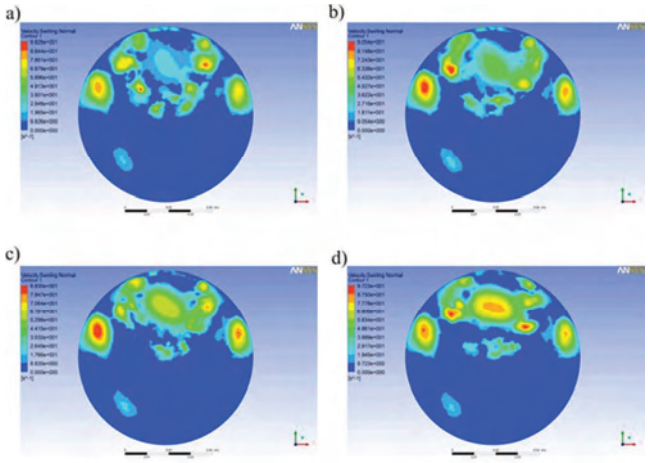


Fig. 13. The distribution of swirl inside the cylinder for charge's flow velocity w = 12 m/s; a) θ = 6 deg, b) θ = 12 deg, c) θ = 18 deg, d) θ = 24 deg

The surface area of the swirl air flow increases because of the tape-twisting angle, and it is also proportional to the increase of the initial air flow velocity. This relation was evaluated using the coefficient swirl area (SA), which is expressed in equation (7):

$$SA = \frac{A_{swirl}}{A} \cdot 100\,\%, \tag{7}$$

where: A_{swirl} – surface area of the swirling air flux; A – surface area of the cross-section of the air flow (cylinder cross-section).

By using a computer application for an analysis of the swirl area we obtained a relation among the swirl area, the initial air flow velocity (w) and the angle of flexible element twisting (θ). This relation was illustrated in Fig. 14.

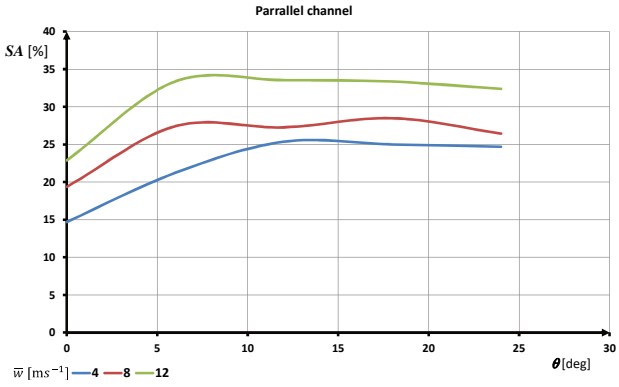


Fig. 14. The characteristic of swirl area (SA) dependence of the twisting angle (θ) and initial air flow velocity (w) – parallel channel

The effect of the air flow velocity and the tape-twisting angle on the swirl area was observed. When the initial air flow velocity increases, the swirl area increases. The numerical analysis result shows that the tape-twisting angle significantly affects the SA, and these two quantities are directly proportional to each other. The results in Fig. 14 show that – when the initial air flow velocity was w = 4 m/s – the SA was maximal for the angle θ ≈ 12 deg. When the initial air flow velocity was w = 12 m/s, the maximal SA

was achieved for the tape-twisting angle $\theta \approx 6$ deg. Thus, when the initial air flow velocity increases, then the twisting angle of the flexible element decreases. Based on these analyses, one can conclude that a dynamic regulation of the tape-twisting angle is not necessary because of the relation between the kinetic energy and the twisting of the flexible element. The coefficient (SA) confirms that there is a possibility of evaluating the in-cylinder charge motion. Moreover, a proposed method of creating the swirl inside the engine cylinder using a flexible element in the intake channel allows us to control the in-cylinder charge motion.

Conclusions

Based on the numerical analysis of the flow system using the inlet system of the engine, we conclude that:

– the geometrical properties of the intake system and the geometry of the combustion chamber geometry of the piston crown significantly affect the kinematics of the in-cylinder charge motion;
– it is possible to generate and control an in-cylinder swirl using a flexible element inside the inlet channel;
– the flexible element inside the inlet channel creates the charge swirl in the cylinder, and the obtained SA can be 50% higher than that in a standard intake system without a flexible element;
– the twisting angle of the flexible element and the initial air flow velocity significantly affect the swirl velocity and the SA value; and
– the proposed method of continuously steering the twisting angle of the flexible element helps us to fully adjust the charge kinematic parameters to actual operating conditions of engines and can easy controlled by engine control unit.

Nomenclature

CI	compression ignition
CFD	computed flow dynamics
CNG	compressed natural gas
SI	spark ignition
SA	swirl area
SR	swirl ratio
TDC	top deat centre
TKE	turbulance kinetic energy
TWO	throttle wide open
w	velocity (for numerical simulation)
θ	tape twisting angle

Bibliography

[1] MERKISZ, J., PIELECHA, J., RADZIMIRSKI, S. New trends in emission control in the European Union. *Springer Tracts on Transportation and Traffic*. 2014, **4**.
[2] ROKOSH, U. The vehicle after treatment systems and on-board diagnosis (in Polish). *WKŁ*. Warszawa 2007.
[3] AMBROZIK, A. The analysis of work cycles of four-stroke piston engine (in Polish). *Wyd. PŚ Kielce*. 2010.
[4] HEYWOOD, J.B. Internal combustion engine fundamentals. *McGraw-Hill*, Singapore 1988.
[5] BENNY, P., GANESAN, V. Flow field development in a direct injection diesel engine with different manifolds. *International Journal of Engineering, Science and Technology*. 2010, **2**(1), 80-91.
[6] KANG, K.Y., REITZ, R.D. The effect of intake valve alignment on swirl generation in a DI diesel engine. *Experimental Thermal and Fluid Science*. 1999, **20**, 94-103.
[7] PIĄTKOWSKI, P. The chosen issues of in-cylinder charge kinematics (in Polish). *Wyd. Ucz. PK*. Koszalin 2013.
[8] PIĄTKOWSKI, P. The impact of kinematics of the airflow on the efficiency of combustion process in piston engines. *Combustion Engines*. 2011, **2**, 82-88.
[9] PIĄTKOWSKI, P. The impact of intake canal geometry on kinematics of load in combustion chamber. *TEKA*. 2012, **12**(1), 89-94.
[10] PIĄTKOWSKI, P., BOHDAL, T. Testing of ecological properties of spark ignition engine fed with LPG mixture. *Annual Set The Environment Protection*. 2011, **XIII**, 607-618.
[11] PIĄTKOWSKI, P., LEWKOWICZ, R. Motrol, 2010, **12**, 115-121.
[12] MARTINS, J., TEIXEIRA, S., COENE, S. Design of an inlet track of a small I.C. engine for SWIRL. *Enhancement Brazil*. 2009.
[13] GOTO, Y., NARUSAWA, K. Combustion stabilization of spark ignition natural gas engine. *JSAE Review*. 1996, **17**, 251-258.
[14] Renault technical info, 2006.

Piotr Piątkowski, DSc., DEng. – Faculty of Mechanical Engineering at Koszalin University of Technology.
e-mail: *Piotr.Piatkowski@tu.koszalin.pl*



Ściegienka Ryszard DSc., DEng. – Faculty of Mechanical Engineering at Koszalin University of Technology.
e-mail: *Ryszard.Sciegienka@tu.koszalin.pl*



Lewkowicz Ryszard, DSc., DEng. – Faculty of Mechanical Engineering at Koszalin University of Technology.
e-mail: *Ryszard.Lewkowicz@tu.koszalin.pl*



Prof. Janusz Mysłowski, DSc., DEng. – Faculty of Mechanical Engineering at Koszalin University of Technology.
e-mail: *Janusz.Myslowski@plusnet.pl*



Article citation info:
WEBER, M. The influence of high efficiency engines and hybrids on exhaust systems. *Combustion Engines*. 2017, **171**(4), 207-210.
DOI: 10.19206/CE-2017-435

Matthias WEBER

CE-2017-435

The influence of high efficiency engines and hybrids on exhaust systems

Increased efficiency of the combustion process itself and low losses in the Engine, lead to lower temperatures in the exhaust line. Combined with the exhaust gas energy recovery as well as the hybridization of the drivetrain, this temperature decrease will require additional efforts for the exhaust gas aftertreatment in future. Current technologies like SCR with urea could only be used in future with additional heating elements or will need to change to different catalysts or gaseous Ammonia, to keep the current efficiency and conversion rates. Catalyst and filter elements with ultra-low backpressure creating additional new challenges for the correct and robust diagnostics of these aftertreatment components and all emission relevant parts and thresholds. New technologies are needed like the direct measurement of the DPF soot loading with radio frequencies or NH_3 sensors to precisely control the ammonia slip for high conversion rates of SCR catalysts.

Key words: *high efficiency engines, low exhaust temperature, NH_3 sensor, low backpressure DPF*

1. Introduction

The increasing efficiency of combustion engines, together with the hybridization of drivetrains, is influencing the aftertreatment system including its control strategies and diagnostics. The reduction of mechanical losses due to use of new lubricants and the cylinder reduction, e.g. from 6 to 5 cylinders for commercial vehicle diesel engines, combined with optimized direct injection strategies, increased injection pressure and advanced fuels, allows the next generation of combustion engines a tremendous increase in efficiency and therefor, also a reduction in CO_2 emissions.

Increased efficiency in the combustion process itself and low losses in the Engine, lead naturally to lower temperatures in the exhaust line. Combined with the exhaust gas energy recovery as well as the hybridization of the drivetrain, this temperature decrease will require additional efforts for the exhaust gas aftertreatment in future. Current technologies like SCR with urea could only be used in future with additional heating elements or will need to change to gaseous ammonia, to keep the current efficiency and conversion rates.

New catalyst and filter elements with ultra-low backpressure contribute to further CO_2 reduction leading to new challenges to perform a correct and robust diagnostics of these aftertreatment components.

To fulfill future emission laws, regarding emission limits and diagnostics of the aftertreatment system, new Sensors like the direct measurement of the DPF soot loading with radio frequencies or NH_3 sensors to precisely control the ammonia slip for high conversion rates of SCR catalysts are needed

2. Current systems (diesel example)

Today's engines are not operating at the most fuel efficient operating points. This is done to reduce the formation of raw emissions, mostly nitrogen oxides. Also, to reduce Particles and to heat the exhaust system, post injections late in the combustion or after combustion are used, leading to a higher temperature of the exhaust gas. The loss of efficiency created with this measure is accepted in general for passenger car applications. For larger engines, like commercial vehicles and non-road mobile machinery (e.g. heavy construction equipment), an additional HC-dosing unit is mounted in the exhaust line to inject fuel in front of the diesel oxidation catalyst (DOC). The fuel is then oxidized in the DOC, leading to a further increase of the exhaust temperature. Prerequisite for this methodology is that the temperature of the DOC is above 200 degrees Celsius. If this temperature cannot be reached, the use of a separate external burner unit to heat up the aftertreatment is needed.

Figure 1 shows an example of a current diesel aftertreatment system. It consists of a diesel oxidation catalyst, diesel particle filter and a SCR-catalyst for NO_x reduction. The potential ammonia slip is treated with a cleanup catalyst combined with the SCR-catalyst.

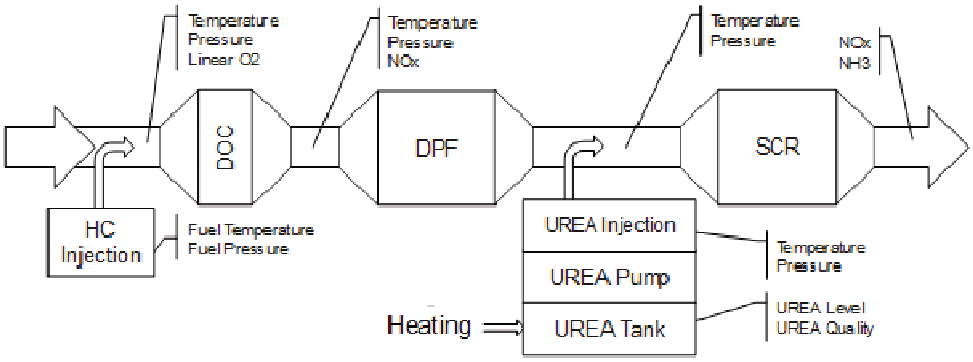


Fig. 1. Current diesel exhaust system example [1]

This aftertreatment systems has a conversion rate depending on the temperature of the exhaust gas and the catalysts. For SCR systems based on urea, the maximum conversion rate is between 200 and 300 degrees Celsius. Below or above this temperature window, this system has lower conversion rates leading to a non-fulfillment of actual emission norms.

The efficiency of the diesel particle filter (DPF) depends on the used materials and technology. Based on the chosen technology, the DPF needs a temperature window either for continuous conversion or to start the regeneration of a loaded filter element. In medium to high load points of the engine, the exhaust gas temperature today is high enough to heat the diesel oxidation catalyst to his light off temperature. This allows the use of additional heating with a post injection in passenger cars, and in addition with a HC dozer for commercial vehicles.

The issue arising here is, that as the efficiency of an engine increase, the exhaust gas temperature of the engine will decrease. This will lead to lower conversion rates and issues to regenerate the diesel particle filter. Once the diesel oxidation catalyst is not getting heated enough, the whole exhaust aftertreatment process is at stake.

3. High efficiency engines

Besides emissions, the next generation of combustion's engines will be optimized also for CO_2 emissions. The efficient combustion of this engines lead to a lower exhaust gas temperature. In addition, exhaust gas energy recovery systems will further reduce the exhaust temperature. This systems convert energy of the exhaust gas into electricity, or transferring it to the coolant water of the engine. Another trend to increase the efficiency is downsizing of the engines and the reduction of the number of cylinders. This lowers the exhaust volume and therefore also the amount of energy available. Furthermore, due to cylinder reduction and new lubricants, the friction of the engines is reduced. The reduction of this engine losses lead to the situation, that in the already critical area of low load with low exhaust gas temperature, the exhaust gas energy is further reduced, as less fuel is needed to keep the engine idling.

Besides classical engine design optimization, hybridization is even for commercial vehicles an upcoming methodology, to increase the overall powertrain efficiency [2]. Energy is recovered by using the electrical motors for regenerative braking. This recovered energy is then used to accelerate the vehicle using an additional electrical engine. This additional engine, assists the combustion engine in the dynamic phase of an acceleration, which is emission critical. Also, according the relation of the vehicle weight and the available electrical torque, vehicles can drive fully electrical for some time, or eradicating the Engine idle with a start/stop functionality completely. These measures are leading to a reduced load, or even to a complete standstill for the combustion engine. As a result, less energy in the exhaust gas for the exhaust system is available.

In future applications, the overall design of the combustion engine including its exhaust system needs to take care of this issue. Engineers must find an optimal operating strategy to balance high efficiency of the combustion engine and low CO_2 against the emissions and the needs of the exhaust system.

4. At the cross road – integrated or standalone

Because of the trend to high efficiency engines, we will see the further integration of the exhaust system into the combustion engine for passenger cars and smaller engines. Oxidation catalyst, NO_x storage catalyst or even the three-way catalyst will be mounted close, or even at the engine inside the engine bay. This will minimize the temperature losses of the exhaust gas before reaching the catalysts or filter elements. The temperature management of the whole system needs to guarantee the needed operating temperature, depending on the operating point of the engine and the produced exhaust gas.

Also, hybrids with increasing capability of driving fully electric laying down extra requirements on this management. Before the combustion engine can take over with medium or full power, there needs to be a heating strategy implemented to get the exhaust system to the required conversion performance. This means, that also the hybrid driving strategy needs to consider the operational status of the exhaust system.

From a controls or operating strategy standpoint of view, this is an issue in classical automotive engineering as the automotive industry is mostly component driven. Distributed functionality based on a system engineering approach to optimize and solve this issue is rare.

For larger engines like trucks, busses or non-road mobile machinery, the exhaust system can be considered as a standalone. Based on the expected emissions, volume stream and allowed back pressure, the active elements can be designed and a feed forward control can best established. Such a stand-alone unit will then request a certain concentration of hydrocarbons and an according temperature for the incoming volume stream and use own heating units, like a HC dozer and oxidation catalysts, electrical heater or separate burner units for further temperature control in the exhaust system.

5. The end of urea?

Most currently used NO_x catalyst systems are using a liquefied solution of urea. This solution is the Injected into the exhaust pipe in front of the SCR catalyst. Besides issues with crystallization at the Injector and aging of the solution, a liquid urea solution needs a certain exhaust gas temperature to create the necessary vapor to release the needed ammonia gas. Lower temperatures limit this process and therefore the distance between urea injector and SCR-catalyst needs to be increased to ensure a proper vaporization. Below 200 degrees Celsius most urea based systems have not sufficient conversion rates to fulfil legal emission limits.

An interesting alternative to this systems was developed by the Danish company AMINEX [3] where ammonia gas is directly stored in a salt. This salt is the used in cartridges in the vehicle, enabling a safe handling of the stored ammonia. The release of the needed ammonia for the aftertreatment system is reached by heating the salt in the cartridges.

Such a system can operate at much lower temperatures as urea based systems as they directly deliver ammonia gas. This makes them an interesting alternative for future aftertreatment systems beyond EURO 6/EURO VI and TIER 4.

6. Missing: systems engineering

Current automotive development is mostly component driven. Major OEM's are structured into engine departments and aftertreatment departments which reflects in the current function- and electronic control unit architecture. For further optimization, systems engineering on vehicle, functional and architectural level will become more and more important. At least in the controls structure of passenger cars, there should be no longer a system combustion engine accompanied by a system aftertreatment. In future, there will be a need to design this as one control system, where combustion engine, aftertreatment components and electrical components are sub systems of the overall driveline. Based on the actual status and capability of all components, it will create the maximum torque with highest possible efficiency.

7. Future aftertreatment systems

Three areas need to be improved for future exhaust systems like the example shown in Figure 2 are the control strategy, diagnostic and the catalysts themselves. As a first step to keep up the conversion rates of today's exhaust gas systems, we will see new sensors and sensor technology. As an example, the usage of a NH_3 sensor, will allow closed loop control of the ammonia slip. This will enable the exhaust system to operate with the maximum urea quantities also on lower temperatures, leading to higher overall conversion rates as with feed forward control strategies.

Also, the urea quality sensor will assist in a more precise calculation of the needed dosing quantity to treat the current NO_x in the exhaust stream. Together with the NH_3 sensor, this results in a more robust and precise dosing strategy with feedback control as we have today.

Using this capability of the SCR system to operate always with its maximum conversion rate, future combustion engines can increase the production of raw emissions like NO_x, leading to better fuel performance and therefore CO_2 reduction.

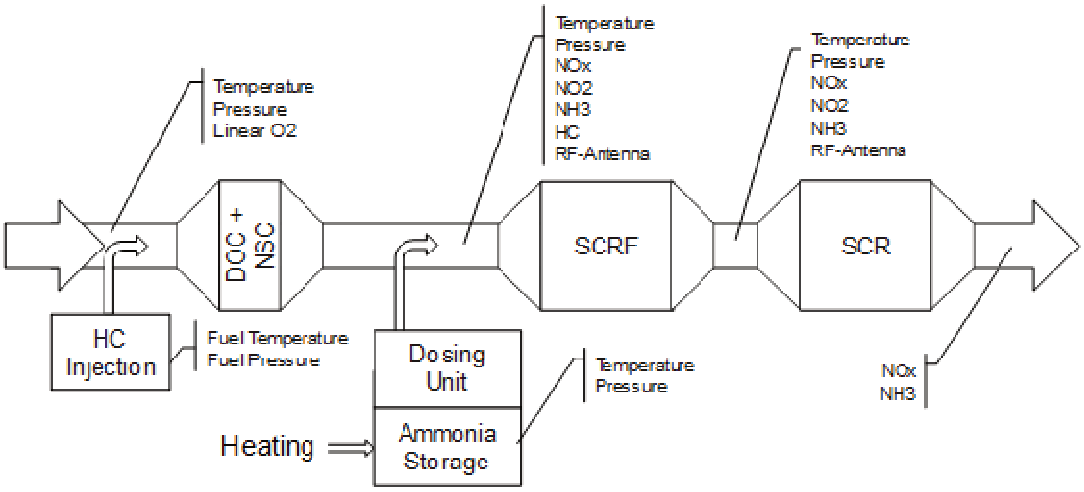


Fig. 2. Future diesel exhaust system example [1]

To establish a feedback control for the regeneration of the diesel particle filter, new sensors like the radio frequency based sensor [4] can be used. With this measurement principle, for the first time in the vehicle, the loading of the filter can be measured and the regeneration will only be performed if necessary. The regeneration based on a maximum time interval, to prohibit damages, is no longer necessary in such systems. This lead overall to a reduced number of regenerations and therefore to lower CO_2 emissions.

To increase the robustness of the aftertreatment diagnostic, especially the diagnostic of the particle filter a particle sensor after the filter can be used. With this sensor, it will be possible to indirectly detect cracks in the filter ceramics due to measurement of the increased mass of particles after the filter element. current diagnostic strategies reaching their detection precision with the introduction of ultra-low backpressure filter ceramics. Diagnosing a crack in this components by pressure drop, is no longer possible.

This is an issue for diagnostics, as a major principle and rule of On Board Diagnostics II is: "If you can't diagnose it, you can't use it". Hence this sensor will open the usage of a variety of low back pressure components.

Regarding future catalysts, we will see active coating for NO_x conversion also on the particle filter itself. This measure aims to increase the available active surface for NO_x conversion (SCR on filter, SCRF). Also, the diesel oxidation catalyst will most likely be combined with a NO_x storage catalyst. This will further increase the NO_x conversion and storage capability, which is needed to reach an effective aftertreatment system shortly after engine start while the exhaust system itself is still heating up. Once the operation temperature is reached; the NO_x storage can be regenerated.

Because of the SCRF element replacing of a classical diesel particle filter, the ammonia gas will be introduced into the exhaust gas stream before the SCRF and not like today after the diesel particle filter. This will increase the complexity of the NO_x conversion control strategy. An additional NH_3 sensor between the SCRF and the SCR

catalyst will most likely be used to enable a feed back control for this configuration.

8. Summary

The overall trend to higher efficiency engines and lower CO_2 emissions, lead to lower temperatures in the exhaust gas aftertreatment system.

This creates the demand for new technologies, like catalysts and additional Sensors, to provide the needed conversion efficiency and conversion rates to fulfill future emission norms and CO_2 targets.

Future control strategies will utilize new and additional sensors, like NH_3 sensor and RF-sensor, to implement closed loop control for regeneration of the particle filter and control of the NO_x conversion rate.

To enable the usage of ultra-low backpressure components, todays diagnostic strategies need to be extended. This can be done by utilizing of urea quality sensors and particle mass sensor into the aftertreatment system.

Nomenclature

DOC	diesel oxidation catalyst
DPF	diesel particle filter
HC	hydrocarbon
NH_3	ammonia
NSC	NO_x storage catalyst
NO_2	nitrogen oxide
NO_x	nitrogen oxides
O_2	oxygen
RF	radio frequence
SCR	selective catalytic reduction
SCRF	SCR on filter

Bibliography

[1] WEBER, M. Exhaust aftertreatment of diesel engines and its OBD. *3rd International Specialist Conference: SENSORS for Exhaust Gas Cleaning and CO_2 Reduction*. Leipzig, Germany.

[2] SHUTTLEWORTH, J. Volvo trucks tests hybrid powertrain for longhaul transport in concept truck. *SAE Article*. articles.sae.org/15330.

[3] JOHANNESSEN, T., SCHMIDT, H., SVAGIN, J. et al. Ammonia storage and delivery systems for automotive NO_x aftertreatment. *SAE Technical Paper*. 2008, 2008-01-1027.

[4] RAGALLER, P., SAPPOK, A., BROMBERG, L. et al. Particulate filter soot load measurements using radio frequency sensors and potential for improved filter management. *SAE Technical Paper*. 2016, 2016-01-0943.

Matthias Weber, Dipl.-Ing. – Managing Director and Founder of Roben Automotive.

e-mail: *Matthias.Weber@roben-automotive.com*



Article citation info:
ŚMIEJA, M., WIERZBICKI, S., MAMALA, J. CAN network in real time on board systems. *Combustion Engines*. 2017, **171**(4), 211-214. DOI:10.19206/CE-2017-436

Michał ŚMIEJA
Sławomir WIERZBICKI
Jarosław MAMALA

CE-2017-436

CAN network in real time on board systems

The network system of data exchange between the various components is an inherent element of every car. Because of the specific and different requirements for data transfer between specific devices, currently used communication protocols have different properties of performance, security, and degree of determinism. The paper presents the increasing complexity of the data exchange system based on the example of the latest requirements for digital tachographs. The article describes also the data transmission initialization methods in the context of network data exchange organization. The hybrid use of time triggering and event triggering mechanisms has been presented in relation to the operation of the CAN network under increased real-time conditions requirements implemented as TTCAN (time triggered CAN).

Key words: *CAN, TTCAN, real time architecture, tachograph, time triggered networks, automotive networks*

Introduction

Electronic systems of modern cars and their networks feature an increasing amount of circulating information as well as diversity in terms of the required level of time determinism or the security.

The network structure optimization must take into account many frequently contradictory criteria such as cost, weight of the system, expandability, and use of hardware and software security mechanisms.

Proper evaluation of the on-board solution is significantly difficult due to the complexity of modern network systems. A visible trend in the construction of automotive communication networks is the tendency for a strong integration of individual network subsystems allowing the exchange of information between any node or node groups across the network. The advantage of such solutions is the easy distribution of information from a single source to multiple receivers / subsystems, as well as the opposite: the possibility of redundant disposing of data from more than one source p. ex. for their verification. The negative consequence of strong network integration, however, is the increase of its vulnerability to unauthorized, and often undesirable, interference [21, 22]. Apart from numerous ways of securing networks based on data encryption [20], one of the simplest methods is to isolate the part of bus that is critical for the security by physical isolation of the bus signal lines or using a gateway as the intermediate element.

An example of a highly autonomous system, based on many communication solutions, is the digital tachograph system described, among others, in [14, 15, 18], based on signal received from the motion sensor coupled to the drive system of the vehicle. Although the improper operation of this system has no direct effect on the vehicle security, the potential consequences of uncontrolled driving times make the relevant regulations and restrictions on its production, operation and transmission very restrictive. Recent regulations, [16, 17] regulating the use of GNSS as a second source of motion data, add to the set of digital network protocols implemented by the ISO/IEC 7816-4:2013 the interface for data exchange between a vehicle unit and an external GNSS device. The smart tachograph described in this document has at least two precise sources of time, location and vehicle speed data.

Use of this information in accordance with the [19] will not be limited to the other car subsystems, but it will also be used in the group of technologies such as intelligent car sharing, fleet management system (FMS), advanced driver assistance system (ADAS) etc. The proposed access to motion data for recipients other than the tachograph recorder is located alternatively directly on the GNSS receiver or as a vehicle unit interface (VU) where it acts as a gate. From this point of view, the tachograph system reduces its autonomous character to function as part of a larger system.

Taking into account the deterministic temporal way of acquiring and using of vehicle motion data as well as the number of potential senders and recipients, it seems appropriate to make greater use of time-deterministic data exchange systems.

Time/event triggering

The current automotive data exchange networks link elements of the complex real-time system.

The effectiveness of such systems depends on both the results of the calculations and the time of their occurrence. The critical parameter for real time systems is the so-called deadline, indicating the time, until which the target specified in the operation of this system is reached. In other words, the execution of actions to be performed must be predictable over time. The problem of proper scheduling of these actions is getting complicated with the increase of amount of them and the restrictions on the data transmission and processing. The automotive mechatronic systems use mainly the serial transmission in which data is transmitted in the form of single bit streams one by one. If the line is busy with a data stream associated with one sender, it locks the flow of messages from others. The deterministic time access to the bus must be guaranteed to any sender being the network nod in order to ensure the real-time system predictability. Messages sent in real-time systems have varying deadline values. Assuming constant transmission speed and the known data packet dimension, the required time of arrival at the destination can be explicitly predicted by the time it begins transmitting. Transmission start is called triggering. In the most

commonly used, in the automotive network, the communication protocol based on the CAN specifications, the initiation of the transmission occurs as a result of a specific event (event triggering). This type of triggering allows a maximum reduction of the response time between the input and output of the selected part of the processing process, provided the sender is free to access the bus. In real conditions, where the network is heavily loaded with data, the time from the occurrence of the event to the action undertaken by the message recipient must be within the significantly extended time deadline range.

Transmission initiation associated with a point in the timeline is called time triggering. In most cases, it is used for parts of a system based on data processed in a recurring manner with a fixed cycle. Under such conditions, the jitter on the assumed moment of receiving the message is minimal and the deadline time is strictly defined. A detailed description of the related issues is described in [1].

The best triggering system selection is the very complex task, and is often taken into consideration at the design stage of the object on which this system is implemented. Increasingly large amounts of data and requirements on the time predictability indicate the growing importance of time-triggering networks. Obviously the advantages of event triggering lead designers and manufacturers to develop solutions that combine both modes of transmission initiation such as FlexRay. An example of the time triggered CAN protocol (TTCAN) which features high adaptability to the most popular in automotive CAN systems, are described later in the article.

Time trigeered CAN

Time Triggered CAN (TTCAN) can be considered as a deterministic temporal extension of the network protocol described in specification that formerly described the data layer. ISO standards ISO 11898, based on the CAN specification, extend the scope of the description to the physical layer [2, 3].

Specific for CAN the way of accessing the bus based on the arbitrary function CSMA/CD implicates a flexible degree of temporal detriment, mainly related to the assignment of the message identifiers to the object. In traditional CAN networks, the access to the bus is highly hierarchical, as the lowest ID has most privileged bus access. Assuming the uniqueness of identifiers, there is no possibility of imposing the equal degree of temporal determinism for the transmission of two different messages. For a classic CAN, the lower limit of deviation from the desired point on the time ax (jitter) can be determined by considering that the node with lowest ID should start transmitting while the transmission of any other message is already proceeding assuming, that the start of transmission can only occur when the line state is IDLE. This may result in, in the worst case, the delay in the transmission equal to bit lengths consisting of a full frame header (29 bits) and a maximal length of the data field provided for the CAN specification, ie 8 x 8 bit. Other elements of the frame such as ACK checksum, etc., have a fixed dimension. The "worst case" assumption should take into account the possibility of adding extra transmission time in conjunction with the occurrence of stuffing bits, which in extreme cases increases the transmission time by about 1/5 (20%).

The Time Triggering CAN (TTCAN) concept is based on so-called The System Matrix, in which the timing of the start of transmission is attributed to the message.

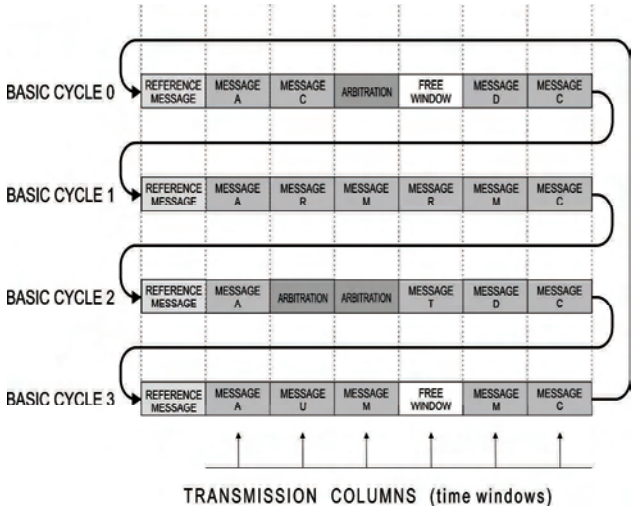


Fig. 1. TTCAN System Matrix

The System Matrix, Illustrated schematically in Fig. 1, describing the full cycle of network data exchange consists on a finite (2^n) number of consequential Basic Cycles, which are defined as rows and a finite number of time windows within a single Basic Cycle which are called columns in the given description. Depending on the way of accessing the TTCAN bus, there are Exclusive time windows and Arbitrating time windows. In order to facilitate possible further extension of the network, there are also planned so-called Free windows which, as the name suggests, are not assigned to any message.

The presence of exclusive time widows is a fundamental feature of TTCAN, giving this network a highly deterministic character. The message attributed to the unique Exclusive time widow is delivered cyclically at specific times because of its constant position in the matrix system. In such cases there is no message hierarchy for bus access. Taking into account the different requirements of the object, in relation to ensuring the proper transmission of the message due to the appropriate type of information, specific messages can be assigned to more than one Exclusive time window. For example, in the diagram shown in Fig. 1 the message A is transmitted in the same frequency as the message C and four times more frequent than the message U.

The arbitrating time windows are used to allow the transmission of significant, though irregular or even occasional messages, while preserving their hierarchy.TTCAN uses here the CAN 2.0 arbitration mechanism, based on the binary bit identifier comparison. Although the size of a specific arbitration window results from the construction of the matrix system (the size of the column imposes the size of the window), there is the possibility to merge the consequential windows of this type, thus giving a window of equal size to their total length.

Every network node, being a frame sender, has information included in the System Matrix, based on which the start of transmission of specific messages is set. The key issue is therefore the need to set up time mechanisms to

synchronize the work of all senders. The basic feature for synchronizing network node work is the so-called Reference message, sent at the beginning of each Basic cycle (see Fig. 1). Reference message is a data frame, transmitted by a node that has Time Master function. The simplest form the reference message data field consists of one data byte, bearing the information about so called Next_Is_Gap. The time master identifier, contained in the reference message, is stored in the memory controller of each network node at the configuration stage so that the message is properly recognized. The receipt of a reference message by each network node initiates a network synchronization process to set the common time base clock in a so-called network time unit (NTU), equal to the nominal time of one bit. Thanks to this process, each of the node knows exactly when times windows, described by System Matrix, begin. The synchronization process is repeated at the beginning of each Basic cycle. As a result, the Cycle_Time is established at the beginning of each basic cycle.

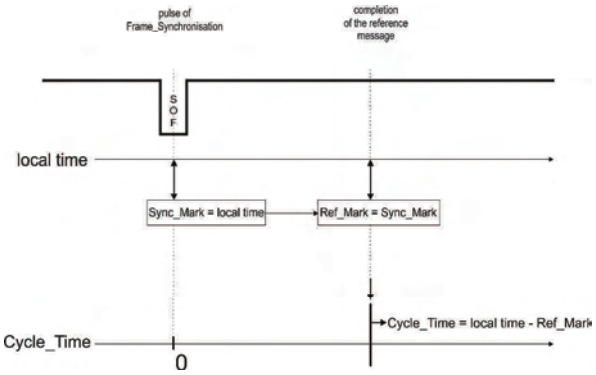


Fig. 2. TTCAN basic cycle synchronisation Level 1

Cycle_time is set to zero at the start of a frame (SOF) bit, and it is incremented during the entire basic cycle. The correct Cycle_Time value appears at the end of the reference message as illustrated in Fig. 2.

The presented synchronization procedure refers to the so-called TTCAN Level 1. In conditions where enhanced synchronization quality, the use of global time or external clock synchronization are required, the Level 2 is used. In level 2 the reference message contains additional information about network time resolution (NTU_Res), discontinuity bit (Disc_Bit) and Master_Ref_Mark (MRM).

In this case NTU _Res refers to NTU based on the physical second. Disc_Bit signals discontinuity in global time with external clock correction. Global time is a uniform timeline for all nodes in the network. Global time view of every node is the sum of the Local Time and the Local Time offset. The local time offset is defined as the difference between the local time and the global time contained in reference message, received by the node, as MRM. The comparison of global time in consecutive basic cycles allows the correction of differences in local NTU caused by, for example, different clock drift (Typical oscillator has an accuracy of 20 to 5 ppm).

The time and the way to send and receive messages in the application is defined by Tx_Trigger and Rx_Trigger, which contains information about the associated time window in the form of so called Time_Marks. The positive result of Time_Mark and Cycle_Time comparison means the occurrence of a specific Time Windows and consequently sending of a specific message or received message handing, as illustrated in Fig. 3.

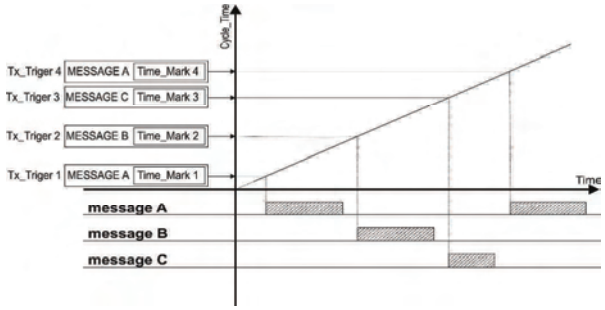


Fig. 3. Scheme of TTCAN message triggering

Summary

The undisputable position of CAN-based communication networks in automotive applications proves their high efficiency and reliability. The fact that CAN is used in so many different applications, such as comfort or driving control systems also confirms their flexibility. However, the scope of on-board systems based on data interchange and processing is constantly growing, what is followed by the evolution of the network structure, and the development and deployment of alternative, to CAN, solutions. Among classic communication networks co-existing in a car, LIN, MOST, FlexRay should be listed. The use of ethernet-based protocols in the automotive industry is also strongly considered and discussed [5, 6]. The reasons for looking for alternative data exchange systems are, for example, costs reduction – Lin development in comfort / body systems, the increase of transmission speeds – MOST, or the need to improve the security and reliability as in FlexRay, dedicated to future X-By-wire solutions. Practical implementations of these protocols indicate, however, that in some cases the achieved results are not satisfactory. As suggested by [10], the transmission baudrate in Flex Ray, assuming the use of all protection features defined for this protocol, doesn't differ significantly from the ones of CAN. Likewise, the cost of using Lin instead of CAN eventually does not show significant savings.

These problems may be addressed by a modification of the CAN data layer protocol for CAN FD [11–13, 24] as well as its implications for the higher layers of the OSI model – TTCAN [7]. The comparison of protocols is presented in [4].

The TTCAN – specific transmission initiation, described in the article, allows in many cases to achieve assumed goals by the existing network structure evolving, without the need to use much more complex protocols such as FlexRay, although some of the mechanisms in the two standards are very similar.

The control of the traffic on the data bus, organized by time transmission initiation control rules introduction allows, for example, similarly as in Flex Ray, to introduce passive Bus Guardian nodes to ensure the correct transmission. The visible feature of TTCAN is the ability to override time triggered transmissions, on which basic cycles are

based, by event triggered one. An example of the event that requires an event-triggering transmission may be the object failure state, what requires the time triggered information about the current circumstances or subsystem state.

Acknowledgement

The article funded under the project entitled "Development of innovative manufacturing technology of motion sensors to a new generation of digital tachographs, according to the common criteria EAL4 +." The subsidy contract No. UDA-POIG.01.04.00-28-004/11-00 under the measure 1.4 Support special projects of the priority axis 1. Research and development of new technologies, Innovative Economy Operational Programme 2007–2013.

Nomenclature

CAN	controller area network	ACK	acknowledge bit
CAN FD	CAN with flexible data-rate	NTU	network time unit
TTCAN	time triggered CAN	SOF	start of a frame
GNSS	global navigation satellite system	NTU_Res	network time resolution
FMS	fleet management system	MRM	master reference mark
ADAS	advanced driver assistance system	NTU_Res	NTU resolution
VU	vehicle unit interface	CSMA/CD	carrier sense multiple access/with collision detection
ID	network identifier		

Bibliography

[1] KOPETZ, H., BAUER, G. The time-triggered architecture. *Proc. IEEE*. 2003, **91**(1), 1120-1126.
[2] OBERMAISSER, R. Reuse of CAN-based legacy applications in time-triggered architectures. *IEEE Transactions on Industrial Informatics*. 2006, **2**(4).
[3] FIJALKOWSKI, B.T. Automotive mechatronics: operational and practical issues, intelligent systems. *Control and Automation: Science and Engineering*. 2011, **47**.
[4] TALBOT, S.C., SHANGPING, R. Comparison of fieldbus systems, CAN, TTCAN, FlexRay and LIN in passenger vehicles. *ICDCSW '09 Proceedings of the 2009 29th IEEE International Conference on Distributed Computing Systems* W*orkshops*. 22-26.06.2009.
[5] HAMMERSCHMIDT, C. Ethernet to gainground in automotive applications. *EETimes*. 03.02.2011.
[6] HANK, P., MULLER, S., VERMESAN, O., Van Den KEYBUS, J. Design automotive ethernet: in-vehicle networking and smart mobility. *Automation & Test in Europe Conference & Exhibition*. 2013.
[7] ABOUBACAR, D. OSI layers in automotive *networks*. IEEE 802.1 Plenary Meeting – Orlando, 2013.03.20.
[8] FRYŚKOWSKI, B., GRZEJSZCZYK, E. Systemy transmisji danych. *WKiŁ,* Warszawa 2010.
[9] MERKISZ, J., MAZUREK, S. Pokładowe systemy diagnostyczne pojazdów samochodowych, *WKiŁ,* Warszawa 2007.
[10] ZIMMERMANN, W., SCHMITGALL, R. Magistrale danych w pojazdach. *WKiŁ*, Warszawa 2008.
[11] BORDOLOI, D., SAMII, S. The frame packing problem for can-FD. *Real-Time Systems Symposium* (RTSS), 2014.
[12] EISELE, H.K., WIENCKOWSKI, N.A. Status and outlook for CAN with flexible data rate. *Vector Congress*. 27.11.2014.
[13] HARTWICH, F. CAN with flexible data-rate. *Proceedings of the 13th international CAN Conference*. Hambach Castle. Germany 2012.
[14] BISHOP, J.W., NORDVIK, J.P. Digital tachograph system European root policy version 2.1 European Communities 2009.
[15] Digital tachograph system European root certification authority certification practices statement version 1.0 European Communities 2004.
[16] Rozporządzenie Parlamentu Europejskiego i Rady (UE) nr 165/2014 z dnia 4 lutego 2014 r.
[17] Rozporządzenie Wykonawcze Komisji (UE) 2016/799 z dnia 18 marca 2016 r. w sprawie wykonania rozporządzenia Parlamentu Europejskiego i Rady (UE) nr 165/2014 ustanawiającego wymogi dotyczące budowy, sprawdzania, instalacji, użytkowania i naprawy tachografów oraz ich elementów składowych.
[18] RYCHTER, M. Budowa i zastosowanie systemu tachografii cyfrowej. *Wydawnictwo ITS*. Warszawa 2011.
[19] Tachograph Forum Meeting 28 November 2016 Bernardo MARTÍNEZ Road Transport Unit (DGMOVE) European Commission.
[20] STALLINGS, W. Cryptography and network security principles and practice fifth edition. *Prentice Hall*. 2011.
[21] SOJA, R. Automotive security: from standards to implementation. Freescale White Paper.
[22] WOLF, M., WEIMERSKIRCH, A., WOLLINGER, T. State of the art: embedding security in vehicles. *EURASIP Journal on Embedded Systems*. 2007.
[23] CAN specification version 2.0. Robert Bosch GmbH, Stuttgart 1991.
[24] CAN with flexible data-rate specification version 1.0. (released April 17th, 2012) Robert Bosch GmbH.
[25] FlexRay communications system protocol specification. version 2.1, revision A.

Michał Śmieja, DEng. – Faculty of Technical Sciences at University of Warmia and Mazury in Olsztyn.

e-mail: *Smieja@uwm.edu.pl*



Jarosław Mamala, DSc., DEng. – Faculty of Mechanical Engineering at Opole University of Technology.

e-mail: *J.Mamala@po.opole.pl*



Sławomir Wierzbicki, DEng. – Faculty of Technical Sciences at University of Warmia and Mazury in Olsztyn.

e-mail: *SlawekW@uwm.edu.pl*



Article citation info:
POJAWA, B. Energetic state parameters measurements of LM 2500 naval gas turbine for modeling and simulation purposes. *Combustion Engines*. 2017, **171**(4), 215-221. DOI: 10.19206/CE-2017-437

Bogdan POJAWA

CE-2017-437

Energetic state parameters measurements of LM 2500 naval gas turbine for modeling and simulation purposes

This article presents examples of results of energetic state parameters measurements of LM 2500 naval gas turbines operated by the Polish Navy. Currently in operation there are four LM 2500-type engines. In the near future, another LM 2500 engine will commence operations, along with a project 661M patrol ship. The energetic state parameters measurements covers the engine start-up process, their operation in idle mode and within the whole range of load variations, as well as stoppage of engine process. The article presents examples of characteristics specific to the above processes, determined based on the results of studies of this kind of engines. The results of these studies will be used to verify the modeling and simulation results of the internal energy processes occurring in this kind of engine.

Key words: *a naval gas turbine, operating characteristic of naval gas turbine, LM 2500, diagnostics, energy research*

1. Introduction

In practical operation of naval power plants, including also naval propulsion systems with naval gas turbines, there is a need for analyzing them and comparing various solutions as well as for evaluating their technical condition [3, 5, 7–9, 16]. At the present time, the operation of engines and broad technical equipment is aimed at increasing their reliability, higher performance and energy efficiency as well as minimizing operating costs and risks to people and the environment. Operational indicators of a naval power plant show its reliability, possibility of overloading main propulsion engines, ship's maneuverability, time between overhauls (TBO), etc. Energy-related indicators on the other hand, e.g. efficiency, individual fuel consumption, power and torque determine the ship's speed through the water, its range, etc. [1–5, 9, 12–14, 16].

Current exploitation systems mostly utilize strategies based on technical condition and overall operating costs. Decisions regarding exploitation in such systems require ongoing assessment of the technical condition of an object in use. Therefore, questions whether an object is functioning properly and what is the forecast for its further operational span are constantly valid. In cases of damage it is necessary to be able to locate it, and to identify the cause. For this purpose, systematic exploitation diagnostics are applied, including energy research. With the formulated measurement results at our disposal, it is possible to determine the characteristics of engines for further modeling and simulation purposes.

Operating characteristic can be best defined as a graphical or an analytical presentation of the relationship between the basic values which define the engine performance, as well as the working medium parameters measured in the specific engine cross-sections, and the values characterizing the working conditions of the engine mated with a specific load. These characteristics can be used for further modeling and simulation of the examined engines [3–5, 7, 10, 16]. Based on modeling and simulation there is a possibility:

- determining whether an object is functioning (or may be functioning) properly − utility diagnoses obtained from the study of the functional properties of an object,
- determining a prognosis relating to the expected lifetime of an object − this is usually done by determining the probability of the correct operation in a given period of time,
- the possibility to locate each damage (obtaining sufficiently accurate operational diagnoses),
- determining the cause of a damage.

The paper identifies the object of the research study and presents the test results concerning the determination of the operating characteristics in steady states of the LM-2500 naval gas turbine being a component of the Oliver Hazard Perry class frigate. Preliminary tests were conducted in the ship's engine room when the ship was at sea. Operating characteristics of the engines were determined on the basis of the measurements recorded over the entire engine load range, from minimum to rated load.

2. Study objective

The objective of the study was to measure the operating parameters of the examined engine with regard to determining functional dependencies of its operating characteristics. These characteristics will be used in further energy modeling and simulations, as well as in diagnostics process this type of engine.

3. Object and methods of study

The LM 2500 naval gas turbines occur in a combined propulsion system (COGAG) installed in the 'Oliver Hazard Perry' missile frigates ORP ″Pułaski″ and ORP ″Kościuszko″. The propulsion system of this frigate consists of two LM 2500 naval gas turbines, reduction gear and shaft line with five-blade adjustable propeller. The total power of this propulsion system amounts to 30.000 kW. The propulsion system enable the following operating modes [18]:

- operation of one engine on the starboard or portside,
- simultaneous operation of two engines on the starboard and portside.

In the near term, an another LM 2500 engine will come into operation together with a 661M patrol boat ORP ″Ślązak″.

LM 2500 naval gas turbine has dual-rotor design, with axial flow of the working mass. It consists of two main components: a gas generator and a power turbine. The gas

generator consists of a 16-stage axial flow compressor, an annular type combustor equipped with 30 injectors and a two-stage high pressure turbine. Downstream of the gas generator there is a 6-stage power turbine which transmits torque to the line shaft through a reduction gear. The power turbine is connected with the gas generator in a thermo-gas-dynamic manner [18]. LM-2500 naval gas turbine is shown in Fig. 1.

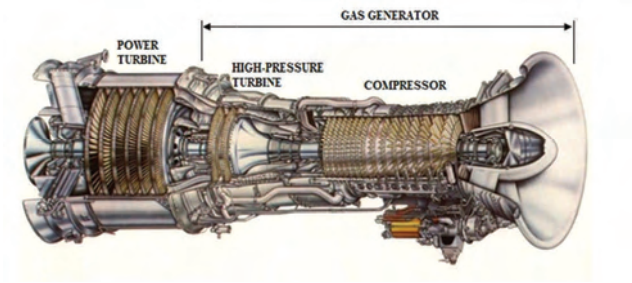


Fig. 1. Cross-section of LM-2500 naval gas turbine [18]

The energy research of naval gas turbines are conducted in order to:

- verify indications of marine control and measurement system,
- determine and assess changes concerning operating parameters of the engine during starting, idling, work with load and during stop (overrun),
- check the correct functioning of the automation system during start-up, while working with load and during stopping the engine,
- check the control parameters according to operational requirements, in particular during idling,
- analyse the operating characteristics of the engine,
- evaluate the fuel system in a steady state,
- assess the technical state of the flow part.

Table 1. Parameters of LM-2500 naval gas turbine measured during the study [18]

parameter designation	measuring range	description of the parameter
n_{GG}	0–12 000 RPM	gas generator speed
n_{PT}	0–5 000 RPM	power turbine speed
p_1	0–16 psia	gas generator inlet air pressure
T_1	–40–150°F	gas generator inlet air temperature
p_{CDP}	0–300 psig	gas generator compressor discharge air pressure
π	0–20	compressor pressure ratio
$p_{4.1}$	0–75 psia	power turbine inlet exhaust gas pressure
$T_{4.1}$	0–2 000°F	power turbine inlet exhaust gas temperature
p_{fuel}	0–1 500 psig	fuel manifold pressure
M	0–35 000 ft·lbf	torque output
P	0–25 000 HP	power output

The study were conducted in motion onboard a two frigates (four engines together), for steady load states, determined on the basis of the gas generator speed over the entire load range of the engine, from minimum to rated load. Engines were loaded in accordance with the propulsion system control program. This program – depending on the preset speed of the ship – selects the optimum setting of propeller pitch and fuel flow and controls the angle of attack of six stages of Variable Stator Vanes (VSV) in the engines' axial compressor. Parameters measured during the study are presented in Table 1.

The schematic diagram of LM-2500 naval gas turbine and the legend describing location of the measured parameters is shown in Fig. 2.

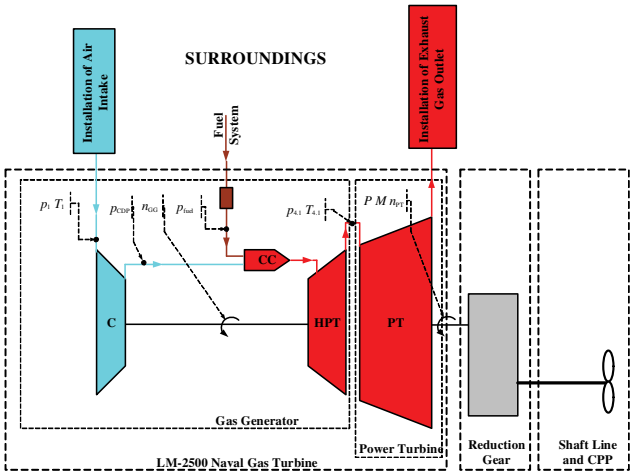


Fig. 2. The schematic diagram of LM-2500 naval gas turbine and the legend describing location of the measured parameters

The parameters were measured simultaneously for both engines, on the load of both engines simultaneous and balanced. The measurements were made using the portable measuring-recording system, Multichannel Recorder type 908416161C and additionally, the operating parameter values were read and recorded from digital displays on the main control panel in the engine control room. The measurements were made for 60 seconds at specific load settings, with the sampling rate of 2 Hz, and then averaged. Measurements were preceded by the calibration of individual measuring circuits including the assessment of their uncertainties. The measuring-recording system during the measurement is shown in Fig. 3.



Fig. 3. The measuring-recording system during the measurement

Parameters were recorded in units of the imperial system of measurement (United States Customary System Units), since in such units measure the measuring instru-

ments on the ship. All registered parameter values are dependent on weather conditions during the study. Therefore, these parameters were reduced to standard reference state using the formulas described in Table 2. Standard reference state are determined by standard pressure 1 atm (101 325 Pa) and standard temperature 288.15 K [17]. Additionally, ambient pressure was taken into account when determin ing absolute pressures.

Table 2. Conversion formulas used to reduce the value of the measured parameters to standard reference state (indexes: R – reduced, M – measured, 0 – ambient) [17]

Parameter	Conversion formula
Power	$P_R = P_M \cdot \frac{101325}{p_0} \cdot \sqrt{\frac{288.15}{T_0}}$
Torque	$M_R = M_M \cdot \frac{101325}{p_0} \cdot \sqrt{\frac{288.15}{T_0}}$
Speed	$n_R = n_M \cdot \sqrt{\frac{288.15}{T_0}}$
Mass Flow Rate	$\dot{m}_R = \dot{m}_M \cdot \frac{101325}{p_0} \cdot \sqrt{\frac{T_0}{288.15}}$
Temperature	$T_R = T_M \cdot \frac{288.15}{T_0}$
Pressure (air, exhaust gas)	$p_R = p_M \cdot \frac{101325}{p_0}$
Hourly Fuel Consumption	$B_{h_R} = B_{h_M} \cdot \frac{101325}{p_0} \cdot \sqrt{\frac{288.15}{T_0}}$
Fuel Pressure	$p_{fuel_R} = p_{fuel_M} \cdot \frac{288.15}{T_0} \cdot \left(\frac{101325}{p_0}\right)^2$

4. Results obtained

4.1. Start-up and stoppage characteristics of the engine and idling

The start-up is a transient process, consisting of a series of dynamic thermal-gaseous processes running simultaneously in all turbine engine fluid-flow machines, aimed at transferring the engine from the idle state to the idle running. In other words, the start-up is the transition from the rotary rim resting state to idle speed. One of the most important requirements for turbine engine starting systems is the automatic, reliable and trouble-free start-up in all weather conditions [10, 18]. Start-up characteristics depend on corresponding adjustments made in the relevant engine and on its technical condition. Therefore, they are individual for every engine within an engine group of a specific type.

Based on the characteristics of the starting and stopping processes of the engine, conclusions may be drawn about correct functioning of the automatic engine start control system, including:

- evaluation of various stages of start-up and correct operation of equipment and installations involved in the start-up process,
- observe the correctness of operation of fuel equipment,
- verify the achievement of required values of the start control parameters in a determined time,
- observe the correctness of the technical condition of the engine bearings,
- carry out the necessary regulations in this regard.

Based on the engine operating parameters recorded in idle running, conclusions may be drawn about the correctness of engine adjustment, as well as the correctness of operation of the fuel equipment. Analysis of the research results is carried out by comparing the measured parameter values with the control parameter values, contained in the operational documentation of the examined engine.

Examples of start-up and stoppage (coasting) characteristics of an engine, recorded during the energetic state parameters measurements of LM 2500 naval gas turbine are presented in Fig. 4–5. Designations of individual control parameters are in accordance with the engine operating parameters contained in Table 1.

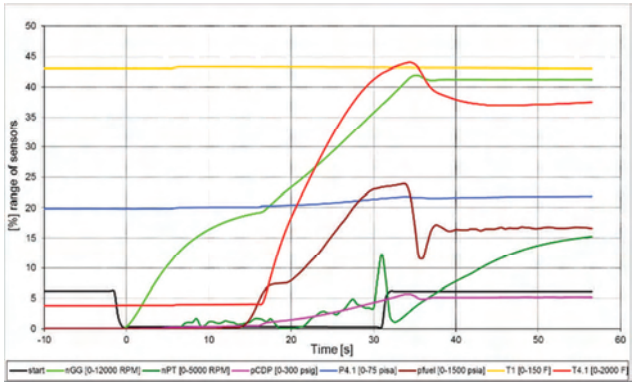


Fig. 4. Course of the relative values of control parameters for start-up of a naval gas turbine LM 2500

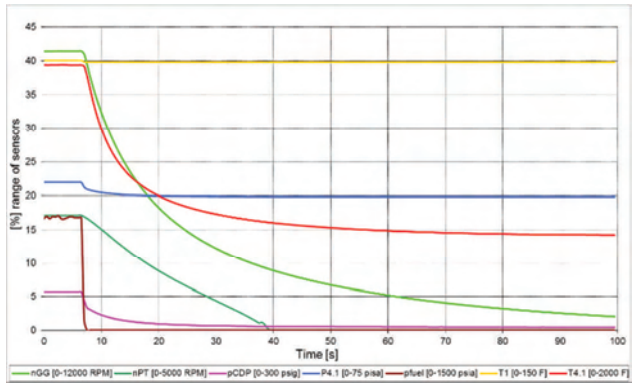


Fig. 5. Course of the relative values of control parameters for the stopping (coasting) of a naval gas turbine LM 2500

4.2. Operating characteristics

Operating characteristics present functional dependencies of between engine operating parameters and the gas generator speed, while maintaining the power turbine speed resulting from its mating to a load being a controllable pitch propeller (CPP). Operating characteristics of the examined engine were determined on the basis of the measurement results from the four engines.

Subsequently, the characteristics obtained were analyzed to determine approximating dependencies. Statistical analysis was used to that end. Statistical analysis is the method of processing data (results of measurements performed according to an assumed program of tests) in order to find regularities in the examined phenomena and to interpret them using the methods employed in mathematical statistics. This facilitates establishing the mathematical function of the examined

object, which may also constitute its mathematical model. The results obtained by means of statistical analysis are the basis for obtaining useful information concerning the examined object and for drawing conclusions from the conducted research. The most common measure of relating the obtained function of the examined object to the measurement results is the coefficient of determination R^2, the average approximation error $\sigma(y)$ (also known as standard deviation) and relative error σ [6, 11, 15]. In addition to the statistical analysis, a substantive analysis of the test results was also carried out. That analysis concerned particularly the validation of the mathematical model obtained for its compliance with the physical phenomena occurring within the relevant examined engine, taking into consideration both theoretical foundations and the principles of operating the engine. In order to approximate the rotational characteristics, least-squares method (LSM) was used, making use of a third-degree polynomials [11, 15]:

$$y = b_0 + b_1 \cdot n_{GG} + b_2 \cdot n_{GG}^2 + b_3 \cdot n_{GG}^3 \qquad (1)$$

for which the coefficient of determination R^2 was the largest [11, 15]. Approximated operating characteristics and the results of the measurements examined engine, recorded for steady-state operation, in relation to gas generator speed n_{GG} are presented in Figs 6–15. The results of statistical analysis of approximated operating characteristics are shown in Table 3.

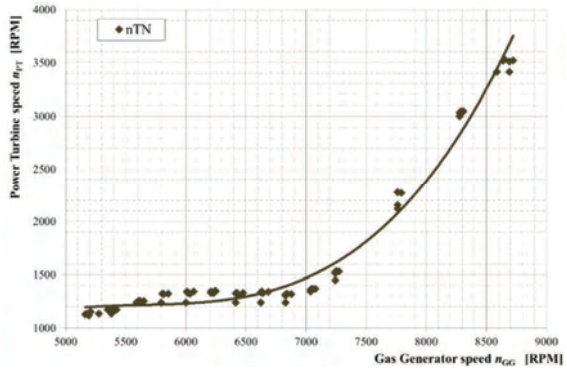


Fig. 6. Approximated function and the results of the measurements of power turbine speed n_{PT}, recorded for steady-state operation of LM-2500 engine, in relation to gas generator speed n_{GG}

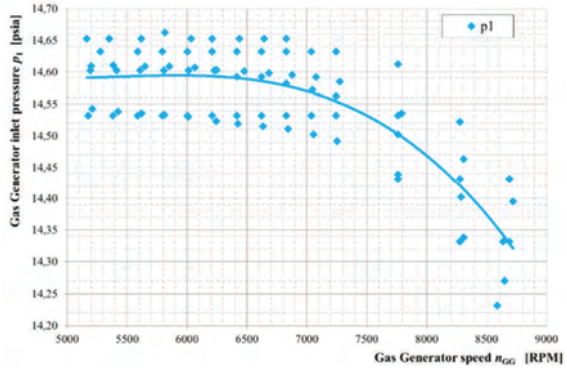


Fig. 7. Approximated function and the results of the measurements of gas generator inlet air pressure p_1, recorded for steady-state operation of LM-2500 engine, in relation to gas generator speed n_{GG}

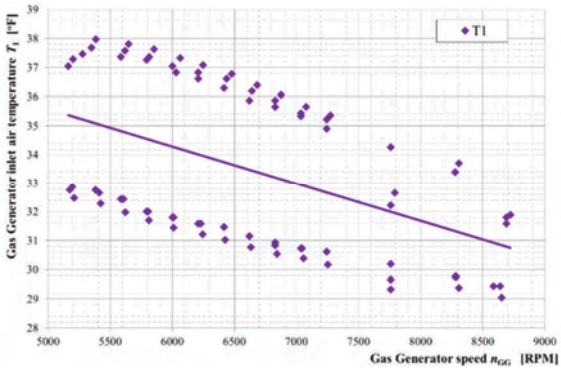


Fig. 8. Approximated function and the results of the measurements of gas generator inlet air temperature T_1, recorded for steady-state operation of LM-2500 engine, in relation to gas generator speed n_{GG}

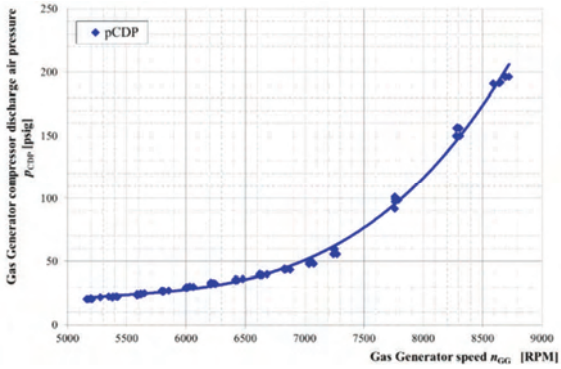


Fig. 9. Approximated function and the results of the measurements of gas generator compressor discharge air pressure p_{CDP}, recorded for steady-state operation of LM-2500 engine, in relation to gas generator speed n_{GG}

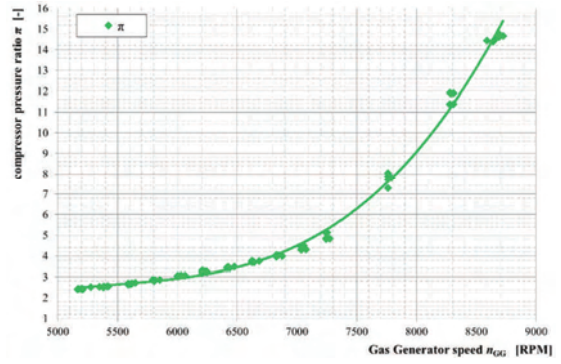


Fig. 10. Approximated function and the results of the measurements of compressor pressure ratio π, recorded for steady-state operation of LM-2500 engine, in relation to gas generator speed n_{GG}

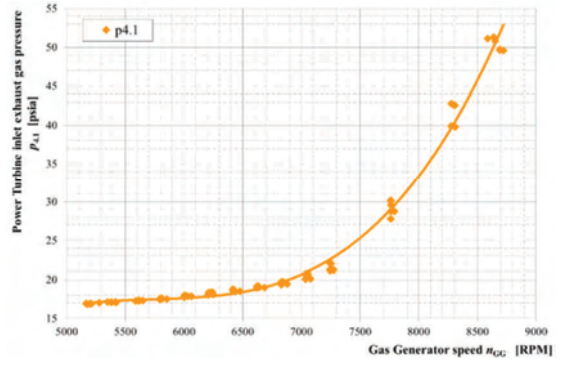


Fig. 11. Approximated function and the results of the measurements of power turbine inlet exhaust gas pressure $p_{4.1}$, recorded for steady-state operation of LM-2500 engine, in relation to gas generator speed n_{GG}

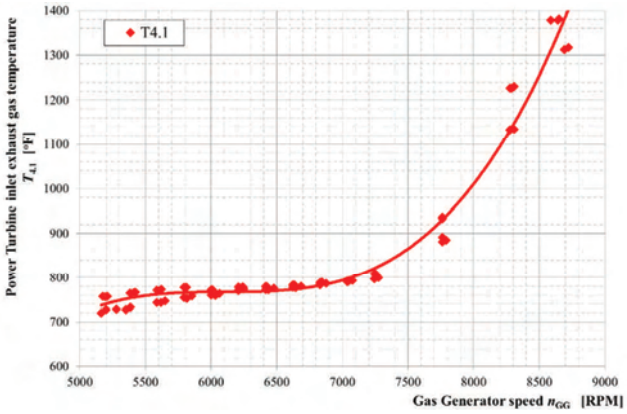


Fig. 12. Approximated function and the results of the measurements of power turbine inlet exhaust gas temperature $T_{4.1}$, recorded for steady-state operation of LM-2500 engine, in relation to gas generator speed n_{GG}

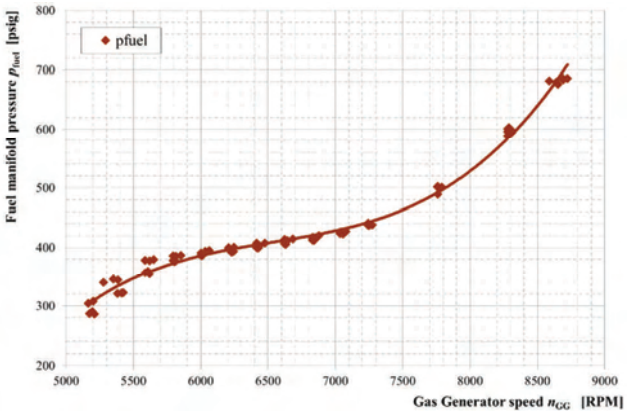


Fig. 13. Approximated function and the results of the measurements fuel manifold pressure p_{fuel}, recorded for steady-state operation of LM-2500 engine, in relation to gas generator speed n_{GG}

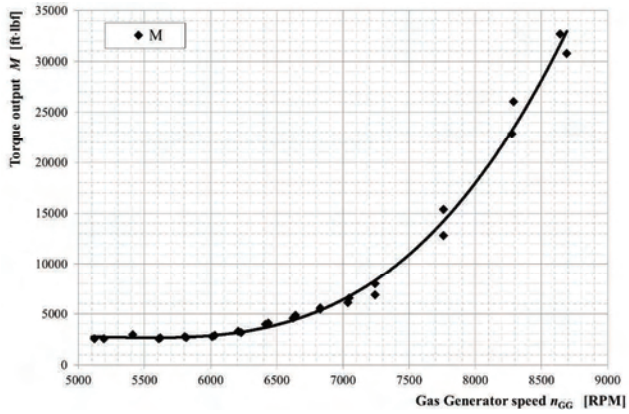


Fig. 14. Approximated function and the results of the measurements of torque output M, recorded for steady-state operation of LM-2500 engine, in relation to gas generator speed n_{GG}

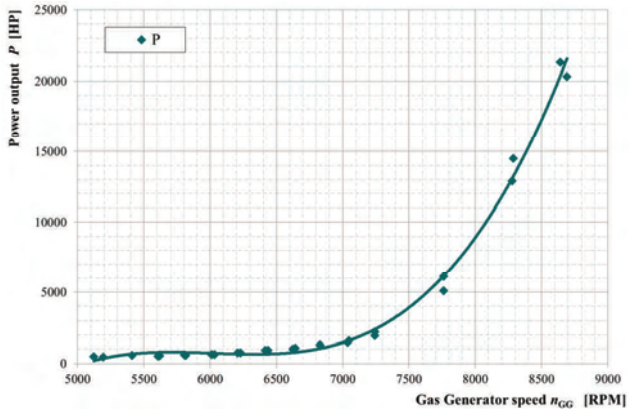


Fig. 15. Approximated function and the results of the measurements of power output P, recorded for steady-state operation of LM-2500 engine, in relation to gas generator speed n_{GG}

Table 3. The results of statistical analysis of approximated operating characteristics

function $y = f(n_{GG})$	coefficients of the polynomial equation				R^2	σ(y)	σ [%]
	b_0	b_1	b_2	b_3			
$n_{PT} = f(n_{GG})$	–13664.92	7.88	$-1.39 \cdot 10^{-3}$	$8.26 \cdot 10^{-8}$	0.9885	108	2.7
$p_1 = f(n_{GG})$	15.83	$-6.99 \cdot 10^{-4}$	$1.30 \cdot 10^{-7}$	$-8.04 \cdot 10^{-12}$	0.8234	0.05	0.4
$T_1 = f(n_{GG})$	42.08	$1.30 \cdot 10^{-3}$	–	–	0.4788	2.4	6.1
$p_{CDP} = f(n_{GG})$	–753.64	$4.15 \cdot 10^{-1}$	$-7.49 \cdot 10^{-5}$	$4.58 \cdot 10^{-9}$	0.9980	3.28	1.3
$\pi = f(n_{GG})$	–54.58	$3.04 \cdot 10^{-2}$	$-5.45 \cdot 10^{-6}$	$3.31 \cdot 10^{-10}$	0.9999	0.24	1.3
$p_{4.1} = f(n_{GG})$	–227.46	$1.27 \cdot 10^{-1}$	$-2.21 \cdot 10^{-5}$	$1.28 \cdot 10^{-9}$	0.9957	0.93	1.7
$T_{4.1} = f(n_{GG})$	–7157.88	3.90	$-6.39 \cdot 10^{-4}$	$3.49 \cdot 10^{-8}$	0.9877	27.8	1.9
$p_{fuel} = f(n_{GG})$	–5756.18	2.75	$-4.15 \cdot 10^{-4}$	$2.11 \cdot 10^{-8}$	0.9952	9.6	2.2
$M = f(n_{GG})$	–102277.48	60.84	$-1.17 \cdot 10^{-2}$	$7.47 \cdot 10^{-7}$	0.9954	868	1.7
$P = f(n_{GG})$	–246467.07	123.85	$-2.06 \cdot 10^{-2}$	$1.14 \cdot 10^{-6}$	0.9968	485	1.9

Analyses of the functions describing operating characteristics of the examined engine show that variation range of the studied operating parameters is in compliance with the specification given by the ship's documentation. The operating characteristic graphs point out to the nonlinear character of the relationships between operating parameters and the engine load. The non–linear character of the said relationships results from the fact that the power turbine is mated to a controllable pitch propeller (CPP). Only the characteristic of the gas generator inlet air temperature T_1 is linear. It is also noticeable that the curves are linear in the range from minimum load to the load at which maximum propeller pitch angle is reached. Maximum propeller pitch angle occurs at the gas generator speed of approximately 7000 RPM. The characteristics also show that a significant increase in engine power output occurs after reaching the maximum propeller pitch angle, when the power turbine is mated with the propeller set at its maximum steady pitch angle. Upon reaching the maximum propeller pitch angle, the engine delivers an output of approximately 2 000 HP, with a maximum power output of 25 000 HP.

4.3. Acceleration and deceleration characteristics

The process of exploitation of naval gas turbines also requires the knowledge of their characteristics in the process of acceleration and deceleration of the engine. These

characteristics represent the change dynamics of various engine parameters at the time of increasing or decreasing a load. On this basis, it is possible to evaluate the prevalence of unstable ranges of engine operation, which may lead to the pumping. The course of changes in an LM 2500 engine selected operating parameters during acceleration and deceleration is presented in Fig. 16–17. Designation of individual parameters is in accordance with the engine operating parameters contained in Table 1.

5. Conclusions

The determined functional dependencies of the LM–2500 naval gas turbine will facilitate analytical determination of engine operating parameters on the basis of gas generator speed, for any ambient parameters. The values of engine operating parameters determined on the basis of the aforementioned dependencies are approximate but their accuracy is sufficient for engineering applications to meet the need of further research concerning this type of engine. In particular, research in the aspect of energy modeling and simulations.

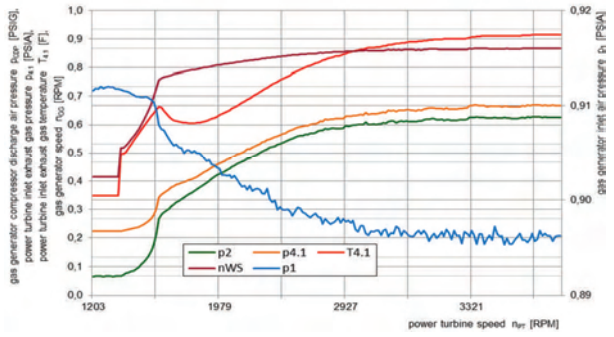


Fig. 16. Changes of LM 2500 engine operating parameters depending on the power turbine speed n_{PT} during acceleration

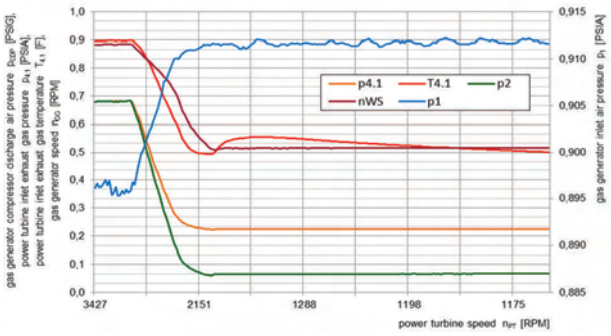


Fig. 17. Changes of LM 2500 engine operating parameters depending on the power turbine speed n_{PT} during deceleration

The possibility of determining engine operating characteristics facilitates their use in the process of diagnostics in its broad sense. Owing to that, there is a possibility of conscious operation of equipment according to its technical condition. Observing the trends present in the changes of the operating characteristics and selected diagnostic symptoms facilitates obtaining data which may be used in the decision–making process related to equipment operation in order to ensure naval combat readiness, as well as to maintenance, adjustment or replacement of engine components and finally, to repairs. That data may also be used to design new engines or upgrade the existing.

Knowledge and experience related to operating characteristics are also used in the process of education and training people responsible for operating of such engines. This is particularly important because incorrect operation often leads to serious failures, which affect the combat readiness of the ship, and also generate large and unexpected costs in the process of ship's operation.

Nomenclature

COGAG	combined gas turbine and gas turbine
CPP	controllable pitch propeller
LSM	least–squares method
TBO	ime between overhauls
VSV	variable stator vanes

Bibliography

[1] FLYNN, D. (eds.)., Thermal power plants –simulation and control. *The Institution of Electrical Engineers*. London 2000.

[2] CUI, J.G., ZHANG, L., WANG, G.H. et al. Fault prediction method of the marine gas turbine based on neural network–Markov. *Applied Mechanics and Materials*. 2014, **538**, 171-174.

[3] GAO, J.H., HUANG, Y.Y. Effect of ambient temperature on three–shaft gas turbine performance under different control strategy. *Advanced Materials Research*. 2012, **424-425**, 276-280.

[4] KIM, K.H. Effects of water and steam injection on thermodynamic performance of gas–turbine systems. *Applied Mechanics and Materials*. 2011, **110-116**, 2109-2116.

[5] CAO, L., LI, S.Y., WANG, Z.T. The study of marine gas turbine power system simulation software development. *Applied Mechanics and Materials*. 2013, **300-301**, 166-171.

[6] MAŃCZAK, K. Design of experiments. *WNT*. Warszawa 1976.

[7] BASHA, M., SHAAHID, S.M., AL-HADHRAMI, L. Impact of gas turbine frame size on efficiency of gas turbine power plants. *Applied Mechanics and Materials*. 2014, **492**, 447-452.

[8] MEYER, R.T., DECARLO, R.A., PEKAREK, S., DOKTORCIK, C. Gas turbine engine behavioral modeling. School of Electrical and Computer Engineering, *Purdue University*. West Lafayette, IN 47907-1288, USA 2014.

[9] FUKUDA, M., HARADA, H., YOKOKAWA, T., KITASHIMA, T. Virtual jet engine system. *Materials Science Forum*. 2010, **638-642**, 2239-2244.

[10] POJAWA, B. The investigation of turbine engine in aspect of output torque control. *Solid State Phenomena*. 2012, **180**, 339-348.

[11] POLAŃSKI, Z. Design of experiments in technique. *PWN*. Warszawa 1984.

[12] WANG, Q., MA, Y.F., HU, X.M. Research on NO_x concentration field distribution of a turbo-jet engine emissions. *Advanced Materials Research*. 2013, **732-733**, 46-51.
[13] MARTINS, R.F., BRANCO, C.M., GONÇALVES–COELHO, A.M., GOMES, E.C. Failure mechanisms on exhaust systems of naval gas turbines. *Materials Science Forum*. 2008, **587-588**, 946-950.
[14] ZHU, R., REN, J.X., LI, F.Q. et al. Thermal and stress field analysis in heavy-duty gas turbine exhaust system. *Advanced Materials Research*. 2012, 516-517, 688-691.
[15] TAYLOR, J.R. Introduction to analysis of measuring error. *PWN*. Warszawa 1999.

Bogdan Pojawa, DEng. – Mechanical and Electrical Engineering Faculty at Polish Naval Academy in Gdynia.

e–mail: *B.Pojawa@amw.gdynia.pl*



[16] QUAN, X.H., QUAN, J.J., HE, H. Modeling and simulation of a certain warship diesel engine based on AMESim. *Applied Mechanics and Materials*. 2014, **496-500**, 760-763.
[17] CENGEL, Y.A., BOLES, M.A. Termodynamics fifth edition in SI units. *McGraw−Hill Higher Education*. New York 2006.
[18] Technical, manual and organizational level maintenance – LM–2500 propulsion gas turbine module of propulsion system of Oliver Hazard Perry class frigate FFG–9. Marine and Industrial Engines and Services Division, *General Electric Company*, Ohio 2003.

Article citation info:
AMBROZIK, A, KURCZYŃSKI, D., ŁAGOWSKI, P., WARIANEK, M. External speed–torque characteristics of Fiat 0.9 TwinAir petrol- and CNG-fuelled engine. *Combustion Engines*. 2017, **171**(4), 222-226. DOI: 10.19206/CE-2017-438

Andrzej AMBROZIK
Dariusz KURCZYŃSKI
Piotr ŁAGOWSKI
Michał WARIANEK

CE-2017-438

External speed–torque characteristics of Fiat 0.9 TwinAir petrol- and CNG-fuelled engine

The paper presents the results of the experimental study of the turbocharged spark ignition Fiat 0.9 TwinAir engine, with indirect, multipoint petrol injection system, powered by petrol and equipped with the injection system of the compressed natural gas (CNG) supplying gas into the intake manifold. The test results provide the comparison of the selected fuel-efficiency, energetic and ecologic indicators of engine work, obtained when it is powered by Pb95 petrol and the CNG gas. The paper compares the external torque-speed characteristics with factory-set engine controllers. Also presented are the concentration levels of harmful gases in the exhaust fumes: carbon monoxide (CO), nitric oxides (NO_x), hydrocarbons (HC) and carbon dioxide (CO_2). Results obtained on the engine powered by CNG are indicating lower power and torque, lower concentration of hazardous gases, in particular carbon monoxide and hydrocarbons as well as significantly lower consumption of the gas when compared to petrol.

Key words: *spark ignition engines, gas engines, gasoline engines, external characteristic, gas engines emissions*

1. Preface

Development of piston combustion engines and the requirements related thereto has manufacturers strive for decreasing the emission of hazardous components of the exhaust gases in order to meet the obligatory emission standards as well as to improve engines energy efficiency [8]. One of the methods to meet the rigorous standards is downsizing and using alternative gas fuels, in particular LPG and CNG. Vehicle owners are using this kind of fuels as they are usually much less expensive than other alternative fuels. Using gases as fuel in spark ignition (SI) engines requires an independent fuel supply system, operated by an additional ECU controller which receives information from the factory petrol supply ECU controller [10]. This paper presents the analysis of results of the selected engine's work parameters, which were obtained as the engine was powered by petrol and CNG. In the CNG fuel supply system, the injectors opening time was controlled on the basis of the signals controlling the petrol injectors [4, 11]. Given the differences between gas fuels and petrol in terms of physical and chemical properties, a scrupulous analysis is required to determine the influence of gas fuels on engine's work characteristics, in particular on the external characteristics, indicating the engine's maximum performance [3]. An important aspect is the attempt of rationalising the algorithm which controls the gas supply systems, commonly used in small turbo-charged petrol engines. The physical and chemical properties of fuels constitute an important area which needs to be studied in order to organise the process of controlling the engine's work. Its assessment and analysis should provide a significant possibility of reducing harmful impact of engines upon natural environment [2]. Another important aspect of improving engine performance are the electronic controls [6]. The results obtained in the tests of the Fiat 0.9 TwinAir engine suggest the necessity of modifying the maps of electronic control unit of the gas powered engine in order to develop required power and correct torque characteristics while maintaining or improving engine's ecological and economical properties at the same time. Using electromagnetic gas injectors controlled by an additional controlling unit allows a good flexibility in managing their opening times. It is also possible to improve the injection advance angle of fuel, depending on engine speed-torque working conditions. Precise dosage of gas fuel as well as maintaining good fuel atomisation provides conditions for proper combustion of the air-fuel mixture and for obtaining high energetic engine efficiency [7]. Using the sequence injection system has also it's disadvantages which is the impossibility of modifying the supercharging control parameters and controlling the inlet valves by the gas controller. It is also not possible to correct the ignition advance angle. Preliminary tests have shown that it is necessary to modify the above-mentioned parameters in order to improve the working characteristics of the engines fuelled by CNG, in particular to increase the power and torque.

2. Test object

The object under test was a two-cylinder, four stroke turbo-charged spark ignition Fiat 0.9 TwinAir engine. It is equipped with a multi-point indirect (MPI) fuel injection system as well as the compressed gas injection system providing the CNG into the intake manifold. The engine uses MultiAir technology, developed by Fiat. This technology allows to control the cylinder fulfilment rate, depending on speed-torque working conditions of the engine. In the Fiat 0.9 engine, cylinder filling process is carried out by means of mechanical -hydraulic timing system, controlling the operation of the engine's inlet valves and turbocharger wastegate [1]. Inlet valve opening is done by the pistons of the hydraulic system, shifted by engine oil located in a variable-volume closed chamber. The chamber volume is changed by electro-hydraulic valves, which are controlled with signals from the engine's electronic control unit.

The tested Fiat 0.9 engine reaches a maximum power of 85 bhp at 5500 rpm and maximum torque of 145 Nm at 1900 rpm. Table 1 presents the basic technical data of the tested engine.

Table 1. Technical data of the Fiat 0.9 TwinAir engine [1]

Parameter	Unit	Value
Cylinder arrangement	–	in-line, vertical
No of cylinders	–	2
Cylinder diameter	mm	80.5
Piston stroke	mm	86
Cylinder capacity	cm^3	875
Compression ratio	–	10 ± 2
Timing system	–	OHC, 4 valves per cylinder

3. CNG fuel supply system in Fiat 0.9 TwinAir engine

Engine under testing was equipped with sequential injection system of compressed natural gas, supplying CNG into the intake manifold. The scheme of the fuel supply system is presented on Fig. 1.

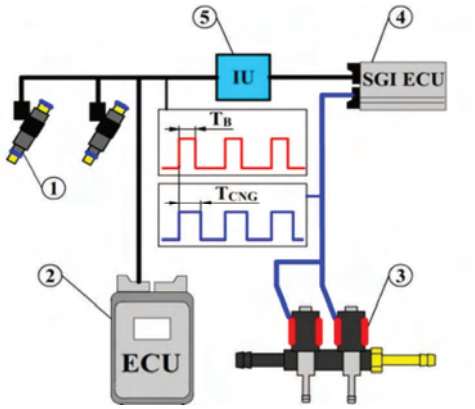


Fig. 1. Scheme of the sequential injector of gas controls [11]: 1 – petrol injector, 2 – engine control unit, 3 – gas injector, 4 – sequential gas injection electronic control unit, 5 – disconnecting injector interface unit, T_B – petrol injector opening time, T_{CNG} – gas injector opening time

Gas injectors are controlled by the electrical signals from additional Stella Elisa controller, manufactured by Elpigaz. The controller receives signals from the petrol injectors, then calculates and corrects the values of opening times according to the following formula [11]:

$$T_{CNG} = \{[T_B + \mathrm{Offset} + f(D) + f(E)\} \cdot f(TR) \cdot f(P) \cdot f(TM)$$

where: T_{CNG} – gas injector opening time, T_B – petrol injector opening time, f(TR) – reducer's temperature dependence correction function, f(TM) – correction function, depending on gas temperature in the fuel rail, f(P) – correction function, depending on actual differential pressure in reducer-vaporiser, f(D) – correction function of fuel – air mixture composition, depending on nozzle diameter, E – correction coefficient, Offset – signal offset in the function of crank shaft angle, depending on the type of gas injectors.

4. Test stand

The tests were carried out on the Automex EMX 100/10000engine test bench, equipped with eddy current brake. The test bench is presented on Fig. 2. The brake control system is linked with the engine's electronic controller and enables setting the speed and torque working conditions of the engine. The measurement system of the test bench enables reading data in real-time and acquisition of measurement data and the engine's working parameters, such as the pressure and temperature of: lubricating oil, the air in air intake system before the turbocharger, the air after the intercooler and the exhaust fumes in the engines exhaust system.



Fig. 2. Test bench of the Fiat 0,9 TwinAir engine

The emission measurements of the key exhaust fumes components were carried out by the AVL DiCom 4000 emission tester. Petrol consumption was measured with the ATMX2040 ODIUT Automex gravimetric fuel gauge, whereas the consumption of the CNG was measured with the Emmerson Elite MicroMotion flow meter, which uses the Coriolis effect. The scheme of the test equipment is presented on Fig. 3.

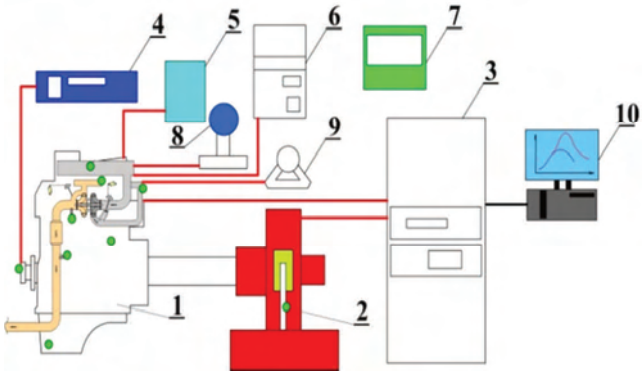


Fig. 3. Test bench scheme: 1 – Fiat 0,9 TwinAir engine, 2 – Automex AMX 100/1000 eddy current brake, 3 – control unit, 4 – AVL IndiSmart 612 cylinder pressure measurement system, 5 –ATMX2040 gravimetric fuel gauge, 6 –AVL DiCom 4000 exhaust analyser, 7 –KTS 540 diagnostic tester, 8 – ABB Sensy Flow air flow meter, 9 – EMERSON Elite gas flow meter, 10 – PC workstation

The test bench also enables to control the engine working parameters and ensures users safety. In addition, the test stand is equipped with a data processing module obtained from measurement files.

5. Characteristics of natural gas as a fuel for powering combustion engines

The spark ignition engines are mainly powered by petrol, which is the mixture of oil hydrocarbons, obtained in oil refining process. The second most popular fuel for spark

ignition engines is the LPG gas, which is a mixture of oil hydrocarbons [9]. The quality requirements of the liquefied propane-butane gases (C_3–C_4) being used as a vehicle fuel are found in the Polish standard PN – EN 589+A1:2012. Over the recent years, the number of vehicles running on natural gas has been growing. There is an increasing amount of drivers who decide to equip their vehicles with the compressed gas fuel installation. The natural gas is one of the elementary natural sources of energy. As a mixture of light organic hydrocarbons, it is considered to be an ecologic fuel. It is about twice as light as air, very easily miscible with air which ensures a homogeneous combustion mixture [8]. The main component of natural gas is methane (CH_4). Engines are powered by the natural gas with high methane content, with the methane mass content exceeding 90% [5]. The gas for powering vehicles may be a gaseous phase (CNG – Compressed Natural Gas) and liquid phase (LNG – Liquified Natural Gas). It is considered to be an environmentally-friendly fuel as it does occur in the free state in nature [13]. A significant advantage of using natural gas as a vehicle fuel is low emission of the carbon dioxide and residual emission of exhaust solid particles. That makes the natural gas an excellent alternative for powering vehicles which are used in towns. The advantageous properties of the natural gas are also found when it rests in vehicle tanks. Unlike petrol or Diesel fuel, the natural gas trapped in a tight tank does not have a negative impact on the natural environment, since it releases no hazardous hydrocarbons to atmosphere. Thus, it is not necessary to use fuel absorber [5, 8]. The basic parameter which differentiates fuels is their chemical composition, determining a correct course of creating combustible mixture and providing the quality of combustible process, defined by such parameters as: ignition delay, combustion time, combustion temperature. These parameters determine the correct work of the engine while maintaining low concentration of hazardous exhaust substances. The key properties of natural gas and petrol are presented in Table 2.

Table 2. Selected properties of petrol and natural gas – comparison [3, 9]

Parameter		Unit	Fuel type	
			Petrol	Natural gas
Calorific value		MJ/kg	42.5–43.5	50
Calorific value of stoichiometric mixture		MJ/m^3	3.5	3.4
Octane number	research		95–98	100
	motor		85–88	110
Air demand for complete combustion		kg	14.7	17.2
Normal conditions density		kg/m^3	715	0.695
Laminar flame speed		m/s	0.3–0.6	0.34
Ignition temperature		°C	480–550	645
Boiling temperature		°C	35–210	–162
Evaporation heat		kJ/kg	350–380	510

The Polish standard specifies the required properties of gas fuels used for powering engines.

One of the advantages of the natural gas in that it does not require being delivered by vehicles to petrol stations located in town centres or towns with gas piping infrastructure, as it may be directly supplied by means of such infrastructure.

The number of vehicles, both in Poland and abroad, which are powered by gas fuels, is increasing. Poland is the leading country in regard to the amount of vehicles fuelled by LPG [13]. The number of CNG-powered vehicles is still low, with a ratio of merely 1.5%. This is mainly due to insufficient infrastructure of petrol stations which allow CNG refuelling. Currently, there are 26 such stations in Poland. The growing interest of using natural gas as a vehicle fuel may be proved by the ongoing extension works of the LNG port in Gdansk. The provisions of the Directive of the European Parliament and the Council 2014/94/EU introduce the strategy of developing infrastructure which allows for refuelling vehicles with natural gas and for increasing the share of alternative fuels on the market. The CNG fuel is increasingly more popular in public transport operators and transport companies [12].

In the future, CNG may revolutionise the fuel market, which is currently aimed at diversification of available oil-based products. In this context, there is another advantage of the CNG worth mentioning – the potential users may be very independent of petrol stations as they may use small compression aggregates to refuel vehicle. This solution, however, is still relatively expensive at the moment due to high prices of such devices.

6. Test schedule

The test schedule comprised the test bench examination of the Fiat 0,9 SGE engine, operating in accordance with the external speed characteristics and with the engine speed of correspondingly: 1500, 2500, 3500, 4500, 5500 and 6000 rpm. The characteristics have been set with the petrol engine fuelled by the lead-free 95 octane petrol (Pb95) as well as with compressed natural gas (CNG). During the tests with petrol fuelling, the engine was operating on the factory map settings of the Fiat 500c model. The external characteristics of the CNG-fuelled engine was carried out with gas injectors being controlled by the Elisa Stella controller, programmed as recommended by the manufacturer.

During the tests, the torque-speed working conditions were set and the measured values included the engine's power and torque, hourly fuel consumption as well as the concentrations of the following exhaust components: carbon monoxide (CO), carbon dioxide (CO_2), nitric oxide (NO_x) and hydrocarbons (HC).

7. Test results

The first external characteristic was made on the engine being fuelled by petrol, the second one – on the engine fuelled by CNG. The characteristics are presented on Fig. 4.

The acquisition system allowed determining the power generated by the engine at specific speed and torque working conditions. On the basis of the obtained characteristics, it has been established that there is a considerable effective power decrease across the entire rotational speed range when it was fuelled by CNG. The maximum effective power of the engine was 55 kW at the engine speed of n = 5300 rpm.

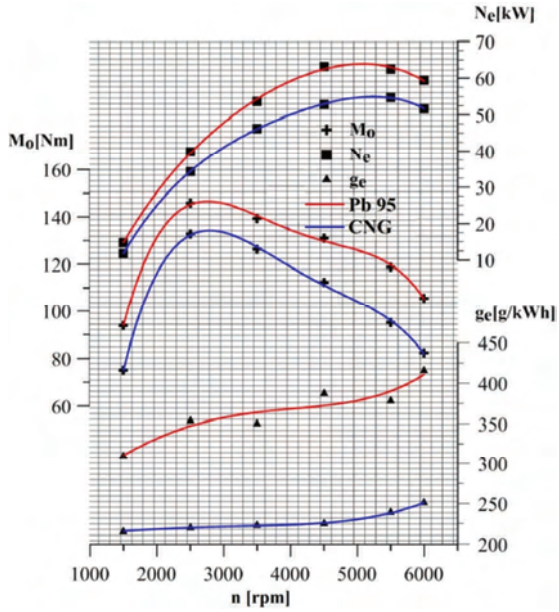


Fig. 4. External torque-speed characteristics of the Fiat 0.9 TwinAir engine, fuelled by Pb 95 petrol and CNG

When powered by petrol, the maximum effective power of the engine was 63 kW at n = 5050 rpm.

The torque of the CNG-powered engine was lower by about 16% when compared to the torque of petrol-fuelled mode.

The specific fuel consumption of the CNG-fuelled engine was decreased by approximately 40%.

The emission of the key exhaust components are presented in Figures 5–8.

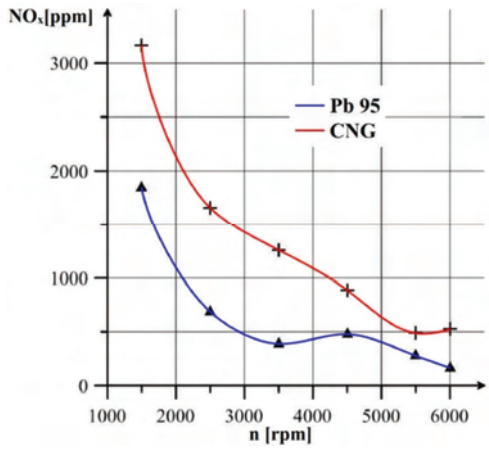


Fig. 5. Concentration of nitric oxides in the Fiat 0.9 TwinAir engine exhaust gases, working with external speed characteristics and fuelled by petrol Pb 95 and CNG

The concentration of the nitric oxides in the exhaust gases of the CNG-fuelled engine increased by max. 48% at the engine speed of n = 1500 rpm. With rotational speed higher than n = 4000 rpm, the concentration of this component was only slightly higher when compared to the concentration obtained with petrol-fuelled engine. In addition, the concentration of hydrocarbons in the CNG-fuelled mode was considerably lower, in particular at low and medium engine speeds.

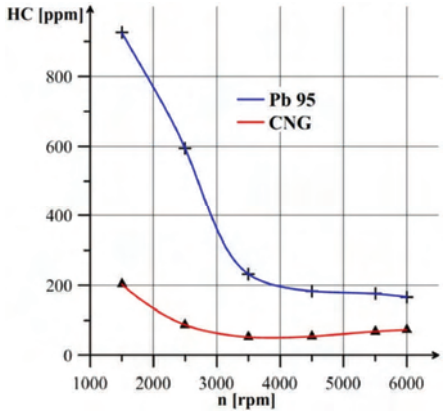


Fig. 6. Concentration of hydrocarbons in the Fiat 0.9 TwinAir engine exhaust gases, working with external speed characteristics and fuelled by petrol Pb 95 and CNG

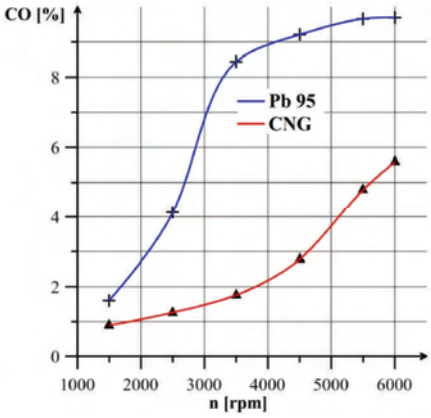


Fig. 7. Concentration of carbon monoxide in the Fiat 0.9 TwinAir engine exhaust gases, working with external speed characteristics and fuelled by petrol Pb 95 and CNG

The result of the engine being powered with CNG was the reduction of the carbon monoxide concentration across the entire range of crankshaft rotational speed as well as slight reduction in the emission of the carbon dioxide in the rotational speed range between n = 1500 and 2700 rpm. In the rotational speed range between n = 3000 and n = 6000, the concentration of carbon dioxide in exhaust fumes of CNG-powered engine was only slightly higher than that of petrol-fuelled engine.

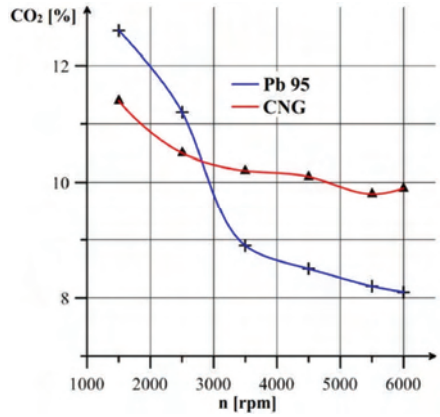


Fig. 8. Concentration of carbon dioxide in the Fiat 0.9 TwinAir engine exhaust gases, working with external speed characteristics and fuelled by petrol Pb 95 and CNG

Conclusions

The current development trends of the internal combustion engines prioritise minimisation of their harmful impact upon natural environment. The efficient method of meeting the rigorous fuel emission standards is powering engines with alternative gas fuels, in particular with natural gas. A significant interest of the researches who examine and assess the engine work figures, as well as positive results of the experiments which test the engines powered by gas fuels prove the rationality of using such fuels in powering all kinds of transport and industrial vehicles.

The results of the Fiat 0.9 TwinAir engine tests reveal both the advantages and drawbacks of the CNG used as a fuel. As regards the impact on natural environment, the tests demonstrate a considerable decrease in concentration of the harmful exhaust components, mainly hydrocarbons and carbon monoxide. On the other hand, the CNG-fuelled engine reached lower power and torque as well as increased emission of nitric oxides and carbon dioxide in higher ranges of crankshaft rotational speed. The CNG-fuelled engine had a much lower specific fuel consumption, which indicates a high energetic efficiency of the combustion process. Fuel consumption has a significant impact in terms of ecology and it is an essential criterion of choosing alternative fuel by vehicle users. Improving work performance in modern combustion engines, which are already very efficient constructions, is a difficult challenge in terms of electronic control of the engine's work processes and it requires an individual approach. Appropriate management of rationalisation of the regulation parameters of the engine powered by gas fuels will considerably enhance the diversification of oil-based fuels. In the future, natural gas may become a primary fuel for powering internal combustion engines.

Nomenclature

CNG	compressed natural gas
LNG	liquified natural gas
LPG	liquified petroleum gas
Pb95	95 octane petrol
MPI	multi point injection
ECU	electronic control unit
IDI	indirect injection
SI	spark ignition

Bibliography

[1] AMBROZIK, A., AMBROZIK, T., KURCZYŃSKI, D., ŁAGOWSKI, P. Conversion of Fiat 0.9 Multiair engine to multi-fuelling. *Journal of Kones*. 2013, **20**(4), 9-15.

[2] AMBROZIK, A., AMBROZIK, T., KURCZYŃSKI, D., ŁAGOWSKI, P. Modern experimental set-up for investigations into strategies for the control and fuelling of spark ignition engines. *Combustion Engines*. 2015, **162**(3).

[3] BACZEWSKI, K., KAŁDOŃSKI, T. Paliwa do silników o zapłonie iskrowym. *Wydawnictwo Komunikacji i Łączności*. Warszawa 2005.

[4] GAJEK, A., JUDA, Z. Czujniki. *Wydawnictwa Komunikacji i Łączności*. Warszawa 2015.

[5] GRZYB, R., KOTOWSKI, W. Nowe wymagania jakościowe na paliwa silnikowe. *Paliwa, Oleje i Smary w Eksploatacji*. 2001, **83**, 5-8.

[6] KNEBA, Z., MAKOWSKI, S. Zasilanie i sterowanie silników. *Wydawnictwo Komunikacji i Łączności*. Warszawa 2004.

[7] MAJERCZYK, A., TAUBERT, S. Układy zasilania gazem propan-butan. *Wydawnictwo Komunikacji i Łączności*, Warszawa 2004.

[8] MERKISZ, J., PIELECHA, I. Wymagania i kierunki rozwoju napędów zasilanych gazem ziemnym CNG/LNG. *Zeszyty naukowe Politechniki Częstochowskiej*, Mechanika **26**, 458-475.

[9] MERKISZ, J., KOZAK, M. Wymagania jakościowe stawiane benzynie przez nowe generacje silników o zapłonie iskrowym. (cz.1, cz. 2). *Paliwa, Oleje i Smary w eksploatacji*. 2002, **104**, 5-8; 2002, **105**, 23-26.

[10] ROMANISZYN, K. Alternatywne zasilanie samochodów benzyną oraz gazami LPG i CNG. *Wydawnictwa Naukowo-Techniczne*, Warszawa 2007.

[11] SKARPETOWSKI, B. Nowoczesne rozwiązania w samochodowych instalacjach gazowych. *Zeszyty naukowe Politechniki Częstochowskiej*. **162**, Mechanika 26, 504-509.

[12] WOŁOSZYN, R. Gaz ziemny jako przyszłościowe paliwo silnikowe w komunikacji miejskiej. *Autobusy*. Radom 2004.

[13] WOŁOSZYN, R., HOFMAN, P. Stacje tankowania gazu ziemnego. *Autobusy: technika, eksploatacja, systemy transportowe*. 2010, **3**, 20-22.

Andrzej Ambrozik, DSc., DEng. – Faculty of Mechatronics and Machine Building at Kielce University of Technology.

e-mail: *SilSpal@tu.kielce.pl*



Dariusz Kurczyński, DEng. – Faculty of Mechatronics and Machine Building at Kielce University of Technology.

e-mail: *KDarek@tu.kielce.pl*



Piotr Łagowski, DEng. – Faculty of Mechatronics and Machine Building at Kielce University of Technology.

e-mail: *P.Lagowski@tu.kielce.pl*



Michał Warianek, MEng. – Faculty of Mechatronics and Machine Building at Kielce University of Technology.

e-mail: *MWarianek@tu.kielce.pl*



Article citation info:
BIELACZYC, P., SZCZOTKA, A., WOODBURN, J. Exhaust emissions of particulate matter from light-duty vehicles – an overview and the current situation. *Combustion Engines*. 2017, **171**(4), 227-238. DOI: 10.19206/CE-2017-439

Piotr BIELACZYC
Andrzej SZCZOTKA
Joseph WOODBURN

CE-2017-439

Exhaust emissions of particulate matter from light-duty vehicles – an overview and the current situation

Emissions of particulate matter associated with the use of light-duty vehicles are an increasingly important topic, with more and more political attention focused on this issue. Now that direct injection Diesel engines feature DPFs, particle emissions from other engine types operating on other fuels are also of great interest. This paper discusses the phenomenon in general, briefly reviews worldwide legislation and emissions limits and presents the results of a laboratory test programme measuring the particle emissions from a range of vehicles. The experimental programme showed that the engine/fuel type has a greater impact on particle emissions than the test conditions.

Key words: *particulate matter, exhaust emissions, PM, PN, chassis dynamometer testing*

1. Introduction

Exhaust emissions of particulate matter are coming under increasing scrutiny as a form of pollution with wide-ranging negative impacts. For decades, discussion of vehicular particulate emissions was limited to exhaust emissions from vehicles with CI (compression ignition – Diesel) engines; this situation has changed and both non-exhaust emissions and exhaust emissions from vehicles with SI (spark ignition – petrol) engines are the subject of intensive research efforts: the advent of petrol engines with direct injection (direct injection spark ignition, DISI) – an engine type prone to somewhat more Diesel-like behaviour regarding particulate emissions – is a major focus.

The specifics of particle formation and release during the combustion cycle are a function of the engine type, fuel chemistry, oil type/chemistry and the engine operating point (including the temperature of the engine and its elements). The chemistry of exhaust particulates depends on the fuel type, oil type and of course engine operating conditions and the type, condition and thermal state of the exhaust gas aftertreatment system (if present). Even where the fuel contribution is zero (during fuel cut-off or when using a zero carbon fuel such a hydrogen), particulate emissions are still detectable, with such emissions deriving from engine oil and metals originating from wear of engine components. Aftertreatment systems dedicated to removing (generally trapping and later destroying) particulate emissions are now commonplace on automotive Diesel engines thanks to the roll-out of DPFs; for the time being, vehicles with other engine types are typically not fitted with such devices, although the petrol equivalent to a DPF (GPF) will be required from September 2017 onwards in the EU.

Legal limits for any type of exhaust emission immediately raise the question of how those emissions will be measured. For decades, a relatively simple laboratory technique has been used, in which a known portion of the diluted exhaust gas is drawn through filter(s) which is (are) weighed before and after the test, generating a particle mass (PM) result. This method remains the main means of enforcement worldwide, although its accuracy is inversely proportional to the quantity of particulate emitted. Increasingly stringent emissions legislation aims to reduce exhaust gas particulate levels – and not only for vehicles featuring Diesel engines. Various authorities have set limits for the mass of particulate (PM) emitted over a legislative driving cycle and the EU has added particle number (PN) limits, now applicable to vehicle with DISI engines. Additionally, there is considerable interest in particulate emissions from engine types traditionally assumed to have negligible particulate emissions – port fuel injected vehicles running on petrol (and even LPG and CNG). In addition to local differences in terms of whether PM and PN (or just PM) is used as the metric of control, test procedures also have an impact on the particle emissions profile and thereby on the final PM/PN results.

An obvious starting point is the driving cycle specified in the legislation: the newly-introduced WLTP with its near-eponymous test cycle (WLTC) is a marked departure from the current EU test cycle (the NEDC). While the new cycle has been designed more with improved CO_2/fuel consumption measurements in mind, it will also be used to measure regulated emissions, including PM and PN and the current Euro 6 limits will not be modified to allow for the new driving cycle. The first phase of both driving cycles can be of special interest – both cycles commence from a cold start and cover between 3 km and 4 km during their respective first phases, but with very different driving profiles. However, apart from the driving cycle, other factors are also relevant (the road load simulation settings applied on the chassis dynamometer, gearshift strategy, test temperature, etc.).

A wide body of work exists on light duty vehicular particulate emissions measured under laboratory conditions. Recently, some studies have begun to report on-road particulate emissions. In recent years virtually all authors have come to employ the PN metric in their investigations, as well as results generated by non-legislative pieces of equipment and techniques. May and co-workers [17] reported on gaseous and solid pollutants measured over various chassis dynamometer cycles, measuring PM and PN via the European legislative methods. They reported impacts on both PM and PN for their test vehicles as the driving cycle

and inertia settings were changed and the results indicated a significant contribution to PN from cold start. Mamakos and Manfredi [15] tested a range of petrol vehicles over the NEDC and CADC (a demanding driving cycle which shares some characteristics with the WLTC), employing a range of advanced particulate measurements strategies. They included a bifuel petrol/CNG vehicle in their studies (NEDC test cycle only), which was found to emit significantly lower numbers of solid particles of diameter >23 nm when running on gaseous fuel than on petrol. Anderson et al. [3] subjected two Euro 6 diesel vehicles to a range of chassis dyno tests, reporting that PM emissions were always under 1 mg/km; PN emissions varied between test cycles and inertia settings with higher PN emissions over the NEDC than the WLTC. Cédric et al. [7] tested several Euro 5 Diesel-DPF and DISI vehicles over multiple driving cycles and reported that cold start was responsible for both a high proportion of PN results and a high proportion of the uncertainty associated with those results. Wei et al. [27] also report finding cold start and high load during the first 200 seconds to be a massive contributor to particulate emissions (measured as PM in their study). They also mentioned significant changes in particle composition as a function of the driving cycle employed, as evidenced by the elemental carbon/organic carbon split.

In their recent study Giechaskiel et al. [11] tested a range of engine technologies both on the chassis dyno and on the road, measuring solid PN using a range of sampling configurations. Vehicle mass (inertia) was varied and was found to have an impact on emissions from a vehicle with a DISI engine. Zhang et al. [29] measured size-classified particle number from direct- and indirect-injection petrol vehicles over the NEDC, again reporting cold start and acceleration to be significant contributors to the PN budget over the entire driving cycle. Whelan et al. [28] quantified the high particulate emissions associated with cold start and warmup of a DISI engine – yet noted that some 95% of the particles (by number) were too small to be measured using the legislative PN setup. Some recent research (e.g. [12], [20], and references therein) has focused on direct-injection petrol engines and the benefits of fitting particulate after-treatment devices (GPFs) to those vehicles, yet as of the time of writing, vehicles fitted with such devices have not yet been rolled out and are generally not market-available.

In addition to legislative measurements/devices, a range of tools is available for R&D purposes, quantifying particles (or some fraction thereof) in terms of number, mass and size distribution (see [2, 11, 18] and references therein for discussions of such hardware and its usage in laboratory testing; see [13] for some inter-instrument comparisons). The experimental section of this paper aims to contribute to the discussion in the field by presenting data obtained from exhaust emissions testing on a range of in-use engine/fuel type combinations, including a vehicle running on CNG, over the NEDC and WLTP, using European legislative techniques (PM/PN) and an additional non-legislative particulate emissions measurement technique (namely an AVL Microsoot sensor). The main variables in the study were the engine/fuel type (varied by test vehicle) and the driving cycle (NEDC, WLTC). Following the test procedures associated with the two test cycles also necessitates using different gearshift points and so the relationship between the speed trace and the engine operating points is another variable. The impact of the chassis dynamometer inertia setting was also investigated. The test vehicle with a Stop&Start system was tested with that system both enabled and disabled. Furthmore, in some cases a non-legislative measurement was performed – AVL's Microsoot sensor (MSS) is a device which measures the mass (not number) concentration of solid particles in real time [21], generally sampling raw exhaust. In the experimental work reported in this paper, such a device was used for some testing and the results are briefly compared to both filter-based PM results and PN results.

Particle emissions from engines have been investigated for decades and regulated since the 1990s (in the EU). Particulates have a range of negative impacts on air quality, human health and the natural and built environments and emissions standards have sought to dramatically reduce emissions of particulates over time. (See [17] and references therein for a discussion of the topic in general and some notes on its history.) The EU was the first jurisdiction to mandate the measurement of solid particle number (PN) and set an emissions limit: 6.0×10^{11} particles/km. This legal requirement means that exhaust emissions laboratories have to be equipped with a condensation particle counter (CPC) meeting the requirements of UNECE Regulation No. 83 [26]. (See [3] and [7] for detailed discussions of legislative PN measurement technique.)

Emissions results (and limits) are distance-specific, meaning they are divided by the distance travelled by the vehicle while the emission took place. During the course of a driving cycle, the vehicle accumulates distance covered according to the integrated speed trace and in doing so emits combustion products, including particulate. At any given moment during the test, these two parameters are usually both evolving – the balance between the instantaneous rate of change of these two factors shall be termed *E* and defined as follows:

$$\mathrm{E} = \frac{\delta\,\mathrm{PN}}{\delta\,\mathrm{S}} \tag{1}$$

where S is the cumulative displacement from the origin – i.e. the distance travelled by the vehicle during the period considered (for example, time elapsed since engine start-up).

As δ S is simply speed, a scalar quantity and negative PN exhaust emissions can be considered unmeasurable, E only takes values ≥ 0. When the vehicle is stationary, but the engine is still running (idling) E reaches ∞. A driving cycle which consisted only of idling would therefore generate a result of ∞ #/km. A driving cycle consisting mainly of idling would likely generate a high PN emission result, even though mean engine load and the amount of fuel consumed would be low. Where present, stop & start (idle stop) systems can have a noticeable impact on PN emissions; self-evidently, for a cycle with no idling at all, the impact of such a system would be nil. Stop events in the cycle speed trace not only involve idling; they also necessitate another pull away event, forcing the usage of low gears to accelerate back up to speed, causing increased fuel con-

sumption and often causing elevated PN emissions. However, fuel-intensive acceleration events warm up the engine more rapidly than constant speed driving and so the proportion of idling is not sufficient information to predict the particulate emissions occurring over a cold start driving cycle.

At any given point in the cycle (i), the values of E given by (1) may be integrated, thereby giving PN accumulated from t = 0 up to point i, divided by the distance covered from t = 0 up to point i (E', as defined in equation 2):

$$E' = \sum_0^i PN \Big/ \sum_0^i \delta S \tag{2}$$

Since PM samples collected on filters only have a resolution of one result per test (or one result per phase), PN results collected at 1 Hz (or more) have a clear advantage in terms of their utility for this type of analysis.

Up to now, particulate emissions have only been regulated under laboratory test conditions over well-defined and widely known test cycles; the notable exception to this is the EU and perhaps some other markets, where on-road limits will be introduced (see comments below and in later sections of this paper).

A summary of these emissions limits and the associated test cycles is presented in Table 1; it is worth recalling that many further countries implement the legislation used in the EU and USA.

Table 1. A summary of particulate emissions control strategies in selected automotive markets

Jurisdiction / legislative stage	PM [mg/km]	PN [#/km]	Applicable test cycle
EU / Euro 6b	4.5	6.0×10^{11} for CI; 6.0×10^{12} for DISI	NEDC
EU / Euro 6c	4.5	6.0×10^{11}	NEDC→WLTC
EU / RDE	Not measured	9.0×10^{11}	RDE-compliant road route
EPA / Tier II ("full useful life", 8 bins)	0.0 - 12.43	None	FTP-75
CARB / Exhaust Mass Emission Standards (2015)	6.21	None	FTP-75
CARB / Particulate Standards (2017-)	1.86	None	FTP-75
CARB / Particulate Standards (2027-)	0.62	None (?)	FTP-75
Japan / Post New Long Term	5.0	None	JC08→WLTC

2. Recent laboratory testing conducted at BOSMAL

2.1. Aim & types of test vehicles used

A series of tests were conducted in late 2016 in order to characterize the emissions from vehicle types other than Diesel with DPF and to compare emissions. The motivation for this was the widespread introduction of DPFs to Diesel and the incoming Diesel-equivalent PN limit for DISI engines. A further motivation was the incoming requirement for RDE testing of vehicles with a CF of 1.5; while no RDE testing is reported in this paper, laboratory test cycles such as the relatively dynamic and demanding WLTC can be informative as regards that topic. Basic data of the test vehicles is given in Table 2.

Table 2. Basic data of the test vehicles used in this study

Vehicle No. / Parameter	1	2	3	4
Vehicle type	PC	PC	PC	PC
Engine type	DISI	CI	SI, CNG	CI
Displacement [dm^3]	~1.5	~2	~1	~1.5
Exhaust emission standard	Euro 6	Euro 5	Euro 6	Euro 6
Aftertreatment system type	TWC	DOC+ DPF	TWC	DOC+ LNT+ DPF
Transmission type, number of gears	Man, 6	Auto, 7	Man, 5	Man, 5
Approx. mileage at start of 2testing [km]	15,000	20,000	3,000	2,500
Particulate measurement systems used	PM, PN	PM, PN	PM, PN, MSS	PM, PN
Additional variables	S&S ON / OFF	S&S ON / OFF	Also tested at constant speed	Dyno inertia varied

2.2. Experimental details

A series of tests was carried out in a climate controlled exhaust emissions laboratory. This test facility meets all the demands of EU Euro 5/6 level legislative requirements, as well as the stipulations of GTR 15 [25]. Each of the test vehicles was tested four times over the driving cycles (but only twice for the constant speed cycle). The vehicles were preconditioned on the chassis dynamometer according to the test procedure associated with each test cycle; external battery charging was performed only before the first preconditioning cycle (and not between emissions tests). The soak time (at 20–25°C) between periods of engine operation was at least 11 hours. The CI vehicles' DPFs were regenerated before commencing testing on a given test cycle (so the first test on each cycle occurred with a very similar state of DPF loading). Oil levels and the onboard computer's estimated oil degradation level were checked to ensure that differences between test runs were as low as reasonably practicable. The Euro 6 CI vehicle with an LNT $DeNO_x$ system was driven over an extended preconditioning cycle to make sure that the system was stable before starting testing.

All testing reported here was performed at 23°C and 45–50% relative humidity, thereby satisfying the ambient condition requirements of the NEDC (current EU legislation [26]), as well as the WLTP (GTR15 [25]).

Three test cycles were employed: the NEDC, the WLTP and, for vehicle 3 only, constant speed (90 km/h in 5th gear). All four test vehicles were tested on the same chassis dynamometer (AVL ROADSIM 48" MIM 4x2 LIGHT TRUCK – twin axle, single roll); emissions measurement and analysis was performed using a Horiba CVS-CFV sampling system, together with a dilution tunnel (Horiba DLT-7020)and a set of Horiba MEXA-7400HRTLE exhaust analysers for measurement of gaseous emissions. Those results are not presented here, but were used to en-

sure test-to-test repeatability and to look for the tell-tale signs of regeneration of the DPF and DeNO$_x$ systems. All the aforementioned devices are controlled by the Horiba VETS-7000NT management system.

Legislative particulate emissions (both mass and number) were measured in accordance with the requirements of [25] and [26]. Specifically, for quantification of PM a single TX40 filter was used to collect a portion of the diluted exhaust gas. (TX40 filters are not without their disadvantages, namely artefacts caused by gaseous emissions which become significant at low particulate emissions levels [8], but their use is permitted according to European legislation [25, 26] and they remain widely used in the automotive industry.) A single TX40 filter was used per test (and not one filter per phase), in line with [25] and [26] and thereby maximising the filter payload and reducing weighing errors. Following the emissions test, the filter was immediately returned to the climate-controlled balance room and allowed to stabilise for at least an hour (between 65 and 80 minutes) before being weighed, again in line with [25] and [26]. For the vehicle running on CNG, this stabilisation period was substantially extended, owing to the increased water content in the exhaust gas and the lower level of particulate emission. For quantification of PN in full accordance with [25] and [26], a Horiba MEXA2000SPCS condensation particle counter (CPC) was used. This device features two-stage internal dilution and a volatile particle remover operating at 350°C; as stipulated by EU legislation, it is specifically designed to measure only solid particles of diameter > 23 nm – see [25] and [26] for details on the response curve and the sample pre-treatment system.

Non-solid (volatile or semi-volatile) particle emissions are measurable using other types of measurement systems, but the results they generate are highly dependent on the sampling procedure [27, 28] (temperature, dilution, residence time) – that fact is the main reason behind their exclusion from legislative PN measurements. The CPC itself has a recommended upper range of 10,000 particles/cm^3; the CPC system's dilution settings were adjusted such that the maximum particle concentration measured during a test did not exceed 4,000-5,000 particles/cm^3. As required by [25] and [26], the PM and PN samples were taken from the emissions system's dilution tunnel at a point where the exhaust gas and the dilution air are very well mixed. Where used, the AVL Microsoot sensor was connected directly to the vehicle's tailpipe (not to the dilution tunnel) and the internal dilution settings were adjusted such that the maximum measured gravimetric concentration did not exceed approximately 40 mg/m^3 during any test (the device's limit is 50 mg/m^3). For the NEDC and WLTP tests, four repeat tests were carried out; two repetitions were deemed sufficient for the constant speed testing, as repeatability was much higher than for the cold start driving cycles. The results presented here refer to the arithmetic mean values obtained from the repeat emissions tests (n = 4; n = 2).

2.3. Results and analysis

All vehicles were found to meet the applicable EU emissions limits when tested over the NEDC. Vehicle 3 (bi-fuel: petrol/CNG, type approved in the EU) is not subject to any particulate emissions limits, but in any case it met the stringent Euro 6 limits for vehicles with CI engines. Test-to-test repeatability of gaseous emissions (most importantly CO_2) was well within normal limits, with low coefficients of variance. Given the stability of the gaseous emissions, particulate emissions are presented here on an "as measured" basis – i.e. no additional repeat tests were carried out, regardless of test-to-test variations in particulate emissions. Results are presented separately for each vehicle.

2.3.1. Vehicle 1

Vehicle 1's legislative particulate emissions were elevated, but within Euro 6 emissions limits when tested over the NEDC. Emissions of both PM and PN (Figures 1 & 2) were significantly higher over the WLTP than the NEDC; PM exceeded the Euro 6 limit over the WLTP. The Stop&Start system showed a clear advantage: when the engine was allowed to stop at idle ("S&S ON") PM emissions were reduced by 47% over the NEDC and 22% over the WLTP; PN emissions were reduced by 30% over the NEDC and 9% over the WLTP compared to when the engine ran at idle ("S&S OFF"). The greater advantage of the Stop&Start system in reducing particulate emissions over the NEDC than the WLTP is in line with the former cycle's higher proportion of idling. That being said, the total proportion of idle time is not the only factor: the timing and number of engine restarts and the warm-up penalty caused by engine shutdown at idle also influence the relative PM and PN results; this applies whether the Stop&Start system is active or inactive.

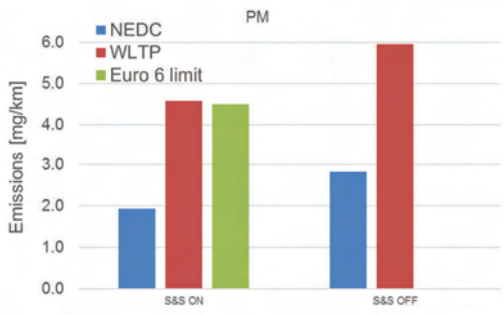


Fig. 1. PM emissions from vehicle 1

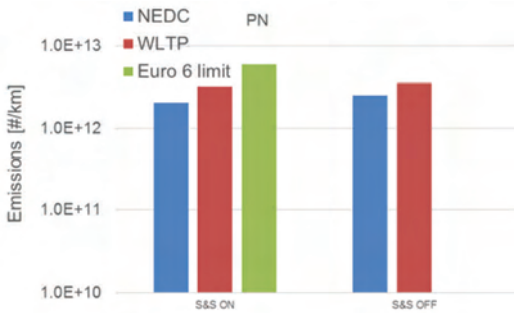


Fig. 2. PN emissions (solid particles only) from vehicle 1 (note the $\log_{10}$ scale)

The magnitude of the emissions from vehicle 1 are reasonably similar to those reported elsewhere [7, 15]. Importantly, when Stop&Start was turned on, the vehicle met the Euro 6 PN limit over the WLTC, despite (presumably) not being calibrated to that cycle.

Particle number measurements were recorded at 1 Hz and the mean traces from the three repeat tests were taken for analysis, as shown in Figure 3.

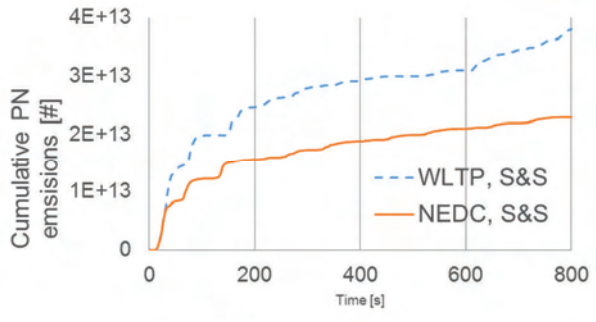


Fig. 3. Cumulative PN emissions (solid particles only) from vehicle 1

As Figure 3 shows, the first 800 seconds of the PN emission profile for the two test cycles differ significantly. However, it should be recalled that emissions limits are distance specific [/km] and so the distance travelled by the vehicle has just as great an impact on the final result as the emissions themselves. Dividing the instantaneous cumulative emissions by the instantiates cumulative distance covered revealed a different tendency, as shown in Figure 4. The higher load of the first ramp of the WLTC Low causes elevated absolute PN emissions compared to the NEDC's UDC phase, but on the other hand there are few stop events and distance is accumulated rather quickly. The result of this is that distance-specific PN emissions rapidly fall to a lower level than those of the NEDC. The length of the first 'ramp' (sub-trip) is important, especially where a Stop&Start system is present – over the WLTC the engine was sufficiently warmed up to allow the Stop&Start system to shut down the engine at the earliest opportunity (98 seconds), whereas over the NEDC this vehicle's engine does not shut down at idle until the second opportunity to do so (which also happens to occur at around 98 seconds). From that point onwards, the Stop & Start system shuts the engine down at every available opportunity and the distance-specific emissions traces over the remainder of the cycle are broadly similar (though not identical).

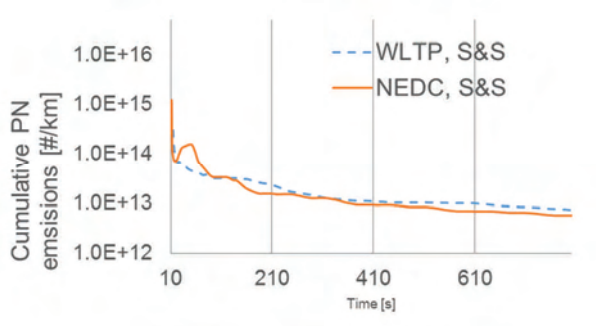


Fig. 4. Distance-specific cumulative PN emissions (solid particles only) from vehicle 1, calculated according to (2). The first 10 seconds have been excluded as distance-specific emissions during that period are ∞

While engine restarts themselves do generate particulates, which add to the PM and PN emitted over the entire test, these startup peaks become progressively smaller as the engine warms up, such that over the entire cycle (both the NEDC and the WLTP) the positive impact of the Stop&Start system on legislative particulate emissions from vehicle 1 is indisputable. Given that vehicle 1 did not feature a dedicated particulate aftertreatment system (GPF), these exhaust emissions trends should be strongly related to the engine out particulate flux, since the potential for substantial accumulation-and-release cycles in the exhaust system is likely to be limited.

2.3.2. Vehicle 2

Vehicle 2's particulate emissions were low, due to it being a Euro 5 CI vehicle fitted with a fully-functioning DPF. However, post-DPF emissions were measurable and differences in PM and PN emissions between the two test cycles used (NEDC, WLTP) were noted, as shown in Figures 5 and 6.

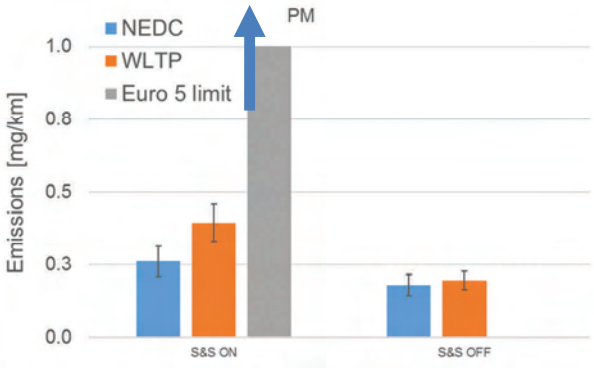


Fig. 5. PM emissions from vehicle 2. Note that the Euro 5 limit (4.5 mg/km) significantly exceeds the y-axis of the figure, being roughly ~10-~20 times the magnitude of the measured PM emissions

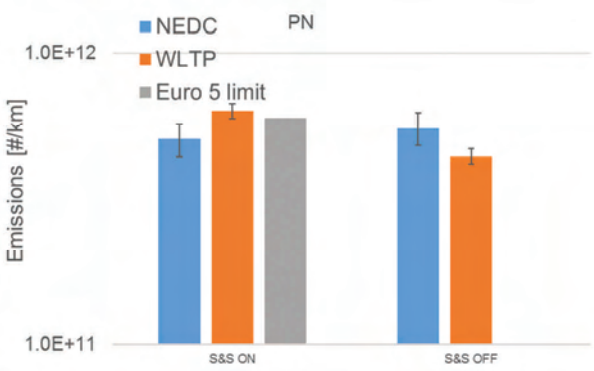


Fig. 6. PN emissions (solid particles only) from vehicle 2

Regarding PM, differences between the two test cycles were only significant where the Stop&Start system was active; with the system deactivated, distance specific emissions were essentially indistinguishable. The PM "penalty" for the WLTP appears to be related to the reduced proportion of idling in that cycle compared to the NEDC and not to engine re-start events (of which there are fewer in the WLTP than in the NEDC). The situation for PN was broadly similar – higher emissions over the WLTP than the NEDC with Stop&Start active; with Stop&Start inactive there was some indication of lower emissions over the WLTP, but the difference was of questionable statistical significance. Somewhat surprisingly, the Stop&Start system

showed no statistically significant advantage regarding reducing legislative particulate emissions over the two test cycles; the emissions eliminated via engine shutdown at idle when using Stop&Start appearing to be cancelled out by emissions from re-start events. However, it is worth repeating that the vehicle featured a DPF and so exhaust emissions do not reveal the full picture. In general, the low emissions levels of DPF-equipped CI engines make the viability of the gravimetric (PM) method questionable.

2.3.3. Vehicle 3

Vehicle 3 was a bi-fuel (petrol/CNG) vehicle, with CNG mode as the default startup option. However, when the temperature of the coolant is < 50°C, startup occurs on petrol and switches over to CNG after approximately 10-20 seconds (depending on the ambient temperature and whether the engine is left to idle or is subject to load). Since solid particulate emissions from the combustion of CNG (where properly metered) are low [10, 19, 22] emissions over the cold start test cycles used (NEDC, WLTP) were dominated by operation on petrol, even though it only accounted for roughly 0.5% to 1% of the engine operation time of the emissions test. A cold start (even at 23°C) features a combination of factors which conspire to increase particulate emissions: cold metal surfaces and lubricant leading to unfavourable thermal conditions and high friction, use of petrol (rather than CNG) and an enriched mixture ($\lambda < 1$).

In terms of the comparison between the two test cycles, there was a clear tendency for higher PM emissions over the WLTP, as shown in Figure 7. However, as Figure 8 shows, legislative PN emissions were virtually indistinguishable, with the difference not significant at the 95% confidence level, although the raw test results for the WLTP were slightly higher than those of the NEDC. In terms of comparisons to other studies measuring legislative particulate emissions from light-duty CNG vehicles, results obtained over the NEDC are study are very similar to those presented in [15]. In [19] particulate emissions (PN and PM) from CNG vehicles are reported to be at similar levels to CI with DPF at low and moderate speeds – a finding broadly confirmed by the results presented here, where emissions lay well within the Euro 5/6 Diesel limits.

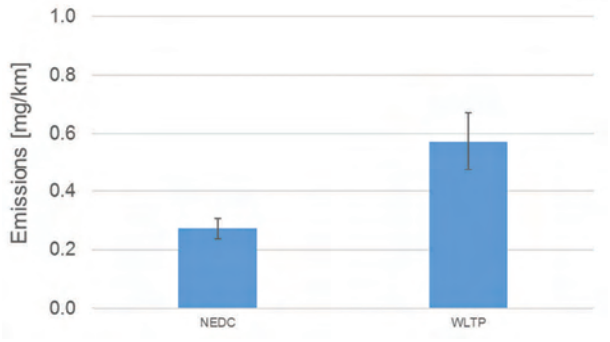


Fig. 7. PM emissions from vehicle 3

Despite the WLTP featuring higher speeds and a greater proportion of driving time at high speeds (say > 90 km/h), this fact did not translate into emissions levels high than CI with DPF (i.e. exceed the Euro 6 limits). In fact, as shown in Figure 9, the cold start phase (#, 'Low') was a much greater contributor to PN emissions than the high speed phase (#4, 'Extra High'). However, care must be taken in comparing these results with those of other studies, as the vehicle's startup strategy (when fuel switchover occurs; whether petrol is used at all when starting the engine at standard laboratory temperatures) may differ substantially from that of vehicles used in other studies.

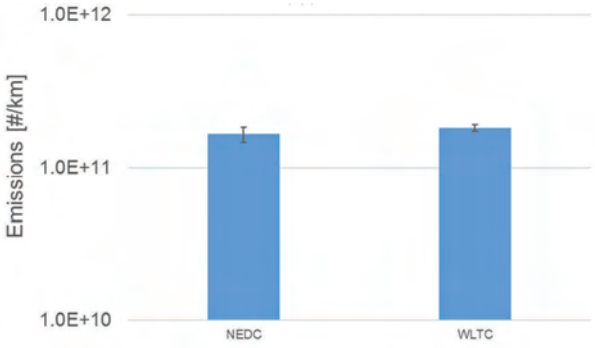


Fig. 8. PN emissions (solid particles only) from vehicle 3

In view of the fact that both cycles contain a cold start and a few seconds' operation on petrol, but that the WLTP's long length (23.2 km) "dilutes" this impact more than the NEDC (11 km), it is somewhat surprising that differences over the entire test cycles are so low (virtually indistinguishable). In an attempt to investigate further, emissions from the individual phases were considered – Figure 9 presents the PN emissions per phase (and per test) for the two test cycles.

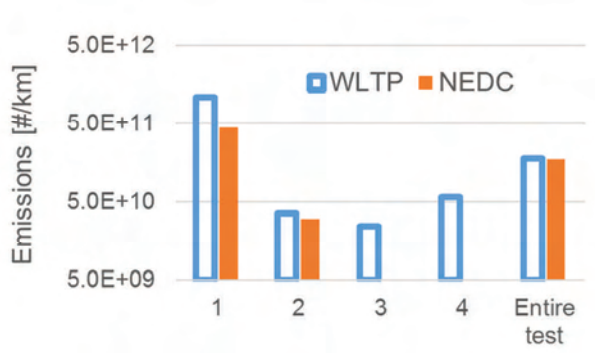


Fig. 9. PN emissions per phase and per test (solid particles only) for vehicle 3 (note that the NEDC consists of only two phases; note also the $\log_{10}$ scale)

The initial phase of both cycles caused the highest PN emissions, linked to the cold start and the fact that the engine starts on a fuel of greater particulate-forming propensity (i.e. petrol), thereafter running on CNG. However, the distance covered by WLTP Low and the NEDC's UDC are unequal (~3 km and ~4 km, respectively) and so the cold start and brief period of operation on petrol are divided by a smaller number of kilometres in the case of the WLTP. Further stages feature no engine operation on petrol whatsoever. The NEDC ends after phase two (EUDC), while the WLTP's third phase has low distance-specific emissions and the fourth phase has PN emissions around a tenth of those from the first phase. The result of the balance be-

tween particles emitted and distance covered means that when the NEDC's two phases and the WLTP's 4 phases are considered, differences all but disappear and the differences in the results for the entire test are barely significant at the 95% confidence level. The presence of phases 2 and 3 in the WLTP (called 'Mid' and 'High', respectively) moderate the final WLTP PN result – particle emissions over those phases are modest, but the number of kilometres covered is relatively high (Mid + High = 11.9 km, i.e. further than the entire NEDC). The High phase commences with the engine already warmed up, features only a single pull-away event, has very limited idling and its maximum speed is moderate (97.4 km/h), with accumulated emissions divided by a distance of just over 7 km – for those reasons, that phase generated the lowest distance-specific PN results of all, causing PN emissions over the entire cycle to be lower than might be expected, based on the dynamic speed trace.

An AVL Microsoot sensor™ (MSS) was also used to investigate exhaust particulate emissions from vehicle 3. This device uses a photoacoustic method to detect light-absorbing particulates (i.e. the carbonaceous fraction) and convert the signal into a mass-based concentration (units: mg/m^3) [21], which can later be multiplied by the measured or calculated exhaust gas flow to yield a mass emission result. Figure 10 shows a comparison of the cumulative MSS particle mass concentration with the cumulative CPC particle count during a WLTP test. For both metrics, it is immediately apparent that the very first portion of the cycle generates the vast majority of particulate emissions. Despite the two devices using very different methods to measure particles and the imperfect overlap between the classes of particle measured by the two instruments, similarities are immediately apparent. As the initial portion of the driving cycle dominates the results returned by both instruments (at least for this test vehicle), Figure 11 shows real-time (non-cumulative) results for the first 50 seconds of the cycle.

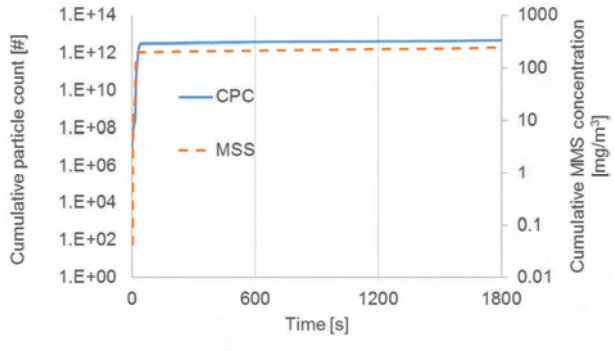


Fig. 10. Cumulative CPC (solid particles only) and MSS readings from vehicle 3 over the WLTP (note the $\log_{10}$ scales on both vertical axes)

The MSS shows two identifiable main peaks – one appearing to be related to the engine startup event and the other to the beginning of the first ramp of the WLTP (which contains the switchover from petrol to CNG, as well as load acceptance and multiple gear changes. The CPC trace shows the startup event and elevated emissions as the driver prepares to execute the first ramp, but the peaks are much less distinct than those returned by the MSS. The more direct response of the MSS is perhaps not unexpected, as the MSS measures directly at the tailpipe with limited internal dilution, while the CPC measures from the dilution tunnel (where the sample is already diluted), with substantial internal dilution (a setting of 1:300 was used for testing vehicle 3). The high Reynolds number of the dilution air-exhaust mixture in the dilution tunnel means that brief peaks in particle emissions are likely to be flattened out to some extent. The MSS was able to measure the first ~30 to ~50 seconds of cycles executed in vehicle 3 well (with good test-to-test repeatability), but thereafter emissions are so low that the device is close to its lower limit of detection for the majority of rest of the cycle (whether NEDC or WLTP), even at very low internal dilution levels (e.g. 1:3). At points later in the test cycles where engine speed was high small peaks measured by the MSS were observed, but test-to-test variability of such peaks was high and their contribution to the overall MSS readings from the entire test was less than 2%.

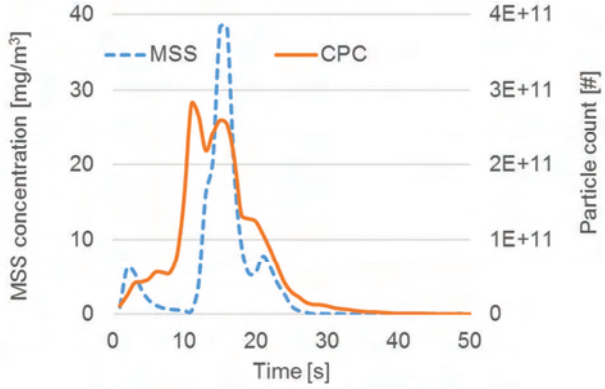


Fig. 11. CPC (solid particles only) and MSS readings over the first 50 seconds of the WLTP, for vehicle 3

Focusing on the first 50 seconds of the two cycles, there are obvious differences between the NEDC and WLTP as regards MSS results (Figures 12a and 12b).

When the four repeat tests are taken into account, test-to-test variations in the first 10 seconds entirely cancel out, such that the startup event and the traces for first few seconds of idling (which are of course identical, regardless of the test cycle in progress) are identical. The first ramp of each cycle is clearly visible and the second peak begins almost simultaneously for both cycles (the difference in the duration of the initial idling time is only 1 second, i.e. within the permitted tolerance of the speed trace). The WLTP's first ramp involves significantly higher speeds than the NEDC's first ramp and uses gears as high as 3rd, while the NEDC's first ramp reaches only 15 km/h and is driven entirely in 1st gear. Integrating the MSS PM readings for the first 50 seconds of the two test cycles reveals that the WLTP produces approximately 40% more particulate quantifiable by MSS than the NEDC does; however, during the first 50 seconds the WLTP covers more than 5 times the distance covered by the first 50 seconds of the NEDC. (Fifty seconds is in fact an arbitrary cut-off point – other ranges could be considered.) The importance of the first 'ramp' (sub-trip) has been mentioned by other authors in the context of gaseous emissions [6, 9].

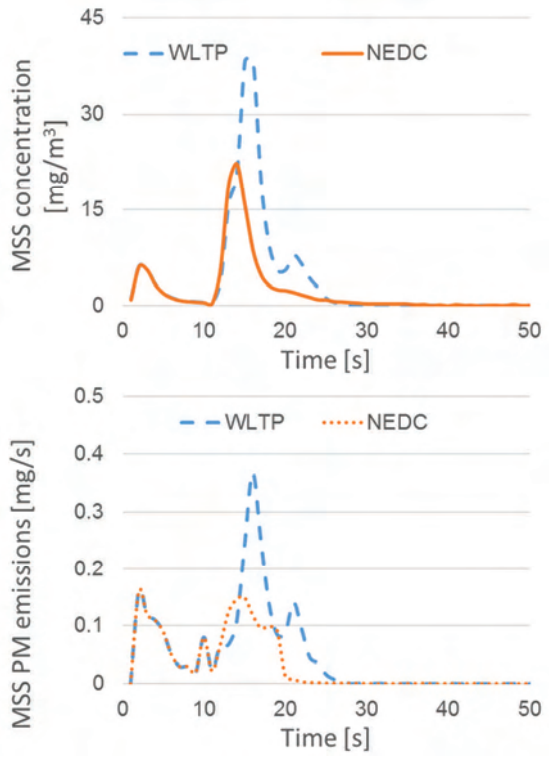


Fig. 12a: Raw MSS readings for the first 50 seconds of the NEDC and WLTP; and 12b: Calculated MSS emissions for the first 50 seconds of the NEDC and WLTP

The observed particle emission behaviour over the first ramp appears to be the result of a combination of effects caused by the cold start, the load associated with the driving trace and the fuel switchover and so it could be further investigated by running the WLTP and NEDC as thermally stabilised hot test cycles, in which case there would be no cold start, no warmup and no fuel switchover. Returning to Figures 11, 12a and 12b, the persistence of relatively high MSS and CPC readings several seconds after the fuel switchover (which always occurred at around 13–15 seconds, during both driving cycles) point to a possible contribution from accumulated impinged liquid fuel. Figure 12b shows the highest mass emissions measured by MSS over the WLTP at 16–17 seconds, after the fuel switchover. Here the authors speculate that the increased exhaust gas flowrate occurring over the first ramp on the WLTP was able to better purge the intake system, resulting in a higher post-fuel switcher over MSS peak over the WLTP than over the NEDC. These speculations provide further motivation to perform the hot testing mentioned in this paragraph.

MSS data were multiplied by the calculated exhaust gas flowrate and divided by the number of kilometres covered to yield an MMS PM result. These results were found to be consistently lower than the PM filter results, with the MSS results numerically equivalent to between 30% and 60% of the mass collected on the filter. The discrepancy in the mass results was lower over the WLTP than over the NEDC, possibly due to PM emissions over the former cycle being numerically higher. As the MSS measures only light-absorbing PM components and as the fuel type (CNG) is a gaseous fuel not prone to PM formation, it is logical that MSS results are lower than filter results and that the correlation is weaker than that reported with other engine/fuel types (e.g. Diesel). The "additional" mass accumulating on the filter was likely due to the presence of water and adsorbed hydrocarbons. When the filters were reweighed following 24–26 hours' stabilization time, the results they yielded were somewhat closer to the MSS results, but the strength of the effect was small – a discrepancy of some 20% to 50% remained between the two sets of results, with high test-to-test variation.

Vehicle 3 was also tested at constant speed (90 km/h in 5th gear, 3 minutes' sampling) as a hot test cycle commencing with the engine already running, following a thorough 42-minute warmup procedure (WLTC, 60 seconds' idling, acceleration to 90 km/h and 90 km/h in 5th gear for 10 minutes). At 90 km/h in 5th gear with the powertrain, tyres, etc. very well warmed up, CNG consumption is at a low level and the engine does not consume any petrol at all; at constant speed there is no inertia to overcome and power demand is highly stable – all of these factors suggest that legislative PM and PN emissions should be low under such conditions. Furthermore, the CNG fuel used for testing had a higher methane number (96) and a chemical analysis revealed only trace levels of compounds containing carbon-carbon double bonds and low levels of sulphur ($\leq$ 8 ppm). Two repeat tests revealed that the MSS was unable to quantify meaningful exhaust emissions at such low levels and so the MSS results from these tests were discarded. PM and PN emissions were quantified successfully, with good agreement between the two tests, generating mean results of 0.04 mg/km and 3.45×10^{10} #/km. Both of these emissions results are roughly an order of magnitude below the emissions measured over the transient cold start driving cycles (NEDC/WLTP).

When correcting for the amount of CNG consumed per km, PM results from the NEDC/WLTP and the constant speed cycle are almost identical, but this was not the case for PN, which was at a much lower level over the constant speed cycle, even when compensating for the reduced quantity fuel consumed per km. This would imply a "lack" of smaller solid particles (which are the type counted by the CPC). For engines burning high quality, low-sulphur CNG the contribution of the lubricating oil to PM and PN can be significant. Given that these PN emissions measured at constant speed are so low, it is interesting that the differences between the NEDC (which features multiple extended periods of constant speed driving) and the WLTP (which features virtually no constant speed driving) were so modest for vehicle 3. Repeating the constant speed test with no warm up (i.e. from a cold start) and at higher load (for example, at 140 km/h and/or applying chassis dyno slope simulation) could provide further insight here, but such data are not available for the time being.

It is also worth reiterating that the PN results presented here were measured in accordance with the EU legislative procedure, which specifically excludes all non-solid particles and solid particles of diameter < 23 nm. Had particles of those kinds been measured for both the NEDC/WLTP cycles and the constant speed test, the ratio of the PN results might have been different. The PN "benefit" associated with combustion of CNG (compared to petrol) has been

reported to reduce as the lower cut-off point of the CPC is reduced [15] – the low PN results found for vehicle 3 at constant speed may have been due to a shift in particle diameter which pushed a significant portion of the particles into the sub-23 nm range and thereby prevented their quantification. Quantifying the size distribution of the exhaust particulate and performing testing at different constant speeds could shed further light on these phenomena.

2.3.4. Vehicle 4

Vehicle 4 met the Euro 6 standard and its DPF-filtered PM/PN emissions easily met Euro 6 limits over under all four test permutations of driving cycle and inertia setting. However, as Figures 13 and 14 show, in some cases the test conditions had a statistically significant impact on the result, although differences were extremely limited in the case of PM. Based on the number of tests performed, the results must be treated with some caution, but certain trends were observed.

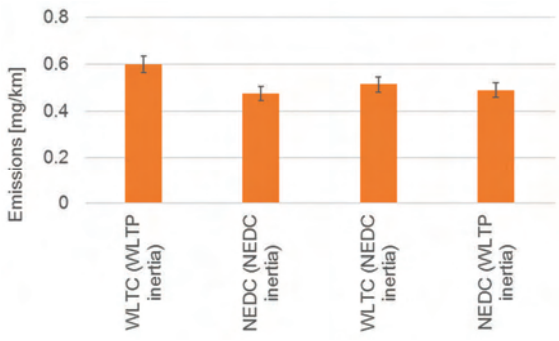


Fig. 13. PM emissions from vehicle 4 for the various test types performed

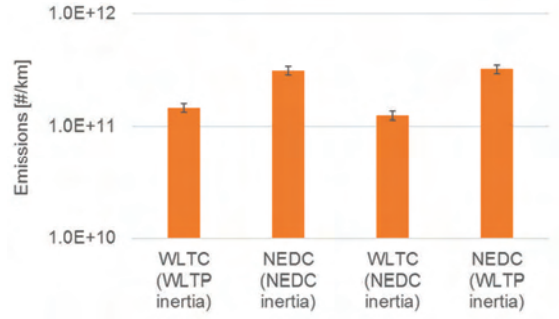


Fig. 14. PN emissions (solid particles only) from vehicle 4 for the various test permutations

The WLTP at the (higher) WLTP-compliant inertia setting caused the highest PM emissions of just under 0.6 mg/km. The NEDC caused the lowest PM emissions and the WLTC performed at the same inertia as the NEDC lay between the two. Performing the NEDC at the WLTP inertia increased the results somewhat, but statistically speaking results were the same as for the NEDC at the (lower) NEDC inertia. Statistically speaking there was no difference between the NEDC results and the WLTC (with NEDC inertia).

Analysing these results, it seems that the combination of the more demanding cycle (WLTC) and the higher inertia causes slightly increased PM emissions in comparison to the NEDC, but that changing *only* the driving cycle or *only* the inertia does not have a meaningful impact on post-DPF PM emissions over the entire test. Regarding PN, the situation was found to be rather different: results were lowest over the WLTC (marginally lower at the lower inertia setting) and results over the NEDC were unequivocally higher (with very little impact of the inertia used during execution of that cycle, which is not totally unexpected, given the many periods of constant speed that cycle contains). Here it appears clear that the test cycle has a greater impact than the inertia settings.

While the WLTC is a more demanding driving cycle with greater total demand for engine power, it also covers much more distance than the NEDC, causing greater dilution of the PN emissions associated with cold start. From the results presented in Figure 14, it can be concluded that for a given driving cycle, increasing the inertia increases PN emissions, but the effect appeared rather modest and of questionable statistical significance given the number of repeat tests performed (4). An increase in PN of 1.8% to 2.5% per 1% inertia increase has been reported for a vehicle with a direct-injection petrol engine [4]. For vehicle 4 the difference between the two inertia values was some 7% and the resulting increase in PN emissions over the WLTP was 15% (i.e. in line with the ~2:1 ratio reported in [4], even though that study reported results from a different engine type). May et al. [17] varied the inertia of their test vehicles, but uncertainty was high and the results were confounded somewhat by the occurrence of DPF regeneration – however, increasing the inertia appeared to sometimes decrease PN emissions, in marked contrast to results presented here.

Over the NEDC the difference was a mere 3%, supporting the theory that the multiple periods of constant speed and relatively gentle accelerations of that cycle minimize the impact of increases in inertia on legislative PN emissions. (Recall that the vehicle has no inertia to overcome at any constant speed – including at zero speed; constant speed and idle conditions account for almost 60% of the NEDC.)

Finally, it is worth underlining that exhaust emissions from this vehicle were DPF-filtered and that the full particulate budget would include the particulate (both PM and PN) which accumulates in the DPF during the various tests performed.

2.3.5. Overall observations from tests performed on vehicle 1-4

It has been very clearly established that overall the WLTP and even its test cycle alone (WLTC) causes much higher NO_x emissions than the NEDC, for a range of vehicle types (see [9, 16] and references therein). Emissions of other pollutants and CO_2/fuel consumption often show more limited changes [5]. The particulate emissions presented in this study showed both increases and decreases, depending on the vehicle in question.

While the WLTP specifies a driving cycle and road load simulation which are arguably much closer to real-world usage than the NEDC, it remains a laboratory cycle carried out under relatively favourable conditions – further testing of a broader range of vehicles is necessary to obtain a complete picture of legislative particulate emissions over the current and incoming driving cycles. A general point re-

garding this study's test vehicles with manual transmissions (i.e. vehicles 1, 3 and 4) and their results obtained over the WLTP is that the gearshift strategy might have a significant impact [4]. While the calculated WLTP gearshifts employed in this study were in full compliance with the most recent version of [25], further investigations could be performed to investigate the impact of subtle differences in the gearshift points on particulate emissions, especially PN.

The current procedure for calculating the gearshifts makes use of a calculated vehicle-specific parameter for the lowest viable engine speed for gears 3 and higher (termed 'n min drive'), a derived value and a concept which may be better suited to Diesel engines than to petrol engines [23, 24]. During accelerations commencing from a low engine speed, the value of this parameter determines when the gears are changed and is thereby crucial in determining engine load and speed (and the behaviour of the turbocharger, if present). The WLTP does permit some flexibility in terms of the application of safety margins, which would likely affect PN emissions to at least some extent.

As noted elsewhere [4], even for a well-defined speed trace with very narrow tolerances, the question of gears and their usage means that the engine speed-load coordinates occurring while meeting that speed trace are far from universal. Much effort has been expended on the derivation of the approach for calculating gearshifts, but the overall emphasis has been more on drivability and (within certain limits) engine load is maximised by using the highest possible gear at a given vehicle speed.

For a given vehicle operating at a given speed, there are sometimes three gears which could physically be used and often two gears which might be selected by an "average driver". Thus, the impact of the gearshift logic and the relationship between calculated gearshift values and their impact on particulate emissions occurring in the real world are topics worthy of dedicated investigation. Finally, it bears repeating that legislative emissions results are distance specific [/km] and so a longer test cycle further dilutes the emissions associated with cold start.

3. Upcoming changes and developments

A highly important upcoming change for the EU and some other markets which broadly follow EU regulations (e.g. China and India) is that of incoming RDE requirements. Recently updated specifications for the EU test procedure mean that PN emissions will be measured for both Diesel and DISI vehicles, with a conformity factor of 1.5 applicable to the limit of 6.0×10^{11} #/km which will apply to both engine types from September 2017, such that the limit is effectively 9.0×10^{11} #/km. However, a decision was also made to include (rather than explicitly exclude) emissions from the cold start event in the calculation process. This makes the application of GPFs virtually a certainty, as emissions must be low under a very wide range of engine operating conditions and ambient conditions, including at high speed and during and following cold start at low ambient temperature.

When the cold start is excluded from the results, RDE PN (and PM) results can be significantly lower than laboratory results from cycles containing a cold start; the inclusion of cold start emissions will change this tendency somewhat, although the fact that for RDE testing the cold start is divided by a very long distance (often 70–90 km; some 3–4 times the distance covered by the WLTC) remains relevant. This issue will most likely dominate the research agenda and scientific debate on the topic addressed in this paper in the EU for some time. Recent indications are that the EU test methodology for the measurement of PN will also be updated to measure solid particles not of diameter > 23 nm, but of diameter >10 nm. Legislation has yet to be drafted, but investigations are underway. Part of the motivation for such a change is the fact that DISI engines generally produce smaller particles than Diesel engines and that the 23 nm cut-off was chosen with Diesel particulate in mind. A further consideration is that all other factors being equal, particle size is inversely proportional to toxicology and concern has been raised over the health impact of particles which are currently not measured.

In China there are indications that PFI vehicles will have to be tested for PN emissions and meet PN limits, with only CNG-fuelled vehicles being exempt. Naturally, the question arises as to whether such an approach might be adopted in other jurisdictions which already employ the PN metric as a standard-setting tool. Finally, there remains the prospect of the USA, Japan (and countries which follow regulations adopted in the aforementioned countries) adopting PN as a metric of control.

The USA has longstanding objections to PN concerning repeatability and the fact that only non-volatile particles are measured, yet Japan and perhaps some other countries could conceivably adopt the PN metric at some point in the next few years. The USA has specified extremely low PM limits of below 1 mg/km, but further decreases in emissions might only be measurable using a number-based approach like PN.

4. Conclusions & summary

This paper has briefly examined the current situation regarding exhaust emissions of particulate matter and their measurement and control, with an emphasis on the situation in the EU. To support this analysis, results obtained in an emissions laboratory were presented. The results of this experimental campaign revealed that overall, it is very difficult to generalize regarding particulate emissions from the vehicles tested, due to their varying engine and fuel types and the presence or absence of a dedicated filter (DPF).

Unlike certain other pollutants (chiefly NO_x) [24, 25], the legislative exhaust particulate emissions from the vehicles tested in this study were not radically changed when moving from the NEDC to the WLTP (even with the application of more demanding road load settings). In some cases, trade-off type behaviour is apparent, where PM can decrease and PN can increase (which is indeed physically possible, as for a given mass of fuel and lubricating oil turned into particulate, the number of particles can vary massively according to the size profile of those particles).

The filter-based PM method was shown to be of limited power in differentiating between test cycles and inertia settings – even when using one filter per test to maximize the payload. The PN count generated by the CPC was a more reliable tool with better sensitivity and it also has the

advantage of higher resolution (1 Hz, or even 10 Hz). The MSS was used for testing on a CNG-powered vehicle with low emissions and proved of use only for the cold start event and the first ramp of the test cycle. However, overall the measurement of emissions from vehicle 3 (CNG) was carried out successfully, despite the legislative PM and PN and the MSS technique not being designed with CNG-powered engines in mind.

In conclusion, as regards upcoming changes, the most significant trends are the levelling of the playing field regarding testing requirements and emissions limits for Diesel and non-Diesel engines and RDE testing under a much wider range of ambient conditions and driving conditions.

Nomenclature

λ	lambda; the ratio of the actual air:fuel ratio to the stoichiometric air:fuel ratio
CF	conformity factor
CI	compression ignition
CNG	compressed natural gas
CPC	condensation particle counter
CVS	constant volume sampling [system]
DOC	diesel oxidation catalyst
DISI	direct injection spark ignition [engine]
DPF	diesel particulate filter
EU	European Union
EUDC	extra-urban driving cycle
FC	fuel consumption
GPF	gasoline particulate filter
GTR15 inertia	Global Technical Regulation No. 15 – the WLTP the setting applied on a chassis dynamometer to simulate the vehicle's resistance to acceleration; closely linked to vehicle mass
LNT	lean NOx trap
MSS	AVL Microsoot sensor ™
n min drive	minimum engine speed when gears 3 and higher are engaged, according to the GTR15
NEDC	New European Driving Cycle
PM	particle mass
PN	particle number
RDE	real driving emissions
S&S	stop&start (idle stop) system
SI	spark ignition
TWC	three-way catalyst
UDC	urban driving cycle (the first phase of the NEDC)
WLTC	worldwide harmonised light duty vehicles test cycle
WLTP	worldwide harmonised light duty vehicles test procedure

Bibliography

[1] ABDUL-KHALEK, I., KITTELSON, D., BREAR, F. The influence of dilution conditions on diesel exhaust particle size distribution measurements. *SAE Technical Paper*. 1999, 1999-01-1142, doi:10.4271/1999-01-1142.

[2] AMARAL, S.S., DE CARVALHO, J.A., COSTA, M.A.M., PINHEIRO, C. An overview of particulate matter measurement instruments. *Atmosphere*. 2015, **6**, 1327-1345, doi: 10.3390/atmos6091327.

[3] ANDERSSON, J., MAY, J., FAVRE, C., BOSTEELS, D. et al. On-road and chassis dynamometer evaluations of emissions from two Euro 6 diesel vehicles. *SAE Int. J. Fuels Lubr*. 2014, **7**(3), doi:10.4271/2014-01-2826.

[4] BAROUCH, G., RICCOBONO, F., VLACHOS, T. et al. Vehicle emission factors of solid nanoparticles in the laboratory and on the road using portable emission measurement systems (PEMS). *Frontiers in Environmental Science*. 2015, **3**, 82, doi:10.3389/fenvs.2015.00082.

[5] BIELACZYC, P., WOODBURN, J., SZCZOTKA, A. Exhaust emissions of gaseous and solid pollutants measured over the NEDC, FTP-75 and WLTC chassis dynamometer driving cycles. *SAE Technical Paper*. 2016, 2016-01-1008, doi:10.4271/2016-01-1008.

[6] BIELACZYC, P., WOODBURN, J., SZCZOTKA, A. A comparison of carbon dioxide exhaust emissions and fuel consumption for vehicles tested over the NEDC, FTP-75 and WLTC chassis dynamometer test cycles. *SAE Technical Paper*. 2015, 2015-01-1065, doi:10.4271/2015-01-1065.

[7] CÉDRIC, L., GORIAUX, M., TASSEL, P. et al. Impact of aftertreatment device and driving conditions on black carbon, ultrafine particle and NOx emissions for Euro 5 diesel and gasoline vehicles. *Transportation Research Procedia*. 2016, **14**, 3079-3088, doi:10.1016/j.trpro.2016.05.454.

[8] CHASE, R., DUSZKIEWICZ, G., RICHERT, J. et al. PM measurement artifact: organic vapor deposition on different filter media. *SAE Technical Paper*. 2004, 2004-01-0967, doi:10.4271/2004-01-0967.

[9] DEMUYNCK, J., BOSTEELS, D., DE PAEPE, M. et al. Recommendations for the new WLTP cycle based on an analysis of vehicle emission measurements on NEDC and CADC. *Energy Policy*. 2012, **49**, 234-242, doi:10.1016/j.enpol.2012.05.081.

[10] EASTWOOD, P. Particulate emissions from vehicles. ISBN: 978-0-470-72455-2, *Wiley*, Chichester 2008.

[11] GIECHASKIEL, B., SCHIEFER, E., SCHINDLER, W., et al. Overview of soot emission measurements instrumentation: from smoke and filter mass to particle number. *SAE Int. J. Engines*. 2013, **6**(1), 10-22, doi:10.4271/2013-01-0138.

[12] KERN, B., SPIESS, S., RICHTER, J. Comprehensive gasoline exhaust gas aftertreatment, an effective measure to minimize the contribution of modern direct injection engines to fine dust and soot emissions? *SAE Technical Paper*. 2014.2014-01-1513, doi:10.4271/2014-01-1513.

[13] KHALED, I., PREMNATH, V. Comparison among DMS 500, EEPS SMPS, MSS, EC/OC, CPMA, using laboratory 'soot' particles. *Cambridge Particle Meeting*. July 3, 2015. www.cambridgeparticlemeeting.org/sites/default/files/Presentations/2015/CPM_Khalek_2015_Comparison%20among%20DMS%20500%20EEPS%20SMPS%20MSS%20ECOC%20CPMA%20using%20laboratory%20%E2%80%9Csoot%E2%80%9D%20particles.pdf (accessed 09.11.2015).

[14] KHALEK, I., KITTELSON, D., BREAR, F. Nanoparticle growth during dilution and cooling of diesel exhaust: exper-

imental investigation and theoretical assessment. *SAE Technical Paper*. 2000, 2000-01-0515, doi:10.4271/2000-01-0515.
[15] MAMAKOS, A., MANFREDI, U. Physical characterization of exhaust particle emissions from late technology gasoline vehicles. *JRC report*. 2012, 72196, doi:10.2788/32371.
[16] MAROTTA, A., PAVLOVIC, J., CIUFFO, B. et al. Gaseous emissions from light-duty vehicles: moving from NEDC to the new WLTP test procedure. *Environmental Science & Technology*. 2015, 49(14), 8315-8322, doi: 10.1021/acs.est.5b01364.
[17] MAY, J., BOSTEELS, D., FAVRE, C. A comparison of light duty vehicle emissions over different test cycles and in real driving conditions. *FISITA*. 2014, F2014-CET-058.
[18] MERKISZ, J., PIELECHA J. Nanoparticle emissions from combustion engines. *Springer*. 2015, doi:10.1007/978-3-319-15928-7.
[19] RISTOVSKI, Z.D., MORAWSKA, L., HITCHINS, J. et al. Particle emissions from compressed natural gas engines. *Journal of Aerosol Science*. 2000, **31**(4), doi:10.1016/S0021-8502(99)00530-3.
[20] SAFFARIPOUR, M., CHAN, T.W., LIU, F. et al. Effect of drive cycle and gasoline particulate filter on the size and morphology of soot particles emitted from a gasoline-direct-injection vehicle. *Environmental Science & Technology*. 2015, **49**(19), 11950-11958, doi:10.1021/acs.est.5b02185.
[21] SCHINDLER, W., HAISCH, C., BECK, H. et al. A photoacoustic sensor system for time resolved quantification of diesel soot emissions. *SAE Technical Paper*. 2004, 2004-01-0968, doi:10.4271/2004-01-0968.
[22] SCHREIBER, D., FORSS, A., MOHR, M., DIMOPOULOS, P. Particle characterisation of modern CNG, gasoline and diesel passenger cars. *SAE Technical Paper*. 2007, 2007-24-0123, doi:10.4271/2007-24-0123.
[23] STEVEN, H. Further modifications on the gearshift calculation tool. *WLTP presentation*. WLTP-DHC-17-02e, 2013, unece.org (accessed 20.12.2016).
[24] STEVEN, H. Status report about the work of the task force on gearshift issues. *WLTP presentation*. WLTP-15-04e, 2016, unece.org (accessed 20.12.2016).
[25] United Nations Economic Commission for Europe. Addendum 15: Global technical regulation No. 15 – Global technical regulation on the Worldwide harmonized Light vehicles Test Procedures. 28.10.2016, www.unece.org/fileadmin/DAM/trans/main/wp29/wp29r-1998agr-rules/ECE-TRANS-180a15app1e.pdf (accessed 18.11.2016).
[26] United Nations Economic Commission for Europe. Addendum 82: Regulation No. 83 Revision 5. 4.02.2015, www.unece.org/fileadmin/DAM/trans/main/wp29/wp29regs/R083r5e.pdf (accessed 4.03.2015).
[27] WEI, Q., AKARD, M., PORTER, S., NAKAMURA, H. The Effect of Drive Cycles on PM emission characteristics from a gasoline vehicle. *SAE Technical Paper*. 2009, 2009-01-1119, doi:10.4271/2009-01-1119.
[28] WHELAN, I., SMITH, W., TIMONEY, D., SAMUEL, S. The effect of engine operating conditions on engine-out particulate matter from a gasoline direct-injection engine during cold-start. *SAE Technical Paper*. 2012, 2012-01-1711, doi:10.4271/2012-01-1711.
[29] ZHANG, X., CHEN, L., LIANG, Z., SHUAI, S. Characterizing particulate matter emissions from GDI and PFI vehicles under transient and cold start conditions. *Fuel*. 2017, **189**, 131-140, doi:10.1016/j.fuel.2016.10.055.

Piotr Bielaczyc, DEng. – Engine Research Department, BOSMAL Automotive Research and Development Institute Ltd in Bielsko-Biała.

e-mail: *Piotr.Bielaczyc@bosmal.com.pl*



Andrzej Szczotka, DEng. – Engine Research Department, BOSMAL Automotive Research and Development Institute Ltd in Bielsko-Biała.

e-mail: *Andrzej.Szczotka@bosmal.com.pl*



Joseph Woodburn, MSci. – Engine Research Department, BOSMAL Automotive Research and Development Institute Ltd in Bielsko-Biała.

e-mail: *Joseph.Woodburn@bosmal.com.pl*



Article citation info:
SITNIK, L.J. Statistic of fuel consumption in test and in natural operation of vehicles. *Combustion Engines*. 2017, **171**(4), 239-244. DOI: 10.19206/CE-2017-440

Lech J. SITNIK

CE-2017-440

Statistic of fuel consumption in test and in natural operation of vehicles

The lowering of carbon dioxide emission is world pursuit which is written in international agreement. It concerns all economy sections, especially motorization. In this last case the lowering is essential, since almost all fuel used for powering vehicles comes from non-renewable resources. Using these fuels means a one-way carbon motion from underground lode to earth atmosphere. This process has to be immediately stopped. For several years there have been taken actions in this direction. There are both legislative and technical actions. However, the reports which were published in 2016 shows that despite the efforts and engagement of considerable means, the effects are mediocre. There has been noticed, that, though the lowering of carbon dioxide emission determined in bench tests has been attained, it is impossible to notice this progress in natural operation of vehicles. The causes of such a state are sought mainly in incompatibility of test conditions to the real operation of vehicles conditions. Assuming that the carbon dioxide emission is (quasi) directly proportional to fuel consumption, in the article there has been proposed the method of solving the problem of removing divergence between test and operational data. There has been suggested the different attitude to bench data analysis and implementation of new calculative procedures in a way to reach the correlation between the test and operating fuel consumption.

Key words: *operation of vehicles, test, fuel consumptions*

1. Introduction

The carbon dioxide emission to atmosphere is constantly increasing, and in the case of car vehicles it happens in the geometrical progress [1].

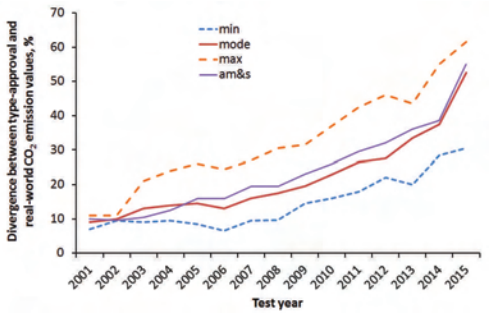


Fig. 1. The increase of carbon dioxide emission from vehicle engines (based on [1])

The increase of carbon dioxide concentration in the atmosphere has to be stopped. Reports published in 2016 shows that despite the efforts and engagement of considerable means, the effects are mediocre. The carbon dioxide emission decrease determined in the bench tests was reached, however, this progress cannot be noticed in the natural operation of vehicles.

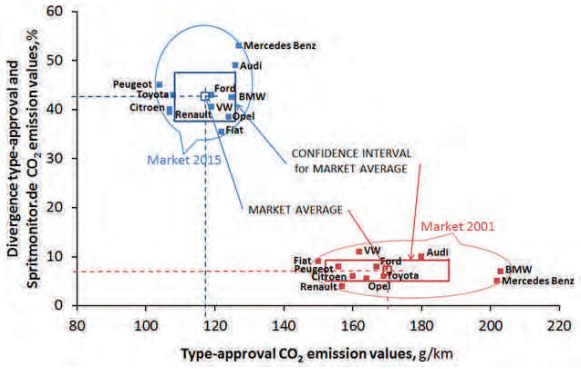


Fig. 2. Test results of carbon dioxide emission in comparison with emission in natural operation (based on [1])

2. The way of determining of fuel consumption in natural operation

The way of determining the fuel consumption in natural operation is not regularized in the European Union.

Most often there are measured:

S_m – vehicle mileage. km, OFC_{sm} – corresponding S_m, operational fuel consumption, dm^3, and then there is calculated, OFC_m – average, operational fuel consumption from the relation:

$$OFC_m=100 \cdot OFC_{sm}/S_m \quad (1)$$

in Europe usually given in $dm^3/100km$ of the travelled route.

The so-called operational fuel consumption (OFC) is usually determined after multiple travelling over the chosen, test route fragments. The fragments are assigned on the generally available streets and roads. E.g. according to Auto Motor und Sport (AMS) magazine, the determining of fuel consumption is made after traveling the test fragments chosen by the editorial office. The fuel consumption determined in this way is indicated as $OFC_{AMS.}$ Moreover, AMS also tests vehicles in the conditions of very spare drive (Sparrunde). The fuel consumptions in these conditions is indicated as OFC_{AMSS}. The fuel consumption determined e.g. from the AMS procedure is not identical with the fuel consumption determined in natural operation. It comes from the fact, that AMS test (as well as other tests of this type) is realized in controlled operation, not in the natural one.

3. The way of determining the fuel consumption in the test conditions

Nowadays, in different world regions, there are used the so-called driving tests, realized on the chassis dynamometers where the fuel consumption of the tested vehicles engines is assigned. In Europe it is currently used the NEDC test (New European Driving Cycle), and in The United States the test FTP is used (Federal Test Procedure), etc. In the nearest future the researches are planned according to the new world test.

The profile of NEDC test velocity presents as follow:

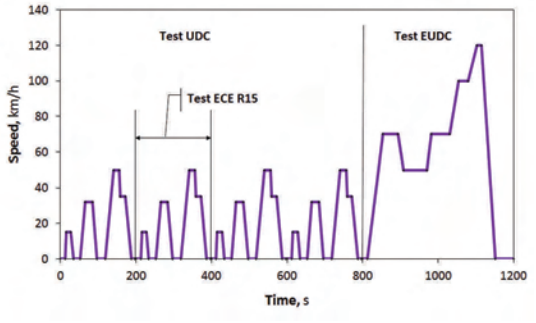


Fig. 3. The profile of NEDC test speed

From the picture it results that the NEDC test is the four time repeated ECE R15 test which is called UDC test (Urban Driving Cycle) plus once repeated EUDC test (Extra Urban Driving Cycle).

The fuel consumption in the NEDC test is determined during vehicle researches in the chassis dynamometer. During researches, the vehicle has to driven in a way that the velocity profile is preserved with very little deviations.

Engines fumes of the researched vehicle are gathered in the special containers (material bags). Their quantity is logged and the quantity of their particular components is assigned. There is also measured the route that is driven during the test.

The test result concerning the fuel consumption does not comes from the direct measurements but comes from the calculations of the following procedure:

There is assumed that the fuel density is indicated according to EN ISO 12185 (or other equivalent method), where in case of:

- petrol or gas oil, the density measurement is made in 15°C;
- LPG and NG – there is used the reference density
  - 0.538 kg/dm^3 in case of LPG
  - 0.654 kg/m^3 in case of NG

If take the indication as follows:

FC – fuel consumption in dm^3/100 km (liters per 100 km) with powering engine by petrol, liquid gas or oil gas or in m^3/100 km (in case of natural gas), THC – planned hydrocarbon emission in g/km of test route, CO – planned carbon oxide emission in g/km of test route, CO_2 – planned carbon dioxide emission in g/km of the test route, D – density of the used fuel, then, the fuel consumption assigned in the test comes from the following calculations:

a) in case of the vehicles with spark engines (OTTO) powered with petrol

$$FC = (0.1154/D) \times [(0.866 \times THC) + (0.429 \times CO) + (0.273 \times CO_2)] \quad (2)$$

b) in case of vehicles with spark engines (OTTO) powered with LPG

$$FC_{norm} = (0.1212/0.538) \times [(0.825 \times THC)+(0.429 \times CO)+(0.273 \times CO_2)] \quad (3)$$

If the composition of fuel is different from the standard one then (2) changes into:

$$FC_{norm} = (0.1212/0.538) \times c_f \times [(0.825 \times THC)+(0.429 \times CO)+(0.273 \times CO_2)] \quad (4)$$

c_f is assigned from the relation: $c_f = 0.825 + 0.0693 \times n_r$, where n_r – actual proportion H/C of the used fuel.

c) in case of vehicles with spark engines (OTTO) powered with NG

$$FC_{norm} = (0.1336/0.654) \times [(0.749 \times THC)+(0.429 \times CO)+(0.273 \times CO_2)] \quad (5)$$

d) in case of vehicles with compression ignition engine (diesel):

$$FC = (0.1155/D) \times [(0.866 \times THC)+(0.429 \times CO)+(0.273 \times \times CO_2)] \quad (6)$$

The fuel consumption assigned in the test is therefore not the result of direct measurement but the recalculations, and is based on the results of the engine fumes components concentration. It has a huge advantage because it enables to release the results from the actual existing chemical composition of fuel. This can, however, lead (and leads) to divergences between the fuel consumption assigned in the tests and in the natural operation.

If we know that emissions of THC and CO are not more than 1% of total emissions, then the quasi linear relationship between fuel consumption and CO_2 emissions results from the above equations

The basic parameters of NEDC tests are following:

Table 1. The basic parameters of NEDC tests

Characteristics	Unit	Test		
		ECE	EUDC	UDC+EUDC=NEDC
Route	km	1.013	6.955	4×1.013+6.955=11.007
Duration	s	195	400	4×195+400=1180
Average velocity	km/h	18.7	62.6	33.6
Maximum velocity	km/h	50	120	120

If take that:

FC_{NEDC} – fuel consumption in NEDC test, dm^3/100 km, FC_{UDC} –fuel consumption in UDC test, dm^3/100 km, FC_{EUDC} –fuel consumption in EUDC test, dm^3/100 km, then, taking into consideration the values from the Table 1, the relation is acquired

$$FC_{NEDC} = 0.368129\ FC_{UDC} + 0.631871\ FC_{EUDC} \quad (7)$$

according to which the value of fuel consumption in the NEDC test may be assigned.

4. The correlation of the fuel consumption assigned in the driving tests and in the operation of vehicles

There has been stated that the fuel consumption in operation is significantly higher than the one given in the tests [2, 15–19]. Because this opinion is based on the reports of numerous research centers or the ones who provide vehicles evaluation (like the AMS editorial office) it is necessary to wonder how to lead to consistency of the test data and operation data.

However, there appears the question whether the correlation of fuel consumption assigned in the tests and in the operation of vehicles may occur at all. Before answering it, there is necessary to pay attention again on the fact that from one side:

- the fuel consumption in the tests is assigned on the way of recalculations, and from the other side,
- the so called operating fuel consumption is assigned in the controlled operation.

Additional doubt which appears, concerns whether the measurements in the controlled operation may be authoritative for the evaluation of fuel consumption in the natural operation. Here, the future works are continuing, but in this moment the data from the controlled operation are taken for the further considerations.

Due to the fact that the present paper concerns presentation of the results correlation method, the data available in the literature will be used in its further part. There has been used the data presented by the editorial office of Auto Motor und Sport. The editorial office leads the usage measurement on chosen test fragments assigning OFC_{AMS} and OFC_{AMSS}

Subsequently, OFC_{AMS} was treated as the equivalent of FC_{UDC} from the UDC test, whereas OFC_{AMSS} as the equivalent of FC_{EUDC} from EUDC tests.

Hence, there has been assumed, that the fuel consumption in controlled operation OFCs will be indicated from the relation

$$OFC_S = 0.368129\ OFC_{AMS} + 0.631871\ OFC_{AMSS} \quad (8)$$

If take that the operating fuel consumption is to be correlated with the test consumption then

$$0.368129\ OFC_{AMS} + 0.631871\ OFC_{AMSS} = OFC_S = b_0 + b_1 * FC_{UDC} + b_2 * FC_{EUDC} \quad (9)$$

As it is visible on the right side of the equation (9) there does not exist the right side of the equation (7). It has been assumed, that there is no premise to stick to the formula (7) resulting from the Table 1 which means that the NEDC test should consist of UDC test plus EUDC test, however, is does not have to be the four times repetition of UDC test plus one repetition of EUDC test.

The usefulness of the assumption according to (9) has been checked by the use of operating data presented by AMS.

The editorial office of the AMS has carried out the measurements of both: cars driven by the spark ignition engines (OTTO), as well as the vehicles with compression ignition engines (DIESEL)

Both entry data and the calculation results are gathered in the tables.

The OFC_{SC} values (the calculated operating fuel consumption) has been determined from the dependence

$$OFC_{SC} = 0.440043\ FC_{UDC} + 0.855818\ FC_{EUDC} - 0.12364 = NFC_{NEDC} \quad (10)$$

which comes out from the Table 2 data with the use of regression analysis. It is worth to once again pay attention, that in the equation (10) the input data are the values of fuel consumption determined in UDC and EUDC tests, thus in the standard measurement tests. According to this fact the fuel consumption NFC_{NEDC} can be treated as the fuel consumption in the "newer" NEDC test.

Table 2. The measurements and calculation results of fuel consumption in the braking and route tests of vehicles with spark ignition engines (Otto)

No	Car (OTTO)	FC_{UDC}	FC_{EUDC}	FC_{NEDC}	OFC_{AMS}	OFC_{AMSS}	OFC_S	OFC_{SC}	Difference $(OFC_S-OFC_{SC})/OFC_S$
		$dm^3/100$ km							%
1	Focus Turnier 1.6 Titanium	7.70	5.00	6.00	10.80	5.70	7.58	7.54	0.44
2	308 SW 1.6 THP Active	9.50	5.20	6.80	10.70	6.00	7.73	8.51	–10.05
3	Astra Sports Tourer 1.4 Turbo	8.40	4.90	6.10	11.10	6.40	8.13	7.77	4.48
4	Twingo 1.2 16V Access	6.70	4.20	5.10	8.80	4.80	6.27	6.42	–2.34
5	i10 1.1 Base	5.80	4.10	4.70	8.40	4.60	6.00	5.94	1.02
6	Alto 1.0 Classic	5.50	3.80	4.40	8.10	4.60	5.89	5.55	5.77
7	M5	14.00	7.60	9.90	18.90	9.60	13.02	12.54	3.70
8	E 63 AMG	13.80	7.50	9.80	18.40	9.70	12.90	12.37	4.15
9	Panamera Turbo	17.00	8.40	11.50	22.50	9.50	14.29	14.55	–1.82
10	458 Italia	19.70	9.70	13.30	25.70	11.70	16.85	16.85	0.04
11	MP4-12C	18.50	7.80	11.70	23.90	9.40	14.74	14.69	0.31
12	Golf 1.4 TSI Comfortline	8.10	5.20	6.30	11.50	5.50	7.71	7.89	–2.36
13	Giulietta 1.4 TB Progression	7.80	4.60	5.80	11.20	5.00	7.28	7.25	0.51
14	Astra 1.4 Turbo Essentia	7.40	4.80	5.90	10.80	5.20	7.26	7.24	0.29
15	Roomster 1.2 TSI Roomster	7.10	4.90	5.70	11.20	5.40	7.54	7.19	4.53
16	Meriva 1.4 EcotecEssentia	8.00	5.00	6.10	10.50	5.50	7.34	7.68	–4.57
17	Grand Modus 1.2 TCE Dyna	7.60	5.00	5.90	10.30	5.90	7.52	7.50	0.27
18	C3 Picasso 1.6 VTi SX Pack	9.40	5.50	6.90	11.30	6.60	8.33	8.72	–4.68
19	Venga 1.6 CVVT M	8.40	5.80	6.70	10.20	5.80	7.42	8.54	–15.05
20	Swift 1.2	6.10	4.40	5.00	9.00	4.90	6.41	6.33	1.30
21	C3 1.4 VTi	7.60	4.80	5.80	9.60	5.20	6.82	7.33	–7.46
22	Ibiza 1.4 MPi	8.00	4.70	5.90	9.90	5.30	6.99	7.42	–6.09
23	i20 1.2	6.50	4.30	5.10	8.90	5.60	6.81	6.42	5.84
24	Focus 1.6 Ti-VCT 16V Trend	8.70	5.40	6.60	11.90	6.60	8.55	8.33	2.63
25	Bravo 1.4 MultiAirDynamic	7.30	4.80	5.70	12.30	5.70	8.13	7.20	11.48
26	i30 1.6 Comfort.	8.00	5.20	6.20	11.60	6.00	8.06	7.85	2.66

There have been obtained surprisingly good factors of equation (10) prediction, which is testified by its regression statistics.

Table 3. Regression statistics of the equation (12) in relation to fuel consumption model of cars with spark ignition engines

Multiple of R	0.989330
Square of R	0.978775
Matched square of R	0.976929
Standard error	0.452155
Observations	26

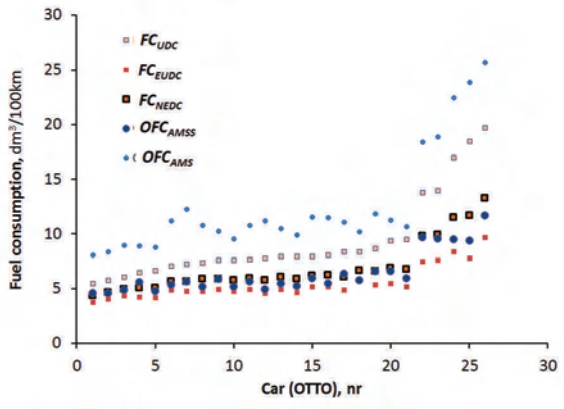


Fig. 4. The research results of fuel consumption in bench tests (FC_{NEDC}, FC_{EUDC} and FC_{UDC}) and in controlled operating tests (OFC_{AMS}, OFC_{AMSS}) of vehicles with spark ignition engines

You can see large variances in the results of the tests and those listed in the pilot operation.

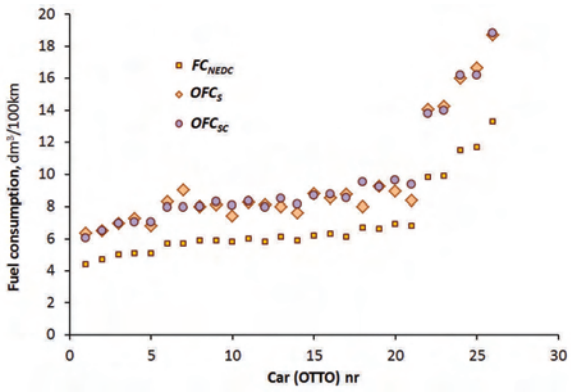


Fig. 5. Fuel consumption FC_{NEDC} and in the road tests OFC_S of vehicles with spark ignition engines

The results obtained in the NEDC test are still different from the operational ones, but if you use the (10) type formula, then the UDC and EUDC (as the newer NEDC test) and the results from the controlled operation almost overlap.

Similar results were obtained in case of vehicles powered by compression ignition engines (diesel).

In the case of vehicles powered by the compression ignition engines (Diesel) there has been also obtained the dependence (11)

$$OFC_{SC} = -0.012954FC_{UDC}+0.964301FC_{EUDC}+2.466235 = \\ = NFC_{NEDC} \quad (11)$$

Analyzing the abovementioned equation there can be stated that in the case of vehicles with compression ignition engines (DIESEL) the fuel consumption assigned in the urban test (UDC) is particularly irrelevant. The essential value is the fuel consumption assigned in the EUDC test.

Also in this case, the obtained prediction factors were not bad (however, they were worse that in the case of vehicles powered by spark ignition engines).

Table 5. Regression statistics of the equation (13) in reference to fuel consumption model of cars with compression ignition engines

Multiple of R	0.851541
Square of R	0.725122
Matched square of R	0.712628
Standard error	0.516375
Observations	47

The data from the abovementioned tables are illustrated in the diagrams.

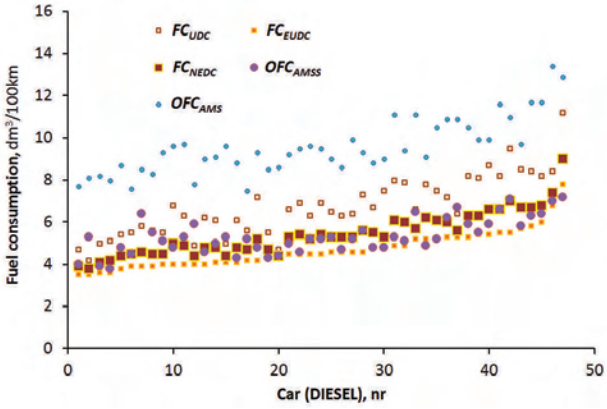


Fig. 6. The research results of fuel consumption in bench tests (FC_{NEDC}, FC_{EUDC} and FC_{UDC}) and in controlled operating tests (OFC_{AMS}, OFC_{AMSS}) of vehicles with compression ignition engines (DIESEL's)

As with OTTO engines, vehicles with Diesel engines also exhibit a fuel consumption balance in tests and in controlled operation.

After the conversion according to the formula (11), the correlation of the results was significantly improved.

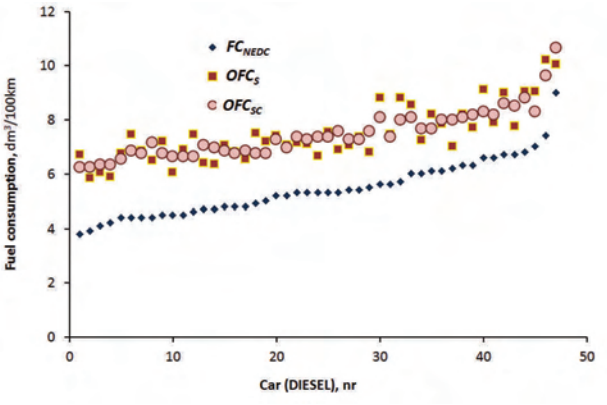


Fig. 7. Correlation of fuel consumption FC_{EUDC} and in road test OFC_S and calculated OFC_{SC} of vehicles with compression ignition engines (DIESEL's)

Table 4. Data concerning fuel consumption in the cars with compression ignition engines (diesel)

No	Car(DIESEL)	FC_{UDC}	FC_{EUDC}	FC_{NEDC}	OFC_{AMS}	OFC_{AMSS}	OFC_S	OFC_{SC}	Difference $(OFC_S-OFC_{SC})/OFC_S$
		$dm^3/100$ km							%
1	A1 1.6 TDI Ambition	4.70	3.50	3.90	7.70	4.00	5.36	5.78	–7.80
2	Cooper D	4.20	3.50	3.80	8.10	5.30	6.33	5.79	8.59
3	320d Efficient Dynamics Edition	5.00	3.60	4.10	8.20	3.90	5.48	5.87	–7.11
4	Polo 1.6 TDI Highline	5.10	3.60	4.20	8.00	3.80	5.35	5.87	–9.83
5	B 180 CDI	5.40	3.80	4.40	8.70	4.80	6.24	6.06	2.81
6	Astra Sports Tourer 1.7 CDTI Enjoy	5.50	3.90	4.50	7.60	4.50	5.64	6.16	–9.12
7	C4 1.6 e-HDiExclusive	5.80	3.90	4.60	8.50	6.40	7.17	6.15	14.24
8	DS3 HDI 110 SportChic	5.60	3.90	4.50	8.30	5.50	6.53	6.15	5.76
9	Zafira Tourer 2.0 CDTiEcoflex Cosmo	5.50	4.00	4.50	9.30	5.10	6.65	6.25	5.93
10	508 SW 2.0 HDiAllure	6.80	4.00	5.00	9.60	4.80	6.57	6.24	5.05
11	Insignia 2.0 CDTI Eco-FLEX Cosmo	6.30	4.00	4.90	9.70	5.30	6.92	6.24	9.80
12	Cee'd 1.6 CRDi M	4.90	4.00	4.40	7.80	5.90	6.60	6.26	5.14
13	C 220 CDI Avantgarde	6.20	4.00	4.80	9.00	4.60	6.22	6.24	–0.38
14	Jetta 2.0 TDI CR Highline	6.10	4.10	4.80	9.10	5.00	6.51	6.34	2.59
15	C-Max 1.6 TDCiTitanium	5.00	4.10	4.40	9.60	5.30	6.88	6.36	7.67
16	Golf 2.0 TDI CR Trendline	6.10	4.10	4.80	8.80	4.30	5.96	6.34	–6.45
17	Auris 1.4 D-4D Premium	5.60	4.20	4.70	7.50	5.20	6.05	6.44	–6.57
18	S60 D3 Summum	7.20	4.20	5.20	9.30	4.80	6.46	6.42	0.52
19	i40 1.7 CRDi Premium	5.50	4.30	4.70	8.50	4.30	5.85	6.54	–11.89
20	Countryman Cooper D	4.70	4.40	4.40	8.60	4.40	5.95	6.65	–11.81
21	Grand C-Max 2.0 TDCi Titanium	6.60	4.50	5.30	9.20	5.00	6.55	6.72	–2.66
22	6 Kombi 2.2 MZR-CD Kirei	6.90	4.50	5.40	9.50	4.60	6.40	6.72	–4.88
23	Passat 2.0 TDI CR Comfortline	6.30	4.50	5.20	9.60	5.20	6.82	6.72	1.40
24	6 Kombi 2.2 MZR-CD Sport	6.90	4.50	5.40	9.50	5.20	6.78	6.72	0.98
25	Touran 2.0 TDI Highline	6.50	4.60	5.30	9.00	5.30	6.66	6.82	–2.34
26	Passat 2.0 TDI DSG Comfortline	6.30	4.60	5.30	8.60	4.70	6.14	6.82	–11.16
27	Mondeo 2.0 TDCi Trend	6.40	4.60	5.30	9.90	5.20	6.93	6.82	1.60
28	Altea 2.0 TDI CR Style	7.30	4.60	5.60	9.30	5.60	6.96	6.81	2.22
29	Lancer 1.8 DI-D Intense	6.70	4.80	5.50	8.80	4.80	6.27	7.01	–11.73
30	SuperbCombi 2.0 TDI Elegance	7.50	4.80	5.30	9.00	4.80	6.35	7.00	–10.27
31	E 250 CDI Kombi	8.00	4.90	6.10	11.10	5.30	7.44	7.09	4.67
32	Insignia Sports Tourer 2.0 CDTi Cosmo	7.90	4.90	6.00	9.40	5.10	6.68	7.09	–6.08
33	530d xDrive	6.60	5.20	5.70	11.10	6.50	8.19	7.40	9.74
34	Superb 2.0 TDI DSG 4x4 Comfort	7.80	5.20	6.20	9.10	4.90	6.45	7.38	–14.48
35	SuperbCombi 2.0 TDI CR	7.50	5.20	6.10	10.50	5.20	7.15	7.38	–3.25
36	A6 3.0 TDI Quattro	7.20	5.30	6.00	10.90	6.20	7.93	7.48	5.63
37	X3 xDrive20d.	6.40	5.30	5.60	10.90	6.70	8.25	7.49	9.12
38	Laguna 2.0 dCi 175 aut. Bose Edition	8.20	5.30	6.30	10.50	5.90	7.59	7.47	1.61
39	Laguna Grandtour 2.0 dCiDynamique	8.10	5.40	6.30	9.90	5.50	7.12	7.57	–6.30
40	3008 2.0 HDi aut. Premium+	8.70	5.40	6.60	9.90	5.90	7.37	7.56	–2.55
41	E 350 CDI 4Matic	8.20	5.50	6.60	11.60	6.60	8.44	7.66	9.21
42	XC60 D5 AWD	9.50	5.50	7.00	11.00	7.10	8.54	7.65	10.41
43	Qashqai 2.0 dCiVisia	8.50	5.70	6.70	9.70	5.80	7.24	7.85	–8.53
44	GLK 220 CDI 4MATIC	8.40	5.80	6.70	11.70	6.30	8.29	7.95	4.07
45	Q5 2.0 TDI Quattro	8.20	6.00	6.80	11.70	6.40	8.35	8.15	2.46
46	ML 350 BlueTEC	8.40	6.80	7.40	13.40	7.00	9.36	8.91	4.72
47	FX30d	11.20	7.80	9.00	12.90	7.20	9.30	9.84	–5.85

4. Conclusions

There exists the urgent need to limit the carbon dioxide emission coming from motorization, and the simplest way to obtain this aim is lowering of operating fuel consumption. There has been noticed, that throughout the last years the reduction of carbon dioxide emission determined in the bench tests was achieved, however, it is not reflected in the natural operation of vehicles. The causes of this state may be found mainly in incompatibility between test conditions and actual vehicles operating conditions.

This article has risen to this issue, concurrently proposing the way of solving the problem.

There has been noticed, that in order to limit the increase of carbon dioxide concentration in the atmosphere, it is necessary to limit the fuel consumption. Therefore, there has been suggested the different attitude to fuel consumption determining in the natural operation, and also broader employing of test data in order to reach the correlation between test and operation fuel consumption.

The appropriate calculating procedure has been proposed.

It has been shown that:

- The results of controlled operating of vehicles may be presented in different form referring to the results of UDC, EUDC or NEDC tests researches.
- The results of fuel consumption researches obtained in the controlled operation of vehicles conditions are possible to correlate with the results of bench test researches.
- There exists satisfactory correlation of fuel consumption research results, determined in the controlled operation

with the results of bench tests- urban UDC and out of city EUDC.
- Because the results of fuel consumption test researches come from the calculations arising from fumes components concentrations, and not directly from the measurements, it seems to be deliberate to implement the further calculating procedures e.g., according to the conception included in this paper, in a way to obtain the correlation of bench tests results with operation researches results.
- The implementation of procedures would enable the real evaluation of operating fuel consumption on the basis standard test researches, without the necessity of change the tests themselves, especially the ones coming in like e.g. WLTP.
- It is deliberate to carry on the further works targeting at reliable fuel consumption evaluation obtaining in natural operation of vehicles and their correlation with bench tests results

The presented research results have been based on relatively sparing experimental references. To broaden the resource of experiment, the continuation of researches seems to be necessary, especially due to the fact, that a new kind of bench test – WLTP is going to be implemented.

Nomenclature

CO	planned carbon oxide emission
CO_2	planned carbon dioxide emission
CNG	compressed natural gas
D	density of the used fuel
DIESEL	compression ignition engine
EUDC	extra urban driving cycle
FC	fuel consumption
FC_{EUDC}	fuel consumption in EUDC test
FC_{NEDC}	fuel consumption in NEDC test
FC_{UDC}	fuel consumption in UDC test
LPG	liquified petrolum gas
NEDC	new European driving cycle
NG	natural gas
OFC_m	average, operational fuel consumption
OFC_{sm}	corresponding S_m, operational fuel consumption
OTTO	spark ignition engine
S_m	vehicle mileage. km,
THC	planned hydrocarbon emission
UDC	urban driving cycle

Bibliography

[1] TIETGE, U., DÍAZ, S., MOCK, P. et al. From laboratory to road. A 2016 update of official and 'real-world' fuel consumption and co_2 values for passenger cars in Europe. White Paper. November 2016, www.theicct.org.

[2] DUDENHÖFFER, F., JOHN, E-M. Studie Kraftstoffverbrauch. Warum der offizielle Kraftstoffverbrauch von Neuwagen erheblich von der Realität abweicht. *ÖkoGlobe-Insituts der Universität Duisburg-Essen.* 2009.

[3] SITNIK, L.J. Theory of cumulative fuel consumption by LPG powered cars. *Journal of KONES.* 2015, **22**(4), 275-280.

[4] DIMITROV, R., MAGDZIAK-TOKŁOWICZ, M., SITNIK, L.J. et al. A comparison of fuel consumption between the new European driving cycle test and the natural operation of a vehicle. *MTM Machines, Technologies, Materials.* 2014, **8**(2), 23-25.

[5] SITNIK, L.J. Theory of cumulative fuel consumption and example for its application. *Trans & MOTAUTO' 14: XXII international scientific-technical conference: proceedings. Section I, Vehicle engines. Application of fuels types. Efficiency.* Scientific-technical union of mechanical engineering, 2014, 17-20.

[6] SITNIK, L.J., MAGDZIAK-TOKŁOWICZ, M., WALKOWIAK, W.W. et al. Comparison of mileage fuel consumption with the natural operation of the three different cycles. *Journal of KONES.* 2014, **21**(4), 439-444.

[7] SITNIK, L.J. Teoria skumulowanego zużycia paliwa i jej aplikacja. *Transport Przemysłowy i Maszyny Robocze.* 2014, **2**, 116-121.

[8] SKRĘTOWICZ, M.D., SITNIK, L.J., KAŹMIERCZAK, A., MAGDZIAK-TOKŁOWICZ, M. Evaluation methods of the impact of motorization on the quality of the atmospheric air. *Journal of KONES.* 2014, **21**(4), 445-452.

[9] KARDASZ, P.Ł. SITNIK, L.J., SZUBERSKI, K., HALLER, P. Ekologiczne skutki motoryzacji. *Autonaprawa.* 2010, **9**, 22-24.

[10] SITNIK, L.J. Some aspect of theory of cumulated fuel consumption. *Journal of KONES.* 2010, **17**(4), 447-453.

[11] SITNIK, L.J. Analiza przebiegów do wymiany oleju silnikowego w eksploatacji naturalnej samochodów. *Journal of KONES.* 2009, **16**(3), 367-373.

[12] SITNIK, L.J. Statystyczna weryfikacja osiągów silników spalinowych. *Journal of KONES.* 2006, **13**(4), 175-182.

[13] SITNIK, L.J. Skumulowane zużycie paliwa. *Archiwum Motoryzacji.* 2004, 7(3), 227-254.

[14] Testy porównawcze www.auto-motor-i-sport.pl/testy/testy-porownawcze.html.

[15] Spritverbrauch: Herstellerangabe gegen Test – Autobild www.autobild.de/artikel/spritverbrauch-herstellerangabegegen-test-1129421.html.

[16] Test: Kraftstoffverbrauch höher als von Herstellern angegeben www.ace.de/der-club/news/test-kraftstoffverbrauch-hoeher-als-von-herstellern-angegeben.html?no_cache=1.

[17] Reale Verbrauchsmessungen Spritverbrauch im Labor und in der Realität www.vcd.org/themen/auto-umwelt/reale-verbrauchsmessungen/.

[18] Vor dem Autokauf den realen Kraftstoffverbrauch ermitteln kurier.at/motor/vor-dem-autokauf-den-realen-kraftstoff-verbrauch-ermitteln/253.857.177.

[19] SpritverbrauchDie große Verbrauchs-Lüge: So stehlen Ihnen Autohersteller 450 Euro pro Jahr www.focus.de/auto/news/kraftstoffverbrauch-die-grosse-verbrauchs-luege-so-stehlen-ihnen-autohersteller-450-euro-pro-jahr_id_4168530.html.

Prof. Lech J. Sitnik, DSc., DEng. – Department Vehicles Engineering at Wroclaw University of Science and Technology.

e-mail: *Lech.Sitnik@pwr.edu.pl*



Article citation info:
KULCZYCKI, A. Theoretical approach to modeling the combustion process in turbine engines fuelled by alternative aviation fuels containing various components/biocomponents. *Combustion Engines*. 2017, **171**(4), 245-249. DOI: 10.19206/CE-2017-441

Andrzej KULCZYCKI

CE-2017-441

Theoretical approach to modeling the combustion process in turbine engines fuelled by alternative aviation fuels containing various components/biocomponents

The aim of this paper is presentation of the possibility of combustion processes modelling so that to better describe the influence of fuels chemistry on fuels combustion. This is important for prediction the behaviour of different alternative fuels in processes in combustion chamber. Currently used mathematical models do not sufficiently take into account the influence of fuels chemical composition on combustion process. The idea of new mathematical model is proposed in this paper. The paper presents the main assumptions of this model and the results of its preliminary verification using MiniJetRig.

Key words: *diesel fuel, jet fuel, mathematical model, combustion process*

1. Introduction

Intensive development of road and air transport leads to respectively increasing air pollution with exhaust gases from internal combustion engines. At global scale, the most important is CO_2 emission, considered as global warming effect cause. At local scale, more important is emission of CO, unburned hydrocarbons, and particle matters, as well as NO_x emission.

Majority of countries have declared implementation the CO_2 emission reduction programs. The fundamental way to achieve the goal is to implement biofuels into road and air transport.

Biofuels and biocomponents have been implemented in road transport for about 20 years. The biocomponents commonly used in fuels are: bioethanol as automotive gasolines component, and FAME as diesel fuel component. The technologies of manufacturing hydrocarbon biofuels designed to be used in CI engines and in aviation turbine engines have been developed for about 10 years. Regarding the chemical structure, the hydrocarbon biofuels are more similar to conventional than bioethanol and FAME. However, the hydrocarbon structure influences the combustion process, hence the operation parameters of engine, and exhaust gas composition.

Research regarding new biocomponents/biofuels, both for CI engines, and for aviation turbine engines demands the development of predicting methods, and assessment the effect of fuels/biofuels chemical composition on combustion process.

The characteristics of combustion process in CI engine indicates strong diversification of reaction chains depending on engine operation conditions, and on energy state of combustion chamber [1]. Similar situation takes place in turbine engines.

Research on dependence of combustion process, and as a consequence, engine operation parameters, and exhaust gases composition, are being carried out at different levels, from macroscopic one (engine tests) to molecular one (tests in laboratory reactors). As a result of such research experimental data are obtained, used then to develop the mathematical models quantitatively describing the relationships between chemical structure of fuels and engine operation parameters as well as exhaust gases composition. The basic problem is how describe quantitatively the chemical structure of fuels, what significantly limits the possibilities of combustion processes modelling.

The aim of this paper is to propose new mathematical model of combustion process, previously developed for another application than combustion process.

2. The analysis of processes in combustion chamber

The fuel combustion in CI engines and in turbine ones is complex process. It should be noticed at least the one process taking place before combustion chamber, i.e. in fuelling system and injector – fuel thermal degradation, and three processes in combustion chamber, such as: atomisation of fuel stream, its vaporization together with further thermal degradation, and combustion.

The separation of elementary processes is needed to analyse the effect of fuels chemical structure and resulting fuel properties on whole complex fuel combustion process. However, such distinct division into elementary processes doesn't fully correspond to the identified processes in engine. Especially it regards to fuel vaporisation and combustion. It is obvious that atomised, but still liquid fuel, in contact with the atmospheric oxygen diffusing into the liquid phase is subjected to initial oxidation reactions that make up long and branched chains of combustion reaction.

Also the combustion process itself is not uniform in whole combustion chamber. Such diversity, caused mainly by heterogeneous thermal state of combustion chamber is recognized as significant reason to create various products of combustion including CO, unburned hydrocarbons and particulate matters.

Next topic, very important for simulation, is term "chemical structure of fuel". It is known that conventional (petroleum) fuels are the mixture of many (even a thousand) hydrocarbons of different chemical structure. The molecules of individual compounds interact of each other. Such interactions affects fuel viscosity, its vaporisation – azeotrope, as well as chemical reactions during combustion process. However the nature of molecular interactions hasn't been sufficiently recognised. In recent years we can notice some interesting information regarding molecular clusters generated in fuels such as aviation turbine ones and diesel fuels, as a result of intermolecular bonds, including van der Waals ones, between the molecules of hydrocarbon

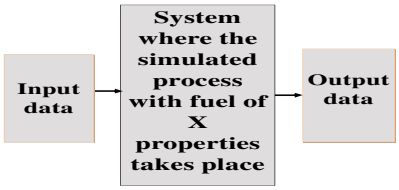
of specific chemical structure. Authors of the publication [2] describe generation of molecular clusters by polycyclic aromatic hydrocarbons (PAH), and point the clusters as the soot source. The molecular cluster are ordered structure of unique properties, different from volumetric properties of fuel treated as the liquid. This regards the energy state and ability to energy transfer [2]. The molecular clusters existing in fuel undoubtedly influence the chemical reactions in combustion process. This is pointed, among others, by authors of [3, 4].

Above mentioned complexity of chemical structure of fuels, as well as complexity of individual processes taking place in combustion chamber, makes simulation of combustion process fundamentally difficult.

3. Currently used mathematical models of combustion process in internal combustion engines

The mathematical models should be useful to predict the influence of fuels chemical structure on combustion process. The mathematical models of combustion processes are generally based on description of relationship between inputs and outputs. Outputs are engines operating parameters, like engine power, thrust, temperature at different points of engine and composition of exhaust gases. All these parameters are measured and output can be determined quantitatively. The problem is with input – fuels chemical structure, which usually is described qualitatively. The chemical reactions are quantitatively describe by thermodynamic relationships and chemical kinetic once. Thermodynamic description operates the thermodynamic parameters (functions) which describe energy state of fuel as a whole. Kinetic equations use such parameters as concentration of chosen reactant – compound which undergoes given reaction. It is very difficult or even impossible to select individual reaction in case the thousand compounds undergo simultaneously similar reactions. Consequently instead of concentration of each compound consisting of fuel the physicochemical properties of fuel are used to quantitatively describe fuel.

The relationships between input – properties of fuel, and output are formulated using different statistical methods. Usually a great number of tested fuels and engine tests results are needed to formulate function describing this relationship.



This method of modelling of combustion process uses the measureable parameters characterising fuel – it is advantage of this method. Weakness of this method is that new, unknown components or additives introduced into the fuel can change the mechanism of combustion process what is not included in the model. In this case the important incompatibility of the model with experimental data takes place. Below two of currently use models are briefly presented.

3.1. The CHEMKIN Model

The CHEMKIN Model is commercial product. It is used to simulate various chemical reactions, both in chemical process as well as in fuel combustion process in internal combustion engines. To simulate reactions with fuel, the model is supported by fuel data base ANSYS. Using this model, it is possible to calculate thermodynamic effects of fuel combustion, hence the amount of heat, pressure change in combustion chamber as function of crank angle, as well as the flame propagation speed and temperature in combustion chamber. These data are further used in calculation of chemical effects of combustion, i.e. in calculation of kinetics of combustion reactions, and creating products of combustion. The Arrhenius equation has been used for kinetic calculations in CHEMKIN model. In this equation, the temperature is the quantity describing the heat supplied to reaction system (RT). According to [4, 5], the average temperature for engine combustion chamber is used in calculations. Such attitude means significant exceptions to the real condition of combustion reaction. It is known [1] that there are different temperatures in different areas of the combustion chamber. It affects the combustion reactions and consequently combustion products, e.g. CO rises mostly by the combustion chamber walls. Accepting the average temperature for whole combustion chamber in CHEMKIN model doesn't accept such effect, so it can lead to significant differences between calculated and experimental CO concentration in exhaust gases.

Author of the publication [6] used the CHEMKIN model for simulation the combustion process in HCCI engine. Such model needs extensive experimental data base, created basing on model fuels ("model-fuel" or "surrogate-fuel"), i.e. the mixtures composed of individual, pure compounds e.g. hydrocarbons. This model covers a lot (up to several hundred) of reactions, making up the chemical reaction chains identified during combustion process. Such reactions have been mostly identified basing on analysis of combustion of individual compounds (mostly hydrocarbons) or their mixtures in reactors. It was found that the reactions identified for individual compound change when another compound is added, e.g. the reaction mechanism determined for pure isooctane has changed after toluene addition. This means major restrictions in using the model which doesn't cover such interaction of fuels components. In many cases, this is the reason for significant discrepancies between the mathematical modelling results and experimental data.

3.2. The SAE Model

The SAE model is part of procedure of analysis and assessment of gas emission from aircraft engines [7], and is used to calculate the emission of CO_2, CO, NO_x and C_xH_y in exhaust gases from aviation turbine engines (jet ones), and in ground applications. This model is based on carbon mass balance. Basis for this model is the following chemical reaction:

$C_nH_mO_pN_qS_r + X[R(O_2) + S(N_2) + T(CO_2) + h(H_2O) + U(CH_4)] \rightarrow P_1(CO_2) + P_2(N_2) + P_3(O_2) + P_4(H_2O) + P_5(CO) + P_6(CxHy) + P_7(NO_2) + P_8(NO) + P_9(SO_2)$

The model doesn't cover processes taking place in the system, i.e. in engine combustion chamber but is based exclusively on relation analysis: input data (fuel + air) – output data (composition of gases from combustion chamber). The relationships used in this model contain many experimentally determined parameters, which values can not be appropriate in case the new, unknown fuels component is tested. The another weakness of this model is that the fuel is characterised by average chemical formula.

Both currently used mathematical models of combustion process describes fuel as one very complex reactant. Consequently it is difficult to predict the influence of new components/biocomponents of fuels on combustion process.

4. The new proposed mathematical model of fuel combustion process

Taking into account:

- all mentioned above weakness of currently use mathematical models of combustion process
- useful of models for predicting the influence of new components/biocomponents or additives added to the fuel on combustion process
- need analysis of the influence of new components on the mechanism of combustion process,

the new model is proposed. This model was previously worked out and tested for another then combustion processes applications. Experience has shown that this model can be useful in mechanisms of various processes analysis and, what seems to be most important, let focus on the one chosen compound or component in very complex mixture an, describe this chosen compound / component influence on complex process, like fuel combustion in engine. It is the reason that this model was chosen to verify the possibility of its application for description of combustion processes.

The assumptions of proposed, new mathematical model of fuels combustion are based on model, developed previously for reactions initiated by heat and mechanical forces [8]. The new model allows to describe directly the impact of selected fuels components or additives on combustion process. The parameter that provides information about similarities or differences of compared combustion processes – for instance combustion process involving Jet fuel with tested component and process involving conventional Jet fuel, is reactivity coefficient α_i. The basing relationship for this model is the following:

$$\alpha_i = \{[f(y) - f_0(y)] / [\phi(y) - \phi_0(y)]\}\, d\phi(y)/df(y) \quad (1)$$

where combustion process is described by two functions of the same variable *y*, linked to the final state of the process. The general dependence (1) has been transformed to dependence (2). It was possible due to f(*y*) was treated as energy supplied from environment to the system and $\phi(y)$ was treated as a part of kinetic equation – reaction rate constant.

$$\alpha_i = (L - L_0)/A \exp[-E_a/(RT+\varepsilon)][(e_0)\cos(k_2L + k_3)]\, t \quad (2)$$

$$C = 1/A\exp[-E_a/(RT+\varepsilon)][(e_0)\cos(k_2L+k_3)]t \quad (3)$$

where: α_i – relative reactivity coefficient of test fuel e.g. in combustion process, L – energy supplied from environment to the system – e.g. combustion chamber where the test fuel is being burnt, L_0 – energy supplied from environment to the system – e.g. combustion chamber where the reference fuel is being burnt, T – temperature, ε – energy supplied to reaction zone, other than heat (RT) – in case of the process is catalytic one, e_0 – stream of the energy emitted by the solid's surface (catalyst), A, k_2, k_3 – constant quantities, t – time.

This relationship describes energy distribution between environment and the system, where observed chemical reaction takes place. Assuming the concept presented in paper [8], equation describing reactivity coefficient can be shown as an relationship of energy streams: energy stream supplied to the system, forcing the process, and energy stream C, supplied to the set of reagent molecules, initiating the chemical reaction.

$$\alpha_i = (E_S - E_{S0})/A \exp[-E_{as}/(RT/t + \varepsilon/t)]\, [(e_0)\cos(bE_S + d)] \quad (4)$$

$$C_S = A \exp[-E_{as}/(RT/t + \varepsilon/t)][(e_0)\cos(bE_S + d)] \quad (5)$$

where: Es, Es_0 – streams of energy supplied to reaction system, accordingly the one having tested reagent, and reference system (index 0) E_{as} – stream of reaction activation energy, T – average temperature of reaction system. According to this equation, energy stream determines the possibility of chemical reaction initiation. The values of these functions change with the change of initial state of the process.

The reactivity coefficient α_i relatively describes the effect of selected reagent on the rate of changes of reaction systems internal energy due to changes in stream of energy supplied to the system.

The aim of research presented in this paper was to see if this model could be used to describe combustion process.

4.1. Methodology of the preliminary verification of the model

The preliminary verification of the proposed model of combustion process was conducted using miniature jet engine, MiniJetRig stand.

The engine operates as reactor in which the combustion process can takes place at various conditions of engine operation. The reactivity coefficient can be determined experimentally by measuring the effect of change in initial energy state of the system on final state, being the result of combustion process.

The MiniJetRig enables temperature measurement in front of the turbine, at different points of combustion chamber, and behind the turbine, as well as fuel consumption, mass flow rate and rotation speed of turbine. The stand is equipped in analytical instruments, which measure the concentration of combustion products, i.e. CO_2, CO, C_xH_y, PM, and NO_x in exhaust gases.

The tests were conducted at the following rotational speed: 39 000, 70 000 and 88 000 rpm in accordance with the procedure developed in Air Force Institute of Technology. At each rotational speed the temperature T_2 and T_{eg} were measured, as well as mass flow rate mf.

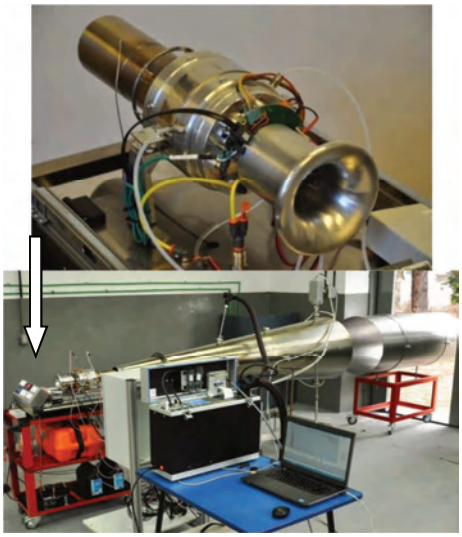


Fig. 1. MiniJetRig testing stand. Source [9]

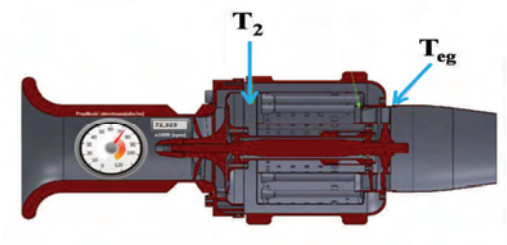


Fig. 2. The scheme of the engine used in verification of the proposed model [9]

The following fuels were tested during preliminary verification of the model:

– conventional mineral Jet A1 as reference fuel
– Blend No. 1 – the mixture of Jet A1 and the blend of synthetic, paraffinic hydrocarbons C15 and C17 added together to Jet A1 in concentration of 10% (V/V)
– Blend No. 2 – the mixture of Jet A1 and the blend of synthetic, paraffinic hydrocarbons C8 and C11 added together to Jet A1 in concentration of 10% (V/V)

The experimentally obtained tests results were used to calculate $\alpha_i = \alpha_{88/39}$ values for tested fuels.

The basic relationship (1), after integration within the limits of the initial and final state of the system gives dependence (6), which was used to calculate $\alpha_i = \alpha_{88/39}$ values for tested fuels.

$$\ln[F(y)_2/F(y)_1] = [1/\alpha_i]\ln[\Phi(y)_2/\Phi(y)_1] \quad (6)$$

where $y = b_{xx}$

$$F(y)_2 = b_{w88} - b_{j88} - b_{w70} + b_{j70} \quad (7)$$

$$F(y)_1 = b_{w70} - b_{j70} - b_{w39} + b_{j39} \quad (8)$$

$$\Phi(y)_2 = b_{w88} - b_{w70} \quad (9)$$

$$\Phi(y)_1 = b_{w70} - b_{w39} \quad (10)$$

It was assumed that:

a) $b_{wxx} = (T_{eg} - T_2)/[(mf)\ (rs)]_{wxx}$

T_{eg} – gas temperature behind the turbine; T_2 – gas temperature in front of the combustion chamber; mf – mass flow rate [g/s]; rs – average engine speed; index w – alternative fuel; index xx – rotational speed, eg. 88,000 rpm;

b) $b_{jxx} = (T_{eg} - T_2)/[(mf)\ (rs)]_{jxx}$

index j – Jet A1 fuel; other signs as above.

The hypothesis that proposed model can be used to describe the influence of different new components on fuels combustion in turbine engine will be verified when:

– values of experimentally determined α_i coefficients will be different for fuels containing different components
– difference between α_i values for fuels containing different components will correspond with experimentally determined difference between chosen results of combustion process, e.g. CO concentration in exhaust gases.

4.2. The results

The data obtained as the results of stand tests are shown in Table 1.

Table 1. The average results of tests on MiniJetRig

Fuel	rs	T_2	T_{eg}	mf
Jet A1	39.000	40.46	569.17	151.18
	70.000	70.30	532.88	220.71
	88.000	98.36	513.12	272.70
Blend No. 1	39.000	38.21	571.53	155.07
	70.000	68.57	527.74	224.88
	88.000	98.16	507.46	282.64
Blend No. 2	39.000	40.59	570.18	151.65
	70.000	68.89	531.19	221.31
	88.000	98.25	512.23	275.15

Basing on the above empirical data the reactivity coefficient $\alpha_{88/39}$ (α_i calculated basing on data for 88,000, 70,000, and 39,000 rpm) for each blend was calculated.

Table 2. Results of reactivity coefficient α_i calculation for two synthetic components

Blends No	Tested fuel	The value of reactivity coefficient $\alpha_{88/39}$
1	Jet A1 + synthetic hydrocarbons C15 and C17	0.241
2	Jet A1 + synthetic hydrocarbons C8 and C11	0.740

This model can further be used for determination the relationship between α_i and concentration of individual exhaust gas components. The results of CO measurements are shown in Table 3.

Table 3. The average results of measurements of CO concentration in exhaust gases

Fuel	rs	CO concentr. [ppm]	$CO_w^* - CO_j^{**}$
Jet A1	39.000	1476.98	–
	70.000	1742.60	–
	88.000	1323.81	–
Blend No.1	39.000	830.62	–646.36
	70.000	1044.53	–698.07
	88.000	513.58	–810.23
Blend No. 2	39.000	1478.85	1.87
	70.000	1716.05	–26.55
	88.000	1725.31	401.50

* CO concentration in exhaust gases in case the tested blends were used
** CO concentration in exhaust gases in case the reference Jet fuel was used

Then, for different engine speeds, the relationship between $\alpha_{88/39}$ and (CO_w – CO_j) was established. The results are shown in Fig. 3.

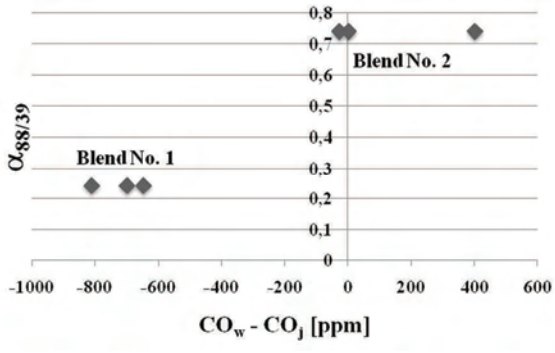


Fig. 3. The relationship between the reactivity coefficient $\alpha_{88/39}$ determined for alternative fuels: Blend 1 and 2 in the MiniJetRig engine, and the difference (CO_w – CO_j) measured at the engine speed of 39000, 70000 and 88000 rpm

5. Conclusions

The results shown above lets conclude that:

– values of experimentally determined $\alpha_{88/39}$ coefficients are different for fuels containing different components (Blend No. 1 and Blend No. 2)

– difference between $\alpha_{88/39}$ values for fuels containing different components correspond with experimentally determined difference between results of combustion process – (CO_w – CO_j).

These results confirm that the proposed model can be used to describe the relation between fuels properties and the results of combustion process.

This is of course a preliminary verification, which leads to further research on this model. Primarily much more fuels should be tested. Than the functional dependence between $\alpha_{88/39}$ and (CO_w – CO_j) should be formulated as well as dependences between $\alpha_{88/39}$ and concentration of other products of combustion (HC, PM, NO_x). On the other hand the $\alpha_{88/39}$ coefficient should be related to chosen physicochemical properties of the fuels.

Nomenclature

CI compression ignition
HCCI homogeneous charge compression ignition
R gas constant (R = 8.3144598(48) $J \cdot mol^{-1} \cdot K^{-1}$)

Bibliography

[1] MERKISZ, J. Ekologiczne problemy silników spalinowych. Tom I. *Wydawnictwo Politechniki Poznańskiej*. Poznań 1998.

[2] GATCHELL, M., ZETTERGREN, H. Knockout driven reactions in complex molecules and their clusters. *Journal of Physics B: Atomic, Molecular and Optical Physics*. 2016, **49**(16), 1-19.

[3] VANHPVE, G., PETIT, G., MINETTI, R. Experimental study of the kinetic interactions in the low-temperature autoignition of hydrocarbon binary mixtures and a surrogate fuel. *Combust. Flame*. 2006, **145** (3), 521-532.

[4] TANAKA, S., AYALA, F., KECK, J.C., HEYWOOD, J.B. Two-stage ignition in HCCI combustion and HCCI control by fuels and additives. *Combustion and Flame*. 2003, **132**, 219-239.

[5] MEEKS, E., ANDO, H., CHOUL, C.P. et al. New modeling approaches using detailed kinetics for advanced engines. *The Seventh International Conference on Modeling and Diagnostics for Advanced Engine Systems (COMODIA 2008)*, 2008, Sapporo, Japan.

[6] PITZ, W.J., CERNANSKY, N.P., DRYER, F.L. et al. Development of an experimental database and chemical kinetic models for surrogate gasoline fuels. *SAE Technical Paper*. 2007, 2007-01-0175.

[7] SAE International; Aerospace recommended practice ARP 1533C. Procedure for the analysis and evaluation of gaseous emission from aircraft engines.

[8] KAJDAS, C., KULCZYCKI, A., OZIMINA, D. A new concept of the mechanism of tribocatalytic reactions induced by mechanical forces. *Tribology International.* 2017, **107**, 144-151.

[9] GAWRON, B., BIAŁECKI, T. The laboratory test rig with miniature jet engine to research aviation fuels combustion process. *Journal of KONBiN*. 2015, **4**(36), 79-89.

Andrzej Kulczycki, DSc. – Air Force Institute of Technology.

e-mail: *Andrzej.Kulczycki@itwl.pl*



Article citation info:
STAWECKI, W., BAJERLEIN, M., DASZKIEWICZ, P. Modern high-resistance alloy steel used in railway transport. *Combustion Engines*. 2017, **171**(4), 250-254. DOI: 10.19206/CE-2017-442

Włodzimierz STAWECKI
Maciej BAJERLEIN
Paweł DASZKIEWICZ

CE-2017-442

Modern high-resistance alloy steel used in railway transport

The article presents an overview of modern steel used in rail transport. Directions for the development of materials, technologies and constructions used in the manufacture of rail vehicles are, on the one hand, determined by the technical and economic requirements of industry and, on the other, by the continued emphasis of environmentalists on reducing fuel consumption and CO_2 emissions. This generates innovation in the use of modern materials, processing methods and new design solutions and results in reduced vehicle weight. More bold forecasts today show that at the current pace of technology development, in the near future the mass of the vehicle will reduce by an average of 30%.

Observing the trends and pace of rail transport development, it can be predicted that existing restrictions on the use of modern materials, such as high prices, technological conditions and difficult automation of large-scale production, can be predicted.

Key words: *construction materials, constantly high strength, rail transport, new metals*

1. Introduction

Similarly to other modes of transport, railway is characterized with certain features that underlie its specificity. Due to the nature of the impact on the functioning and advancement of this mode of transport, its individual characteristics can be divided into stimulating and de-stimulating ones. Among the properties that positively influence this mode of transport we may include:

- capability of carriage of great mass of cargo at a time (both in terms of weight of a single load and the total weight of the entire train);
- capability of carriage of a high number of passengers at a time (long distance routes – depending on the class of the compartment – from 54 to 72 seats in a single car, regional trains up to approx. 280 seats in a multiple train set or even more in multiple sets);
- capability of carriage of goods and passengers on long distance routes;
- limited negative impact on the natural environment in terms of energy consumption and exhaust emissions [1].

In Poland, railway transport can be divided into three basic subsystems: inter-agglomeration, regional and in-agglomeration transit. It is assumed that the aim of the application of modern technologies in railway transport is to stop the current trend of reduced share of railway in the transport market and to lead to a sustainable development, i.e. ensuring maximum possible utilization of railway for carriage purposes, to which it is best designed.

The formation of self-government railway business entities, particularly the appearance of private companies on the market interested in providing transport services in railway regional passenger carriage is a symptom that this activity may turn out economically attractive and that it may thrive under the condition of stable, long-term financing of the initial deficit generated by this activity (Fig.1). The chances for development are the greatest in the area of agglomeration transport due to a competitive advantage over other modes of transport.

Following the analysis of the current condition of railway transport in Poland along with the SWOT analysis performed by the authors, it was observed that the most impactful decelerating factor is the degradation of infrastructure. The consequence of this degradation is low maximum speeds on the majority of the railway network. In many cases the speeds are much lower than the original speeds that were once applicable. There are also many speed limits on the routes. Both, the reduced maximum speeds and the introduced speed limits make the traveling times significantly extended compared to the shortest times obtained historically. The planned actions aim at a substantial improvement of the infrastructure and, as a consequence, boost the competitiveness of railway transport by increasing the cruising speeds (Fig. 2) and using modern steel as the fundamental building material of modern railway vehicles. The above will lay foundations for the development of new quality of transport of passengers and cargo.

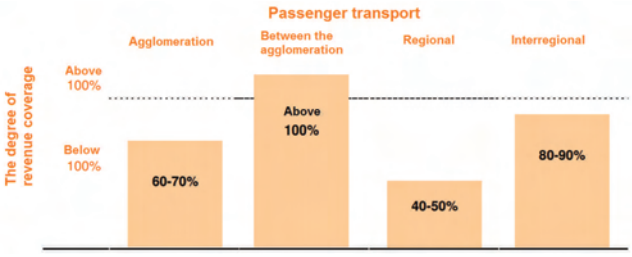


Fig. 1. Matrix of cost coverage with revenues in individual segments of the market of passenger carriage

2. Analysis of strength and plasticity of metal sheets

2.1. Regulations

The requirements of modern industry force a search for new building materials for production of metal sheets of high strength and good parameters in terms of technological plastification, allowing a reduction of the vehicle weight and rational energy consumption. A growing attention is drawn to low density alloys on the Aluminium (Al) and Magnesium (Mg) matrix and composite polymer plastics. The economic reasons and efficiency of recycling as well as the possibility of obtainment of a wide range of mechanical and technological properties result in metal sheets constituting over 65% of the vehicle weight.

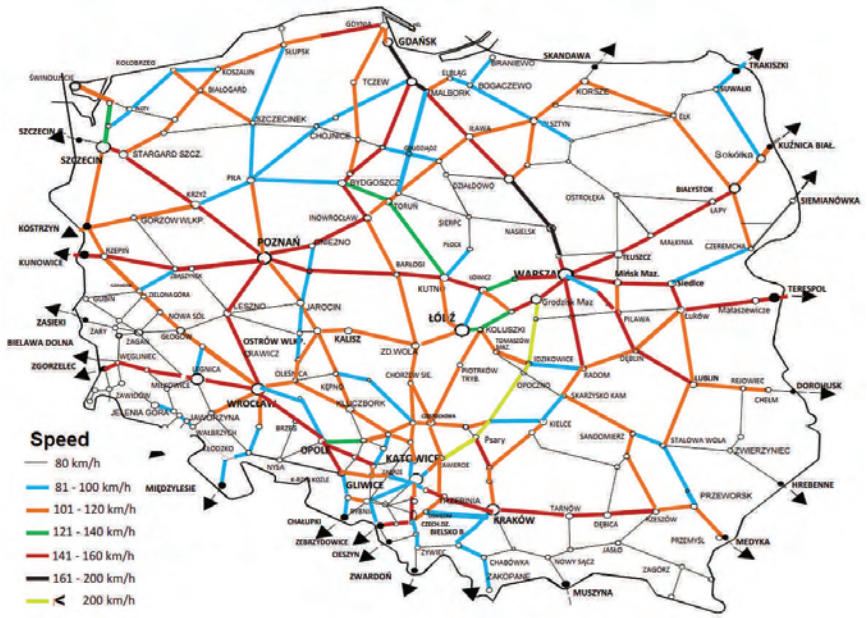


Fig. 2. Polish rail network and its maximum admissible speeds [3]

The last decade saw a rapid advancement in the development and production of modern steels used in transport for body and undercarriage components of railway vehicles. We may observe a dynamic development of high-strength types of steel that allow a reduction of the thickness of the applied steel metal sheets, hence the consumption of energy. Modern types of steel are characterized by multiphase microstructure that ensures a good balance between the strength properties and the plastic properties while the steel sheets are good in terms of technological plastification. In the further part of the paper, the authors analyze the principles of design of the chemical composition and microstructure of multiphase steels in the context of obtainment of the required mechanical and technological properties as well as final application of steel metal sheets in crucial load-bearing components of the tram bogies.

Currently, various types of deep drawn steel and HSLA steels are applied in the construction of railway vehicle bodies. The replacement of soft steels with steels of higher strength allows the application of thinner metal sheets. In fact, the weight of the railway carriages remains the same, as the reduction of mass resulting from the application of thinner high-strength metal sheets is compensated with additional equipment fitted to increase safety, comfort etc. A characteristic feature of conventional steels is the decreasing plasticity of sheets with the increasing strength (Fig. 3). An increase in the strength properties is relatively easy to obtain in a variety of ways: increased content of Carbon (C), increased hardenability by introducing alloy elements, solid solution strengthening, precipitation strengthening or deformation strengthening. The fundamental problem is to ensure the increased strength of metal sheets without a significant deterioration of plasticity. These requirements are met by modern types of high-strength DP, TRIP and CP steels of multiphase microstructure (Fig. 3). A significant contribution in the advancement of modern steel sheets for the industry was made by international projects, in which numerous steel industry companies participated. The optimization of the weight of the body and the undercarriage became possible thanks to a complex application of steel of a good combination of strength and technological plasticity, modern methods of element forming and innovative technologies of joining individual body components.

The response of the material designers to the demand of the industry was the development of new groups of steels of a wide range of strength and plasticity related properties (Fig. 3). According to the nomenclature, these steels have been divided into three groups: LSS (Low-Strength Steels), HSS (High-Strength Steels) – steels of the plasticity boundary between 210 and 550 MPa and tensile strength between 270 and 700 MPa, and UHSS (Ultra High-Strength Steels) [4].

Along with the increase in the share of the hard structural component, i.e. perlite, bainite, martensite, the strength properties increase and the plastic properties decrease (Fig. 3).

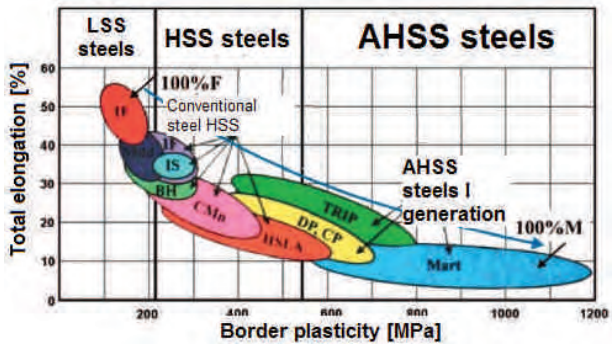


Fig. 3. Comparison of the mechanical properties of conventional HSS steels and modern AHSS steels used in transport [2]

A slightly higher plasticity (than that resulting from the parabolic trend line) have DP, CP and TRIP steels from the

group of AHSS (Advanced High Strength Steels) of the first generation. The AHSS steels are defined as multiphase steels of the tensile strength of Rm greater than 500 MPa and contain different shares of ferrite, bainite, martensite and residual austenite. They are marked as XX aaa/bbb, which denotes the type of steel and minimum Re and Rm values. For example, DP 350/600 denotes a dual phase steel of the minimum plastic boundary of 350 MPa and the tensile strength of 600 MPa. The interaction among the structural components of different properties is the reason for good results in deformation strengthening, which distinguishes the AHSS steels from conventional HSS steels. These steels have been briefly described below. Only modern types of high-strength multiphase steels (AHSS) will be subject to analysis.

Conventional deep drawn mild steels are the most frequently applied deep drawn steels in the automotive industry for a variety of body closing components. Depending on the carbon content (0.02–0.12%) they have different drawing class. Aside from impurities Sulphur (S) and Phosphorus (P) they contain only carbon and from 0.25 to 0.6% Manganese (Mn). They are most often made as cold rolled steels and annealed in top hat furnaces or are subject to lengthwise annealing. The obtained tensile strength range is from 270 to 400 MPa and the total extension – from 40 to 28%. The main parameters characterizing the drawability of steels are the coefficient of normal anisotropy r and the deformation strengthening exponent n [7, 8].

IF (Interstitial Free) steels. These steels contain a minimum amount of Carbon (C) and Nitrogen (N) internodal elements (~0.003%), silicon and approx. 0.02% Nb and/or 0.02% Ti that fully bond Nitrogen (N) and Carbon (C) in stable carbonitrides. From the analysis of Fig. 4, it results that they exhibit the highest plasticity out of all steels and extremely good deep drawability. Ultra low carbon and nitrogen content is obtained following a vacuum degasification. The mechanical properties of deep drawn steels (IF) are characterized by the effective plasticity boundary Rp0.2 from 140 to 220 MPa, tensile strength Rm from 230 to 300 MPa, extension A from 37 to 50% and the coefficient of normal anisotropy up to 2.4.

2.2. Analysis of conventional high-strength steels

HS-IF (High-Strength Interstitial Free) steels. These are IF type steels additionally solution-strengthened by an increased concentration of Phosphorus (P) (up to 0.03%), Boron (B) (up to 0.003%) and Manganese (Mn) up to 1.2%. Their tensile strength may reach 390 MPa. BH (Bake Hardenable) steels are siliconless steels, containing below 0.03% Carbon (C), 0.1–0.5% Manganese (Mn) and up to 0.02% Niobium (Nb), very often containing increased concentration (0.03%) of Phosphorus (P) resulting in an increased strength and coefficient of sheet normal anisotropy. Beside the strengthening during cold deformation, the vehicle components made from BH sheets (e.g. doors, trunk covers) are also strengthened during paint curing, usually taking place at the temperature of 170°C for 20 min, thus, boosting the plasticity and strength boundary by approx. 20–40 MPa. The idea behind this strengthening is the increase in the density of dislocation after the process of deep drawing and segregation of atoms of carbon in the paint-curing process. BH steel sheets are characterized by plasticity boundary Rp0.2 from 180 to 240 MPa, tensile strength Rm from 310 to 360 MPa, extension A from 42 to 36% and the coefficient of normal anisotropy of approx. 1.6. IS (Isotropic) steels have a chemical composition and mechanical properties that are similar to the HS-IF steel (Fig. 3). They are characterized by a ferritic microstructure and their coefficient of planar anisotropy is $\Delta r = 0$. This means that steel sheets exhibit isotropic properties during drawing, which allows an obtainment of a molding without the characteristic 'ears'. Carbon (C)–Manganese (Mn) steels are classic steels of mass usage of the ferritic-perlitic microstructure, usually containing below 0.1% Carbon (C) and up to 1.5% Manganese (Mn) [6, 8].

2.3. HSLA (high strength low alloy) steel analysis

HSL steels are steels originating from the Carbon (C)–Manganese (Mn) steels. They contain micro-additives of high affinity to carbon and nitrogen, i.e. of the content of Niobium (Nb), Titanium (Ti), Vanadium (V) below 0.1%. Metallic elements form dispersive particles of carbonitrides with Carbon (C) and Nitrogen (N) during hot plastic processing, precipitation-strengthening the steel and limiting the growth of austenitic grains during hot plate rolling, thus enabling the obtainment of fine-grained structure of the product.

Modern multiphase high-strength steels – the schematic presentation of the microstructure of modern types of multiphase high-strength steels has been shown in Fig. 4 that also presents the approximate range of extension and tensile strength, obtained by individual groups of steel. In reality, it is possible to obtain a very wide range of mechanical properties depending on the applied production technology, thermal processing parameters etc. Table 1 presents the chemical composition of typical multiphase steels.

DP (Dual Phase) steels – these are dual phase steels, in which small islands of martensite are evenly distributed in the ferrite matrix (Fig. 4) and the share of martensite is usually 15 to 30%. The content of carbon in the steel is 0.05 to 0.18%, silicon – from 0.1 to 0.6% and Manganese (Mn) – from 1 to 2%.

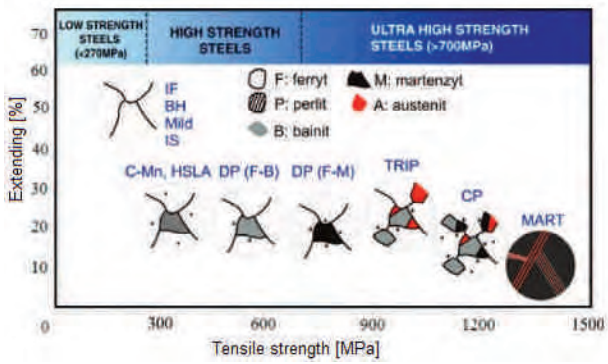


Fig. 4. Schematic presentation of the microstructure of different types of conventional and multiphase steels in transport [6]

Very often, in order to improve the hardenability, Chromium (Cr) and Molybdenum (Mo) are applied (1, 6, 7). The properties of dual phase steels depend on the share,

hardness and distribution of martensite as well as on the ferrite hardness and distribution of its grains. They behave like a composite material, in which ferrite constitutes the matrix guaranteeing good plastic properties while martensite is the component that increase the strength. The ferritic martensitic structure can be obtained either through thermal processing of steel sheets after cold rolling or through the application of controlled chilling immediately after completion of hot rolling. A characteristic feature of DP steels is the lack of a clear plasticity boundary (lower and upper) and the Lüders deformation on the extension curve. These features are particularly important for metal sheet subject to drawing as well as other operations of technological forming. In the final stage of the thermal processing of metal sheets a martensitic transformation occurs of austenite distributed in the form of islands in the ferrite. During the martensitic transformation, which causes an increase in the volume, around the martensite occurs an area of compressive stress and new dislocations are generated (Fig. 5). It is important that these dislocations are capable of moving at the initial stage of plastic deformation, which explains the lack of clear plasticity boundary. The presence of hard islands of martensite is decisive of a deformation strengthening in the steel at the initial stage of plastic deformation, which delays the initiation of the sample narrowing in the tensile trial and thinning of the sheets during drawing. As a result, DP steels are characterized with a good combination of strength and drawability and a low value of the Rp0.2/Rm quotient [5].

2.4. TRIP (transformation induced plasticity) steels

These are steels composed of the ferritic matrix, in which bainitic-austenitic islands are located. Typical TRIP steels contain 0.2% Carbon (C), 1.5% Manganese (Mn) and 1.5% Silicon (Si) (Table 1).

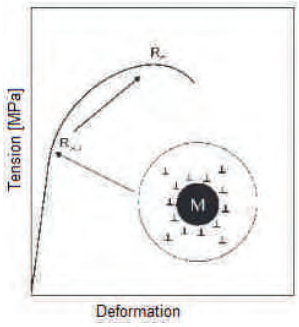


Fig. 5. Schematic presentation of the extension curve [5]

Such a combination of elements ensures the share of austenite on the level of 10 to 15%, provided that the thermal processing was properly carried out. The presence of silicon has fundamental importance, as it slows down the precipitation of carbides during strength of the steel sheets in terms of bainitic transformation. In this way, carbon is not 'consumed' by carbides, but enriches the austenite to the content enabling a reduction of the temperature of the start of the martensitic transformation Ms below the room temperature, and, consequently, stabilization of the residual austenite. Unfortunately, Silicon (Si) generates problems during metal sheet galvanization, because the compounds forming on the surface do not ensure appropriate wettability of the sheets by liquid zinc. For this reason, steels containing Aluminium (Al) and/or Phosphorus (P) (Table 1) are also developed, which has a positive effect on the carbide inhibition (Fig. 7).

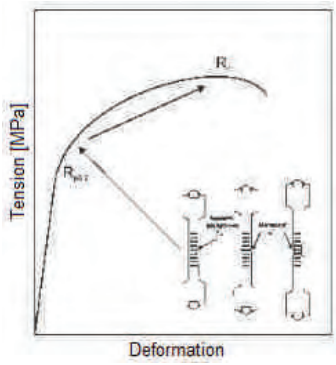


Fig. 6. Schematic presentation of the TRIP multiphase steel extension curve along with the schematics of deformation-induced martensitic transformation [5]

A characteristic feature of TRIP steels is the martensite transformation occurring during the sheet technological forming. The martensite transformation of residual austenite occurs gradually as the deformation increases. This transformation occurring in subsequent points of the molding prevents localization of the deformation and, at the same time, leads to heavy deformation strengthening (Fig. 6). This leads to a simultaneous increase of the Rm value and the delay of the initiation of the neck forming in the extension trial (and thinning of the sheet during drawing), thus leading to the obtainment of large even extension elongation evenly. A particularly beneficial combination of high-strength and plasticity is the main feature of multiphase TRIP steels [6, 7].

DP (F-B) (Ferritic-Bainitic) steels – these are dual phase steels containing bainitic islands instead of martensite (Fig. 2.2). A smaller difference in the hardness among the structural components, compared to the DP (F-M) steels, makes them particularly good for forming of the sheet edges and flanges and ensures good fatigue strength.

CP (Complex Phase) steels – these are steels containing fine-grained ferrite, bainite, martensite and residual austenite (Fig. 2.2). They are usually hot-rolled and additionally strengthened by dispersive particles of Niobium (Nb) and Titanium (Ti). The increase in the steel hardenability is ensured by additions of Chromium (Cr) and Molybdenum (Mo) (Table 1). They exhibit particularly good energy absorption properties under dynamic loads.

HF (Hot-Formed) steels these are usually low-cost steels of the composition corresponding to 22MnB5 (Table 1). They are best for hot drawing of components of complicated shapes (B pillar, bumpers) and then press tempering. In the said processes a very good deformability of austenite is used, and the ready component has the properties corresponding to those of steel of tempered martensite. The components are protected against oxidation by Aluminium (Al) – Silicon (Si) layers.

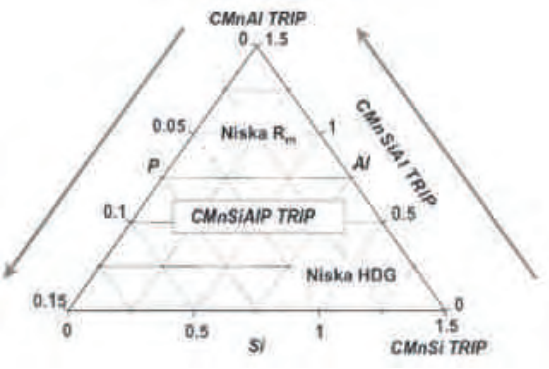


Fig. 7. The influence of the alloy elements on selected microstructural features and mechanical and technological properties of multiphase steels [6]

Table 1.Chemical composition of typical multiphase steels

Type of steel	C	Mn	Si	Al	Mo	Cr	Other
DP1 (F-M)	0,10	1,50	0,10	-	-	0,8	-
DP2 (F-M)	0,10	1,50	0,25	-	0,15	-	0,1 Ti, B
TRIP1	0,20	1,50	1,50	-	-	-	-
TRIP2	0,24	1,50	0,25	1,50	0,15	-	-
DP3 (F-B)	0,07	0,80	0,50	-	-	-	0,03 Nb
CP	0,15	1,50	0,25	-	0,20	0,30	Ti, Nb, B
HF	0,22	1,25	0,20	-	-	-	0,003 B
MART	0,05-0,2	1,50	0,20	-	-	-	-

MART (Martensitic) steels – These are steels of the microstructure of martensite, sometimes containing a small share of bainite and/or residual austenite (Fig. 7). They are characterized by the best strength properties that mainly depend on the carbon content in the steel. Due to the extension lower than 10%, their plastic deformation is possible only when rolled.

3. Conclusions

The development trends in material technologies and designs applied in the production of railway vehicles are determined by the technical and economic requirements imposed by the industry as well as a continuous pressure of environmentalists regarding the reduction of fuel consumption and the emissions of CO_2. This spurs innovativeness in the application of modern materials, methods of their processing and in novel design solutions and reduces the weight of the vehicles. More daring forecasts hail that, at the current technology advancement rate, in the nearest future the weight of a vehicle will be reduced by 30 % on average.

A very important aspect in the process of design and application of modern materials is the system of recycling of used vehicles. The manufactures of the rolling stock when designing their vehicles must allow for the need to recycle the vehicle at the end of its life cycle. This is observed through the application of recyclable materials, marking of the materials and proper material combinations (the latter will facilitate its later dismantling and segregation of material fractions). By doing so, the rolling stock recyclability index may reach up to 95%, similarly to on-road vehicles. The actual recyclability index will depend on many factors such as the existing infrastructure of material recycling facilities, availability of recycling technologies (particularly modern materials), demand for recycled materials and parts for reuse, legislation imposed on business entities with a view to obtaining certain recyclability levels as well as the expectations and environment related policy of the rolling stock operators [2].

When observing the trends and the advancement of the railway transport, we may fore-cast that there still exist limitations as to the application of modern materials (high price, technological specificity, difficult automation of serial production). Looking at the automotive market, however, it appears these limitations are soon to be overcome.

Bibliography

[1] HOLTZER, M. Procesy metalurgiczne i odlewnicze stopów żelaza., *Wydawnictwo Naukowe PWN*. Warszawa 2013.
[2] KORZYŃSKI, M. Nonconventional finishing technologies. *Wydawnictwo Naukowe PWN*. Warszawa 2013.
[3] LIPIŃSKI, T., WACH, A. The effect of fine non-metallic inclusions on the fatigue strength of structural steel. *Archives of metallurgy and materials*. 2015, **60**(1).
[4] MERKISZ-GURANOWSKA, A., DASZKIEWICZ, P., MERKISZ, J. et al. Zrównoważona polityka odzysku materiałów z taboru kolejowego wycofanego z eksploatacji. *Najnowsze technologie w transporcie szynowym*. Józefów 2014.
[5] PIETRZAK, K., PIETRZAK, O. Ekonomiczne i organizacyjne aspekty transportu kolejowego. Bydgoszcz 2013.
[6]. ROGAL, Ł., KORPAŁA, G., DUTKIEWICZ, J. Evolution of microstructure in 100Cr6 steel after cooling from a thixoforming temperature to bainitic transformation ranges. *Materials science and engineering a-structural materials properties microstructure and processing*. 2015, **624**.
[7] Master plan dla transportu kolejowego w Polsce do 2030 roku. *Ministerstwo Nauki i Szkolnictwa Wyższego*.

Włodzimierz Stawecki, Ph.D. – Managing Director of the Rail Vehicles Institute TABOR in Poznan.

e-mail: *Sekretariat@tabor.com.pl*



Pawel Daszkiewicz, DEng. – Rail Vehicles Institute "TABOR" in Poznan.

e-mail: *P.Daszkiewicz@tabor.com.pl*



Maciej Bajerlein, DSc., DEng. – Faculty of Machines and Transport at Poznan University of Technology.

e-mail: *Maciej.Bajerlein@put.poznan.pl*



Article citation info:
AMBROSEWICZ-WALACIK, M., TAŃSKA, M., WALACIK, M., NITKIEWICZ, S. Production of fuel blends from diesel oil and waste products. *Combustion Engines*. 2017, **171**(4), 255-258. DOI: 10.19206/CE-2017-443

Marta AMBROSEWICZ-WALACIK
Małgorzata TAŃSKA
Marek WALACIK
Szymon NITKIEWICZ

CE-2017-443

Production of fuel blends from diesel oil and waste products

The aim of the study was to evaluate the physico-chemical parameters of the fuel blends consist of a diesel oil and waste products, such as a pyrolytic oil from car tires and a frying oil. The samples were characterized by the kinematic viscosity at 40°C, density at 15°C, acid value, sulphur content, temperature of flash point and temperature of cold filter plugging point. The obtained results indicated that the fraction of the pyrolysis oil due to the very low temperature of flash-point and high sulphur content is a difficult material to use in the biofuels sector. While the sulphur content of that material may be reduced by the desulphurisation, whereas the increasing temperature of flash point, which greatly influenced the low value of this parameter for the mixture, is problematic. What is more, a high degree of oxidation of the frying oil determined too low stability of the produced methyl esters, and thus the fuel blends.

Key words: *fuel blends, diesel oil, pyrolytic oil, frying oil, transestrification, physico-chemical properties*

1. Introduction

The main hydrocarbon deposits (petroleum, natural gas) in Poland are located in Podkarpacie, Wielkopolska, in Lubuskie region and in Pomorze [1]. One of the main leaders of the exploration and production of petroleum on land is the Polskie Górnictwo Naftowe i Gazownictwo (PGNiG). The mining oscillates at the level of 1.2 million tons of the petroleum per year, which covers only a few percent of the annual demand. In turn, the main leader in the production of petroleum in the Baltic Sea leads the Lotus Group, which has in its possession two deposits of production, allowing to mined 7 000 barrels of the crude oil per day. Mateusz Cabak, an employee of the Lotos company, reported that the Polish sea hidden beneath about 30 million tons of the crude oil, and therefore the search for this product are continued. According to "The balance of mineral deposits in Poland as of 31.12.2015" prepared by the Polish Geological Institute – Polish Research Institute, it was stated that the amount of mined resources in Poland is 139.84 billion cubic meters for natural gas; 23.22 million tons for crude petroleum; 27.04 billion tons for lignite and 59.79 bilions tons for coal. It was estimated that crude oil production covers only 3.5 percent of the national demand, while production of natural gas 1/3. Only the mining of lignite and coal covers the annual Polish demand. However, as it is well known the conventional energy resources are non-renewable, and their resources will be depleted [2]. In the same time, the share of renewables will increase almost twice in comparison to 2010, and it will be equal to those of the nuclear power and petroleum. As GUS report presented, in 2014 the usage of electricity on 1 inhabitant was the highest in the Silesian Voivodeship (5 579.9 kWh), and the lowest in Podlaskie (2 367.61 kWh) [3]. The equivalent use of raw materials such as a rapeseed, soybean or sunflower for consumption and fuel purposes and a lack of the satisfactory programs to support the production of biofuels affect the doubtful profitability of the production. However, the quantitative targets "3 x 20%" established for 2020 by the European Union, which impose, among others, the increase of the use of the renewable energy sources to 20% of the total energy consumption in the EU, including their use in transport to 10%, oblige the members to continuously increase the share of bio- components in conventional fuels. Among the main objectives of the energy policy concerning the use of renewable energy sources are: an increase the share of renewable energy sources in the final energy consumption to at least 15% in 2020 and further growth in the coming years; a gradually increase of biofuels share in the transport fuel market up to 10% in 2020 and a reduction of usage of first generation biofuels; an increase the degree of diversification of supply sources and the creation of appropriate conditions for the development of locally available raw materials. In terms of the use of biomass the attention is primarily turned to the use of more efficient energy solutions, for example, an usage of different methods of gassing and processing into liquid fuels, with particular focus on the second generation biofuels. Currently, the increased interest in the use of waste materials can also be observed. Due to the economic and ecological reasons, it seems to be reasonable to use residual fats and oils. However, the application of these raw materials is associated with prior processes of oil purification, which are sometimes complex and expensive [4]. However, despite the low price encouraging their use, they are a "difficult" raw material for the biodiesel production. Namely, waste vegetable and animal fats are characterised by the increased content of free fatty acids, water, solid contaminants, phosphorus compounds and polymers, which impede and sometimes prevent the transesterification process [5]. Moreover, the main problem of the use of these materials is related to a lack of an appropriate legislation to support their collection from catering establishments, which amount, in 2014, was estimated at 65 509, including 16 473 restaurants, 23 634 bars, canteens 4014 and eateries 21 761 [3,6]. From an ecological point of view, use of the other waste materials, or plastic solid waste (PSW) and waste tyres also seems an important issue [7]. The last group includes pyrolysis, which is defined as controlled burning or heating (400–700°C) of a material in the absence of oxygen. Organic components of a raw material are decomposed, generating liquid and gaseous products that can be used as fuels, while

inorganic ingredients remain practically unaltered and free of binding organic matter [8, 9]. A similar composition of pyrolytic oil and petroleum indicates the possibility of application of these materials in the production of alternative fuels; therefore, technologies for processing waste tyres are constantly being improved [10]. In 2016 in Poland, 47 of the of waste incinerators were reported. These places may contribute to the recovery of the valuable products, including fuel. Due to the above the aim of presented work was to determine the possibility of use a ternary mixture as a power source for diesel engines.

2. Material and analitical methods

The research materials were 3 different samples: a diesel fuel purchased on the commercial fuel stations in 2016, in Olsztyn; a pyrolysis oil sample, that was collected from a private investor and a waste oil obtained from regional point of catering. In the first stage of an experimental part the pyrolytic oil and waste frying oil had to be properly prepared for later use. In the case of the pyrolytic oil the distillation process was used to obtain a medium fraction of naphta, which served as one of a component of fuel mixture. Firstly, the sample was heated to 160°C whereby the light fraction of naphta was separated (2%). Then the temperature was gradually increased to approx. 204°C, what allowed to isolate approx. 49% of medium fraction. In turn, the frying oil was analysed in terms of the hydrolysis degree (acid value by PN-EN14104:2004P, %FFA share of free fatty acids), oxidation degree (peroxide value according to PN-EN ISO 3960:2012P) and fatty acid composition (PN-EN ISO 12966-4:2015-07E') (Table 1). The results of the analysis led to the conclusion that the appropriate transesterification method will be the acid-base reaction. The above decision was related to the high acid value (7.24 mg KOH/g).

Table 1. Characterization of the frying oil

Distriminats	Frying oil
Acid value (mg KOH/g)	7.24
% FFA	3.62
Peroxide value (mEq O_2/kg oil)	12.07
Composition of fatty acids (%)	
– myristic $C_{14:0}$	0.15
– palmitic $C_{16:0}$	7.57
– palmitoleic $C_{16:1}$	0.21
– stearic $C_{18:0}$	3.26
– oleic $C_{18:1}$	76.86
– linoleic $C_{18:2}$	7.78
– linolenic $C_{18:3}$	0.48
– arachidic $C_{20:0}$	0.88
– eicosenoic $C_{20:1}$	1.88
– behenic $C_{22:0}$	0.27
	0.86

Description of the transestrification proces

In the first stage of the transestrification to 200 g of a heated oil (up to 60°C) 224 ml of a methanol and 2% of H_2SO_4 (v/v) were added. The reaction was at 60°C during 1.5 h. After the reaction the mixture was subjected to the sedimentation for 24 h, in order to obtained the upper ester phase. Then the separated phase was poured into glass flasks and the second stage of transesterification was carried out – 0.5% of a potassium hydroxide was dissolved in 27.0 ml of a methanol and then added to ester phase. The reaction was carried out at 60°C for 0.5 h. The ester phase after the second stage of the reaction was isolated as described above. The yield of the ester production was determined with using the thin liquid chromatography (TLC) technique (85.29%) (Fig. 1).



Fig. 1. TLC chromatogram of esters obtained by the double base-acid transesterification

After preparing the components of the mixture, each of them has been analysed in terms of a kinematic viscosity at 40°C (ISO 3104), density at 15°C (ISO 12185), temperature of flash point (PN-EN ISO 3679), temperature of cold filter plugging point (EN 116), sulphur content (EN ISO 20884) and oxidation stability (ISO 14112) (Table 2).

Table 2. Characteristics of the prepared raw materials

Discriminants	Fraction of pyrolytic oil	Esters of frying oil	Diesel oil
Viscosity at 40 °C (mm^2/s)	1.05	3.63	3.05
Density at 15 °C (kg/m^3)	870	878	835
Flash point (°C)	12	194	56
Cold filter plugging point (°C)	< –30	–1	–18
Acid value (mg KOH/g)	3.56	0.04	0.049
Sulphur content (%)	1.22	0.004	0.005
Oxidative stability (h)	> 20	1.44	20.63

Analysing the results of the study it was found that in case of the methyl esters derived from the frying oil, most quality parameters met the requirements of PN EN 14214+A1:2014-04. An exception was only the oxidation stability, which the minimum limit has been increased from 6 to 8 h. What is more, taking into account the yield of the methyl esters production it was found that 85.29% is not enough satisfying result. The sample of the diesel oil did not show any irregularities. One the other hand, most of the determined parameters for the medium fraction of naphta did not meet requirements of the quality standards for the diesel fuel and methyl esters. Noteworthy were especially too low the temperature of flash point, that determine the safety use of the fuel samples, as well as an increased the free fatty acids content and sulphur content. The presented results indicating, that the analysed medium fraction of naphta should not be used as an individual fuel, however it is believed that it can be use as one of the minor components of the fuel mixtures.

After conducting the physico-chemical characteristics of the prepared components 4 fuel mixtures were prepared, in proportions presented in Table 3.

Table 3. Composition of the fuel blends (% v/v)

Fuels blends	Fraction of pyrolytic oil	Esters of frying oil	Diesel oil
FB_1	1.0	49.5	49.5
FB_2	1.0	69.0	39.0
FB_3	2.0	49.0	49.0
FB_4	2.0	60.0	39.0

3. Results and discusion

It was found that almost all of the analysed physico-chemical parameters for the fuel blends, except for the viscosity, density, temperature of cold filter plugging, did not meet requirements of the European Union standards.

Duo to too low value of the temperature of flash point, it would not be possible to direct these samples for the general use. Despite the high share of the frying oil methyl esters (flash point – 190°C) and diesel oil (flash point – 56°C), the addition of even a small amount of pyrolytic fraction significant decreased the value of that parameter (Table 4). It is believed that it was related to the volatile compounds of the medium fraction of the pyrolytic car oil.

The value of the cold filter plugging point can be considered as acceptable (the lowest one –5°C for FB_3 sample and the highest one –2°C for both FB_1 and FB_2 samples), when spring and summer periods are concerned. It is believed that high share of saturated acid in frying oil has important effect of high temperature of that parameter. Muniyappa et al. (1996), found that that methyl esters from a beef tallow oil were characterized by the high cold point, what was involved with high concentration of saturated fatty acid methyl esters [11]. Mittelbach and Remschmidt (2004), Wang et al. (2012) and Chuah et al. (2016) explained that during biodiesel cooling, the first fraction to precipitate is the stearic and palmitic methyl esters [12–14]. What is more, these components constitute a substantial share of the material that are recovered from the clogged biodiesel fuel filters.

The next unacceptable parameter of the analysed fuel blends was sulphur content. As PN EN 14214+A1:2014-04 and PN-EN 590: 2013-12 standards determine the highest acceptable sulphur content is 10 ppm. The analysed fuel blends were characterized by the 6-fold (FB_1 and FB_2 samples) and 12-fold (FB_3 and FB_4 samples) higher content of that compound (Table 4). Bocheński and Bocheńska (2005) reported that the sulphur contained in the fuel products has a significant impact on its corrosive action, but also on the lubricity of the fuel and the formation of sulphur oxides [15]. Olesiak and Stępień (2008) found that the reduced amount of sulphur and aromatic hydrocarbons in fuels has a positive effect from the ecological point of view, however these compounds are characterized by the good anti-wear properties, and their removal has significant effect on the deterioration of lubricity of fuel, what is also results in the deterioration of the engine work [16].

Table 4. Characteristics of the prepared fuel blends

Discriminants	Fuels blends			
	FB_1	FB_2	FB_3	FB_4
Viscosity at 40 °C (mm^2/s)	3.30	3.38	2.93	3.21
Density at 15 °C (kg/m^3)	853	848	849	852
Flash point (°C)	37	36	31	29
Cold filter plugging point (°C)	–2	–2	–5	–4
Sulphur content (ppm)	61.0	63.1	122.9	121.9
Oxidative stability (h)	3.23	1.73	3.43	2.23

The oxidative stability of the fuel blends was determined by a low stability of the frying oil methyl esters (1.44 h, Table 2). The value of that parameter ranged from 1.73 h for FB_2 sample to 3.43 h for FB_3 sample (Table 4). The higher share of the frying oil esters, the lower resistance to oxidation (Table 3, 4). The degradation of the diesel fuels is generally due to the oxidation. The main signs of the oxidative stability decrease are an increased acid value and viscosity, as well as the formation of gums and sediments. The first stage of the oxidation process is associated with the hydroperoxides formation. That reaction is caused by the addition of an oxygen molecule to a carbon atom adjacent to a C=C double bond. During the oxidation process the peroxides break away to form aldehydes and short-chain acids. Free radicals can be also generated by peroxides. These newly formed compounds promote the polymerization and crosslinking among the olefinic molecules [17]. As the cited authors found the oxidation reactivity is in an inverse correlation with the degree of C=C bonds in the fuel. Jakóbiec and Ambrozik (2008) found that the main external factors influenced the oxidative stability of motor fuels, including the vegetable oil methyl esters, are an increasing temperature, presence of air, light, oxygen and metals that catalyse the oxidation process. In turn, the internal factors determining the susceptibility to oxidation are related to the chemical composition and quality of raw material, as well as the conditions of the transesterification [18].

4. Conclusions

The prepared fuel blends met 3 from 6 of the requirements for analysed parameters. Among them the viscosity, density and temperature of cold filter plugging point should be listed. It is worth to mention, that even 1% addition of the medium fraction of naphta, distilled from the pyrolytic car oil, characterized by a very low temperature of flash point caused the significant decrease of that parameter values for the fuel blends. What is more, stated in the presented work a high sulphur content in the naphta sample had an influence on the increased amount of that compound in the composed blends, significantly exceeding permissible level (10 ppm). Therefore, it is believed the desulfurization process of the pyrolytic oil would be needed to reduce increased sulphur content. On the other hand, noticed for the frying oil methyl esters a low oxidative stability determined an unacceptable value of that parameter for analysed ternary samples. For that reason, it is found that the produced methyl esters of the frying oil were not a suitable raw material for the biofuels production, because of the high share of easily oxidising fatty acids and high value of the peroxide value.

Bibliography

[1] CEBULA, P. Samowystarczalność energetyczna Polski. *Nowy Dziennik – Polish Daily News*. www.dziennik.com/publicystyka/artykul/samowystarczalnosc-energetyczna-polski (publ. 25.08. 2016) (accessed 10.01.2017).

[2] BARTOSIK, M., KAMRAT, W., KAŹMIERKOWSKI, M. et al. Bezpieczeństwo elektroenergetyczne pokoleń. *Przegląd Elektrotechniczny*. 2016, **92**(8), 268-282.

[3] GUS 2015. Główny Urząd Statystyczny 2015. *Mały rocznik statystyczny Polski*. 2015, 175.

[4] KARMAKAR, A., KARMAKAR, S., MUKHERJEE, S. Properties of various plants and animals feedstocks for biodiesel production. *Bioresour. Technol.* 2010, **101**(19), 201-210.

[5] TAŃSKA, M., ROTKIEWICZ, D., BĄC□EK, N. Adsorpcyjne oczyszczanie tłuszczów posmaż□i□zy□h przeznaczonych do produkcji biodiesla. *Przyroda Nauka Technologie*. 2012, **6**, 1-11.

[6] KUPCZYK, A., MANTEUFFEL, W., RUCIŃSKI, D., WIŚ□IEWSKI, G. Analiza rynku paliw płynnych pochodzenia roślinnego do celów energetycznych. 2008, IEO na zlecenie EC Rzeszów.

[7] LUO, G., SUTO, T., YASU, S., KATO, K. Catalytic degradation of high density polyethylene and polypropylene into liquid fuel in a powder-particle fluidized bed. *Polymer Degradation and Stability*. 2007, **70**(1), 97-102.

[8] PANDA, A.K., SINGH, R.K., MISHRA, D.K. Renewable and Sustainable Energy Review.

[9] ADRADOS, A., DE MARCO, I., CABALLERO, A. et al. Pyrolysis of plastic packaging waste: a comparison of plastic residuals from material recovery facilities with simulated plastic waste. *Waste Manage*. 2012, **32**(5), 826-832.

[10] SUROVKA, D., PERTILE, E., LORENZ, T. et al. Potencjalny odzysk energii z produktów pirolitycznej obróbki odpadów. I□ynieria *Mineralna*. 2012, **13**(2), 43-48.

[11] MUNIYAPPA, P.R., BRAMMER, S.C., NOUREDDINI, H. Improved conversion of plant oils and animal fats into biodiesel and co-product. *Bioresour. Technol.* 1996, **56**(1), 19-24.

[12] MITTELBACH, M., REMSCHMIDT, C. Biodiesel: *The Comprehensive Handbook Boersedruck GmbH*. 2004, Vienna, Austria.

[13] WANG, L.B., YU, H.Y., HE, X.H., LIU, R.Y. Influence of fatty acid composition of woody biodiesel plants on the fuel properties. *J. Fuel Chem. Technol.* 2012, **40**(4), 397-404.

[14] CHUAH, L.F., YUSUP, S. AZIZ, A.R.A. et al. Influence of fatty acid content in non-edible oil for biodiesel properties. *Clean Technol. Environ. Policy*. 2016, **18**(2), 473-482.

[15] BOCHEŃSKI, C.J., BOCHEŃSKA, A. Badania mieszaniny oleju napędowego z estrami metylowymi oleju rzepakowego. *MOTROL*. 2005, **7**, 24-34.

[16] OLESIAK, S., STĘPIEŃ, Z. Zagadnienia smarności ciekłych paliw silnikowych. *Czasopismo Techniczne Mechanika*. 2008, **105**(7), 251-263.

[17] TANG, H., SALLEY, S.O., NG, K.Y.S. Michigan Ohio University Transportation Center Subtitle: Improved oxidative stability of biodiesel fuels: antioxidant research and development. Report No: MIOH UTC AF4p2-5 2011-Final MDOT Report No: RC1545, 2011, 1-46.

[18] JAKÓBIEC, J., AMBROZIK, A. Wybrane właściwości fizykochemiczne i użytkowe estrów metylowych kwasów tłuszczowych oleju rzepakowego jako paliwa silnikowego. *Inżynieria Rolnicza*. 2008, 9(107), 107-115.

Marta Ambrosewicz-Walacik, DEng. – Faculty of the Technical Sciences, University of Warmia and Mazury in Olsztyn.

e-mail: *Marta.Ambrosewicz@uwm.edu.pl*



Marek Walacik, DEng. – Faculty of Geodesy, Geospatial and Civil Engineering, University of Warmia and Mazury in Olsztyn.

e-mail: *Marek.Walacik@uwm.edu.pl*



Małgorzata Tańska, DEng. – Faculty of Food Sciences, University of Warmia and Mazury in Olsztyn.

e-mail: *M.Tanska@uwm.edu.pl*



Szymon Nitkiewicz, MSc. – Faculty of the Technical Sciences, University of Warmia and Mazury in Olsztyn.

e-mail: *Szymon.Nitkiewicz@uwm.edu.pl*



Article citation info:
BOROWCZYK, T., SPADŁO, M. The issues of designing of construction features of the internal combustion cam engine. *Combustion Engines*. 2017, **171**(4), 259-264. DOI: 10.19206/CE-2017-444

Tomasz BOROWCZYK
Mikołaj SPADŁO

CE-2017-444

The issues of designing of construction features of the internal combustion cam engine

On the pages of the article described cam-piston mechanism developed as an alternative to piston crank mechanism. The main feature of this mechanism is that the piston is dwell in the TDC by the 30°CA and thus allows combustion of the fuel in constant volume. Authors presented the process of designing an analytical cam. The starting point for the calculation was the displacement of piston graph and the limits of acceleration and velocity values obtained. The results of strength calculations of the cam with regard to fatigue problems are also presented. Calculations were carried out in order to reduce the weight of the cam. For this purpose, the Finite Element Method was used.

Key words: *cam engine, analitical cam, dynamic analysis, fatigue strength, finite element method*

1. Introduction

The most common form of conversion of piston displacement to rotary motion is the crank-piston mechanism (CrPM).

This mechanism has several advantages: compact design, low number of components, low complexity, high durability in heavy load. The schematic diagram of the crank-piston mechanism used in internal combustion engines (ICE) is shown in Fig. 1.

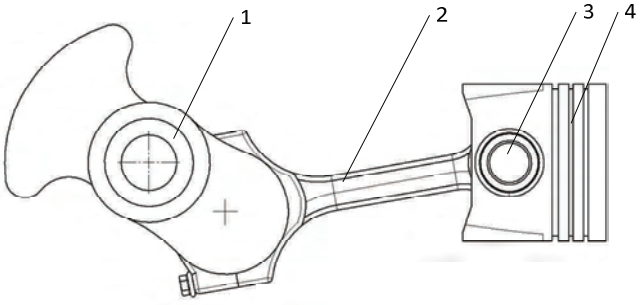


Fig. 1. Crank-piston mechanism: 1 – crankshaft, 2 – connecting rod, 3 – piston pin, 4 – piston

In the discussed mechanism the displacement of the piston $x(\varphi)$ realizes the motion according to the relation (1):

$$x(\varphi) = R\left[(1-\cos\varphi) + \frac{\lambda}{4}(1-\cos 2\varphi)\right] \quad (1)$$

were: R – crank radius, φ – crank angle, l – connecting rod length, $\lambda = \frac{l}{R}$

From the above equation it follows that the displacement is related to trigonometric relationships with the geometric parameters of the system. Because the feature of trigonometric functions (sin and cos) is their continuity and variability, the course of the piston's movement is even and smooth. In addition, this feature also applies to derivatives of displacement: velocity and acceleration. Movement of a mechanism with such characteristics, which is advantageous for mechanical reasons, is less adapted to other phenomena occurring in ICE. This is referred inter alia to: cylinder filling, compression, exhaust, camshaft and valve cooperation, and most in relation to the combustion phenomena. Therfore, in the last few years, it has been noted that scientists and engineers have been pushing for changes to the existing CrPM or to change at the ideological level. One of the proposed methods is to use a cam-piston mechanism (CPM). The drawing of this mechanism is shown in the Fig. 2.

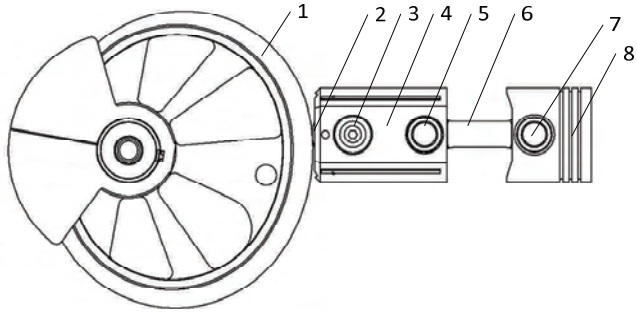


Fig. 2. Cam-piston mechanism (desctiption in the text)

In these systems, a drive cam (1) cooperates with the roller-bearing (2) mounted on a pin (3) which is associated with the piston rod (4) connected to the piston (8) by means of the connector (6) with has two more pins (5), (7). Historically one of the first uses of the CPM was Daniela's 1906 cam engine [1]. The feature of the CPM is the lack of a clear connection between the cam and the roller bearings. Therefore, an additional structural design should be used in the CPM to enable the reciprocating motion of the piston rod assembly with the cam. In ICE, this may be an element that co-operates with a recess in the lateral face of the cam or in a multi-cylinder engine, a stabilizing mechanism (for example, in the Fairchild-Caminez airplane engine [2]). From a mechanical point of view, the complexity of CPM is greater than CrPM. However, considering that the displacement of the piston is due to the outline of the cam, it can be adapted, for example, to duration of the combustion process or to the limit heat flux by the cylinder wall. Many theoretical papers have been produced in this subject, eg [3–5]. Optimizing methods are used to determine the curvature of the cam, usually by selecting the appropriate weight for the phenomena described by mathematical formulas. In addition, aspects related to the kinetics and dynamics of the

piston movement, as well as the strength aspects, are taken into account. This subject is described in this article. However, a discussion of the outline was adopted, which was not determined only by the limitations of thermodynamic nature. It was assumed that the piston in the TDC should be stopped by a certain angle of rotation of the cam. Below is a description of the outline and the strength aspects of the adopted cam.

2. Determining the outline of the cam

There are many methods of determining the outline of the cam, with detailed description in the literature of the subject eg. [6–8]. The issue can be solved directly by proposing a cam profile defined eg by arcs, and then calculating the displacement, velocity, and acceleration. In addition, using the Mulitibody Dynamics method, the outline process can be automated using a feedback loop that returns specific geometric parameters of the curves (such as radii and arc lengths). By using the directly method, it may be that the search for the optimum is time consuming and often also limited.

The second way is to solve the inverse problem, ie with the assumed movement, speed and acceleration, determine the outline of the cam. In this way, the so-called *Analytical Cam*. If the displacement of the cam is related to the angle of rotation (the most common case) the result of the outline is obtained in polar variables. In practice, often used ready-made functions representing a particular type of movement. For example, it may be harmonic or cycloidal motion. Note that harmonic or cycloidal motion describes the trigonometric relationships, and thus (as mentioned above) make the motion smooth and even. Algebraic and diagrammatic representation of these types of motion are shown in Fig. 3.

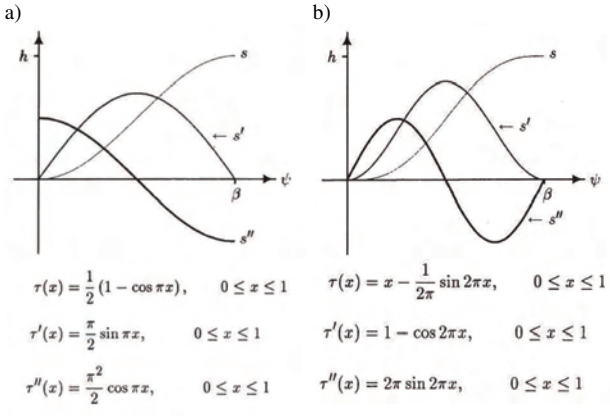


Fig. 3. Displacement, velocity and acceleration in: a) harmonic, b) cycloidal motion [8]

Notice that the displacement in harmonic motion is proportional to the cosine function and in the cycloidal motion to the sinus function. The sinus function (with the changed sign) is a derivative of the cosine function. In other words, it is also known that if at the point the system has continuous derivatives (eg first and second derivatives), that is, they take the same value, the increment of a given quantity takes place more evenly. This relationship can be seen clearly when comparing the harmonic and cycloid velocity graph near the origin of the coordinate system (Fig. 2a and 2b).

However, it is not always possible to "fit" the existing and practically described types of motion to a specific application of the cam profile. One of the methods is to assume the course of the displacement and describe the mathematical relationship. In addition to the trigonometric functions, polynomial functions or spline curves can be used. For they are differentiable functions and comfortable during the search for a solution. An additional feedback method can also be used between the analyzed movements of deceplecament, speed and acceleration to conclude some compromise and optimization.

In this publication the authors present an analytical method, the motion parameters are described by polynomial functions whose base was appropriately modified trigonometric function. The starting point was the need to take into account the outline of the cam constant radius, which is in line standing piston TDC by 30°CA. Changing the outline of the cam so that the piston's proper movement was not over 360°CA (as in the traditional CrPM) but at 330°CA. The additional restriction was taken into account by the need for a relatively mild increase in acceleration after dwell in TDC to avoid impact loads. For the base function of assumed harmonic motion as discussed above (see. Fig. 3a). However, in this case, the acceleration at the start point is the maximum value, which is not acceptable. As a result of a series of attempts, it was found that the displacement would be described by a grade 12 polynomial, whose course is based on the 12 characteristic points that belong to the graphs describing the motion of the cam. The general form of the polynomial shown in the following relationship:

$$\tau(x) = a_0 + a_1 x + a_2 x^2 + \ldots + a_n x^n \qquad (2)$$

The solution to the problem is to find polynomial coefficients from a_0 to a_{11}. To this end, for each point of the characteristic equation must be placed for which the independent variable is the angle of rotation and the dependent variable the value of the displacement, velocity and acceleration. It should be added that the considered cam has a symmetrical profile, so it is justified to consider half of the cam movement. In this case it is the movement of the piston from the TDC to the BDC.

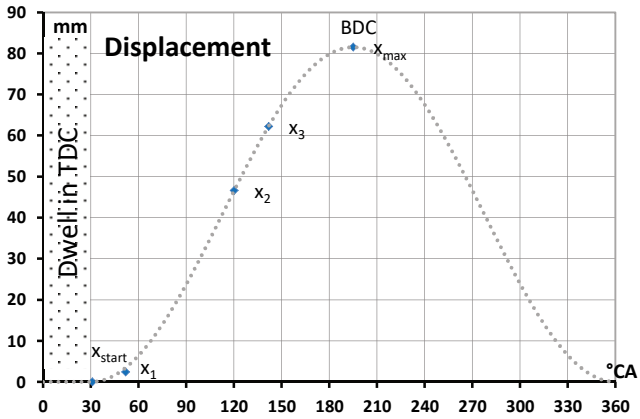


Fig. 4. Characteristic points of displacement (blue points) against the background of the base function (gray line)

Thus, for the displacement, characteristic points were created which, in the background of the displacement described by the harmonic function, are shown in Fig. 4. Minimal point x_{start} in which the downward movement begins after stopping in TDC, compatible with the base function. The degree of polynomial growth between x_{start} and x_1 depends on the number of derivatives that have the same value at this point. Point x_1 does not lie on the base function. The position of the point x_1 (52°CA) forces the polynomial to have an even more benign increase. The following characteristic points (x_2, x_3, x_{max}) belong to the base function. It is easy to see that in order for a polynomial to accurately reproduce the base function, more points are needed. Limiting their numbers makes it possible to select characteristic points not only related to the displacement, but related to speed and acceleration. You can go to the description of the speed points by discussing the x_{max} point. At this point, the polynomial describing the displacement should take the maximum value. The first derivative achieves zero value so the speed should be zero. As a consequence, the next characteristic point is the x_{max} point but applied to the velocity graph (Fig. 5). Since at this point the speed is zero, and it relates to a derivative of the displacement.

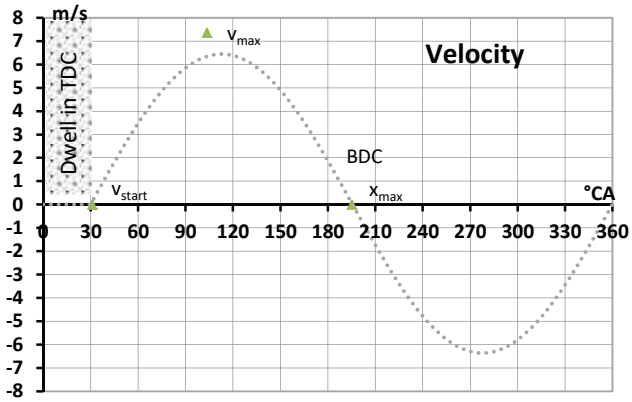


Fig. 5. Characteristic points of velocity (green points) against the background of the base function (gray line)

Since at this point the speed is zero, and it relates to a derivative of the displacement of the additional support of a polynomial (the following equation in the system of equations 12). For 103° it was determined that the speed should have a maximum value. Before solving the system of equations, it was not defined how much it should be. So a similar procedure was used for the one described above. Namely zero of the first derivative of the speed (acceleration) provides for obtaining the maximum speed v_{max} at a point. Above, it was mentioned that at the starting point (for the 30°CA) is required for continuity for the second derivative included. The next characteristic point must take the same value as x_{start}, and thus: $x_{start} = v_{start} = 0$. The same value at this point has acceleration $a_{start} = 0$ (Fig. 6). Acceptance of zero acceleration at this point deviates significantly from base acceleration, which at this point assumes a maximum value (1000 m/s^2). It is primarily for this reason could not be accepted harmonic motion to determine the outline of the cam. In point a_{start} can be taken further by the value of derivatives 0 to further slow down the growth of the function. In this case it was considered that the increase was satisfactory. At the next characteristic point a_{max} was given a specific angle parameter and the acceleration value. After performing a series of simulations solution and the constraints imposed by the other maximum value of the acceleration was set at 1330 m/s^2 at the 56°CA. In amin also applied to a specific solution regarding the acceleration, which is at –1350 m/s^2. The smoothed run in the area of the point is obtained by the condition of the continuity of the third derivative (jerk).

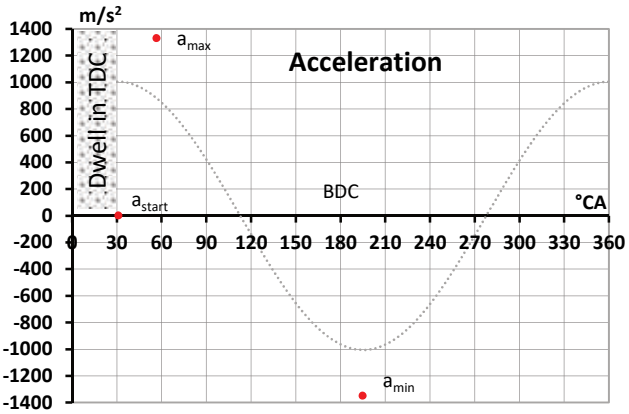


Fig. 6. Characteristic points of acceleration (red points) against the background of the base function (gray line)

The smoothed run in the area of the point is obtained by the condition of the continuity of the third derivative (jerk). This condition also causes the transition to a turning point between delay and acceleration to be smooth. The created system of equations was solved by the inverse matrix. In this method, the system of equations is written in matrix form: **Ma = B**, where matrix **M** is a matrix of polynomial coefficients, matrix **a** of unknown matrix and **B** is solutions matrix. Considering the previously defined characteristic points and their values, as well as the fact that the output function is a polynomial τ(x) of degree 12, a derivative of a polynomial of degree 11, a second derivative of a polynomial of degree 10 and respectively the third derivative of a polynomial of degree 9, the system of equations written in the matrix form is as follows:

$$\begin{bmatrix} \tau(x_{pocz}) \\ \tau'(x_{pocz}) \\ \tau''(x_{pocz}) \\ \tau(x_1) \\ \tau(x_2) \\ \tau(x_3) \\ \tau(x_{max}) \\ \tau'(x_{max}) \\ \tau''(x_{max}) \\ \tau'''(x_{max}) \\ \tau''(v_{max}) \\ \tau'''(a_{max}) \end{bmatrix} * \begin{bmatrix} a_0 \\ a_1 \\ a_2 \\ a_3 \\ a_4 \\ a_5 \\ a_6 \\ a_7 \\ a_8 \\ a_9 \\ a_{10} \\ a_{11} \end{bmatrix} = \begin{bmatrix} f(x_{pocz}) \\ f'(x_{pocz}) \\ f''(x_{pocz}) \\ f(x_1) \\ f(x_2) \\ f(x_3) \\ f(x_{max}) \\ f'(x_{max}) \\ f''(x_{max}) \\ f'''(x_{max}) \\ f''(v_{max}) \\ f'''(a_{max}) \end{bmatrix} \quad (3)$$

According to the adopted methodology, the solution of the equations is a matrix solution (designated polynomial

coefficients describing the displacement of the piston) determined from the relationship: $\mathbf{a = M^{-1} B}$. The calculated and base polynomials are shown in the graphical interpretation in Fig. 7.

The described methodology for determining the individual points of interest results in a smoother increase in displacement after the piston is stationary at TDC (30–90°). Then, practically until the maximum stroke is reached, the course of the polynomial approximates the course of the base function. However, there are some exceptions in the range of the obtained inflection points.

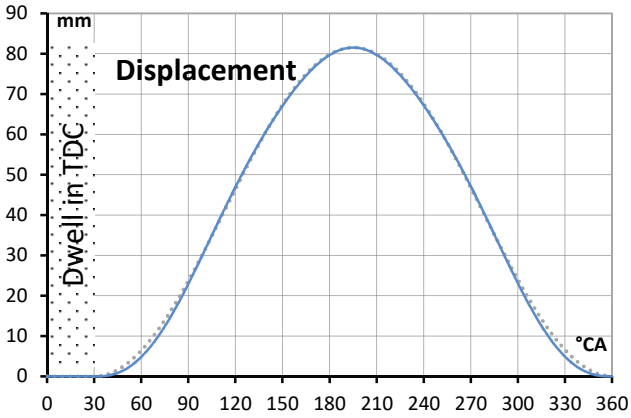


Fig. 7. Calculated displeacement (red line) against the background of the base function (gray line)

More complete description can be obtained by observing the course of the other two quantities: velocity and acceleration. It is preferable to observe them on a single graph (Fig. 8).

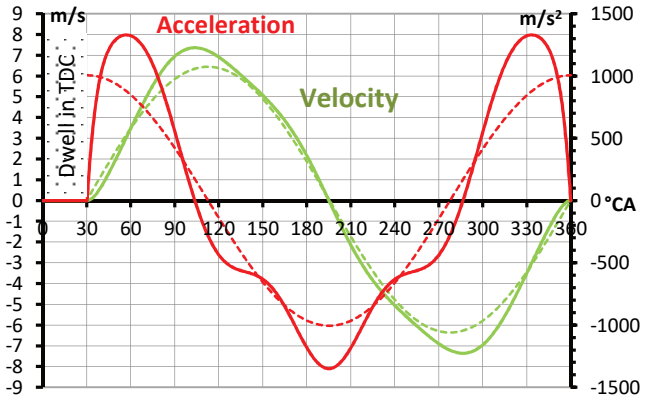


Fig. 8. Calculated velocity and acceleration against the background of the base functions

The even movement of the piston in the vicinity of the TDC, which is mentioned many times, causes the velocity and acceleration of the piston to flow smoothly. The calculated maximum speed at point v_{max} (for 103°CA) is 7.35 m/s. Naturally, this point acceleration value is zero. The TDC also imposed specific conditions for the acceleration achieved and its smoothing (the condition of a continuous third derivative). Adopting this condition explains both the inflection points on the displacement graph and the velocity and acceleration line between 103° and 195°. After obtaining a zero value at 103°, the acceleration must be adjusted to the minimum value of –1350 m/s^2. It can be estimated that acceleration could be developed more smoothly, without jerk, but at the expense of obtaining a minimum value at a higher level (absolute value). Changing the zero point of acceleration (maximum speed) eg 120° would also change acceleration and no jerk also. Computational simulations also indicate that in such a situation the maximum velocity will increase. Since the polynomial of degree 12, taking the point x_1 for angle values instead of 52° eg. 57° can lead to much greater deviation from the base function of all three sizes, and consequently to the adoption of a more complex outline of cam. The final outline of the cam, derived from the displacement of the piston, after changing the polarized to cartesian coordinates, is shown in Fig. 9.

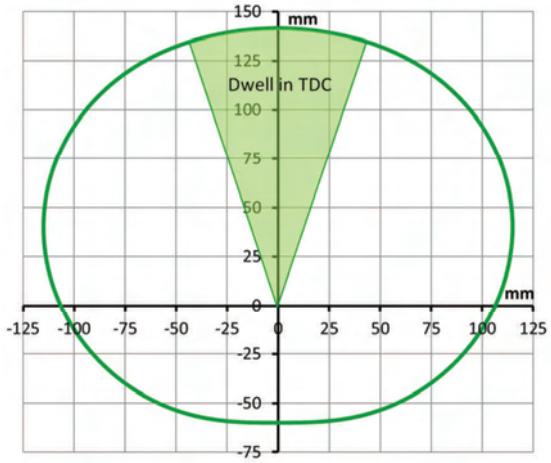


Fig. 9. Final result of cam's outline

3. Strength test of the cam

The engine drive system was subject to strength tests using the finite element method. The tests were performed to assess the structural strength of the object. The question of the strength rating of the track surface layer was consciously omitted. This aspect was the subject of other analyzes, which wasn't presented here.

Three-dimensional parabolic, quadrilateral finite elements (Fig. 10) were used to construct the computational model. The strength of the spline connection was determined using simple mathematical relationships, known in the specialistics literature [9]. At the location of the grooves was left a hole with internal diameter of the spline. Then translation ability of all the nodes lying on such cylinder was blocked.

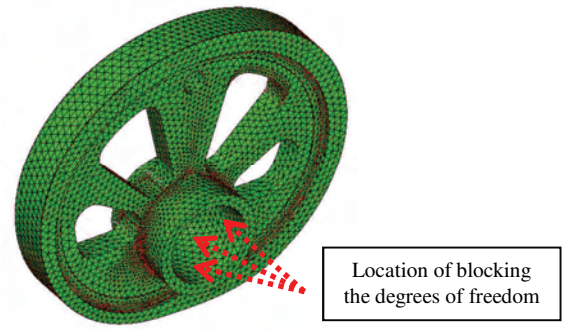


Fig. 10. Computational model of the cam

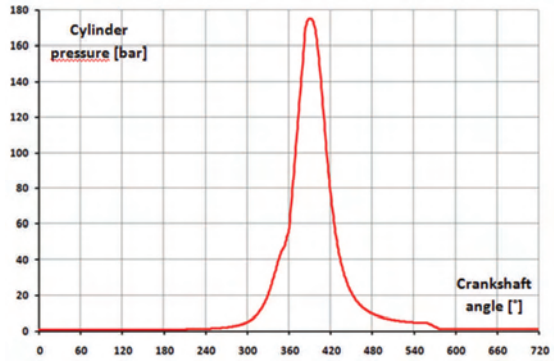
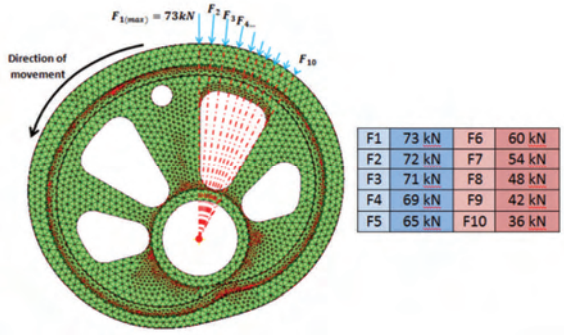


Fig. 11. Pressure inside the cylinder as a function of the angle of rotation of the crankshaft

The loads were modeled using concentrated forces. These forces was applied at right angles to the track. Variability of loads resulting from combustion process was considered (Fig 11.). The maximum load value is 73 kN for a crankshaft angle of 390˚, measured from TDC. Strength studies was started since then. Subsequently the stresses were evaluated with a step of 3° up to 420 (Fig. 12).



F1	73 kN	F6	60 kN
F2	72 kN	F7	54 kN
F3	71 kN	F8	48 kN
F4	69 kN	F9	42 kN
F5	65 kN	F10	36 kN

Fig. 12. Loads which was implemented in strength analysis of the cam

The forces acting on the system induce a complex state of stress. Wherein the greatest stresses occur in the cam section above the opening. This area is largely subject to bending. The selection of the geometric parameters of the crosssection, including the determination of its height, was the most important objective of the analysis. The computational model was prepared so that multivariate analysis could be carried out for different heights. Hence, four volumes were separated, which were filled with finite elements according to the diagram depicted on Fig 13.

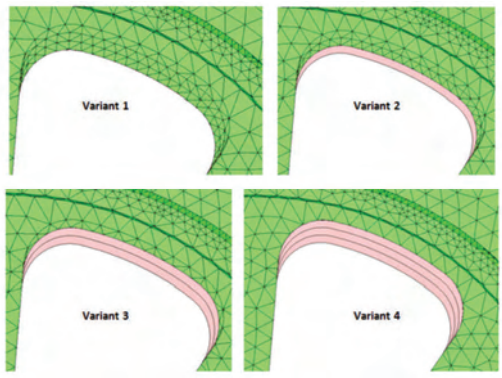


Fig. 13. Four variants of the hole shape

Below the results of calculations for two variants (1 and 4) was presented. Images depict maps of reduced tension according to Huber-Mises-Henck's hypothesis (Fig. 14 and Fig. 15). H-M-H stresses for variant 1 reach a maximum of 240 MPa, while for variant 4 about 300 MPa. These stresses accumulate in the rounding of the hole and can cause fatigue effects in this area. Due to the dominance of bending, it is necessary to select the material which has a endurance limit for bending more than 300 MPa. This feature has 18 HGT steel. Thus the carrying capacity of the cam does not deviate from the classical crank-rod system for similar mass. The system is capable of carrying heavy loads.



Fig. 14. Stress map H-M-H for variant 1 - displacement of nodes at a scale of 400: 1



Fig. 15. Stress map H-M-H for variant 4 - displacement of nodes at a scale of 400: 1

Reduction of weight and moment of inertia is important in mechanism with high rotational speed. The presented strength test method allowed to define the shape of the cam (especially the defining of shape of openings). Removing the material will have a positive effect on the dynamics of movement. This treatment will reduce the weight of the counterweight, which is very desirable. The amplitude of the vibration of the whole engine is reduced. In addition, the applied strength verification technique, based on the finite element method, allowed to determine the geometric parameters of the cam which do not affect the ability to

define the intended path of the piston movement. In particular, the thickness and width of the contact plane, the height of the lining and the radius of the roundings were determined. Strength indicators of material were also determined.

It is noted that the method applied is simplified (among others due to imperfections in the shape mapping, deviations from the actual material indicators, numerical method of solving the task). Hence, these are preliminary calculations. Prior to placing an object on the market, further analyzes and tests should be done.

4. Summary

The article describes the CPM as an alternative to the CrPM. The main feature of the designed CPM is the piston dwell in the TDC for 30°CA. This feature introduces significant modifications to the combustion process in the ICE. It enables: greater use of energy potential of low calorie fuels, impact on combustion kinetics and reduction of toxic compounds in exhaust gases. Performing this type of mechanism requires the use of appropriate design methods: an analytical design of the cam outline with kinematic limitations and the use of advanced FEM stress-strain estimation methods to select its geometric parameters for overpiston pressure distribution. When designing outline of the cam, the focus was on achieving a smooth and even motion of the piston. For this purpose, an analytical method with the implementation of polynomial functions was used. The smooth motion of the piston was obtained by limiting the value of the motion parameters as well as the continuity of the derivatives at the characteristic points. The beneficial effect of this method was most evident at the time of acceleration from a standstill cam at TDC. The applied calculation method allow multiple kinematic equations to solve and make interaction between the various parameters in order to have a smoother course of the modeled size. The strength tests made it possible to reduce the mass of the cam, hence it was possible to select low weight masses and low moment of inertia. The procedure for selecting the counterweight, flywheel and endurance of cam's surface layer will be presented in future publications of the authors.

Nomenclature

ICE	internal combustion engine
CrPM	crank-piston mechanism
CPM	cam-piston mechanism
TDC	top dead centre
BDC	bottom dead centre
CA	crank angle

Bibliography

[1] www.douglasself.com (Online).
[2] www.google.com.gt/patents/US1711260 (Online).
[3] GE, Y., CHEN, L., SUN, F. Optimal paths of piston motion of irreversible diesel cycle for minimum entropy generation. *Thermal Science*. 2011, **15**(4), 975-993.
[4] BURZLER, K.H. Optimal piston paths for diesel engines. *Thermodynamics of Energy Conversion and Transport*. 2000, 7.
[5] BADESCU, V. Optimal piston motion for maximum net output work of Daniel cam. *Energy Conversion and Management*. 2015, **101**, 181-202.
[6] American Can Company, Cam Design, Emmerson, 1961.
[7] ANGELES, J., LOPEZ-CAJUN, C.S. Optimization of cam mechanism. *Springer Science*, Business Media Dordrecht, 1991.
[8] NORTON, R.L. Cam design. Design of machinery. *McGraw-Hill*, 1999, 8.
[9] DIETRICH, M. Podstawy budowy maszyn. *PWN*. Warszawa 1988.

Tomasz Borowczyk, DEng – Faculyy of Machines and Transport at Poznań University of Technology.

e-mail: *TomaszBorowczyk@wp.pl*



Mikołaj Spadło, DEng – Faculty of Machines and Transport at Poznań University of Technology.

e-mail: *MikolajSpadlo@gmail.com*



Article citation info:
SZCZEPAŃSKI, T., SKARBEK-ŻABKIN, A., DZIEDZIAK, P. Impact of the road conditions on the amount of braking energy. *Combustion Engines*. 2017, **171**(4), 265-268. DOI: 10.19206/CE-2017-445

Tomasz SZCZEPAŃSKI
Anna SKARBEK-ŻABKIN
Paweł DZIEDZIAK

CE-2017-445

Impact of the road conditions on the amount of braking energy

The issue of energy recuperation is increasingly found in modern cars (both electric and hybrid, as well as powered by a combustion engine only). Road conditions are one of the essential factors determining the appropriateness of using certain design solutions in braking energy recovery systems. This article presents an analysis of road conditions prevailing in a large urban agglomeration together with an evaluation of their usefulness for utilizing the braking energy. Road tests were carried out for this purpose, and their analysis used the Monte Carlo method to determine the pseudo-accidental courses.

Key words: *energy recuperation, Monte Carlo method, braking energy, road tests*

1. Introduction

The issue of energy recuperation is increasingly found in modern cars. The braking energy recovery systems are used in hybrid, electric and combustion engine vehicles. In the latter ones, an alternator is used to convert the kinetic energy into electrical energy, and the recovered energy is used to power the car's current receivers, such as traffic lights. In combustion engine cars, the issue of energy recuperation is being developed by BMW, which introduced Efficient Dynamics technology in 2007. In the case of electric and hybrid cars, braking energy recovery is used much earlier [2, 3, 6]. In view of the dynamic development of technologies conducive to improving the environmental performance of cars and their energy efficiency, it seems to be expedient to run a research aimed at optimizing the performance of energy recovery systems.

Road conditions are one of the basic factors determining the appropriateness of using certain construction solutions in the braking energy recovery systems. It is them that the amount of energy that can be recovered depends on as well as how it is distributed over time [3]. This article presents an analysis of road conditions prevailing in large urban agglomeration (Warsaw) together with an evaluation of their usefulness for the use of braking energy. The road tests were performed for this purpose, and their analysis used the Monte Carlo method to determine pseudo-accidental waveforms.

2. The road tests

The Renault Clio passenger car equipped with a self-ignition engine was used. The vehicle's empty weight was 1100 kg and with the driver and passenger – 1230 kg. The study was conducted in the city of Warsaw in the afternoon, as the traffic intensity increased. The route was selected accordingly in such a way as to engage in different traffic condition: from low traffic intensity to a high one (up to street congestion). The parameter measured was speed of the car. The OBD system in the vehicle was used for the measurement, and the OBD CarChip Pro reader was used for the recording. The sampling frequency of the recorded physical quantities was 1 Hz, and the measurement resolution was 1 km/h.

Within a two-day study, more than 17,000 measurement points were registered in total. The total test drive time was 4 hours and 47 minutes. The total distance traveled included 115.46 km. The average driving speed was 24 km/h and the maximum speed was 89 km/h. The engine average rotation speed was 1158 rpm, the maximum value was 2874 rpm and the minimal registered value was706 rpm.

Figures 1–3. show examples of the speed variation of a car in different urban driving. Fig. 1 corresponds to driving in the highest traffic, Fig. 2. driving in moderate traffic (without traffic congestion), Fig. 3. driving in the lightest traffic.

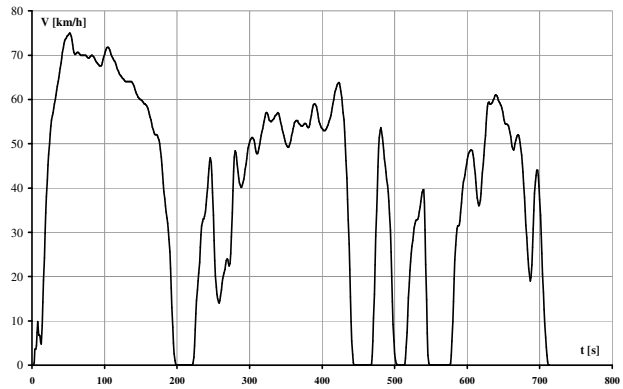


Fig. 1. The car speed variation at the greatest traffic intensity

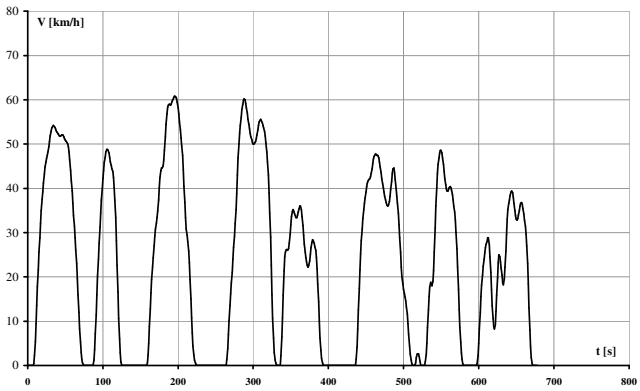


Fig. 2. The car speed variation at the average traffic intensity

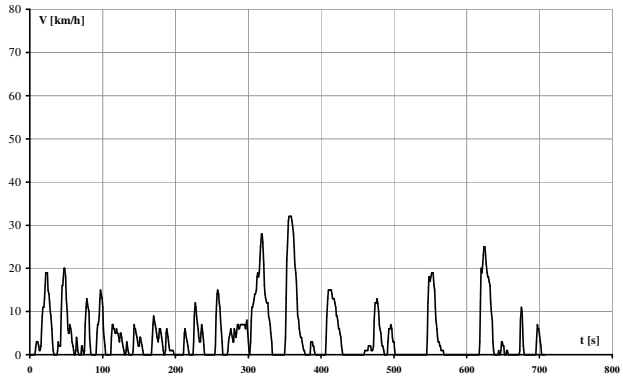


Fig. 3. The car speed variation at the lightest traffic intensity

The Figures 1–3, show a variation in the nature of the driving. The differences relate to both the speed achieved, the rate of speed changes (acceleration achieved), and the frequency of speed variations. Each type of traffic will be associated with other possibilities of the energy recuperation. Of course, the question occurs about a clear measure of the nature of the traffic. A few approaches to this issue will be covered later in this article.

3. Braking energy

In the discrete field, the kinetic power of a car at a given measuring point can be calculated from (1)

$$N_i = 0.5 \cdot m \cdot \left(V_i^2 - V_{i-1}^2\right) \cdot T^{-1} \tag{1}$$

where: N – kinetic power, m – mass of the vehicle, V – driving speed, i – current measuring point, T – sampling period. Of course, the power possible to be recovered only during deceleration. The formula (1) assumes the form (2)

$$N_i = \begin{cases} -0.5 \cdot m \cdot \left(V_i^2 - V_{i-1}^2\right) \cdot T^{-1} \text{ for } V_i - V_{i-1} < 0 \\ 0 \text{ for } V_i - V_{i-1} \geq 0 \end{cases} \tag{2}$$

In practice, such calculated braking power of a car can not be fully recuperated due to the movement resistance. The power of movement resistance is shown below, where formula (3) shows the rolling resistance and formula (4) the power of air resistance [4]:

$$N_t = f_t \cdot \left(1 + A_d \cdot V_i^2\right) \cdot m \cdot 9.81 \cdot V_i \tag{3}$$

$$N_p = 0.047 \cdot C_x \cdot A \cdot V_i^3 \tag{4}$$

where: f_t – essential rolling resistance coefficient, A_d – additional rolling resistance coefficient, C_x – air resistance coefficient, A – vehicle's surface area.

Figures 4–6 shows the variation of the braking power and the combined resistance power of the car corresponding to the three previously presented traffic segments. The braking energy can be identified with the field under the power curve.

In the case of lower intensity traffic where higher driving speeds are achieved, higher braking power values are present, but at the same time higher resistance power values. In order to quantify the above phenomena, it seems necessary to introduce some formalism describing traffic conditions.

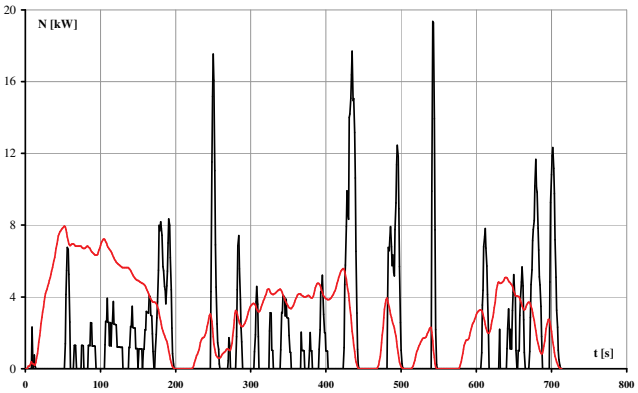


Fig. 4. Kinetic power variation (black color) and resistance power (red color) of the movement at the maximum traffic intensity

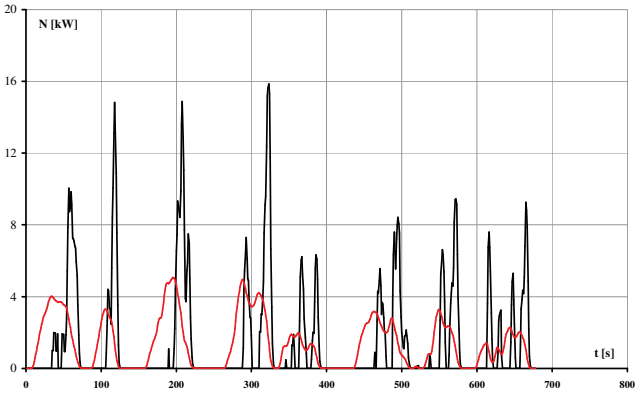


Fig. 5. The kinetic power (black color) and resistance power (red color) of the movement at the average traffic intensity

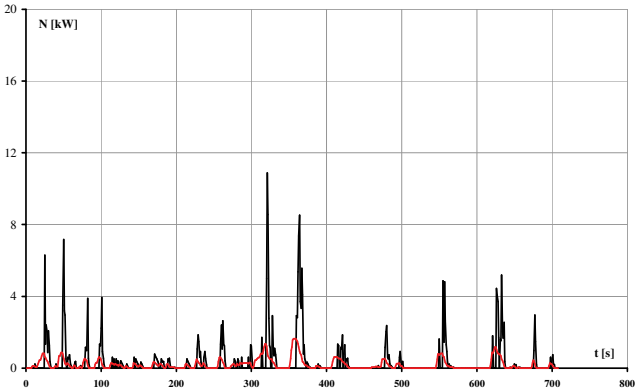


Fig. 6. The kinetic power (black color) and resistance power (red color) of the movement at the lightest traffic intensity

4. Analysis of the traffic conditions

Monte Carlo method [1, 5] was used to analyze traffic conditions. It involves drawing random fragments of the stochastic process. In the case in question, these fragments were of a given length, and the parent process was the compounded course of speed of the car recorded in the road tests. As a result, a collection of pseudo-accidental processes has emerged, whose properties can be considered independently. Then, for each part of the process, a zero-dimensional characteristic was defined, representing a quantitative description of traffic conditions. It served as a criterion for evaluating road conditions.

Subsequently, the pseudo-random processes drawn were sorted out in relation to the accepted criterion. For each process, the variations of the braking power, movement resistance power, and the braking power decreased by the movement resistance power, and the average values of those variations, were calculated. Finally, the relationships of mean values of braking power, movement resistance and braking power decreased by the power of motion resistance were established in respect to the adopted criteria describing the nature of traffic conditions. Calculations were made in a Java program environment. The number of pseudo-random processes was 100, and the length of each process was 300 s (300 measurement points).

An important issue was the choice of the zero-dimensional characteristic representing the criterion describing the road traffic. The simplest solution was to use the vehicle' speed average value. Fig. 7 shows the relationship between the average braking power and the average driving speed for pseudo-random processes of driving a car obtained by Monte Carlo method. The average power value is proportional to the braking energy in a given traffic segment.

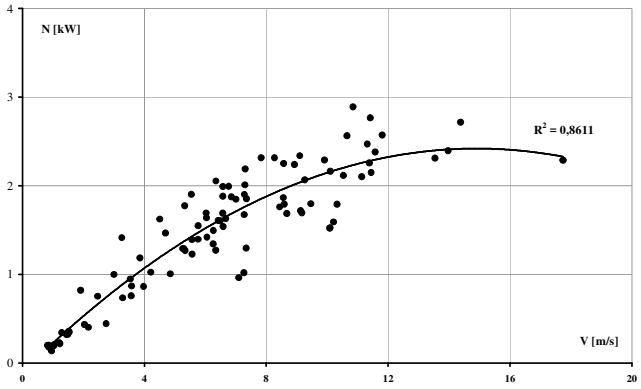


Fig. 7. The relationship between the average braking power and the average car speed

The graph above shows the correlation between the average power and average speed, but this relationship is nonlinear and distinctly fuzzy (the determination factor is 0.8611 in this case). This is understandable because the braking power also depends on other factors, including, among the others, the braking intensity, whose measure may be the average deceleration delay. Figure 8 shows the relationship between the average braking power and the average braking delay calculated according to formula (5)

$$a_h = \begin{cases} -\frac{1}{n}\sum_{i=1}^{n} a_i \text{ for } a < 0 \\ 0 \text{ for } a \geq 0 \end{cases} \quad (5)$$

where: a_h – braking delay, a – acceleration of the car, n – number of measurement points in the process under consideration.

As in the previous case, there is some correlation visible between the average delay and the average braking power, but it is of clearly limited character. The determination coefficient for this correlation is even smaller, and equal to 0.5898. In view of the positive correlation shown in Figures 7 and 8, it seems appropriate to use the criterion for assessing traffic conditions that combines speed and driving delay information. In the road vehicle operating tests, the commonly used zero-dimensional characteristic is the product of average speed and the average positive acceleration. By analogy to this solution, it is proposed to use the product of average speed and average driving delay. Figure 9 shows the relationship between the average braking power and the product of the average speed and the average delay.

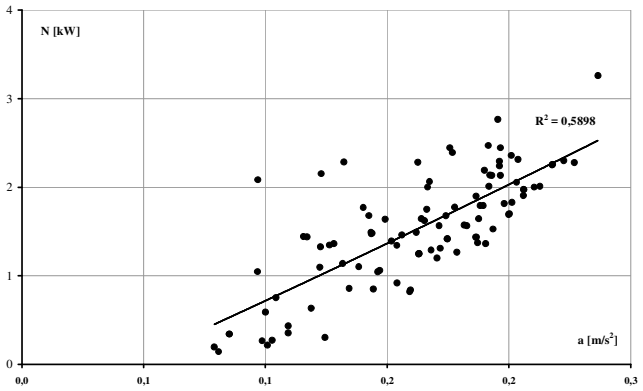


Fig. 8. Relationship between the average braking power and the average vehicle delay

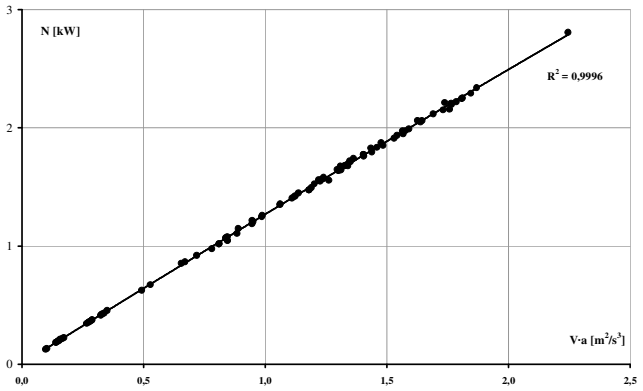


Fig. 9. Correlation of the average braking power as the function of the product of average speed and average car delay

The graph above clearly shows a correlation between the values in question. The determination factor is 0.9996. It seems that the last zero-dimensional characteristic is the best criterion for assessing road conditions. The average speed of a car carries information about the amount of energy required for a single stoppage of the vehicle, whereas the average delay indicates the speed of the braking process, and indirectly also about its frequency.

Fig. 10 shows the mean power of the motion resistance as the function of the product of the average velocity and mean delay, and in Fig. 11. in the same function, the braking power decreased by the power of motion resistance is shown.

The average braking power decreased by the movement resistance power, shown in Figure 11, is not so strongly correlated to the product of average speed and average delay, as it was apparent in the case of braking power alone

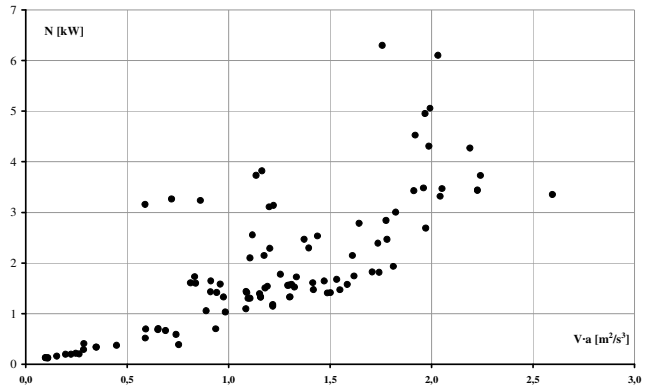


Fig. 10. The average power of movement resistance as a function of the product of the average speed and the average car delay

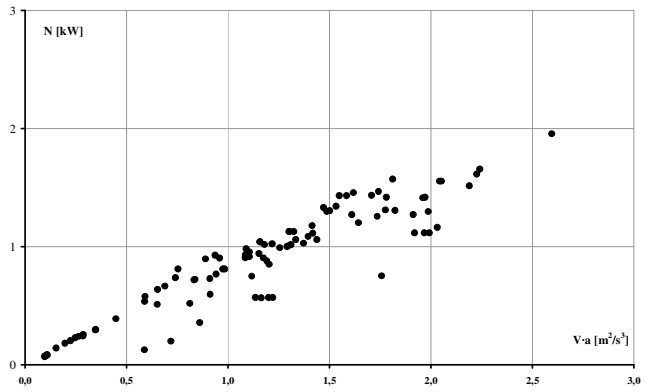


Fig. 11. The average braking power decreased by the movement resistance power as the function of the product of the average speed and the average car delay

(seen in Fig. 9). The reason for this is the lower correlation of the movement resistance power with the product of velocity and delay, which can be observed in Fig. 10., for the movement resistance power is strongly correlated with the speed of the vehicle alone.

5. Summary

In this paper several indicators have been proposed to describe the road conditions in a statistical sense. These include: the average speed, the average deceleration delay and product of average speed and average deceleration delay. In the next, dependence between the road conditions described this way and the braking energy available in the recuperation process was sought.

Average braking power reduced by the motion resistance power is a key piece of information about how much energy can be used in practice by means of a recuperation system. Of course, not all of the energy is actually recoverable due to the limitations inherent in the constructional characteristics of modern vehicles. It is, however, an indicator for assessing traffic conditions in terms of energy.

There is a clear differentiation in the power theoretically possible to recover under different traffic conditions. Braking power decreased by the movement resistance power ranges from 0.2 kW to almost 2 kW. The average power set for the entire road test is approximately 1 kW.

This gives some idea about the design of recuperation systems that are installed more and more often in cars. This proves, among other things, that it is expedient to use braking energy recovery only in cars powered by an internal combustion engine. The recovered average power of 1 kW can be used in modern cars by such receivers as: lights, control systems, fuel pump power supply, cooling liquid pumps and oil pumps. In such a case, it is not necessary to power the car using the recovered braking energy for its full use.

Bibliography

[1] CHŁOPEK, Z., LASKOWSKI, P. Pollutant emission characteristics determined using the Monte Carlo Metod. *Eksploatacja i Niezawodność – Maintenance and Reliability*. 2009, **2**(42).

[2] FICE, M. Hamowanie rekuperacyjne w miejskim pojeździe hybrydowym z napędem na koła tylne. *Prace Naukowe Politechniki Śląskiej*. Elektryka. 2013.

[3] HOFMAN, T. Framework for combined control and design optimization of hybrid vehicle propulsion systems. *Ph.D. dissertation*. Eindhoven University of Technology, Eindhoven 2007.

[4] LANZENDOERFER, J., SZCZEPANIAK, C. Teoria ruchu samochodu. *WKiŁ*, Warszawa 1980.

[5] LASKOWSKI, P. Vehicle nitric oxides emission characteristics determined using the monte carlo method. *Zeszyty Naukowe Instytut Pojazdów*. 2017, **1**(110).

[6] SZUMANOWSKI, A. Hybrid electric vehicle drives design. Edition based on urban buses. *Wydawnictwo ITE*. Warszawa-Radom 2006.

Tomasz Szczepański, DEng. – Motor Transport Institute.

e-mail: *Tomasz.Szczepanski@its.waw.pl*



Dziedziak Paweł, MEng. – Diagnostics and Servicing Process Department in Motor Transport Institute.

e-mail: *PawelDziedziak@its.waw.pl.*



Anna Skarbek-Żabkin, MEng. – Motor Transport Institute.

e-mail: *Anna.Skarbek@its.waw.pl*



Article citation info:
CISEK, J. The influence of non-cooled exhaust gas recirculation on the diesel engine parameters. *Combustion Engines*. 2017, **171**(4), 269-273. DOI: 10.19206/CE-2017-446

Jerzy CISEK

CE-2017-446

The influence of non-cooled exhaust gas recirculation on the diesel engine parameters

This paper presents the results of the diesel engine research on the energy performance, components of exhaust gases and smoke and parameters related to the supply system for VW 1.9 TDI working in 2 modes: with standard, non-cooled EGR system, and without this system. All of measurements were carried out on the some engine speed – 2000 rpm (speed of maximum engine torque) and various engine loads. It was found that the serial engine control unit switches the EGR system off above 150 Nm engine load (Mo_{max} = 295 Nm). In this range of load the engine running with EGR is characterized by higher fuel consumption (lower total efficiency) ca. 5%, compared with engine without EGR. Concentration of NO_x in exhaust gases was lower up to 45% but, at the same time, exhaust gas smoke and concentration of carbon oxides were strongly increasing. It can be seen that EGR system increases the temperature (up to 110°C) and changes the composition of air-exhaust gas in the intake manifold. One of reason of this fact is self-changing start of injection. Additional effect of EGR is lower air pressure behind turbocharger, because the flow of exhaust gases (into EGR) is taken before the turbine.

Key words: *diesel engine, exhaust gases, EGR*

1. Introduction and methodology of research

In the domain of diesel engines, the emission of carbon monoxide (CO) and unburned hydrocarbons (HC) does not pose a serious threat to the development of their structure. It is different from the emission of nitrogen oxides (NO_x) and particulates matter (PM) [1]. One of the common methods used by manufacturers of internal combustion engines is to reduce the NO_x concentration in exhaust gases by means of external exhaust gas recirculation (EGR). In a large number of engines, this is a non-cooled EGR [3, 4]. However, the question is whether the use of EGR significantly affects other parameters of engine operation (directly or indirectly), and if so, how it affects the engine itself and its user.

From the review of domestic and foreign literature it is clear that the effect of EGR on diesel engine performance is quite well studied. However, most publications do not deal with the energy parameters and composition of the engine exhaust gases (working with/without EGR) with the parameters of the indicator graphs and the rate of heat release. Detailed analysis of bibliographic data would exceed the volume potential of this publication. The purpose of the author was to determine the impact of the EGR on the specific operation of the propulsion engine (VW 1.9TDI AJM) tested, inter alia because of the use of this engine for other research purposes.

This article, and its second part, on the impact of EGR on the parameters of indicator graphs and the rate of heat release in the engine cylinder, is an attempt to answer this question. The study was carried out using the popular VW 1.9 TDI engine in the AJM version (with injection unit), popular in Europe, in passenger cars and light commercial vehicles. This article describes the influence of engine load (at max torque speed 2000 rpm) on the basic engine parameters and exhaust composition. In the study were used Schenk's engine dynamometer, AVL Fuel Balance and AVL Bench Emission System CEB II for measuring the concentration of gaseous components. In addition, the air temperature collected by the engine, the air temperature behind the turbocharger, the inter-cooler and the intake manifold (behind the EGR valve) were measured. The exhaust gas temperature was measured before and after the turbocharger. For comprehensive analysis, the impact of the engine load on the boost pressure and the onset of fuel injection. In the second part of the article, the AVL Indimeter 617D was also used to determine and analyze the fast-changing pressure in the engine cylinder (as a function of the engine crankshaft rotation angle) and to calculate the rate of heat release. In each of these cases the engine worked in two operating modes:

– MODE I – with factory preset of EGR,
– MODE II – without exhaust gas recirculation (EGR).

2. Experimental

2.1. Energy parameters of the engine

A common parameter used to determine the current degree of exhaust gas recirculation is the percentage of opening of the EGR valve. The value of this parameter was measured using the VCDS diagnostic interface communicating with the engine controller via the OBD2 connector of the engine used. Changes to the EGR valve opening as a function of engine load (torque Mo) are shown in Fig. 1. It can be seen that the highest values of exhaust gas recirculation correspond to the lowest engine loads. Although the NO_x concentration in the exhaust then is not high but the low fuel consumption makes it possible to replace the clean air (consumed by the engine) with significant amounts of exhaust gas. With a higher engine load (over 100 Nm – about 1/3 of the maximum torque), the EGR valve turns off by the engine controller to completely disable the exhaust gas recirculation at 175 Nm. High engine load is characterized by high NO_x concentration and exhaust gas recirculation would be most needed at that time, however, high fuel consumption requires large amounts of clean air, not mixed with exhaust gases within the EGR. Data shown in Fig. corresponds to the operation of the engine according to I MODE – factory setting of EGR. In II MODE, the percentage of opening of the EGR valve is 0%.

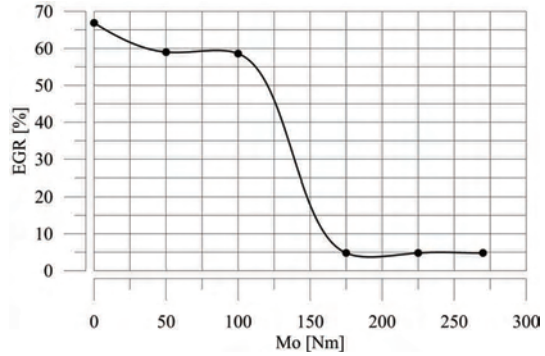


Fig. 1. Influence of engine load on factory change of opening of exhaust gas recirculation valve (EGR)

A parameter that clearly shows the difference between the engine operation with and without the EGR system is the temperature at the intake manifold (Fig. 2). During operation of the engine without exhaust gas recirculation, the temperature of the intake manifold slightly increases over the entire engine load range, not exceeding 55˚C. This is caused by an increase in the charge pressure then. When operating the engine with the factory-set EGR, can see that the maximum EGR valve opening temperature is up to 108°C. Only when the engine load increases, when the EGR valve is closed by the engine controller, the temperature of the intake manifold approaches the values achieved without this system. It can therefore be stated that the use of the EGR system significantly influences the temperature of the intake manifold. This phenomenon is due to the fact that when the EGR valve is open, hot gases are introduced into the intake manifold, which cause the temperature to rise.

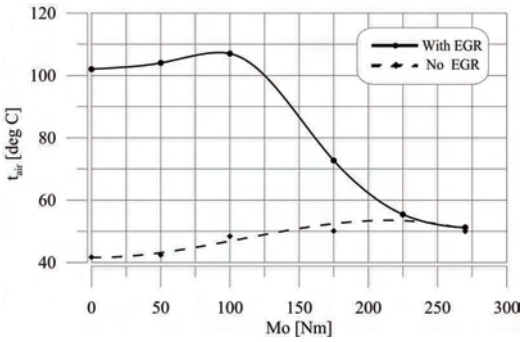


Fig. 2. Influence of the engine load on the temperature inside the intake manifold of engine operating with/without EGR

A large increase in temperature in the engine intake manifold working with the factory opening of the EGR valve compared to the EGR switched off is a disadvantage because this temperature is added to the combustion temperature. For this reason, the cooled EGR system, used in modern engine designs, reduces the NO_x concentration in the exhaust gas more effectively than not cooled EGR does.

The operation of the exhaust gas recirculation also affects the variation of the fuel gas temperature before the turbocharger, as a function of the engine load. In the area of small and medium engine loads, when the controller makes the EGR system on, the exhaust gas temperature before the turbine is significantly lower. This is due to the fact that a large proportion of the exhaust, within the EGR, it is delivered to the intake manifold, so the kinetic energy of the exhaust before the turbine decreases then. Because the measure of kinetic energy of gas is, among others, the temperature of this gas, the reduction of exhaust gas energy with the EGR switched on, leads to a reduction of the exhaust gas temperature in front of the turbine, as illustrated in Fig. 3.

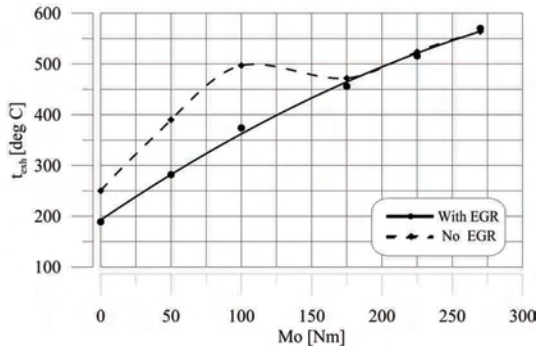


Fig. 2. Influence of the engine load on the exhaust gas temperature before the turbine of engine operating with/without EGR

The turbine exhaust gas stream (energy) is reduced by the exhaust gas flow to the engine intake manifold working with the open EGR valve [2]. For this reason, the boost pressure (p_d) in the engine running with the EGR system switched on is lower than the air pressure behind the engine charger running without EGR. This is shown in Fig. 3.

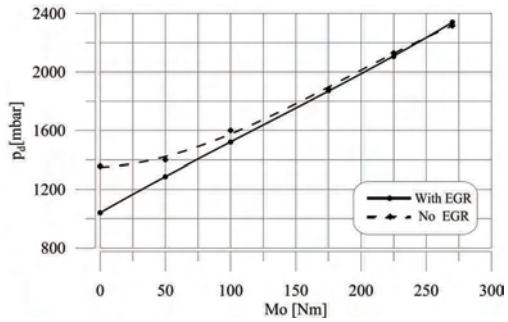


Fig. 3. Influence of engine load on the air pressure after the turbocharger of engine operating with/without EGR

Obviously, the difference in air pressure behind the charger for the engine running with/without EGR also results in other air temperatures behind the turbocharger, as shown in Fig. 4.

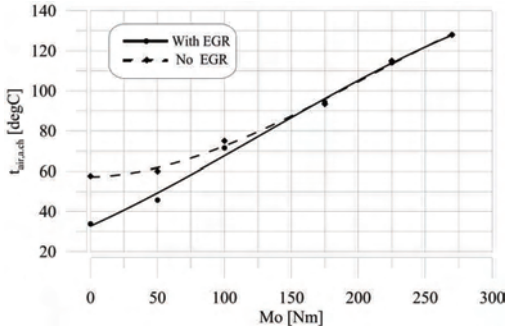


Fig. 4. Influence of the engine load on the air temperature after the turbocharger of engine operating with/without EGR

The reduced air temperature behind the compressor for the exhaust gas recirculation engine is of no importance since, as shown in Fig. 2, the air in the intake manifold blended with hot exhaust gases and the air temperature taken into the engine cylinder is significantly higher than that of the engine running without EGR.

Increasing the temperature of the intake manifold gas and lowering the pressure behind the turbocharger (reduction of charge density) and, above all, the lower purity air stream consumed by the engine running the exhaust gas recirculation, naturally reduces the excess air ratio value (Fig. 5). With heavy engine loads (175 Nm and higher), the λ values are the same for both engine operating modes, as the EGR valve closes with the engine controller. On the other hand, with lower engine loads, the EGR effect would have to be separated into two stages of engine operation: idle run and partial loads.

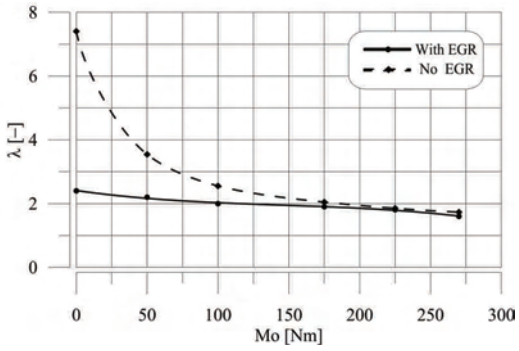


Fig. 5. Influence of the engine load on the excess air ratio λ for engine operating with/without EGR

For idle run (Mo = 0 Nm) in the cylinder of the diesel engine operating without the EGR system, in the combustion process the huge mass of air is disproportional to the low fuel dose (λ = 7.4). This is an unfavorable composition of the fuel-air mixture due to the engine's thermal efficiency. In addition, so much air, which largely does not take part in the oxidation of the fuel, is a thermodynamic ballast, which unnecessarily receives part of the heat intended for performance and lifts the heat from the exhaust. This is an undoubted waste of energy. Therefore, for idle run, adding a portion of the exhaust to the air in the intake manifold reduces the fuel consumption (Fig. 6) by decreasing the volumetric efficiency η_v (Fig. 7), which in turn reduces the excessively high value of the excess air ratio λ (Fig. 5).

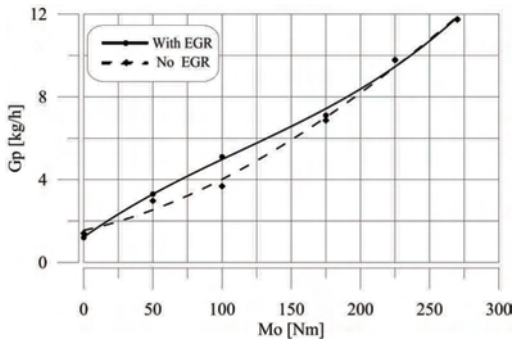


Fig. 6. Influence of the engine load on the fuel consumption Gp for engine operating with/without EGR

With partial engine loads (in this case, up to 175 Nm) the use of EGR, resulting in a reduction in the amount of clean air in the engine cylinder (due to the need of reducing the NO_x concentration in the exhaust gases), worsens the course of the combustion process. This is clearly evident in the overall efficiency of the engine running with/without EGR (Fig. 8). As the result of the work of EGR, with engine load of 50 Nm, the overall efficiency of the engine running without EGR is reduced from 32% to 25% after switching the exhaust gas recirculation on. Percentage reduction in overall efficiency (22 percentage points) is automatically means an increase in fuel consumption (Fig. 6). This should not be surprising, since the structural or regulatory methods that reduce NO_x emissions in the exhaust gases unfortunately have an adverse effect on the overall efficiency of the engine, too.

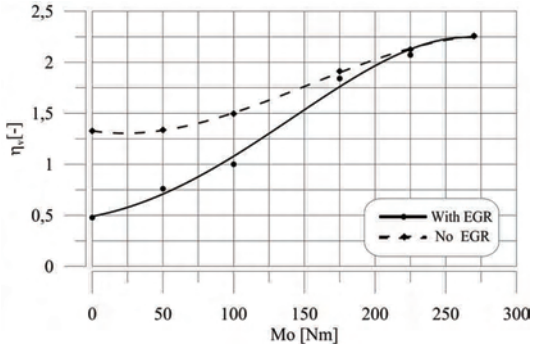


Fig. 7. Influence of the engine load on the volumetric efficiency η_v of engine cylinder for engine operating with/without EGR

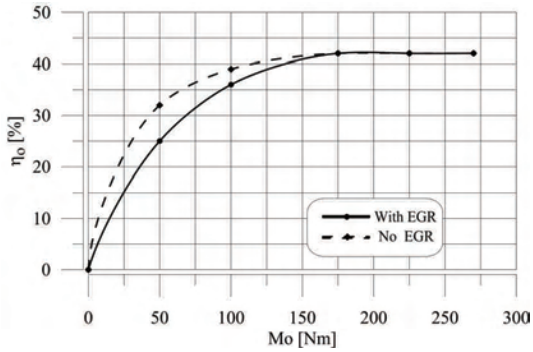


Fig. 8. Influence of the engine load on the engine efficiency η_o for engine operating with/without EGR

The research on the impact of the exhaust gases recirculation on the composition of the exhaust gases was started from the NO_x concentration in the exhaust gas, because that is what the EGR system was created for. From the data shown in Fig. 9, it is clear that within the engine load range at which the factory EGR operates, the NO_x concentration in the exhaust gases is reduced by up to 45% compared to that of the non-EGR engine.

Since the impact of the engine load on NO_x concentration in the exhaust gas is very high (60 ppm – 1200 ppm), to further analyze the effect of EGR on the concentration of this exhaust gas component, see below (Fig. 9b) bar charts separately for selected engine loads.

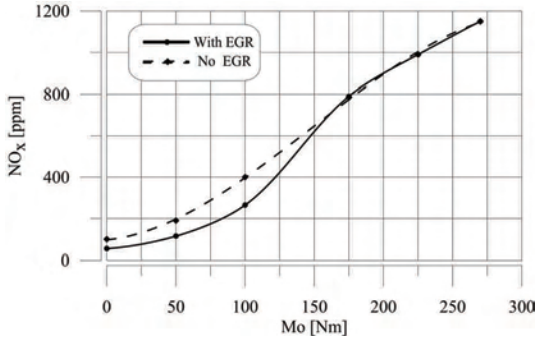


Fig. 9. Influence of the engine load on the NO_x concentration in exhaust gases for engine operating with/without EGR

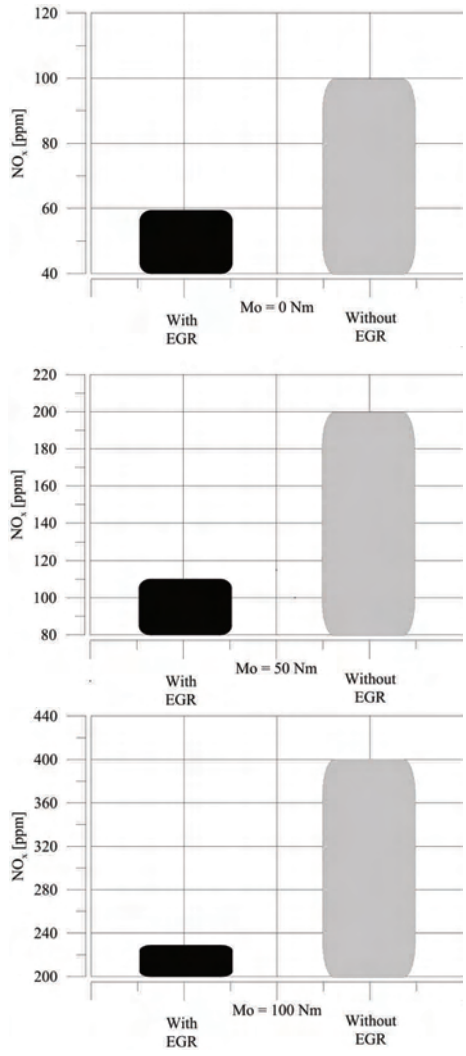


Fig. 9b. Influence of the engine load (within the range of the EGR activity) on the NO_x concentration in exhaust gases for engine operating with/without EGR

Unfortunately, as mentioned earlier, in terms of high engine loads, where the concentration of nitrogen oxides is the greatest, the engine controller must shut the system down because of the high demand for clean air used to burn high fuel dose.

As a matter of principle, exhaust gases recirculation might seem to be the result of the reduction of NO_x concentration in the exhaust gases for an EGR engine only because of the limited availability of oxygen, oxygenating the nitrogen from the air. Of course, this is not just the EGR mechanism. A more detailed analysis of this phenomenon will be carried out in the second part of the article, which shows the effect of EGR on the course of indicator graphs and rate of heat release in the engine cylinder working with/without exhaust gas recirculation.

Carbon monoxide is a typical incomplete combustion product that comes into being by global or local oxygen deficiency. Since the exhaust gases recirculation is intended to reduce the amount of oxygen in the engine cylinder, it must therefore lead to an increase in the CO concentration in the engine exhaust gases. This is shown in Fig. 10.

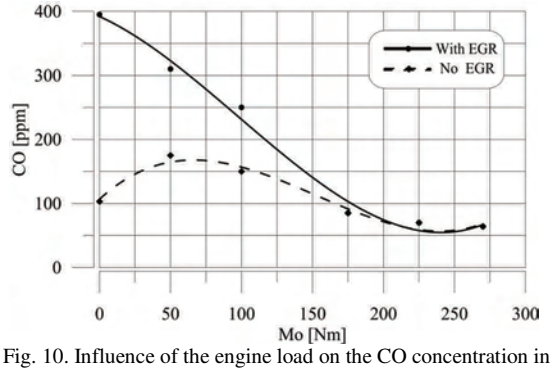


Fig. 10. Influence of the engine load on the CO concentration in exhaust gases for engine operating with/without EGR

As far as the engine load, at which the EGR valve is open is concerned, the CO concentration in the exhaust gases is greater by 75–40% compared to the carbon monoxide concentration in the exhaust gases of the non exhaust gas recirculation engine. However, the increase in CO concentration in the exhaust of the contemporary CI engine is not a problem, as these engines are equipped with an oxidation catalytic convertor which, at values of $\lambda > 2$ (Fig. 5) effectively catalyzes carbon monoxide.

In the exhaust gas used in the testing of the VW 1.9 TDI engine, under test conditions, the unburned hydrocarbons concentration, both with and without the EGR system varies from just a few dozen ppm. Of course, it is larger for an open EGR valve. This is mainly due to not limiting the amount of oxygen in the engine cylinder working with the EGR, which results in a reduction in combustion temperature. One reason for the lower maximum combustion temperature in the case of an EGR engine is the shortening of self-ignition delay (τ_s), but the analysis of this phenomenon will be carried out in the second part of the article on the effect of EGR on the parameters of the graphs and the velocity of heat generation. As with the carbon monoxide concentration, unburned HC emissions do not pose a problem to those oxidation catalytic convertors operating at big excess air ratio λ. A more serious problem, however, is the effect of exhaust gas recirculation on the smoke exhaust of diesel engine. This is shown in Fig. 11.

This phenomenon is unfavorable because as the exhaust smoke increases, the emission of particulate matter (PM) increases too. This is typical of most engine methods that reduce NO_x concentration in exhaust gases. Reducing the maximum combustion temperature to reduce NO_x emis-

sions also reduces the efficiency of the combustion of the particulate matter generated in the engine cylinder, which increases the PM emissions in the exhaust gas of the diesel engine. Of course, in another stage of the combustion process, nitrogen oxides are formed (mainly in the kinetic combustion stage), and in another stage, the resulting PM particles are burned up, but the analysis of these phenomena is shown in the second part of this article.

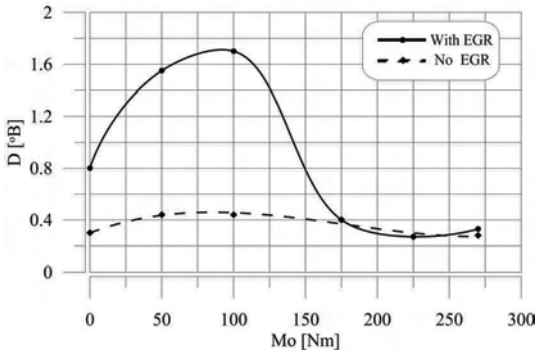


Fig. 11. Smoke exhaust D of diesel engine operating with/without EGR

3. Conclusions

In conclusion, the use of non-cooled exhaust gas recirculation in a diesel engine (compared to an engine without EGR) results in:

- on the idle run of the engine – reduced hourly fuel consumption,
- as regards small and medium loadings of the engine, EGR increases an hourly fuel consumption, which results in a reduction in the overall efficiency of the engine by up to 20% compared to the engine without exhaust gas recirculation,
- as regards engine load where the exhaust gases recirculation system is turned on, a clear EGR effect reducing the nitrogen oxide concentration in the exhaust gases (up to 45%) can be observed. However, at the highest engine loads, when nitrogen oxides are generated the most, it is not possible to use an exhaust gas recirculation system (due to the high engine demand for large amounts of air needed for burning a large dose of fuel)
- applying an EGR system increases the CO concentration by as much as 70% compared to engine operation with closed exhaust gases recirculation valve. However, in CI engines this is not a problem, due to the high efficiency of the catalytic oxidation reactors,
- in CI engines, the decrease in nitrogen oxide emissions is accompanied by increasing smoke exhaust and particulate PM emissions. With the exhaust gases recirculation system, an increase of over 70% is observed. This requires the use of post-processed methods for purifying particulate matter such as FAP or DPF filters,
- the exhaust gases recirculation system is a method that performs its function in the small area and average engine load with respect to the reduction of NOx concentration in exhaust gases at this point. The EGR, however, adversely affects a number of engine energy parameters and the concentration of other harmful exhaust gases,
- the comparison of the indicator graphs and the rate of heat release in the engine cylinder operating with/without the EGR will allow a deeper analysis of the causal effect of exhaust gas recirculation on the actual diesel engine work cycle (second part of the article).

Nomenclature

CI	compression ignition
CO	carbon monoxide
D	exhaust smoke
EGR	exhaust gas recirculation
G_p	fuel consumption
HC	unburned hydrocarbons
Mo	engine torque
NO_x	nitrogen oxides
PM	particulate matter
p_d	air pressure after the turbocharger
t_{air}	temperature inside the intake manifold
$t_{air,a.ch}$	air temperature after the turbocharger
t_{exh}	exhaust gas temperature before the turbine
λ	excess air ratio
η_v	volumetric efficiency of engine cylinder
η_o	total efficiency of engine cylinder
τ_s	self-ignition delay

Bibliography

[1] MERKISZ, J. Ekologiczne problemy silników spalinowych. Tom 1. *Wydawnictwo Politechniki Poznańskiej.* Poznań 1998.

[2] HEYWOOD, J.B. Internal combustion engine fundamentals. *McGraw-Hill Book Company*, Series In mechanical engineering, USA, 1988.

[3] MYSZKOWSKI, S. Recyrkulacja spalin w silnikach cz.1. Dodatek techniczny do wiadomości *Inter Cars S.A.* 2010, **35**.

[4] CIEŚLIK, W., BOROWSKI, P., PIELECHA, I. et al. System recyrkulacji spalin we współczesnych konstrukcjach silnikowych. *Logistyka.* 2014, **3**.

Jerzy Cisek, DSc. DEng. – Faculty of Mechanical Engineering at Cracow University of Technology.

e-mail: *JCisek@pk.edu.pl*



Article citation info:
BALAWENDER, K., KONIECZNY, D., KUSZEWSKI, H. et al. The effect of physicochemical properties of fuels on ecological parameters of a diesel engine. *Combustion Engines*. 2017, **171**(4), 274-278. DOI: 10.19206/CE-2017-447

Krzysztof BALAWENDER
Dariusz KONIECZNY
Hubert KUSZEWSKI
Kazimierz LEJDA
Krzysztof LEW
Paweł WOJEWODA

CE-2017-447

The effect of physicochemical properties of fuels on ecological parameters of a diesel engine

The objective of the research results of which are presented in this paper was to determine the effect of selected physicochemical properties of fuels on ecological parameters of a diesl engine. Physicochemical parameters of fuel have a decisive effect on correct functioning, operating parameters, and cleanliness of the exhaust gas emitted to the environment by any combustion engine. Results of physicochemical studies can be useful in developing fuels blends of specific properties, whereas results obtained in the course of tests carried out on an engine test bench allow to optimize parameters of the fuel injection process with the aim to reduce emissions of toxic compounds to atmosphere.

Key words: *fuel properties, diesel engine, ecological parameters*

1. Introduction

Until quite recently, toxicity of fuels were considered only from the point of view of hazards to human health and life. Nowadays, the problem is considered from the perspective of protection of the whole nature. Information about toxic properties of any specific fuel must be disclosed in the Material Safety Data Sheet according to EU Directive 91/155/EEC [4, 7].

Adverse effects of fuels used in transport on natural environment can be both direct and indirect. As far as the direct environmental effect are concerned, the effects can be categorized as follows [1, 3]:

- pollution of ecosystems,
- toxic effects on living organisms,
- persistence in the environment.

Indirect effects on the natural environment are related mainly to toxic product of combustion of engine fuels which, according to applicable normative instruments, include: carbon oxide (CO), nitrogen oxides (NO_x), hydrocarbons (HC), and particulate matter (PM). Apart from that, exhaust gases contain many toxic compounds which are not subject to any limits. For instance, 65 chemical compounds have been identified in diesel fuel, including 14 mutagenic polycyclic aromatic compounds of which 9 are considered carcinogenic [1, 6, 10].

Fuels containing fractions with high boiling point are characterized with increased emission of particulate matter, more exhaust smoke, and lower content of nitrogen oxides. The effect of presence of heavy fractions in the fuel on emissions is of indirect nature, via an increased tendency to develop the carbon deposit on injector nozzles and in combustion chamber. This in turn disrupts the course of the combustion process and leads to decrease of its effectiveness, increase of emissions of unburned hydrocarbons, carbon oxide, and particulate matter. To prevent this, fuels are treated with suitable washing detergents.

Another factors affecting toxicity of exhaust gases are fuel viscosity and density, as these parameters have a direct effect on the volume of the fuel charge delivered to the combustion chamber and the quality of spraying which are decisive for the course of combustion process. On the other hand, higher fuel density results in increased emissions of particulate matter, especially in transient operating conditions of combustion engines [1, 2, 5, 8, 9, 12].

A particularly harmful component of fuels is sulfur presence of which is the cause of emission of sulfur oxides, particulate matter, and nitrogen oxides to atmosphere. In the course of combustion process occurring in engine, sulfur contained in fuel is oxidized to SO_2 which, oxidized subsequently to SO_3, can react with water produced in the same combustion process and create sulfuric acid. Sulfur dioxide and trioxide, emitted together with the exhaust gas to the atmosphere, are the cause of the so-called acid rains. Moreover, sulfur acid is the cause of corrosion attacking engine components [1, 11].

Fuels containing aromatic hydrocarbons in their formulations show also an adverse effect on cleanliness of engine exhaust gases. Increased quantity of these hydrocarbons in fuel contributes to increased emissions of nitrogen compounds and particulate matter [11].

2. Experimental setup and methodology

The measuring devices used to determine basic parameters of fuels selected for testing (Figs 1–3) included instruments constituting research equipment of the Consumable Materials Laboratory run by the Department of Combustion Engines and Transport, Rzeszow University of Technology [5]. The present paper presents result obtained for commercially available diesel fuel (ONH), FAME (Fatty Acid Methyl Esters) (B100), and a blend containing 40% of rape oil and 60% of commercially available diesel fuel (OR40). Much wider range of fuel blends configurations was presented in [7] where it has been found that the OR40 blend is characterized with the highest usefulness among the other tested fuels. Therefore this paper presents results obtained for this configuration.

a) b) c)

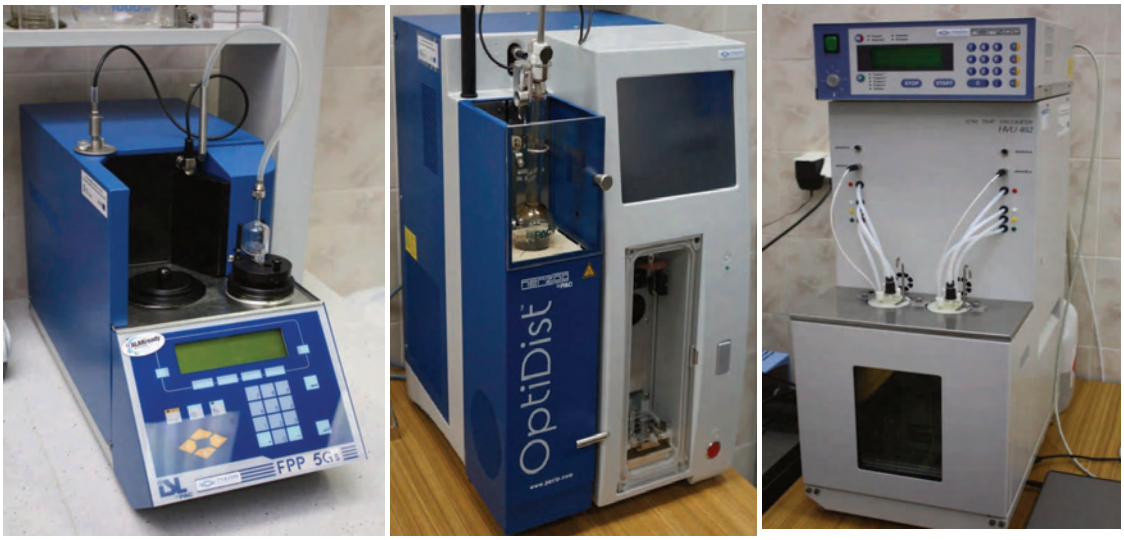


Fig. 1. Research devices: (a) FPP 5Gs Automated Cold Filter Plugging Point Analyzer; (b) OptiDist Automated Distillation Analyzer for Refining; (c) HVU 482 Automated Ubbelohde Viscometer

a) b)



Fig. 2. Research devices: (a) Cetane ID 510 Cetane Analyzer; (b) IKA C200 Automated Bomb Calorimeter

a) b)



Fig. 3. Research devices: (a) HFP 339 Pensky-Martens Flash Point Analyzer; (b) DMA 4500 M Accurate Density Meter

Parameters of the tested fuels as far as the required measurements are concerned, were determined according to procedures defined in applicable standards.

To study the effect of fuel on ecological-related parameters, a single-cylinder diesel test engine of SB3.1/CR type was used equipped with a fuel injection system of Common Rail type allowing to inject five fuel charges per engine working cycle at different injection pressures, developed in the Department of Combustion Engines and Transport, Rzeszow University of Technology. The engine is a modified version of the experimental engine SB3.1 designed and constructed by the Communication Equipment Research and Development Center in Mielec (Fig. 4). Technical details of SB3.1 engine are presented in Table 1.

Table 1. Technical specification of SB3.1 with original fuel system [9]

Parameter type	Parameter value
Number of cylinder	1
Number of strokes	4
Cooling system	liquid
Piston stroke	146 mm
Cylinder diameter	127 mm
Displacement volume	1850 cm^3
Compression ratio	15.75
Engine rated power	23 kW
Rated speed	2200 rpm
Maximum torque	110 Nm
Speed at maximum torque	1600 rpm
Engine rotation sense (as seen from flywheel side)	CCW
Oil lubrication system	circulating forced
Valve clearance on cold engine	0.5 mm
Injector opening static pressure	16.67 + 0.49 MPa

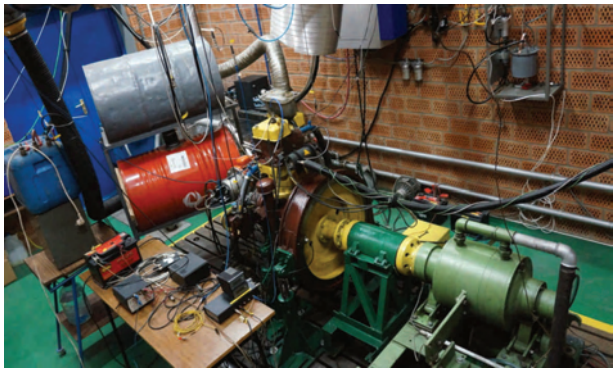


Fig. 4. SB-3.1 single-cylinder experimental engine equipped with CR-type fuel system

After completion of preliminary engine tests aimed at determination of measuring points, the actual tests were carried out for engine performance characteristics the course of which is one of the most important features used in comparative and functional analyses concerning combustion engines. The criterion adopted for the maximum load applied to the test engine, at constant injection pressure (100 MPa) and injection advance angle (18° CA), was the smoke opacity value of 25 HRT. Individual measuring points were selected for rotational speeds in the range 1200–1600 rpm with step of 100 rpm. The selected parameter was the injection duration (injector controlling pulse duration time). The determined measuring points are listed in Table 2.

Table 2. The engine control parameters determined in the course of research

No.	Engine speed n [rpm]	Injection duration t_{is} [μs]
1.	1200	3150
2.	1300	3000
3.	1400	2750
4.	1500	2600
5.	1600	2600

The soot content in exhaust gases was measured with the use of AVL Micro Soot Sensor measuring system (Fig. 5). Fig. 6 is a screenshot of the program window used to record the soot content in exhaust gases.



Fig. 5. AVL Micro Soot Sensor system for measuring soot concentrations in the exhaust gases

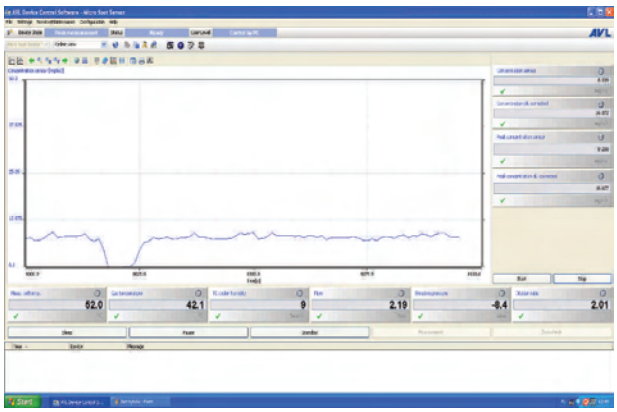


Fig. 6. A view of program window used to record soot concentration in exhaust gases [7]

3. Results and discussion

As a result of the performed research, values of the following physicochemical properties characterizing the fuels selected for the assessment were measured: density at 15°C; flash point; cold filter plugging point (CFPP); kinematic viscosity at 40°C; derived cetane number (DCN); and fraction composition. The obtained results are presented in Table 3.

Table 3. Parameters of the tested fuels

Fuel parameters		Unit	ONH	B100	OR40
Density at 15°C		g/cm^3	0.83411	0.88343	0.86849
Flash point		°C	59	149.5	66.5
CFPP		°C	–29	–22	–17
Kinematic viscosity at 40°C		mm^2/s	2.9491	4.3288	7.8408
Higher heating value		MJ/kg	43037	37417	40516
DCN		–	53.1	52.27	51.06
Fractional composition	E250	vol%	40	0	24
	E350	vol%	96	90	93
	T95	°C	345	354	–

According to the adopted objective, engine tests allowed to determine the effect of physicochemical properties of selected fuels on environment parameters of diesel engines. Based on the recorded ecological-related parameters of the engine, such as concentration of hydrocarbons, nitrogen oxides and soot, corresponding charts were made (Figs. 7–9).

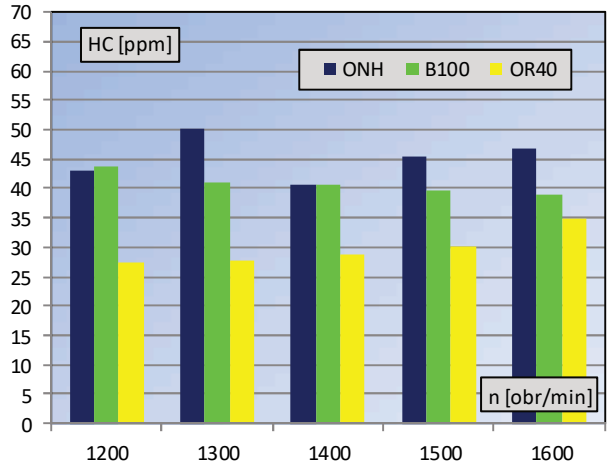


Fig. 7. Concentration of hydrocarbons HC in exhaust gases for test engine performance characteristics

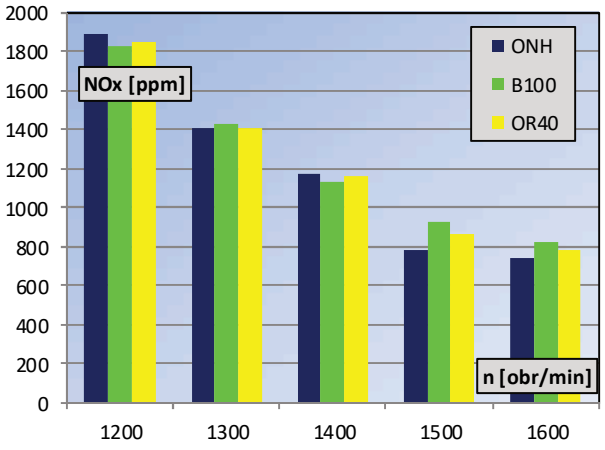


Fig. 8. Concentration of nitrogen oxides NO_x in exhaust gases for test engine performance characteristics

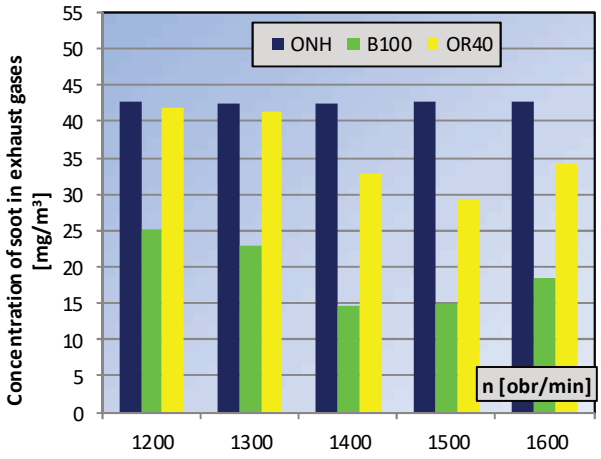


Fig. 9. Concentration of soot in exhaust gases for test engine performance characteristics

Figs 7–9 presents results of test with three fuel types (ONH, B100, OR40) in which concentrations of hydrocarbons, nitrogen oxides, and soot in exhaust gases were determined. Analysis of the results revealed that concentration of nitrogen oxides in the exhaust gases increases with decreasing engine speed. This follows from the fact that the decrease of the engine speed was accompanied by an increase of the load which in turn resulted in an increase of the exhaust gases temperature and the related increase of nitrogen oxides emissions.

For given engine speed, the injection duration was selected so that the force applied to the brake reached its maximum at the assumed smoke opacity of exhaust gas on the level of 25 HRT corresponding to concentration of soot in the exhaust gases of about 42 mg/m^3 (which can be clearly seen in Fig. 9). Determination of the parameter was performed for ONH diesel fuel which was selected a reference fuel. Under the adopted assumptions, concentration of soot in exhaust gases for the other two fuels was lower, though varied, depending on the engine speed.

4. Summary and conclusions

Properties of substitution fuels which can be potentially used in diesel engines, are usually compared to those of regular diesel fuel. Results of determination of physicochemical properties of fuels and experiments carried out on the engine test bench were used to assess the effect of individual fuel parameters on ecological-related parameters of the test engine.

An important parameter of fuels is their viscosity which significantly affects both the fuel spraying and combustion process and as a consequence, concentration of toxic components in exhaust gases.

The results presented in Figs 7–9 show that relatively small decrease of the derived cetane number results in reduction of hydrocarbons HC and soot content in exhaust gases; as far as concentration of nitrogen oxides NO_x is concerned, increase of the autoignition delay result in a slight increase of the parameter (compared to the increase of the combustion delay time and reduction of the derived cetane number value which show more distinct effect on the increase of concentration of nitrogen oxides).

Bibliography

[1] BACZEWSKI, K., KAŁDOŃSKI, T. Paliwa do silników o zapłonie samoczynnym. *WKŁ*, Warszawa 2008.

[2] BALAWENDER, K., KUSZEWSKI, H., LEJDA, K., LEW K. The study on injection parameters of selected alternative fuels used in diesel engines. *IOP Conf. Series: Materials Science and Engineering*. 2016, **148**, 012070.

[3] JAWORSKI, A., KUSZEWSKI, H., LEW, K., USTRZYCKI, A. Ocena przydatności paliw zastępczych do silników o ZS autobusów miejskich na podstawie wybranych parametrów wtrysku. *Systemy i Środki Transportu Samochodowego*. Monografia pod redakcją naukową Kazimierza Lejdy, Transport'12, 2012, **3**, 143-148, Rzeszów.

[4] JAWORSKI, A., KUSZEWSKI, H., USTRZYCKI, A. Wpływ biododatków na parametry energetyczne paliw stosowanych w spalinowych napędach środków transportu. *Międzynarodowa Konferencja Naukowa w Kijowie*. ВІСНИК. 2011, **23**, 95-100, Kijów.

[5] LEJDA, K. Selected problems of fuel supply in high-speed diesel engines. *Published by Meta.* Lvov, 2004, 225.

[6] LEJDA, K., KUSZEWSKI, H., LEW, K. Wpływ właściwości fizykochemicznych paliw na parametry operacyjne silnika o ZS. *Combustion Engines*. 2015, **162**(3), 915-920.

[7] LEW, K. Opracowanie kryteriów doboru paliw do specyfiki napędów wykorzystywanych w komunikacji miejskiej. *Rozprawa doktorska*. Poznań 2014.

[8] ORZECHOWSKI, Z., PRYWER, J. Rozpylanie cieczy w urządzeniach energetycznych. *Wydawnictwa Naukowo-Techniczne*. Warszawa 1994.

[9] UZDOWSKI, M. Problematyka wykorzystania paliw alternatywnych do zasilania silników trakcyjnych. *MOTROL*. 2008, 143-146.

[10] WIŚLICKI, B. Eksploatacja silników Diesla w aspektach ochrony środowiska w Polsce. *Paliwa, Oleje i Smary w Eksploatacji*. 2000, **73**, 34-38.

[11] Worldwide Fuel Charter, September 2006.

[12] ZABŁOCKI, M. Wtrysk i spalanie paliwa w silnikach wysokoprężnych. *Wydawnictwo Komunikacji i Łączności*. Warszawa 1976.

Krzysztof Balawender, DEng. – Faculty of Mechanical Engineering and Aeronautics at Rzeszów University of Technology.



Dariusz Konieczny, MEng. – Faculty of Mechanical Engineering and Aeronautics at Rzeszów University of Technology.



Hubert Kuszewski, DEng. – Faculty of Mechanical Engineering and Aeronautics at Rzeszów University of Technology.



Prof. Kazimierz Lejda, DSc., DEng. – Faculty of Mechanical Engineering and Aeronautics at Rzeszów University of Technology.



Krzysztof Lew, DEng. – Faculty of Mechanical Engineering and Aeronautics at Rzeszów University of Technology.



Paweł Wojewoda, DEng. – Faculty of Mechanical Engineering and Aeronautics at Rzeszów University of Technology.



Article citation info:
SZYMAŃSKI, G.M., MISZTAL, W. Analysis of measurement points sensitivity of vibration signals on the stand of jet engine. *Combustion Engines*. 2017, **171**(4), 279-282. DOI: 10.19206/CE-2017-448

Grzegorz M. SZYMAŃSKI
Wojciech MISZTAL

CE-2017-448

Analysis of measurement points sensitivity of vibration signals on the stand of jet engine

The diagnostic testing of internal combustion engine can be made by using working processes and methods which take advantage of leftover processes. Working processes give information about general condition of internal combustion engine. Leftover processes give information about condition of particular subassemblies and kinematic couples; hence they are used as autonomous processes or as processes supporting other diagnostic methods. Methods based on analysis of vibrations and noise changes to determine technical condition of object are named as vibroacoustic diagnostics. In papers about vibroacoustic diagnostics of engine, problems connected with difficulty to select test point and to define diagnostic parameters containing essential information about engine's condition, are most often omitted. Selection of engine's working parameters and conditions of taking measurements or recording vibration signal are usually based on references, researcher's experience or intuition. General assumptions about taking measurements of signal closest to its source are most often used. This paper presents a new approach to vibroacoustic diagnostics of jet engine. Selection of measurement points of vibration signals on the basis of tests stand results was suggested and perform a sensitivity analysis of measurement points on the engine support.

Key words: *vibration signal, jet engine*

1. Introduction

In the capacity of drive units in the aircraft among other things the jet engines of high power rating are used. Diagnosing of their technical condition enables to carry out an overhaul policy conditioned by technical condition, to prevent most of unplanned outages and by detecting defects in early stage, to decrease significantly the scope and the cost of overhaul and service. Safety of transportation and their timelines constitute a separate issue.

To assess technical condition and working conditions (functional and operation parameters) of combustion engine, parameters and characteristics of vibration signal generated by combustion engine [1–3] are more and more often used. However, receiving from vibrations diagnostically useful information is not easy. It is difficult to identify and to deduct the technical or working condition of engine's part or subassembly on the basis of commonly used parameters and characteristics of vibroacoustic signal (VA), stems, among others, from complex nature of vibrations generated by engine, processes proceeding inside, coexistence of many sources of vibrations and complex kinetics.

This study hereafter will show the problem of choosing on the engine support the point of acquisition of the vibration signals for diagnostic testing (for the aspect engine power assessing).

2. Choosing the measurement point of the vibration signals

The following values describe working processes used in diagnostic testing of combustion engines: power, torque, reaction torque, instantaneous angular speed and turning angle of crankshaft etc. They are used as conceptualized parameters of technical condition of an engine. To assess technical condition of combustion engine, parameters of accompanying processes, working processes and parameters of processes used in nondestructive tests (e.g. ultrasounds) are used as a vector signal.

Parameters of accompanying processes (vibrations, noise, thermal processes, wear etc.) are used to diagnose detailed technical condition of engine and to localize failures. In diagnostic testing of jet engine, vibroacoustic processes (vibrations, noise) are the often used accompanying processes.

Because of placing the vibration transducers has strong influence on the results received after diagnostic signals analysis, in the course of drawing up a method for the diagnostic testing the important thing is choosing the point of vibration signal acquisition. In extreme case the place of vibration measurement improperly chosen might give wrong conclusions about the technical condition of jet engine.

3. Research methodology

Jet engine F100-PW-229 were the research object. This engine is used, among others, to drive aircrafts F16. It is an afterburning turbofan engine. Research concerning sensitivity of measurements points was carried out according to active experiment. Active experiment consists in purposeful change of input or disturbing parameters and observing influence of those changes on input parameters. Power of engine was taken as input parameter and vibration accelerations of jet engine's test stand are taken as output parameters.

The vibration transducers type 4513 and 8344 [7, 8] made by Brüel & Kjær company were chosen following the instructions comprised in the study [4, 5] and their frequency band was up to 10 kHz (for 4514) and up to 3 kHz (for 8344). In the course of diagnostic testing the signals in the band range from 0.1 Hz to 51.2 kHz were recorded. The sampling frequency was adjusted to the value of 131072 Hz and the accelerometers were mounted on the engine support by glue. To choose the places of measurement a principle that the transducer should be put in the place accessible and closest to the area where the working engine generate the vibration signals was taken [1, 6].To recording the vibration signals three pieces of the vibration converters (P1, P2, P3)

were used. Measurements were made for the following power settings: Idle, Middle (Mid), Afterburner min (AB Min), Afterburner max (AB Max).

Figure 1 presents a view the engine on the test stand while Figure 2 – the spatial orientation of the transducers for vibration measurements and the places of their mounting on tested object. To recording the vibration signals a Multi-Analyzer PULSE made by the Brüel & Kjær company was used. The view of the measurement equipment on the test stand is shown in Figure 3.

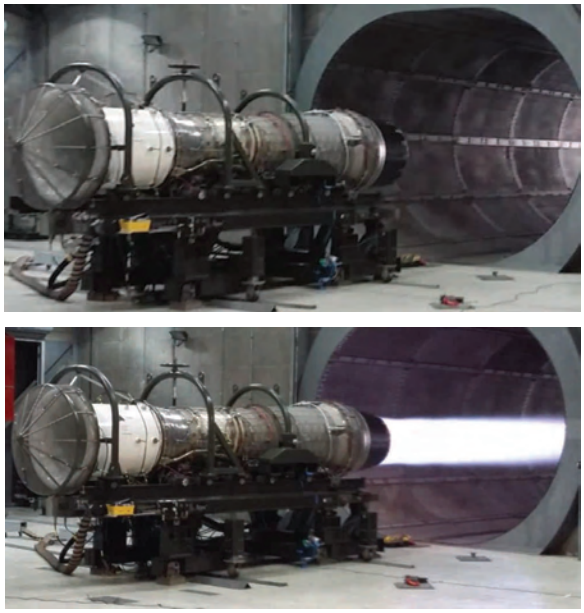


Fig. 1. View of the engine F100-PW-229 on the test stand

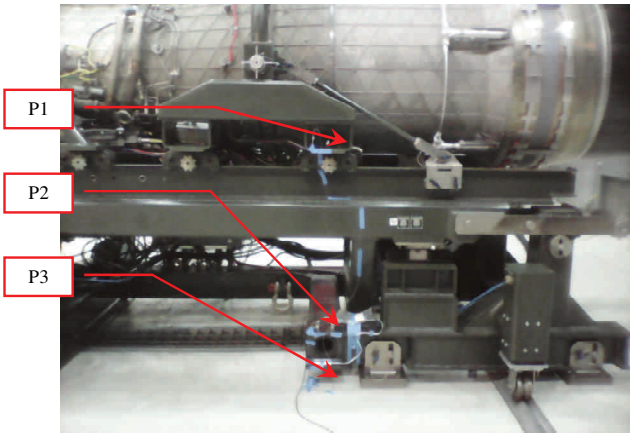


Fig. 2. Distribution of acceleration transducers on the test stand, engine F100-PW-229

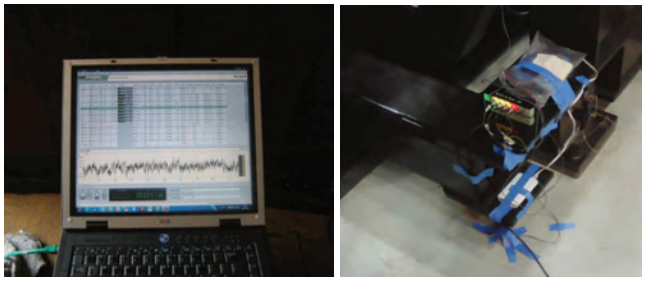


Fig. 3. View of the measurement equipment on the test stand

The device shown in Figure 3 enables the registration of the quick-changeable runs parallel on 17 ducts with the dynamics up to 160 dB.

4. Analysis of test results

To make selection of the best point of signal acquisition for assessing the power of engine, the tests of the engine stand were made and they consisted in impacting of the engine power for the test stand. To eliminate the casual errors and to obtain the averaging result, the operation described above was repeated several times. The aim was to determine such a vibration signals measurement place which would allow to make assessment of the impacting change of engine power for vibration signal. The analysis of the signals recorded were made in PULSE REFLEX [9] environment. The used software enabled to carry out an analysis of three signals at the same time. Such an analysis variant gave opportunity to determine the influence of the dynamical impacts in on the signals synchronously recorded in three different measurement points.

Selected tests results for determining the acquisition point of the vibration acceleration signals are shown in figures 4–7. Figure 4 shows the time histories of vibration signals for different measurement points with markers defining state of engine power during test.

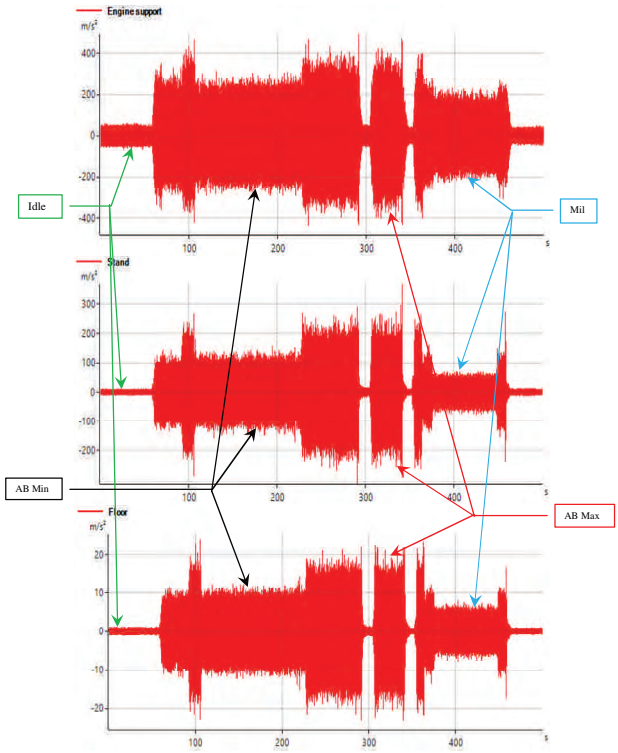


Fig. 4. Time histories of vibration signals for different measurement points

Figure 5 shows the averaging amplitude spectrums of the vibration acceleration signals synchronously recorded in three different measurement points. The demonstrated spectrums are the results of the analysis of vibration signals being outcome of the different power settings. In this figure the results are grouped by terms of settings power.

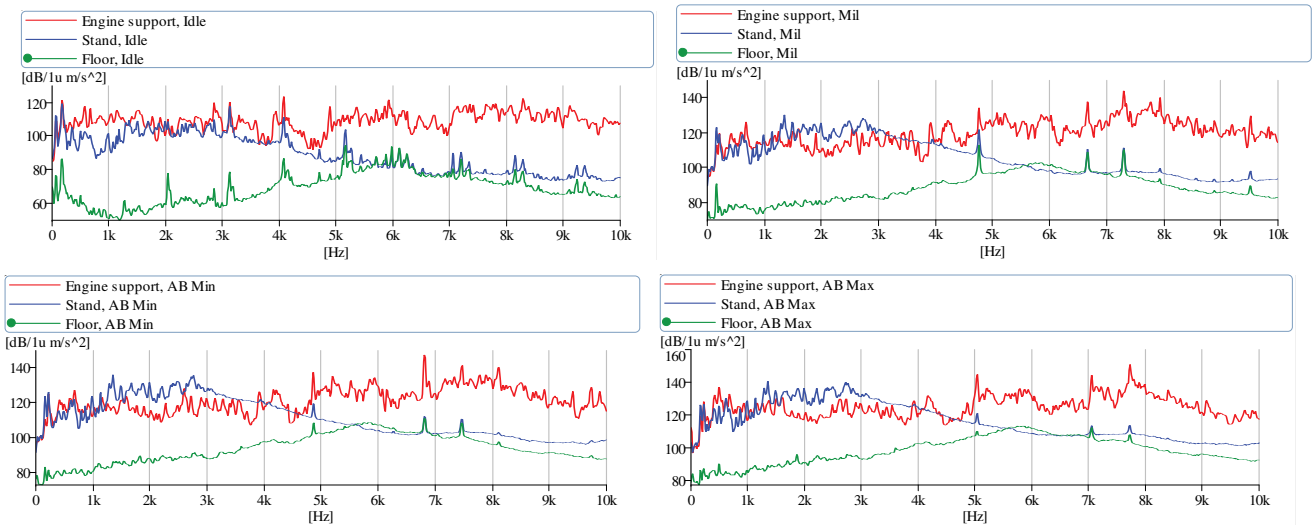


Fig. 5. The averaging amplitude spectrums of the vibration accelerations

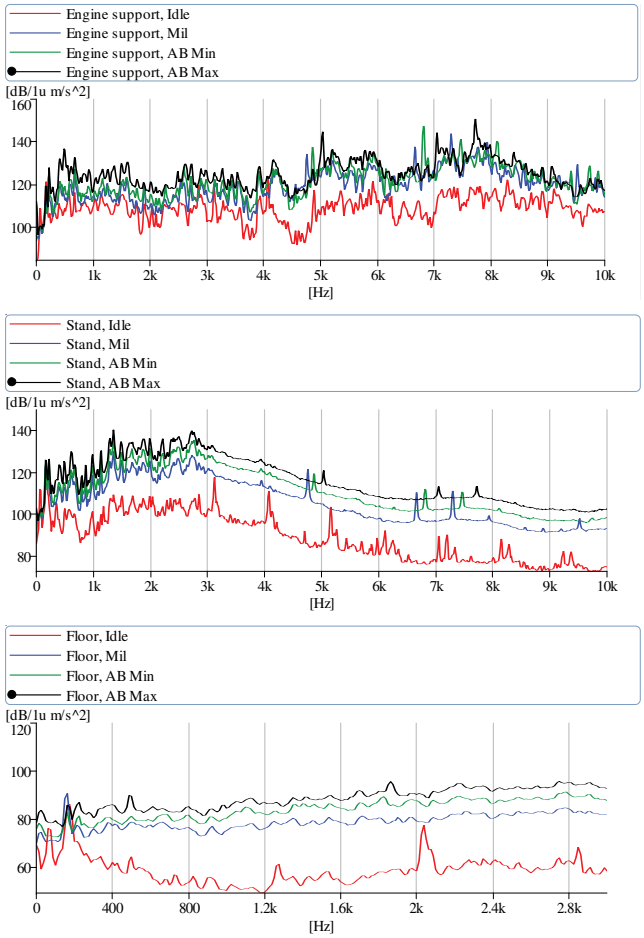


Fig. 6. The averaging amplitude spectrums of the vibration accelerations

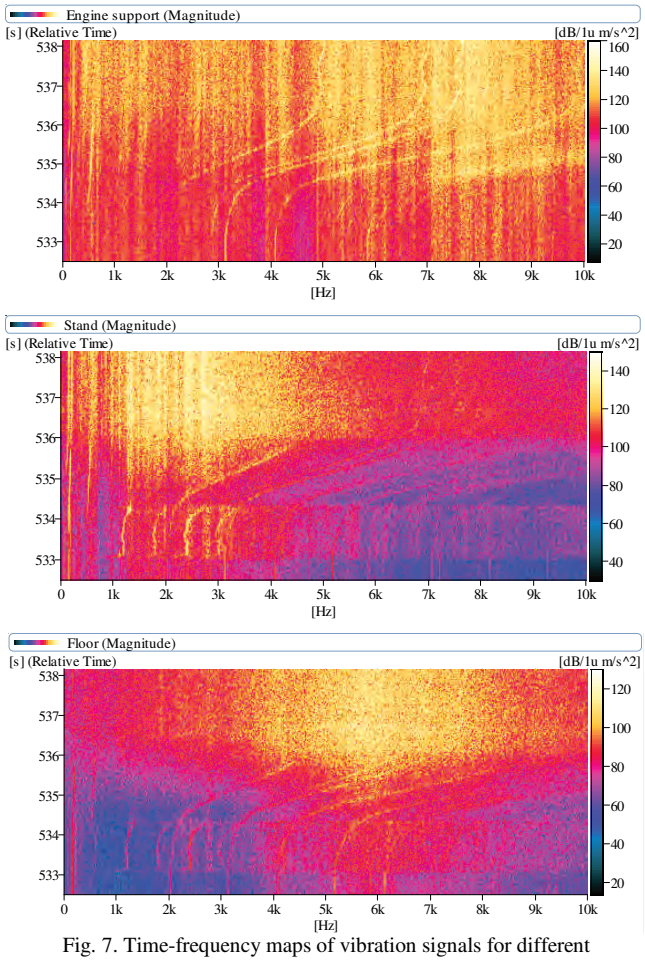


Fig. 7. Time-frequency maps of vibration signals for different measurement points

Figure 6 shows the average amplitude spectrum of vibration acceleration signals recorded at three different measurement points. In this illustration the results are grouped by measurement points.

The time-frequency analysis for the motor acceleration test from Idle to AB Max is shown in Figure 7. Visible frequency changes in time are the result of changes in the revolution speed of the engine shaft.

From the characteristics shown in Figures 4–7, it appears that to assess the action of power in an engine tested, the best thing is to apply the point P1 or P2 because they are characterized by the better dynamics than point P3. Measurement point P1 is better than P2, for analysis concerning with natural frequencies of system. Whereas point P2 is good to frequencies analysis related with

kinematics. To make an assessment of the engine power, point P3 is much less useful.

5. Conclusion

This paper shows a method which supports the choosing of the vibration signals acquisition points, it is based on an analysis of the test signals. This paper demonstrated that in the course of working out the test method is not enough to consider only the specialist literature and/or the some researcher's experience.

In described case all three measurement points met the requirements described in specialist literature, i.e. they were placed closest to the vibration source and they were easy accessible. However, to make an assessment of the power of engine, by the frequency characteristics analysis on the basis of test signals, point P1 and P2 was chosen.

Through the analysis of the presented test results it was found that the point of acquisition of the vibration signals, described as P3 should not be used for making an assessment of the engine power, because it is characterized by the low dynamics in the changes in the characteristics of spectrum test signals.

It is possible to use measurement point P3 for making a diagnosis of the other processes in jet engine. However, it is necessary first to make tests for proving the usefulness of this measurement point for a diagnostic testing.

Acknowledgements

This work was supported by Statutory Activities fund of the Institute of Combustion Engines and Transport, PUT (PL) 05/52/DSPB/0259.

Bibliography

[1] NIZIŃSKI, S., MICHALSKI, R. Diagnostyka obiektów technicznych. *Biblioteka Problemów Eksploatacji Polskie Towarzystwo Diagnostyki Technicznej*. Katedra Eksploatacji Pojazdów i Maszyn Wydziału Nauk Technicznych Uniwersytetu Warmińsko-Mazurskiego w Olsztynie. Instytut Technologii Eksploatacji w Radomiu, 2002.

[2] CZECHYRA, B., SZYMAŃSKI, G.M., TOMASZEWSKI, F. Assessment of camvalves clearance in internal combustion engine based on parameters of vibration – methodological assumption. *Combustion Engines*. 2004, **118**(1).

[3] SZYMAŃSKI, G.M. Analiza możliwości zastosowania wybranych charakterystyk sygnału drganiowego do diagnostyki silnika spalinowego. *Rozprawa doktorska*. Politechnika Poznańska, Poznań 2005.

[4] OSIECKI, J., ZIEMBA, S. Podstawy pomiarów drgań mechanicznych. *Państwowe Wydawnictwo Naukowe*. Warszawa 1968.

[5] SERRIDGE, M., LICHT, T.R. Piezoelectric accelerometers and vibration preamplifiers. *Brüel & Kjær*. 1987.

[6] ŻÓŁTOWSKI, B., ĆWIK, Z. Leksykon diagnostyki technicznej. *ATR*. Bydgoszcz 1996.

[7] 4513A – Piezoelectric IEPE accelerometer. 2017. www.bksv.com/media/doc/Bp2065.pdf.

[8] 8344A – Piezoelectric TEDS accelerometer. 2017 www.bksv.com/en/products/transducers/vibration/Vibration-transducers/accelerometers/8344.

[9] Pulse Analysis Software. 2017. www.bksv.com/en/products/PULSE-analysis-software.

Grzegorz M. Szymański, DSc., DEng. – Faculty of Machines and Transport at Poznań University of Technology.

e-mail: *Grzegorz.M.Szymanski@put.poznan.pl*



Capt. Wojciech Misztal, DEng. – 31st Tactical Air Base, Poznan-Krzesiny.



Article citation info:
CISEK, J. The influence of non-cooled exhaust gas recirculation on the indicator diagrams and heat release parameters in diesel engine cylinder. *Combustion Engines*. 2017, **171**(4), 283-288. DOI: 10.19206/CE-2017-449

Jerzy CISEK

CE-2017-449

The influence of non-cooled exhaust gas recirculation on the indicator diagrams and heat release parameters in diesel engine cylinder

This paper presents the results of the diesel engine research on the indicator and heat realized diagrams for VW 1.9 TDI working in 2 modes: with standard, non-cooled EGR system, and without this system. All of measurement was carried out on the some engine speed – 2000 rpm (speed of maximum engine torque) and various engine load. Some of the analyzed parameters were read directly from the measurement systems (e.g. indicator diagrams) or engine controller (e.g. start of injection) and the rest of them had to be calculated. The calculation of rate of heat release ($\delta Q/d\alpha$) was based on the well-known mathematical model. When the exhaust gas recirculation valve is open, the maximum of combustion pressure and rate of maximum kinetic heat release $(\delta Q_k/d\alpha)_{max}$ are smaller than when the valve is closed. These facts are connected with the shorter self-combustion delay for engine working with EGR. But this is also associated with reduction of the rate of maximum diffusion heat release $(\delta Q_d/d\alpha)_{max}$, which means that more particulates (PM) are excreted into the atmosphere. This fact explains e.g. significantly higher smog of exhaust gases for diesel engine which works with EGR system. The analysis results show that exhaust gas recirculation system slightly deteriorates the energetic parameters of VW 1.9 TDI engine, but, at the same time, significantly reduces the level of toxic nitrogen oxides in exhaust gases.

Key words: *diesel engine, exhaust gases, EGR, indicator diagrams, rate of heat release*

1. Introduction

This article is a continuation of the article CE-2017-446, which analyzed the influence of non-cooled exhaust gas recirculation on the diesel engine parameters. Tested Diesel engine VW 1.9 TDI worked in two operating modes:

– MODE I – with factory preset of EGR
– MODE II – without exhaust gas recirculation (EGR)

Data shown in Fig. 1 corresponds to the operation of the engine according to MODE I – factory setting of EGR. In MODE II, the percentage of opening of the EGR valve is 0% for all of range of engine torque.

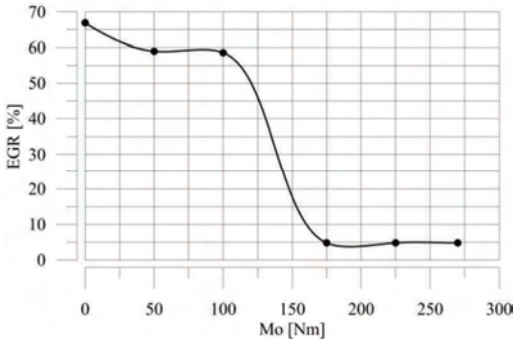


Fig. 1. Influence of engine load on factory change of opening of exhaust gas recirculation valve (EGR)

According to article CE-2017-446, the use of EGR reduces fuel consumption only at engine idle (compared to engine without EGR). At medium loadings of the engine, EGR increases hourly fuel consumption up to 20%, compared to the engine without exhaust gas recirculation. In this range of engine load, EGR effect reducing the nitrogen oxide concentration in the exhaust gases up to 45% can be observed. Applying an EGR system increases the CO concentration by as much as 70% compared to engine operation with closed exhaust gases recirculation valve. With the exhaust gases recirculation system, an increase of exhaust smoke (by Bosch method) over 70% was observed.

Because the comparison of the indicator graphs and the rate of heat realize in the engine cylinder operating with/without the EGR will allow a deeper study of the causal effect of exhaust gas recirculation, this paper analysis processes inside cylinder of engine working with and without EGR system.

2. Indicator diagrams parameters

Under the work conditions of the tested engine, the cylinder pressure is a function of the crankshaft angle, engine load and operating mode: with/without EGR. For these conditions, measurements of a number of open graphs were made and the differential characteristic, shown graphically in Fig. 2, were made. Each indicator graph is the average of 60 consecutive engine cycles, so that obtained results are representative, in spite of the natural fluctuations that result in subsequent engine cycles. It can be seen that the differential pressure in the engine cylinder working with/without EGR occurs only in the range from idle run to about 175 Nm. Above this load, the engine controller switches the EGR system off, due to the combustion of high fuel volumes that require air not mixed with the exhaust fumes in the intake manifold. This load range obviously coincides with the course of the closure characteristics of the EGR valves shown in Fig. 1.

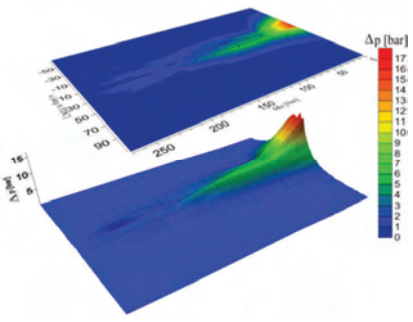


Fig. 2. Influence of crank angle of engine and engine load on pressure changing inside engine cylinder as a result of EGR valve closing

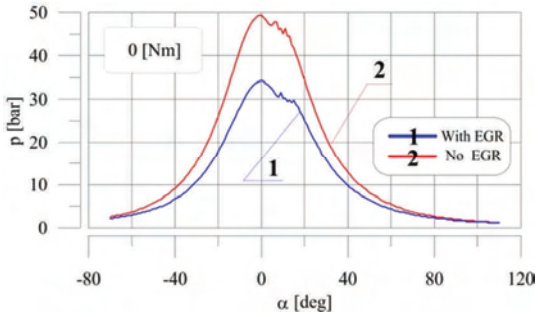


Fig. 3. Influence of the engine crank angle on the pressure inside engine cylinder for engine operating with/without EGR at torque 0 Nm

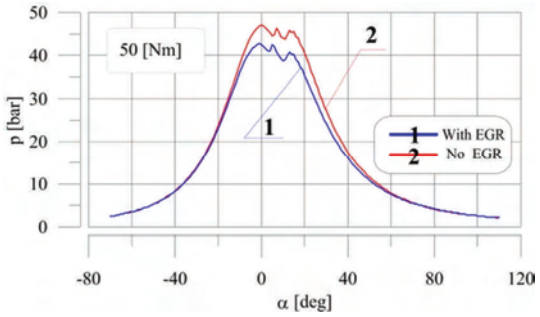


Fig. 4. Influence of the engine crank angle on the pressure inside engine cylinder for engine operating with/without EGR at torque 50 Nm

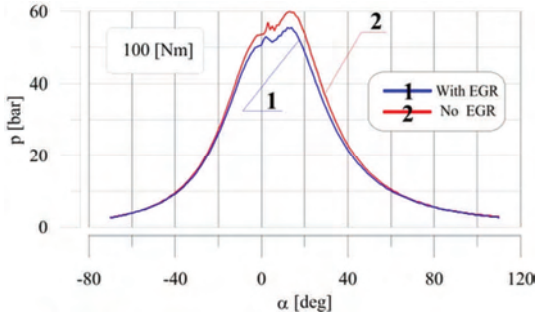


Fig. 5. Influence of the engine crank angle on the pressure inside engine cylinder for engine operating with/without EGR at torque 100 Nm

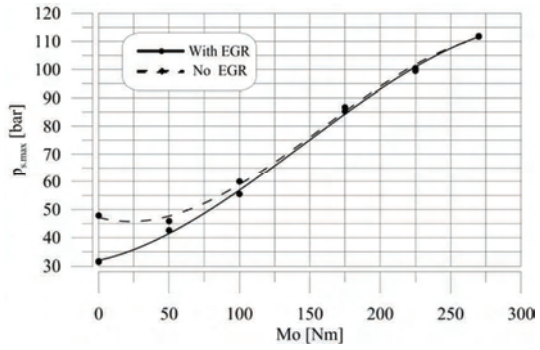


Fig. 6. Influence of the engine load on max pressure inside engine cylinder for engine operating with/without EGR

In order to analyze the pressure values in the engine cylinder working with/without EGR better, open indicator graphs were show for the 3 selected engine loads: 0 Nm, 50 Nm and 100 Nm, that is, in the engine work range where the EGR valve is open. This is shown in Figs 3–5. Clearly, in each of these cases, the pressure corresponding to the combustion process is significantly smaller for the engine operating with the exhaust gases recirculation. In reference to the maximum combustion pressure as a function of the engine load, this is shown in Fig. 6.

The greatest reduction in maximum combustion pressure $p_{s,max}$ resulting in the opening of the EGR valve, occurs on the idle run of the engine. Then $p_{s,max}$ for the engine operating at the factory EGR setting is about 60% lower than the pressure in the engine cylinder working without exhaust gas recirculation. Of course, the lower pressure is associated with a lower maximum combustion temperature, which is one of the main causes of the formation of NO_x in the engine cylinder, and later emission of the exhaust gas. At higher engine loads (engine torque), when the engine control unit (ECU) closes the EGR valve, the difference in maximum combustion pressure in the engine cylinder working with/without EGR is lower, because it is about 10%. This, however, ensures that the combustion process is carried out at lower temperatures, so that the NOx concentration in the exhaust gas is about 48% lower for the EGR engine compared to the non-EGR engine.

The NO_x concentration generated in the engine cylinder is shown not as much by the average combustion temperature (associated with the combustion pressure), as maximum combustion temperature, which also depends strongly on the max. rate of combustion pressure $(dp/d\alpha)_{max}$, shown in Fig.7.

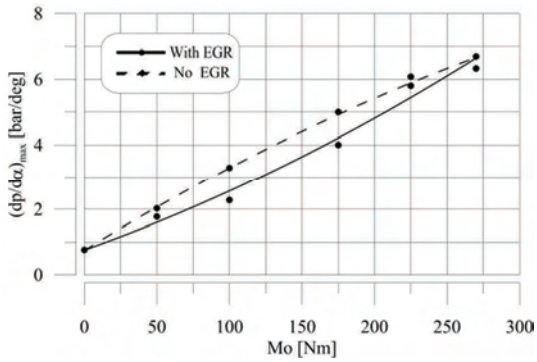


Fig. 7. Influence of the engine load on max rate of combustion pressure $(dp/d\alpha)_{max}$ for engine operating with/without EGR

From these data it is clear that for idle run of the engine (Mo = 0 Nm), the difference between maximal combustion pressure in the engine cylinder working with/without EGR is 60%, $(dp/da)_{max}$ is almost the same. For this reason, the NO_x flue gas concentration for the engine working with/without EGR is only 50 ppm. On the other hand, for a engine load Mo = 100 Nm, at which the difference in maximum combustion pressure for an engine running with/without EGR is only 8%, the difference $(dp/d\alpha)_{max}$ is the highest and equals 37%. At this point, the EGR system is most likely to reduce NO_x concentration (Fig. 8), because it does so up to about ca. 180 ppm (48%). A significant conclusion from this part of the study confirms that the reduction of NO_x concentration in the exhaust gas is not only related to the reduction of the maximum combustion pressure $p_{s,max}$, but also to the reduction of the maximum rise of pressure $(dp/da)_{max}$.

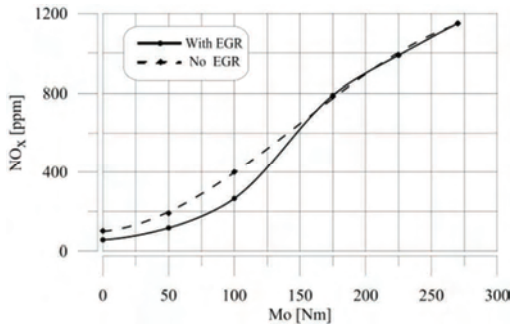


Fig. 8. Influence of the engine load on the NO_x concentration in exhaust gases for engine operating with/without EGR

Using the VCDS diagnostic interface, it was found that the start of fuel injection into the engine cylinder working with the EGR system occurred slightly earlier (ca. 1 deg) than for an EGR – disabled engine. This may be due to the difference in the density of the working medium (chemical composition and the temperature of pure air or air mixed with the exhaust gases), which shows itself in differences in the compression pressures shown in Figs 3–5, which is the back pressure with respect to the fuel injection. In the case of an EGR engine, the early start of fuel injection, however, does not result in self-ignition delay (τ_s), despite the beginning of the fuel injection to the pressure of the work factor that was much lower then (Figs 3–5). This is because the temperature of the air mixed with the hot exhaust, in the non-cooled EGR, is higher. Due to this physical phenomenon, the propensity for self-ignition of fuel (for an EGR engine) is greater and the start of self-ignition α_{ps} (Fig. 10) occurs much earlier, which leads to shortening self-ignition delay (τ_s) then – Fig. 11.

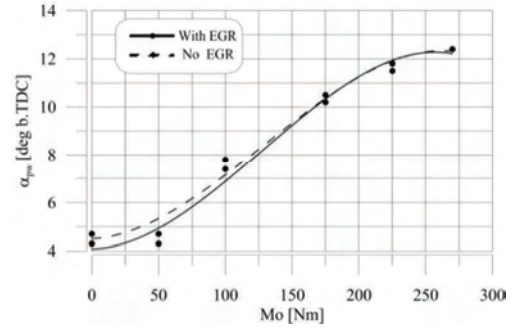


Fig. 9. Influence of the engine load on start of injection α_{pw} for engine operating with/without EGR

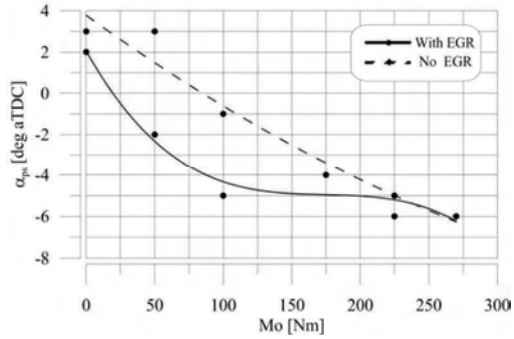


Fig. 10. Influence of the engine load on start of combustion α_{ps} for engine operating with/without EGR

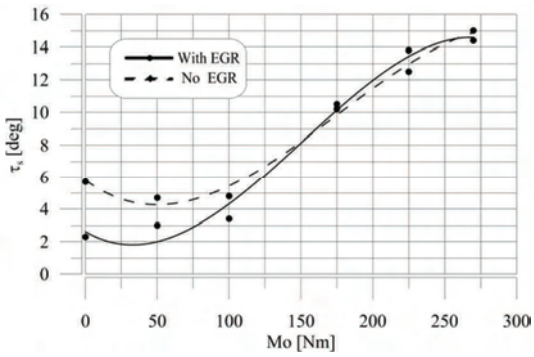


Fig. 11. Influence of the engine load delay of self-ignition τ_s for engine operating with/without EGR

In the range of small and medium loads of the engine working with the EGR, the delay of self-ignition is smaller by about 2˚deg. Reducing the self-ignition delay reduces the time between the start of fuel injection and self-ignition, so that less fuel accumulates in the combustion chamber until self-ignition. This leads to less explosive self-ignition of fuel, which means less dynamic combustion. This results in less crankshaft system dynamic load, reduced combustion noise and lower combustion pressure rise $(dp/d\alpha)_{max}$ and a lower maximum combustion temperature, resulting in a lower concentration of nitrogen oxides in the exhaust gas of the engine operating with EGR.

2. Rate of heat release

As the maximum temperature in the engine cylinder is a consequence of the combustion process, the effect of exhaust gas recirculation on the rate of heat release was also analyzed. This is particularly important for the analysis of the influence of structural and/or setup and/or fuel parameters on emissions of exhaust gas components. It appears that from the point of view of the composition of the exhaust gases (and also thermal efficiency of the engine), not only the value of the combustion temperature, but also its run-in time as a function of combustion time, is directly related to the distribution of the rate of heat release as a function of the angle of crankshaft rotation. The rate of heat release, with the breakdown of the kinetic and diffusion burns (Fig. 12), as commonly known; is it shows which combustion phase is responsible for the NO_x concentration and which one is responsible for the PM emissions in the engine exhaust gases.

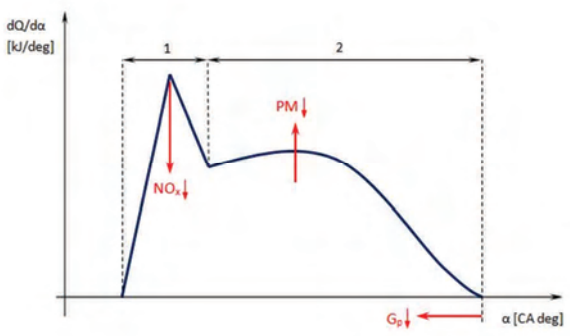


Fig. 12. Schema of the rate of heat release in a diesel engine: 1 – kinetic combustion phase 2 – diffusion combustion phase

The function of the rate of heat release, shown in Fig. 12, is a typical progress of CI engine in which the start of fuel injection was optimized due to the total efficiencies of the engine. This course is characterized by a high rate of kinetic combustion and a low rate of diffusion combustions. Because of the very strong reduction of emission intensity of NO_x in the exhaust gases over the last 20 years, modern CI engines use a delay of start of injection (compared to the optimal state for engine total efficiency). The later start of the injection takes place into a more compressed working medium with a higher temperature, which in turn facilitates fuel spontaneous combustion, thus reducing the delay of self-ignition of fuel (τ_s). As explained earlier, the reduction of self-ignition delay leads to less dynamic combustion, with a lower rate of heat release in the first uncontrolled combustion phase, just after the self-ignition of the fuel. There was also pilot-injection used in the engine tests, which further reduces the maximum rate of kinetic combustion. In this situation, the max rate of kinetic combustion is less than the max rate of diffusion combustion. This is advantageous in terms of reducing NO_x emissions in the flue gas (by reducing the maximum combustion temperature), but it also alleviates the maximum rate of heat released in the diffusion phase of combustion. This is a disadvantage due to the Particle Matter emission and the exhaust smoke. Diesel particle matter, mainly composed of carbon blacks, is produced in the engine's cylinder, under the conditions of reduced rate of heat release in diffusion combustion. In the final balance this process increases PM emission in exhaust gases of CI engine.

Unfortunately, it is similar in the case of exhaust gas recirculation: the decrease of self-ignition (τ_s – Fig. 11) reduces max rate of heat release at kinetic combustion (thanks to which the emission of NO_x in exhaust gases is reduced) and at the same time, rate of heat release at diffusion phase of combustion is reduced too, which significantly increases exhaust smoke and particulate matter emission.

This situation is shown in the graph of the rate of heat release as a function of the crank angle of engine working with/without EGR – Figs 13–15. In the engine range of load, where the factory EGR system works, it can be seen in the graph that the rate of heat release is lower for the engine with the open EGR valve than for the engine with EGR disabled. Thus, the EGR, which reduced the max kinetic heat release $(dQ_k/d\alpha)_{max}$ – Fig. 16, reduced the diffusion heat release $(dQ_d/d\alpha)_{max}$ as well – Fig. 17. According to the reasoning presented earlier, this unfortunately increases the emission of PM and exhaust smoke D, as shown in Fig. 18.

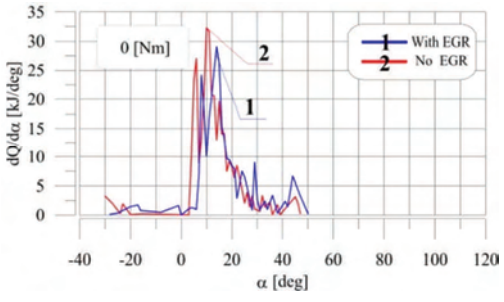


Fig. 13. Influence of the engine crank angle on the rate of heat release inside cylinder for engine operating with/without EGR at torque 0 Nm

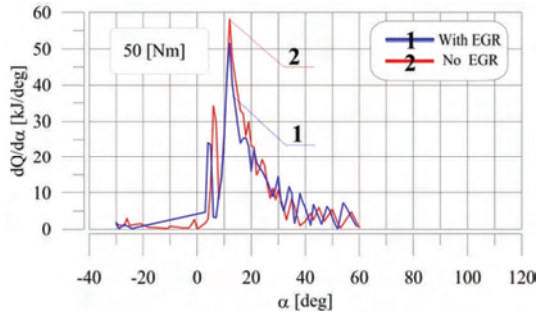


Fig. 14. Influence of the engine crank angle on the rate of heat release inside cylinder for engine operating with/without EGR at torque 50 Nm

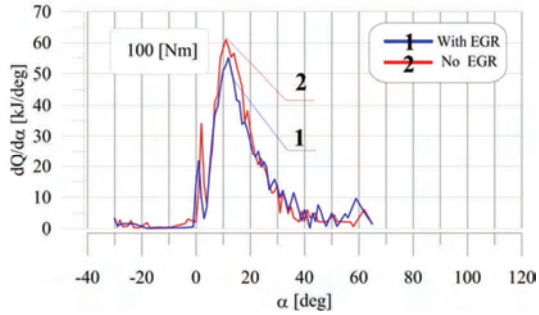


Fig. 15. Influence of the engine crank angle on the rate of heat release inside cylinder for engine operating with/without EGR at torque 100 Nm

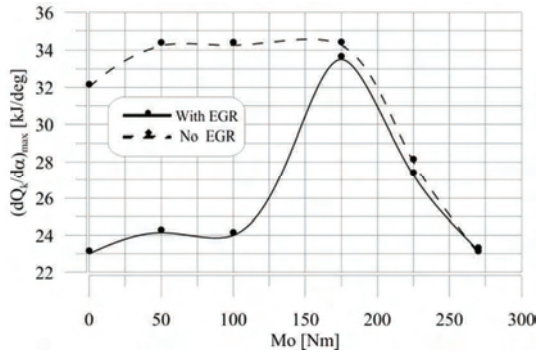


Fig. 16. Influence of the engine load on max rate of kinetic heat release $(dQ_k/d\alpha)_{max}$ for engine operating with/without EGR

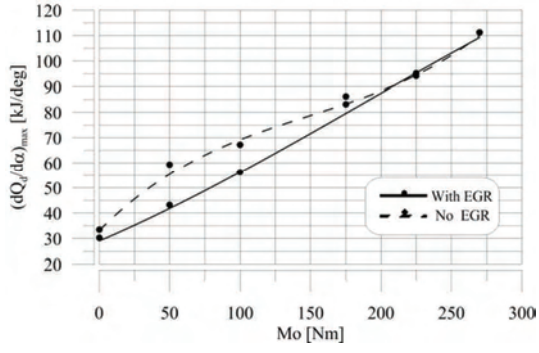


Fig. 17. Influence of the engine load on max rate of diffusion heat release $(dQ_d/d\alpha)_{max}$ for engine operating with/without EGR

As it has already been mentioned, most of the technical, structural, setup and fuel compositions, if they lead to a reduction in NO_x emissions, increase PM emissions and vice versa. This is due to the mechanisms of formation of nitrogen oxides and particulate matter under combustion

conditions in the cylinder of an internal combustion engine. The effect of mutual correlation, under these conditions, is schematically illustrated in Fig.19.

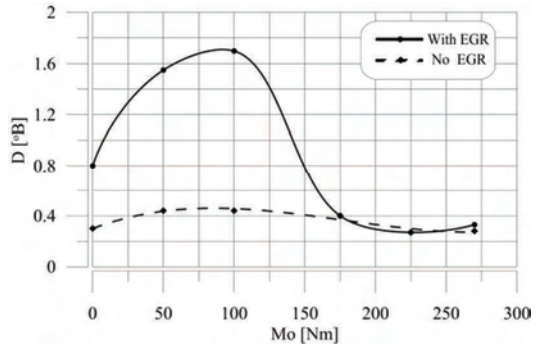


Fig. 18. Smoke exhaust D of diesel engine operating with/without EGR

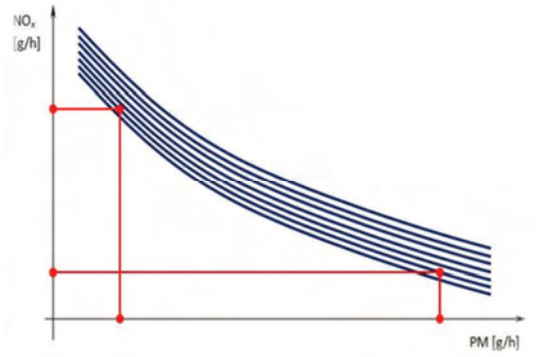


Fig. 19. The correlation between emission intensity of PM and emission intensity of nitrogen oxides emissions (NO_x) in diesel engine exhaust gases

Another fact (in addition to decrease of the delay of self-ignition), which in the case of exhaust gas recirculation reduces the maximum combustion temperature, is availability of oxygen involved in the combustion process, which is smaller then. Since a part of the clean air in the intake manifold is then replaced by exhaust gases, the amount of oxygen in both the engine cylinder and exhaust gas is reduced – Fig. 20.

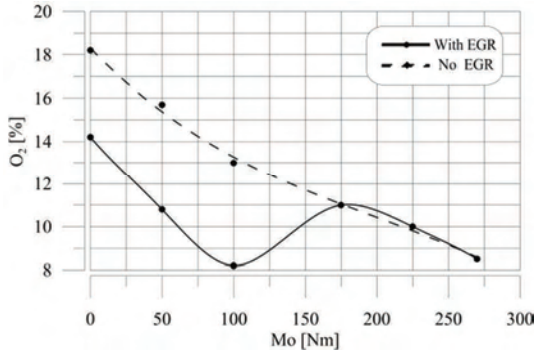


Fig. 20. Influence of the engine load on the O_2 concentration in exhaust gases for engine operating with/without EGR

Another factor that, in the case of exhaust gas recirculation, reduces the combustion temperature and thereby reduces the NO_x concentration in the exhaust gases is that there is much more carbon dioxide in the EGR engine cylinder than in the non-EGR engine. This is because in the delivered load of the engine cylinder there already is CO_2 from the previous engine cycle (within EGR). As the amount of CO_2 in the engine cylinder increases, the concentration of this compound in the engine exhaust is also increased, as illustrated in Fig. 21.

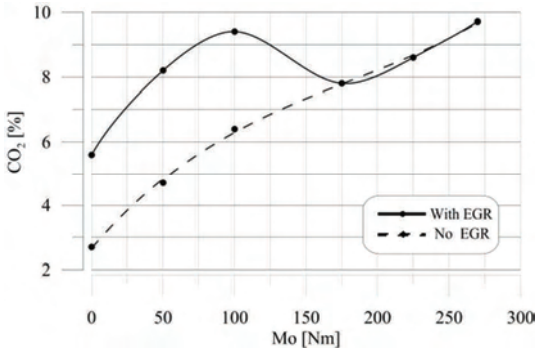


Fig. 21. Influence of the engine load on the CO_2 concentration in exhaust gases for engine operating with/without EGR

The increase in CO_2 concentration in the combustion process has a double effect on the reduction of the combustion temperature (and NO_x in the engine exhaust):

– The process of thermal dissociation of CO_2 is an endothermic process. The heat received from the working medium in the engine cylinder to decay CO_2 reduces the maximum combustion temperature. From the data [1], however, it appears that heat losses due to dissociation of particles at engine operating temperatures are virtually negligible. Even at temperatures above 2000 K they take ca. 0.5% of the heat supplied in the fuel.
– CO_2 molecules form specific thermodynamic ballast. They absorb heat (in the physical sense) that could be consumed by increasing the internal energy of the working medium, doing work, or by combining nitrogen with oxygen, and thus producing additional NO_x.

From the statistical treatment of the rate of heat release graphs (Figs 13–15), the end of the combustion process in the ignition engine with/without exhaust gas recirculation is also not the same. This is shown in the graph in Fig. 22.

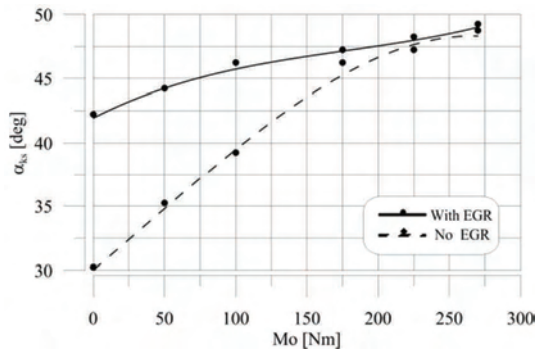


Fig. 22. Influence of the engine load on the end of combustion α_{ks} for engine operating with/without EGR

The later end of the combustion process for an EGR engine involves practically all of the aforementioned phenomena: the availability of oxygen and the greater share of CO_2 in the engine cylinder, shorter delay of self-ignition, lower rate of kinematic and diffusion heat release and more

chronic burning, which is a more low temperature process than for the non-EGR engine.

Conclusions

The use of non-cooled exhaust gas recirculation in CI engines in relation to indicator diagrams and rates of heat release results in (compared to engines without EGR):

1. reducing the pressure of the compressed working medium in the engine cylinder (before the self-combustion of fuel),
2. reduction of maximum combustion pressure $p_{s,max}$ by approx. 60% at idle run of the engine and approx. 10% at partial loads of the engine,
3. decrease in the maximum rate of combustion pressure $(dp/d\alpha)_{max}$ up to 37% at 1/3 of maximum engine torque. In this point of engine work decrease of NO_x, as a result of the EGR system action, is even 48%,
4. shortening the delay of self-ignition, mainly as a physical effect of the mixing of hot exhaust gases with the air in the engine intake manifold,
5. decrease in both max rate of kinetic $(dQ_k/d\alpha)_{max}$ and diffusion $(dQ_d/d\alpha)_{max}$ heat release. Unfortunately, the reduction in the rate of diffusion combustion results in a decrease in the amount of soot burned in the engine cylinder, which in the general balance increases PM emission and exhaust smoke,
6. reduction of oxygen availability and increase of CO_2 concentration in the engine cylinder significantly reduce the speed and combustion temperature, which is one of the reasons of the lower NOx emission in the engine exhaust,
7. later end of the combustion process, which also contributes to a more low-temperature combustion process.

Nomenclature

CO_2	concentration of carbon dioxides
CI	compression ignition
D	exhaust smoke
EGR	exhaust gas recirculation
ECU	
Mo	engine torque
NOx	concentration of nitrogen oxides
O_2	concentration of oxygen
PM	particulate matter
p	pressure inside engine cylinder
$p_{s,max}$	maximum combustion pressure
$(dp/d\alpha)_{max}$	max rate of combustion pressure
$(dQ_k/da)_{max}$	max rate of kinetic heat release
$(dQ_d/da)_{max}$	max rate of diffusion heat release
α	crank angle
α_{pw}	start of fuel injection
α_{ps}	start of self-injection
α_{ks}	end of combustion
τ_s	delay of self-ignition

Bibliography

[1] HEYWOOD, J.B. Internal combustion engine fundamentals. *McGraw-Hill.* Series in Mechanical Engineering. 1988.

[2] WIMMER, A., GLASER, J. Indykowanie silnika. *AVL.* Warszawa 2004.

[3] MERKISZ, J. Ekologiczne problemy silników spalinowych. Tom 1. *Wydawnictwo Politechniki Poznańskiej*. Poznań 1998.

[4] MYSZKOWSKI, S. Recyrkulacja spalin w silnikach cz. 1. *Dodatek techniczny do wiadomości Inter Cars S.A*. 2010, **35**.

[5] CIEŚLIK, W., BOROWSKI, P., PIELECHA, I. et al. System recyrkulacji spalin we współczesnych konstrukcjach silnikowych. *Logistyka*. 2014, **3**.

Jerzy Cisek, DSc. DEng. – Faculty of Mechanical Engineering at Cracow University of Technology.

e-mail: *JCisek@pk.edu.pl*

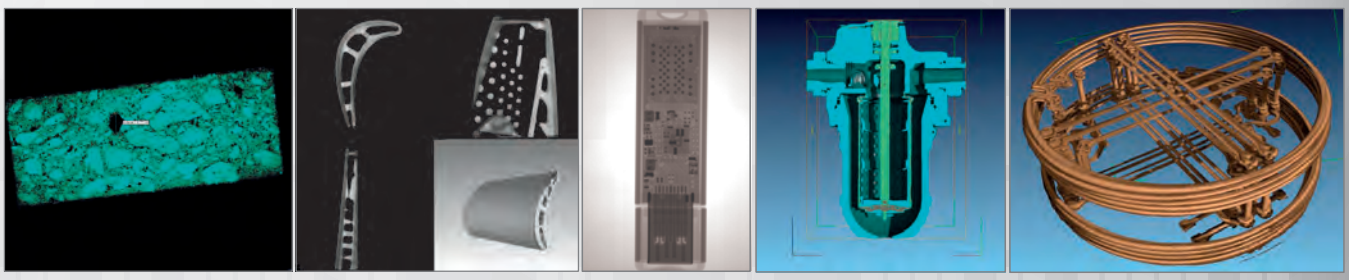


INSTYTUT TECHNICZNY WOJSK LOTNICZYCH

ul. Księcia Bolesława 6, 01-494 Warszawa, skr. poczt. 96
tel.: 261 851 300; tel./faks: 261 851 313
www.itwl.pl e-mail: poczta@itwl.pl

Tomograf komputerowy (CT) – badanie nieniszczące NDT

Instytut Techniczny Wojsk Lotniczych oferuje usługi z zakresu badań tomografem komputerowym. Badania prowadzone są na tomografie typu v/tome/x m 300 firmy GE o max. mocy lampy 300kV/500W. Urządzenie posiada również lampę do nanotomografii o mocy 80kV/15W.

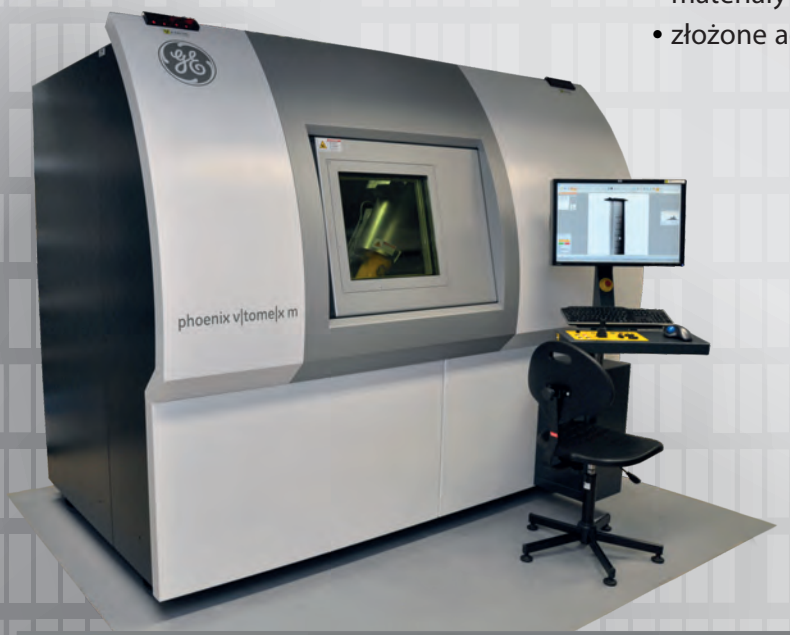


Prowadzimy prace badawcze obejmujące swym zakresem materiały takie jak:

- stopy tytanu
- stale
- materiały kompozytowe
- beton
- guma

Urządzenie umożliwia prowadzenie badań z zakresu:

- wykrywania defektów o rozmiarach powyżej 0,5 µm z wykorzystaniem lampy 180 kV
- materiałów o bardzo dużej gęstości (np. łopatki turbin silników lotniczych) z wykorzystaniem lampy o mocy 300 kV
- układy elektroniczne (scalone)
- materiały pirotechniczne
- złożone agregaty lotnicze

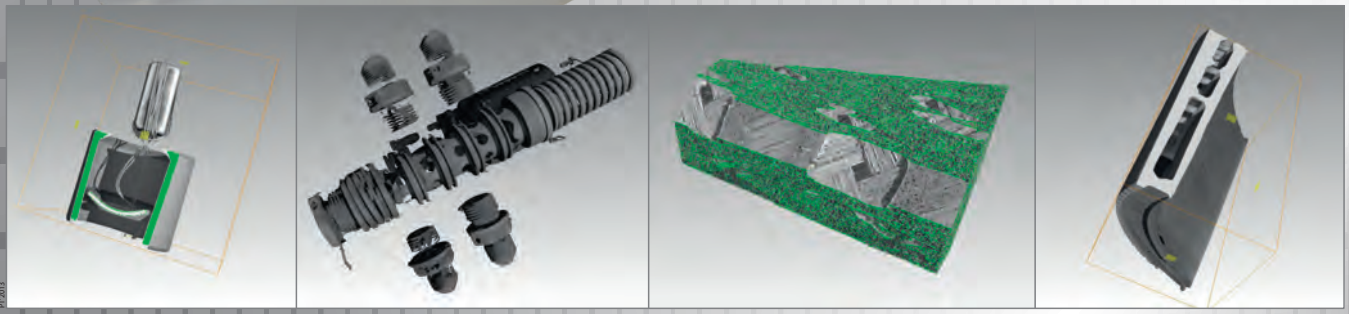


Masa badanych elementów do 50 kg.
Wymiary orientacyjne 50×50×60 cm.

Posiadamy wysoko wykwalifikowany, certyfikowany personel.

Kontakt bezpośredni:
Zakład Silników Lotniczych
tel.: +48 261 851 334; fax: +48 261 851 338
e-mail: jaroslaw.spychala@itwl.pl

Zapraszamy do współpracy!





Publisher:

Polish Scientific Society of Combustion Engines

Combustion Engines

Polskie Towarzystwo Naukowe Silników Spalinowych







ISSN: 2300-9896

www.combustion-engines.eu